

# Multiplicity Dependence of $\sigma_{\psi(2S)}/\sigma_{J/\psi}$ in $pp$ collision at $\sqrt{s} = 13$ TeV

Xianglei Zhu, Youen Kang, Li Xu, Chenzhi Dong.

*Tsinghua University*

## Abstract

Using a data sample with an integrated Luminosity of  $658 \text{ pb}^{-1}$  collected by the LHCb detector in the LHC operations in 2016, ratio of production cross section of  $\psi(2S)$  over  $J/\psi$  as a function of multiplicity was measured in proton-proton collisions at a centre-of-mass energy  $\sqrt{s} = 13$  TeV. A multiplicity-dependent modification of the ratio has been observed for prompt mesons when there is an overlap between the rapidity ranges where the multiplicity and the charmonia production are measured. No evident modification of same significance for that of non-prompt component is observed. The ratio as a function of multiplicity is compared to co-mover model and show agreements except in low multiplicity region. The ratio and ratio as a function of  $p_T$  are compared to other measurements in different collision systems, which shows a good agreement.



# 1 Contents

2	<b>1 Introduction</b>	3
3	<b>2 Data and Monte Carlo samples</b>	4
4	2.1 Data . . . . .	4
5	2.2 Monte Carlo . . . . .	4
6	<b>3 Candidate Reconstruction and selection</b>	5
7	3.1 Trigger and Turbo stream selection . . . . .	5
8	3.2 Offline Selection . . . . .	6
9	<b>4 Ratio of Cross-Section Determination</b>	7
10	4.1 Double Differential Cross-Section . . . . .	7
11	4.2 Ratio of Cross-Section . . . . .	9
12	<b>5 Signal Extraction</b>	10
13	5.1 Determination of the prompt and detached signal yields . . . . .	10
14	<b>6 Efficiency determination</b>	13
15	6.1 Geometrical acceptance . . . . .	15
16	6.2 Reconstruction-selection efficiency . . . . .	16
17	6.3 Muon identification efficiency . . . . .	18
18	6.4 Trigger efficiency . . . . .	19
19	6.5 Total efficiency . . . . .	20
20	6.6 Variation due to different reweight samples . . . . .	20
21	<b>7 Systematic Uncertainties</b>	21
22	7.1 Signal extraction . . . . .	23
23	7.1.1 Signal mass shape . . . . .	23
24	7.1.2 Fit to $t_z$ background . . . . .	24
25	7.1.3 Fit to $t_z$ signal . . . . .	25
26	7.2 Trigger efficiency . . . . .	25
27	7.3 Tracking efficiency . . . . .	28
28	7.4 MuonID efficiency . . . . .	29
29	7.5 MC sample size . . . . .	30
30	7.6 Other systematic uncertainties . . . . .	30
31	<b>8 Bin Width Correction</b>	31
32	<b>9 Results</b>	33
33	9.1 $\psi(2S)$ -to- $J/\psi$ ratio as functions of multiplicity . . . . .	33
34	9.2 $\psi(2S)$ -to- $J/\psi$ ratio in different $p_T$ regions . . . . .	35
35	9.3 $\psi(2S)$ -to- $J/\psi$ ratio in different $y$ regions . . . . .	37
36	9.4 Comparisons with other measurements . . . . .	38
37	<b>10 Conclusion</b>	40
38	<b>A Tables of ratio</b>	40

<sup>39</sup>	<b>B</b> Tables of the fit results in each kinematic bin	<b>48</b>
<sup>40</sup>	<b>C</b> Efficiency tables	<b>80</b>
<sup>41</sup>	<b>D</b> Fitting plots in each kinematic bin	<b>92</b>
<sup>42</sup>	<b>References</b>	<b>207</b>

## 43 1 Introduction

44 In normal matter, quarks and gluons are confined within particles called hadrons, such  
45 as protons and neutrons. However, at extremely high temperatures and densities, such  
46 as those that existed shortly after the Big Bang or in high-energy particle collisions, the  
47 strong force that binds quarks and gluons together becomes weaker. It results in the  
48 creation of a new form of matter Quark Gluon Plasma (QGP) in which the partons are  
49 evolving quasi freely. The measurement of quarkonia suppression is considered a probe of  
50 QGP. In such a hot and dense state, the existence of a large density of free color charges  
51 will lead to a color screening of quark and anti-quark binding, hence, the dissociation of  
52 quarkonium [1].

53 But before we interpret any phenomena observed in hot, dense QCD matter, baseline  
54 measurements need to be performed in the small system such as  $pp$  collisions in which  
55 no QGP is in principle produced. With the increasing charged-particle multiplicity, a  
56 transition from normal density to a relatively high-density environment serves as a probe  
57 for how quarkonium production suppression is affected by the charged particle multiplicity.

58 Quarkonia suppression can be detected by measuring nuclear modification factors. This  
59 factor is computed by measuring quarkonia yields in heavy-ion collisions and compared  
60 to the yield measured in  $pp$  collisions scaled by the number of nucleons. The PHENIX  
61 collaboration measured the nuclear modification factor of  $J/\psi$  in dAu collisions at 200  
62 GeV [2] and observed a significative suppression while no QGP production is expected.  
63 More recent results by LHCb also confirm this suppression [3] in the nuclear modification  
64 factor measured using  $p\text{Pb}$  collisions. However, this suppression can be explained by  
65 different effects such as the nuclear Parton Distribution functions (nPDFs) of the colliding  
66 heavy-ion [4], quarkonia energy loss [5] or interaction with co-moving particles [6]. The  
67 latter effect would affect quarkonia from two excited states differently, as they have  
68 different binding energy, and would have a stronger influence when the multiplicity of the  
69 collisions is high. The effect governing heavy quark production is expected to be similar  
70 for charmonium with the same content.

71 As we mentioned above, quarkonia suppressions in  $pp$  collisions have been traditionally  
72 served as a baseline measurement when searching QGP. While more and more signatures  
73 of QGP has been observed in small systems such as high-multiplicity  $pp$  collisions. For  
74 examples, ALICE collaboration has reported a measurement of strangeness enhancement  
75 in high-multiplicity  $pp$  collisions at  $\sqrt{s} = 7$  TeV [7] and CMS collaboration found a high  
76 degree of collectivity flow in high-multiplicity  $pp$  collisions at  $\sqrt{s} = 13$  TeV [8]. The  
77 possible existence of QGP in high-multiplicity  $pp$  collisions could also have an effect on  
78 the suppressions of charmonia since color Debye Screening effect will prevent quark from  
79 forming a quarkonium with an anti-quark. Quarkonia with same content but different  
80 energy levels may dissociate at different temperatures. Those with higher energy levels  
81 have a weaker bound will dissociate first compared to the lower-levels in QGP, which  
82 will cause a similar effect on the ratio of  $\sigma_{\psi(2S)}/\sigma_{J/\psi}$ . Hence, a further calculation from  
83 co-mover model prediction is needed to verify the sources of different suppressions, if exist.

84 The analysis proceeds as follows: Samples of  $J/\psi$  and  $\psi(2S)$  are selected from 13 TeV  
85  $pp$  collisions data collected in 2016, by fitting the invariant mass spectrum of oppositely  
86 charged muons. Prompt and non-prompt components are separated by fitting the pseudo  
87 proper-time in multiple bins of multiplicity. Then the yields are corrected by the efficiencies  
88 from different sources. Then the ratio of production is calculated in each multiplicity

89 bin to come to a final result. Three variables, PVNTRACKS, nForwardTracks and  
90 nBackwardTracks, are used as proxy for the multiplicity of the  $pp$  collisions. PVNTRACKS  
91 is the number of tracks used to reconstruct the primary vertex, and nBackTracks is the  
92 number of tracks in the backward directions. PVNTRACKS is the global multiplicity of  
93 the  $pp$  collisions while nForwardTracks is the multiplicity measured in the same phase  
94 space as the two charmonia. Some correlations between the ratio and nForwardTracks  
95 can appear and due to that, the use of nBackTracks, allows to reduce this effect.

## 96 2 Data and Monte Carlo samples

### 97 2.1 Data

98 The study here uses  $pp$  collision data collected by the LHCb detector at a center-of-mass  
99 energy of 13 TeV in 2016 with a corresponding luminosity of  $658 \pm 13 \text{ pb}^{-1}$ . To enlarge  
100 the sample size, two different TCKs 0x1138160F and 0x11381612 of both MagUp and  
101 MagDown were used. In this analysis, only muon triggers are used, and both TCKs have  
102 identical criteria for muon selection. The bookkeeping paths for the mdst file for both  
103  $J/\psi$  and  $\psi(2S)$  are as follows:

- 104 • MagUp /LHCb/Collision16/Beam6500GeV-VeloClosed-MagUp/Real  
105 Data/Turbo03a/94000000/LEPTONS.MDST
- 106 • MagDown /LHCb/Collision16/Beam6500GeV-VeloClosed-MagDown/Real  
107 Data/Turbo03a/94000000/LEPTONS.MDST

108 The NoBias data is used for normalization of multiplicity. The bookkeeping path for the  
109 mdst file is:

- 110 • /LHCb/Collision16/Beam6500GeV-VeloClosed-MagDown/Real  
111 Data/Reco16/96000000/FULL.DST

### 112 2.2 Monte Carlo

113 To study the efficiency, full simulation Monte Carlo samples with about 20 M candidates  
114 for  $J/\psi$  and 10 M for  $\psi(2S)$ . The bookKeeping path for them are:

- 115 •  $J/\psi$ 
  - 116 – MagUp /MC/2016/24142001/Beam6500GeV-2016-MagUp-Nu1.6-25ns-  
117 Pythia8/Sim09b/Trig0x6138160F/Reco16/Turbo03/  
118 Stripping26NoPrescalingFlagged/ALLSTREAMS.DST
  - 119 – MagDown /MC/2016/24142001/Beam6500GeV-2016-MagDown-Nu1.6-25ns-  
120 Pythia8/Sim09b/Trig0x6138160F/Reco16/Turbo03/  
121 Stripping26NoPrescalingFlagged/ALLSTREAMS.DST
- 122 •  $\psi(2S)$ 
  - 123 – MagUp: /MC/2016/28142001/Beam6500GeV-2016-MagDown-Nu1.6-25ns-  
124 Pythia8/Sim09i/Trig0x6139160F/Reco16/Turbo03a/  
125 Stripping28r2NoPrescalingFlagged/ALLSTREAMS.DST

126 – MagDown: /MC/2016/28142001/Beam6500GeV-2016-MagUp-Nu1.6-25ns-  
 127 Pythia8/Sim09i/Trig0x6139160F/Reco16/Turbo03/  
 128 Stripping28r2NoPrescalingFlagged/ALLSTREAMS.DST

129 In the simulation,  $pp$  collisions are generated using Pythia [9] with a specific LHCb  
 130 configuration [10]. Decays of hadronic particles are described by EvtGen [11], in which  
 131 final state radiation is generated using Photos [12]. The interaction of the generated  
 132 particles with the detector and its response are implemented using the Geant4 toolkit [13]  
 133 as described in Ref. [14]. The prompt charmonium production is simulated in Pythia with  
 134 contributions from both the leading order color-singlet and color-octet mechanisms [10,  
 135 15], and the charmonium is generated without polarization. To study the geometrical  
 136 acceptance, two samples of 100 k candidates generator level Monte Carlo are produced for  
 137 both  $J/\psi$  and  $\psi(2S)$  respectively. Since the acceptance is only a function of kinematic  
 138 variables, hence, it is universal for all multiplicity regions. Under the binning scheme in  
 139 Sec 4, the sample size is fairly enough.

## 140 3 Candidate Reconstruction and selection

### 141 3.1 Trigger and Turbo stream selection

142 The reconstruction and preselection of  $J/\psi$  and  $\psi(2S)$  candidates for real data were based  
 143 on the Turbo stream. The LHCb trigger system consists of three levels. The first level  
 144 ( $L0$ ) is designed to retain the instreaming data rate from detector read-outs up to 1  
 145 MHz, at which the LHC bunch crossing rate is 40 MHz. The  $L0$ -triggered data is input  
 146 to the first stage of the software trigger (HLT1), which then performs a partial event  
 147 reconstruction to filter out potentially signals of interest in the inflow data. The second  
 148 stage of the software trigger (HLT2) performs a full event reconstruction to further remove  
 149 backgrounds. This analysis is based on  $L0Dimuon$  and  $Hlt1DiMuonHighMass$  for both  $J/\psi$   
 150 and  $\psi(2S)$ . And  $Hlt2DiMuonJPsiTrubo$  for  $J/\psi$  and  $Hlt2DiMuonPsi2STrubo$  for  $\psi(2S)$ .  
 The online selections for the trigger are summarized in Table 1 for both  $J/\psi$  and  $\psi(2S)$ .

Table 1: Summary of Trigger Lines

trigger line	main cuts
$L0Dimuon$	$nSPDHits < 900$
$Hlt1DiMuonHighMass$	track $p_T > 300$ MeV/c track $p > 6000$ MeV/c $M_{\mu^+\mu^-} > 2700$ MeV/c <sup>2</sup> Muon ID: IsMuon
$Hlt2DiMuonJPsiTrubo$ $Hlt2DiMuonPsi2STrubo$	$(3096.9 - 120)$ MeV/c $< m_{J/\psi} < (3096.9 + 120)$ MeV/c $(3686.09 - 120)$ MeV/c $< m_{\psi(2S)} < (3686.09 + 120)$ MeV/c track $\chi^2/ndf < 4$ vertex $\chi^2/ndf < 25$

### 152 3.2 Offline Selection

153 The offline selections are applied to both  $J/\psi$  and  $\psi(2S)$  candidates to reduce the combinatorial background to a reasonable level and ensure the good quality of the signal-extraction  
 154 fit. First, each event is required to have exactly one primary vertex (PV) reconstructed  
 155 to avoid track contributions from multiple PVs that occur in the same beam crossing  
 156 (pile-up).  $J/\psi$  and  $\psi(2S)$  candidates are formed from pairs of oppositely charged tracks  
 157 reconstructed in the full tracking system (long tracks). We require the ghost probability  
 158 for each track ( $\mu^+$  and  $\mu^-$ ) to be less than 0.3. Both two tracks must have a transverse  
 159 momentum  $p_T$  above 1200 MeV/ $c$ , pass muon identification , and have a good quality of  
 160 the track fit ( $\chi^2/\text{ndf} < 3$ ). The pseudo-rapidity of each muon is required to be in the range  
 161  $2.0 < \eta < 4.9$ . A Particle identification (PID) is performed to identify muon candidates  
 162 ( $\text{DLLmu} > 2$ ). The two muons are required to form a good vertex by restricting the vertex  
 163 fit quality  $\text{Prob}(\chi^2/\text{ndf}) > 0.5\%$ . The pseudo-proper time is defined as  
 164

$$t_z = \frac{(z_X - z_{\text{PV}}) \times m_X}{p_z}, \quad (1)$$

165 where  $X$  is  $J/\psi$  or  $\psi(2S)$ ,  $z_X$  is the z position of the decay vertex,  $z_{\text{PV}}$  that of the primary  
 166 vertex,  $p_z$  the measured momentum along the beam axis z, and  $m_X$  the known mass for  
 167  $J/\psi$  and  $\psi(2S)$  [16]. This variable was found to give a good approximation of the b-hadron  
 168 decay proper time: given that b-hadrons are not fully reconstructed, the momentums of  
 169  $J/\psi$  and  $\psi(2S)$  are used instead of the exact b-hadron momentum.  $t_z$  is calculated event  
 170 by event with uncertainty no more than 0.3ps. In the analysis, it is required to be in the  
 171 range  $-10 < t_z < 10$  ps. Prompt component and component-from-b can be separated by  
 172 the different behaviors in the pseudo-proper time  $t_z$ . The full offline selection criteria are  
 summarized in Table 2. The restriction of vertex  $\chi^2/\text{ndf} < 7.8794$  is chosen so that the

Table 2: Summary of Offline Selections

Quantity	Requirement
nPVs	= 1
$z_{\text{PV}}$	$> -60$ mm (for PVNTRACKS as multiplicity variable) $> -30$ mm (for nBackTracks as multiplicity variable)
vertex $\chi^2/\text{ndf}$	$< 7.8794$
mass window	$m_{J/\psi} \pm 120$ MeV/ $c^2$ $m_{\psi(2S)} \pm 120$ MeV/ $c^2$
PID	IsMuon, $\text{DLLmu} > 2$ $\text{probNNmu} > 0.8$
muon $\eta$	$2 < \eta < 4.9$
track ghost prob.	$< 0.3$
$t_z$	$-10 \text{ ps} < t_z < 10 \text{ ps}$
$t_z$ uncertainty	$< 0.3$ ps

173  
 174 P-Value is exactly 0.005. For PID selection, we set  $\text{DLLmu} > 2$  to reduce combinatorial  
 175 background for both  $J/\psi$  and  $\psi(2S)$ . And  $\text{probNNmu} > 0.8$  is further applied since it

can largely reduce the combinatorial background for  $\psi(2S)$  at high multiplicity and low  $p_T$  bins. Here we restrict  $z_{\text{PV}}$  to be larger than -60 mm in order to maintain equivalent VELO acceptance. From Figure 1 we can see that for  $z_{\text{PV}} < -60$  mm (as indicated by the black, red, and green points), there is a clear deviation from the other curves toward lower track multiplicity. This is due to events producing tracks that do not enter the VELO acceptance. Therefore, in this analysis, we restrict our primary vertex z range to  $z_{\text{PV}} > -60$  mm. If nBackTracks is used as multiplicity variables, the restriction is further modified to  $z_{\text{PV}} > -30$  mm, and no restriction needs to be made for nForwardTracks as multiplicity variable, which can be seen in Fig. 1.

## 4 Ratio of Cross-Section Determination

### 4.1 Double Differential Cross-Section

The determination of the double-differential production cross-section requires knowledge of the numbers of prompt and non-prompt signals of  $J/\psi$  and  $\psi(2S)$  in bins of the kinematic variables  $y$  and  $p_T$ , and multiplicity bin. This is done by performing a simultaneous fit to the distributions of the dimuon invariant mass and the pseudo-proper time  $t_z$  in each bin. The  $t_z$  of promptly produced signals has zero lifetime, while the  $t_z$  distribution for the non-prompt signal is approximately exponential as seen from the simulation. The pseudo-proper time  $t_z$  allows us to statistically separate the prompt signal from that created in decays of b-hadrons. The double differential cross-section for prompt  $J/\psi$  and  $J/\psi$  from- $b$  production in a given ( $p_T$ ,  $y$ ) bin with multiplicity in a certain range is defined as

$$\frac{d^2\sigma_{J/\psi}}{dydp_T} = \frac{N(J/\psi \rightarrow \mu^+\mu^-)}{\mathcal{L} \times \epsilon_{\text{tot}} \times \mathcal{B}(J/\psi \rightarrow \mu^+\mu^-) \times \Delta y \times \Delta p_T}. \quad (2)$$

And for  $\psi(2S)$

$$\frac{d^2\sigma_{\psi(2S)}}{dydp_T} = \frac{N(\psi(2S) \rightarrow \mu^+\mu^-)}{\mathcal{L} \times \epsilon_{\text{tot}} \times k \cdot \mathcal{B}(\psi(2S) \rightarrow e^+e^-) \times \Delta y \times \Delta p_T}. \quad (3)$$

where

- $N$  is either the number of prompt  $\psi(2S)$  or  $\psi(2S)$  from  $b$ -hadron signals of  $J/\psi$  or  $\psi(2S)$  reconstructed through the dimuon decay channel. They are obtained by the fits;
- $\mathcal{L}$  is the integrated luminosity;
- $\epsilon_{\text{tot}}$  is the total efficiency in that particular  $p_T - y$  bin with PVNTRACKS in a certain range, for both prompt and non-prompt and both  $J/\psi$  and  $\psi(2S)$  respectively;
- $k$  is the phase space factor which is assumed to be unit under the assumption of lepton universality. The lepton universality is a reasonable assumption under the current statistical precision;
- $\mathcal{B}(J/\psi \rightarrow \mu^+\mu^-) = (5.961 \pm 0.033)\%$  is the branching fraction of the decay  $J/\psi \rightarrow \mu^+\mu^-$ , quoted from the PDG 2022 review [16].

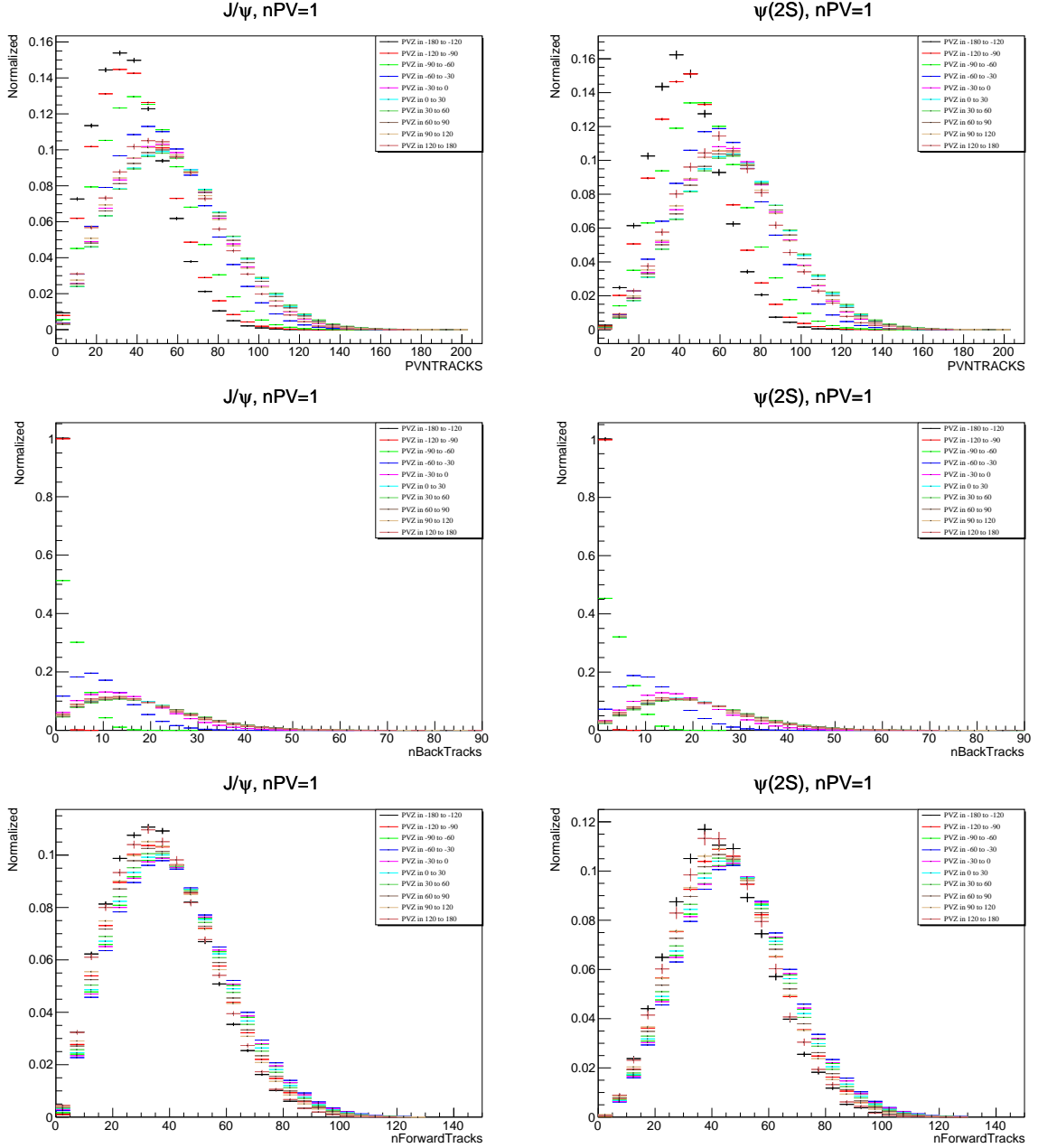


Figure 1: Distribution of PVNTRACKS, nBackTracks and nForwardTracks under  $nPVs = 1$  for  $J/\psi$  (left) and  $\psi(2S)$  (right). The clear deviation shows for  $z_{PV}$  smaller than a certain range so that we subtract that part of data for equivalence of VELO acceptance.

210     •  $\mathcal{B}(\psi(2S) \rightarrow e^+e^-) = (7.93 \pm 0.17) \times 10^{-3}$  is the branching fraction of the decay  
 211      $\psi(2S) \rightarrow e^+e^-$ , quoted from the PDG 2022 review [16]. The dielectron branching  
 212     fraction is used since it has a much smaller uncertainty than the dimuon one;

- 213     •  $\Delta p_T$  is the bin width of the transverse momentum;  
 214     •  $\Delta y$  is the bin width of the rapidity.

215     In the measurement of modification of  $b$  quark hadronization in high-multiplicity  $pp$   
 216     collision at  $\sqrt{s} = 13$  TeV shows that, ratio of cross sections  $\sigma_{B_s^0}/\sigma_{B^0}$  versus normalized  
 217     multiplicity behaves differently according to the choices of multiplicity variable [17]. That  
 218     motivates us to measure how the ratio changes with different multiplicity variables. The  
 219     following boundaries are used for the binning scheme of  $p_T$ ,  $y$  and different multiplicity  
 220     variables. To remove the contribution from photon-production charmonium, we remove  
 221     the production for  $p_T < 0.3$  GeV/ $c$ :

- 222     •  $p_T$  boundaries [GeV/ $c$ ]: 0.3, 2, 4, 6, 8, 20;  
 223     •  $y$  boundaries: 2.0, 2.8, 3.5, 4.5;  
 224     • For multiplicity (each at a time)  
     – PVNTRACKS: 4, 20, 45, 70, 95, 200. (At least 4 tracks required.)  
     – nBackTracks: 0, 8, 15, 22, 30, 80.  
     – nForwardTracks: 0, 12, 24, 36, 48, 130.

228     There is a wider bin in high  $p_T$  and multiplicity region, and the scheme of  $y$  is not exactly  
 229     evenly distributed for the sake of significant signal numbers for fitting in each bin. And this  
 230     binning scheme is common for both  $J/\psi$  and  $\psi(2S)$ . To see how charmonium suppression  
 231     is affected by charged particle multiplicity, we normalize the ratio of production to see  
 232     the trend. The multiplicity variables are normalized by their respective mean value from  
 233     an unbiased data sample from the same year. Here we divide them by the mean values  
 234     from NoBias data rather than just the mean values in their trigger lines is due to the  
 235     fact that the trigger line may influence the distribution of charged particle multiplicity.  
 236     So the x-coordinate represents 'how many times is the multiplicity to the mean value of  
 237     multiplicity from NoBias data'. Since the multiplicity distributions in high-energy hadron  
 238     collisions is a KNO variable [18], which is, after normalized, the distribution of a certain  
 239     collision system has the same distribution of a certain multiplicity variable. By scaling  
 240     we change the multiplicity variable as a scale of how many times the mean number of  
 241     charged particle multiplicity, so that the results are compatible with other results.

## 242     4.2 Ratio of Cross-Section

243     In each multiplicity region, we have defined the double differential cross-section in kinetic  
 244     bin ( $p_T, y$ ) above. Then the ratio of double differential cross-section is determined as  
 245     follows

$$\frac{\sigma(p_T, y)_{\psi(2S)}}{\sigma(p_T, y)_{J/\psi}} = \frac{N_{\psi(2S)}(p_T, y, \epsilon)}{N_{J/\psi}(p_T, y, \epsilon)} \times \frac{\epsilon_{\text{tot}, J/\psi}(p_T, y)}{\epsilon_{\text{tot}, \psi(2S)}(p_T, y)} \times \frac{\mathcal{B}_{J/\psi \rightarrow \mu^+\mu^-}}{k \times \mathcal{B}_{\psi(2S) \rightarrow e^+e^-}}, \quad (4)$$

where the bin widths for  $p_T$  and  $y$  are canceled out, so as the luminosity term. While when calculating the ratio of differential cross-section, the bin widths of  $p_T$  and  $y$  are no longer canceled out since the binning scheme is not uniform. Hence, the ratio of the cross-section is determined as follows,

$$\frac{\Sigma_{(p_T,y)}\sigma_{\psi(2S)}(p_T, y)}{\Sigma_{(p_T,y)}\sigma_{J/\psi}(p_T, y)} = \frac{\Sigma_{(p_T,y)}(\Delta p_T \times \Delta y \times N_{\psi(2S)}(p_T, y)/\epsilon_{\text{tot},\psi(2S)}(p_T, y))}{\Sigma_{(p_T,y)}(\Delta p_T \times \Delta y \times N_{J/\psi}(p_T, y)/\epsilon_{\text{tot},J/\psi}(p_T, y))} \times \frac{\mathcal{B}_{J/\psi \rightarrow \mu^+ \mu^-}}{k \times \mathcal{B}_{\psi(2S) \rightarrow e^+ e^-}}. \quad (5)$$

In a small kinetic bin, the efficiency  $\epsilon_{\text{tot}}$  is assumed to be constant, and thus a single number with corresponding uncertainty is provided. The efficiency for prompt non-prompt signals is calculated separately for  $J/\psi$  and  $\psi(2S)$ . And since our scheme is not significantly small, a re-weight in  $p_T$ - $y$  spectrum is performed when calculating the efficiency.

## 5 Signal Extraction

The total number of  $J/\psi$  and  $\psi(2S)$  signals is determined from an extended unbinned maximum likelihood fit to the invariant mass distribution of the selected candidates. The fit models for both  $J/\psi$  and  $\psi(2S)$  are the same, which we consider the previous studies of  $J/\psi$  production at 13 TeV [19] and  $\psi(2S)$  production at 13 TeV [20]. The only strategy for both is as follows.

In the fit the component of the background is modelled with an exponential function

$$f_{\text{bkg}}(m) = a_0 e^{-p_0 \cdot m}. \quad (6)$$

The signal component is described by the sum of two Crystal Ball (CB) functions [21]. The CB function is defined as:

$$f_{\text{CB}}(m; \mu, \sigma, \alpha, n) = \begin{cases} \left(\frac{n}{|\alpha|}\right)^n e^{-\frac{1}{2}\alpha^2} \left(\frac{n}{|\alpha|} - |\alpha| - \frac{m-\mu}{\sigma}\right)^{-n} & \frac{m-\mu}{\sigma} < -|\alpha| \\ \exp\left(-\frac{1}{2}\left(\frac{m-\mu}{\sigma}\right)^2\right) & \frac{m-\mu}{\sigma} > -|\alpha|. \end{cases}, \quad (7)$$

which combines a Gaussian core (described by the parameters  $\mu$  and  $\sigma$ ) and one tail on the left (described by the parameters  $\alpha$  and  $n$ ). The tails in CB functions are used to model the radiative effects, which leads to more candidates with lower invariant masses. Not all parameters of the CB functions are free when fitting data. Some parameters are fixed or parameterized. For both  $J/\psi$  and  $\psi(2S)$ , the two CB functions share one common mean value  $\mu$  and have different widths  $\sigma_1$  and  $\sigma_2$ , and  $\alpha$  is parameterized from simulation as a function of the  $\sigma$ :  $\alpha = 2.066 \pm 0.0085\sigma - 0.00011\sigma^2$ , which applies to both CB functions. Furthermore, for  $\psi(2S)$  only,  $\sigma_1$  and  $\sigma_2$  are parameterized as a linear function:  $\sigma_2 = 25.7 + \sigma_1$  and the fraction of the narrower CB function is fixed at 0.96. For the tail parameters,  $n$  is fixed to unity from physics [22]. Therefore, there are merely two free parameters for the signal shape,  $\mu$  and  $\sigma_1$ . The strategy followed the previous study of  $J/\psi$  and  $\psi(2S)$  production at 13 TeV [19, 20]. The invariant mass fit is performed in each  $p_T - y$  and PVNTRACKS bin of the candidate.

### 5.1 Determination of the prompt and detached signal yields

To determine the signal yields of prompt and from- $b$  components separately, the  $t_z$  distribution is used. In each kinematic and multiplicity bin, an unbinned extended

maximum likelihood fit to the two-dimension distributions of invariant mass  $m(\mu^+\mu^-)$  and  $t_z$  is performed to separate prompt component from that from  $b$ .

At the generator level, the  $t_z$  distribution of the prompt component is a Dirac delta function,  $\delta(t_z)$ , while that from  $b$  follows an exponential function as seen from simulation. For  $J/\psi$  and  $\psi(2S)$  signals, the detector resolution is taken into account by convolving a resolution function, which is described by the sum of two Gaussian functions,

$$f_{\text{resolution}}(t_z; \mu, S_1, S_2, \beta) = \frac{\beta}{\sqrt{2\pi}S_1\sigma} e^{-\frac{(t_z-\mu)^2}{2S_1^2\sigma^2}} + \frac{1-\beta}{\sqrt{2\pi}S_2\sigma} e^{-\frac{(t_z-\mu)^2}{2S_2^2\sigma^2}}. \quad (8)$$

The parameter  $\sigma$  is the event-by-event uncertainty of  $t_z$ , calculated by combining the estimated uncertainties of the  $J/\psi$  and  $\psi(2S)$  decay vertex and the associated PV. Besides,  $S_1$  and  $S_2$  are two scale factors to correct the non-perfect estimation of the  $t_z$  uncertainty, the parameter  $\mu$  is the bias of the  $t_z$  measurement, and  $\beta$  is the fraction of one of the two Gaussians. In the fitting procedure, all the resolution parameters are floated. For some ( $p_T, y$ , PVNTRACKS) bin, the count for signal yield for  $\psi(2S)$  or  $J/\psi$  is significantly low that fit will fail for too many free parameters, and we may set  $\beta = 0$ , which is, only one Gaussian function is used to describe the resolution.

It is possible that the reconstructed candidate is associated with a "wrong" PV. This can happen either because the real PV that produces the candidate failed to be reconstructed, and the candidate was associated with the nearest reconstructed PV in the event, or because a wrong PV is accidentally close to the candidate. For the latter case, the positions of the reconstructed and the true PV are correlated, which results in a Gaussian-like  $t_z$  distribution with a width much larger than the detection resolution. This effect can be described by adding a third Gaussian with a much larger width than the resolution function. However, it is found from simulation that including the wide Gaussian in the resolution does not change the fitted parameters significantly because the fraction of this component is quite small,  $\leq 1\%$  as seen from studies in Ref. [19]. Therefore, the third wide Gaussian is not used in the fit function. For the former case that the true PV is not reconstructed, the true PV and wrongly associated PV are not correlated, which results in a long tail in the  $t_z$  distribution that can be modeled using the next-event method for both  $J/\psi$  and  $\psi(2S)$ . The next-event method is applied directly on data sample. The next-event pseudo-proper time,  $t_z^{\text{next}}$ , for each candidate, is calculated combining the candidate with the closest PV of another (next) event as

$$t_z^{\text{next}} = \frac{(z_{\mu\mu} - z_{\text{PV}}^{\text{next}}) \times m_{\mu\mu}}{p_z}, \quad (9)$$

where  $z_{\text{PV}}^{\text{next}}$  is the  $z$ -coordinate of the nearest PV of the next selected event. The tail distribution is extracted in each bin separately and not convolved with resolution functions since the distribution is much wider than the resolution and very smooth in the whole  $t_z$  region. It should be noted that since the requirement of PV reconstruction is loose, using at least 4 VELO tracks, the probability to reconstruct the true PV is very high ( $> 99\%$ ).

The candidates in the mass sidebands, where  $m_{\mu^+\mu^-}$  is at least 60 MeV/c away from the mass of  $J/\psi$  and  $\psi(2S)$ , are used as the background control sample to model the  $t_z$  distribution of the background. The background control sample consists of random combinations of muons from semi-leptonic  $b$  and  $c$  decays, which tend to produce positive  $t_z$  values, as well as mis-reconstructed tracks from decays-in-flight of kaons and pions,

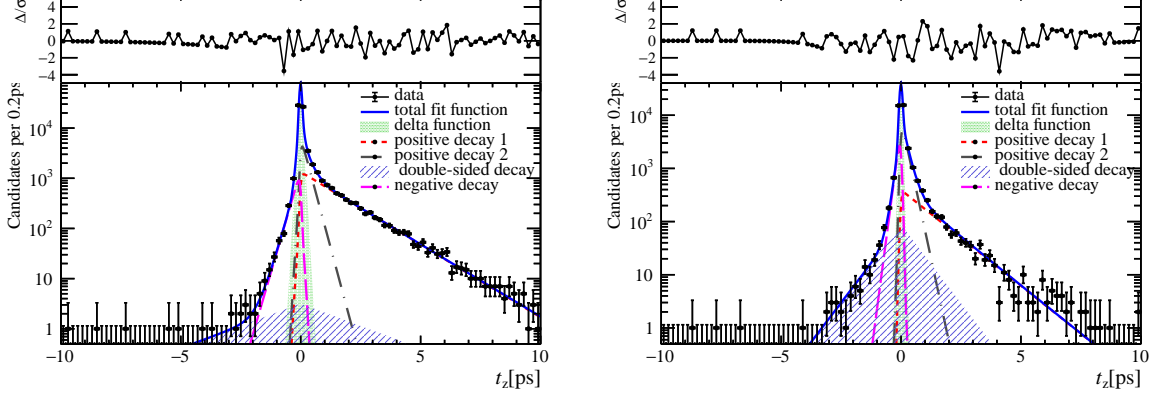


Figure 2:  $t_z$  background fit for PVNTRACKS from 20 to 40,  $y$  from 2 to 2.8, and  $p_T$  from 2  $\text{GeV}/c$  to 4  $\text{GeV}/c$ . The left is that of  $J/\psi$  and the right is of  $\psi(2S)$ .

which contribute both to positive and negative  $t_z$  values. The  $t_z$  distribution of the background is therefore modeled with an empirical function, composed of a Dirac delta function and five exponentials (three for positive  $t_z$  and two for negative  $t_z$ , with one positive  $t_z$  and one negative sharing the same slope parameter). This function is convolved with the sum of two Gaussian functions as a resolution function, which has different parameters as for signals,<sup>1</sup>,

$$f_{\text{background}} = \left[ (1 - f_1 - f_2 - f_3 - f_4) \delta(t_z) + \theta(t_z) \left( \frac{f_1}{\tau_1} e^{-t_z/\tau_1} + \frac{f_2}{\tau_2} e^{-t_z/\tau_2} \right) + \theta(-t_z) \left( \frac{f_3}{\tau_3} e^{t_z/\tau_3} + \frac{f_4}{2\tau_4} e^{-|t_z|/\tau_4} \right) \right] * \left( \frac{\beta'}{\sqrt{2\pi S'_1} \sigma} e^{-\frac{(t_z-\mu)^2}{2S'^2_1 \sigma^2}} + \frac{1-\beta'}{\sqrt{2\pi S'_2} \sigma} e^{-\frac{(t_z-\mu)^2}{2S'^2_2 \sigma^2}} \right). \quad (10)$$

The parameters in Eq. 10 are determined by fitting the  $t_z$  distribution of background control sample defined above (in each kinematical bin of  $J/\psi$  and  $\psi(2S)$ ), and are fixed for the final fits. In Fig. 2, the  $t_z$  distribution of the background in the kinematic range  $p_T \in [2, 4] \text{ GeV}/c$ ,  $y \in [2.0, 2.8]$  and PVNTRACKS  $\in [20, 40]$  is shown, superposed by a fit using Eq. 10. In total, the eventual function for the  $t_z$  fit is:

$$F_{t_z}(t_z; n_{\text{prompt}}, n_{\text{tail}}, n_{\text{bdecay}}, n_{\text{bkg}}, \mu, S_1, S_2, \beta, \tau_b) = \left( n_{\text{prompt}} \delta(t_z) + \frac{n_{\text{bdecay}}}{\tau_b} e^{-t_z/\tau_b} \right) * f_{\text{resolution}}(t_z; \mu, S_1, S_2, \beta) + n_{\text{tail}} f_{\text{tail}}(t_z) + n_{\text{bkg}} f_{\text{background}}(t_z), \quad (11)$$

where  $n_{\text{bkg}}$ ,  $n_{\text{prompt}}$ ,  $n_{\text{bdecay}}$  and  $n_{\text{tail}}$  are the number of background, prompt components, components from  $b$  and wrong PV events, respectively.

Because the requirement of the PV reconstruction is loose, and the PV is not refitted by removing the VELO segments of the muon tracks, it is reasonable to assume that prompt components and components from  $b$  have equal probability to be assigned with a wrong PV. Therefore, the fractions of the prompt and from  $b$  components in  $n_{\text{tail}}$  is

<sup>1</sup>The uncertainty on the background vertex is usually worse than that for the signal vertex.

336 equal to the fraction  $\frac{n_{\text{prompt}}}{n_{\text{bdecay}} + n_{\text{prompt}}}$  and  $\frac{n_{\text{bdecay}}}{n_{\text{bdecay}} + n_{\text{prompt}}}$ . Even if the shape is extracted from  
 337 data including the background candidate, the fit result  $n_{\text{tail}}$  should only contain prompt  
 338 and non-prompt signals. First, the shape of the PDF due to the wrong-PV effect should  
 339 be the same no matter from which sample we extract it. Then, the wrong-PV effect for  
 340 background candidates should be merged in the background PDF, which means the  $n_{\text{tail}}$   
 341 part in the total PDF should be specifically for signal candidates. And in this analysis,  
 342 we only care about the ratio of prompt and from  $b$ , where  $n_{\text{tail}}$  in each kinetic bin and  
 343 multiplicity bin accounts for about 0.1% of  $n_{\text{bdecay}} + n_{\text{prompt}}$ , which results in an even  
 344 more negligible influence on the ratio in Sec 4. In this case, we can ignore the subtle  
 345 contribution to  $n_{\text{bdecay}}$  and  $n_{\text{prompt}}$  from  $n_{\text{tail}}$ .

346 The two-dimensional fit to the invariant mass and the lifetime in the kinematic range  
 347  $4 \text{ GeV}/c < p_T < 6 \text{ GeV}/c$ ,  $2.0 < y < 2.8$  and multiplicity bin  $20 \leq \text{PVNTRACKS} < 40$   
 348 is shown in Fig. 3, with the red shaded area being prompt components, and the cyan  
 349 shaded area being components from  $b$ , the dots with vertical error bar are data points,  
 350 the violet dashed lines are the combinatorial background, the green dashed lines are the  
 351 components by wrong PV (which are invisible in the graph of projection on mass) and  
 352 the blue lines are the total fit functions. During the  $t_z$ -mass combined fitting procedure,  
 353 the parameters of mass signal shape ( $\mu_{\text{mass}}, \sigma_{\text{mass}}, p_0$ ) are floated within a certain times  
 354 of their uncertainties from the 1D mass fit for the final fits of  $J/\psi$ . While for  $\psi(2S)$ , due  
 355 to the limitation of number of candidates, the parameters are fixed. According to the  
 356 comparison of two fitting strategies upon  $J/\psi$ , no significant difference between errors of  
 357 prompt and non-prompt signals are observed ( 0.1%).

## 358 6 Efficiency determination

359 The total efficiency  $\epsilon_{\text{tot}}$  is determined independently in each kinetic bin and multiplicity  
 360 bin. The expression is as follows,

$$\epsilon_{\text{tot}} = \epsilon_{\text{acc}} \times \epsilon_{\text{Reco\&Sel}} \times \epsilon_{\text{MuonID}} \times \epsilon_{\text{Trigger}}. \quad (12)$$

361 The Monte Carlo samples for both prompt and non-prompt signals of  $J/\psi$  and  $\psi(2S)$  are  
 362 divided according to the multiplicity binning schemes in Sec. 4. For different multiplicity  
 363 regions based on division upon different multiplicity variables, efficiencies are calculated  
 364 in the same way as follows, which is calculated in the same binning scheme for kinematic  
 365 variables  $p_T$  and  $y$ . The truth-matching fail rates for both  $J/\psi$  and  $\psi(2S)$  are around 0.4%,  
 366 which is negligible compared to the statistical and systematic uncertainties after division  
 367 to get the ratio. And in the simulated sample, the efficiency of prompt components and  
 368 components from  $b$ -hadron decay is calculated separately. Since we have already separated  
 369 the data and MC in a multiplicity bin, the bin width of  $p_T$  and  $y$  is not significantly  
 370 small that the efficiency can be treated as constant in a certain kinetic bin, hence, all  
 371 the efficiencies are corrected by reweighting the distribution of  $p_T$ - $y$  spectrum of MC to  
 372 that of s-weighted data which contains only signal by sPlot method [23]. Also, the effect  
 373 due to the difference in the distribution of multiplicity is corrected by reweighting the  
 374 distribution of multiplicity variables of MC to that of s-weighted data which contains only  
 375 signal. Since there are differences in the distribution of  $p_T$ - $y$  spectrum and multiplicity  
 376 variables for prompt and non-prompt signals, before calculating efficiencies, we reweight

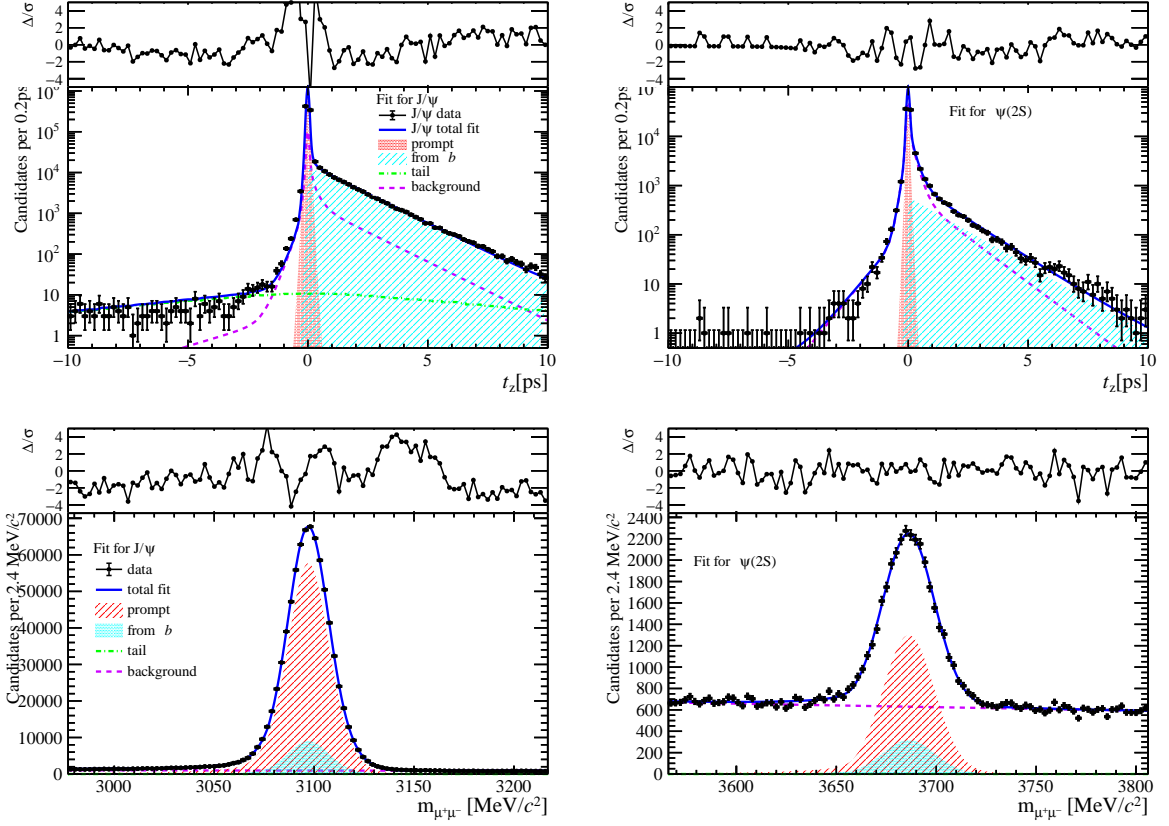


Figure 3: Projection in  $t_z$  and mass spectrum of  $t_z$ -mass fit for PVNTRACKS from 20 to 40,  $y$  from 2 to 2.8, and  $pt$  from  $2 \text{ GeV}/c$  to  $4 \text{ GeV}/c$ . The left is that of  $J/\psi$  and the right is of  $\psi(2S)$ .

377 the  $p_T$ - $y$  and multiplicity distributions separately for prompt and non-prompt signals, as  
 378 shown in Figs 4.

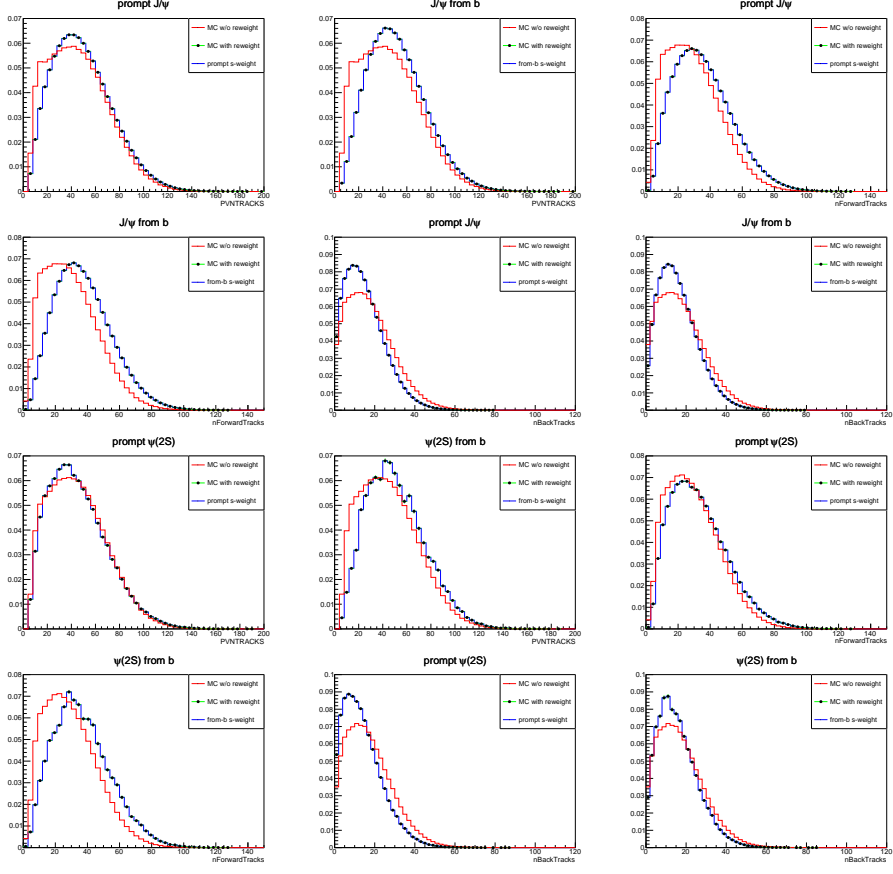


Figure 4: Reweighting the multiplicity distribution to match MC to s-weighted data, the first two rows are reweight of  $J/\psi$  and the rest two rows are of  $\psi(2S)$ .

379 For  $J/\psi p_T$ - $y$  reweight, the results cut in each  $y$  region for  $J/\psi$  is shown in Figs 5. And  
 380 the result for  $\psi(2S)$  is shown in Figs 6.

## 381 6.1 Geometrical acceptance

382 The geometrical acceptance in each kinematic bin is defined as

$$\epsilon_{\text{acc}} \equiv \frac{N(p_T, y) \text{ with both } \mu \text{ in LHCb acceptance}}{N(p_T, y)}. \quad (13)$$

383 The LHCb acceptance means the polar angle  $[10, 400]$  mrad defined with respect to the  
 384 direction of LHCb  $z$ -axis, before the effect of the magnetic field. The efficiency  $\epsilon_{\text{acc}}$  is  
 385 determined using a simulated sample at the generator level. In Fig. 7, the efficiency in each  
 386  $p_T$  and  $y$  bin of  $J/\psi$  and  $\psi(2S)$  mesons for  $PVZ > -60\text{mm}$  and  $nPVs = 1$  are presented.  
 387 The geometrical acceptances for prompt production and production from  $b$ -hadron decay  
 388 are calculated separately for both  $J/\psi$  and  $\psi(2S)$ . And since the geometrical acceptance  
 389 is only a function of kinematic variables, we assume that there is no difference between  
 390 the geometrical acceptance between different multiplicity regions.

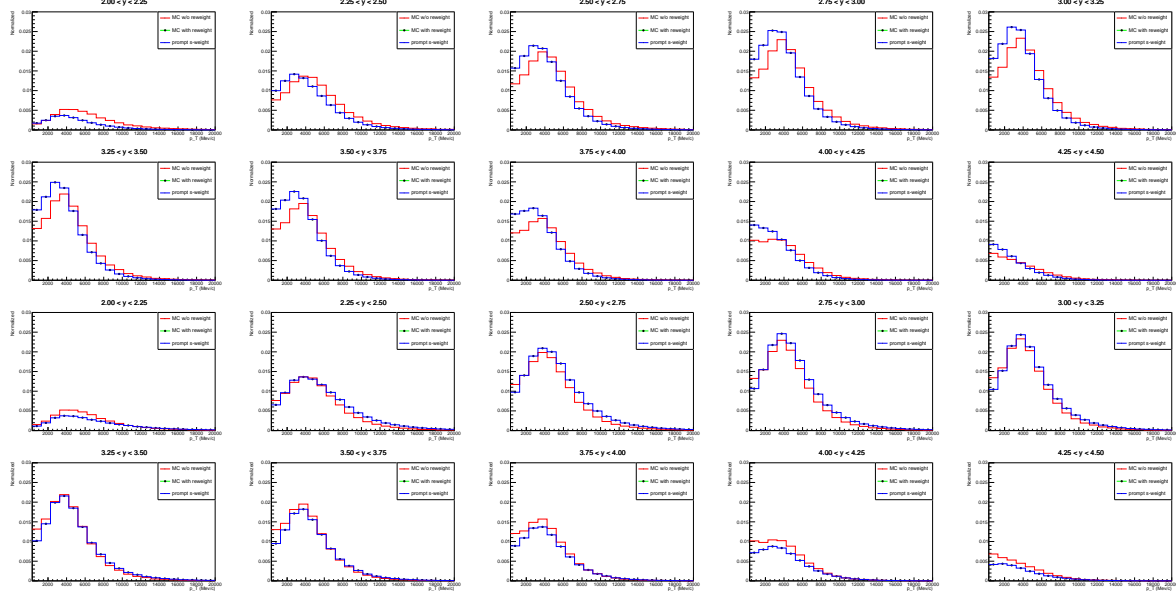


Figure 5: Reweight the  $p_T$ - $y$  distribution to match MC to s-weight data. The first two rows are results of prompt  $J/\psi$  and the rest two rows are that of non-prompt  $J/\psi$ .

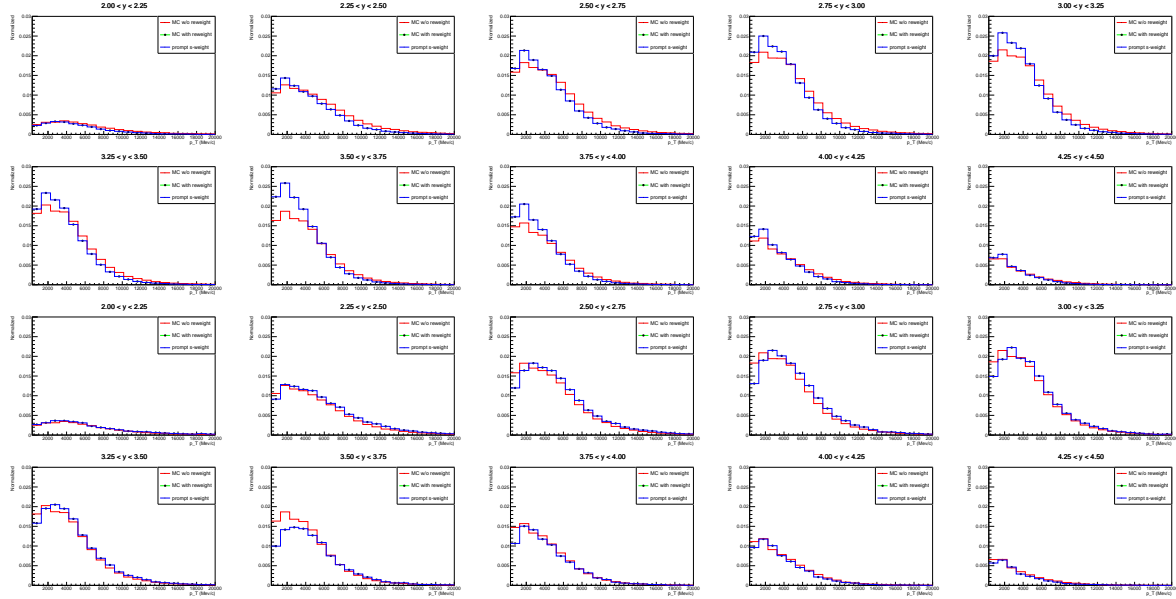


Figure 6: Reweight the  $p_T$ - $y$  distribution to match MC to s-weight data. The first two rows are results of prompt  $\psi(2S)$  and the rest two rows are that of non-prompt  $\psi(2S)$ .

## 391 6.2 Reconstruction-selection efficiency

392 The reconstruction and selection efficiency in each kinematic bin is estimated as

$$\epsilon_{\text{Reco\&Sel}} \equiv \frac{N(p_T, y) \text{ reconstructed and selected (w/o } \mu \text{ ID)}}{N(p_T, y) \text{ with both } \mu \text{ in LHCb acceptance}}. \quad (14)$$

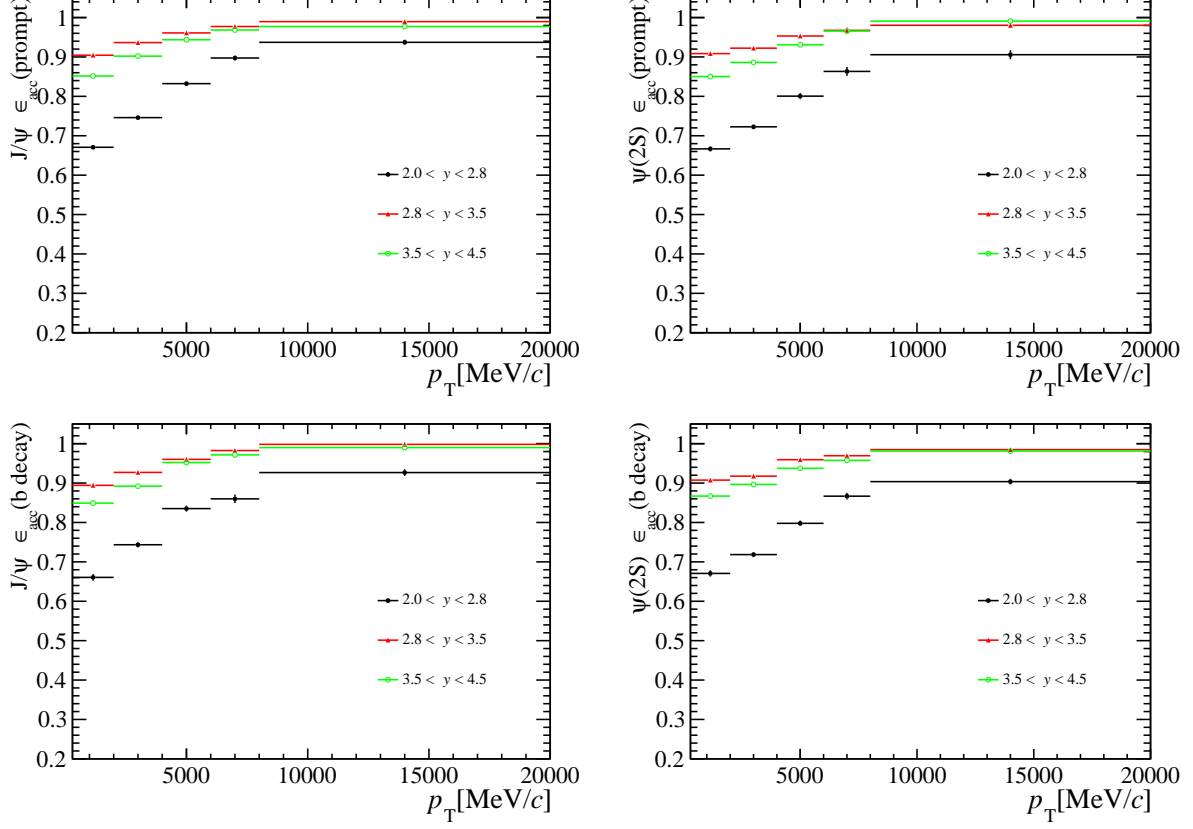


Figure 7: Efficiency of geometrical acceptance for both  $J/\psi$  and  $\psi(2S)$  for PVNTRACKS in 4 to 20, where the left is that of  $J/\psi$  and the right is of  $\psi(2S)$ . The first row is that of prompt signals and the second row is that of non-prompt signals.

393 It includes the efficiency of reconstructing the two muon tracks and the selection of the  
 394 signals, with the selection criteria listed in Table 2 (excluding muon identification and  
 395 the trigger). Then the reconstruction efficiency is further corrected using the data-over-  
 396 simulation single tracking efficiency ratio. The ratio of tracking efficiencies for a single  
 397 track in data and simulation determined with the Long Tag-Probe method [24] is shown  
 398 in Fig. 8, which was given by the tracking group.

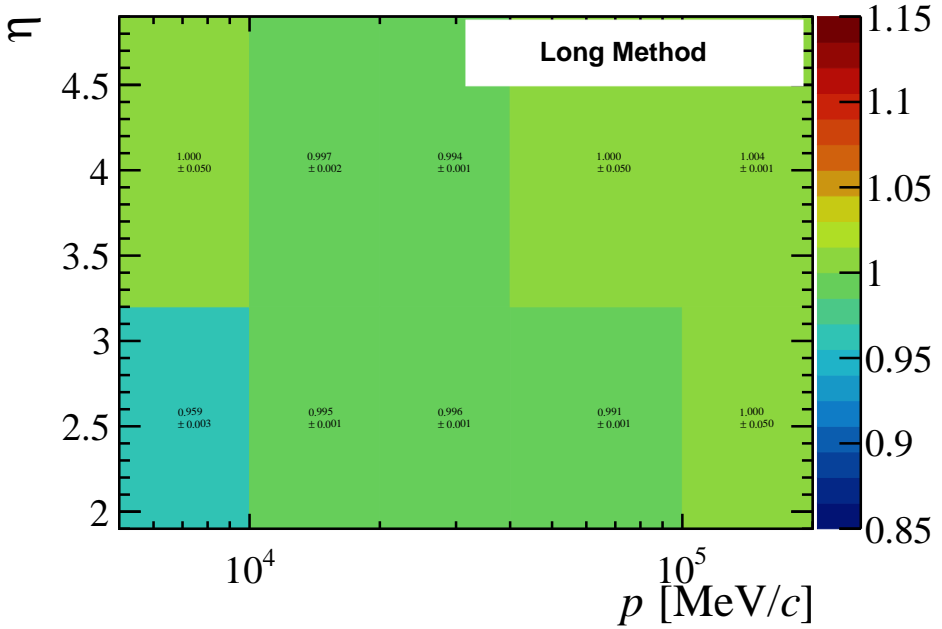


Figure 8: Tracking efficiency ratio between data and MC2016 simulation in bins of  $p_\mu$  and  $\eta_\mu$  of the muon.

399 For a given event the correction factor is determined by multiplying the efficiency  
 400 ratios for each of the tracks in the final state. The reweight for prompt and non-prompt  
 401 signals are done separately with the sWeight extracted from two-dimensional fit. For each  
 402  $p_T$  and  $y$  bin, the efficiency of  $\epsilon_{\text{Reco\&Sel}}$  is shown in Fig. 9 for PVNTRACKS between 4 to  
 403 20. Results in other multiplicity regions are shown in Sec C.

### 404 6.3 Muon identification efficiency

405 The muon identification requirement used in this analysis is `IsMuon == 1&&DLLmu >`  
 406 `2&&ProbNNmu > 0.8`. The efficiency is introduced by

$$\epsilon_{\text{MuonID}} \equiv \frac{N(p_T, y) \text{ selected including } \mu\text{ID requirement}}{N(p_T, y) \text{ reconstructed and selected (w/o } \mu\text{ID)}}. \quad (15)$$

407 The Muon ID efficiency is obtained using simulated samples and calibrated with the  
 408 data using the PIDCalib package. The full simulated samples used here are selected by all  
 409 the selections except the muon ID and the trigger. The selected samples are the same as  
 410 the ones used in the reconstruction and selection. As estimating the reconstruction and  
 411 selection efficiency, we first reweight the multiplicity variable according to the variable  
 412 we used to divide the multiplicity, and  $p_T$ - $y$  spectrum. The muon ID efficiency in each  
 413 ( $p_T, y$ ) bin is then calculated by averaging the muon ID efficiency of each candidate in the  
 414 bin, which is the product of the muon ID efficiencies of the two muons from the efficiency  
 415 table, obtained from the PIDCalib package, according to their  $(p, \eta, \text{nSPDhits})$  values.  
 416 The formula is

$$\bar{\epsilon}(p_T, y) = \frac{\sum \epsilon_{\mu^+}(p_{\mu^+}, \eta_{\mu^+}, \text{nSPDhits}) \epsilon_{\mu^-}(p_{\mu^-}, \eta_{\mu^-}, \text{nSPDhits})}{N_{\text{res\&sel}}}. \quad (16)$$

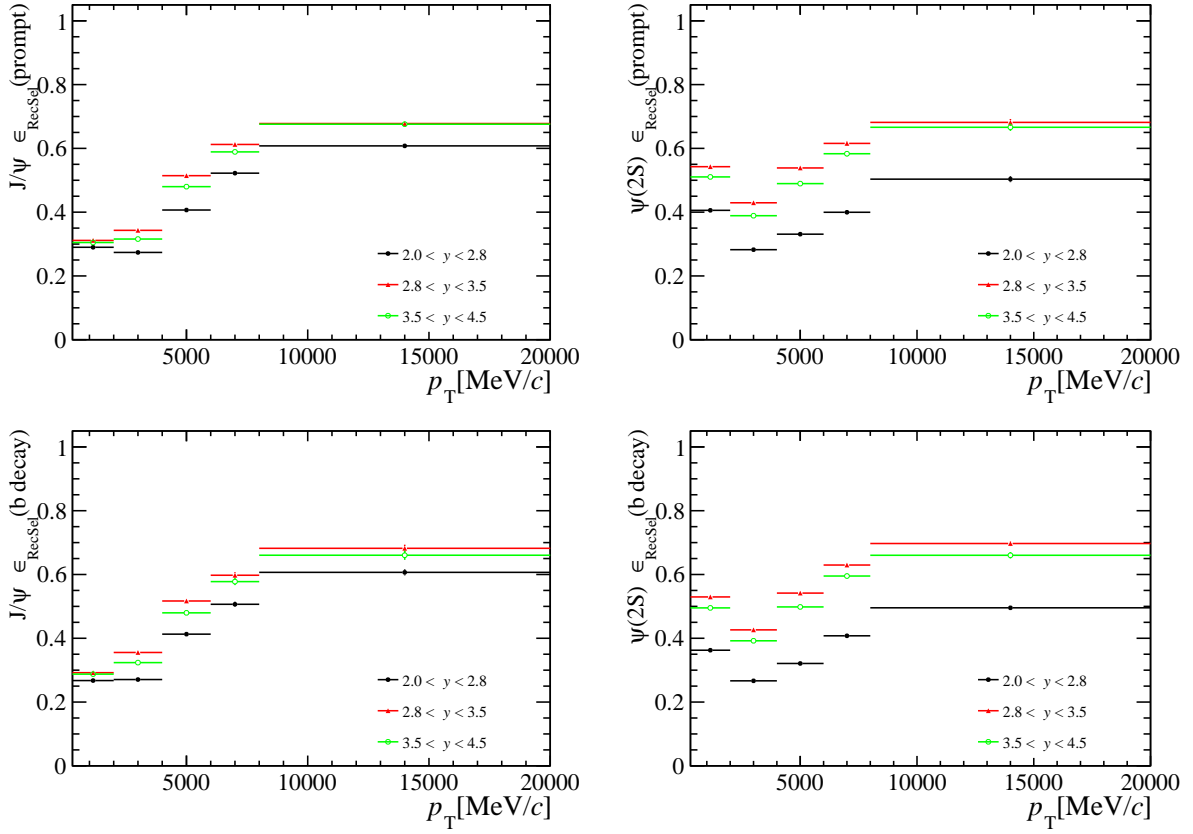


Figure 9: Efficiency of reconstruction and selection (excluding muon identification and the trigger) for both  $J/\psi$  and  $\psi(2S)$  for PVNTRACKS in 4 to 20, where the left is that of  $J/\psi$  and the right is of  $\psi(2S)$ . The first row is that of prompt signals and the second row is that of non-prompt signals.

417 where  $\epsilon_{\mu^+}(p_{\mu^+}, \eta_{\mu^+}, \text{nSPDhits})$  and  $\epsilon_{\mu^-}(p_{\mu^-}, \eta_{\mu^-}, \text{nSPDhits})$  are the muon ID efficiencies  
 418 obtained from the efficiency table. The efficiency table we used here is from the calibration  
 419 sample which contains  $J/\psi$  candidates taken in the same period and the average efficiency  
 420 over the whole period is used. One 3-Dimensional efficiency table dedicated to the muon  
 421 ID selection is obtained from this calibration sample in bins of the muon ( $p, \eta, \text{nSPDhits}$ )  
 422 using the tag-and-probe method. The MagDown and MagUp efficiencies are calculated  
 423 separately. For the muon candidates whose  $(p, \eta, \text{nSPDhits})$  are out of the range of the  
 424 calibration sample, we simply set the value to be one due to the fact that the production  
 425 in those bins is significantly small. For each  $p_T$  and  $y$  bin, the efficiency of  $\epsilon_{\text{MuonID}}$  is  
 426 shown in Fig. 10. Results in other multiplicity regions are shown in Sec C.

## 427 6.4 Trigger efficiency

428 The trigger efficiency in each kinematic bin is defined as

$$\epsilon_{\text{Trigger}} \equiv \frac{N(p_T, y) \text{ triggered}}{N(p_T, y) \text{ selected including } \mu\text{ID requirement}} \quad (17)$$

429 Here the triggers include both TOS requirements of `L0DiMuon`, `Hlt1DiMuonHighMass` for  
 430 both, and `Hlt2DiMuonJPsiTurbo` for  $J/\psi$  and `Hlt2DiMuonPsi2STurbo` for  $\psi(2S)$ , respec-

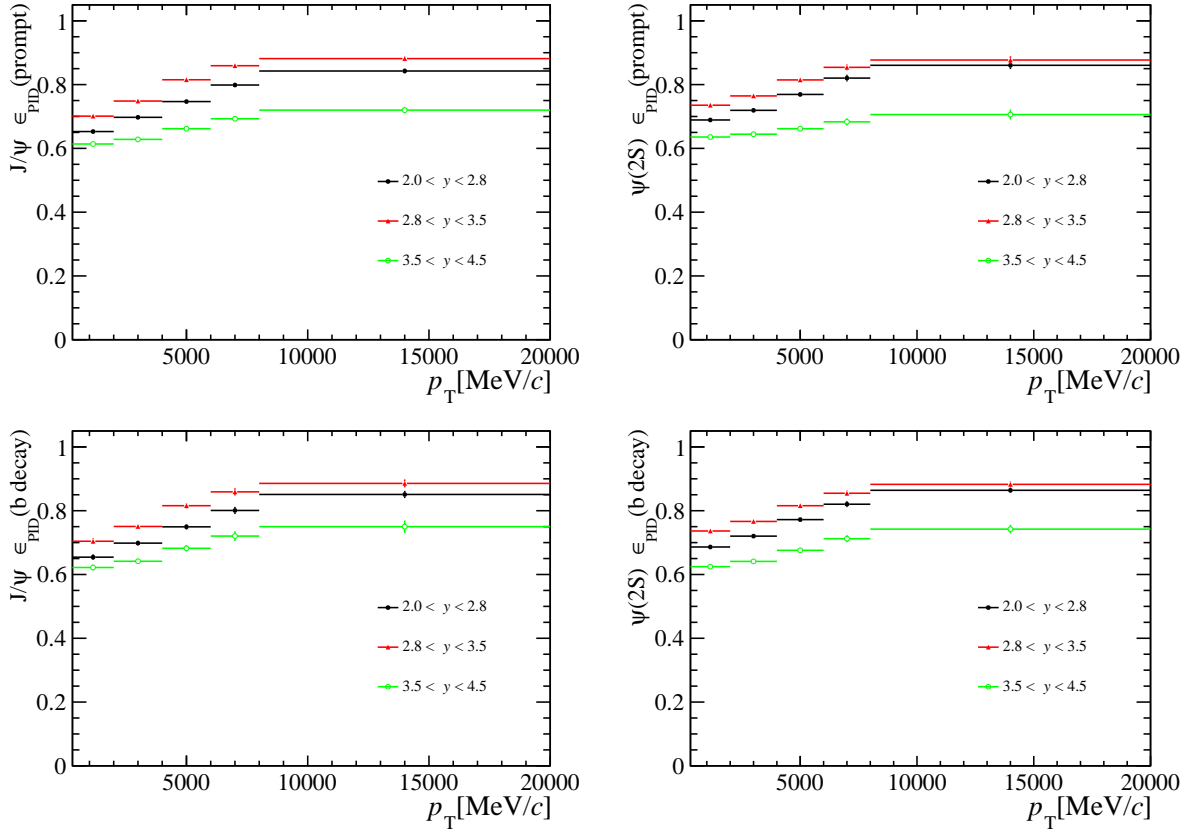


Figure 10: PID efficiencies for both  $J/\psi$  and  $\psi(2S)$  for PVNTRACKS in 4 to 20, where the left is that of  $J/\psi$  and the right is of  $\psi(2S)$ . The first row is that of prompt signals and the second row is that of non-prompt signals.

tively. Only `LODiMuon` and `Hlt1DiMuonHighMass` contribute actually to the efficiency because the `Hlt2DiMuonJPsiTurbo` and `Hlt2DiMuonPsi2STurbo` is almost fully efficient due to the facts that the offline selections are tighter. For each  $p_T$  and  $y$  bin, the efficiencies of  $\epsilon_{\text{Trigger}}$  for both  $J/\psi$  and  $\psi(2S)$  from different sources for PVNTRACKS between 4 to 20 are shown in Fig. 11. Results in other multiplicity regions are shown in Sec C.

## 436 6.5 Total efficiency

The total efficiencies  $\epsilon_{\text{tot}}$  for  $J/\psi$  and  $\psi(2S)$  from different sources for PVNTRACKS between 4 to 20 are shown in Fig. 12. Results in other multiplicity regions are shown in Sec C. The separate efficiencies for prompt and non-prompt signals are used to calculate the final cross-section.

## 441 6.6 Variation due to different reweight samples

Since the multiplicity-dependent breakup effects may vary with  $(p_T, y)$ , the two-dimensional  $(p_T, y)$  distribution may differ in different multiplicity region. To study this effect, the  $(p_T, y)$  spectra are prepared for three different multiplicity classes:

- 445 • Data sample with all selections of PVNTRACKS.

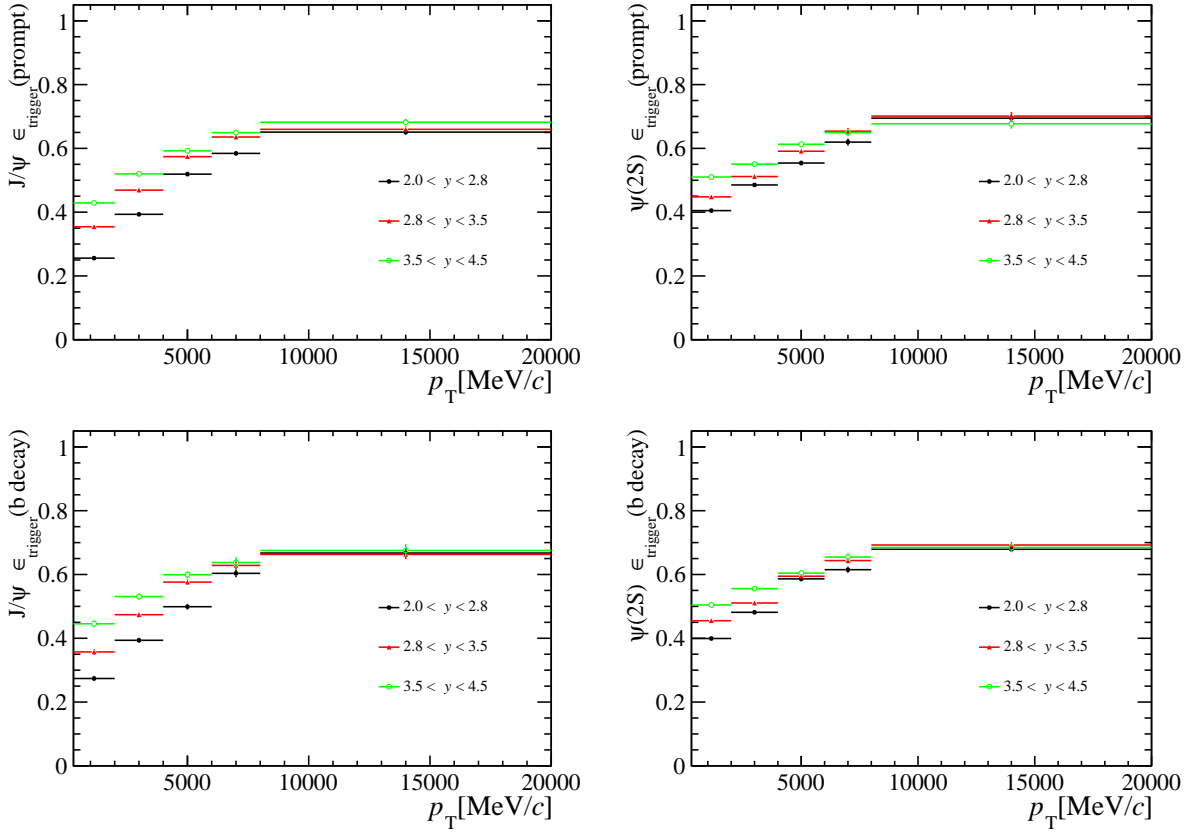


Figure 11: Trigger efficiencies for both  $J/\psi$  and  $\psi(2S)$  for PVNTRACKS in 4 to 20, where the left is that of  $J/\psi$  and the right is of  $\psi(2S)$ . The first row is that of prompt signals and the second row is that of non-prompt signals.

- Data sample with PVNTRACKS $\geq 60$  as high-multiplicity sample, where 60 is the bin edge of the second to last bin of  $p_T$  binning scheme.
  - Data sample with PVNTRACKS $< 60$  as low-multiplicity sample.
- The  $(p_T, y)$  distributions of high- and low-multiplicity samples are shown in Figs. 13. With this two samples for  $(p_T, y)$  reweight, we can calculate the ratio of total efficiencies for both prompt and non-prompt  $J/\psi$  and  $\psi(2S)$  in each multiplicity region. And after comparing the newly calculated ratio of total efficiencies with the original one, we record the variation in each  $(p_T, y, \text{PVNTRACKS})$  bin in form of a certain time of statistical uncertainty in that bin. And the result is shown in Figs 14. It's clearly shown that all the variations are within uncertainties, where the center values and uncertainties for ratio of efficiencies are from the results reweighted by the full-multiplicity sample.

## 7 Systematic Uncertainties

The ratio of production of  $\psi(2S)$  to  $J/\psi$  in a certain  $(p_T, y)$  is defined in equation 4, which is universal for both prompt components and components from  $b$ -hadron decay in each multiplicity bin and Systematic uncertainties of various sources are combined through the error propagation formula in each bin. While when calculating the systematic

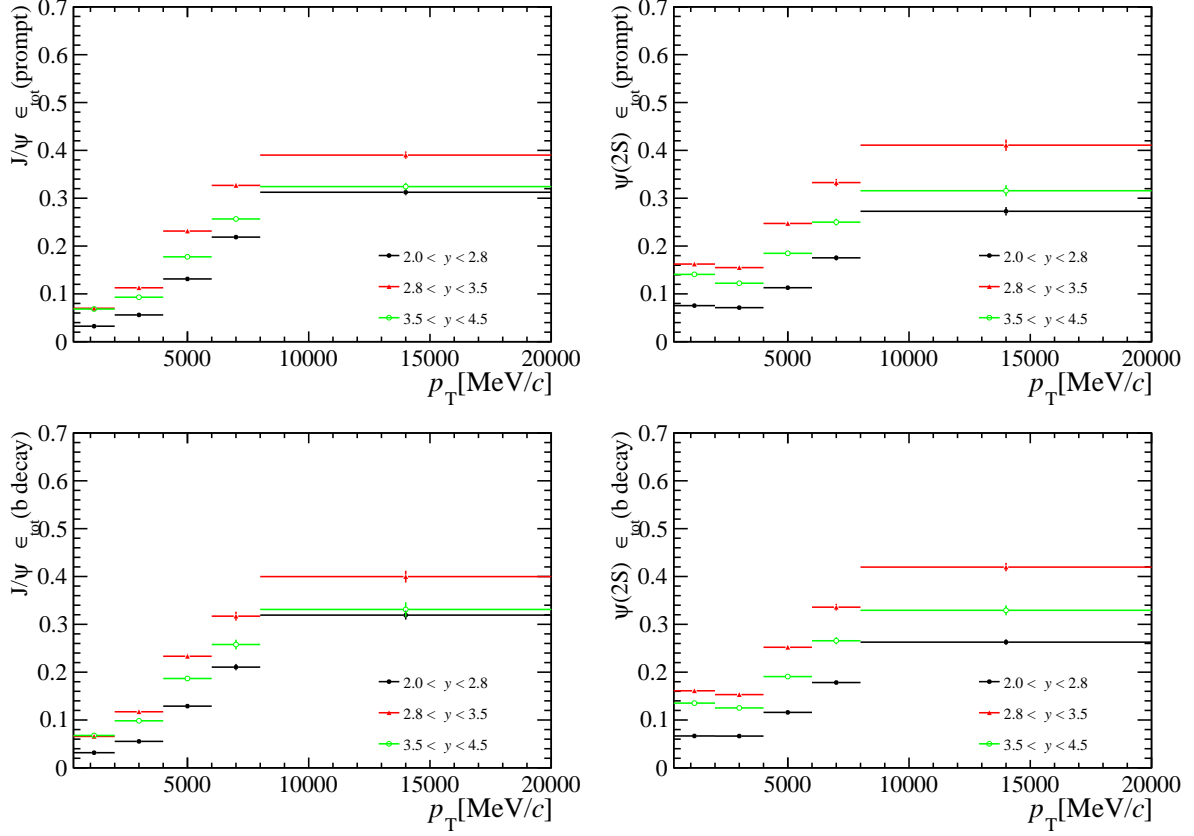


Figure 12: Total efficiencies for both  $J/\psi$  and  $\psi(2S)$  for PVNTRACKS in 4 to 20, where the left is that of  $J/\psi$  and the right is of  $\psi(2S)$ . The first row is that of prompt signals and the second row is that of non-prompt signals.

uncertainties of the ratio of integrated production, the bin size is no more canceled and we need to take into account the production as weight in each bin. The ratio of integrated production is defined in equation 5. The form of expression for the ratio of integrated production is not a simple production or division (it is a division of sums). So when studying the systematic uncertainties, a simple and straightforward way is calculating the uncertainties of  $\frac{\Sigma_{(p_T,y)} \sigma_{\psi(2S)}(p_T,y)}{\Sigma_{(p_T,y)} \sigma_{J/\psi}(p_T,y)}$  itself, which is for example, if we calculate the uncertainty of the fit model, instead of combining the uncertainties from different bins, we directly calculate how much  $\frac{\Sigma_{(p_T,y)} \sigma_{\psi(2S)}(p_T,y)}{\Sigma_{(p_T,y)} \sigma_{J/\psi}(p_T,y)}$  would vary when we change the fit model. For the uncertainties which are independent of bins, we can combine them through the error propagation formula, i.e. the Systematic uncertainty due to MC sample size. The following sources of systematic uncertainties are considered. And the systematic uncertainties are calculated separately in each multiplicity bin. For the rest of the part, we only show the results for the first multiplicity bin, which is  $4 \leq \text{PVNTRACKS} < 20$ .

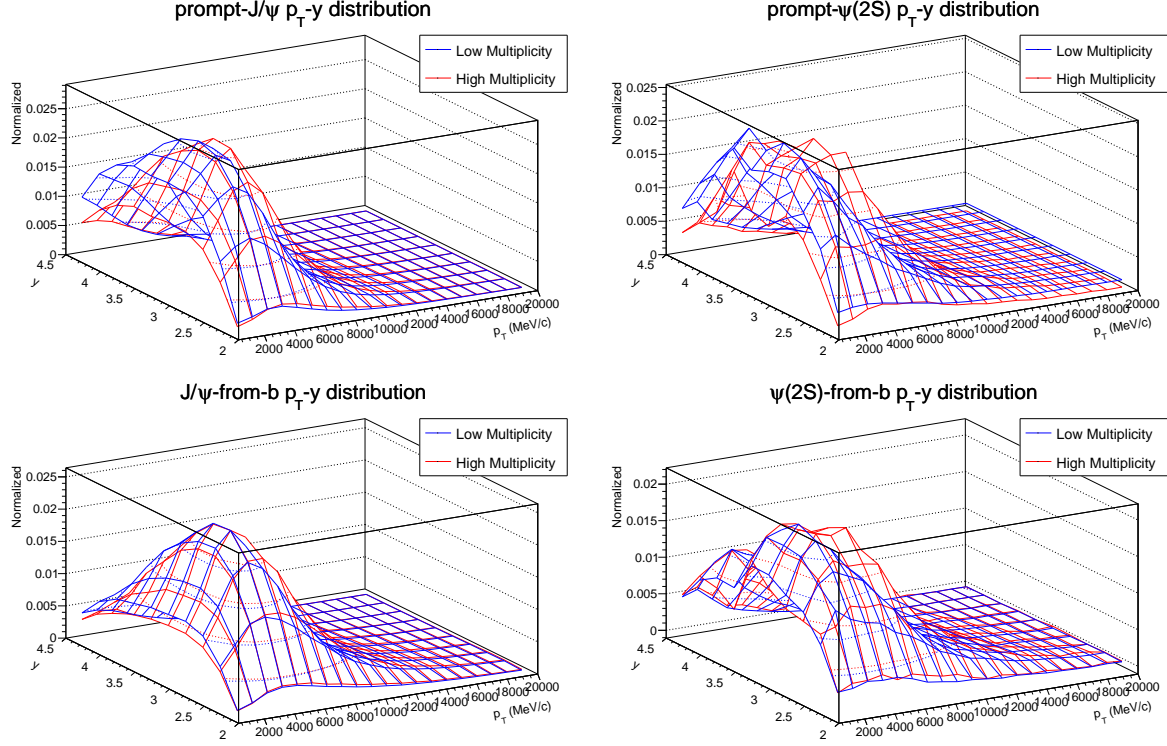


Figure 13: Two-dimensional ( $p_T$ ,  $y$ ) distribution for prompt and non-prompt  $J/\psi$  and  $\psi(2S)$  of different samples (high-multiplicity sample in red).

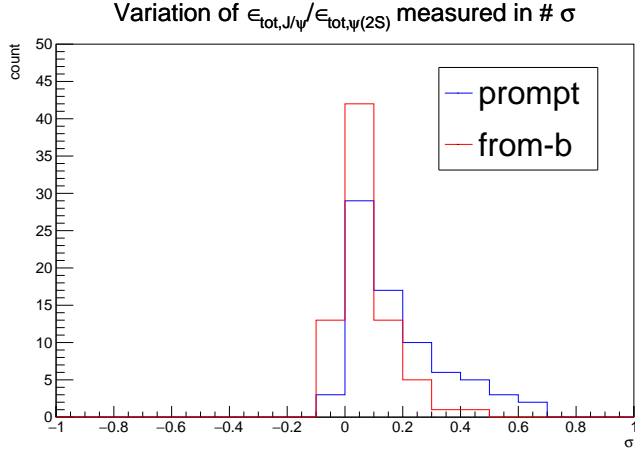


Figure 14: Distribution of the variation due to different reweight samples recorded in times of the statistical uncertainty.

## 475 7.1 Signal extraction

### 476 7.1.1 Signal mass shape

477 Using the sum of two Crystal Ball functions parametrized as described in Section 5 could  
 478 bias the signal yields. For an alternative, the signal invariant mass is also fitted with  
 479 the model which is extracted from the kernel-estimated distribution from the simulated

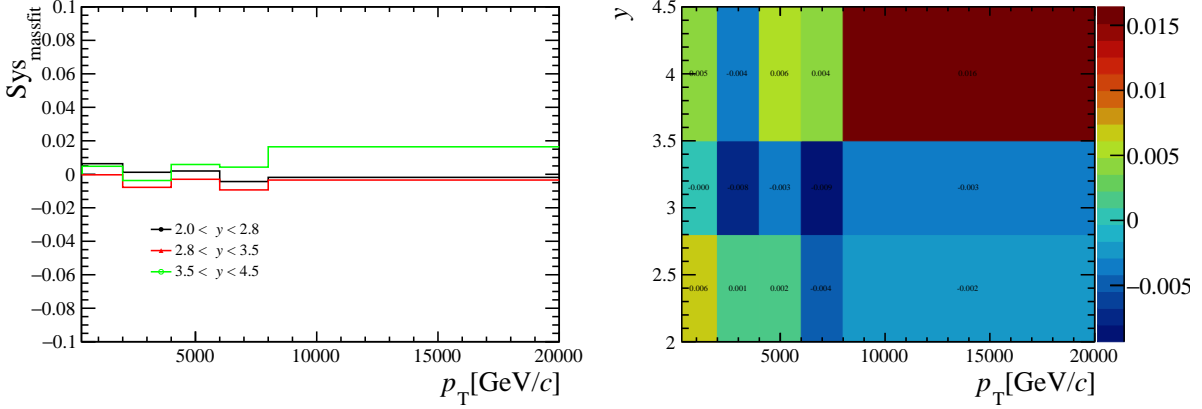


Figure 15: The systematic uncertainty of ratio of production due to the fit model in each bin for PVNTRACKS from 4 to 20. It is common for both prompt components and components from  $b$ -hadron decay.

sample bin dependently. In order to account for the resolution difference between data and simulation, a Gaussian function (all the parameters float during the fit procedure) is used to smear the shape of the signals. The study is performed in each kinematic bin, and the signal yields from the default fit and alternative fit are compared. For both  $J/\psi$  and  $\psi(2S)$ , we change the fit model to get uncertainties for both and then calculate the uncertainties through the error propagation formula. The detailed results of systematic uncertainty for ratio in each single  $p_T$  and  $y$  bin and PVNTRACKS from 4 to 20 are shown in Fig. 15. The result is common for both prompt components and components from  $b$ -hadron decay since when we fit the mass spectrum, we fit both components simultaneously. For the ratio of integrated production, we change the fit model and calculate a new value with equation 5. The variation between the new ratio and the original one is quoted as systematic uncertainty for ratio of integrated production due to mass fit model.

### 7.1.2 Fit to $t_z$ background

There are several scenarios that could deviate the fitted  $b$  fraction from its true value:

- Imperfect modeling of the detector resolution of  $t_z$ . Since the shape of prompt  $\psi(2S)$  is dominated by the resolution, a defective description of the resolution could make the prompt  $J/\psi$  and  $\psi(2S)$  distribution not fitted very well, and thus will affect the fitted fraction of components from  $b$ . To study this effect, a third wide Gaussian is added to the resolution function. It is found that the difference of the fitted  $F_b$  between the default fit and the new fit is negligible.
- Systematic uncertainty related to the background description. In the nominal procedure, the fit explicitly models the background distribution using the mass sidebands. As an alternative, the parameters of the  $t_z$  distribution for the background are obtained by the sPlot technique for both  $J/\psi$  and  $\psi(2S)$  and are fixed in the  $t_z$  fit.

For each  $p_T$  and  $y$  bin, the systematic uncertainties are calculated by combining the uncertainties from  $J/\psi$  and  $\psi(2S)$ . For the ratio of integrated production, similarly, as

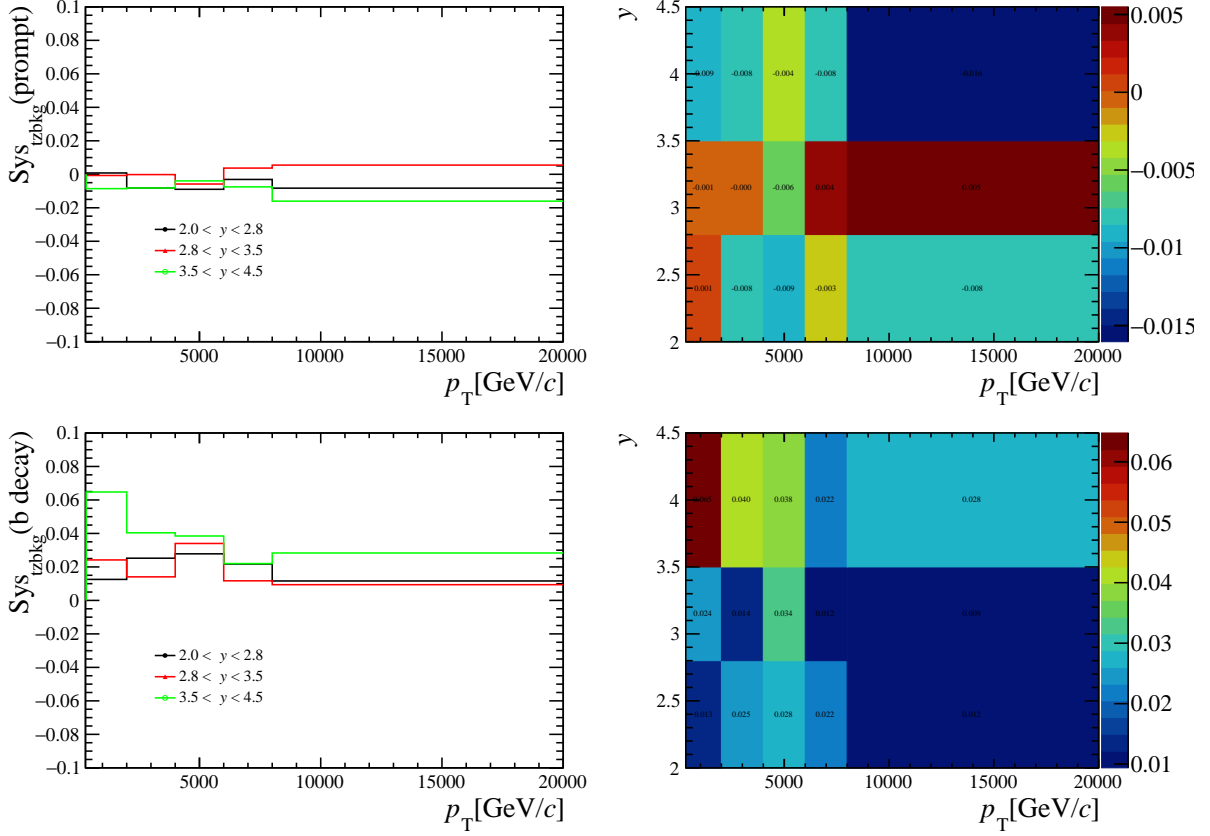


Figure 16: The systematic uncertainty of ratio of production due to  $t_z$  background fit model in each bin for PVNTRACKS from 4 to 20. The first row is that of prompt components and the second row is that of components from  $b$ -hadron decay.

above, we change the fit model for  $t_z$  background for both  $J/\psi$  and  $\psi(2S)$  to calculate a new value and quote the variation as a systematic uncertainty. The uncertainties for prompt components and components from  $b$ -hadron decay are calculated separately. The results in a single bin are shown in figure 16.

### 7.1.3 Fit to $t_z$ signal

For the imperfect modeling of detector resolution, we fit the  $t_z$  spectrum on MC and then compare the yields of prompt components to the real counts in MC. The variation is quoted as systematic uncertainty due to imperfect modeling of the  $t_z$  signal model. When fitting the  $t_z$  spectrum on MC for  $J/\psi$  or  $\psi(2S)$ , we should take care that one or two Gaussian functions should be used depending on the number of Gaussian functions we are using when fitting  $t_z$  spectrum on data in a certain ( $p_T, y$ , PVNTRACKS) bin. The systematic uncertainties of ratio in different bins 17 are listed for PVNTRACKS from 4 to 20.

## 7.2 Trigger efficiency

The trigger efficiency in simulation is cross-checked with data, and the resulting difference in the ratio of production between simulation and data is quoted as a systematic uncertainty.

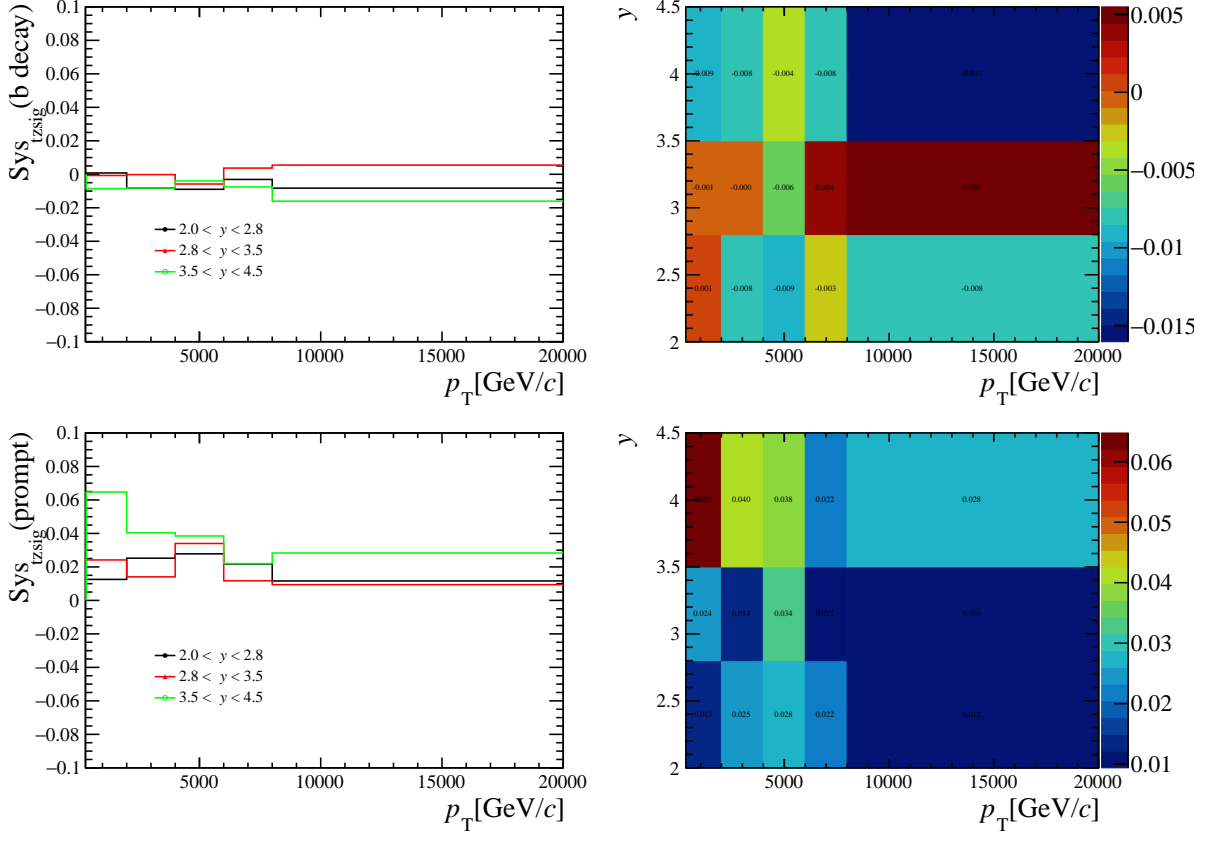


Figure 17: The systematic uncertainty of ratio of production due to  $t_z$  signal fit model in each bin for PVNTRACKS from 4 to 20. The first row is that of prompt components and the second row is that of components from  $b$ -hadron decay.

523 For both L0DiMuon and Hlt1DiMuonHighMass the TISTOS method is used to evaluate  
 524 the efficiency for L0DiMuon&&Hlt1DiMuonHighMass both in simulation and data. We  
 525 use L0Global and Hlt1Global as the TIS line. As the data sample size is limited by the  
 526 number of the TIS events of  $\psi(2S)$  sample, we only consider the uncertainty in different  
 527 multiplicity bins. By comparing the difference between the calculated efficiencies using  
 528 TISTOS method in data and MC, we construct an estimate of the difference in trigger  
 529 efficiency calculate by MC and the true trigger efficiency. It is shown in Figs. 18.

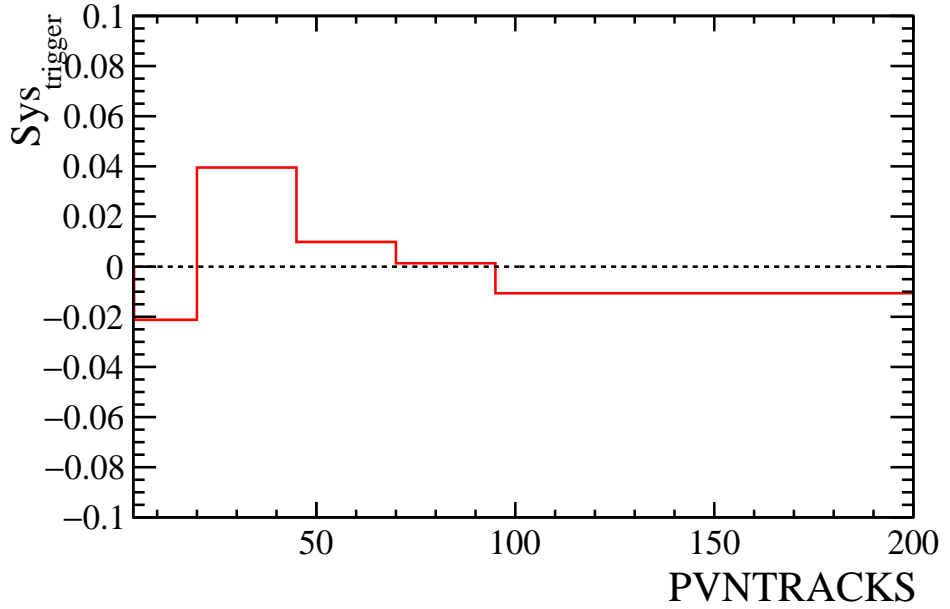


Figure 18: Summary of Systematic Uncertainties of ratio due to uncertainty of  $\epsilon_{\text{trigger}}$  in different multiplicity region.

530 To compare the ratio as a function of  $p_T$  with other measurements in different collision  
 531 systems, we also find the systematic uncertainties in different  $p_T$  bins, where we integrate  
 532 over the multiplicity and rapidity dimensions due to the limit of TIS sample size. It is  
 533 shown in Figs. 19.

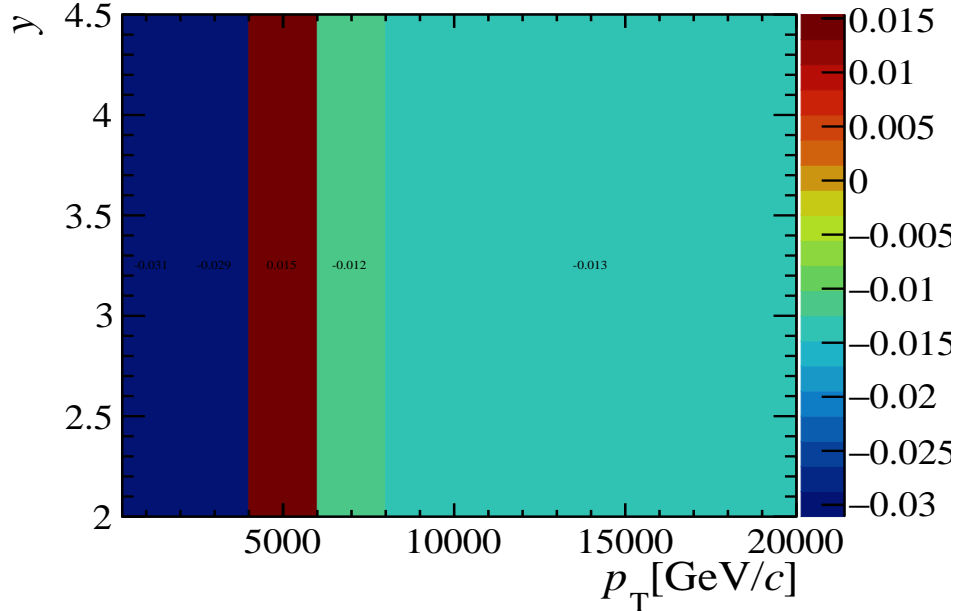


Figure 19: Summary of Systematic Uncertainties of ratio due to uncertainty of  $\epsilon_{\text{trigger}}$ .

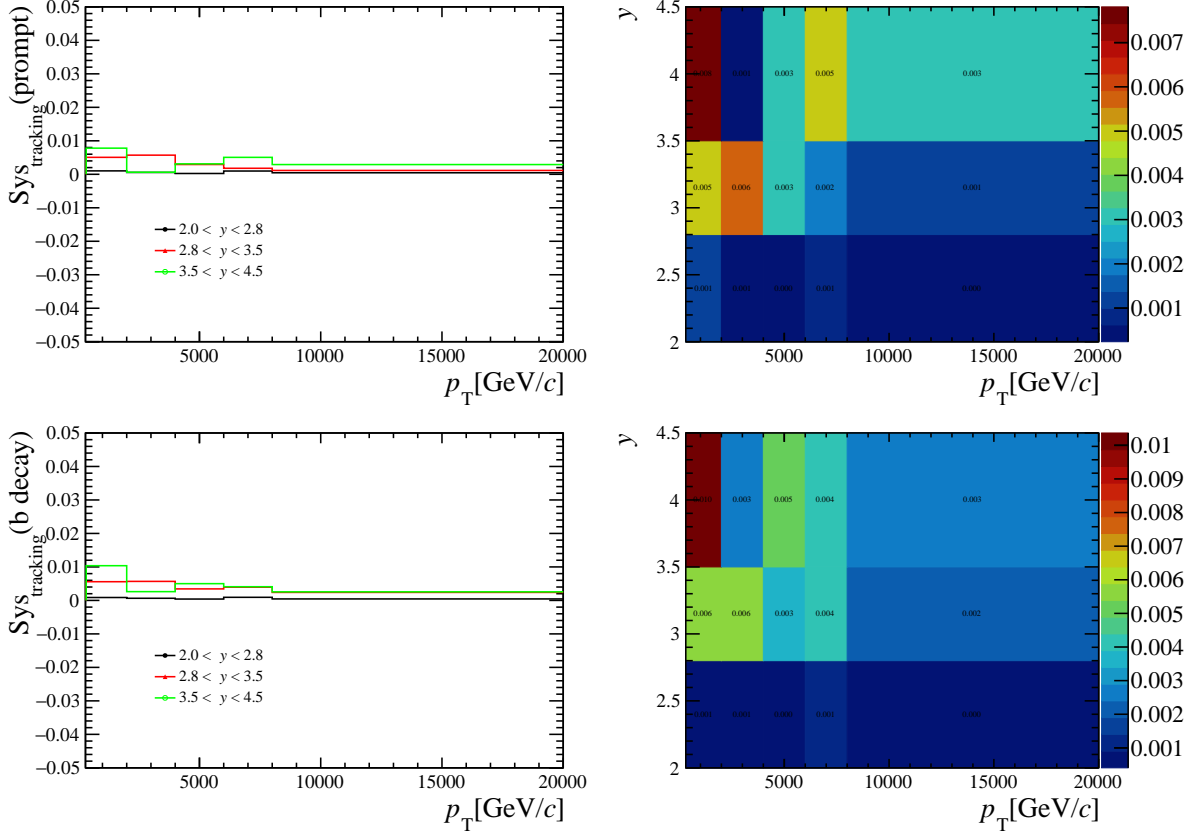


Figure 20: The systematic uncertainty of ratio of production due to the uncertainty of track table in each bin for PVNTRACKS from 4 to 20. The first row is that of prompt components and the second row is that of components from  $b$ -hadron decay.

### 534 7.3 Tracking efficiency

535 There are two sources of systematic uncertainties associated with the track reconstruction  
536 efficiency.

537 One is the statistical uncertainty of the ratios due to the limited sample size used to  
538 obtain the tracking correction table. This part could be obtained by toy studies: Two  
539 hundred experiments were performed where the efficiency for each bin in the  $p$  and  $\eta$   
540 was sampled from Fig. 8 by Gaussian distributions with the corresponding central value  
541 as the mean and the uncertainty as the width; For each experiment, the reconstruction  
542 and selection efficiency of prompt components and components from  $b$ -hadron decay in  
543 different bins could be obtained with the sampled efficiency correction table, and hence  
544 we can calculate two hundred values for ratio in a single bin or any integrated region;  
545 Finally, using a gaussian function to fit the two hundred of results, and the sigma divided  
546 by the mean value of the fit result is quoted as the relative uncertainty. The relative  
547 uncertainty in each bin for prompt components and components from  $b$ -hadron decay for  
548 PVNTRACKS from 4 to 20 is shown in figure 20.

549 Another one is the choice of event multiplicity variable. This systematic uncertainty  
550 is provided by the tracking group. The tracking experts indicate that the choice of  
551 the multiplicity variable (nTracks, nSPDHits, or others) is relevant for deciding the  
552 systematics. They studied this effect and suggest 0.8% per track, as detailed in Ref. [25].

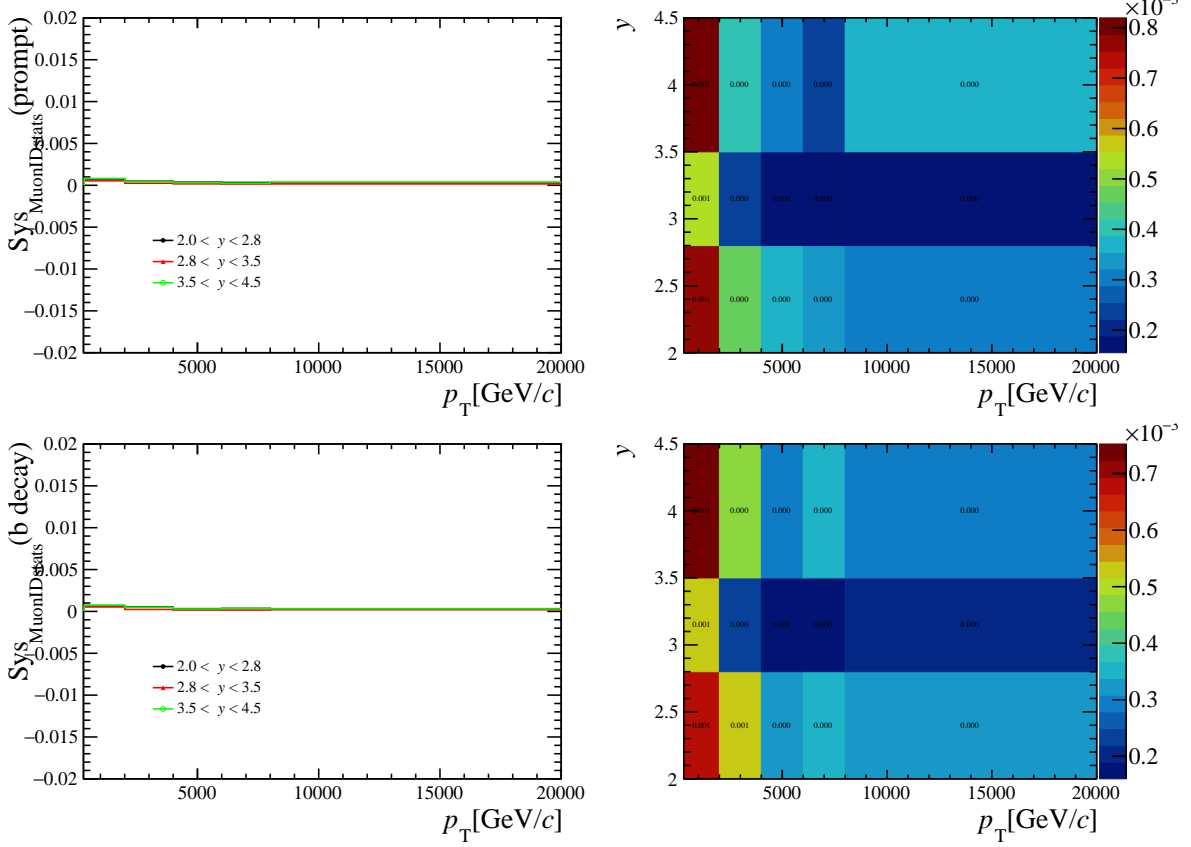


Figure 21: The systematic uncertainty of ratio of production due to the statistical uncertainty of PID efficiency in each bin for PVNTRACKS from 4 to 20. The first row is that of prompt components and the second row is that of components from  $b$ -hadron decay.

553 But when we calculate the ratio between  $J/\psi$  and  $\psi(2S)$ , the uncertainty due to the choice  
 554 of multiplicity variable is canceled out since we use the same table for calculating both  
 555  $J/\psi$  and  $\psi(2S)$ .

## 556 7.4 MuonID efficiency

557 The systematic uncertainty due to MuonID includes the following contributions:

- 558 • The statistical uncertainty is due to the finite size of the calibration sample. To  
 559 estimate the systematic uncertainty due to the limited calibration sample size, we  
 560 first generate two hundred tables of efficiencies from the original table, where the  
 561 efficiency in each bin of each table is randomly sampled from a Gaussian distribution  
 562 using the central value as the mean and the uncertainty as the width. Then, we  
 563 obtain two hundred efficiency values from the generated efficiency tables, hence, we  
 564 calculated two hundred productions of  $J/\psi$  and  $\psi(2S)$  in each  $p_T$ - $y$  bin in different  
 565 multiplicity region and their ratios. Finally, we fit the distribution of the two  
 566 hundred ratios (in a single bin and integrated region) with a Gaussian function.  
 567 The ratio between the width and the mean value of the fitted Gaussian function is  
 568 quoted as a systematic uncertainty, which is summarized in figure 21.
- 569 • Uncertainty due to binning scheme of the calibration sample, studied by varying the

570 binning method in  $p_\mu$ ,  $\eta_\mu$ , and nSPDHits respectively. The default one and the two  
 571 alternative binning schemes could be found below. The nominal binning scheme of  
 572 the muon ID efficiency for muons we use to calculate the muon ID efficiency of  $J/\psi$   
 573 and  $\psi(2S)$  mesons is defined:

- 574 –  $p_\mu$  boundaries [ GeV/c ]: 3, 6, 8, 10, 12, 13, 14, 15, 16, 18, 20, 24, 28, 32, 40, 60,  
 575 70, 80, 90, 100, 200, 1000
- 576 –  $\eta$  boundaries: 2.0, 2.5, 3.0, 3.5, 4.0, 4.5, 4.9
- 577 – nSPDhits boundaries: 0, 200, 400, 1000.

578 One of the two alternative binning schemes is defined:

- 579 –  $p_\mu$  boundaries [ GeV/c ]: 5, 7, 9, 11, 12, 13, 14, 15, 17, 19, 23, 27, 32, 40, 55, 65,  
 580 75, 85, 95, 150, 200, 1000
- 581 –  $\eta$  boundaries: 2.0, 2.4, 2.9, 3.4, 3.9, 4.4, 4.9
- 582 – nSPDhits boundaries: 0, 300, 500, 1000.

583 The other one binning schemes is defined:

- 584 –  $p_\mu$  boundaries [ GeV/c ]: 3, 5.5, 7.5, 9.5, 11.5, 12.5, 13.5, 14.5, 15.5, 17.5, 19.5,  
 585 23.5, 27.5, 32, 38, 48, 58, 68, 78, 88, 98, 198, 1000
- 586 –  $\eta$  boundaries: 2.0, 2.6, 3.1, 3.6, 4.1, 4.6, 4.9
- 587 – nSPDhits boundaries: 0, 150, 480, 1000.

588 The maximum difference between the two new ratios calculated by new efficiency and  
 589 the original ratio is quoted as the systematic uncertainty. The relative uncertainties  
 590 for the ratio in each bin for PVNTRACKS from 4 to 20 are summarized in Fig 22.

## 591 7.5 MC sample size

592 The limited size of the simulation sample used to determine the efficiencies is a source of  
 593 systematic uncertainties. The uncertainty of ratio due to MC sample size in different bin  
 594 for PVNTRACKS from 4 to 20 are summarized in Fig 23.

## 595 7.6 Other systematic uncertainties

- 596 • The uncertainty of  $\mathcal{B}(J/\psi \rightarrow \mu^+\mu^-) = (5.961 \pm 0.033)\%$  and  $\mathcal{B}(\psi(2S) \rightarrow e^+e^-) =$   
 597  $(7.93 \pm 0.17) \times 10^{-3}$  are canceled when we only care the normalized ratio.
- 598 • The relative uncertainty of the luminosity is canceled out when calculating the ratio  
 599 of production cross-section.
- 600 • A fraction of events is lost because of the QED radiative tail. But when calculating  
 601 the ratio of production, the effects for  $J/\psi$  and  $\psi(2S)$  are canceled out.

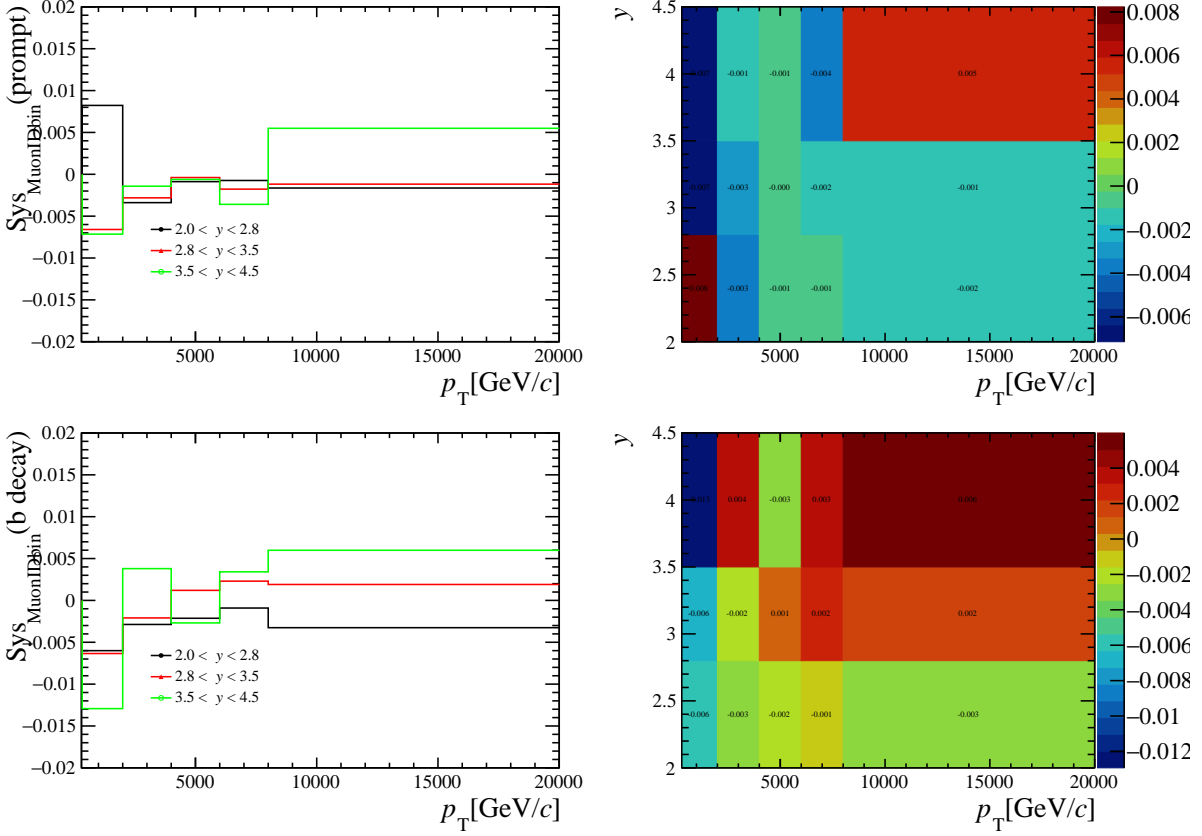


Figure 22: The systematic uncertainty of ratio of production due to the binning scheme of calibration sample in each bin for PVNTRACKS from 4 to 20. The first row is that of prompt components and the second row is that of components from  $b$ -hadron decay.

## 8 Bin Width Correction

As shown in Fig. 4, the distributions of multiplicity skew a lot so that in a certain bin, the center of the bin may not represent an ideal horizontal coordinate for plotting the results, especially for the small and large multiplicity regions. To study the effect, 10000 fitting trials are done in Monte Carlo. In each trial, in a certain multiplicity region of the three different binning schemes (PVNTRACKS, nForwardTracks, and nBackTracks), we randomly sample the mean values of the multiplicity region from a Gaussian sampling, within each bin, mean being the content of the bin and width being the error of the bin. Then we fit the 10000 mean values with gaussian distribution to get the central values and uncertainties. To choose a point at which to plot the data, we make the average value of the central values we get from the fit. Since the data point is a ratio between two species,  $J/\psi$ , and  $\psi(2S)$ , the average value for the ratio is weighted by the inverse of the square of the uncertainties (following the PDG weighted average procedure). An example is shown in Fig. 24.

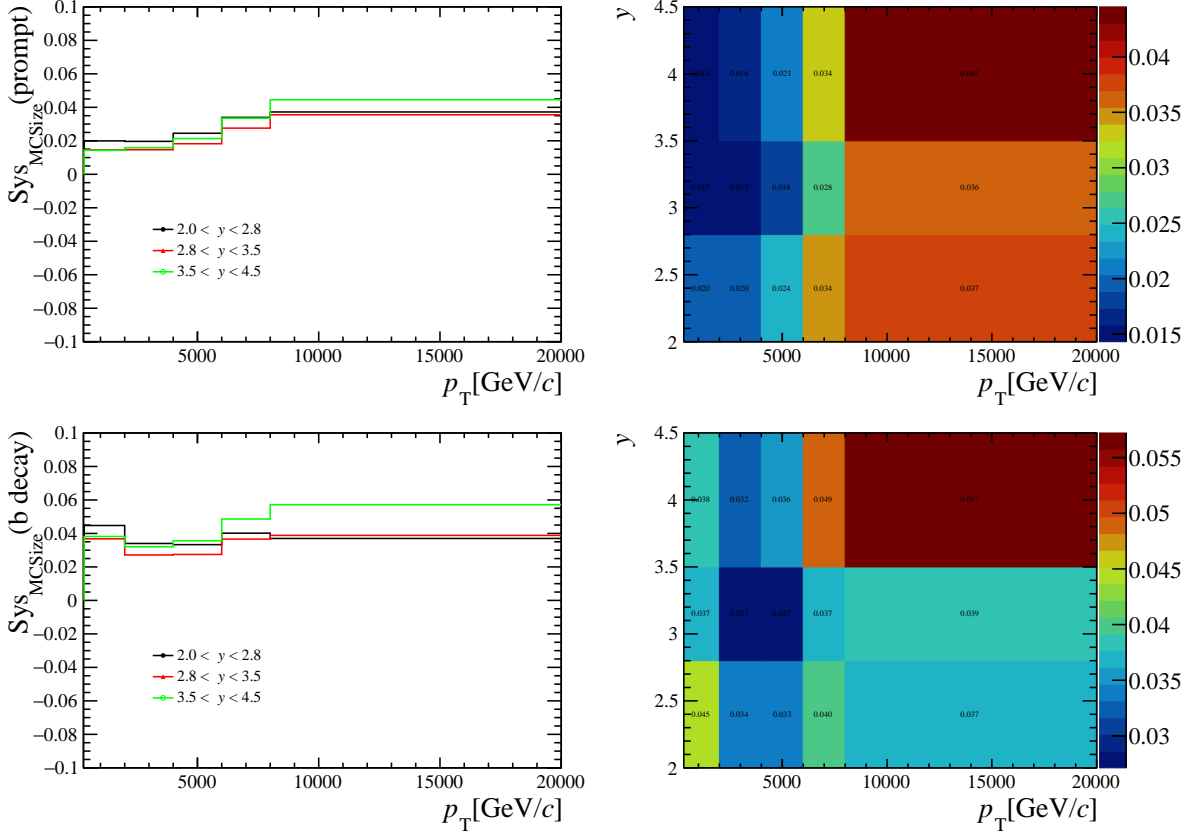


Figure 23: The systematic uncertainty of ratio of production due to limit sample size in each bin for PVNTRACKS from 4 to 20. The first row is that of prompt components and the second row is that of components from  $b$ -hadron decay.

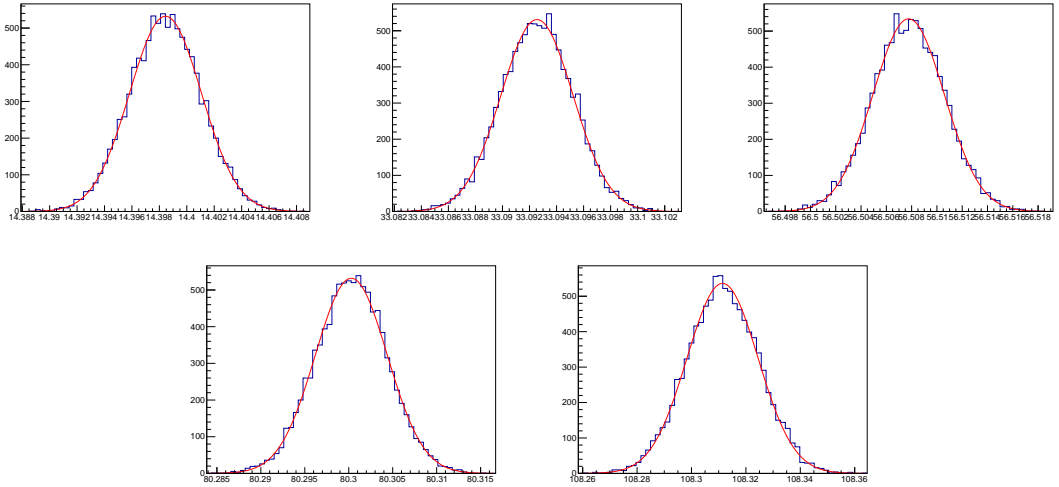


Figure 24: The distribution of mean value of PVNTRACKS for prompt  $J/\psi$  signal in each multiplicity region, which are  $4 \leq \text{PVNTRACKS} < 20, 20 \leq \text{PVNTRACKS} < 45, 45 \leq \text{PVNTRACKS} < 70, 70 \leq \text{PVNTRACKS} < 95, 95 \leq \text{PVNTRACKS} < 200$ .

616 After finding the proper horizontal coordinates in each multiplicity region, they are  
 617 further normalized by dividing the mean value of that into no-biased data. Finally, the  
 618 horizontal coordinates for each species are summarized in Table 3.

Table 3: The horizontal coordinates for different binning schemes.

PVNTRACKS	4-20	20-45	45-70	70-95	95-200
prompt	0.5571	1.2791	2.1836	3.1028	4.1852
from $b$	0.5758	1.2971	2.1861	3.1010	4.1776
nForwardTracks	0-12	12-24	24-36	36-48	48-130
prompt	0.5404	1.1143	1.8135	2.5216	3.7005
from $b$	0.5415	1.1290	1.8179	2.5229	3.6889
nBackTracks	0-8	8-15	15-22	22-30	30-80
prompt	0.4630	1.1746	1.8747	2.6175	3.7708
from $b$	0.4938	1.1793	1.8767	2.6183	3.7710

## 619 9 Results

### 620 9.1 $\psi(2S)$ -to- $J/\psi$ ratio as functions of multiplicity

621 With the signal yields determined from the fitting to dimuon invariant mass distributions,  
 622 the efficiencies estimated from simulation and calibrated control sample, and the systematic  
 623 uncertainties, the ratio of  $\psi(2S)$  and  $J/\psi$  production cross-sections are measured in each  
 624 kinematic and multiplicity bin. By integrating the double differential results over  $p_T$  ( $y$ )  
 625 one can obtain the ratio as functions of  $y(p_T)$ . And also the normalized ratio of total  
 626 cross-sections as a function of normalized multiplicity can be obtained by integrating  
 627 the double differential results over  $p_T$  and  $y$  bins. The normalization of ratio is achieved  
 628 simply by dividing the ratio in each multiplicity bin by the over-all ratio in integrated  
 629 multiplicity region. The normalized ratio of integrated production over  $p_T$ - $y$  as a function  
 630 of PVNTRACKS is shown in Fig 25. We can see a decreasing trend for the ratio of  
 631 prompt production with multiplicity getting larger. While for the ratio of production from  
 632  $b$ -hadron decay, no significantly decreasing trend is observed. The ratio of production  
 633 is also measured as a function of nBackTracks and nForwardTracks (see Figure 26),  
 634 which are two mutual subsets of PVNTRACKS representing numbers of backward and  
 635 forward tracks respectively. The ratio of production from  $b$ -hadron decay is roughly  
 636 independent of multiplicity under three different kinds of schemes. The decreasing trend  
 637 for the ratio versus nBackTracks is much slower than the other two. This indicates  
 638 that the relative suppression is correlated with the local particle multiplicity since an  
 639 independent multiplicity variable leads to a slower decrease. It is within expectation since  
 640  $\psi(2S)$  has a larger radius and lower bounding energy so a preferential dissociation may  
 641 happen when interacting with the co-moving matters after the collisions. Theoretically,  
 642 nBackTracks is a multiplicity variable independent of the measured ratio, and the ratio  
 643 should roughly be the same in different multiplicity regions. But nBackTracks is not fully  
 644 independent since there is a correlation between nForwardTracks and nBackTracks with

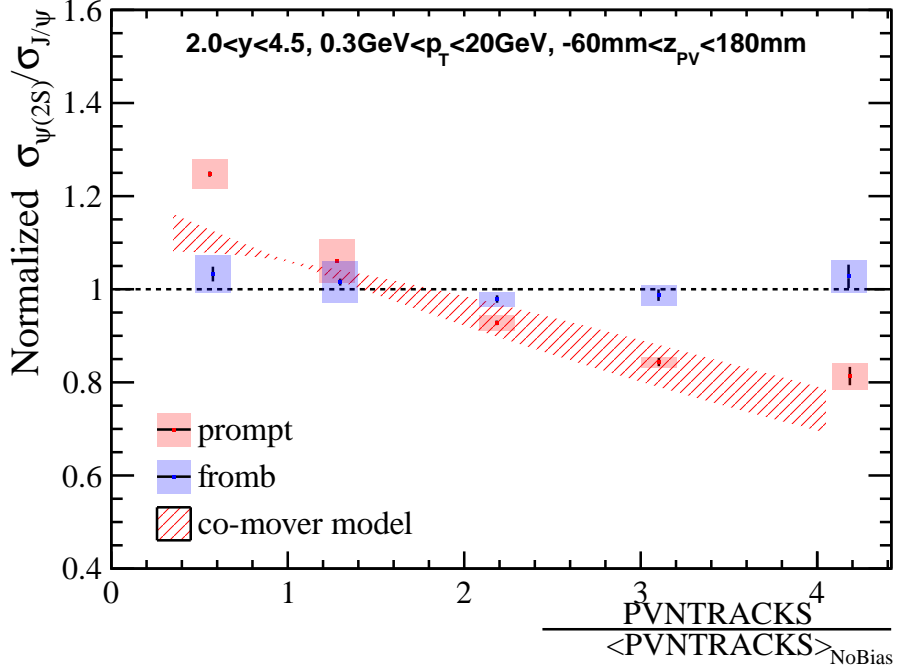


Figure 25: The ratio of integrated production over  $p_T$ - $y$  as a function of PVNTRACKS.

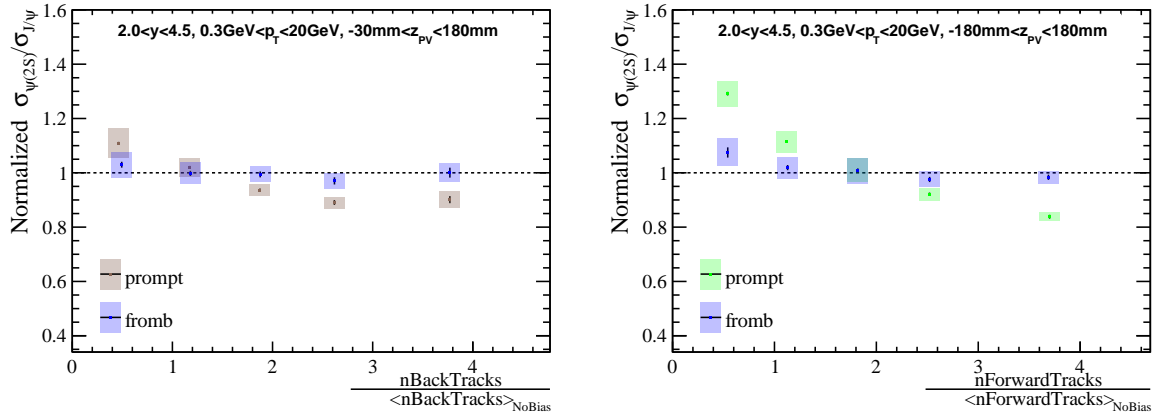


Figure 26: The ratio of integrated production over  $p_T$ - $y$  as a function of nBackTracks and nForwardTracks.

645 a correlation factor of 0.54 for  $J/\psi$  and 0.51 for  $\psi(2S)$ . To study the effect produced by  
 646 the correlation between nBackTracks and nForwardTracks, we measure the mean values  
 647 of nForwardTracks in each nBackTracks bin for both prompt  $J/\psi$  and  $\psi(2S)$ . Then we  
 648 follow the procedures in Sec 8 to calculate the x-coordinates of nForwardTracks in each  
 649 nBackTracks bin. Finally, the normalized ratios in different nBackTracks bin is migrated  
 650 to the plot of nForwardTracks in Figs. 27. We find a good agreement on the decreasing  
 651 trend, which means the dependence of normalized  $\psi(2S)$ -to- $J/\psi$  ratio on nBackTracks  
 652 could result from the correlation between nBackTracks and nForwardTracks.

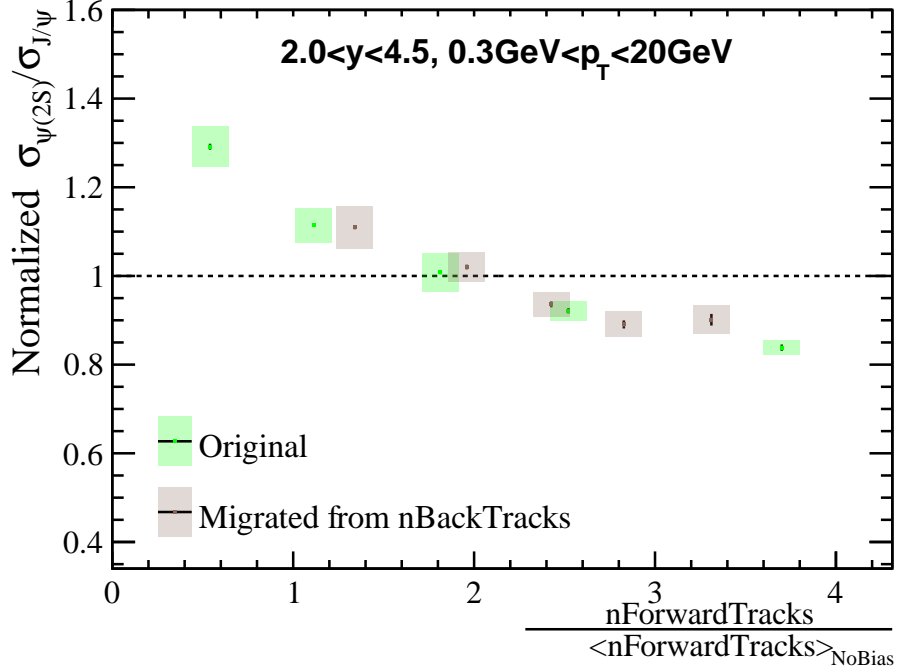


Figure 27: Data points on nBackTracks are migrated to plot of nForwardTracks by find the mean value of nForwardTracks in each nBackTracks bin.

## 653    9.2 $\psi(2S)$ -to- $J/\psi$ ratio in different $p_T$ regions

654    In Sec 8 we have discussed how to find appropriate horizontal coordinates for the  $\psi(2S)$ -to-  
 655     $J/\psi$  ratio in  $2.0 < y < 4.5$  and  $0.3 \text{ GeV}/c < p_T < 20 \text{ GeV}/c$ . The multiplicity distributions  
 656    in different  $p_T$  ranges are significantly different. Hence, for all the results in different  
 657     $p_T$  ranges, we need to repeat the procedures in Sec 8 to find appropriate horizontal  
 658    coordinates for plotting. And the final results in different  $p_T$  ranges are shown in Fig 28,  
 659    Fig 29 and Fig 30. In three binning schemes for multiplicity, the ratios share the same  
 660    property that, in low  $p_T$  region, the preferential suppression of  $\psi(2S)$  is higher than that  
 661    in higher  $p_T$  region.

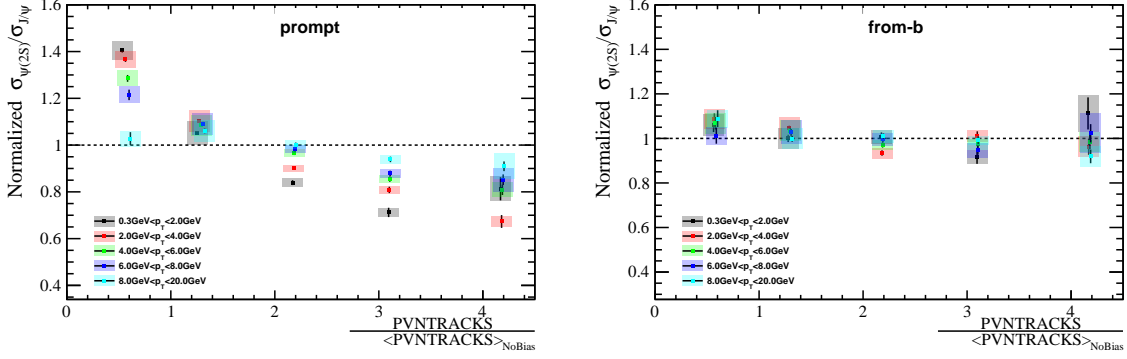


Figure 28: Ratio of  $\psi(2S)$  to  $J/\psi$  in different  $p_T$  region when multiplicity is divided in PVN-TRACKS

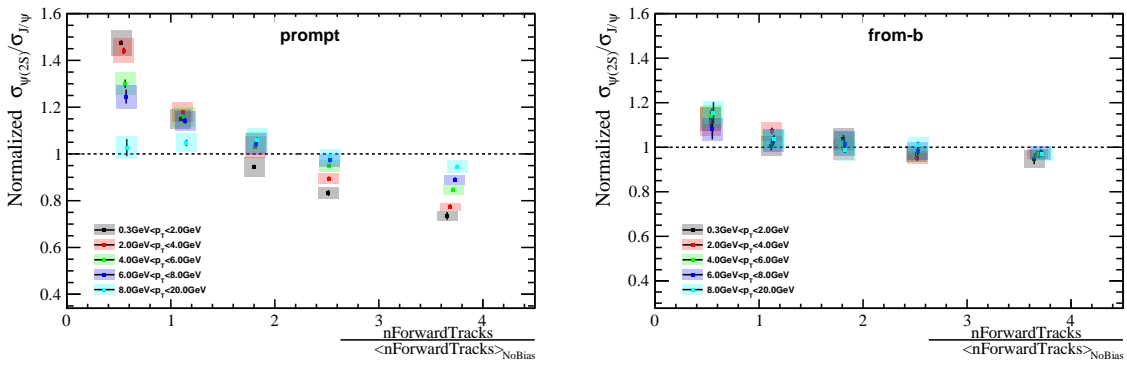


Figure 29: Ratio of  $\psi(2S)$  to  $J/\psi$  in different  $p_T$  region when multiplicity is divided in nForward-Tracks

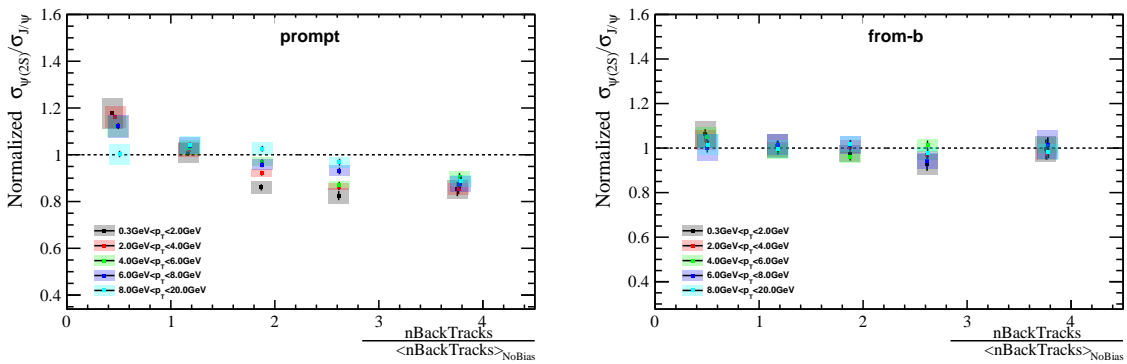


Figure 30: Ratio of  $\psi(2S)$  to  $J/\psi$  in different  $p_T$  region when multiplicity is divided in nBackTracks

### 9.3 $\psi(2S)$ -to- $J/\psi$ ratio in different $y$ regions

The results for ratio in different rapidity bins are given in Figs 31 when taking PVN-TRACKS as a multiplicity variable. And the results for nForwardTracks and nBackTracks are given in Figs 32 and Figs 33. The results show that there is no significant difference in different rapidity regions, for both prompt and non-prompt signals.

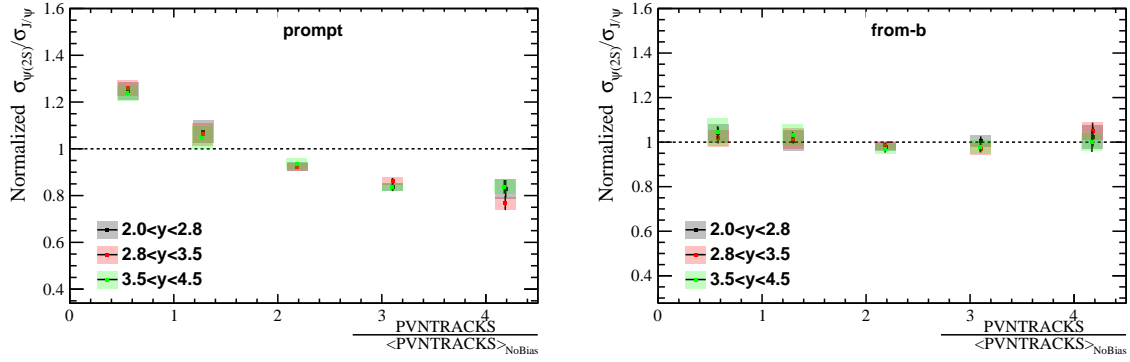


Figure 31: Ratio of  $\psi(2S)$  to  $J/\psi$  in different  $y$  region when multiplicity is divided in PVN-TRACKS

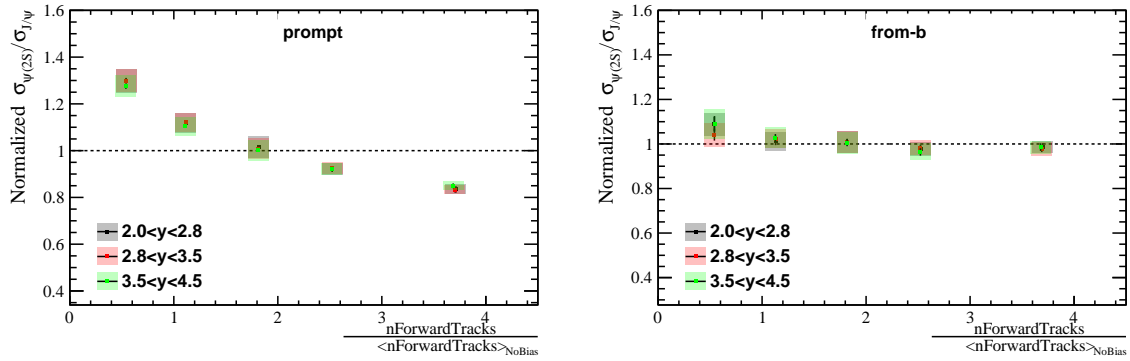


Figure 32: Ratio of  $\psi(2S)$  to  $J/\psi$  in different  $y$  region when multiplicity is divided in nForward-Tracks

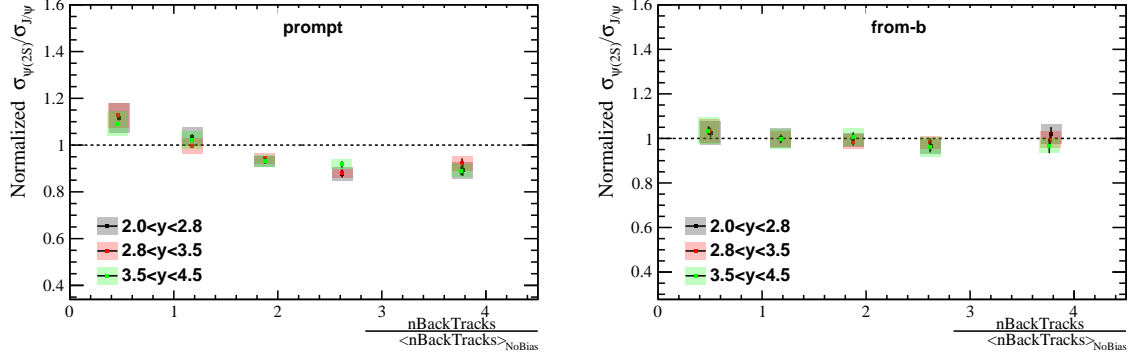


Figure 33: Ratio of  $\psi(2S)$  to  $J/\psi$  in different  $y$  region when multiplicity is divided in nBackTracks

#### 9.4 Comparisons with other measurements

Measurements of  $\mathcal{B}_{\psi(2S)}/\sigma_{\psi(2S)}$  over  $\mathcal{B}_{J/\psi}/\sigma_{J/\psi}$  have been done in different collision systems at different center-of-mass energies. Results show that the value of the ratio is roughly independent of the collision systems and energies. We multiply the ratio of  $\sigma_{\psi(2S)}/\sigma_{J/\psi}$  by the ratio of their branching fractions and add our measurements to the plot as follows, we find our measurements having a good agreement with others in Figs 34 and Figs 35.

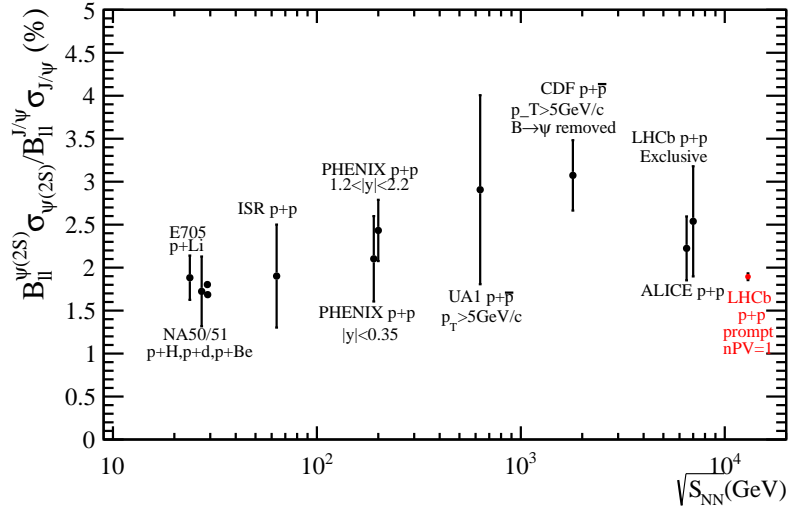


Figure 34: Comparisons of world data on the ratio of  $\psi(2S)/J/\psi$  measons in dilepton decays [26–34].

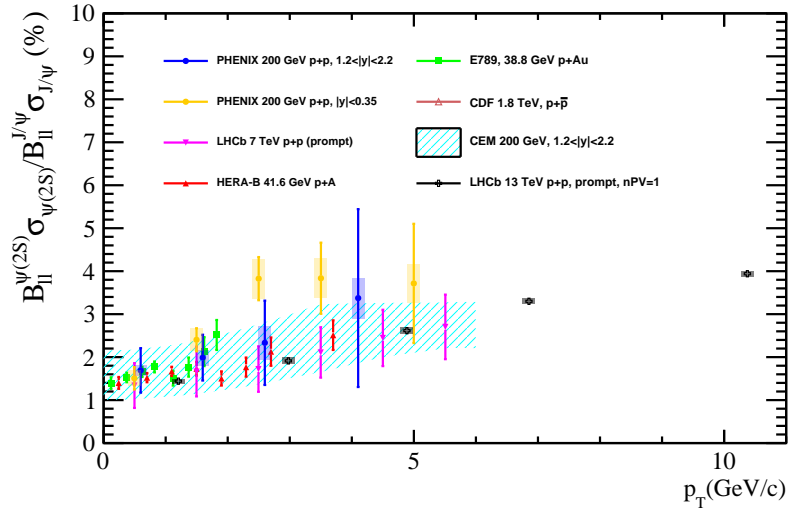


Figure 35: Comparisons of world data on the ratio of  $\psi(2S)/J/\psi$  mesons as a function of  $p_T$  in dilepton decays [26–34].

## 673 10 Conclusion

674 The ratio of production cross-sections of  $\psi(2S)$  to  $J/\psi$  in proton-proton collisions at a  
 675 center-of-mass energy  $\sqrt{s} = 13$  TeV are reported with a data sample corresponding to  
 676 an integrated luminosity of  $658 \pm 13 \text{ pb}^{-1}$ , collected by the LHCb detector in 2016. The  
 677 normalized ratio of  $\psi(2S)$ -to- $J/\psi$  production, as functions of  $p_T$  and  $y$  in different  $p_T$   
 678 and  $y$  regions, are measured as well as in the total region of  $0 \text{ GeV} < p_T < 20 \text{ GeV}$  and  
 679  $2.0 < y < 4.5$  for prompt production and production from  $b$ -hadron decay. We see an  
 680 obvious decreasing trend for prompt production as a function of PVNTRACKS and  
 681 nForwardTracks and a slower decrease as a function of nBackTracks. For the ratio of  
 682 production from  $b$ -hadron decay, there is no independence shown.

## 683 A Tables of ratio

### 684 1 Taking PVNTRACKS as multiplicity variable

Table 4: Ratio(%) of double differential production cross-section for prompt  $\psi(2S)$  to  $J/\psi$  in bins of  $(p_T, y)$ . The first uncertainties are statistical, the second are the systematic uncertainties, for  $0 \leq \text{PVNTRACKS} < 20$ .

$p_T$ (GeV/c)	prompt		
	$2 < y < 2.8$	$2.8 < y < 3.5$	$3.5 < y < 4.5$
0-2	$14.95 \pm 0.19 \pm 0.54$	$15.18 \pm 0.15 \pm 0.44$	$15.54 \pm 0.15 \pm 0.48$
2-4	$20.45 \pm 0.30 \pm 0.72$	$18.97 \pm 0.22 \pm 0.54$	$19.49 \pm 0.24 \pm 0.56$
4-6	$29.18 \pm 0.60 \pm 1.02$	$23.22 \pm 0.39 \pm 0.68$	$22.75 \pm 0.45 \pm 0.75$
6-8	$34.60 \pm 1.08 \pm 1.45$	$26.74 \pm 0.76 \pm 0.97$	$27.89 \pm 0.93 \pm 1.16$
8-20	$33.05 \pm 1.39 \pm 1.52$	$27.67 \pm 1.19 \pm 1.15$	$29.83 \pm 1.65 \pm 1.70$
from $b$			
$p_T$ (GeV/c)	$2 < y < 2.8$	$2.8 < y < 3.5$	$3.5 < y < 4.5$
0-2	$21.88 \pm 1.19 \pm 1.16$	$19.99 \pm 0.91 \pm 1.01$	$21.04 \pm 1.16 \pm 1.74$
2-4	$28.29 \pm 1.17 \pm 1.37$	$27.02 \pm 0.90 \pm 1.09$	$27.60 \pm 1.11 \pm 1.56$
4-6	$32.89 \pm 1.53 \pm 1.61$	$29.53 \pm 1.13 \pm 1.46$	$33.70 \pm 1.57 \pm 1.98$
6-8	$34.89 \pm 2.10 \pm 1.88$	$31.70 \pm 1.69 \pm 1.41$	$32.33 \pm 2.23 \pm 1.96$
8-20	$43.93 \pm 2.36 \pm 1.97$	$39.96 \pm 2.16 \pm 1.77$	$39.78 \pm 2.95 \pm 2.80$

Table 5: Ratio(%) of double differential production cross-section for prompt  $\psi(2S)$  to  $J/\psi$  in bins of  $(p_T, y)$ . The first uncertainties are statistical, the second are the systematic uncertainties, for  $20 \leq \text{PVNTRACKS} < 45$ .

prompt			
$p_T$ (GeV/c)	$2 < y < 2.8$	$2.8 < y < 3.5$	$3.5 < y < 4.5$
0-2	$11.50 \pm 0.14 \pm 0.54$	$10.92 \pm 0.11 \pm 0.55$	$11.62 \pm 0.11 \pm 0.63$
2-4	$16.48 \pm 0.17 \pm 0.74$	$15.33 \pm 0.13 \pm 0.65$	$15.81 \pm 0.14 \pm 0.67$
4-6	$22.41 \pm 0.25 \pm 0.98$	$20.68 \pm 0.18 \pm 0.86$	$20.62 \pm 0.21 \pm 0.88$
6-8	$29.18 \pm 0.40 \pm 1.41$	$26.20 \pm 0.32 \pm 1.14$	$25.11 \pm 0.38 \pm 1.16$
8-20	$35.01 \pm 0.53 \pm 1.65$	$29.31 \pm 0.43 \pm 1.35$	$28.46 \pm 0.54 \pm 1.39$

from $b$			
$p_T$ (GeV/c)	$2 < y < 2.8$	$2.8 < y < 3.5$	$3.5 < y < 4.5$
0-2	$19.03 \pm 0.57 \pm 1.04$	$20.24 \pm 0.49 \pm 0.98$	$20.72 \pm 0.56 \pm 1.14$
2-4	$26.92 \pm 0.55 \pm 1.30$	$25.65 \pm 0.43 \pm 1.24$	$27.27 \pm 0.56 \pm 1.37$
4-6	$34.28 \pm 0.68 \pm 1.58$	$28.18 \pm 0.49 \pm 1.33$	$29.32 \pm 0.67 \pm 1.55$
6-8	$34.61 \pm 0.83 \pm 1.89$	$32.17 \pm 0.71 \pm 1.57$	$34.12 \pm 1.02 \pm 2.38$
8-20	$41.47 \pm 0.84 \pm 1.99$	$36.17 \pm 0.78 \pm 1.78$	$34.52 \pm 1.04 \pm 1.80$

Table 6: Ratio(%) of double differential production cross-section for prompt  $\psi(2S)$  to  $J/\psi$  in bins of  $(p_T, y)$ . The first uncertainties are statistical, the second are the systematic uncertainties, for  $45 \leq \text{PVNTRACKS} < 70$ .

prompt			
$p_T$ (GeV/c)	$2 < y < 2.8$	$2.8 < y < 3.5$	$3.5 < y < 4.5$
0-2	$9.04 \pm 0.22 \pm 0.27$	$8.79 \pm 0.18 \pm 0.20$	$9.42 \pm 0.16 \pm 0.29$
2-4	$13.03 \pm 0.21 \pm 0.29$	$12.38 \pm 0.16 \pm 0.24$	$13.53 \pm 0.17 \pm 0.29$
4-6	$20.18 \pm 0.28 \pm 0.52$	$17.62 \pm 0.21 \pm 0.33$	$18.83 \pm 0.23 \pm 0.44$
6-8	$25.17 \pm 0.38 \pm 0.68$	$23.94 \pm 0.31 \pm 0.52$	$23.65 \pm 0.37 \pm 0.60$
8-20	$31.32 \pm 0.43 \pm 0.84$	$29.02 \pm 0.41 \pm 0.71$	$27.94 \pm 0.50 \pm 0.88$

from $b$			
$p_T$ (GeV/c)	$2 < y < 2.8$	$2.8 < y < 3.5$	$3.5 < y < 4.5$
0-2	$20.93 \pm 0.68 \pm 0.83$	$18.99 \pm 0.56 \pm 0.81$	$19.55 \pm 0.62 \pm 0.70$
2-4	$23.54 \pm 0.54 \pm 0.68$	$24.22 \pm 0.45 \pm 0.68$	$23.76 \pm 0.55 \pm 0.87$
4-6	$31.83 \pm 0.66 \pm 0.82$	$26.85 \pm 0.49 \pm 0.78$	$27.46 \pm 0.67 \pm 1.16$
6-8	$32.65 \pm 0.77 \pm 1.03$	$31.71 \pm 0.69 \pm 1.02$	$34.16 \pm 0.96 \pm 1.55$
8-20	$39.44 \pm 0.74 \pm 1.12$	$37.75 \pm 0.73 \pm 1.14$	$38.58 \pm 1.07 \pm 1.71$

Table 7: Ratio(%) of double differential production cross-section for prompt  $\psi(2S)$  to  $J/\psi$  in bins of  $(p_T, y)$ . The first uncertainties are statistical, the second are the systematic uncertainties, for  $70 \leq \text{PVNTRACKS} < 95$ .

prompt			
$p_T$ (GeV/c)	$2 < y < 2.8$	$2.8 < y < 3.5$	$3.5 < y < 4.5$
0-2	$7.71 \pm 0.44 \pm 0.28$	$7.89 \pm 0.34 \pm 0.23$	$7.55 \pm 0.28 \pm 0.51$
2-4	$11.29 \pm 0.37 \pm 0.34$	$11.58 \pm 0.31 \pm 0.28$	$12.18 \pm 0.30 \pm 0.45$
4-6	$17.92 \pm 0.43 \pm 0.56$	$15.68 \pm 0.31 \pm 0.33$	$16.52 \pm 0.36 \pm 0.47$
6-8	$23.07 \pm 0.54 \pm 0.78$	$20.16 \pm 0.43 \pm 0.57$	$21.77 \pm 0.52 \pm 0.75$
8-20	$29.65 \pm 0.59 \pm 1.14$	$27.43 \pm 0.55 \pm 0.95$	$25.27 \pm 0.66 \pm 1.00$

from $b$			
$p_T$ (GeV/c)	$2 < y < 2.8$	$2.8 < y < 3.5$	$3.5 < y < 4.5$
0-2	$17.74 \pm 1.03 \pm 1.07$	$17.59 \pm 0.80 \pm 0.75$	$19.41 \pm 0.99 \pm 0.83$
2-4	$26.99 \pm 0.92 \pm 0.95$	$24.29 \pm 0.69 \pm 0.73$	$25.62 \pm 0.89 \pm 1.23$
4-6	$32.36 \pm 0.99 \pm 1.04$	$26.84 \pm 0.71 \pm 0.89$	$26.85 \pm 0.95 \pm 1.18$
6-8	$31.96 \pm 1.12 \pm 1.24$	$31.70 \pm 1.01 \pm 1.27$	$28.69 \pm 1.32 \pm 1.59$
8-20	$41.22 \pm 1.06 \pm 1.22$	$35.64 \pm 1.01 \pm 1.35$	$34.33 \pm 1.47 \pm 1.58$

Table 8: Ratio(%) of double differential production cross-section for prompt  $\psi(2S)$  to  $J/\psi$  in bins of  $(p_T, y)$ . The first uncertainties are statistical, the second are the systematic uncertainties, for  $95 \leq \text{PVNTRACKS} < 200$ .

prompt			
$p_T$ (GeV/c)	$2 < y < 2.8$	$2.8 < y < 3.5$	$3.5 < y < 4.5$
0-2	$9.91 \pm 1.05 \pm 0.83$	$7.13 \pm 0.79 \pm 0.46$	$8.93 \pm 0.77 \pm 0.69$
2-4	$9.18 \pm 0.74 \pm 0.55$	$9.23 \pm 0.59 \pm 0.41$	$10.99 \pm 0.61 \pm 0.51$
4-6	$17.20 \pm 0.86 \pm 1.02$	$14.79 \pm 0.61 \pm 0.67$	$15.31 \pm 0.66 \pm 1.08$
6-8	$22.16 \pm 1.04 \pm 1.89$	$19.04 \pm 0.78 \pm 1.61$	$22.02 \pm 1.00 \pm 1.60$
8-20	$28.98 \pm 1.05 \pm 3.43$	$26.00 \pm 0.93 \pm 1.53$	$24.66 \pm 1.17 \pm 1.84$

from $b$			
$p_T$ (GeV/c)	$2 < y < 2.8$	$2.8 < y < 3.5$	$3.5 < y < 4.5$
0-2	$23.68 \pm 2.65 \pm 3.06$	$20.28 \pm 1.84 \pm 1.65$	$21.47 \pm 2.45 \pm 2.05$
2-4	$24.12 \pm 1.55 \pm 1.89$	$25.31 \pm 1.39 \pm 1.30$	$24.29 \pm 1.61 \pm 1.71$
4-6	$30.40 \pm 1.81 \pm 4.41$	$28.96 \pm 1.41 \pm 1.84$	$28.78 \pm 1.85 \pm 2.25$
6-8	$35.56 \pm 2.30 \pm 3.36$	$36.19 \pm 1.99 \pm 4.02$	$25.80 \pm 2.46 \pm 2.30$
8-20	$35.20 \pm 1.79 \pm 2.74$	$33.68 \pm 1.78 \pm 1.74$	$37.92 \pm 2.77 \pm 3.21$

685 **2 Taking nBackTracks as multiplicity variable**

Table 9: Ratio(%) of double differential production cross-section for prompt  $\psi(2S)$  to  $J/\psi$  in bins of  $(p_T, y)$ . The first uncertainties are statistical, the second are the systematic uncertainties, for  $0 \leq \text{nBackTracks} < 8$ .

		prompt		
$p_T$ (GeV/c)		$2 < y < 2.8$	$2.8 < y < 3.5$	$3.5 < y < 4.5$
0-2		$12.78 \pm 0.18 \pm 0.89$	$12.48 \pm 0.14 \pm 0.66$	$12.88 \pm 0.13 \pm 0.75$
2-4		$17.26 \pm 0.23 \pm 0.81$	$16.40 \pm 0.18 \pm 0.68$	$16.36 \pm 0.18 \pm 0.66$
4-6		$23.45 \pm 0.36 \pm 1.07$	$21.17 \pm 0.26 \pm 0.87$	$20.84 \pm 0.29 \pm 0.88$
6-8		$30.78 \pm 0.62 \pm 1.63$	$26.87 \pm 0.47 \pm 1.26$	$26.21 \pm 0.53 \pm 1.31$
8-20		$32.25 \pm 0.71 \pm 1.68$	$28.28 \pm 0.60 \pm 1.42$	$27.93 \pm 0.76 \pm 1.46$
from $b$				
$p_T$ (GeV/c)		$2 < y < 2.8$	$2.8 < y < 3.5$	$3.5 < y < 4.5$
0-2		$21.71 \pm 0.88 \pm 2.39$	$20.83 \pm 0.72 \pm 1.38$	$21.28 \pm 0.82 \pm 1.67$
2-4		$26.41 \pm 0.79 \pm 1.31$	$26.46 \pm 0.63 \pm 1.29$	$26.41 \pm 0.75 \pm 1.35$
4-6		$34.65 \pm 1.00 \pm 1.70$	$29.13 \pm 0.71 \pm 1.39$	$30.13 \pm 0.95 \pm 1.69$
6-8		$33.39 \pm 1.23 \pm 2.17$	$31.37 \pm 1.02 \pm 1.85$	$33.99 \pm 1.40 \pm 2.61$
8-20		$41.81 \pm 1.26 \pm 2.03$	$36.94 \pm 1.11 \pm 2.00$	$35.45 \pm 1.45 \pm 2.12$

Table 10: Ratio(%) of double differential production cross-section for prompt  $\psi(2S)$  to  $J/\psi$  in bins of  $(p_T, y)$ . The first uncertainties are statistical, the second are the systematic uncertainties, for  $8 \leq \text{nBackTracks} < 15$ .

		prompt		
$p_T$ (GeV/c)		$2 < y < 2.8$	$2.8 < y < 3.5$	$3.5 < y < 4.5$
0-2		$10.88 \pm 0.21 \pm 0.53$	$10.31 \pm 0.17 \pm 0.40$	$11.35 \pm 0.16 \pm 0.55$
2-4		$15.30 \pm 0.24 \pm 0.56$	$13.74 \pm 0.18 \pm 0.43$	$14.85 \pm 0.19 \pm 0.47$
4-6		$21.98 \pm 0.33 \pm 0.78$	$18.69 \pm 0.23 \pm 0.60$	$19.23 \pm 0.27 \pm 0.64$
6-8		$27.76 \pm 0.49 \pm 1.19$	$25.11 \pm 0.38 \pm 0.91$	$24.65 \pm 0.47 \pm 1.04$
8-20		$33.44 \pm 0.60 \pm 1.44$	$28.62 \pm 0.51 \pm 1.09$	$29.46 \pm 0.66 \pm 1.52$
from $b$				
$p_T$ (GeV/c)		$2 < y < 2.8$	$2.8 < y < 3.5$	$3.5 < y < 4.5$
0-2		$21.38 \pm 0.82 \pm 1.35$	$19.44 \pm 0.63 \pm 1.01$	$19.59 \pm 0.71 \pm 1.30$
2-4		$25.22 \pm 0.68 \pm 1.05$	$24.62 \pm 0.53 \pm 0.91$	$26.11 \pm 0.70 \pm 1.00$
4-6		$32.12 \pm 0.80 \pm 1.27$	$27.71 \pm 0.60 \pm 1.04$	$28.15 \pm 0.81 \pm 1.36$
6-8		$33.65 \pm 0.99 \pm 1.64$	$33.25 \pm 0.88 \pm 1.46$	$32.86 \pm 1.20 \pm 2.38$
8-20		$39.68 \pm 0.95 \pm 1.75$	$37.19 \pm 0.94 \pm 1.58$	$35.36 \pm 1.31 \pm 2.08$

Table 11: Ratio(%) of double differential production cross-section for prompt  $\psi(2S)$  to  $J/\psi$  in bins of  $(p_T, y)$ . The first uncertainties are statistical, the second are the systematic uncertainties, for  $15 \leq n\text{BackTracks} < 22$ .

prompt			
$p_T$ (GeV/c)	$2 < y < 2.8$	$2.8 < y < 3.5$	$3.5 < y < 4.5$
0-2	$8.97 \pm 0.27 \pm 0.32$	$9.42 \pm 0.23 \pm 0.32$	$9.58 \pm 0.21 \pm 0.39$
2-4	$13.41 \pm 0.28 \pm 0.34$	$12.68 \pm 0.22 \pm 0.27$	$13.57 \pm 0.24 \pm 0.36$
4-6	$20.29 \pm 0.38 \pm 0.55$	$17.52 \pm 0.27 \pm 0.39$	$18.62 \pm 0.33 \pm 0.48$
6-8	$25.76 \pm 0.52 \pm 0.90$	$23.21 \pm 0.41 \pm 0.69$	$22.37 \pm 0.49 \pm 0.78$
8-20	$32.96 \pm 0.62 \pm 1.24$	$28.41 \pm 0.55 \pm 0.91$	$28.58 \pm 0.73 \pm 1.04$

from $b$			
$p_T$ (GeV/c)	$2 < y < 2.8$	$2.8 < y < 3.5$	$3.5 < y < 4.5$
0-2	$18.28 \pm 0.84 \pm 0.91$	$19.54 \pm 0.74 \pm 0.91$	$21.70 \pm 0.89 \pm 1.02$
2-4	$26.99 \pm 0.78 \pm 0.89$	$24.53 \pm 0.61 \pm 0.84$	$24.61 \pm 0.76 \pm 1.15$
4-6	$31.88 \pm 0.91 \pm 1.02$	$25.95 \pm 0.64 \pm 1.11$	$27.80 \pm 0.93 \pm 1.13$
6-8	$35.26 \pm 1.08 \pm 1.48$	$31.24 \pm 0.93 \pm 1.30$	$32.19 \pm 1.34 \pm 1.96$
8-20	$40.96 \pm 1.06 \pm 1.57$	$36.60 \pm 1.00 \pm 1.41$	$37.63 \pm 1.47 \pm 1.93$

Table 12: Ratio(%) of double differential production cross-section for prompt  $\psi(2S)$  to  $J/\psi$  in bins of  $(p_T, y)$ . The first uncertainties are statistical, the second are the systematic uncertainties, for  $22 \leq n\text{BackTracks} < 30$ .

prompt			
$p_T$ (GeV/c)	$2 < y < 2.8$	$2.8 < y < 3.5$	$3.5 < y < 4.5$
0-2	$8.84 \pm 0.42 \pm 0.38$	$8.44 \pm 0.31 \pm 0.30$	$9.44 \pm 0.30 \pm 0.62$
2-4	$12.34 \pm 0.39 \pm 0.44$	$11.70 \pm 0.29 \pm 0.25$	$13.21 \pm 0.32 \pm 0.31$
4-6	$17.14 \pm 0.46 \pm 0.52$	$16.60 \pm 0.35 \pm 0.39$	$17.25 \pm 0.42 \pm 0.48$
6-8	$24.94 \pm 0.65 \pm 1.00$	$21.02 \pm 0.49 \pm 0.65$	$23.60 \pm 0.66 \pm 0.93$
8-20	$30.78 \pm 0.71 \pm 1.12$	$27.47 \pm 0.66 \pm 0.91$	$26.57 \pm 0.84 \pm 1.39$

from $b$			
$p_T$ (GeV/c)	$2 < y < 2.8$	$2.8 < y < 3.5$	$3.5 < y < 4.5$
0-2	$19.08 \pm 1.06 \pm 1.17$	$18.33 \pm 0.91 \pm 0.95$	$18.24 \pm 1.04 \pm 1.54$
2-4	$24.53 \pm 0.93 \pm 0.87$	$24.59 \pm 0.75 \pm 0.65$	$24.82 \pm 0.98 \pm 0.96$
4-6	$34.04 \pm 1.14 \pm 1.13$	$27.68 \pm 0.83 \pm 0.92$	$28.05 \pm 1.18 \pm 1.49$
6-8	$30.65 \pm 1.25 \pm 1.21$	$30.66 \pm 1.13 \pm 1.30$	$31.91 \pm 1.65 \pm 1.99$
8-20	$38.03 \pm 1.20 \pm 1.20$	$36.79 \pm 1.24 \pm 1.45$	$35.96 \pm 1.79 \pm 2.19$

Table 13: Ratio(%) of double differential production cross-section for prompt  $\psi(2S)$  to  $J/\psi$  in bins of  $(p_T, y)$ . The first uncertainties are statistical, the second are the systematic uncertainties, for  $30 \leq n\text{BackTracks} < 80$ .

prompt			
$p_T$ (GeV/c)	$2 < y < 2.8$	$2.8 < y < 3.5$	$3.5 < y < 4.5$
0-2	$10.05 \pm 0.65 \pm 0.70$	$8.74 \pm 0.49 \pm 0.34$	$8.60 \pm 0.43 \pm 0.40$
2-4	$11.00 \pm 0.52 \pm 0.40$	$12.93 \pm 0.46 \pm 0.58$	$13.28 \pm 0.44 \pm 0.39$
4-6	$19.54 \pm 0.67 \pm 0.72$	$15.82 \pm 0.44 \pm 0.45$	$17.01 \pm 0.52 \pm 0.70$
6-8	$21.82 \pm 0.78 \pm 1.10$	$21.98 \pm 0.68 \pm 1.17$	$21.93 \pm 0.79 \pm 0.90$
8-20	$28.63 \pm 0.87 \pm 1.25$	$25.73 \pm 0.78 \pm 0.98$	$22.99 \pm 0.96 \pm 1.05$
from $b$			
$p_T$ (GeV/c)	$2 < y < 2.8$	$2.8 < y < 3.5$	$3.5 < y < 4.5$
0-2	$20.03 \pm 1.60 \pm 1.77$	$19.62 \pm 1.20 \pm 1.13$	$20.23 \pm 1.49 \pm 1.20$
2-4	$26.02 \pm 1.26 \pm 1.00$	$23.62 \pm 1.01 \pm 0.83$	$24.16 \pm 1.25 \pm 0.91$
4-6	$33.55 \pm 1.45 \pm 1.31$	$28.41 \pm 1.07 \pm 1.14$	$27.64 \pm 1.44 \pm 1.67$
6-8	$35.20 \pm 1.81 \pm 2.00$	$34.75 \pm 1.62 \pm 2.78$	$27.33 \pm 2.10 \pm 2.32$
8-20	$40.75 \pm 1.57 \pm 1.72$	$33.67 \pm 1.46 \pm 1.26$	$34.87 \pm 2.28 \pm 1.82$

### 686 3 Taking nForwardTracks as multiplicity variable

Table 14: Ratio(%) of double differential production cross-section for prompt  $\psi(2S)$  to  $J/\psi$  in bins of  $(p_T, y)$ . The first uncertainties are statistical, the second are the systematic uncertainties, for  $0 \leq n\text{ForwardTracks} < 12$ .

prompt			
$p_T$ (GeV/c)	$2 < y < 2.8$	$2.8 < y < 3.5$	$3.5 < y < 4.5$
0-2	$16.01 \pm 0.22 \pm 0.69$	$15.86 \pm 0.18 \pm 0.62$	$16.07 \pm 0.18 \pm 0.64$
2-4	$21.67 \pm 0.37 \pm 0.92$	$19.67 \pm 0.27 \pm 0.76$	$20.59 \pm 0.31 \pm 0.80$
4-6	$28.37 \pm 0.70 \pm 1.21$	$24.31 \pm 0.51 \pm 1.00$	$23.25 \pm 0.58 \pm 1.01$
6-8	$34.96 \pm 1.38 \pm 1.75$	$27.17 \pm 1.00 \pm 1.31$	$28.99 \pm 1.26 \pm 1.47$
8-20	$33.65 \pm 1.77 \pm 1.87$	$27.14 \pm 1.59 \pm 1.41$	$28.53 \pm 2.28 \pm 2.00$
from $b$			
$p_T$ (GeV/c)	$2 < y < 2.8$	$2.8 < y < 3.5$	$3.5 < y < 4.5$
0-2	$22.02 \pm 1.35 \pm 1.27$	$21.28 \pm 1.08 \pm 1.27$	$23.51 \pm 1.43 \pm 1.48$
2-4	$29.87 \pm 1.36 \pm 1.82$	$26.89 \pm 1.03 \pm 1.41$	$27.32 \pm 1.33 \pm 2.18$
4-6	$35.66 \pm 1.82 \pm 1.71$	$30.86 \pm 1.42 \pm 1.81$	$35.67 \pm 1.97 \pm 2.15$
6-8	$36.27 \pm 2.50 \pm 2.10$	$35.57 \pm 2.18 \pm 2.07$	$34.00 \pm 2.92 \pm 2.13$
8-20	$48.13 \pm 3.00 \pm 2.48$	$40.55 \pm 2.76 \pm 2.12$	$39.03 \pm 3.58 \pm 3.07$

Table 15: Ratio(%) of double differential production cross-section for prompt  $\psi(2S)$  to  $J/\psi$  in bins of  $(p_T, y)$ . The first uncertainties are statistical, the second are the systematic uncertainties, for  $12 \leq n\text{ForwardTracks} < 24$ .

prompt			
$p_T$ (GeV/c)	$2 < y < 2.8$	$2.8 < y < 3.5$	$3.5 < y < 4.5$
0-2	$12.52 \pm 0.16 \pm 0.51$	$12.00 \pm 0.12 \pm 0.45$	$12.79 \pm 0.12 \pm 0.51$
2-4	$17.29 \pm 0.20 \pm 0.69$	$16.64 \pm 0.15 \pm 0.61$	$16.81 \pm 0.16 \pm 0.62$
4-6	$24.11 \pm 0.32 \pm 0.95$	$21.80 \pm 0.23 \pm 0.81$	$22.20 \pm 0.27 \pm 0.84$
6-8	$30.99 \pm 0.54 \pm 1.38$	$27.27 \pm 0.42 \pm 1.07$	$25.82 \pm 0.50 \pm 1.08$
8-20	$34.20 \pm 0.69 \pm 1.46$	$28.33 \pm 0.59 \pm 1.21$	$28.99 \pm 0.77 \pm 1.33$

from $b$			
$p_T$ (GeV/c)	$2 < y < 2.8$	$2.8 < y < 3.5$	$3.5 < y < 4.5$
0-2	$19.02 \pm 0.69 \pm 1.00$	$20.54 \pm 0.60 \pm 0.90$	$20.53 \pm 0.69 \pm 1.05$
2-4	$27.70 \pm 0.70 \pm 1.17$	$26.41 \pm 0.55 \pm 1.15$	$27.35 \pm 0.69 \pm 1.20$
4-6	$33.87 \pm 0.87 \pm 1.40$	$28.73 \pm 0.63 \pm 1.24$	$28.92 \pm 0.85 \pm 1.66$
6-8	$34.24 \pm 1.10 \pm 1.97$	$31.66 \pm 0.95 \pm 1.53$	$36.00 \pm 1.40 \pm 2.05$
8-20	$42.40 \pm 1.14 \pm 1.83$	$36.58 \pm 1.06 \pm 1.62$	$37.08 \pm 1.47 \pm 1.96$

Table 16: Ratio(%) of double differential production cross-section for prompt  $\psi(2S)$  to  $J/\psi$  in bins of  $(p_T, y)$ . The first uncertainties are statistical, the second are the systematic uncertainties, for  $24 \leq n\text{ForwardTracks} < 36$ .

prompt			
$p_T$ (GeV/c)	$2 < y < 2.8$	$2.8 < y < 3.5$	$3.5 < y < 4.5$
0-2	$10.25 \pm 0.19 \pm 0.50$	$9.94 \pm 0.15 \pm 0.45$	$10.47 \pm 0.14 \pm 0.49$
2-4	$15.01 \pm 0.21 \pm 0.74$	$14.06 \pm 0.16 \pm 0.63$	$15.27 \pm 0.17 \pm 0.69$
4-6	$22.14 \pm 0.30 \pm 1.03$	$19.72 \pm 0.21 \pm 0.88$	$19.45 \pm 0.24 \pm 0.89$
6-8	$27.15 \pm 0.43 \pm 1.36$	$24.99 \pm 0.34 \pm 1.15$	$24.87 \pm 0.42 \pm 1.26$
8-20	$34.19 \pm 0.55 \pm 1.69$	$29.95 \pm 0.48 \pm 1.41$	$28.70 \pm 0.59 \pm 1.56$

from $b$			
$p_T$ (GeV/c)	$2 < y < 2.8$	$2.8 < y < 3.5$	$3.5 < y < 4.5$
0-2	$20.86 \pm 0.70 \pm 1.14$	$19.55 \pm 0.57 \pm 1.06$	$20.70 \pm 0.66 \pm 1.15$
2-4	$24.64 \pm 0.59 \pm 1.30$	$25.44 \pm 0.49 \pm 1.22$	$25.49 \pm 0.61 \pm 1.24$
4-6	$33.39 \pm 0.75 \pm 1.71$	$28.38 \pm 0.55 \pm 1.50$	$28.53 \pm 0.75 \pm 1.59$
6-8	$34.21 \pm 0.91 \pm 1.88$	$32.26 \pm 0.78 \pm 1.66$	$33.53 \pm 1.12 \pm 2.48$
8-20	$39.71 \pm 0.87 \pm 2.00$	$36.66 \pm 0.85 \pm 1.87$	$34.49 \pm 1.16 \pm 2.10$

Table 17: Ratio(%) of double differential production cross-section for prompt  $\psi(2S)$  to  $J/\psi$  in bins of  $(p_T, y)$ . The first uncertainties are statistical, the second are the systematic uncertainties, for  $36 \leq n\text{ForwardTracks} < 48$ .

prompt			
$p_T$ (GeV/c)	$2 < y < 2.8$	$2.8 < y < 3.5$	$3.5 < y < 4.5$
0-2	$8.97 \pm 0.27 \pm 0.34$	$8.91 \pm 0.21 \pm 0.28$	$9.18 \pm 0.19 \pm 0.35$
2-4	$12.98 \pm 0.25 \pm 0.40$	$12.24 \pm 0.20 \pm 0.35$	$13.34 \pm 0.21 \pm 0.40$
4-6	$19.67 \pm 0.33 \pm 0.66$	$17.34 \pm 0.24 \pm 0.48$	$18.71 \pm 0.27 \pm 0.62$
6-8	$25.22 \pm 0.45 \pm 0.91$	$24.19 \pm 0.37 \pm 0.77$	$22.53 \pm 0.43 \pm 0.93$
8-20	$30.83 \pm 0.52 \pm 1.17$	$29.39 \pm 0.48 \pm 1.01$	$26.80 \pm 0.58 \pm 1.10$

from $b$			
$p_T$ (GeV/c)	$2 < y < 2.8$	$2.8 < y < 3.5$	$3.5 < y < 4.5$
0-2	$19.55 \pm 0.82 \pm 0.94$	$18.95 \pm 0.68 \pm 0.89$	$18.66 \pm 0.73 \pm 0.97$
2-4	$24.04 \pm 0.66 \pm 0.87$	$24.03 \pm 0.55 \pm 0.86$	$24.57 \pm 0.67 \pm 0.97$
4-6	$32.21 \pm 0.79 \pm 1.18$	$26.33 \pm 0.56 \pm 0.83$	$27.16 \pm 0.79 \pm 1.37$
6-8	$32.09 \pm 0.91 \pm 1.37$	$33.16 \pm 0.85 \pm 1.31$	$31.59 \pm 1.13 \pm 2.03$
8-20	$38.94 \pm 0.89 \pm 1.47$	$37.14 \pm 0.87 \pm 1.45$	$39.10 \pm 1.30 \pm 1.88$

Table 18: Ratio(%) of double differential production cross-section for prompt  $\psi(2S)$  to  $J/\psi$  in bins of  $(p_T, y)$ . The first uncertainties are statistical, the second are the systematic uncertainties, for  $48 \leq n\text{ForwardTracks} < 130$ .

prompt			
$p_T$ (GeV/c)	$2 < y < 2.8$	$2.8 < y < 3.5$	$3.5 < y < 4.5$
0-2	$7.83 \pm 0.35 \pm 0.31$	$7.63 \pm 0.28 \pm 0.31$	$8.44 \pm 0.25 \pm 0.25$
2-4	$10.93 \pm 0.30 \pm 0.35$	$10.96 \pm 0.24 \pm 0.28$	$11.58 \pm 0.23 \pm 0.29$
4-6	$18.12 \pm 0.35 \pm 0.63$	$15.04 \pm 0.24 \pm 0.35$	$16.48 \pm 0.28 \pm 0.60$
6-8	$23.28 \pm 0.44 \pm 0.83$	$19.97 \pm 0.32 \pm 0.54$	$22.83 \pm 0.42 \pm 0.82$
8-20	$29.91 \pm 0.46 \pm 0.98$	$27.16 \pm 0.41 \pm 1.04$	$25.68 \pm 0.51 \pm 1.07$

from $b$			
$p_T$ (GeV/c)	$2 < y < 2.8$	$2.8 < y < 3.5$	$3.5 < y < 4.5$
0-2	$19.00 \pm 0.87 \pm 1.09$	$17.31 \pm 0.66 \pm 1.00$	$19.72 \pm 0.79 \pm 0.85$
2-4	$24.67 \pm 0.68 \pm 0.83$	$24.22 \pm 0.55 \pm 0.70$	$24.98 \pm 0.68 \pm 0.83$
4-6	$30.68 \pm 0.76 \pm 0.98$	$27.65 \pm 0.57 \pm 0.94$	$27.95 \pm 0.74 \pm 1.13$
6-8	$32.93 \pm 0.89 \pm 1.21$	$32.79 \pm 0.78 \pm 1.22$	$29.56 \pm 1.01 \pm 1.59$
8-20	$39.20 \pm 0.79 \pm 1.35$	$35.10 \pm 0.75 \pm 1.30$	$34.72 \pm 1.11 \pm 1.71$

687 **B Tables of the fit results in each kinematic bin**

688 **1 Tables of two dimensional fit for  $t_z$**

689 For each kinematic and multiplicity bin of  $J/\psi$  and  $\psi(2S)$  candidates, the mass fitted  
690 value of  $\mu_{mass}$  (mean value of narrower Gaussian),  $\sigma_{mass}$  (width of narrower Gaussian),  
691  $n_{sig}$  (signal yields),  $n_{bkg}$  (background number),  $1000p_0$  (parameter in exponential function)  
692 and  $t_z$ -mass combine fitted value  $\beta$  (fraction of first Gaussian of signal resolution function),  
693  $1000\mu_{t_z}$  (bias of  $t_z$  distribution),  $S(1, 2)_{t_z}$  ( $\sigma_{1,2}$  of first/second Gaussian resolution function  
694 convolved with the  $t_z$  function),  $\tau_b$  (effective  $b$ -hadron lifetime),  $n_{bkg}$ ,  $n_{prompt}$  (number of  
695 prompt  $\psi(2S)$ ),  $n_{b-decay}$  (number of  $\psi(2S)$ -from- $b$ ) and  $n_{tail}$  (number of events in tail)  
696 are given below. For those bin where only one Gaussian function is used to describe the  
697 detector resolution, only  $S_2$  is recorded.

Table 19: The parameters of the invariant mass and  $t_z$  fit for  $J/\psi$ , including the fitted yields and the shape parameters for different  $p_T$  bins in the rapidity bin  $2.0 < y < 2.8$  and multiplicity bin  $0 < PVNTRACKS < 20$ .

$J/\psi$ parameters	$p_T$ (GeV/c)				
	0-2	2-4	4-6	6-8	8-20
$\mu_{mass}$	$3097.7 \pm 0.0$	$3097.1 \pm 0.0$	$3097.1 \pm 0.0$	$3096.9 \pm 0.1$	$3096.9 \pm 0.1$
$\sigma_{mass}$	$16.3 \pm 0.4$	$17.5 \pm 0.5$	$10.8 \pm 0.1$	$22.8 \pm 4.5$	$19.9 \pm 1.1$
$n_{sig}$	$237806 \pm 530$	$214317 \pm 496$	$115291 \pm 360$	$45943 \pm 253$	$29342 \pm 181$
$n_{bkg}$	$30467 \pm 271$	$17008 \pm 221$	$5854 \pm 142$	$1975 \pm 141$	$1353 \pm 68$
$1000 * p_0$	$0.42 \pm 0.09$	$-0.88 \pm 0.13$	$-0.00 \pm 0.24$	$-1.21 \pm 0.43$	$-1.49 \pm 0.50$
$1000 * \mu_{tz}$	$-8.1 \pm 0.1$	$-7.1 \pm 0.1$	$-4.8 \pm 0.2$	$-3.2 \pm 0.2$	$-1.4 \pm 0.3$
$S1_{tz}$	$1.34 \pm 0.02$	$0.81 \pm 0.01$	$1.48 \pm 0.04$	$0.89 \pm 0.02$	$1.62 \pm 0.15$
$S2_{tz}$	$0.74 \pm 0.01$	$1.36 \pm 0.03$	$0.86 \pm 0.01$	$1.46 \pm 0.07$	$0.97 \pm 0.03$
$\beta_{tz}$	$0.32 \pm 0.01$	$0.76 \pm 0.02$	$0.19 \pm 0.02$	$0.80 \pm 0.05$	$0.16 \pm 0.07$
$\tau_b$	$1.62 \pm 0.02$	$1.62 \pm 0.01$	$1.51 \pm 0.01$	$1.50 \pm 0.02$	$1.46 \pm 0.02$
$n_{prompt}$	$219797 \pm 494$	$189247 \pm 454$	$95656 \pm 321$	$35068 \pm 194$	$19202 \pm 144$
$n_{fromb}$	$14590 \pm 149$	$23770 \pm 175$	$19024 \pm 153$	$10587 \pm 113$	$9975 \pm 108$
$n_{tail}$	$2829 \pm 79$	$792 \pm 43$	$285 \pm 26$	$116 \pm 16$	$71 \pm 12$

Table 20: The parameters of the invariant mass and  $t_z$  fit for  $\psi(2S)$ , including the fitted yields and the shape parameters for different  $p_T$  bins in the rapidity bin  $2.0 < y < 2.8$  and multiplicity bin  $0 < PVNTRACKS < 20$ .

$\psi(2S)$ parameters	$p_T$ (GeV/c)				
	0-2	2-4	4-6	6-8	8-20
$\mu_{mass}$	$3686.8 \pm 0.2$	$3686.2 \pm 0.2$	$3685.6 \pm 0.3$	$3685.1 \pm 0.4$	$3686.6 \pm 0.5$
$\sigma_{mass}$	$12.7 \pm 0.2$	$13.1 \pm 0.2$	$13.6 \pm 0.3$	$14.3 \pm 0.4$	$14.5 \pm 0.4$
$n_{sig}$	$10688 \pm 157$	$7583 \pm 118$	$3894 \pm 76$	$1696 \pm 48$	$1217 \pm 40$
$n_{bkg}$	$27087 \pm 203$	$10614 \pm 130$	$2818 \pm 69$	$801 \pm 38$	$489 \pm 30$
$1000 * p_0$	$-0.49 \pm 0.09$	$-0.27 \pm 0.14$	$-0.00 \pm 0.28$	$-0.30 \pm 0.54$	$-0.85 \pm 0.70$
$1000 * \mu_{tz}$	$-10.0 \pm 0.8$	$-8.3 \pm 0.8$	$-7.0 \pm 1.0$	$-5.5 \pm 1.4$	$-1.9 \pm 1.4$
$S1_{tz}$	$0.59 \pm 0.06$	$0.76 \pm 0.05$	$0.85 \pm 0.04$	$1.60 \pm 0.37$	$1.38 \pm 0.26$
$S2_{tz}$	$1.16 \pm 0.07$	$1.29 \pm 0.16$	$1.88 \pm 0.33$	$0.89 \pm 0.08$	$0.79 \pm 0.15$
$\beta_{tz}$	$0.45 \pm 0.10$	$0.73 \pm 0.13$	$0.84 \pm 0.07$	$0.19 \pm 0.16$	$0.40 \pm 0.28$
$\tau_b$	$1.79 \pm 0.10$	$1.57 \pm 0.07$	$1.55 \pm 0.07$	$1.55 \pm 0.09$	$1.62 \pm 0.09$
$n_{prompt}$	$9739 \pm 134$	$6476 \pm 101$	$3165 \pm 67$	$1289 \pm 40$	$742 \pm 31$
$n_{fromb}$	$884 \pm 47$	$1079 \pm 43$	$731 \pm 34$	$416 \pm 24$	$473 \pm 25$
$n_{tail}$	$93 \pm 17$	$23 \pm 9$	$8 \pm 5$	$5 \pm 3$	$0 \pm 1$

Table 21: The parameters of the invariant mass and  $t_z$  fit for  $J/\psi$ , including the fitted yields and the shape parameters for different  $p_T$  bins in the rapidity bin  $2.8 < y < 3.5$  and multiplicity bin  $0 < PVNTRACKS < 20$ .

$J/\psi$ parameters	$p_T$ (GeV/c)				
	0-2	2-4	4-6	6-8	8-20
$\mu_{mass}$	$3096.8 \pm 0.0$	$3096.5 \pm 0.0$	$3096.3 \pm 0.0$	$3096.1 \pm 0.1$	$3095.9 \pm 0.1$
$\sigma_{mass}$	$10.2 \pm 0.1$	$16.5 \pm 0.4$	$16.2 \pm 0.5$	$17.4 \pm 0.7$	$16.9 \pm 0.8$
$n_{sig}$	$387202 \pm 674$	$354703 \pm 634$	$171777 \pm 436$	$54934 \pm 245$	$26814 \pm 172$
$n_{bkg}$	$49040 \pm 341$	$28117 \pm 274$	$7963 \pm 161$	$1967 \pm 85$	$1100 \pm 62$
$1000 * p_0$	$0.37 \pm 0.08$	$-0.72 \pm 0.10$	$-0.00 \pm 0.21$	$-1.17 \pm 0.44$	$-0.45 \pm 0.59$
$1000 * \mu_{tz}$	$-5.7 \pm 0.1$	$-5.9 \pm 0.1$	$-4.9 \pm 0.1$	$-3.1 \pm 0.2$	$-2.7 \pm 0.2$
$S1_{tz}$	$1.49 \pm 0.02$	$1.55 \pm 0.03$	$0.93 \pm 0.01$	$2.44 \pm 0.19$	$2.01 \pm 0.22$
$S2_{tz}$	$0.86 \pm 0.01$	$0.90 \pm 0.01$	$1.71 \pm 0.06$	$0.98 \pm 0.01$	$0.97 \pm 0.02$
$\beta_{tz}$	$0.22 \pm 0.01$	$0.16 \pm 0.01$	$0.89 \pm 0.01$	$0.04 \pm 0.01$	$0.07 \pm 0.03$
$\tau_b$	$1.56 \pm 0.02$	$1.56 \pm 0.01$	$1.52 \pm 0.01$	$1.50 \pm 0.02$	$1.47 \pm 0.02$
$n_{prompt}$	$355733 \pm 629$	$314555 \pm 586$	$144035 \pm 393$	$42799 \pm 214$	$18164 \pm 140$
$n_{fromb}$	$22068 \pm 192$	$36502 \pm 220$	$26276 \pm 180$	$11740 \pm 118$	$8496 \pm 99$
$n_{tail}$	$8089 \pm 131$	$2494 \pm 75$	$811 \pm 42$	$185 \pm 20$	$78 \pm 13$

Table 22: The parameters of the invariant mass and  $t_z$  fit for  $\psi(2S)$ , including the fitted yields and the shape parameters for different  $p_T$  bins in the rapidity bin  $2.8 < y < 3.5$  and multiplicity bin  $0 < PVNTRACKS < 20$ .

$\psi(2S)$ parameters	$p_T$ (GeV/c)				
	0-2	2-4	4-6	6-8	8-20
$\mu_{mass}$	$3685.8 \pm 0.2$	$3685.5 \pm 0.2$	$3685.2 \pm 0.3$	$3684.8 \pm 0.4$	$3685.1 \pm 0.6$
$\sigma_{mass}$	$13.6 \pm 0.2$	$14.2 \pm 0.2$	$14.6 \pm 0.2$	$15.9 \pm 0.4$	$17.1 \pm 0.6$
$n_{sig}$	$17903 \pm 207$	$12751 \pm 159$	$5906 \pm 95$	$2100 \pm 53$	$1208 \pm 41$
$n_{bkg}$	$43575 \pm 262$	$19484 \pm 179$	$4172 \pm 86$	$722 \pm 38$	$363 \pm 28$
$1000 * p_0$	$-0.50 \pm 0.07$	$-0.46 \pm 0.11$	$-0.00 \pm 0.23$	$-0.74 \pm 0.58$	$-1.41 \pm 0.83$
$1000 * \mu_{tz}$	$-6.0 \pm 0.6$	$-6.0 \pm 0.6$	$-6.9 \pm 0.7$	$-4.5 \pm 1.0$	$-4.6 \pm 1.2$
$S1_{tz}$	$1.38 \pm 0.11$	$1.15 \pm 0.09$	$0.90 \pm 0.02$	$1.72 \pm 0.25$	$7.44 \pm 2.34$
$S2_{tz}$	$0.79 \pm 0.04$	$0.68 \pm 0.12$	$2.29 \pm 0.27$	$0.87 \pm 0.05$	$0.93 \pm 0.03$
$\beta_{tz}$	$0.36 \pm 0.10$	$0.62 \pm 0.20$	$0.90 \pm 0.02$	$0.19 \pm 0.09$	$0.03 \pm 0.01$
$\tau_b$	$1.61 \pm 0.09$	$1.67 \pm 0.06$	$1.73 \pm 0.07$	$1.65 \pm 0.09$	$1.54 \pm 0.08$
$n_{prompt}$	$16115 \pm 173$	$11003 \pm 134$	$4774 \pm 81$	$1555 \pm 44$	$724 \pm 30$
$n_{fromb}$	$1383 \pm 63$	$1684 \pm 56$	$1105 \pm 42$	$532 \pm 27$	$481 \pm 25$
$n_{tail}$	$324 \pm 30$	$60 \pm 14$	$40 \pm 10$	$8 \pm 5$	$4 \pm 3$

Table 23: The parameters of the invariant mass and  $t_z$  fit for  $J/\psi$ , including the fitted yields and the shape parameters for different  $p_T$  bins in the rapidity bin  $3.5 < y < 4.5$  and multiplicity bin  $0 < PVNTRACKS < 20$ .

$J/\psi$ parameters	$p_T$ (GeV/c)				
	0-2	2-4	4-6	6-8	8-20
$\mu_{mass}$	$3096.2 \pm 0.0$	$3095.9 \pm 0.0$	$3095.9 \pm 0.0$	$3095.9 \pm 0.1$	$3096.0 \pm 0.2$
$\sigma_{mass}$	$19.1 \pm 0.3$	$19.1 \pm 0.3$	$20.7 \pm 0.4$	$23.3 \pm 1.2$	$28.4 \pm 1.6$
$n_{sig}$	$449859 \pm 724$	$308192 \pm 590$	$129805 \pm 381$	$39684 \pm 213$	$18026 \pm 146$
$n_{bkg}$	$33188 \pm 328$	$15424 \pm 236$	$4428 \pm 140$	$1256 \pm 85$	$598 \pm 62$
$1000 * p_0$	$-0.05 \pm 0.10$	$-0.95 \pm 0.15$	$-0.00 \pm 0.31$	$-1.87 \pm 0.58$	$-0.70 \pm 0.90$
$1000 * \mu_{tz}$	$4.0 \pm 0.1$	$0.3 \pm 0.1$	$-1.2 \pm 0.1$	$-1.5 \pm 0.2$	$-0.9 \pm 0.3$
$S1_{tz}$	$0.95 \pm 0.00$	$1.74 \pm 0.04$	$1.87 \pm 0.07$	$0.94 \pm 0.01$	$2.32 \pm 0.27$
$S2_{tz}$	$1.94 \pm 0.04$	$0.92 \pm 0.00$	$0.94 \pm 0.01$	$1.76 \pm 0.12$	$0.96 \pm 0.01$
$\beta_{tz}$	$0.90 \pm 0.01$	$0.13 \pm 0.01$	$0.09 \pm 0.01$	$0.90 \pm 0.02$	$0.05 \pm 0.01$
$\tau_b$	$1.45 \pm 0.02$	$1.52 \pm 0.01$	$1.47 \pm 0.01$	$1.42 \pm 0.02$	$1.42 \pm 0.02$
$n_{prompt}$	$408504 \pm 673$	$274907 \pm 547$	$110875 \pm 346$	$31804 \pm 185$	$12899 \pm 119$
$n_{fromb}$	$22251 \pm 212$	$27849 \pm 199$	$17173 \pm 150$	$7418 \pm 96$	$4944 \pm 77$
$n_{tail}$	$16775 \pm 179$	$3618 \pm 87$	$980 \pm 46$	$189 \pm 20$	$81 \pm 13$

Table 24: The parameters of the invariant mass and  $t_z$  fit for  $\psi(2S)$ , including the fitted yields and the shape parameters for different  $p_T$  bins in the rapidity bin  $3.5 < y < 4.5$  and multiplicity bin  $0 < PVNTRACKS < 20$ .

$\psi(2S)$ parameters	$p_T$ (GeV/c)				
	0-2	2-4	4-6	6-8	8-20
$\mu_{mass}$	$3685.2 \pm 0.2$	$3684.7 \pm 0.2$	$3685.0 \pm 0.4$	$3684.9 \pm 0.6$	$3685.4 \pm 1.1$
$\sigma_{mass}$	$16.9 \pm 0.2$	$17.6 \pm 0.2$	$18.2 \pm 0.4$	$19.0 \pm 0.6$	$22.0 \pm 1.1$
$n_{sig}$	$18795 \pm 201$	$10774 \pm 141$	$4311 \pm 82$	$1497 \pm 46$	$763 \pm 36$
$n_{bkg}$	$26302 \pm 219$	$9755 \pm 137$	$2233 \pm 68$	$493 \pm 34$	$319 \pm 29$
$1000 * p_0$	$-0.68 \pm 0.09$	$-0.77 \pm 0.15$	$-0.00 \pm 0.33$	$-0.95 \pm 0.72$	$-1.06 \pm 0.90$
$1000 * \mu_{tz}$	$2.7 \pm 0.6$	$0.6 \pm 0.7$	$-2.3 \pm 0.9$	$-0.2 \pm 1.3$	$-0.7 \pm 1.7$
$S1_{tz}$	-	$0.94 \pm 0.01$	$1.39 \pm 0.20$	$0.94 \pm 0.05$	$4.38 \pm 1.98$
$S2_{tz}$	$1.00 \pm 0.01$	$2.80 \pm 0.31$	$0.84 \pm 0.07$	$2.06 \pm 0.51$	$0.98 \pm 0.04$
$\beta_{tz}$	0	$0.93 \pm 0.01$	$0.31 \pm 0.17$	$0.89 \pm 0.07$	$0.02 \pm 0.02$
$\tau_b$	$1.37 \pm 0.08$	$1.62 \pm 0.07$	$1.63 \pm 0.08$	$1.83 \pm 0.12$	$1.51 \pm 0.11$
$n_{prompt}$	$16604 \pm 163$	$9356 \pm 119$	$3488 \pm 68$	$1145 \pm 38$	$499 \pm 27$
$n_{fromb}$	$1292 \pm 68$	$1282 \pm 51$	$790 \pm 36$	$340 \pm 22$	$261 \pm 19$
$n_{tail}$	$687 \pm 38$	$160 \pm 20$	$35 \pm 9$	$3 \pm 3$	$3 \pm 2$

Table 25: The parameters of the invariant mass and  $t_z$  fit for  $J/\psi$ , including the fitted yields and the shape parameters for different  $p_T$  bins in the rapidity bin  $2.0 < y < 2.8$  and multiplicity bin  $20 < PVNTRACKS < 40$ .

$J/\psi$ parameters	$p_T$ (GeV/c)				
	0-2	2-4	4-6	6-8	8-20
$\mu_{mass}$	$3097.6 \pm 0.0$	$3097.1 \pm 0.0$	$3097.0 \pm 0.0$	$3096.9 \pm 0.0$	$3096.8 \pm 0.0$
$\sigma_{mass}$	$15.3 \pm 0.3$	$15.3 \pm 0.2$	$10.3 \pm 0.1$	$18.0 \pm 0.4$	$20.5 \pm 0.6$
$n_{sig}$	$490090 \pm 844$	$646733 \pm 901$	$460671 \pm 734$	$225677 \pm 506$	$181913 \pm 455$
$n_{bkg}$	$237902 \pm 678$	$154406 \pm 565$	$50891 \pm 359$	$14076 \pm 211$	$8914 \pm 185$
$1000 * p_0$	$0.53 \pm 0.03$	$-0.54 \pm 0.04$	$-0.00 \pm 0.07$	$-0.88 \pm 0.15$	$-0.91 \pm 0.20$
$1000 * \mu_{tz}$	$-9.8 \pm 0.1$	$-8.0 \pm 0.1$	$-5.1 \pm 0.1$	$-3.0 \pm 0.1$	$-1.1 \pm 0.1$
$S1_{tz}$	$1.62 \pm 0.03$	$1.74 \pm 0.04$	$1.58 \pm 0.03$	$1.62 \pm 0.04$	$1.83 \pm 0.04$
$S2_{tz}$	$0.95 \pm 0.01$	$0.95 \pm 0.00$	$0.93 \pm 0.01$	$0.95 \pm 0.01$	$0.99 \pm 0.01$
$\beta_{tz}$	$0.19 \pm 0.02$	$0.11 \pm 0.01$	$0.17 \pm 0.01$	$0.20 \pm 0.02$	$0.19 \pm 0.01$
$\tau_b$	$1.55 \pm 0.01$	$1.51 \pm 0.01$	$1.44 \pm 0.01$	$1.38 \pm 0.01$	$1.34 \pm 0.01$
$n_{prompt}$	$438453 \pm 741$	$559394 \pm 811$	$379786 \pm 652$	$174770 \pm 438$	$122377 \pm 366$
$n_{fromb}$	$47748 \pm 265$	$85003 \pm 332$	$79474 \pm 313$	$50071 \pm 246$	$58895 \pm 264$
$n_{tail}$	$1983 \pm 75$	$600 \pm 44$	$163 \pm 23$	$93 \pm 17$	$78 \pm 14$

Table 26: The parameters of the invariant mass and  $t_z$  fit for  $\psi(2S)$ , including the fitted yields and the shape parameters for different  $p_T$  bins in the rapidity bin  $2.0 < y < 2.8$  and multiplicity bin  $20 < PVNTRACKS < 40$ .

$\psi(2S)$ parameters	$p_T$ (GeV/c)				
	0-2	2-4	4-6	6-8	8-20
$\mu_{mass}$	$3686.5 \pm 0.2$	$3686.2 \pm 0.2$	$3686.1 \pm 0.2$	$3685.4 \pm 0.2$	$3685.8 \pm 0.2$
$\sigma_{mass}$	$12.4 \pm 0.3$	$13.0 \pm 0.2$	$13.5 \pm 0.2$	$14.1 \pm 0.2$	$15.5 \pm 0.2$
$n_{sig}$	$18098 \pm 343$	$19193 \pm 275$	$13623 \pm 176$	$7651 \pm 113$	$7403 \pm 104$
$n_{bkg}$	$221791 \pm 567$	$110208 \pm 408$	$30533 \pm 219$	$7585 \pm 113$	$3963 \pm 86$
$1000 * p_0$	$-0.53 \pm 0.03$	$-0.45 \pm 0.04$	$-0.00 \pm 0.08$	$-0.58 \pm 0.17$	$-1.10 \pm 0.24$
$1000 * \mu_{tz}$	$-11.2 \pm 0.9$	$-8.0 \pm 0.7$	$-6.7 \pm 0.6$	$-5.1 \pm 0.6$	$-1.4 \pm 0.6$
$S1_{tz}$	$0.72 \pm 0.06$	$3.47 \pm 0.40$	$1.36 \pm 0.16$	$2.04 \pm 0.22$	$1.65 \pm 0.25$
$S2_{tz}$	$1.24 \pm 0.07$	$0.95 \pm 0.01$	$0.87 \pm 0.05$	$0.93 \pm 0.03$	$0.94 \pm 0.07$
$\beta_{tz}$	$0.40 \pm 0.11$	$0.04 \pm 0.01$	$0.26 \pm 0.14$	$0.14 \pm 0.04$	$0.28 \pm 0.15$
$\tau_b$	$1.67 \pm 0.05$	$1.58 \pm 0.03$	$1.53 \pm 0.03$	$1.53 \pm 0.04$	$1.43 \pm 0.03$
$n_{prompt}$	$15277 \pm 264$	$15378 \pm 219$	$10456 \pm 143$	$5632 \pm 93$	$4696 \pm 81$
$n_{fromb}$	$2771 \pm 90$	$3784 \pm 86$	$3201 \pm 70$	$2028 \pm 54$	$2679 \pm 61$
$n_{tail}$	$56 \pm 16$	$6 \pm 7$	$12 \pm 6$	$7 \pm 4$	$12 \pm 5$

Table 27: The parameters of the invariant mass and  $t_z$  fit for  $J/\psi$ , including the fitted yields and the shape parameters for different  $p_T$  bins in the rapidity bin  $2.8 < y < 3.5$  and multiplicity bin  $20 < PVNTRACKS < 40$ .

$J/\psi$ parameters	$p_T$ (GeV/c)				
	0-2	2-4	4-6	6-8	8-20
$\mu_{mass}$	$3096.8 \pm 0.0$	$3096.5 \pm 0.0$	$3096.2 \pm 0.0$	$3096.1 \pm 0.0$	$3095.9 \pm 0.0$
$\sigma_{mass}$	$15.5 \pm 0.3$	$16.1 \pm 0.2$	$16.4 \pm 0.3$	$17.7 \pm 0.4$	$19.4 \pm 0.6$
$n_{sig}$	$775131 \pm 1052$	$1049320 \pm 1161$	$671368 \pm 879$	$266271 \pm 544$	$165299 \pm 431$
$n_{bkg}$	$360004 \pm 832$	$238027 \pm 726$	$60308 \pm 402$	$12795 \pm 207$	$7259 \pm 167$
$1000 * p_0$	$0.31 \pm 0.03$	$-0.63 \pm 0.03$	$-0.00 \pm 0.07$	$-0.84 \pm 0.17$	$-0.56 \pm 0.23$
$1000 * \mu_{tz}$	$-6.1 \pm 0.1$	$-5.8 \pm 0.1$	$-4.6 \pm 0.1$	$-3.5 \pm 0.1$	$-2.3 \pm 0.1$
$S1_{tz}$	$2.39 \pm 0.06$	$1.78 \pm 0.03$	$1.72 \pm 0.03$	$1.71 \pm 0.04$	$0.94 \pm 0.01$
$S2_{tz}$	$1.00 \pm 0.00$	$0.96 \pm 0.00$	$0.95 \pm 0.00$	$0.95 \pm 0.01$	$1.64 \pm 0.05$
$\beta_{tz}$	$0.05 \pm 0.00$	$0.10 \pm 0.01$	$0.12 \pm 0.01$	$0.14 \pm 0.01$	$0.83 \pm 0.02$
$\tau_b$	$1.55 \pm 0.01$	$1.50 \pm 0.00$	$1.42 \pm 0.00$	$1.38 \pm 0.01$	$1.33 \pm 0.01$
$n_{prompt}$	$697291 \pm 938$	$913033 \pm 1038$	$559686 \pm 788$	$209353 \pm 476$	$115515 \pm 354$
$n_{fromb}$	$69202 \pm 327$	$130343 \pm 414$	$108037 \pm 365$	$55499 \pm 258$	$48992 \pm 240$
$n_{tail}$	$5208 \pm 117$	$1508 \pm 66$	$622 \pm 42$	$169 \pm 23$	$61 \pm 13$

Table 28: The parameters of the invariant mass and  $t_z$  fit for  $\psi(2S)$ , including the fitted yields and the shape parameters for different  $p_T$  bins in the rapidity bin  $2.8 < y < 3.5$  and multiplicity bin  $20 < PVNTRACKS < 40$ .

$\psi(2S)$ parameters	$p_T$ (GeV/c)				
	0-2	2-4	4-6	6-8	8-20
$\mu_{mass}$	$3685.5 \pm 0.2$	$3685.1 \pm 0.2$	$3685.3 \pm 0.2$	$3684.8 \pm 0.2$	$3685.1 \pm 0.3$
$\sigma_{mass}$	$13.8 \pm 0.2$	$14.2 \pm 0.2$	$14.9 \pm 0.2$	$15.7 \pm 0.2$	$16.5 \pm 0.2$
$n_{sig}$	$28687 \pm 444$	$31235 \pm 361$	$20786 \pm 217$	$9840 \pm 126$	$6960 \pm 101$
$n_{bkg}$	$323713 \pm 702$	$175404 \pm 524$	$40981 \pm 260$	$7302 \pm 115$	$3409 \pm 82$
$1000 * p_0$	$-0.52 \pm 0.03$	$-0.51 \pm 0.04$	$-0.00 \pm 0.07$	$-0.41 \pm 0.18$	$-0.83 \pm 0.26$
$1000 * \mu_{tz}$	$-6.7 \pm 0.7$	$-6.1 \pm 0.5$	$-5.1 \pm 0.4$	$-3.7 \pm 0.5$	$-2.3 \pm 0.5$
$S1_{tz}$	$1.27 \pm 0.07$	$1.23 \pm 0.06$	$1.70 \pm 0.18$	$2.12 \pm 0.25$	$1.87 \pm 0.32$
$S2_{tz}$	$0.72 \pm 0.06$	$0.76 \pm 0.05$	$0.90 \pm 0.03$	$0.96 \pm 0.02$	$0.94 \pm 0.04$
$\beta_{tz}$	$0.56 \pm 0.10$	$0.55 \pm 0.11$	$0.19 \pm 0.06$	$0.11 \pm 0.03$	$0.14 \pm 0.07$
$\tau_b$	$1.58 \pm 0.04$	$1.56 \pm 0.03$	$1.56 \pm 0.03$	$1.45 \pm 0.04$	$1.50 \pm 0.04$
$n_{prompt}$	$23890 \pm 334$	$25190 \pm 279$	$16542 \pm 178$	$7441 \pm 103$	$4626 \pm 79$
$n_{fromb}$	$4293 \pm 119$	$5907 \pm 110$	$4279 \pm 83$	$2369 \pm 59$	$2328 \pm 57$
$n_{tail}$	$195 \pm 29$	$13 \pm 12$	$25 \pm 9$	$20 \pm 7$	$3 \pm 3$

Table 29: The parameters of the invariant mass and  $t_z$  fit for  $J/\psi$ , including the fitted yields and the shape parameters for different  $p_T$  bins in the rapidity bin  $3.5 < y < 4.5$  and multiplicity bin  $20 < PVNTRACKS < 40$ .

$J/\psi$ parameters	$p_T$ (GeV/c)				
	0-2	2-4	4-6	6-8	8-20
$\mu_{mass}$	$3096.2 \pm 0.0$	$3095.9 \pm 0.0$	$3095.7 \pm 0.0$	$3095.8 \pm 0.0$	$3095.9 \pm 0.1$
$\sigma_{mass}$	$12.9 \pm 0.1$	$20.1 \pm 0.3$	$13.9 \pm 0.2$	$22.1 \pm 0.4$	$26.2 \pm 0.6$
$n_{sig}$	$841376 \pm 1078$	$860732 \pm 1023$	$491085 \pm 753$	$186930 \pm 461$	$106604 \pm 357$
$n_{bkg}$	$181147 \pm 709$	$99415 \pm 535$	$27054 \pm 322$	$6955 \pm 181$	$4212 \pm 159$
$1000 * p_0$	$0.02 \pm 0.04$	$-0.73 \pm 0.05$	$-0.00 \pm 0.11$	$-1.10 \pm 0.24$	$-0.91 \pm 0.32$
$1000 * \mu_{tz}$	$4.4 \pm 0.1$	$0.6 \pm 0.1$	$-1.1 \pm 0.1$	$-1.0 \pm 0.1$	$-0.8 \pm 0.1$
$S1_{tz}$	$1.92 \pm 0.03$	$1.64 \pm 0.02$	$1.67 \pm 0.03$	$1.79 \pm 0.04$	$1.61 \pm 0.05$
$S2_{tz}$	$0.96 \pm 0.00$	$0.93 \pm 0.00$	$0.93 \pm 0.00$	$0.94 \pm 0.01$	$0.92 \pm 0.01$
$\beta_{tz}$	$0.10 \pm 0.01$	$0.15 \pm 0.01$	$0.15 \pm 0.01$	$0.12 \pm 0.01$	$0.17 \pm 0.02$
$\tau_b$	$1.46 \pm 0.01$	$1.44 \pm 0.01$	$1.39 \pm 0.01$	$1.35 \pm 0.01$	$1.30 \pm 0.01$
$n_{prompt}$	$759321 \pm 954$	$759083 \pm 931$	$416720 \pm 677$	$151382 \pm 406$	$78543 \pm 295$
$n_{fromb}$	$65800 \pm 332$	$93412 \pm 360$	$70479 \pm 301$	$34188 \pm 206$	$27361 \pm 182$
$n_{tail}$	$10867 \pm 156$	$2606 \pm 82$	$639 \pm 41$	$117 \pm 19$	$25 \pm 8$

Table 30: The parameters of the invariant mass and  $t_z$  fit for  $\psi(2S)$ , including the fitted yields and the shape parameters for different  $p_T$  bins in the rapidity bin  $3.5 < y < 4.5$  and multiplicity bin  $20 < PVNTRACKS < 40$ .

$\psi(2S)$ parameters	$p_T$ (GeV/c)				
	0-2	2-4	4-6	6-8	8-20
$\mu_{mass}$	$3684.8 \pm 0.2$	$3684.6 \pm 0.2$	$3684.3 \pm 0.2$	$3684.8 \pm 0.3$	$3684.1 \pm 0.4$
$\sigma_{mass}$	$16.8 \pm 0.2$	$17.3 \pm 0.2$	$18.7 \pm 0.2$	$20.0 \pm 0.3$	$21.5 \pm 0.4$
$n_{sig}$	$28682 \pm 365$	$25522 \pm 281$	$14838 \pm 175$	$6550 \pm 105$	$4331 \pm 85$
$n_{bkg}$	$148091 \pm 502$	$69097 \pm 350$	$16006 \pm 179$	$3685 \pm 90$	$2012 \pm 70$
$1000 * p_0$	$-0.66 \pm 0.04$	$-0.51 \pm 0.06$	$-0.00 \pm 0.12$	$-1.18 \pm 0.26$	$-1.30 \pm 0.36$
$1000 * \mu_{tz}$	$0.8 \pm 0.6$	$-1.0 \pm 0.5$	$-0.5 \pm 0.5$	$-0.9 \pm 0.6$	$-2.4 \pm 0.7$
$S1_{tz}$	$1.14 \pm 0.04$	$1.36 \pm 0.07$	$0.91 \pm 0.02$	$3.37 \pm 0.41$	$1.86 \pm 0.29$
$S2_{tz}$	$0.66 \pm 0.07$	$0.79 \pm 0.03$	$1.81 \pm 0.24$	$0.94 \pm 0.02$	$0.87 \pm 0.04$
$\beta_{tz}$	$0.71 \pm 0.09$	$0.37 \pm 0.07$	$0.87 \pm 0.05$	$0.07 \pm 0.01$	$0.16 \pm 0.06$
$\tau_b$	$1.60 \pm 0.05$	$1.45 \pm 0.03$	$1.52 \pm 0.04$	$1.56 \pm 0.05$	$1.48 \pm 0.05$
$n_{prompt}$	$24402 \pm 271$	$20920 \pm 219$	$12035 \pm 141$	$5031 \pm 86$	$2985 \pm 65$
$n_{fromb}$	$3783 \pm 112$	$4396 \pm 98$	$2732 \pm 69$	$1503 \pm 50$	$1302 \pm 44$
$n_{tail}$	$309 \pm 32$	$98 \pm 17$	$20 \pm 8$	$3 \pm 3$	$5 \pm 3$

Table 31: The parameters of the invariant mass and  $t_z$  fit for  $J/\psi$ , including the fitted yields and the shape parameters for different  $p_T$  bins in the rapidity bin  $2.0 < y < 2.8$  and multiplicity bin  $40 < PVNTRACKS < 60$ .

$J/\psi$ parameters	$p_T$ (GeV/c)				
	0-2	2-4	4-6	6-8	8-20
$\mu_{mass}$	$3097.6 \pm 0.0$	$3097.1 \pm 0.0$	$3097.0 \pm 0.0$	$3096.9 \pm 0.0$	$3096.8 \pm 0.0$
$\sigma_{mass}$	$16.4 \pm 0.5$	$15.8 \pm 0.3$	$16.9 \pm 0.3$	$18.7 \pm 0.5$	$19.3 \pm 0.5$
$n_{sig}$	$436651 \pm 959$	$679122 \pm 1022$	$542622 \pm 833$	$291868 \pm 587$	$260436 \pm 550$
$n_{bkg}$	$506941 \pm 995$	$350218 \pm 846$	$111695 \pm 512$	$26924 \pm 282$	$15820 \pm 241$
$1000 * p_0$	$0.55 \pm 0.02$	$-0.43 \pm 0.03$	$-0.00 \pm 0.05$	$-0.46 \pm 0.10$	$-0.64 \pm 0.14$
$1000 * \mu_{tz}$	$-10.2 \pm 0.1$	$-8.4 \pm 0.1$	$-5.4 \pm 0.1$	$-2.9 \pm 0.1$	$-1.2 \pm 0.1$
$S1_{tz}$	$2.16 \pm 0.08$	$1.78 \pm 0.04$	$1.65 \pm 0.03$	$1.79 \pm 0.04$	$1.95 \pm 0.03$
$S2_{tz}$	$1.04 \pm 0.01$	$0.98 \pm 0.00$	$0.95 \pm 0.01$	$0.98 \pm 0.01$	$1.03 \pm 0.01$
$\beta_{tz}$	$0.11 \pm 0.01$	$0.13 \pm 0.01$	$0.19 \pm 0.01$	$0.17 \pm 0.01$	$0.19 \pm 0.01$
$\tau_b$	$1.55 \pm 0.01$	$1.47 \pm 0.01$	$1.39 \pm 0.01$	$1.33 \pm 0.01$	$1.31 \pm 0.01$
$n_{prompt}$	$382521 \pm 756$	$578687 \pm 864$	$444986 \pm 724$	$227236 \pm 505$	$179176 \pm 446$
$n_{fromb}$	$50976 \pm 283$	$97906 \pm 361$	$95828 \pm 347$	$63629 \pm 279$	$80398 \pm 310$
$n_{tail}$	$1013 \pm 59$	$295 \pm 33$	$113 \pm 21$	$33 \pm 11$	$47 \pm 12$

Table 32: The parameters of the invariant mass and  $t_z$  fit for  $\psi(2S)$ , including the fitted yields and the shape parameters for different  $p_T$  bins in the rapidity bin  $2.0 < y < 2.8$  and multiplicity bin  $40 < PVNTRACKS < 60$ .

$\psi(2S)$ parameters	$p_T$ (GeV/c)				
	0-2	2-4	4-6	6-8	8-20
$\mu_{mass}$	$3685.6 \pm 0.5$	$3686.1 \pm 0.3$	$3686.2 \pm 0.2$	$3686.1 \pm 0.2$	$3686.2 \pm 0.2$
$\sigma_{mass}$	$12.9 \pm 0.5$	$13.2 \pm 0.3$	$13.5 \pm 0.2$	$14.3 \pm 0.2$	$15.5 \pm 0.2$
$n_{sig}$	$13827 \pm 482$	$17326 \pm 378$	$14038 \pm 229$	$9128 \pm 141$	$10065 \pm 128$
$n_{bkg}$	$478372 \pm 835$	$258952 \pm 620$	$75485 \pm 338$	$17330 \pm 168$	$7910 \pm 119$
$1000 * p_0$	$-0.56 \pm 0.02$	$-0.53 \pm 0.03$	$-0.00 \pm 0.05$	$-0.75 \pm 0.11$	$-0.88 \pm 0.17$
$1000 * \mu_{tz}$	$-17.2 \pm 1.9$	$-8.2 \pm 0.3$	$-6.8 \pm 0.7$	$-4.2 \pm 0.6$	$-1.5 \pm 0.5$
$S1_{tz}$	$5.61 \pm 1.32$	$1.09 \pm 0.02$	$0.73 \pm 0.08$	$1.91 \pm 0.34$	$1.97 \pm 0.23$
$S2_{tz}$	$1.01 \pm 0.04$	$0.02 \pm 0.01$	$1.27 \pm 0.08$	$0.96 \pm 0.04$	$0.92 \pm 0.03$
$\beta_{tz}$	$0.06 \pm 0.02$	$0.98 \pm 0.00$	$0.41 \pm 0.13$	$0.15 \pm 0.07$	$0.20 \pm 0.06$
$\tau_b$	$1.76 \pm 0.05$	$1.51 \pm 0.03$	$1.53 \pm 0.03$	$1.47 \pm 0.04$	$1.48 \pm 0.03$
$n_{prompt}$	$10797 \pm 373$	$13191 \pm 283$	$10402 \pm 180$	$6657 \pm 114$	$6471 \pm 100$
$n_{fromb}$	$2803 \pm 102$	$3894 \pm 94$	$3556 \pm 77$	$2453 \pm 61$	$3590 \pm 71$
$n_{tail}$	$1 \pm 34$	$29 \pm 12$	$5 \pm 6$	$4 \pm 4$	$5 \pm 4$

Table 33: The parameters of the invariant mass and  $t_z$  fit for  $J/\psi$ , including the fitted yields and the shape parameters for different  $p_T$  bins in the rapidity bin  $2.8 < y < 3.5$  and multiplicity bin  $40 < PVNTRACKS < 60$ .

$J/\psi$ parameters	$p_T$ (GeV/c)				
	0-2	2-4	4-6	6-8	8-20
$\mu_{mass}$	$3096.8 \pm 0.0$	$3096.5 \pm 0.0$	$3096.2 \pm 0.0$	$3096.0 \pm 0.0$	$3095.9 \pm 0.0$
$\sigma_{mass}$	$15.3 \pm 0.3$	$16.1 \pm 0.3$	$11.5 \pm 0.1$	$18.9 \pm 0.4$	$20.8 \pm 0.5$
$n_{sig}$	$675810 \pm 1117$	$1078240 \pm 1259$	$780100 \pm 974$	$339639 \pm 623$	$235358 \pm 517$
$n_{bkg}$	$728497 \pm 1141$	$515614 \pm 1012$	$123996 \pm 541$	$23101 \pm 268$	$11644 \pm 209$
$1000 * p_0$	$0.28 \pm 0.02$	$-0.48 \pm 0.02$	$-0.00 \pm 0.05$	$-0.77 \pm 0.12$	$-0.84 \pm 0.18$
$1000 * \mu_{tz}$	$-6.2 \pm 0.1$	$-5.8 \pm 0.1$	$-4.6 \pm 0.1$	$-3.4 \pm 0.1$	$-2.1 \pm 0.1$
$S1_{tz}$	$2.12 \pm 0.07$	$0.95 \pm 0.00$	$1.65 \pm 0.02$	$0.95 \pm 0.01$	$1.80 \pm 0.05$
$S2_{tz}$	$1.00 \pm 0.00$	$1.70 \pm 0.02$	$0.94 \pm 0.00$	$1.66 \pm 0.07$	$0.97 \pm 0.01$
$\beta_{tz}$	$0.09 \pm 0.01$	$0.86 \pm 0.01$	$0.17 \pm 0.01$	$0.82 \pm 0.03$	$0.14 \pm 0.01$
$\tau_b$	$1.54 \pm 0.01$	$1.46 \pm 0.00$	$1.38 \pm 0.00$	$1.34 \pm 0.01$	$1.30 \pm 0.01$
$n_{prompt}$	$596476 \pm 941$	$926437 \pm 1092$	$646380 \pm 864$	$267792 \pm 546$	$167095 \pm 428$
$n_{fromb}$	$73048 \pm 341$	$146080 \pm 443$	$129515 \pm 403$	$70054 \pm 292$	$67013 \pm 282$
$n_{tail}$	$2565 \pm 88$	$792 \pm 51$	$307 \pm 33$	$85 \pm 17$	$46 \pm 12$

Table 34: The parameters of the invariant mass and  $t_z$  fit for  $\psi(2S)$ , including the fitted yields and the shape parameters for different  $p_T$  bins in the rapidity bin  $2.8 < y < 3.5$  and multiplicity bin  $40 < PVNTRACKS < 60$ .

$\psi(2S)$ parameters	$p_T$ (GeV/c)				
	0-2	2-4	4-6	6-8	8-20
$\mu_{mass}$	$3686.0 \pm 0.4$	$3685.4 \pm 0.3$	$3685.2 \pm 0.2$	$3685.2 \pm 0.2$	$3684.8 \pm 0.2$
$\sigma_{mass}$	$13.9 \pm 0.4$	$14.5 \pm 0.3$	$14.9 \pm 0.2$	$15.5 \pm 0.2$	$16.6 \pm 0.2$
$n_{sig}$	$20788 \pm 600$	$27776 \pm 490$	$21457 \pm 278$	$11529 \pm 150$	$9754 \pm 124$
$n_{bkg}$	$654636 \pm 997$	$388057 \pm 775$	$92705 \pm 386$	$15503 \pm 163$	$6203 \pm 109$
$1000 * p_0$	$-0.49 \pm 0.02$	$-0.49 \pm 0.02$	$-0.00 \pm 0.05$	$-0.43 \pm 0.12$	$-0.97 \pm 0.19$
$1000 * \mu_{tz}$	$-11.9 \pm 1.4$	$-5.6 \pm 0.8$	$-4.8 \pm 0.5$	$-4.4 \pm 0.5$	$-2.5 \pm 0.4$
$S1_{tz}$	$0.94 \pm 0.03$	-	$1.23 \pm 0.07$	-	$1.73 \pm 0.20$
$S2_{tz}$	$7.17 \pm 0.73$	$0.99 \pm 0.02$	$0.72 \pm 0.07$	$1.02 \pm 0.01$	$0.91 \pm 0.04$
$\beta_{tz}$	$0.93 \pm 0.01$	0	$0.61 \pm 0.12$	0	$0.22 \pm 0.07$
$\tau_b$	$1.87 \pm 0.05$	$1.57 \pm 0.03$	$1.52 \pm 0.03$	$1.44 \pm 0.03$	$1.42 \pm 0.03$
$n_{prompt}$	$16822 \pm 447$	$21291 \pm 362$	$16292 \pm 215$	$8322 \pm 117$	$6384 \pm 96$
$n_{fromb}$	$3951 \pm 123$	$6024 \pm 119$	$4931 \pm 92$	$3045 \pm 68$	$3313 \pm 68$
$n_{tail}$	$25 \pm 17$	$0 \pm 0$	$20 \pm 9$	$13 \pm 7$	$8 \pm 5$

Table 35: The parameters of the invariant mass and  $t_z$  fit for  $J/\psi$ , including the fitted yields and the shape parameters for different  $p_T$  bins in the rapidity bin  $3.5 < y < 4.5$  and multiplicity bin  $40 < PVNTRACKS < 60$ .

$J/\psi$ parameters	$p_T$ (GeV/c)				
	0-2	2-4	4-6	6-8	8-20
$\mu_{mass}$	$3096.2 \pm 0.0$	$3095.8 \pm 0.0$	$3095.7 \pm 0.0$	$3095.8 \pm 0.0$	$3095.9 \pm 0.1$
$\sigma_{mass}$	$18.4 \pm 0.2$	$20.2 \pm 0.3$	$21.6 \pm 0.3$	$24.5 \pm 0.8$	$26.3 \pm 0.6$
$n_{sig}$	$701162 \pm 1033$	$857704 \pm 1067$	$557631 \pm 817$	$233139 \pm 532$	$148215 \pm 425$
$n_{bkg}$	$317118 \pm 826$	$183127 \pm 681$	$45849 \pm 395$	$11086 \pm 246$	$6050 \pm 195$
$1000 * p_0$	$0.06 \pm 0.03$	$-0.58 \pm 0.04$	$-0.00 \pm 0.08$	$-1.01 \pm 0.18$	$-0.56 \pm 0.27$
$1000 * \mu_{tz}$	$4.4 \pm 0.1$	$0.6 \pm 0.1$	$-1.0 \pm 0.1$	$-1.0 \pm 0.1$	$-0.8 \pm 0.1$
$S1_{tz}$	$1.88 \pm 0.03$	$1.69 \pm 0.03$	$1.64 \pm 0.03$	$1.74 \pm 0.04$	$1.91 \pm 0.06$
$S2_{tz}$	$0.96 \pm 0.00$	$0.94 \pm 0.00$	$0.93 \pm 0.00$	$0.95 \pm 0.01$	$0.97 \pm 0.01$
$\beta_{tz}$	$0.12 \pm 0.01$	$0.14 \pm 0.01$	$0.17 \pm 0.01$	$0.14 \pm 0.01$	$0.10 \pm 0.01$
$\tau_b$	$1.47 \pm 0.01$	$1.42 \pm 0.01$	$1.36 \pm 0.01$	$1.32 \pm 0.01$	$1.27 \pm 0.01$
$n_{prompt}$	$623808 \pm 906$	$747348 \pm 952$	$470080 \pm 730$	$188959 \pm 457$	$110802 \pm 351$
$n_{fromb}$	$67427 \pm 336$	$103379 \pm 382$	$83024 \pm 329$	$42450 \pm 231$	$36329 \pm 211$
$n_{tail}$	$5351 \pm 116$	$1304 \pm 61$	$347 \pm 35$	$81 \pm 18$	$23 \pm 9$

Table 36: The parameters of the invariant mass and  $t_z$  fit for  $\psi(2S)$ , including the fitted yields and the shape parameters for different  $p_T$  bins in the rapidity bin  $3.5 < y < 4.5$  and multiplicity bin  $40 < PVNTRACKS < 60$ .

$\psi(2S)$ parameters	$p_T$ (GeV/c)				
	0-2	2-4	4-6	6-8	8-20
$\mu_{mass}$	$3684.8 \pm 0.4$	$3684.8 \pm 0.3$	$3685.0 \pm 0.3$	$3683.8 \pm 0.3$	$3684.6 \pm 0.4$
$\sigma_{mass}$	$17.1 \pm 0.4$	$17.4 \pm 0.3$	$18.8 \pm 0.3$	$20.1 \pm 0.3$	$21.9 \pm 0.4$
$n_{sig}$	$20451 \pm 463$	$22376 \pm 347$	$15497 \pm 210$	$7646 \pm 122$	$5878 \pm 103$
$n_{bkg}$	$257562 \pm 672$	$133387 \pm 481$	$30952 \pm 244$	$6438 \pm 117$	$3163 \pm 89$
$1000 * p_0$	$-0.60 \pm 0.03$	$-0.48 \pm 0.04$	$-0.00 \pm 0.09$	$-0.64 \pm 0.19$	$-0.62 \pm 0.28$
$1000 * \mu_{tz}$	$3.0 \pm 1.1$	$-1.0 \pm 0.7$	$-0.2 \pm 0.5$	$-3.6 \pm 0.6$	$-1.5 \pm 0.6$
$S1_{tz}$	$7.58 \pm 0.98$	$1.42 \pm 0.10$	$2.55 \pm 0.25$	$2.22 \pm 0.33$	$0.96 \pm 0.02$
$S2_{tz}$	$0.97 \pm 0.02$	$0.80 \pm 0.04$	$0.90 \pm 0.02$	$0.92 \pm 0.03$	$3.57 \pm 0.67$
$\beta_{tz}$	$0.03 \pm 0.01$	$0.34 \pm 0.08$	$0.12 \pm 0.02$	$0.11 \pm 0.03$	$0.95 \pm 0.01$
$\tau_b$	$1.67 \pm 0.05$	$1.53 \pm 0.04$	$1.57 \pm 0.04$	$1.46 \pm 0.04$	$1.40 \pm 0.04$
$n_{prompt}$	$16699 \pm 326$	$18072 \pm 260$	$12526 \pm 166$	$5837 \pm 97$	$4168 \pm 80$
$n_{fromb}$	$3510 \pm 119$	$4256 \pm 102$	$2920 \pm 74$	$1784 \pm 54$	$1697 \pm 51$
$n_{tail}$	$135 \pm 25$	$61 \pm 14$	$12 \pm 6$	$3 \pm 3$	$11 \pm 6$

Table 37: The parameters of the invariant mass and  $t_z$  fit for  $J/\psi$ , including the fitted yields and the shape parameters for different  $p_T$  bins in the rapidity bin  $2.0 < y < 2.8$  and multiplicity bin  $60 < PVNTRACKS < 80$ .

$J/\psi$ parameters	$p_T$ (GeV/c)				
	0-2	2-4	4-6	6-8	8-20
$\mu_{mass}$	$3097.6 \pm 0.0$	$3097.1 \pm 0.0$	$3097.0 \pm 0.0$	$3096.9 \pm 0.0$	$3096.8 \pm 0.0$
$\sigma_{mass}$	$16.1 \pm 0.8$	$15.1 \pm 0.3$	$15.9 \pm 0.3$	$18.6 \pm 0.5$	$19.8 \pm 0.5$
$n_{sig}$	$267225 \pm 883$	$448309 \pm 875$	$382752 \pm 717$	$214554 \pm 508$	$201541 \pm 484$
$n_{bkg}$	$558965 \pm 1035$	$400046 \pm 847$	$125905 \pm 508$	$27797 \pm 267$	$14401 \pm 216$
$1000 * p_0$	$0.52 \pm 0.02$	$-0.41 \pm 0.02$	$-0.00 \pm 0.04$	$-0.53 \pm 0.10$	$-0.69 \pm 0.15$
$1000 * \mu_{tz}$	$-10.4 \pm 0.2$	$-8.6 \pm 0.1$	$-5.4 \pm 0.1$	$-2.9 \pm 0.1$	$-0.9 \pm 0.1$
$S1_{tz}$	$2.72 \pm 0.14$	$1.85 \pm 0.04$	$1.89 \pm 0.04$	$1.87 \pm 0.04$	$2.07 \pm 0.04$
$S2_{tz}$	$1.09 \pm 0.01$	$0.99 \pm 0.01$	$0.98 \pm 0.01$	$0.99 \pm 0.01$	$1.05 \pm 0.01$
$\beta_{tz}$	$0.08 \pm 0.01$	$0.15 \pm 0.01$	$0.14 \pm 0.01$	$0.18 \pm 0.01$	$0.19 \pm 0.01$
$\tau_b$	$1.55 \pm 0.01$	$1.45 \pm 0.01$	$1.36 \pm 0.01$	$1.33 \pm 0.01$	$1.28 \pm 0.01$
$n_{prompt}$	$232323 \pm 642$	$380383 \pm 736$	$314302 \pm 625$	$168684 \pm 441$	$141030 \pm 398$
$n_{fromb}$	$33019 \pm 236$	$66174 \pm 302$	$67044 \pm 293$	$45130 \pm 236$	$59726 \pm 269$
$n_{tail}$	$379 \pm 38$	$120 \pm 25$	$50 \pm 18$	$38 \pm 12$	$20 \pm 9$

Table 38: The parameters of the invariant mass and  $t_z$  fit for  $\psi(2S)$ , including the fitted yields and the shape parameters for different  $p_T$  bins in the rapidity bin  $2.0 < y < 2.8$  and multiplicity bin  $60 < PVNTRACKS < 80$ .

$\psi(2S)$ parameters	$p_T$ (GeV/c)				
	0-2	2-4	4-6	6-8	8-20
$\mu_{mass}$	$3686.2 \pm 1.0$	$3686.7 \pm 0.5$	$3685.8 \pm 0.4$	$3686.0 \pm 0.3$	$3685.7 \pm 0.3$
$\sigma_{mass}$	$16.1 \pm 1.4$	$12.8 \pm 0.5$	$14.3 \pm 0.4$	$14.4 \pm 0.4$	$16.0 \pm 0.3$
$n_{sig}$	$8930 \pm 643$	$10836 \pm 396$	$9947 \pm 240$	$6169 \pm 135$	$7555 \pm 118$
$n_{bkg}$	$527298 \pm 965$	$299953 \pm 668$	$88043 \pm 369$	$19836 \pm 179$	$8150 \pm 121$
$1000 * p_0$	$-0.56 \pm 0.02$	$-0.57 \pm 0.03$	$-0.00 \pm 0.05$	$-0.39 \pm 0.10$	$-0.47 \pm 0.17$
$1000 * \mu_{tz}$	$-29.5 \pm 3.0$	$-11.8 \pm 1.8$	$-5.1 \pm 1.1$	$-3.9 \pm 0.9$	$-1.0 \pm 0.6$
$S1_{tz}$	$4.38 \pm 0.61$	-	$1.41 \pm 0.13$	$1.58 \pm 0.19$	$1.90 \pm 0.20$
$S2_{tz}$	$0.72 \pm 0.06$	$1.06 \pm 0.04$	$0.77 \pm 0.10$	$0.86 \pm 0.08$	$0.92 \pm 0.06$
$\beta_{tz}$	$0.20 \pm 0.04$	0	$0.57 \pm 0.15$	$0.38 \pm 0.15$	$0.32 \pm 0.09$
$\tau_b$	$1.75 \pm 0.07$	$1.53 \pm 0.04$	$1.53 \pm 0.04$	$1.39 \pm 0.04$	$1.38 \pm 0.03$
$n_{prompt}$	$5993 \pm 410$	$7826 \pm 290$	$7373 \pm 185$	$4481 \pm 105$	$4958 \pm 92$
$n_{fromb}$	$2061 \pm 96$	$2654 \pm 82$	$2459 \pm 67$	$1711 \pm 52$	$2576 \pm 60$
$n_{tail}$	$0 \pm 3$	$0 \pm 0$	$0 \pm 27$	$4 \pm 4$	$3 \pm 3$

Table 39: The parameters of the invariant mass and  $t_z$  fit for  $J/\psi$ , including the fitted yields and the shape parameters for different  $p_T$  bins in the rapidity bin  $2.8 < y < 3.5$  and multiplicity bin  $60 < PVNTRACKS < 80$ .

$J/\psi$ parameters	$p_T$ (GeV/c)				
	0-2	2-4	4-6	6-8	8-20
$\mu_{mass}$	$3096.7 \pm 0.0$	$3096.4 \pm 0.0$	$3096.2 \pm 0.0$	$3096.0 \pm 0.0$	$3095.9 \pm 0.0$
$\sigma_{mass}$	$14.9 \pm 0.4$	$16.0 \pm 0.3$	$17.2 \pm 0.3$	$17.3 \pm 0.4$	$20.0 \pm 0.7$
$n_{sig}$	$405557 \pm 979$	$702107 \pm 1084$	$545048 \pm 838$	$247263 \pm 535$	$179523 \pm 455$
$n_{bkg}$	$768142 \pm 1150$	$559381 \pm 1016$	$130930 \pm 537$	$22834 \pm 249$	$10384 \pm 196$
$1000 * p_0$	$0.28 \pm 0.02$	$-0.43 \pm 0.02$	$-0.00 \pm 0.04$	$-0.75 \pm 0.11$	$-0.57 \pm 0.18$
$1000 * \mu_{tz}$	$-6.4 \pm 0.1$	$-5.8 \pm 0.1$	$-4.7 \pm 0.1$	$-3.3 \pm 0.1$	$-2.1 \pm 0.1$
$S1_{tz}$	$2.63 \pm 0.10$	$1.79 \pm 0.04$	$1.75 \pm 0.03$	$1.74 \pm 0.04$	$1.66 \pm 0.04$
$S2_{tz}$	$1.03 \pm 0.00$	$0.97 \pm 0.00$	$0.96 \pm 0.00$	$0.96 \pm 0.01$	$0.94 \pm 0.01$
$\beta_{tz}$	$0.07 \pm 0.01$	$0.14 \pm 0.01$	$0.16 \pm 0.01$	$0.18 \pm 0.01$	$0.23 \pm 0.02$
$\tau_b$	$1.52 \pm 0.01$	$1.45 \pm 0.01$	$1.35 \pm 0.01$	$1.31 \pm 0.01$	$1.26 \pm 0.01$
$n_{prompt}$	$355240 \pm 786$	$601042 \pm 922$	$452449 \pm 738$	$196187 \pm 469$	$129268 \pm 378$
$n_{fromb}$	$46794 \pm 282$	$97191 \pm 367$	$89648 \pm 338$	$49714 \pm 247$	$49236 \pm 242$
$n_{tail}$	$1151 \pm 61$	$331 \pm 37$	$153 \pm 25$	$45 \pm 12$	$22 \pm 10$

Table 40: The parameters of the invariant mass and  $t_z$  fit for  $\psi(2S)$ , including the fitted yields and the shape parameters for different  $p_T$  bins in the rapidity bin  $2.8 < y < 3.5$  and multiplicity bin  $60 < PVNTRACKS < 80$ .

$\psi(2S)$ parameters	$p_T$ (GeV/c)				
	0-2	2-4	4-6	6-8	8-20
$\mu_{mass}$	$3685.7 \pm 0.7$	$3685.3 \pm 0.5$	$3685.5 \pm 0.3$	$3685.0 \pm 0.3$	$3684.7 \pm 0.3$
$\sigma_{mass}$	$13.2 \pm 0.8$	$14.9 \pm 0.5$	$15.4 \pm 0.3$	$16.1 \pm 0.3$	$17.3 \pm 0.3$
$n_{sig}$	$10286 \pm 584$	$16490 \pm 523$	$14089 \pm 280$	$7898 \pm 139$	$7094 \pm 112$
$n_{bkg}$	$687393 \pm 1009$	$423794 \pm 825$	$103660 \pm 410$	$16423 \pm 167$	$5856 \pm 106$
$1000 * p_0$	$-0.53 \pm 0.02$	$-0.46 \pm 0.02$	$-0.00 \pm 0.05$	$-0.36 \pm 0.12$	$-0.38 \pm 0.20$
$1000 * \mu_{tz}$	$-8.1 \pm 2.3$	$-5.1 \pm 1.5$	$-4.8 \pm 0.7$	$-5.0 \pm 0.6$	$-2.8 \pm 0.5$
$S1_{tz}$	$1.50 \pm 0.07$	-	$1.25 \pm 0.07$	$1.99 \pm 0.28$	$2.16 \pm 0.28$
$S2_{tz}$	$0.38 \pm 0.05$	$1.06 \pm 0.03$	$0.65 \pm 0.08$	$0.94 \pm 0.04$	$0.94 \pm 0.03$
$\beta_{tz}$	$0.67 \pm 0.06$	0	$0.68 \pm 0.10$	$0.19 \pm 0.06$	$0.14 \pm 0.04$
$\tau_b$	$1.88 \pm 0.07$	$1.56 \pm 0.04$	$1.49 \pm 0.03$	$1.45 \pm 0.04$	$1.49 \pm 0.04$
$n_{prompt}$	$7767 \pm 426$	$12237 \pm 366$	$10589 \pm 208$	$5826 \pm 111$	$4691 \pm 86$
$n_{fromb}$	$2468 \pm 102$	$4039 \pm 103$	$3480 \pm 80$	$2058 \pm 57$	$2392 \pm 57$
$n_{tail}$	$0 \pm 0$	$9 \pm 7$	$14 \pm 9$	$3 \pm 3$	$13 \pm 6$

Table 41: The parameters of the invariant mass and  $t_z$  fit for  $J/\psi$ , including the fitted yields and the shape parameters for different  $p_T$  bins in the rapidity bin  $3.5 < y < 4.5$  and multiplicity bin  $60 < PVNTRACKS < 80$ .

$J/\psi$ parameters	$p_T$ (GeV/c)				
	0-2	2-4	4-6	6-8	8-20
$\mu_{mass}$	$3096.2 \pm 0.0$	$3095.8 \pm 0.0$	$3095.7 \pm 0.0$	$3095.7 \pm 0.0$	$3095.8 \pm 0.1$
$\sigma_{mass}$	$19.6 \pm 0.5$	$19.4 \pm 0.3$	$21.4 \pm 0.3$	$24.7 \pm 0.9$	$26.3 \pm 0.7$
$n_{sig}$	$406374 \pm 889$	$542622 \pm 886$	$375045 \pm 682$	$165798 \pm 453$	$109964 \pm 371$
$n_{bkg}$	$298511 \pm 826$	$182844 \pm 652$	$44105 \pm 367$	$9557 \pm 222$	$5207 \pm 181$
$1000 * p_0$	$0.06 \pm 0.03$	$-0.62 \pm 0.04$	$-0.00 \pm 0.08$	$-0.80 \pm 0.19$	$-0.17 \pm 0.29$
$1000 * \mu_{tz}$	$4.4 \pm 0.1$	$0.5 \pm 0.1$	$-1.0 \pm 0.1$	$-1.0 \pm 0.1$	$-0.5 \pm 0.1$
$S1_{tz}$	$1.85 \pm 0.05$	$1.60 \pm 0.03$	$1.74 \pm 0.03$	$1.83 \pm 0.06$	$1.77 \pm 0.07$
$S2_{tz}$	$0.95 \pm 0.01$	$0.92 \pm 0.01$	$0.93 \pm 0.00$	$0.96 \pm 0.01$	$0.96 \pm 0.01$
$\beta_{tz}$	$0.14 \pm 0.01$	$0.19 \pm 0.01$	$0.17 \pm 0.01$	$0.14 \pm 0.01$	$0.15 \pm 0.02$
$\tau_b$	$1.46 \pm 0.01$	$1.40 \pm 0.01$	$1.34 \pm 0.01$	$1.28 \pm 0.01$	$1.24 \pm 0.01$
$n_{prompt}$	$358421 \pm 722$	$470562 \pm 776$	$316379 \pm 607$	$134539 \pm 389$	$83259 \pm 306$
$n_{fromb}$	$42547 \pm 271$	$67900 \pm 312$	$55991 \pm 272$	$29924 \pm 195$	$25832 \pm 179$
$n_{tail}$	$2392 \pm 82$	$578 \pm 43$	$157 \pm 25$	$59 \pm 14$	$0 \pm 2$

Table 42: The parameters of the invariant mass and  $t_z$  fit for  $\psi(2S)$ , including the fitted yields and the shape parameters for different  $p_T$  bins in the rapidity bin  $3.5 < y < 4.5$  and multiplicity bin  $60 < PVNTRACKS < 80$ .

$\psi(2S)$ parameters	$p_T$ (GeV/c)				
	0-2	2-4	4-6	6-8	8-20
$\mu_{mass}$	$3684.9 \pm 0.6$	$3685.8 \pm 0.5$	$3684.8 \pm 0.4$	$3684.1 \pm 0.4$	$3684.9 \pm 0.5$
$\sigma_{mass}$	$17.2 \pm 0.7$	$18.1 \pm 0.5$	$18.5 \pm 0.4$	$19.4 \pm 0.4$	$22.3 \pm 0.5$
$n_{sig}$	$11429 \pm 443$	$12870 \pm 336$	$9353 \pm 191$	$5032 \pm 107$	$4155 \pm 88$
$n_{bkg}$	$245094 \pm 655$	$134309 \pm 484$	$31981 \pm 243$	$6255 \pm 113$	$2764 \pm 80$
$1000 * p_0$	$-0.67 \pm 0.03$	$-0.60 \pm 0.04$	$-0.00 \pm 0.08$	$-0.86 \pm 0.19$	$-1.12 \pm 0.30$
$1000 * \mu_{tz}$	$3.6 \pm 1.9$	$-2.0 \pm 1.2$	$-0.1 \pm 0.8$	$-0.1 \pm 0.8$	$-0.0 \pm 0.7$
$S1_{tz}$	$1.54 \pm 0.10$	$1.29 \pm 0.08$	$2.14 \pm 0.31$	$2.05 \pm 0.31$	$2.36 \pm 0.41$
$S2_{tz}$	$0.66 \pm 0.04$	$0.68 \pm 0.06$	$0.86 \pm 0.03$	$0.89 \pm 0.04$	$0.92 \pm 0.03$
$\beta_{tz}$	$0.54 \pm 0.07$	$0.54 \pm 0.10$	$0.17 \pm 0.05$	$0.15 \pm 0.05$	$0.12 \pm 0.04$
$\tau_b$	$1.70 \pm 0.07$	$1.49 \pm 0.04$	$1.54 \pm 0.04$	$1.41 \pm 0.05$	$1.32 \pm 0.05$
$n_{prompt}$	$9284 \pm 302$	$10109 \pm 246$	$7294 \pm 147$	$3871 \pm 84$	$2919 \pm 69$
$n_{fromb}$	$2184 \pm 96$	$2821 \pm 85$	$2085 \pm 63$	$1199 \pm 44$	$1241 \pm 44$
$n_{tail}$	$47 \pm 18$	$40 \pm 12$	$0 \pm 2$	$10 \pm 6$	$3 \pm 3$

Table 43: The parameters of the invariant mass and  $t_z$  fit for  $J/\psi$ , including the fitted yields and the shape parameters for different  $p_T$  bins in the rapidity bin  $2.0 < y < 2.8$  and multiplicity bin  $80 < PVNTRACKS < 200$ .

$J/\psi$ parameters	$p_T$ (GeV/c)				
	0-2	2-4	4-6	6-8	8-20
$\mu_{mass}$	$3097.5 \pm 0.0$	$3097.1 \pm 0.0$	$3097.0 \pm 0.0$	$3096.8 \pm 0.0$	$3096.8 \pm 0.0$
$\sigma_{mass}$	$16.7 \pm 1.0$	$15.6 \pm 0.8$	$16.1 \pm 0.5$	$17.8 \pm 0.6$	$19.3 \pm 0.8$
$n_{sig}$	$161677 \pm 840$	$287506 \pm 865$	$256438 \pm 626$	$148719 \pm 433$	$144313 \pm 418$
$n_{bkg}$	$593211 \pm 1067$	$435890 \pm 947$	$136808 \pm 522$	$28958 \pm 260$	$12951 \pm 207$
$1000 * p_0$	$0.52 \pm 0.02$	$-0.41 \pm 0.02$	$-0.00 \pm 0.04$	$-0.47 \pm 0.09$	$-0.64 \pm 0.15$
$1000 * \mu_{tz}$	$-10.8 \pm 0.2$	$-8.6 \pm 0.1$	$-5.3 \pm 0.1$	$-2.8 \pm 0.1$	$-0.9 \pm 0.1$
$S1_{tz}$	$3.27 \pm 0.16$	$2.24 \pm 0.08$	$1.89 \pm 0.05$	$1.98 \pm 0.05$	$2.03 \pm 0.05$
$S2_{tz}$	$1.14 \pm 0.01$	$1.04 \pm 0.01$	$1.00 \pm 0.01$	$1.02 \pm 0.01$	$1.06 \pm 0.01$
$\beta_{tz}$	$0.08 \pm 0.01$	$0.11 \pm 0.01$	$0.18 \pm 0.01$	$0.19 \pm 0.01$	$0.22 \pm 0.02$
$\tau_b$	$1.54 \pm 0.02$	$1.43 \pm 0.01$	$1.34 \pm 0.01$	$1.29 \pm 0.01$	$1.25 \pm 0.01$
$n_{prompt}$	$140717 \pm 559$	$244398 \pm 631$	$212257 \pm 531$	$118470 \pm 375$	$103033 \pm 343$
$n_{fromb}$	$19779 \pm 192$	$41864 \pm 247$	$43192 \pm 239$	$29655 \pm 193$	$40639 \pm 223$
$n_{tail}$	$215 \pm 31$	$52 \pm 16$	$58 \pm 15$	$15 \pm 7$	$17 \pm 9$

Table 44: The parameters of the invariant mass and  $t_z$  fit for  $\psi(2S)$ , including the fitted yields and the shape parameters for different  $p_T$  bins in the rapidity bin  $2.0 < y < 2.8$  and multiplicity bin  $80 < PVNTRACKS < 200$ .

$\psi(2S)$ parameters	$p_T$ (GeV/c)				
	0-2	2-4	4-6	6-8	8-20
$\mu_{mass}$	$3687.4 \pm 1.8$	$3687.9 \pm 0.8$	$3686.5 \pm 0.6$	$3686.5 \pm 0.5$	$3686.1 \pm 0.3$
$\sigma_{mass}$	$14.2 \pm 2.4$	$12.4 \pm 1.0$	$13.4 \pm 0.6$	$14.5 \pm 0.5$	$15.8 \pm 0.4$
$n_{sig}$	$4201 \pm 594$	$5891 \pm 404$	$5701 \pm 234$	$3961 \pm 129$	$5069 \pm 106$
$n_{bkg}$	$562864 \pm 954$	$329810 \pm 698$	$98510 \pm 384$	$21789 \pm 185$	$8567 \pm 122$
$1000 * p_0$	$-0.57 \pm 0.02$	$-0.53 \pm 0.03$	$-0.00 \pm 0.05$	$-0.33 \pm 0.10$	$-0.48 \pm 0.16$
$1000 * \mu_{tz}$	$19.4 \pm 9.8$	$-6.8 \pm 3.8$	$-5.9 \pm 1.9$	$-3.2 \pm 1.3$	$-1.5 \pm 0.8$
$S1_{tz}$	-	$1.46 \pm 0.12$	$5.83 \pm 1.11$	$1.58 \pm 0.16$	$1.51 \pm 0.19$
$S2_{tz}$	$1.54 \pm 0.10$	$0.51 \pm 0.14$	$0.99 \pm 0.04$	$0.70 \pm 0.10$	$0.89 \pm 0.11$
$\beta_{tz}$	0	$0.75 \pm 0.12$	$0.07 \pm 0.02$	$0.53 \pm 0.12$	$0.47 \pm 0.21$
$\tau_b$	$1.71 \pm 0.09$	$1.56 \pm 0.06$	$1.72 \pm 0.06$	$1.32 \pm 0.05$	$1.43 \pm 0.04$
$n_{prompt}$	$2981 \pm 421$	$4293 \pm 291$	$4211 \pm 180$	$2825 \pm 99$	$3284 \pm 81$
$n_{fromb}$	$1141 \pm 78$	$1643 \pm 68$	$1505 \pm 55$	$1132 \pm 44$	$1762 \pm 50$
$n_{tail}$	$0 \pm 34$	$11 \pm 7$	$4 \pm 4$	$4 \pm 4$	$0 \pm 1$

Table 45: The parameters of the invariant mass and  $t_z$  fit for  $J/\psi$ , including the fitted yields and the shape parameters for different  $p_T$  bins in the rapidity bin  $2.8 < y < 3.5$  and multiplicity bin  $80 < PVNTRACKS < 200$ .

$J/\psi$ parameters	$p_T$ (GeV/c)				
	0-2	2-4	4-6	6-8	8-20
$\mu_{mass}$	$3096.7 \pm 0.0$	$3096.4 \pm 0.0$	$3096.2 \pm 0.0$	$3096.0 \pm 0.0$	$3095.9 \pm 0.0$
$\sigma_{mass}$	$17.1 \pm 1.3$	$16.3 \pm 0.4$	$16.8 \pm 0.4$	$19.0 \pm 0.5$	$19.5 \pm 0.6$
$n_{sig}$	$239858 \pm 1021$	$438711 \pm 958$	$357609 \pm 716$	$167698 \pm 449$	$126006 \pm 384$
$n_{bkg}$	$769931 \pm 1254$	$572102 \pm 1025$	$134489 \pm 539$	$21713 \pm 236$	$8438 \pm 173$
$1000 * p_0$	$0.30 \pm 0.02$	$-0.38 \pm 0.02$	$-0.00 \pm 0.04$	$-0.53 \pm 0.11$	$-0.18 \pm 0.20$
$1000 * \mu_{tz}$	$-6.7 \pm 0.2$	$-6.0 \pm 0.1$	$-4.8 \pm 0.1$	$-3.6 \pm 0.1$	$-2.1 \pm 0.1$
$S1_{tz}$	$1.99 \pm 0.05$	$1.70 \pm 0.04$	$1.85 \pm 0.04$	$1.82 \pm 0.04$	$1.93 \pm 0.06$
$S2_{tz}$	$0.97 \pm 0.01$	$0.95 \pm 0.01$	$0.98 \pm 0.01$	$0.97 \pm 0.01$	$0.99 \pm 0.01$
$\beta_{tz}$	$0.20 \pm 0.01$	$0.22 \pm 0.02$	$0.17 \pm 0.01$	$0.19 \pm 0.02$	$0.18 \pm 0.02$
$\tau_b$	$1.53 \pm 0.01$	$1.42 \pm 0.01$	$1.34 \pm 0.01$	$1.26 \pm 0.01$	$1.23 \pm 0.01$
$n_{prompt}$	$210122 \pm 669$	$375729 \pm 776$	$298561 \pm 617$	$134541 \pm 394$	$92644 \pm 322$
$n_{fromb}$	$27978 \pm 223$	$60210 \pm 295$	$56854 \pm 273$	$32206 \pm 200$	$32633 \pm 199$
$n_{tail}$	$558 \pm 44$	$185 \pm 29$	$79 \pm 17$	$28 \pm 10$	$8 \pm 5$

Table 46: The parameters of the invariant mass and  $t_z$  fit for  $\psi(2S)$ , including the fitted yields and the shape parameters for different  $p_T$  bins in the rapidity bin  $2.8 < y < 3.5$  and multiplicity bin  $80 < PVNTRACKS < 200$ .

$\psi(2S)$ parameters	$p_T$ (GeV/c)				
	0-2	2-4	4-6	6-8	8-20
$\mu_{mass}$	$3684.8 \pm 1.2$	$3685.1 \pm 0.8$	$3684.8 \pm 0.5$	$3685.0 \pm 0.4$	$3684.9 \pm 0.4$
$\sigma_{mass}$	$12.6 \pm 1.1$	$15.3 \pm 1.0$	$14.7 \pm 0.5$	$15.7 \pm 0.4$	$17.0 \pm 0.4$
$n_{sig}$	$6027 \pm 529$	$9605 \pm 535$	$8336 \pm 267$	$4972 \pm 127$	$4710 \pm 98$
$n_{bkg}$	$686320 \pm 974$	$436750 \pm 845$	$109219 \pm 415$	$17198 \pm 169$	$5665 \pm 102$
$1000 * p_0$	$-0.54 \pm 0.02$	$-0.48 \pm 0.02$	$-0.00 \pm 0.04$	$-0.35 \pm 0.11$	$-0.30 \pm 0.20$
$1000 * \mu_{tz}$	$-14.4 \pm 3.0$	$-4.2 \pm 2.3$	$-6.2 \pm 1.2$	$-3.0 \pm 0.9$	$-4.6 \pm 0.7$
$S1_{tz}$	$1.76 \pm 0.13$	$1.54 \pm 0.11$	$7.78 \pm 1.44$	$2.01 \pm 0.30$	$2.10 \pm 0.28$
$S2_{tz}$	$0.40 \pm 0.05$	$0.49 \pm 0.07$	$1.00 \pm 0.03$	$0.86 \pm 0.05$	$0.89 \pm 0.05$
$\beta_{tz}$	$0.59 \pm 0.07$	$0.61 \pm 0.08$	$0.05 \pm 0.01$	$0.22 \pm 0.07$	$0.23 \pm 0.07$
$\tau_b$	$1.62 \pm 0.11$	$1.66 \pm 0.05$	$1.54 \pm 0.05$	$1.36 \pm 0.05$	$1.36 \pm 0.04$
$n_{prompt}$	$4965 \pm 394$	$7101 \pm 377$	$6276 \pm 205$	$3552 \pm 99$	$3188 \pm 75$
$n_{fromb}$	$1362 \pm 94$	$2450 \pm 85$	$2098 \pm 66$	$1396 \pm 47$	$1504 \pm 47$
$n_{tail}$	$111 \pm 21$	$0 \pm 2$	$0 \pm 3$	$10 \pm 6$	$3 \pm 4$

Table 47: The parameters of the invariant mass and  $t_z$  fit for  $J/\psi$ , including the fitted yields and the shape parameters for different  $p_T$  bins in the rapidity bin  $3.5 < y < 4.5$  and multiplicity bin  $80 < PVNTRACKS < 200$ .

$J/\psi$ parameters	$p_T$ (GeV/c)				
	0-2	2-4	4-6	6-8	8-20
$\mu_{mass}$	$3096.2 \pm 0.0$	$3095.8 \pm 0.0$	$3095.7 \pm 0.0$	$3095.7 \pm 0.1$	$3096.0 \pm 0.1$
$\sigma_{mass}$	$18.7 \pm 0.6$	$20.0 \pm 0.6$	$22.6 \pm 0.6$	$22.4 \pm 0.6$	$27.4 \pm 0.9$
$n_{sig}$	$227398 \pm 721$	$324957 \pm 744$	$236955 \pm 563$	$107639 \pm 360$	$73454 \pm 304$
$n_{bkg}$	$267128 \pm 748$	$169685 \pm 631$	$39301 \pm 346$	$7735 \pm 172$	$3642 \pm 151$
$1000 * p_0$	$0.08 \pm 0.03$	$-0.52 \pm 0.04$	$-0.00 \pm 0.08$	$-0.65 \pm 0.21$	$-0.82 \pm 0.33$
$1000 * \mu_{tz}$	$4.2 \pm 0.2$	$0.4 \pm 0.1$	$-0.7 \pm 0.1$	$-1.1 \pm 0.1$	$-0.7 \pm 0.2$
$S1_{tz}$	$0.95 \pm 0.01$	$1.61 \pm 0.04$	$1.79 \pm 0.04$	$1.96 \pm 0.07$	$2.05 \pm 0.08$
$S2_{tz}$	$1.93 \pm 0.06$	$0.92 \pm 0.01$	$0.94 \pm 0.01$	$0.98 \pm 0.01$	$0.98 \pm 0.01$
$\beta_{tz}$	$0.84 \pm 0.01$	$0.22 \pm 0.02$	$0.18 \pm 0.01$	$0.13 \pm 0.01$	$0.12 \pm 0.01$
$\tau_b$	$1.45 \pm 0.01$	$1.39 \pm 0.01$	$1.32 \pm 0.01$	$1.26 \pm 0.01$	$1.21 \pm 0.01$
$n_{prompt}$	$199891 \pm 574$	$281687 \pm 623$	$201145 \pm 492$	$88086 \pm 317$	$56662 \pm 254$
$n_{fromb}$	$24735 \pm 212$	$40667 \pm 245$	$34100 \pm 215$	$18721 \pm 155$	$16189 \pm 142$
$n_{tail}$	$997 \pm 55$	$252 \pm 31$	$96 \pm 18$	$15 \pm 8$	$18 \pm 9$

Table 48: The parameters of the invariant mass and  $t_z$  fit for  $\psi(2S)$ , including the fitted yields and the shape parameters for different  $p_T$  bins in the rapidity bin  $3.5 < y < 4.5$  and multiplicity bin  $80 < PVNTRACKS < 200$ .

$\psi(2S)$ parameters	$p_T$ (GeV/c)				
	0-2	2-4	4-6	6-8	8-20
$\mu_{mass}$	$3683.4 \pm 1.3$	$3685.0 \pm 0.7$	$3684.2 \pm 0.5$	$3684.5 \pm 0.6$	$3684.3 \pm 0.6$
$\sigma_{mass}$	$17.3 \pm 1.7$	$17.8 \pm 0.8$	$18.3 \pm 0.6$	$21.2 \pm 0.7$	$22.7 \pm 0.6$
$n_{sig}$	$5406 \pm 455$	$7494 \pm 326$	$5755 \pm 172$	$3187 \pm 98$	$2739 \pm 76$
$n_{bkg}$	$221991 \pm 650$	$127565 \pm 476$	$29993 \pm 232$	$5611 \pm 109$	$2207 \pm 72$
$1000 * p_0$	$-0.65 \pm 0.03$	$-0.44 \pm 0.04$	$-0.00 \pm 0.09$	$-0.34 \pm 0.20$	$-1.11 \pm 0.33$
$1000 * \mu_{tz}$	$-10.6 \pm 2.9$	$1.8 \pm 2.2$	$-1.3 \pm 1.1$	$-1.6 \pm 1.0$	$-1.3 \pm 0.7$
$S1_{tz}$	$1.50 \pm 0.27$	-	$2.37 \pm 0.31$	$2.65 \pm 0.32$	$0.07 \pm 0.04$
$S2_{tz}$	$0.56 \pm 0.05$	$1.07 \pm 0.04$	$0.81 \pm 0.04$	$0.86 \pm 0.03$	$1.04 \pm 0.03$
$\beta_{tz}$	$0.26 \pm 0.11$	0	$0.23 \pm 0.05$	$0.17 \pm 0.03$	$0.02 \pm 0.01$
$\tau_b$	$1.29 \pm 0.07$	$1.56 \pm 0.06$	$1.49 \pm 0.05$	$1.45 \pm 0.08$	$1.18 \pm 0.05$
$n_{prompt}$	$3790 \pm 281$	$5483 \pm 227$	$4516 \pm 132$	$2550 \pm 75$	$2012 \pm 57$
$n_{fromb}$	$1482 \pm 91$	$1705 \pm 69$	$1339 \pm 51$	$653 \pm 35$	$712 \pm 34$
$n_{tail}$	$98 \pm 17$	$2 \pm 16$	$0 \pm 1$	$0 \pm 2$	$0 \pm 4$

698 **Tables of  $t_z$  background fit**

699 The  $t_z$  background fitted value of,  $\beta$  (fraction of first Gaussian of background resolution  
700 function),  $1000\mu_{tzbkg}$  (bias of background  $t_z$  distribution),  $S(1, 2)_{tzbkg}$  ( $\sigma'_{1,2}$  correct factor of  
701 first/second Gaussian resolution function which will be convolved with the  $t_z$  background  
702 function),  $\tau_{1,2,3,4}$ (exponentials parameters),  $f_{1,2,3,4}$ (fraction of each exponentials compo-  
703 nent) are given below. In some kinetic and multiplicity bin, some ratio of component(s)  
704 is set to be 0 since due to the limit size of sample and extremely low proportion for the  
705 certain component(s).

Table 49: The parameters of  $t_z$  background fit for  $J/\psi$  in the rapidity bin  $2.0 < y < 2.8$  and multiplicity bin  $0 < PVNTRACKS < 20$ .

$J/\psi$ parameters	$p_T$ (GeV/c)				
	0-2	2-4	4-6	6-8	8-20
$\tau_1$	$1.62 \pm 0.08$	$1.49 \pm 0.05$	$1.56 \pm 0.05$	$1.48 \pm 0.05$	$1.51 \pm 0.06$
$\tau_2$	$0.25 \pm 0.02$	$0.19 \pm 0.03$	$0.15 \pm 0.05$	-	-
$\tau_3$	$0.13 \pm 0.01$	$0.16 \pm 0.01$	$0.35 \pm 0.03$	$0.18 \pm 0.03$	$0.34 \pm 0.09$
$\tau_4$	$1.69 \pm 0.30$	$2.05 \pm 0.55$	-	-	-
$f_1$	$0.084 \pm 0.005$	$0.174 \pm 0.007$	$0.286 \pm 0.009$	$0.411 \pm 0.011$	$0.541 \pm 0.014$
$f_2$	$0.139 \pm 0.005$	$0.077 \pm 0.007$	$0.049 \pm 0.010$	0	0
$f_3$	$0.058 \pm 0.007$	$0.051 \pm 0.005$	$0.036 \pm 0.004$	$0.042 \pm 0.009$	$0.013 \pm 0.003$
$f_4$	$0.010 \pm 0.002$	$0.005 \pm 0.001$	0	0	0
$1000 * \mu_{tzbk}$	$-5.2 \pm 0.8$	$-6.5 \pm 0.8$	$-5.2 \pm 1.1$	$-3.8 \pm 1.5$	$-3.1 \pm 1.6$
$\beta_{tzbk}$	0	0	0	0	0
$S1_{tzbk}$	-	-	-	-	-
$S2_{tzbk}$	$0.92 \pm 0.01$	$0.94 \pm 0.01$	$1.00 \pm 0.02$	$1.05 \pm 0.04$	$1.15 \pm 0.04$

Table 50: The parameters of  $t_z$  background fit for  $\psi(2S)$  in the rapidity bin  $2.0 < y < 2.8$  and multiplicity bin  $0 < PVNTRACKS < 20$ .

$\psi(2S)$ parameters	$p_T$ (GeV/c)				
	0-2	2-4	4-6	6-8	8-20
$\tau_1$	$0.91 \pm 0.06$	$1.33 \pm 0.16$	$1.19 \pm 0.07$	$0.05 \pm 0.03$	$1.23 \pm 0.11$
$\tau_2$	$0.16 \pm 0.01$	$0.27 \pm 0.03$	-	$1.32 \pm 0.11$	-
$\tau_3$	$0.13 \pm 0.01$	$0.14 \pm 0.02$	$0.33 \pm 0.04$	$0.21 \pm 0.04$	$0.47 \pm 0.14$
$\tau_4$	$2.34 \pm 0.54$	$2.22 \pm 0.60$	-	-	-
$f_1$	$0.103 \pm 0.008$	$0.074 \pm 0.012$	$0.234 \pm 0.012$	$0.129 \pm 0.088$	$0.417 \pm 0.029$
$f_2$	$0.196 \pm 0.010$	$0.154 \pm 0.011$	0	$0.366 \pm 0.024$	0
$f_3$	$0.078 \pm 0.009$	$0.081 \pm 0.012$	$0.076 \pm 0.010$	$0.115 \pm 0.023$	$0.049 \pm 0.015$
$f_4$	$0.008 \pm 0.002$	$0.014 \pm 0.003$	0	0	0
$1000 * \mu_{tzbk}$	$-7.3 \pm 1.1$	$-4.3 \pm 1.3$	$-2.1 \pm 2.0$	$-10.7 \pm 6.4$	$0.6 \pm 3.0$
$\beta_{tzbk}$	0	0	0	0	0
$S1_{tzbk}$	-	-	-	-	-
$S2_{tzbk}$	$0.87 \pm 0.02$	$0.95 \pm 0.02$	$1.15 \pm 0.04$	$0.96 \pm 0.10$	$1.10 \pm 0.09$

Table 51: The parameters of  $t_z$  background fit for  $J/\psi$  in the rapidity bin  $2.8 < y < 3.5$  and multiplicity bin  $0 < PVNTRACKS < 20$ .

$J/\psi$ parameters	$p_T$ (GeV/c)				
	0-2	2-4	4-6	6-8	8-20
$\tau_1$	$1.45 \pm 0.06$	$1.55 \pm 0.05$	$1.50 \pm 0.04$	$1.47 \pm 0.05$	$1.36 \pm 0.06$
$\tau_2$	$0.22 \pm 0.01$	$0.22 \pm 0.02$	-	-	-
$\tau_3$	$0.16 \pm 0.01$	$0.17 \pm 0.01$	$3.85 \pm 1.69$	$1.04 \pm 0.16$	$0.46 \pm 0.10$
$\tau_4$	$6.70 \pm 1.64$	$2.54 \pm 0.50$	$0.20 \pm 0.01$	-	-
$f_1$	$0.092 \pm 0.004$	$0.150 \pm 0.005$	$0.281 \pm 0.006$	$0.414 \pm 0.011$	$0.483 \pm 0.015$
$f_2$	$0.159 \pm 0.005$	$0.119 \pm 0.005$	0	0	0
$f_3$	$0.052 \pm 0.004$	$0.062 \pm 0.004$	$0.003 \pm 0.001$	$0.023 \pm 0.004$	$0.022 \pm 0.005$
$f_4$	$0.010 \pm 0.001$	$0.009 \pm 0.001$	$0.121 \pm 0.007$	0	0
$1000 * \mu_{tzbg}$	$-5.4 \pm 0.6$	$-6.7 \pm 0.6$	$-7.6 \pm 0.7$	$-7.7 \pm 1.3$	$-3.1 \pm 1.5$
$\beta_{tzbg}$	0	0	0	0	0
$S1_{tzbg}$	-	-	-	-	-
$S2_{tzbg}$	$0.97 \pm 0.01$	$0.99 \pm 0.01$	$1.03 \pm 0.02$	$1.23 \pm 0.03$	$1.17 \pm 0.04$

Table 52: The parameters of  $t_z$  background fit for  $\psi(2S)$  in the rapidity bin  $2.8 < y < 3.5$  and multiplicity bin  $0 < PVNTRACKS < 20$ .

$\psi(2S)$ parameters	$p_T$ (GeV/c)				
	0-2	2-4	4-6	6-8	8-20
$\tau_1$	$0.91 \pm 0.05$	$1.30 \pm 0.17$	$0.87 \pm 0.04$	$0.27 \pm 0.11$	$1.46 \pm 0.15$
$\tau_2$	$0.18 \pm 0.01$	$0.25 \pm 0.02$	-	$1.29 \pm 0.17$	-
$\tau_3$	$0.16 \pm 0.01$	$0.21 \pm 0.01$	$0.44 \pm 0.04$	$0.18 \pm 0.03$	$0.57 \pm 0.18$
$\tau_4$	$5.54 \pm 1.25$	$3.62 \pm 2.13$	-	-	-
$f_1$	$0.105 \pm 0.007$	$0.073 \pm 0.011$	$0.260 \pm 0.010$	$0.119 \pm 0.050$	$0.405 \pm 0.034$
$f_2$	$0.207 \pm 0.008$	$0.215 \pm 0.010$	0	$0.293 \pm 0.049$	0
$f_3$	$0.062 \pm 0.004$	$0.077 \pm 0.005$	$0.095 \pm 0.008$	$0.128 \pm 0.025$	$0.053 \pm 0.017$
$f_4$	$0.009 \pm 0.001$	$0.005 \pm 0.002$	0	0	0
$1000 * \mu_{tzbg}$	$-4.4 \pm 0.8$	$-5.3 \pm 1.0$	$-5.4 \pm 1.6$	$-1.4 \pm 3.4$	$1.5 \pm 3.5$
$\beta_{tzbg}$	0	0	0	0	0
$S1_{tzbg}$	-	-	-	-	-
$S2_{tzbg}$	$0.98 \pm 0.01$	$1.07 \pm 0.02$	$1.29 \pm 0.04$	$1.10 \pm 0.09$	$1.23 \pm 0.12$

Table 53: The parameters of  $t_z$  background fit for  $J/\psi$  in the rapidity bin  $3.5 < y < 4.5$  and multiplicity bin  $0 < PVNTRACKS < 20$ .

$J/\psi$ parameters	$p_T$ (GeV/c)				
	0-2	2-4	4-6	6-8	8-20
$\tau_1$	$1.25 \pm 0.05$	$1.48 \pm 0.05$	$1.55 \pm 0.07$	$1.40 \pm 0.06$	$1.37 \pm 0.07$
$\tau_2$	$0.21 \pm 0.01$	$0.19 \pm 0.02$	$0.24 \pm 0.05$	-	-
$\tau_3$	$0.18 \pm 0.01$	$0.18 \pm 0.01$	$0.14 \pm 0.02$	$0.44 \pm 0.07$	$0.62 \pm 0.19$
$\tau_4$	$4.40 \pm 0.44$	$3.36 \pm 0.64$	$2.93 \pm 0.73$	-	-
$f_1$	$0.126 \pm 0.006$	$0.174 \pm 0.006$	$0.240 \pm 0.013$	$0.365 \pm 0.012$	$0.424 \pm 0.016$
$f_2$	$0.184 \pm 0.007$	$0.130 \pm 0.008$	$0.086 \pm 0.011$	0	0
$f_3$	$0.066 \pm 0.005$	$0.074 \pm 0.006$	$0.082 \pm 0.010$	$0.033 \pm 0.006$	$0.014 \pm 0.004$
$f_4$	$0.025 \pm 0.002$	$0.013 \pm 0.002$	$0.015 \pm 0.003$	0	0
$1000 * \mu_{tzbk}$	$0.5 \pm 1.0$	$-3.2 \pm 1.0$	$-5.1 \pm 1.3$	$-7.8 \pm 1.6$	$-3.7 \pm 2.0$
$\beta_{tzbk}$	0	0	0	0	0
$S1_{tzbk}$	-	-	-	-	-
$S2_{tzbk}$	$1.01 \pm 0.01$	$1.06 \pm 0.01$	$1.08 \pm 0.02$	$1.23 \pm 0.04$	$1.30 \pm 0.05$

Table 54: The parameters of  $t_z$  background fit for  $\psi(2S)$  in the rapidity bin  $3.5 < y < 4.5$  and multiplicity bin  $0 < PVNTRACKS < 20$ .

$\psi(2S)$ parameters	$p_T$ (GeV/c)				
	0-2	2-4	4-6	6-8	8-20
$\tau_1$	$0.23 \pm 0.02$	$1.47 \pm 0.11$	$1.33 \pm 0.10$	$0.05 \pm 0.17$	$1.30 \pm 0.18$
$\tau_2$	$0.97 \pm 0.06$	$0.27 \pm 0.02$	-	$1.11 \pm 0.11$	-
$\tau_3$	$0.18 \pm 0.01$	$0.65 \pm 0.05$	-	$0.65 \pm 0.19$	$0.45 \pm 0.17$
$\tau_4$	$6.07 \pm 1.51$	-	$0.29 \pm 0.02$	-	-
$f_1$	$0.254 \pm 0.012$	$0.103 \pm 0.011$	$0.206 \pm 0.017$	$0.178 \pm 0.107$	$0.264 \pm 0.031$
$f_2$	$0.147 \pm 0.015$	$0.276 \pm 0.014$	0	$0.388 \pm 0.031$	0
$f_3$	$0.069 \pm 0.006$	$0.049 \pm 0.004$	0	$0.044 \pm 0.013$	$0.040 \pm 0.015$
$f_4$	$0.013 \pm 0.002$	0	$0.284 \pm 0.027$	0	0
$1000 * \mu_{tzbk}$	$5.1 \pm 1.4$	$-3.1 \pm 1.8$	$3.7 \pm 2.4$	$-10.9 \pm 7.6$	$-1.6 \pm 2.6$
$\beta_{tzbk}$	0	0	0	0	0
$S1_{tzbk}$	-	-	-	-	-
$S2_{tzbk}$	$1.09 \pm 0.02$	$1.24 \pm 0.03$	$1.21 \pm 0.06$	$1.19 \pm 0.12$	$0.97 \pm 0.07$

Table 55: The parameters of  $t_z$  background fit for  $J/\psi$  in the rapidity bin  $2.0 < y < 2.8$  and multiplicity bin  $20 < PVNTRACKS < 40$ .

$J/\psi$ parameters	$p_T$ (GeV/c)				
	0-2	2-4	4-6	6-8	8-20
$\tau_1$	$1.43 \pm 0.03$	$1.51 \pm 0.03$	$1.39 \pm 0.02$	$1.47 \pm 0.04$	$1.34 \pm 0.03$
$\tau_2$	$0.25 \pm 0.01$	$0.25 \pm 0.01$	$0.11 \pm 0.01$	$0.17 \pm 0.04$	$0.07 \pm 0.02$
$\tau_3$	$0.36 \pm 0.03$	$0.23 \pm 0.02$	$0.11 \pm 0.01$	$0.11 \pm 0.02$	$0.22 \pm 0.02$
$\tau_4$	$3.12 \pm 0.73$	$1.74 \pm 0.33$	$0.61 \pm 0.08$	$0.71 \pm 0.14$	-
$f_1$	$0.050 \pm 0.002$	$0.081 \pm 0.002$	$0.180 \pm 0.003$	$0.296 \pm 0.008$	$0.454 \pm 0.008$
$f_2$	$0.115 \pm 0.002$	$0.083 \pm 0.003$	$0.105 \pm 0.007$	$0.066 \pm 0.007$	$0.069 \pm 0.019$
$f_3$	$0.011 \pm 0.001$	$0.022 \pm 0.002$	$0.068 \pm 0.004$	$0.060 \pm 0.006$	$0.037 \pm 0.003$
$f_4$	$0.002 \pm 0.000$	$0.002 \pm 0.000$	$0.018 \pm 0.004$	$0.015 \pm 0.005$	0
$1000 * \mu_{tzbkg}$	$-7.2 \pm 0.2$	$-6.4 \pm 0.2$	$-6.0 \pm 0.5$	$-2.7 \pm 0.7$	$-6.2 \pm 1.2$
$\beta_{tzbkg}$	$0.13 \pm 0.01$	$0.20 \pm 0.02$	0	0	0
$S1_{tzbkg}$	$2.60 \pm 0.09$	$1.93 \pm 0.08$	-	-	-
$S2_{tzbkg}$	$1.02 \pm 0.01$	$0.94 \pm 0.01$	$1.02 \pm 0.01$	$1.09 \pm 0.02$	$1.16 \pm 0.03$

Table 56: The parameters of  $t_z$  background fit for  $\psi(2S)$  in the rapidity bin  $2.0 < y < 2.8$  and multiplicity bin  $20 < PVNTRACKS < 40$ .

$\psi(2S)$ parameters	$p_T$ (GeV/c)				
	0-2	2-4	4-6	6-8	8-20
$\tau_1$	$1.08 \pm 0.04$	$0.26 \pm 0.01$	$1.35 \pm 0.06$	$0.24 \pm 0.03$	$1.23 \pm 0.04$
$\tau_2$	$0.24 \pm 0.01$	$1.33 \pm 0.07$	$0.14 \pm 0.01$	$1.58 \pm 0.12$	-
$\tau_3$	$0.25 \pm 0.02$	$0.24 \pm 0.02$	$0.10 \pm 0.01$	$0.37 \pm 0.03$	$0.23 \pm 0.02$
$\tau_4$	$1.40 \pm 0.26$	$1.23 \pm 0.24$	$0.53 \pm 0.08$	-	-
$f_1$	$0.036 \pm 0.002$	$0.115 \pm 0.004$	$0.061 \pm 0.004$	$0.160 \pm 0.011$	$0.342 \pm 0.010$
$f_2$	$0.128 \pm 0.003$	$0.026 \pm 0.002$	$0.153 \pm 0.008$	$0.114 \pm 0.011$	0
$f_3$	$0.019 \pm 0.002$	$0.022 \pm 0.003$	$0.109 \pm 0.010$	$0.068 \pm 0.005$	$0.092 \pm 0.009$
$f_4$	$0.003 \pm 0.001$	$0.004 \pm 0.001$	$0.032 \pm 0.009$	0	0
$1000 * \mu_{tzbkg}$	$-6.8 \pm 0.3$	$-6.4 \pm 0.3$	$-4.6 \pm 0.8$	$-4.2 \pm 1.1$	$1.9 \pm 1.3$
$\beta_{tzbkg}$	$0.19 \pm 0.02$	$0.17 \pm 0.02$	0	0	0
$S1_{tzbkg}$	$2.16 \pm 0.11$	$2.17 \pm 0.12$	-	-	-
$S2_{tzbkg}$	$1.01 \pm 0.01$	$1.00 \pm 0.01$	$1.03 \pm 0.02$	$1.21 \pm 0.03$	$1.27 \pm 0.04$

Table 57: The parameters of  $t_z$  background fit for  $J/\psi$  in the rapidity bin  $2.8 < y < 3.5$  and multiplicity bin  $20 < PVNTRACKS < 40$ .

$J/\psi$ parameters	$p_T$ (GeV/c)				
	0-2	2-4	4-6	6-8	8-20
$\tau_1$	$1.28 \pm 0.02$	$1.47 \pm 0.02$	$1.47 \pm 0.03$	$1.45 \pm 0.03$	$1.35 \pm 0.03$
$\tau_2$	$0.20 \pm 0.00$	$0.24 \pm 0.01$	$0.27 \pm 0.03$	$0.11 \pm 0.02$	$0.05 \pm 0.01$
$\tau_3$	$0.32 \pm 0.02$	$0.25 \pm 0.01$	$0.27 \pm 0.02$	$0.13 \pm 0.01$	$0.08 \pm 0.02$
$\tau_4$	$3.92 \pm 0.59$	$1.57 \pm 0.23$	$2.74 \pm 0.85$	$1.20 \pm 0.23$	$0.44 \pm 0.09$
$f_1$	$0.055 \pm 0.001$	$0.080 \pm 0.002$	$0.174 \pm 0.005$	$0.317 \pm 0.007$	$0.438 \pm 0.007$
$f_2$	$0.135 \pm 0.002$	$0.094 \pm 0.003$	$0.076 \pm 0.005$	$0.088 \pm 0.008$	$0.073 \pm 0.018$
$f_3$	$0.012 \pm 0.001$	$0.026 \pm 0.002$	$0.036 \pm 0.003$	$0.062 \pm 0.004$	$0.055 \pm 0.008$
$f_4$	$0.003 \pm 0.000$	$0.003 \pm 0.001$	$0.002 \pm 0.001$	$0.010 \pm 0.003$	$0.021 \pm 0.007$
$1000 * \mu_{tzbg}$	$-5.2 \pm 0.2$	$-6.0 \pm 0.2$	$-6.6 \pm 0.3$	$-7.4 \pm 0.7$	$-6.2 \pm 1.0$
$\beta_{tzbg}$	$0.13 \pm 0.01$	$0.18 \pm 0.01$	$0.18 \pm 0.01$	0	0
$S1_{tzbg}$	$2.43 \pm 0.08$	$2.35 \pm 0.08$	$2.62 \pm 0.19$	-	-
$S2_{tzbg}$	$1.01 \pm 0.01$	$0.99 \pm 0.01$	$1.01 \pm 0.01$	$1.06 \pm 0.02$	$1.03 \pm 0.03$

Table 58: The parameters of  $t_z$  background fit for  $\psi(2S)$  in the rapidity bin  $2.8 < y < 3.5$  and multiplicity bin  $20 < PVNTRACKS < 40$ .

$\psi(2S)$ parameters	$p_T$ (GeV/c)				
	0-2	2-4	4-6	6-8	8-20
$\tau_1$	$0.88 \pm 0.03$	$0.21 \pm 0.01$	$1.28 \pm 0.05$	$0.16 \pm 0.02$	$1.17 \pm 0.04$
$\tau_2$	$0.18 \pm 0.01$	$0.99 \pm 0.05$	$0.15 \pm 0.01$	$1.29 \pm 0.07$	-
$\tau_3$	$0.29 \pm 0.02$	$0.29 \pm 0.02$	$0.09 \pm 0.01$	$0.26 \pm 0.02$	$0.25 \pm 0.02$
$\tau_4$	$3.24 \pm 0.42$	$3.59 \pm 1.02$	$0.49 \pm 0.04$	-	-
$f_1$	$0.054 \pm 0.002$	$0.121 \pm 0.004$	$0.062 \pm 0.003$	$0.175 \pm 0.013$	$0.368 \pm 0.011$
$f_2$	$0.157 \pm 0.003$	$0.042 \pm 0.003$	$0.169 \pm 0.007$	$0.162 \pm 0.010$	0
$f_3$	$0.015 \pm 0.001$	$0.028 \pm 0.002$	$0.120 \pm 0.009$	$0.107 \pm 0.007$	$0.090 \pm 0.009$
$f_4$	$0.002 \pm 0.000$	$0.002 \pm 0.000$	$0.066 \pm 0.008$	0	0
$1000 * \mu_{tzbg}$	$-4.4 \pm 0.2$	$-5.4 \pm 0.3$	$-5.5 \pm 0.6$	$-5.3 \pm 1.1$	$-0.4 \pm 1.2$
$\beta_{tzbg}$	$0.87 \pm 0.01$	$0.20 \pm 0.01$	0	0	0
$S1_{tzbg}$	$1.04 \pm 0.01$	$2.49 \pm 0.10$	-	-	-
$S2_{tzbg}$	$2.66 \pm 0.10$	$1.00 \pm 0.01$	$1.09 \pm 0.02$	$1.21 \pm 0.03$	$1.34 \pm 0.05$

Table 59: The parameters of  $t_z$  background fit for  $J/\psi$  in the rapidity bin  $3.5 < y < 4.5$  and multiplicity bin  $20 < PVNTRACKS < 40$ .

$J/\psi$ parameters	$p_T$ (GeV/c)				
	0-2	2-4	4-6	6-8	8-20
$\tau_1$	$1.38 \pm 0.03$	$1.47 \pm 0.03$	$1.41 \pm 0.03$	$1.39 \pm 0.03$	$1.39 \pm 0.03$
$\tau_2$	$0.25 \pm 0.01$	$0.27 \pm 0.02$	$0.16 \pm 0.01$	$0.11 \pm 0.02$	$0.10 \pm 0.02$
$\tau_3$	$0.40 \pm 0.03$	$0.32 \pm 0.02$	$0.14 \pm 0.01$	$0.18 \pm 0.02$	$0.09 \pm 0.02$
$\tau_4$	$5.86 \pm 1.27$	$4.44 \pm 1.37$	$0.98 \pm 0.15$	$1.86 \pm 1.00$	$0.51 \pm 0.15$
$f_1$	$0.082 \pm 0.002$	$0.118 \pm 0.003$	$0.220 \pm 0.004$	$0.298 \pm 0.007$	$0.351 \pm 0.008$
$f_2$	$0.165 \pm 0.004$	$0.108 \pm 0.004$	$0.124 \pm 0.006$	$0.096 \pm 0.012$	$0.065 \pm 0.012$
$f_3$	$0.013 \pm 0.001$	$0.022 \pm 0.002$	$0.098 \pm 0.005$	$0.053 \pm 0.005$	$0.057 \pm 0.009$
$f_4$	$0.004 \pm 0.000$	$0.002 \pm 0.000$	$0.010 \pm 0.002$	$0.004 \pm 0.002$	$0.014 \pm 0.007$
$1000 * \mu_{tzbg}$	$4.2 \pm 0.4$	$-2.0 \pm 0.4$	$-5.9 \pm 0.6$	$-5.7 \pm 1.1$	$-2.4 \pm 1.0$
$\beta_{tzbg}$	$0.19 \pm 0.01$	$0.79 \pm 0.01$	0	0	0
$S1_{tzbg}$	$2.46 \pm 0.07$	$1.02 \pm 0.01$	-	-	-
$S2_{tzbg}$	$1.01 \pm 0.01$	$2.57 \pm 0.10$	$1.07 \pm 0.01$	$1.17 \pm 0.02$	$1.18 \pm 0.03$

Table 60: The parameters of  $t_z$  background fit for  $\psi(2S)$  in the rapidity bin  $3.5 < y < 4.5$  and multiplicity bin  $20 < PVNTRACKS < 40$ .

$\psi(2S)$ parameters	$p_T$ (GeV/c)				
	0-2	2-4	4-6	6-8	8-20
$\tau_1$	$0.92 \pm 0.03$	$1.45 \pm 0.07$	$1.45 \pm 0.08$	$0.99 \pm 0.04$	$1.20 \pm 0.06$
$\tau_2$	$0.21 \pm 0.01$	$0.31 \pm 0.01$	$0.22 \pm 0.02$	-	-
$\tau_3$	$0.35 \pm 0.03$	$0.64 \pm 0.05$	$0.15 \pm 0.02$	$0.30 \pm 0.03$	$0.21 \pm 0.03$
$\tau_4$	$5.27 \pm 1.19$	-	$0.62 \pm 0.11$	-	-
$f_1$	$0.087 \pm 0.005$	$0.045 \pm 0.004$	$0.096 \pm 0.008$	$0.295 \pm 0.011$	$0.341 \pm 0.014$
$f_2$	$0.210 \pm 0.005$	$0.163 \pm 0.005$	$0.214 \pm 0.011$	0	0
$f_3$	$0.016 \pm 0.002$	$0.012 \pm 0.001$	$0.109 \pm 0.009$	$0.088 \pm 0.009$	$0.074 \pm 0.011$
$f_4$	$0.003 \pm 0.000$	0	$0.042 \pm 0.015$	0	0
$1000 * \mu_{tzbg}$	$3.0 \pm 0.5$	$1.4 \pm 0.5$	$-3.3 \pm 1.1$	$3.6 \pm 1.7$	$2.7 \pm 1.5$
$\beta_{tzbg}$	$0.78 \pm 0.01$	$0.22 \pm 0.01$	0	0	0
$S1_{tzbg}$	$1.02 \pm 0.01$	$3.30 \pm 0.11$	-	-	-
$S2_{tzbg}$	$2.52 \pm 0.08$	$1.10 \pm 0.01$	$1.22 \pm 0.03$	$1.49 \pm 0.05$	$1.29 \pm 0.05$

Table 61: The parameters of  $t_z$  background fit for  $J/\psi$  in the rapidity bin  $2.0 < y < 2.8$  and multiplicity bin  $40 < PVNTRACKS < 60$ .

$J/\psi$ parameters	$p_T$ (GeV/c)				
	0-2	2-4	4-6	6-8	8-20
$\tau_1$	$1.30 \pm 0.03$	$1.41 \pm 0.02$	$1.40 \pm 0.02$	$1.43 \pm 0.03$	$0.08 \pm 0.02$
$\tau_2$	$0.21 \pm 0.00$	$0.20 \pm 0.01$	$0.17 \pm 0.01$	$0.12 \pm 0.02$	$1.32 \pm 0.02$
$\tau_3$	$0.31 \pm 0.02$	$0.23 \pm 0.01$	$0.17 \pm 0.01$	$0.07 \pm 0.01$	$0.20 \pm 0.01$
$\tau_4$	$1.99 \pm 0.32$	$1.53 \pm 0.22$	$0.93 \pm 0.12$	$0.39 \pm 0.04$	-
$f_1$	$0.032 \pm 0.001$	$0.048 \pm 0.001$	$0.114 \pm 0.002$	$0.220 \pm 0.005$	$0.083 \pm 0.012$
$f_2$	$0.114 \pm 0.002$	$0.083 \pm 0.002$	$0.080 \pm 0.004$	$0.093 \pm 0.006$	$0.406 \pm 0.007$
$f_3$	$0.011 \pm 0.001$	$0.019 \pm 0.001$	$0.043 \pm 0.004$	$0.105 \pm 0.013$	$0.045 \pm 0.003$
$f_4$	$0.002 \pm 0.000$	$0.002 \pm 0.000$	$0.007 \pm 0.002$	$0.040 \pm 0.008$	0
$1000 * \mu_{tzbg}$	$-8.2 \pm 0.2$	$-6.8 \pm 0.2$	$-5.7 \pm 0.3$	$-1.7 \pm 0.8$	$-4.5 \pm 0.9$
$\beta_{tzbg}$	$0.15 \pm 0.01$	$0.17 \pm 0.01$	$0.24 \pm 0.04$	0	0
$S1_{tzbg}$	$2.58 \pm 0.06$	$2.17 \pm 0.06$	$1.82 \pm 0.13$	-	-
$S2_{tzbg}$	$1.08 \pm 0.01$	$1.01 \pm 0.01$	$0.97 \pm 0.02$	$1.06 \pm 0.02$	$1.20 \pm 0.02$

Table 62: The parameters of  $t_z$  background fit for  $\psi(2S)$  in the rapidity bin  $2.0 < y < 2.8$  and multiplicity bin  $40 < PVNTRACKS < 60$ .

$\psi(2S)$ parameters	$p_T$ (GeV/c)				
	0-2	2-4	4-6	6-8	8-20
$\tau_1$	$0.20 \pm 0.01$	$1.09 \pm 0.04$	$0.22 \pm 0.01$	$1.53 \pm 0.08$	$1.03 \pm 0.03$
$\tau_2$	$0.94 \pm 0.03$	$0.20 \pm 0.01$	$1.23 \pm 0.07$	$0.12 \pm 0.01$	-
$\tau_3$	$0.29 \pm 0.02$	$0.23 \pm 0.02$	$0.22 \pm 0.02$	$0.08 \pm 0.01$	$0.21 \pm 0.01$
$\tau_4$	$2.67 \pm 0.38$	$1.20 \pm 0.27$	$1.27 \pm 0.25$	$0.39 \pm 0.05$	-
$f_1$	$0.118 \pm 0.002$	$0.022 \pm 0.001$	$0.090 \pm 0.004$	$0.071 \pm 0.004$	$0.263 \pm 0.007$
$f_2$	$0.028 \pm 0.001$	$0.104 \pm 0.003$	$0.030 \pm 0.002$	$0.153 \pm 0.011$	0
$f_3$	$0.014 \pm 0.001$	$0.020 \pm 0.002$	$0.036 \pm 0.004$	$0.133 \pm 0.018$	$0.085 \pm 0.007$
$f_4$	$0.002 \pm 0.000$	$0.002 \pm 0.001$	$0.005 \pm 0.001$	$0.058 \pm 0.012$	0
$1000 * \mu_{tzbg}$	$-8.6 \pm 0.2$	$-7.5 \pm 0.2$	$-5.5 \pm 0.3$	$-2.4 \pm 1.1$	$1.5 \pm 0.9$
$\beta_{tzbg}$	$0.86 \pm 0.01$	$0.84 \pm 0.01$	$0.79 \pm 0.02$	0	0
$S1_{tzbg}$	$1.09 \pm 0.01$	$1.04 \pm 0.01$	$1.02 \pm 0.01$	-	-
$S2_{tzbg}$	$2.58 \pm 0.07$	$2.32 \pm 0.09$	$2.26 \pm 0.11$	$1.11 \pm 0.02$	$1.40 \pm 0.03$

Table 63: The parameters of  $t_z$  background fit for  $J/\psi$  in the rapidity bin  $2.8 < y < 3.5$  and multiplicity bin  $40 < PVNTRACKS < 60$ .

$J/\psi$ parameters	$p_T$ (GeV/c)				
	0-2	2-4	4-6	6-8	8-20
$\tau_1$	$1.31 \pm 0.03$	$1.46 \pm 0.02$	$1.51 \pm 0.03$	$1.31 \pm 0.02$	$1.27 \pm 0.02$
$\tau_2$	$0.20 \pm 0.00$	$0.19 \pm 0.01$	$0.27 \pm 0.02$	$0.06 \pm 0.01$	$0.03 \pm 0.00$
$\tau_3$	$0.28 \pm 0.01$	$0.20 \pm 0.01$	$0.24 \pm 0.02$	$0.07 \pm 0.01$	$0.05 \pm 0.01$
$\tau_4$	$2.08 \pm 0.30$	$0.93 \pm 0.06$	$1.08 \pm 0.17$	$0.37 \pm 0.05$	$0.27 \pm 0.04$
$f_1$	$0.032 \pm 0.001$	$0.047 \pm 0.001$	$0.118 \pm 0.003$	$0.269 \pm 0.005$	$0.405 \pm 0.006$
$f_2$	$0.127 \pm 0.002$	$0.093 \pm 0.002$	$0.069 \pm 0.003$	$0.139 \pm 0.027$	$0.196 \pm 0.048$
$f_3$	$0.013 \pm 0.001$	$0.027 \pm 0.002$	$0.036 \pm 0.003$	$0.099 \pm 0.008$	$0.085 \pm 0.011$
$f_4$	$0.002 \pm 0.000$	$0.007 \pm 0.001$	$0.005 \pm 0.002$	$0.038 \pm 0.010$	$0.040 \pm 0.009$
$1000 * \mu_{tzbg}$	$-5.4 \pm 0.2$	$-6.1 \pm 0.1$	$-5.8 \pm 0.2$	$-5.9 \pm 1.2$	$-8.8 \pm 1.9$
$\beta_{tzbg}$	$0.15 \pm 0.01$	$0.81 \pm 0.01$	$0.19 \pm 0.01$	0	0
$S1_{tzbg}$	$2.37 \pm 0.05$	$1.00 \pm 0.01$	$2.77 \pm 0.10$	-	-
$S2_{tzbg}$	$1.03 \pm 0.00$	$2.25 \pm 0.05$	$1.05 \pm 0.01$	$1.02 \pm 0.03$	$0.94 \pm 0.03$

Table 64: The parameters of  $t_z$  background fit for  $\psi(2S)$  in the rapidity bin  $2.8 < y < 3.5$  and multiplicity bin  $40 < PVNTRACKS < 60$ .

$\psi(2S)$ parameters	$p_T$ (GeV/c)				
	0-2	2-4	4-6	6-8	8-20
$\tau_1$	$0.17 \pm 0.00$	$0.19 \pm 0.00$	$0.18 \pm 0.01$	$1.39 \pm 0.07$	$0.16 \pm 0.02$
$\tau_2$	$0.82 \pm 0.02$	$1.09 \pm 0.03$	$1.38 \pm 0.05$	$0.12 \pm 0.01$	$1.26 \pm 0.06$
$\tau_3$	$0.27 \pm 0.01$	$0.18 \pm 0.01$	$0.13 \pm 0.02$	$0.08 \pm 0.01$	$0.19 \pm 0.01$
$\tau_4$	$2.32 \pm 0.19$	$0.66 \pm 0.04$	$0.52 \pm 0.04$	$0.39 \pm 0.04$	-
$f_1$	$0.144 \pm 0.002$	$0.111 \pm 0.002$	$0.103 \pm 0.005$	$0.089 \pm 0.005$	$0.160 \pm 0.013$
$f_2$	$0.037 \pm 0.001$	$0.022 \pm 0.001$	$0.032 \pm 0.002$	$0.168 \pm 0.011$	$0.210 \pm 0.012$
$f_3$	$0.015 \pm 0.001$	$0.029 \pm 0.002$	$0.047 \pm 0.006$	$0.141 \pm 0.015$	$0.100 \pm 0.008$
$f_4$	$0.002 \pm 0.000$	$0.011 \pm 0.002$	$0.037 \pm 0.006$	$0.086 \pm 0.015$	0
$1000 * \mu_{tzbg}$	$-4.9 \pm 0.2$	$-5.2 \pm 0.2$	$-5.5 \pm 0.3$	$-2.3 \pm 1.0$	$-4.0 \pm 1.0$
$\beta_{tzbg}$	$0.15 \pm 0.01$	$0.79 \pm 0.01$	$0.75 \pm 0.02$	0	0
$S1_{tzbg}$	$2.50 \pm 0.06$	$1.02 \pm 0.01$	$1.03 \pm 0.02$	-	-
$S2_{tzbg}$	$1.05 \pm 0.00$	$2.27 \pm 0.06$	$2.41 \pm 0.13$	$1.12 \pm 0.03$	$1.24 \pm 0.04$

Table 65: The parameters of  $t_z$  background fit for  $J/\psi$  in the rapidity bin  $3.5 < y < 4.5$  and multiplicity bin  $40 < PVNTRACKS < 60$ .

$J/\psi$ parameters	$p_T$ (GeV/c)				
	0-2	2-4	4-6	6-8	8-20
$\tau_1$	$1.32 \pm 0.03$	$1.43 \pm 0.02$	$1.44 \pm 0.04$	$1.35 \pm 0.03$	$1.23 \pm 0.02$
$\tau_2$	$0.24 \pm 0.01$	$0.24 \pm 0.01$	$0.34 \pm 0.05$	$0.09 \pm 0.01$	-
$\tau_3$	$0.42 \pm 0.03$	$0.30 \pm 0.01$	$0.30 \pm 0.04$	$0.11 \pm 0.01$	$0.23 \pm 0.02$
$\tau_4$	$3.41 \pm 0.58$	$2.34 \pm 0.61$	$2.01 \pm 0.69$	$0.78 \pm 0.15$	-
$f_1$	$0.058 \pm 0.002$	$0.085 \pm 0.002$	$0.165 \pm 0.006$	$0.286 \pm 0.006$	$0.364 \pm 0.005$
$f_2$	$0.154 \pm 0.003$	$0.100 \pm 0.003$	$0.061 \pm 0.006$	$0.106 \pm 0.012$	0
$f_3$	$0.012 \pm 0.001$	$0.024 \pm 0.002$	$0.024 \pm 0.003$	$0.093 \pm 0.007$	$0.032 \pm 0.003$
$f_4$	$0.003 \pm 0.000$	$0.001 \pm 0.000$	$0.003 \pm 0.001$	$0.011 \pm 0.003$	0
$1000 * \mu_{tzbkg}$	$4.7 \pm 0.3$	$-1.4 \pm 0.3$	$-4.3 \pm 0.4$	$-4.9 \pm 0.9$	$-0.8 \pm 0.7$
$\beta_{tzbkg}$	$0.81 \pm 0.01$	$0.75 \pm 0.01$	$0.25 \pm 0.01$	0	0
$S1_{tzbkg}$	$1.02 \pm 0.01$	$1.00 \pm 0.01$	$2.97 \pm 0.10$	-	-
$S2_{tzbkg}$	$2.48 \pm 0.06$	$2.44 \pm 0.06$	$1.05 \pm 0.01$	$1.11 \pm 0.02$	$1.39 \pm 0.02$

Table 66: The parameters of  $t_z$  background fit for  $\psi(2S)$  in the rapidity bin  $3.5 < y < 4.5$  and multiplicity bin  $40 < PVNTRACKS < 60$ .

$\psi(2S)$ parameters	$p_T$ (GeV/c)				
	0-2	2-4	4-6	6-8	8-20
$\tau_1$	$0.82 \pm 0.03$	$0.27 \pm 0.01$	$1.29 \pm 0.06$	$1.19 \pm 0.07$	$1.05 \pm 0.04$
$\tau_2$	$0.19 \pm 0.01$	$1.26 \pm 0.05$	$0.16 \pm 0.01$	$0.16 \pm 0.02$	-
$\tau_3$	$0.39 \pm 0.02$	$0.54 \pm 0.03$	$0.11 \pm 0.01$	$0.25 \pm 0.02$	$0.32 \pm 0.03$
$\tau_4$	$5.54 \pm 1.42$	-	$0.49 \pm 0.06$	-	-
$f_1$	$0.069 \pm 0.004$	$0.124 \pm 0.004$	$0.070 \pm 0.004$	$0.167 \pm 0.012$	$0.309 \pm 0.011$
$f_2$	$0.172 \pm 0.004$	$0.036 \pm 0.002$	$0.190 \pm 0.008$	$0.189 \pm 0.016$	0
$f_3$	$0.012 \pm 0.001$	$0.015 \pm 0.001$	$0.127 \pm 0.008$	$0.094 \pm 0.008$	$0.070 \pm 0.008$
$f_4$	$0.002 \pm 0.000$	0	$0.045 \pm 0.010$	0	0
$1000 * \mu_{tzbkg}$	$2.4 \pm 0.4$	$0.1 \pm 0.3$	$-3.0 \pm 0.8$	$-4.2 \pm 1.5$	$1.0 \pm 1.3$
$\beta_{tzbkg}$	$0.81 \pm 0.01$	$0.77 \pm 0.01$	0	0	0
$S1_{tzbkg}$	$1.06 \pm 0.01$	$1.09 \pm 0.01$	-	-	-
$S2_{tzbkg}$	$2.71 \pm 0.07$	$3.10 \pm 0.07$	$1.18 \pm 0.02$	$1.34 \pm 0.04$	$1.40 \pm 0.04$

Table 67: The parameters of  $t_z$  background fit for  $J/\psi$  in the rapidity bin  $2.0 < y < 2.8$  and multiplicity bin  $60 < PVNTRACKS < 80$ .

$J/\psi$ parameters	$p_T$ (GeV/c)				
	0-2	2-4	4-6	6-8	8-20
$\tau_1$	$0.20 \pm 0.00$	$1.43 \pm 0.03$	$1.44 \pm 0.03$	$1.42 \pm 0.03$	$1.32 \pm 0.02$
$\tau_2$	$1.26 \pm 0.03$	$0.19 \pm 0.01$	$0.18 \pm 0.01$	$0.10 \pm 0.01$	$0.06 \pm 0.01$
$\tau_3$	$0.29 \pm 0.02$	$0.20 \pm 0.01$	$0.19 \pm 0.01$	$0.07 \pm 0.01$	$0.04 \pm 0.00$
$\tau_4$	$1.45 \pm 0.21$	$1.05 \pm 0.10$	$1.13 \pm 0.17$	$0.36 \pm 0.04$	$0.31 \pm 0.03$
$f_1$	$0.110 \pm 0.002$	$0.031 \pm 0.001$	$0.070 \pm 0.002$	$0.170 \pm 0.004$	$0.345 \pm 0.006$
$f_2$	$0.023 \pm 0.001$	$0.081 \pm 0.002$	$0.076 \pm 0.004$	$0.110 \pm 0.008$	$0.145 \pm 0.024$
$f_3$	$0.012 \pm 0.001$	$0.020 \pm 0.001$	$0.034 \pm 0.003$	$0.121 \pm 0.017$	$0.136 \pm 0.022$
$f_4$	$0.002 \pm 0.000$	$0.004 \pm 0.001$	$0.005 \pm 0.001$	$0.040 \pm 0.009$	$0.042 \pm 0.006$
$1000 * \mu_{tzbg}$	$-8.3 \pm 0.2$	$-7.1 \pm 0.2$	$-5.4 \pm 0.3$	$-1.8 \pm 0.9$	$-2.1 \pm 1.6$
$\beta_{tzbg}$	$0.83 \pm 0.01$	$0.20 \pm 0.01$	$0.80 \pm 0.02$	0	0
$S1_{tzbg}$	$1.11 \pm 0.01$	$2.15 \pm 0.06$	$1.03 \pm 0.01$	-	-
$S2_{tzbg}$	$2.55 \pm 0.05$	$1.02 \pm 0.01$	$2.17 \pm 0.11$	$1.10 \pm 0.02$	$1.03 \pm 0.04$

Table 68: The parameters of  $t_z$  background fit for  $\psi(2S)$  in the rapidity bin  $2.0 < y < 2.8$  and multiplicity bin  $60 < PVNTRACKS < 80$ .

$\psi(2S)$ parameters	$p_T$ (GeV/c)				
	0-2	2-4	4-6	6-8	8-20
$\tau_1$	$0.85 \pm 0.03$	$0.17 \pm 0.01$	$0.18 \pm 0.01$	$0.10 \pm 0.01$	$0.13 \pm 0.02$
$\tau_2$	$0.18 \pm 0.00$	$0.88 \pm 0.04$	$1.12 \pm 0.13$	$1.55 \pm 0.11$	$1.38 \pm 0.07$
$\tau_3$	$0.25 \pm 0.01$	$0.25 \pm 0.01$	$0.24 \pm 0.02$	$0.06 \pm 0.01$	$0.20 \pm 0.01$
$\tau_4$	$1.97 \pm 0.21$	$2.22 \pm 0.46$	$2.14 \pm 0.72$	$0.35 \pm 0.03$	-
$f_1$	$0.023 \pm 0.001$	$0.095 \pm 0.003$	$0.086 \pm 0.005$	$0.161 \pm 0.013$	$0.154 \pm 0.013$
$f_2$	$0.116 \pm 0.002$	$0.020 \pm 0.001$	$0.023 \pm 0.003$	$0.037 \pm 0.003$	$0.142 \pm 0.009$
$f_3$	$0.017 \pm 0.001$	$0.018 \pm 0.001$	$0.030 \pm 0.003$	$0.177 \pm 0.029$	$0.097 \pm 0.007$
$f_4$	$0.002 \pm 0.000$	$0.001 \pm 0.000$	$0.003 \pm 0.001$	$0.086 \pm 0.013$	0
$1000 * \mu_{tzbg}$	$-8.8 \pm 0.2$	$-7.6 \pm 0.2$	$-6.3 \pm 0.3$	$-1.2 \pm 1.3$	$-3.4 \pm 1.0$
$\beta_{tzbg}$	$0.81 \pm 0.01$	$0.81 \pm 0.01$	$0.81 \pm 0.01$	0	0
$S1_{tzbg}$	$1.10 \pm 0.01$	$1.06 \pm 0.01$	$1.05 \pm 0.01$	-	-
$S2_{tzbg}$	$2.35 \pm 0.05$	$2.26 \pm 0.07$	$2.47 \pm 0.12$	$1.06 \pm 0.03$	$1.26 \pm 0.03$

Table 69: The parameters of  $t_z$  background fit for  $J/\psi$  in the rapidity bin  $2.8 < y < 3.5$  and multiplicity bin  $60 < PVNTRACKS < 80$ .

$J/\psi$ parameters	$p_T$ (GeV/c)				
	0-2	2-4	4-6	6-8	8-20
$\tau_1$	$1.26 \pm 0.03$	$0.18 \pm 0.00$	$1.45 \pm 0.03$	$1.35 \pm 0.03$	$1.33 \pm 0.03$
$\tau_2$	$0.19 \pm 0.00$	$1.40 \pm 0.02$	$0.17 \pm 0.01$	$0.08 \pm 0.01$	$0.07 \pm 0.01$
$\tau_3$	$0.26 \pm 0.01$	$0.20 \pm 0.01$	$0.15 \pm 0.01$	$0.07 \pm 0.01$	$0.06 \pm 0.01$
$\tau_4$	$1.48 \pm 0.16$	$0.97 \pm 0.07$	$0.79 \pm 0.08$	$0.37 \pm 0.04$	$0.30 \pm 0.04$
$f_1$	$0.024 \pm 0.001$	$0.087 \pm 0.002$	$0.087 \pm 0.002$	$0.218 \pm 0.004$	$0.350 \pm 0.007$
$f_2$	$0.121 \pm 0.002$	$0.033 \pm 0.001$	$0.089 \pm 0.005$	$0.132 \pm 0.010$	$0.102 \pm 0.013$
$f_3$	$0.013 \pm 0.001$	$0.027 \pm 0.002$	$0.059 \pm 0.006$	$0.123 \pm 0.011$	$0.113 \pm 0.014$
$f_4$	$0.003 \pm 0.000$	$0.006 \pm 0.001$	$0.012 \pm 0.002$	$0.040 \pm 0.007$	$0.035 \pm 0.009$
$1000 * \mu_{tzbg}$	$-5.6 \pm 0.1$	$-5.8 \pm 0.1$	$-5.7 \pm 0.2$	$-5.2 \pm 0.7$	$-2.6 \pm 1.0$
$\beta_{tzbg}$	$0.82 \pm 0.01$	$0.22 \pm 0.01$	$0.73 \pm 0.03$	0	0
$S1_{tzbg}$	$1.04 \pm 0.00$	$2.21 \pm 0.05$	$0.99 \pm 0.02$	-	-
$S2_{tzbg}$	$2.28 \pm 0.04$	$1.01 \pm 0.01$	$2.02 \pm 0.16$	$1.04 \pm 0.02$	$1.03 \pm 0.03$

Table 70: The parameters of  $t_z$  background fit for  $\psi(2S)$  in the rapidity bin  $2.8 < y < 3.5$  and multiplicity bin  $60 < PVNTRACKS < 80$ .

$\psi(2S)$ parameters	$p_T$ (GeV/c)				
	0-2	2-4	4-6	6-8	8-20
$\tau_1$	$0.69 \pm 0.02$	$0.17 \pm 0.00$	$1.25 \pm 0.07$	$1.41 \pm 0.08$	$0.11 \pm 0.02$
$\tau_2$	$0.14 \pm 0.00$	$1.00 \pm 0.04$	$0.22 \pm 0.01$	$0.11 \pm 0.01$	$1.11 \pm 0.06$
$\tau_3$	$0.26 \pm 0.01$	$0.20 \pm 0.01$	$0.21 \pm 0.02$	$0.07 \pm 0.01$	$0.19 \pm 0.01$
$\tau_4$	$2.63 \pm 0.19$	$0.78 \pm 0.08$	$0.94 \pm 0.15$	$0.38 \pm 0.04$	-
$f_1$	$0.036 \pm 0.002$	$0.098 \pm 0.003$	$0.022 \pm 0.002$	$0.060 \pm 0.004$	$0.186 \pm 0.017$
$f_2$	$0.136 \pm 0.002$	$0.017 \pm 0.001$	$0.085 \pm 0.004$	$0.159 \pm 0.010$	$0.164 \pm 0.011$
$f_3$	$0.014 \pm 0.001$	$0.026 \pm 0.002$	$0.048 \pm 0.003$	$0.172 \pm 0.018$	$0.113 \pm 0.009$
$f_4$	$0.002 \pm 0.000$	$0.007 \pm 0.001$	$0.008 \pm 0.003$	$0.082 \pm 0.014$	0
$1000 * \mu_{tzbg}$	$-5.6 \pm 0.2$	$-5.4 \pm 0.2$	$-5.7 \pm 0.3$	$-2.3 \pm 0.9$	$-5.5 \pm 1.2$
$\beta_{tzbg}$	$0.84 \pm 0.01$	$0.79 \pm 0.01$	$0.24 \pm 0.01$	0	0
$S1_{tzbg}$	$1.06 \pm 0.00$	$1.04 \pm 0.01$	$2.63 \pm 0.11$	-	-
$S2_{tzbg}$	$2.53 \pm 0.05$	$2.40 \pm 0.05$	$1.06 \pm 0.01$	$1.09 \pm 0.03$	$1.27 \pm 0.04$

Table 71: The parameters of  $t_z$  background fit for  $J/\psi$  in the rapidity bin  $3.5 < y < 4.5$  and multiplicity bin  $60 < PVNTRACKS < 80$ .

$J/\psi$ parameters	$p_T$ (GeV/c)				
	0-2	2-4	4-6	6-8	8-20
$\tau_1$	$1.23 \pm 0.03$	$1.40 \pm 0.03$	$1.38 \pm 0.03$	$1.35 \pm 0.03$	$1.33 \pm 0.04$
$\tau_2$	$0.21 \pm 0.01$	$0.24 \pm 0.01$	$0.13 \pm 0.01$	$0.11 \pm 0.01$	$0.15 \pm 0.03$
$\tau_3$	$0.49 \pm 0.03$	$0.31 \pm 0.02$	$0.11 \pm 0.01$	$0.08 \pm 0.01$	$0.10 \pm 0.01$
$\tau_4$	$5.53 \pm 2.05$	$1.20 \pm 0.22$	$0.51 \pm 0.05$	$0.38 \pm 0.06$	$0.53 \pm 0.19$
$f_1$	$0.048 \pm 0.002$	$0.060 \pm 0.002$	$0.141 \pm 0.003$	$0.236 \pm 0.006$	$0.294 \pm 0.010$
$f_2$	$0.143 \pm 0.003$	$0.092 \pm 0.003$	$0.141 \pm 0.006$	$0.123 \pm 0.011$	$0.087 \pm 0.010$
$f_3$	$0.010 \pm 0.001$	$0.021 \pm 0.002$	$0.118 \pm 0.006$	$0.111 \pm 0.014$	$0.060 \pm 0.009$
$f_4$	$0.001 \pm 0.000$	$0.003 \pm 0.001$	$0.027 \pm 0.005$	$0.032 \pm 0.010$	$0.007 \pm 0.005$
$1000 * \mu_{tzbg}$	$4.7 \pm 0.3$	$-0.9 \pm 0.3$	$-4.3 \pm 0.6$	$-4.4 \pm 1.1$	$-2.5 \pm 0.9$
$\beta_{tzbg}$	$0.80 \pm 0.01$	$0.77 \pm 0.01$	0	0	0
$S1_{tzbg}$	$1.03 \pm 0.01$	$1.03 \pm 0.01$	-	-	-
$S2_{tzbg}$	$2.52 \pm 0.05$	$2.58 \pm 0.07$	$1.10 \pm 0.01$	$1.12 \pm 0.03$	$1.28 \pm 0.03$

Table 72: The parameters of  $t_z$  background fit for  $\psi(2S)$  in the rapidity bin  $3.5 < y < 4.5$  and multiplicity bin  $60 < PVNTRACKS < 80$ .

$\psi(2S)$ parameters	$p_T$ (GeV/c)				
	0-2	2-4	4-6	6-8	8-20
$\tau_1$	$0.18 \pm 0.01$	$0.25 \pm 0.01$	$1.28 \pm 0.07$	$0.16 \pm 0.02$	$1.06 \pm 0.05$
$\tau_2$	$0.79 \pm 0.03$	$1.19 \pm 0.06$	$0.17 \pm 0.01$	$1.16 \pm 0.09$	-
$\tau_3$	$0.38 \pm 0.03$	$0.40 \pm 0.02$	$0.14 \pm 0.01$	$0.20 \pm 0.01$	$0.21 \pm 0.02$
$\tau_4$	$4.01 \pm 0.90$	-	$0.66 \pm 0.10$	-	-
$f_1$	$0.159 \pm 0.004$	$0.109 \pm 0.004$	$0.045 \pm 0.004$	$0.209 \pm 0.015$	$0.263 \pm 0.012$
$f_2$	$0.054 \pm 0.003$	$0.026 \pm 0.002$	$0.182 \pm 0.007$	$0.107 \pm 0.011$	0
$f_3$	$0.014 \pm 0.001$	$0.018 \pm 0.001$	$0.114 \pm 0.006$	$0.112 \pm 0.009$	$0.085 \pm 0.010$
$f_4$	$0.002 \pm 0.000$	0	$0.022 \pm 0.006$	0	0
$1000 * \mu_{tzbg}$	$2.7 \pm 0.4$	$-0.2 \pm 0.3$	$-3.1 \pm 0.7$	$-4.8 \pm 1.3$	$0.8 \pm 1.4$
$\beta_{tzbg}$	$0.20 \pm 0.01$	$0.75 \pm 0.01$	0	0	0
$S1_{tzbg}$	$2.56 \pm 0.07$	$1.07 \pm 0.01$	-	-	-
$S2_{tzbg}$	$1.06 \pm 0.01$	$2.77 \pm 0.07$	$1.23 \pm 0.02$	$1.25 \pm 0.04$	$1.40 \pm 0.05$

Table 73: The parameters of  $t_z$  background fit for  $J/\psi$  in the rapidity bin  $2.0 < y < 2.8$  and multiplicity bin  $80 < PVNTRACKS < 200$ .

$J/\psi$ parameters	$p_T$ (GeV/c)				
	0-2	2-4	4-6	6-8	8-20
$\tau_1$	$1.20 \pm 0.04$	$0.17 \pm 0.00$	$1.46 \pm 0.04$	$1.34 \pm 0.04$	$1.23 \pm 0.03$
$\tau_2$	$0.19 \pm 0.00$	$1.32 \pm 0.03$	$0.16 \pm 0.01$	$0.08 \pm 0.01$	$0.05 \pm 0.01$
$\tau_3$	$0.26 \pm 0.02$	$0.19 \pm 0.01$	$0.16 \pm 0.02$	$0.06 \pm 0.01$	$0.04 \pm 0.00$
$\tau_4$	$1.25 \pm 0.15$	$1.03 \pm 0.09$	$0.80 \pm 0.10$	$0.34 \pm 0.05$	$0.20 \pm 0.01$
$f_1$	$0.016 \pm 0.001$	$0.081 \pm 0.003$	$0.041 \pm 0.001$	$0.122 \pm 0.003$	$0.292 \pm 0.006$
$f_2$	$0.103 \pm 0.002$	$0.020 \pm 0.001$	$0.079 \pm 0.005$	$0.167 \pm 0.015$	$0.138 \pm 0.022$
$f_3$	$0.012 \pm 0.001$	$0.021 \pm 0.002$	$0.039 \pm 0.005$	$0.139 \pm 0.018$	$0.229 \pm 0.053$
$f_4$	$0.003 \pm 0.001$	$0.004 \pm 0.001$	$0.008 \pm 0.002$	$0.039 \pm 0.011$	$0.078 \pm 0.009$
$1000 * \mu_{tzbg}$	$-8.8 \pm 0.2$	$-7.6 \pm 0.2$	$-5.5 \pm 0.3$	$-4.1 \pm 0.9$	$2.6 \pm 2.7$
$\beta_{tzbg}$	$0.82 \pm 0.01$	$0.78 \pm 0.01$	$0.75 \pm 0.02$	0	0
$S1_{tzbg}$	$1.14 \pm 0.01$	$1.05 \pm 0.01$	$1.03 \pm 0.01$	-	-
$S2_{tzbg}$	$2.72 \pm 0.05$	$2.18 \pm 0.05$	$2.07 \pm 0.09$	$1.09 \pm 0.03$	$0.98 \pm 0.05$

Table 74: The parameters of  $t_z$  background fit for  $\psi(2S)$  in the rapidity bin  $2.0 < y < 2.8$  and multiplicity bin  $80 < PVNTRACKS < 200$ .

$\psi(2S)$ parameters	$p_T$ (GeV/c)				
	0-2	2-4	4-6	6-8	8-20
$\tau_1$	$0.85 \pm 0.04$	$0.98 \pm 0.05$	$0.17 \pm 0.01$	$0.10 \pm 0.01$	$1.38 \pm 0.09$
$\tau_2$	$0.17 \pm 0.00$	$0.17 \pm 0.01$	$1.00 \pm 0.06$	$1.32 \pm 0.10$	$0.10 \pm 0.02$
$\tau_3$	$0.26 \pm 0.01$	$0.18 \pm 0.01$	$0.17 \pm 0.02$	$0.08 \pm 0.01$	$0.06 \pm 0.02$
$\tau_4$	$1.77 \pm 0.21$	$0.67 \pm 0.07$	$0.73 \pm 0.15$	$0.48 \pm 0.07$	$0.35 \pm 0.05$
$f_1$	$0.019 \pm 0.001$	$0.011 \pm 0.001$	$0.075 \pm 0.005$	$0.170 \pm 0.012$	$0.085 \pm 0.007$
$f_2$	$0.111 \pm 0.002$	$0.089 \pm 0.003$	$0.016 \pm 0.002$	$0.029 \pm 0.003$	$0.161 \pm 0.021$
$f_3$	$0.014 \pm 0.001$	$0.020 \pm 0.002$	$0.036 \pm 0.005$	$0.150 \pm 0.019$	$0.143 \pm 0.030$
$f_4$	$0.002 \pm 0.000$	$0.006 \pm 0.001$	$0.007 \pm 0.003$	$0.034 \pm 0.009$	$0.085 \pm 0.022$
$1000 * \mu_{tzbg}$	$-9.9 \pm 0.2$	$-7.8 \pm 0.2$	$-5.9 \pm 0.3$	$-3.4 \pm 1.0$	$-0.1 \pm 1.5$
$\beta_{tzbg}$	$0.80 \pm 0.01$	$0.78 \pm 0.01$	$0.73 \pm 0.03$	0	0
$S1_{tzbg}$	$1.14 \pm 0.01$	$1.08 \pm 0.01$	$1.03 \pm 0.02$	-	-
$S2_{tzbg}$	$2.58 \pm 0.05$	$2.24 \pm 0.06$	$2.15 \pm 0.12$	$1.14 \pm 0.03$	$1.16 \pm 0.05$

Table 75: The parameters of  $t_z$  background fit for  $J/\psi$  in the rapidity bin  $2.8 < y < 3.5$  and multiplicity bin  $80 < PVNTRACKS < 200$ .

$J/\psi$ parameters	$p_T$ (GeV/c)				
	0-2	2-4	4-6	6-8	8-20
$\tau_1$	$0.13 \pm 0.00$	$0.18 \pm 0.00$	$1.43 \pm 0.03$	$1.38 \pm 0.04$	$1.30 \pm 0.03$
$\tau_2$	$1.13 \pm 0.02$	$1.38 \pm 0.03$	$0.16 \pm 0.01$	$0.08 \pm 0.01$	$0.05 \pm 0.01$
$\tau_3$	$0.09 \pm 0.00$	$0.21 \pm 0.01$	$0.13 \pm 0.01$	$0.05 \pm 0.01$	$0.04 \pm 0.01$
$\tau_4$	$0.66 \pm 0.02$	$0.97 \pm 0.07$	$0.51 \pm 0.05$	$0.35 \pm 0.03$	$0.28 \pm 0.03$
$f_1$	$0.190 \pm 0.002$	$0.083 \pm 0.002$	$0.055 \pm 0.002$	$0.143 \pm 0.004$	$0.306 \pm 0.007$
$f_2$	$0.020 \pm 0.001$	$0.021 \pm 0.001$	$0.075 \pm 0.004$	$0.148 \pm 0.010$	$0.152 \pm 0.029$
$f_3$	$0.087 \pm 0.002$	$0.024 \pm 0.001$	$0.051 \pm 0.005$	$0.165 \pm 0.021$	$0.160 \pm 0.026$
$f_4$	$0.011 \pm 0.001$	$0.006 \pm 0.001$	$0.020 \pm 0.004$	$0.067 \pm 0.009$	$0.056 \pm 0.011$
$1000 * \mu_{tzbg}$	$-6.5 \pm 0.2$	$-6.1 \pm 0.1$	$-5.1 \pm 0.2$	$-3.6 \pm 0.9$	$-3.7 \pm 1.7$
$\beta_{tzbg}$	0	$0.79 \pm 0.01$	$0.78 \pm 0.01$	0	0
$S1_{tzbg}$	-	$1.05 \pm 0.01$	$1.06 \pm 0.01$	-	-
$S2_{tzbg}$	$1.09 \pm 0.00$	$2.37 \pm 0.05$	$2.42 \pm 0.09$	$1.04 \pm 0.03$	$0.98 \pm 0.04$

Table 76: The parameters of  $t_z$  background fit for  $\psi(2S)$  in the rapidity bin  $2.8 < y < 3.5$  and multiplicity bin  $80 < PVNTRACKS < 200$ .

$\psi(2S)$ parameters	$p_T$ (GeV/c)				
	0-2	2-4	4-6	6-8	8-20
$\tau_1$	$0.16 \pm 0.00$	$0.67 \pm 0.03$	$0.21 \pm 0.01$	$0.11 \pm 0.02$	$0.10 \pm 0.01$
$\tau_2$	$0.90 \pm 0.02$	$0.15 \pm 0.01$	$1.18 \pm 0.09$	$1.43 \pm 0.12$	$1.30 \pm 0.08$
$\tau_3$	$0.54 \pm 0.02$	$0.23 \pm 0.01$	$0.23 \pm 0.02$	$0.08 \pm 0.01$	$0.21 \pm 0.02$
$\tau_4$	-	$1.58 \pm 0.13$	$1.03 \pm 0.28$	$0.37 \pm 0.05$	-
$f_1$	$0.119 \pm 0.002$	$0.021 \pm 0.002$	$0.068 \pm 0.004$	$0.156 \pm 0.012$	$0.216 \pm 0.019$
$f_2$	$0.021 \pm 0.001$	$0.090 \pm 0.003$	$0.015 \pm 0.002$	$0.034 \pm 0.004$	$0.121 \pm 0.008$
$f_3$	$0.007 \pm 0.000$	$0.023 \pm 0.001$	$0.036 \pm 0.003$	$0.150 \pm 0.014$	$0.089 \pm 0.008$
$f_4$	0	$0.003 \pm 0.000$	$0.005 \pm 0.003$	$0.056 \pm 0.015$	0
$1000 * \mu_{tzbg}$	$-5.4 \pm 0.2$	$-6.0 \pm 0.2$	$-5.1 \pm 0.3$	$-2.9 \pm 0.8$	$-5.3 \pm 1.2$
$\beta_{tzbg}$	$0.83 \pm 0.00$	$0.78 \pm 0.01$	$0.76 \pm 0.01$	0	0
$S1_{tzbg}$	$1.10 \pm 0.00$	$1.06 \pm 0.01$	$1.11 \pm 0.01$	-	-
$S2_{tzbg}$	$2.86 \pm 0.04$	$2.47 \pm 0.05$	$2.85 \pm 0.10$	$1.19 \pm 0.03$	$1.28 \pm 0.04$

Table 77: The parameters of  $t_z$  background fit for  $J/\psi$  in the rapidity bin  $3.5 < y < 4.5$  and multiplicity bin  $80 < PVNTRACKS < 200$ .

$J/\psi$ parameters	$p_T$ (GeV/c)				
	0-2	2-4	4-6	6-8	8-20
$\tau_1$	$1.23 \pm 0.04$	$1.30 \pm 0.04$	$1.31 \pm 0.03$	$1.43 \pm 0.05$	$1.31 \pm 0.04$
$\tau_2$	$0.22 \pm 0.01$	$0.20 \pm 0.01$	$0.11 \pm 0.01$	$0.13 \pm 0.02$	$0.11 \pm 0.02$
$\tau_3$	$0.50 \pm 0.04$	$0.28 \pm 0.02$	$0.10 \pm 0.01$	$0.08 \pm 0.01$	$0.13 \pm 0.01$
$\tau_4$	$6.02 \pm 3.49$	$2.29 \pm 0.92$	$0.43 \pm 0.05$	$0.41 \pm 0.08$	$1.21 \pm 0.97$
$f_1$	$0.034 \pm 0.002$	$0.047 \pm 0.002$	$0.114 \pm 0.003$	$0.191 \pm 0.008$	$0.280 \pm 0.009$
$f_2$	$0.127 \pm 0.003$	$0.092 \pm 0.004$	$0.158 \pm 0.008$	$0.151 \pm 0.012$	$0.101 \pm 0.014$
$f_3$	$0.008 \pm 0.001$	$0.026 \pm 0.002$	$0.118 \pm 0.007$	$0.138 \pm 0.016$	$0.065 \pm 0.009$
$f_4$	$0.001 \pm 0.000$	$0.001 \pm 0.000$	$0.036 \pm 0.008$	$0.025 \pm 0.009$	$0.002 \pm 0.002$
$1000 * \mu_{tzbg}$	$5.0 \pm 0.3$	$-1.0 \pm 0.3$	$-4.6 \pm 0.7$	$-3.0 \pm 1.3$	$-2.3 \pm 1.2$
$\beta_{tzbg}$	$0.20 \pm 0.01$	$0.75 \pm 0.01$	0	0	0
$S1_{tzbg}$	$2.57 \pm 0.05$	$1.04 \pm 0.01$	-	-	-
$S2_{tzbg}$	$1.05 \pm 0.01$	$2.43 \pm 0.06$	$1.11 \pm 0.01$	$1.13 \pm 0.03$	$1.29 \pm 0.03$

Table 78: The parameters of  $t_z$  background fit for  $\psi(2S)$  in the rapidity bin  $3.5 < y < 4.5$  and multiplicity bin  $80 < PVNTRACKS < 200$ .

$\psi(2S)$ parameters	$p_T$ (GeV/c)				
	0-2	2-4	4-6	6-8	8-20
$\tau_1$	$0.19 \pm 0.01$	$0.91 \pm 0.05$	$1.27 \pm 0.09$	$0.20 \pm 0.02$	$1.08 \pm 0.07$
$\tau_2$	$0.95 \pm 0.03$	$0.19 \pm 0.01$	$0.15 \pm 0.01$	$1.38 \pm 0.13$	-
$\tau_3$	$0.51 \pm 0.03$	$0.28 \pm 0.02$	$0.12 \pm 0.01$	$0.21 \pm 0.02$	$0.14 \pm 0.02$
$\tau_4$	-	$2.39 \pm 0.83$	$0.60 \pm 0.10$	-	-
$f_1$	$0.145 \pm 0.004$	$0.027 \pm 0.002$	$0.030 \pm 0.003$	$0.172 \pm 0.014$	$0.224 \pm 0.013$
$f_2$	$0.033 \pm 0.002$	$0.108 \pm 0.005$	$0.167 \pm 0.007$	$0.080 \pm 0.010$	0
$f_3$	$0.009 \pm 0.001$	$0.027 \pm 0.003$	$0.128 \pm 0.007$	$0.096 \pm 0.009$	$0.100 \pm 0.016$
$f_4$	0	$0.001 \pm 0.001$	$0.023 \pm 0.007$	0	0
$1000 * \mu_{tzbg}$	$2.6 \pm 0.4$	$-1.1 \pm 0.4$	$-2.4 \pm 0.7$	$-6.2 \pm 1.2$	$1.7 \pm 1.7$
$\beta_{tzbg}$	$0.80 \pm 0.01$	$0.73 \pm 0.02$	0	0	0
$S1_{tzbg}$	$1.08 \pm 0.01$	$1.05 \pm 0.02$	-	-	-
$S2_{tzbg}$	$2.74 \pm 0.06$	$2.41 \pm 0.10$	$1.21 \pm 0.02$	$1.33 \pm 0.04$	$1.52 \pm 0.05$

706 **C Efficiency tables**

707 **C.1 Geometrical Acceptance (Universal for three multiplicity  
708 binning schemes)**

Table 79: The efficiency  $\epsilon_{\text{acc}}$  in different bins of  $p_{\text{T}}$  and  $y$  for prompt  $J/\psi$  mesons for PVZ>-60mm.

$p_{\text{T}}$ ( GeV/c )	$2 < y < 2.8$	$2.8 < y < 3.5$	$3.5 < y < 4.5$
0-2	$0.671 \pm 0.004$	$0.904 \pm 0.003$	$0.852 \pm 0.003$
2-4	$0.746 \pm 0.004$	$0.936 \pm 0.002$	$0.902 \pm 0.003$
4-6	$0.832 \pm 0.005$	$0.961 \pm 0.003$	$0.944 \pm 0.003$
6-8	$0.897 \pm 0.006$	$0.977 \pm 0.004$	$0.968 \pm 0.004$
8-20	$0.937 \pm 0.007$	$0.990 \pm 0.003$	$0.977 \pm 0.005$

Table 80: The efficiency  $\epsilon_{\text{acc}}$  in different bins of  $p_{\text{T}}$  and  $y$  for prompt  $\psi(2S)$  mesons for PVZ>-60mm.

$p_{\text{T}}$ ( GeV/c )	$2 < y < 2.8$	$2.8 < y < 3.5$	$3.5 < y < 4.5$
0-2	$0.667 \pm 0.007$	$0.908 \pm 0.005$	$0.850 \pm 0.005$
2-4	$0.723 \pm 0.006$	$0.922 \pm 0.004$	$0.886 \pm 0.005$
4-6	$0.801 \pm 0.008$	$0.953 \pm 0.005$	$0.931 \pm 0.006$
6-8	$0.863 \pm 0.011$	$0.967 \pm 0.007$	$0.966 \pm 0.007$
8-20	$0.906 \pm 0.011$	$0.980 \pm 0.006$	$0.991 \pm 0.005$

Table 81: The efficiency  $\epsilon_{\text{acc}}$  in different bins of  $p_{\text{T}}$  and  $y$  for  $J/\psi$  from b hardron decay mesons for PVZ>-60mm.

$p_{\text{T}}$ ( GeV/c )	$2 < y < 2.8$	$2.8 < y < 3.5$	$3.5 < y < 4.5$
0-2	$0.661 \pm 0.008$	$0.894 \pm 0.006$	$0.849 \pm 0.007$
2-4	$0.743 \pm 0.007$	$0.927 \pm 0.005$	$0.892 \pm 0.006$
4-6	$0.835 \pm 0.008$	$0.960 \pm 0.005$	$0.952 \pm 0.006$
6-8	$0.860 \pm 0.011$	$0.983 \pm 0.005$	$0.972 \pm 0.007$
8-20	$0.927 \pm 0.008$	$0.998 \pm 0.002$	$0.990 \pm 0.005$

Table 82: The efficiency  $\epsilon_{\text{acc}}$  in different bins of  $p_{\text{T}}$  and  $y$  for  $\psi(2S)$  from b hardron decay mesons for PVZ>-60mm.

$p_{\text{T}}$ ( GeV/c )	$2 < y < 2.8$	$2.8 < y < 3.5$	$3.5 < y < 4.5$
0-2	$0.671 \pm 0.008$	$0.908 \pm 0.006$	$0.867 \pm 0.007$
2-4	$0.718 \pm 0.006$	$0.918 \pm 0.005$	$0.897 \pm 0.005$
4-6	$0.798 \pm 0.007$	$0.959 \pm 0.004$	$0.937 \pm 0.006$
6-8	$0.867 \pm 0.008$	$0.969 \pm 0.005$	$0.958 \pm 0.007$
8-20	$0.904 \pm 0.007$	$0.985 \pm 0.004$	$0.981 \pm 0.005$

## 709 2 Efficiency of reconstruction and selection

710 In different PVNTRACKS region:

Table 83: The efficiency  $\epsilon_{\text{MuonID}}$  for  $J/\psi$  prompt signals in different  $(p_{\text{T}}, y)$  bins.

0 $\leq$ PVNTRACKS < 20					
$p_{\text{T}}$ ( GeV/c )	0-2	2-4	4-6	6-8	8-20
$2.0 < y < 2.8$	$0.653 \pm 0.003$	$0.697 \pm 0.003$	$0.747 \pm 0.004$	$0.799 \pm 0.006$	$0.843 \pm 0.008$
$2.8 < y < 3.5$	$0.701 \pm 0.003$	$0.748 \pm 0.003$	$0.815 \pm 0.004$	$0.859 \pm 0.006$	$0.881 \pm 0.008$
$3.5 < y < 4.5$	$0.614 \pm 0.003$	$0.628 \pm 0.003$	$0.662 \pm 0.004$	$0.693 \pm 0.007$	$0.720 \pm 0.010$
20 $\leq$ PVNTRACKS < 45					
$p_{\text{T}}$ ( GeV/c )	0-2	2-4	4-6	6-8	8-20
$2.0 < y < 2.8$	$0.651 \pm 0.002$	$0.696 \pm 0.002$	$0.748 \pm 0.003$	$0.799 \pm 0.004$	$0.843 \pm 0.004$
$2.8 < y < 3.5$	$0.699 \pm 0.002$	$0.747 \pm 0.002$	$0.814 \pm 0.002$	$0.860 \pm 0.003$	$0.882 \pm 0.004$
$3.5 < y < 4.5$	$0.613 \pm 0.002$	$0.626 \pm 0.002$	$0.659 \pm 0.003$	$0.688 \pm 0.004$	$0.715 \pm 0.005$
45 $\leq$ PVNTRACKS < 70					
$p_{\text{T}}$ ( GeV/c )	0-2	2-4	4-6	6-8	8-20
$2.0 < y < 2.8$	$0.634 \pm 0.003$	$0.685 \pm 0.003$	$0.741 \pm 0.003$	$0.794 \pm 0.004$	$0.839 \pm 0.004$
$2.8 < y < 3.5$	$0.681 \pm 0.003$	$0.734 \pm 0.002$	$0.806 \pm 0.003$	$0.852 \pm 0.004$	$0.877 \pm 0.004$
$3.5 < y < 4.5$	$0.599 \pm 0.002$	$0.618 \pm 0.002$	$0.652 \pm 0.003$	$0.681 \pm 0.004$	$0.708 \pm 0.005$
70 $\leq$ PVNTRACKS < 95					
$p_{\text{T}}$ ( GeV/c )	0-2	2-4	4-6	6-8	8-20
$2.0 < y < 2.8$	$0.610 \pm 0.004$	$0.667 \pm 0.004$	$0.729 \pm 0.004$	$0.785 \pm 0.006$	$0.831 \pm 0.006$
$2.8 < y < 3.5$	$0.655 \pm 0.004$	$0.716 \pm 0.003$	$0.792 \pm 0.004$	$0.842 \pm 0.005$	$0.869 \pm 0.006$
$3.5 < y < 4.5$	$0.579 \pm 0.004$	$0.602 \pm 0.003$	$0.642 \pm 0.004$	$0.671 \pm 0.006$	$0.696 \pm 0.007$
95 $\leq$ PVNTRACKS < 200					
$p_{\text{T}}$ ( GeV/c )	0-2	2-4	4-6	6-8	8-20
$2.0 < y < 2.8$	$0.588 \pm 0.008$	$0.652 \pm 0.008$	$0.720 \pm 0.009$	$0.776 \pm 0.011$	$0.827 \pm 0.011$
$2.8 < y < 3.5$	$0.632 \pm 0.008$	$0.698 \pm 0.007$	$0.779 \pm 0.008$	$0.833 \pm 0.010$	$0.863 \pm 0.011$
$3.5 < y < 4.5$	$0.560 \pm 0.007$	$0.591 \pm 0.007$	$0.628 \pm 0.008$	$0.660 \pm 0.012$	$0.688 \pm 0.014$

Table 84: The efficiency  $\epsilon_{\text{MuonID}}$  for  $\psi(2S)$  prompt signals in different  $(p_T, y)$  bins.

$0 \leq \text{PVNTRACKS} < 20$					
$p_T$ ( GeV/c )	0-2	2-4	4-6	6-8	8-20
$2.0 < y < 2.8$	$0.689 \pm 0.004$	$0.719 \pm 0.005$	$0.769 \pm 0.007$	$0.820 \pm 0.011$	$0.861 \pm 0.012$
$2.8 < y < 3.5$	$0.735 \pm 0.003$	$0.764 \pm 0.004$	$0.815 \pm 0.006$	$0.854 \pm 0.009$	$0.877 \pm 0.012$
$3.5 < y < 4.5$	$0.636 \pm 0.003$	$0.644 \pm 0.004$	$0.662 \pm 0.006$	$0.683 \pm 0.011$	$0.706 \pm 0.016$
$20 \leq \text{PVNTRACKS} < 45$					
$p_T$ ( GeV/c )	0-2	2-4	4-6	6-8	8-20
$2.0 < y < 2.8$	$0.687 \pm 0.003$	$0.719 \pm 0.004$	$0.771 \pm 0.005$	$0.819 \pm 0.006$	$0.861 \pm 0.006$
$2.8 < y < 3.5$	$0.734 \pm 0.003$	$0.764 \pm 0.003$	$0.813 \pm 0.004$	$0.854 \pm 0.005$	$0.878 \pm 0.006$
$3.5 < y < 4.5$	$0.634 \pm 0.003$	$0.644 \pm 0.003$	$0.661 \pm 0.004$	$0.684 \pm 0.006$	$0.710 \pm 0.008$
$45 \leq \text{PVNTRACKS} < 70$					
$p_T$ ( GeV/c )	0-2	2-4	4-6	6-8	8-20
$2.0 < y < 2.8$	$0.674 \pm 0.004$	$0.709 \pm 0.004$	$0.763 \pm 0.005$	$0.816 \pm 0.007$	$0.857 \pm 0.007$
$2.8 < y < 3.5$	$0.720 \pm 0.003$	$0.752 \pm 0.003$	$0.804 \pm 0.004$	$0.850 \pm 0.006$	$0.874 \pm 0.006$
$3.5 < y < 4.5$	$0.625 \pm 0.003$	$0.635 \pm 0.004$	$0.652 \pm 0.005$	$0.671 \pm 0.007$	$0.699 \pm 0.008$
$70 \leq \text{PVNTRACKS} < 95$					
$p_T$ ( GeV/c )	0-2	2-4	4-6	6-8	8-20
$2.0 < y < 2.8$	$0.654 \pm 0.007$	$0.692 \pm 0.007$	$0.751 \pm 0.008$	$0.806 \pm 0.010$	$0.850 \pm 0.010$
$2.8 < y < 3.5$	$0.698 \pm 0.005$	$0.735 \pm 0.006$	$0.792 \pm 0.007$	$0.837 \pm 0.009$	$0.865 \pm 0.009$
$3.5 < y < 4.5$	$0.605 \pm 0.005$	$0.622 \pm 0.006$	$0.642 \pm 0.007$	$0.666 \pm 0.010$	$0.697 \pm 0.012$
$95 \leq \text{PVNTRACKS} < 200$					
$p_T$ ( GeV/c )	0-2	2-4	4-6	6-8	8-20
$2.0 < y < 2.8$	$0.636 \pm 0.014$	$0.679 \pm 0.015$	$0.742 \pm 0.018$	$0.800 \pm 0.022$	$0.846 \pm 0.019$
$2.8 < y < 3.5$	$0.679 \pm 0.012$	$0.723 \pm 0.012$	$0.784 \pm 0.014$	$0.833 \pm 0.018$	$0.854 \pm 0.017$
$3.5 < y < 4.5$	$0.589 \pm 0.012$	$0.613 \pm 0.012$	$0.631 \pm 0.015$	$0.663 \pm 0.021$	$0.681 \pm 0.023$

Table 85: The efficiency  $\epsilon_{\text{MuonID}}$  for  $J/\psi$  from b signals in different  $(p_T, y)$  bins.

$p_T$ ( GeV/c )	0 $\leq$ PVNTRACKS < 20				
	0-2	2-4	4-6	6-8	8-20
2.0 $< y <$ 2.8	0.654 $\pm$ 0.009	0.698 $\pm$ 0.008	0.749 $\pm$ 0.008	0.801 $\pm$ 0.011	0.851 $\pm$ 0.011
2.8 $< y <$ 3.5	0.704 $\pm$ 0.009	0.751 $\pm$ 0.007	0.816 $\pm$ 0.008	0.859 $\pm$ 0.011	0.886 $\pm$ 0.012
3.5 $< y <$ 4.5	0.622 $\pm$ 0.009	0.642 $\pm$ 0.008	0.682 $\pm$ 0.010	0.720 $\pm$ 0.015	0.750 $\pm$ 0.020
20 $\leq$ PVNTRACKS < 45					
$p_T$ ( GeV/c )	0-2	2-4	4-6	6-8	8-20
	0.650 $\pm$ 0.005	0.696 $\pm$ 0.004	0.748 $\pm$ 0.005	0.799 $\pm$ 0.006	0.848 $\pm$ 0.005
2.0 $< y <$ 2.8	0.700 $\pm$ 0.005	0.748 $\pm$ 0.004	0.815 $\pm$ 0.004	0.859 $\pm$ 0.005	0.883 $\pm$ 0.005
3.5 $< y <$ 4.5	0.620 $\pm$ 0.005	0.637 $\pm$ 0.004	0.676 $\pm$ 0.005	0.713 $\pm$ 0.007	0.742 $\pm$ 0.008
45 $\leq$ PVNTRACKS < 70					
$p_T$ ( GeV/c )	0-2	2-4	4-6	6-8	8-20
	0.632 $\pm$ 0.006	0.684 $\pm$ 0.005	0.740 $\pm$ 0.005	0.793 $\pm$ 0.006	0.843 $\pm$ 0.005
2.0 $< y <$ 2.8	0.678 $\pm$ 0.006	0.733 $\pm$ 0.004	0.805 $\pm$ 0.004	0.851 $\pm$ 0.006	0.876 $\pm$ 0.005
3.5 $< y <$ 4.5	0.602 $\pm$ 0.006	0.626 $\pm$ 0.005	0.668 $\pm$ 0.005	0.706 $\pm$ 0.007	0.732 $\pm$ 0.008
70 $\leq$ PVNTRACKS < 95					
$p_T$ ( GeV/c )	0-2	2-4	4-6	6-8	8-20
	0.609 $\pm$ 0.009	0.668 $\pm$ 0.007	0.729 $\pm$ 0.007	0.784 $\pm$ 0.008	0.839 $\pm$ 0.007
2.0 $< y <$ 2.8	0.652 $\pm$ 0.008	0.714 $\pm$ 0.006	0.792 $\pm$ 0.006	0.842 $\pm$ 0.008	0.870 $\pm$ 0.008
3.5 $< y <$ 4.5	0.585 $\pm$ 0.008	0.609 $\pm$ 0.007	0.663 $\pm$ 0.008	0.698 $\pm$ 0.010	0.721 $\pm$ 0.011
95 $\leq$ PVNTRACKS < 200					
$p_T$ ( GeV/c )	0-2	2-4	4-6	6-8	8-20
	0.589 $\pm$ 0.017	0.649 $\pm$ 0.013	0.719 $\pm$ 0.013	0.778 $\pm$ 0.016	0.833 $\pm$ 0.012
2.0 $< y <$ 2.8	0.629 $\pm$ 0.016	0.699 $\pm$ 0.012	0.782 $\pm$ 0.012	0.830 $\pm$ 0.015	0.861 $\pm$ 0.013
3.5 $< y <$ 4.5	0.568 $\pm$ 0.016	0.598 $\pm$ 0.013	0.649 $\pm$ 0.015	0.684 $\pm$ 0.019	0.712 $\pm$ 0.020

Table 86: The efficiency  $\epsilon_{\text{MuonID}}$  for  $\psi(2S)$  from b signals in different  $(p_T, y)$  bins.

$0 \leq \text{PVNTRACKS} < 20$					
$p_T$ ( GeV/c )	0-2	2-4	4-6	6-8	8-20
$2.0 < y < 2.8$	$0.686 \pm 0.007$	$0.720 \pm 0.007$	$0.772 \pm 0.007$	$0.820 \pm 0.009$	$0.864 \pm 0.008$
$2.8 < y < 3.5$	$0.736 \pm 0.006$	$0.766 \pm 0.006$	$0.816 \pm 0.006$	$0.855 \pm 0.008$	$0.883 \pm 0.009$
$3.5 < y < 4.5$	$0.625 \pm 0.007$	$0.641 \pm 0.006$	$0.676 \pm 0.008$	$0.712 \pm 0.011$	$0.742 \pm 0.013$
$20 \leq \text{PVNTRACKS} < 45$					
$p_T$ ( GeV/c )	0-2	2-4	4-6	6-8	8-20
$2.0 < y < 2.8$	$0.684 \pm 0.004$	$0.719 \pm 0.004$	$0.770 \pm 0.004$	$0.820 \pm 0.005$	$0.865 \pm 0.004$
$2.8 < y < 3.5$	$0.734 \pm 0.004$	$0.764 \pm 0.003$	$0.815 \pm 0.003$	$0.855 \pm 0.004$	$0.881 \pm 0.004$
$3.5 < y < 4.5$	$0.623 \pm 0.004$	$0.640 \pm 0.004$	$0.668 \pm 0.004$	$0.701 \pm 0.006$	$0.739 \pm 0.006$
$45 \leq \text{PVNTRACKS} < 70$					
$p_T$ ( GeV/c )	0-2	2-4	4-6	6-8	8-20
$2.0 < y < 2.8$	$0.668 \pm 0.005$	$0.707 \pm 0.004$	$0.762 \pm 0.004$	$0.815 \pm 0.005$	$0.859 \pm 0.004$
$2.8 < y < 3.5$	$0.717 \pm 0.004$	$0.749 \pm 0.004$	$0.805 \pm 0.004$	$0.846 \pm 0.004$	$0.874 \pm 0.004$
$3.5 < y < 4.5$	$0.610 \pm 0.004$	$0.627 \pm 0.004$	$0.659 \pm 0.005$	$0.689 \pm 0.006$	$0.730 \pm 0.006$
$70 \leq \text{PVNTRACKS} < 95$					
$p_T$ ( GeV/c )	0-2	2-4	4-6	6-8	8-20
$2.0 < y < 2.8$	$0.649 \pm 0.007$	$0.691 \pm 0.007$	$0.751 \pm 0.007$	$0.805 \pm 0.008$	$0.852 \pm 0.006$
$2.8 < y < 3.5$	$0.696 \pm 0.006$	$0.735 \pm 0.005$	$0.792 \pm 0.006$	$0.838 \pm 0.007$	$0.865 \pm 0.006$
$3.5 < y < 4.5$	$0.589 \pm 0.007$	$0.617 \pm 0.006$	$0.651 \pm 0.007$	$0.681 \pm 0.009$	$0.713 \pm 0.009$
$95 \leq \text{PVNTRACKS} < 200$					
$p_T$ ( GeV/c )	0-2	2-4	4-6	6-8	8-20
$2.0 < y < 2.8$	$0.632 \pm 0.015$	$0.680 \pm 0.013$	$0.740 \pm 0.014$	$0.800 \pm 0.015$	$0.846 \pm 0.011$
$2.8 < y < 3.5$	$0.679 \pm 0.013$	$0.721 \pm 0.011$	$0.780 \pm 0.011$	$0.829 \pm 0.013$	$0.859 \pm 0.012$
$3.5 < y < 4.5$	$0.579 \pm 0.013$	$0.605 \pm 0.012$	$0.641 \pm 0.014$	$0.664 \pm 0.017$	$0.705 \pm 0.017$

711 In different nBackTracks region:

Table 87: The efficiency  $\epsilon_{\text{Trigger}}$  for  $J/\psi$  prompt signals in different  $(p_T, y)$  bins.

$0 \leq n_{\text{BackTracks}} < 8$					
$p_T$ ( GeV/c )	0-2	2-4	4-6	6-8	8-20
$2.0 < y < 2.8$	$0.259 \pm 0.003$	$0.395 \pm 0.003$	$0.518 \pm 0.004$	$0.595 \pm 0.006$	$0.659 \pm 0.007$
$2.8 < y < 3.5$	$0.356 \pm 0.003$	$0.473 \pm 0.003$	$0.579 \pm 0.004$	$0.649 \pm 0.006$	$0.662 \pm 0.007$
$3.5 < y < 4.5$	$0.428 \pm 0.003$	$0.523 \pm 0.003$	$0.600 \pm 0.004$	$0.650 \pm 0.006$	$0.675 \pm 0.008$
$8 \leq n_{\text{BackTracks}} < 15$					
$p_T$ ( GeV/c )	0-2	2-4	4-6	6-8	8-20
$2.0 < y < 2.8$	$0.269 \pm 0.003$	$0.406 \pm 0.003$	$0.527 \pm 0.004$	$0.596 \pm 0.005$	$0.650 \pm 0.006$
$2.8 < y < 3.5$	$0.361 \pm 0.003$	$0.475 \pm 0.003$	$0.583 \pm 0.003$	$0.636 \pm 0.005$	$0.678 \pm 0.006$
$3.5 < y < 4.5$	$0.440 \pm 0.003$	$0.524 \pm 0.003$	$0.597 \pm 0.004$	$0.652 \pm 0.005$	$0.685 \pm 0.007$
$15 \leq n_{\text{BackTracks}} < 22$					
$p_T$ ( GeV/c )	0-2	2-4	4-6	6-8	8-20
$2.0 < y < 2.8$	$0.266 \pm 0.003$	$0.408 \pm 0.003$	$0.524 \pm 0.004$	$0.592 \pm 0.005$	$0.668 \pm 0.006$
$2.8 < y < 3.5$	$0.375 \pm 0.003$	$0.477 \pm 0.003$	$0.589 \pm 0.003$	$0.648 \pm 0.005$	$0.676 \pm 0.006$
$3.5 < y < 4.5$	$0.434 \pm 0.004$	$0.528 \pm 0.003$	$0.607 \pm 0.004$	$0.647 \pm 0.006$	$0.682 \pm 0.007$
$22 \leq n_{\text{BackTracks}} < 30$					
$p_T$ ( GeV/c )	0-2	2-4	4-6	6-8	8-20
$2.0 < y < 2.8$	$0.278 \pm 0.004$	$0.409 \pm 0.004$	$0.535 \pm 0.004$	$0.601 \pm 0.006$	$0.661 \pm 0.006$
$2.8 < y < 3.5$	$0.374 \pm 0.004$	$0.486 \pm 0.003$	$0.584 \pm 0.004$	$0.642 \pm 0.006$	$0.681 \pm 0.007$
$3.5 < y < 4.5$	$0.441 \pm 0.004$	$0.529 \pm 0.004$	$0.599 \pm 0.004$	$0.647 \pm 0.006$	$0.685 \pm 0.008$
$30 \leq n_{\text{BackTracks}} < 80$					
$p_T$ ( GeV/c )	0-2	2-4	4-6	6-8	8-20
$2.0 < y < 2.8$	$0.282 \pm 0.004$	$0.413 \pm 0.004$	$0.541 \pm 0.005$	$0.601 \pm 0.006$	$0.668 \pm 0.007$
$2.8 < y < 3.5$	$0.377 \pm 0.004$	$0.495 \pm 0.004$	$0.591 \pm 0.004$	$0.655 \pm 0.006$	$0.692 \pm 0.007$
$3.5 < y < 4.5$	$0.431 \pm 0.005$	$0.537 \pm 0.004$	$0.607 \pm 0.005$	$0.647 \pm 0.007$	$0.663 \pm 0.008$

Table 88: The efficiency  $\epsilon_{\text{Trigger}}$  for  $\psi(2S)$  prompt signals in different  $(p_{\text{T}}, y)$  bins.

$0 \leq \text{nBackTracks} < 8$					
$p_{\text{T}}$ ( GeV/c )	0-2	2-4	4-6	6-8	8-20
$2.0 < y < 2.8$	$0.404 \pm 0.004$	$0.489 \pm 0.005$	$0.571 \pm 0.007$	$0.629 \pm 0.010$	$0.699 \pm 0.011$
$2.8 < y < 3.5$	$0.454 \pm 0.004$	$0.513 \pm 0.004$	$0.593 \pm 0.006$	$0.640 \pm 0.009$	$0.694 \pm 0.010$
$3.5 < y < 4.5$	$0.513 \pm 0.004$	$0.561 \pm 0.005$	$0.615 \pm 0.006$	$0.643 \pm 0.010$	$0.681 \pm 0.012$
$8 \leq \text{nBackTracks} < 15$					
$p_{\text{T}}$ ( GeV/c )	0-2	2-4	4-6	6-8	8-20
$2.0 < y < 2.8$	$0.410 \pm 0.005$	$0.498 \pm 0.005$	$0.573 \pm 0.007$	$0.636 \pm 0.009$	$0.683 \pm 0.009$
$2.8 < y < 3.5$	$0.459 \pm 0.004$	$0.523 \pm 0.004$	$0.602 \pm 0.005$	$0.634 \pm 0.008$	$0.680 \pm 0.009$
$3.5 < y < 4.5$	$0.517 \pm 0.004$	$0.563 \pm 0.005$	$0.612 \pm 0.006$	$0.667 \pm 0.009$	$0.673 \pm 0.011$
$15 \leq \text{nBackTracks} < 22$					
$p_{\text{T}}$ ( GeV/c )	0-2	2-4	4-6	6-8	8-20
$2.0 < y < 2.8$	$0.425 \pm 0.005$	$0.491 \pm 0.006$	$0.581 \pm 0.007$	$0.636 \pm 0.009$	$0.678 \pm 0.009$
$2.8 < y < 3.5$	$0.464 \pm 0.004$	$0.526 \pm 0.005$	$0.597 \pm 0.006$	$0.639 \pm 0.008$	$0.679 \pm 0.009$
$3.5 < y < 4.5$	$0.516 \pm 0.005$	$0.554 \pm 0.005$	$0.614 \pm 0.007$	$0.648 \pm 0.009$	$0.673 \pm 0.011$
$22 \leq \text{nBackTracks} < 30$					
$p_{\text{T}}$ ( GeV/c )	0-2	2-4	4-6	6-8	8-20
$2.0 < y < 2.8$	$0.416 \pm 0.006$	$0.490 \pm 0.007$	$0.593 \pm 0.008$	$0.640 \pm 0.011$	$0.697 \pm 0.010$
$2.8 < y < 3.5$	$0.460 \pm 0.005$	$0.526 \pm 0.005$	$0.596 \pm 0.007$	$0.652 \pm 0.009$	$0.683 \pm 0.010$
$3.5 < y < 4.5$	$0.518 \pm 0.006$	$0.548 \pm 0.006$	$0.603 \pm 0.008$	$0.637 \pm 0.011$	$0.674 \pm 0.012$
$30 \leq \text{nBackTracks} < 80$					
$p_{\text{T}}$ ( GeV/c )	0-2	2-4	4-6	6-8	8-20
$2.0 < y < 2.8$	$0.424 \pm 0.007$	$0.499 \pm 0.008$	$0.587 \pm 0.009$	$0.650 \pm 0.011$	$0.703 \pm 0.011$
$2.8 < y < 3.5$	$0.456 \pm 0.006$	$0.523 \pm 0.006$	$0.605 \pm 0.007$	$0.645 \pm 0.010$	$0.690 \pm 0.011$
$3.5 < y < 4.5$	$0.513 \pm 0.007$	$0.561 \pm 0.007$	$0.616 \pm 0.009$	$0.663 \pm 0.012$	$0.704 \pm 0.013$

Table 89: The efficiency  $\epsilon_{\text{Trigger}}$  for  $J/\psi$  from b signals in different  $(p_T, y)$  bins.

$0 \leq n\text{BackTracks} < 8$					
$p_T$ ( GeV/c )	0-2	2-4	4-6	6-8	8-20
$2.0 < y < 2.8$	$0.268 \pm 0.008$	$0.404 \pm 0.007$	$0.520 \pm 0.008$	$0.605 \pm 0.010$	$0.674 \pm 0.009$
$2.8 < y < 3.5$	$0.353 \pm 0.008$	$0.478 \pm 0.007$	$0.595 \pm 0.007$	$0.628 \pm 0.010$	$0.667 \pm 0.011$
$3.5 < y < 4.5$	$0.438 \pm 0.009$	$0.526 \pm 0.008$	$0.609 \pm 0.009$	$0.653 \pm 0.012$	$0.666 \pm 0.014$
$8 \leq n\text{BackTracks} < 15$					
$p_T$ ( GeV/c )	0-2	2-4	4-6	6-8	8-20
$2.0 < y < 2.8$	$0.274 \pm 0.007$	$0.407 \pm 0.006$	$0.530 \pm 0.007$	$0.608 \pm 0.008$	$0.676 \pm 0.007$
$2.8 < y < 3.5$	$0.373 \pm 0.007$	$0.477 \pm 0.006$	$0.586 \pm 0.006$	$0.643 \pm 0.008$	$0.685 \pm 0.008$
$3.5 < y < 4.5$	$0.428 \pm 0.008$	$0.536 \pm 0.007$	$0.605 \pm 0.008$	$0.654 \pm 0.010$	$0.691 \pm 0.011$
$15 \leq n\text{BackTracks} < 22$					
$p_T$ ( GeV/c )	0-2	2-4	4-6	6-8	8-20
$2.0 < y < 2.8$	$0.274 \pm 0.007$	$0.405 \pm 0.006$	$0.528 \pm 0.007$	$0.606 \pm 0.008$	$0.687 \pm 0.007$
$2.8 < y < 3.5$	$0.389 \pm 0.008$	$0.487 \pm 0.006$	$0.587 \pm 0.006$	$0.642 \pm 0.008$	$0.683 \pm 0.009$
$3.5 < y < 4.5$	$0.438 \pm 0.009$	$0.527 \pm 0.007$	$0.611 \pm 0.008$	$0.666 \pm 0.011$	$0.692 \pm 0.012$
$22 \leq n\text{BackTracks} < 30$					
$p_T$ ( GeV/c )	0-2	2-4	4-6	6-8	8-20
$2.0 < y < 2.8$	$0.263 \pm 0.008$	$0.407 \pm 0.007$	$0.536 \pm 0.007$	$0.608 \pm 0.009$	$0.667 \pm 0.008$
$2.8 < y < 3.5$	$0.378 \pm 0.009$	$0.485 \pm 0.007$	$0.588 \pm 0.007$	$0.650 \pm 0.009$	$0.683 \pm 0.009$
$3.5 < y < 4.5$	$0.432 \pm 0.010$	$0.535 \pm 0.008$	$0.601 \pm 0.009$	$0.662 \pm 0.012$	$0.672 \pm 0.012$
$30 \leq n\text{BackTracks} < 80$					
$p_T$ ( GeV/c )	0-2	2-4	4-6	6-8	8-20
$2.0 < y < 2.8$	$0.273 \pm 0.009$	$0.422 \pm 0.007$	$0.534 \pm 0.008$	$0.611 \pm 0.010$	$0.687 \pm 0.008$
$2.8 < y < 3.5$	$0.387 \pm 0.009$	$0.496 \pm 0.007$	$0.597 \pm 0.007$	$0.659 \pm 0.009$	$0.671 \pm 0.009$
$3.5 < y < 4.5$	$0.445 \pm 0.011$	$0.532 \pm 0.009$	$0.603 \pm 0.010$	$0.664 \pm 0.012$	$0.686 \pm 0.013$

Table 90: The efficiency  $\epsilon_{\text{Trigger}}$  for  $\psi(2S)$  from b signals in different  $(p_T, y)$  bins.

$0 \leq n_{\text{BackTracks}} < 8$					
$p_T$ (GeV/c)	0-2	2-4	4-6	6-8	8-20
$2.0 < y < 2.8$	$0.396 \pm 0.007$	$0.497 \pm 0.006$	$0.592 \pm 0.007$	$0.627 \pm 0.008$	$0.684 \pm 0.007$
$2.8 < y < 3.5$	$0.449 \pm 0.006$	$0.506 \pm 0.005$	$0.594 \pm 0.006$	$0.648 \pm 0.008$	$0.686 \pm 0.008$
$3.5 < y < 4.5$	$0.519 \pm 0.007$	$0.567 \pm 0.006$	$0.603 \pm 0.007$	$0.648 \pm 0.010$	$0.692 \pm 0.010$
$8 \leq n_{\text{BackTracks}} < 15$					
$p_T$ (GeV/c)	0-2	2-4	4-6	6-8	8-20
$2.0 < y < 2.8$	$0.404 \pm 0.006$	$0.499 \pm 0.006$	$0.594 \pm 0.006$	$0.640 \pm 0.007$	$0.699 \pm 0.006$
$2.8 < y < 3.5$	$0.464 \pm 0.005$	$0.517 \pm 0.005$	$0.594 \pm 0.005$	$0.636 \pm 0.006$	$0.688 \pm 0.006$
$3.5 < y < 4.5$	$0.519 \pm 0.006$	$0.559 \pm 0.006$	$0.620 \pm 0.006$	$0.659 \pm 0.008$	$0.681 \pm 0.008$
$15 \leq n_{\text{BackTracks}} < 22$					
$p_T$ (GeV/c)	0-2	2-4	4-6	6-8	8-20
$2.0 < y < 2.8$	$0.419 \pm 0.006$	$0.506 \pm 0.006$	$0.584 \pm 0.006$	$0.659 \pm 0.007$	$0.696 \pm 0.006$
$2.8 < y < 3.5$	$0.457 \pm 0.006$	$0.521 \pm 0.005$	$0.601 \pm 0.005$	$0.647 \pm 0.007$	$0.683 \pm 0.006$
$3.5 < y < 4.5$	$0.526 \pm 0.007$	$0.562 \pm 0.006$	$0.612 \pm 0.007$	$0.643 \pm 0.008$	$0.675 \pm 0.008$
$22 \leq n_{\text{BackTracks}} < 30$					
$p_T$ (GeV/c)	0-2	2-4	4-6	6-8	8-20
$2.0 < y < 2.8$	$0.417 \pm 0.007$	$0.510 \pm 0.007$	$0.595 \pm 0.007$	$0.651 \pm 0.008$	$0.686 \pm 0.006$
$2.8 < y < 3.5$	$0.465 \pm 0.007$	$0.523 \pm 0.006$	$0.597 \pm 0.006$	$0.650 \pm 0.007$	$0.690 \pm 0.007$
$3.5 < y < 4.5$	$0.531 \pm 0.008$	$0.563 \pm 0.007$	$0.619 \pm 0.007$	$0.658 \pm 0.009$	$0.686 \pm 0.009$
$30 \leq n_{\text{BackTracks}} < 80$					
$p_T$ (GeV/c)	0-2	2-4	4-6	6-8	8-20
$2.0 < y < 2.8$	$0.400 \pm 0.008$	$0.502 \pm 0.007$	$0.586 \pm 0.008$	$0.640 \pm 0.008$	$0.706 \pm 0.007$
$2.8 < y < 3.5$	$0.475 \pm 0.007$	$0.527 \pm 0.006$	$0.596 \pm 0.007$	$0.646 \pm 0.008$	$0.679 \pm 0.007$
$3.5 < y < 4.5$	$0.521 \pm 0.008$	$0.568 \pm 0.008$	$0.613 \pm 0.008$	$0.636 \pm 0.010$	$0.672 \pm 0.010$

712 In different nForwardTracks region:

Table 91: The efficiency  $\epsilon_{\text{tot}}$  for  $J/\psi$  prompt signals in different  $(p_T, y)$  bins.

$0 \leq \text{nForwardTracks} < 12$					
$p_T$ ( GeV/c )	0-2	2-4	4-6	6-8	8-20
$2.0 < y < 2.8$	$0.032 \pm 0.000$	$0.056 \pm 0.001$	$0.131 \pm 0.002$	$0.218 \pm 0.004$	$0.307 \pm 0.006$
$2.8 < y < 3.5$	$0.070 \pm 0.001$	$0.112 \pm 0.001$	$0.231 \pm 0.002$	$0.330 \pm 0.005$	$0.392 \pm 0.008$
$3.5 < y < 4.5$	$0.068 \pm 0.001$	$0.093 \pm 0.001$	$0.176 \pm 0.002$	$0.252 \pm 0.005$	$0.325 \pm 0.008$
$12 \leq \text{nForwardTracks} < 24$					
$p_T$ ( GeV/c )	0-2	2-4	4-6	6-8	8-20
$2.0 < y < 2.8$	$0.033 \pm 0.000$	$0.057 \pm 0.001$	$0.132 \pm 0.001$	$0.224 \pm 0.003$	$0.314 \pm 0.004$
$2.8 < y < 3.5$	$0.070 \pm 0.001$	$0.116 \pm 0.001$	$0.235 \pm 0.002$	$0.325 \pm 0.003$	$0.396 \pm 0.005$
$3.5 < y < 4.5$	$0.068 \pm 0.001$	$0.095 \pm 0.001$	$0.178 \pm 0.001$	$0.258 \pm 0.003$	$0.319 \pm 0.005$
$24 \leq \text{nForwardTracks} < 36$					
$p_T$ ( GeV/c )	0-2	2-4	4-6	6-8	8-20
$2.0 < y < 2.8$	$0.033 \pm 0.000$	$0.057 \pm 0.001$	$0.133 \pm 0.001$	$0.218 \pm 0.003$	$0.317 \pm 0.004$
$2.8 < y < 3.5$	$0.071 \pm 0.001$	$0.115 \pm 0.001$	$0.230 \pm 0.002$	$0.328 \pm 0.003$	$0.401 \pm 0.004$
$3.5 < y < 4.5$	$0.067 \pm 0.001$	$0.094 \pm 0.001$	$0.178 \pm 0.002$	$0.254 \pm 0.003$	$0.314 \pm 0.004$
$36 \leq \text{nForwardTracks} < 48$					
$p_T$ ( GeV/c )	0-2	2-4	4-6	6-8	8-20
$2.0 < y < 2.8$	$0.032 \pm 0.000$	$0.055 \pm 0.001$	$0.128 \pm 0.001$	$0.215 \pm 0.003$	$0.306 \pm 0.004$
$2.8 < y < 3.5$	$0.070 \pm 0.001$	$0.114 \pm 0.001$	$0.232 \pm 0.002$	$0.325 \pm 0.004$	$0.397 \pm 0.005$
$3.5 < y < 4.5$	$0.066 \pm 0.001$	$0.094 \pm 0.001$	$0.176 \pm 0.002$	$0.247 \pm 0.003$	$0.306 \pm 0.005$
$48 \leq \text{nForwardTracks} < 130$					
$p_T$ ( GeV/c )	0-2	2-4	4-6	6-8	8-20
$2.0 < y < 2.8$	$0.031 \pm 0.001$	$0.054 \pm 0.001$	$0.129 \pm 0.002$	$0.214 \pm 0.003$	$0.305 \pm 0.005$
$2.8 < y < 3.5$	$0.066 \pm 0.001$	$0.109 \pm 0.001$	$0.223 \pm 0.002$	$0.310 \pm 0.004$	$0.392 \pm 0.005$
$3.5 < y < 4.5$	$0.063 \pm 0.001$	$0.090 \pm 0.001$	$0.169 \pm 0.002$	$0.239 \pm 0.004$	$0.303 \pm 0.005$

Table 92: The efficiency  $\epsilon_{\text{tot}}$  for  $\psi(2S)$  prompt signals in different  $(p_T, y)$  bins.

<u>0≤nForwardTracks&lt;12</u>					
$p_T$ ( GeV/c )	0-2	2-4	4-6	6-8	8-20
$2.0 < y < 2.8$	$0.075 \pm 0.001$	$0.071 \pm 0.001$	$0.116 \pm 0.003$	$0.170 \pm 0.005$	$0.272 \pm 0.009$
$2.8 < y < 3.5$	$0.163 \pm 0.002$	$0.155 \pm 0.002$	$0.246 \pm 0.004$	$0.334 \pm 0.008$	$0.413 \pm 0.013$
$3.5 < y < 4.5$	$0.140 \pm 0.002$	$0.122 \pm 0.002$	$0.183 \pm 0.004$	$0.246 \pm 0.008$	$0.313 \pm 0.013$
<u>12≤nForwardTracks&lt;24</u>					
$p_T$ ( GeV/c )	0-2	2-4	4-6	6-8	8-20
$2.0 < y < 2.8$	$0.075 \pm 0.001$	$0.072 \pm 0.001$	$0.118 \pm 0.002$	$0.185 \pm 0.004$	$0.264 \pm 0.006$
$2.8 < y < 3.5$	$0.167 \pm 0.002$	$0.157 \pm 0.002$	$0.245 \pm 0.003$	$0.329 \pm 0.005$	$0.409 \pm 0.007$
$3.5 < y < 4.5$	$0.143 \pm 0.002$	$0.124 \pm 0.001$	$0.184 \pm 0.003$	$0.255 \pm 0.005$	$0.317 \pm 0.007$
<u>24≤nForwardTracks&lt;36</u>					
$p_T$ ( GeV/c )	0-2	2-4	4-6	6-8	8-20
$2.0 < y < 2.8$	$0.074 \pm 0.001$	$0.071 \pm 0.001$	$0.113 \pm 0.002$	$0.183 \pm 0.004$	$0.260 \pm 0.006$
$2.8 < y < 3.5$	$0.163 \pm 0.002$	$0.155 \pm 0.002$	$0.241 \pm 0.003$	$0.320 \pm 0.005$	$0.396 \pm 0.007$
$3.5 < y < 4.5$	$0.141 \pm 0.002$	$0.122 \pm 0.001$	$0.186 \pm 0.003$	$0.241 \pm 0.005$	$0.309 \pm 0.006$
<u>36≤nForwardTracks&lt;48</u>					
$p_T$ ( GeV/c )	0-2	2-4	4-6	6-8	8-20
$2.0 < y < 2.8$	$0.075 \pm 0.001$	$0.071 \pm 0.001$	$0.113 \pm 0.002$	$0.182 \pm 0.005$	$0.263 \pm 0.006$
$2.8 < y < 3.5$	$0.161 \pm 0.002$	$0.154 \pm 0.002$	$0.242 \pm 0.003$	$0.315 \pm 0.006$	$0.384 \pm 0.007$
$3.5 < y < 4.5$	$0.137 \pm 0.002$	$0.120 \pm 0.002$	$0.177 \pm 0.003$	$0.245 \pm 0.005$	$0.310 \pm 0.007$
<u>48≤nForwardTracks&lt;130</u>					
$p_T$ ( GeV/c )	0-2	2-4	4-6	6-8	8-20
$2.0 < y < 2.8$	$0.073 \pm 0.002$	$0.067 \pm 0.001$	$0.113 \pm 0.003$	$0.171 \pm 0.005$	$0.255 \pm 0.006$
$2.8 < y < 3.5$	$0.155 \pm 0.003$	$0.147 \pm 0.002$	$0.237 \pm 0.004$	$0.320 \pm 0.007$	$0.385 \pm 0.008$
$3.5 < y < 4.5$	$0.132 \pm 0.002$	$0.118 \pm 0.002$	$0.172 \pm 0.003$	$0.229 \pm 0.006$	$0.307 \pm 0.008$

Table 93: The efficiency  $\epsilon_{\text{tot}}$  for  $J/\psi$  from b signals in different  $(p_T, y)$  bins.

$0 \leq \text{nForwardTracks} < 12$					
$p_T$ ( GeV/c )	0-2	2-4	4-6	6-8	8-20
$2.0 < y < 2.8$	$0.033 \pm 0.001$	$0.055 \pm 0.001$	$0.131 \pm 0.003$	$0.211 \pm 0.007$	$0.318 \pm 0.009$
$2.8 < y < 3.5$	$0.066 \pm 0.002$	$0.114 \pm 0.003$	$0.235 \pm 0.005$	$0.314 \pm 0.009$	$0.415 \pm 0.013$
$3.5 < y < 4.5$	$0.070 \pm 0.002$	$0.095 \pm 0.003$	$0.190 \pm 0.005$	$0.268 \pm 0.011$	$0.311 \pm 0.016$
$12 \leq \text{nForwardTracks} < 24$					
$p_T$ ( GeV/c )	0-2	2-4	4-6	6-8	8-20
$2.0 < y < 2.8$	$0.029 \pm 0.001$	$0.057 \pm 0.001$	$0.133 \pm 0.002$	$0.208 \pm 0.004$	$0.327 \pm 0.006$
$2.8 < y < 3.5$	$0.067 \pm 0.001$	$0.120 \pm 0.002$	$0.234 \pm 0.003$	$0.328 \pm 0.005$	$0.406 \pm 0.007$
$3.5 < y < 4.5$	$0.065 \pm 0.001$	$0.099 \pm 0.002$	$0.186 \pm 0.003$	$0.269 \pm 0.006$	$0.322 \pm 0.008$
$24 \leq \text{nForwardTracks} < 36$					
$p_T$ ( GeV/c )	0-2	2-4	4-6	6-8	8-20
$2.0 < y < 2.8$	$0.031 \pm 0.001$	$0.056 \pm 0.001$	$0.134 \pm 0.002$	$0.212 \pm 0.004$	$0.317 \pm 0.005$
$2.8 < y < 3.5$	$0.068 \pm 0.001$	$0.118 \pm 0.002$	$0.237 \pm 0.003$	$0.324 \pm 0.005$	$0.408 \pm 0.006$
$3.5 < y < 4.5$	$0.064 \pm 0.001$	$0.097 \pm 0.002$	$0.188 \pm 0.003$	$0.263 \pm 0.005$	$0.328 \pm 0.007$
$36 \leq \text{nForwardTracks} < 48$					
$p_T$ ( GeV/c )	0-2	2-4	4-6	6-8	8-20
$2.0 < y < 2.8$	$0.029 \pm 0.001$	$0.054 \pm 0.001$	$0.126 \pm 0.002$	$0.204 \pm 0.004$	$0.317 \pm 0.005$
$2.8 < y < 3.5$	$0.070 \pm 0.002$	$0.118 \pm 0.002$	$0.222 \pm 0.003$	$0.325 \pm 0.006$	$0.400 \pm 0.006$
$3.5 < y < 4.5$	$0.063 \pm 0.002$	$0.096 \pm 0.002$	$0.184 \pm 0.003$	$0.253 \pm 0.006$	$0.335 \pm 0.007$
$48 \leq \text{nForwardTracks} < 130$					
$p_T$ ( GeV/c )	0-2	2-4	4-6	6-8	8-20
$2.0 < y < 2.8$	$0.028 \pm 0.001$	$0.054 \pm 0.001$	$0.126 \pm 0.003$	$0.202 \pm 0.005$	$0.309 \pm 0.006$
$2.8 < y < 3.5$	$0.063 \pm 0.002$	$0.110 \pm 0.002$	$0.225 \pm 0.004$	$0.309 \pm 0.006$	$0.382 \pm 0.007$
$3.5 < y < 4.5$	$0.060 \pm 0.002$	$0.094 \pm 0.002$	$0.173 \pm 0.004$	$0.247 \pm 0.006$	$0.306 \pm 0.007$

Table 94: The efficiency  $\epsilon_{\text{tot}}$  for  $\psi(2S)$  from b signals in different  $(p_T, y)$  bins.

$0 \leq n\text{ForwardTracks} < 12$					
$p_T$ ( GeV/c )	0-2	2-4	4-6	6-8	8-20
$2.0 < y < 2.8$	$0.067 \pm 0.002$	$0.067 \pm 0.001$	$0.117 \pm 0.003$	$0.184 \pm 0.005$	$0.263 \pm 0.006$
$2.8 < y < 3.5$	$0.157 \pm 0.003$	$0.154 \pm 0.003$	$0.246 \pm 0.004$	$0.326 \pm 0.007$	$0.422 \pm 0.009$
$3.5 < y < 4.5$	$0.136 \pm 0.003$	$0.126 \pm 0.003$	$0.197 \pm 0.004$	$0.266 \pm 0.008$	$0.345 \pm 0.011$
$12 \leq n\text{ForwardTracks} < 24$					
$p_T$ ( GeV/c )	0-2	2-4	4-6	6-8	8-20
$2.0 < y < 2.8$	$0.068 \pm 0.001$	$0.070 \pm 0.001$	$0.116 \pm 0.002$	$0.183 \pm 0.003$	$0.266 \pm 0.004$
$2.8 < y < 3.5$	$0.159 \pm 0.002$	$0.157 \pm 0.002$	$0.249 \pm 0.003$	$0.329 \pm 0.004$	$0.413 \pm 0.005$
$3.5 < y < 4.5$	$0.137 \pm 0.002$	$0.127 \pm 0.002$	$0.188 \pm 0.003$	$0.251 \pm 0.004$	$0.329 \pm 0.006$
$24 \leq n\text{ForwardTracks} < 36$					
$p_T$ ( GeV/c )	0-2	2-4	4-6	6-8	8-20
$2.0 < y < 2.8$	$0.067 \pm 0.001$	$0.070 \pm 0.001$	$0.115 \pm 0.002$	$0.181 \pm 0.003$	$0.269 \pm 0.004$
$2.8 < y < 3.5$	$0.158 \pm 0.002$	$0.152 \pm 0.002$	$0.245 \pm 0.003$	$0.321 \pm 0.004$	$0.408 \pm 0.004$
$3.5 < y < 4.5$	$0.135 \pm 0.002$	$0.123 \pm 0.002$	$0.186 \pm 0.003$	$0.250 \pm 0.004$	$0.322 \pm 0.005$
$36 \leq n\text{ForwardTracks} < 48$					
$p_T$ ( GeV/c )	0-2	2-4	4-6	6-8	8-20
$2.0 < y < 2.8$	$0.066 \pm 0.002$	$0.068 \pm 0.001$	$0.113 \pm 0.002$	$0.184 \pm 0.003$	$0.266 \pm 0.004$
$2.8 < y < 3.5$	$0.153 \pm 0.003$	$0.153 \pm 0.002$	$0.244 \pm 0.003$	$0.314 \pm 0.005$	$0.394 \pm 0.005$
$3.5 < y < 4.5$	$0.132 \pm 0.002$	$0.123 \pm 0.002$	$0.180 \pm 0.003$	$0.246 \pm 0.005$	$0.313 \pm 0.006$
$48 \leq n\text{ForwardTracks} < 130$					
$p_T$ ( GeV/c )	0-2	2-4	4-6	6-8	8-20
$2.0 < y < 2.8$	$0.064 \pm 0.002$	$0.065 \pm 0.001$	$0.109 \pm 0.002$	$0.174 \pm 0.004$	$0.261 \pm 0.004$
$2.8 < y < 3.5$	$0.152 \pm 0.003$	$0.147 \pm 0.002$	$0.237 \pm 0.003$	$0.303 \pm 0.005$	$0.385 \pm 0.005$
$3.5 < y < 4.5$	$0.125 \pm 0.003$	$0.119 \pm 0.002$	$0.180 \pm 0.003$	$0.238 \pm 0.005$	$0.304 \pm 0.006$

## 713 D Fitting plots in each kinematic bin

### 714 1 Separated by PVNTRACKS

715 For each kinematic bin of  $J/\psi$  and  $\psi(2S)$  candidates, the two-dimensional fit to the  
 716 invariant mass and the lifetime are shown below. The left is the invariant mass and the  
 717 right is pseudo-proper decay time fit results. The first row in each figure set is that of  $J/\psi$   
 718 and the second row is that of  $\psi(2S)$ .

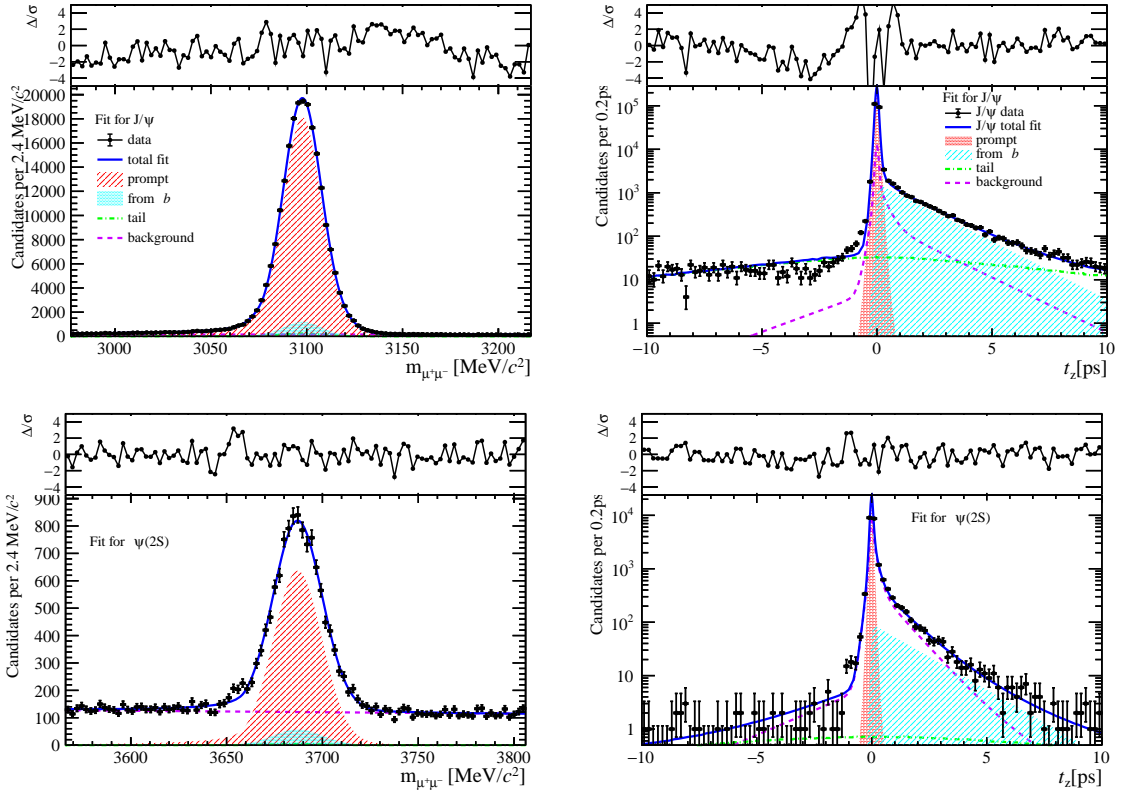


Figure 36: Fit results in  $0 \text{ GeV}/c < p_T < 2 \text{ GeV}/c$ ,  $2.0 < y < 2.8$  and  $0 \leq \text{PVNTRACKS} < 20$ .

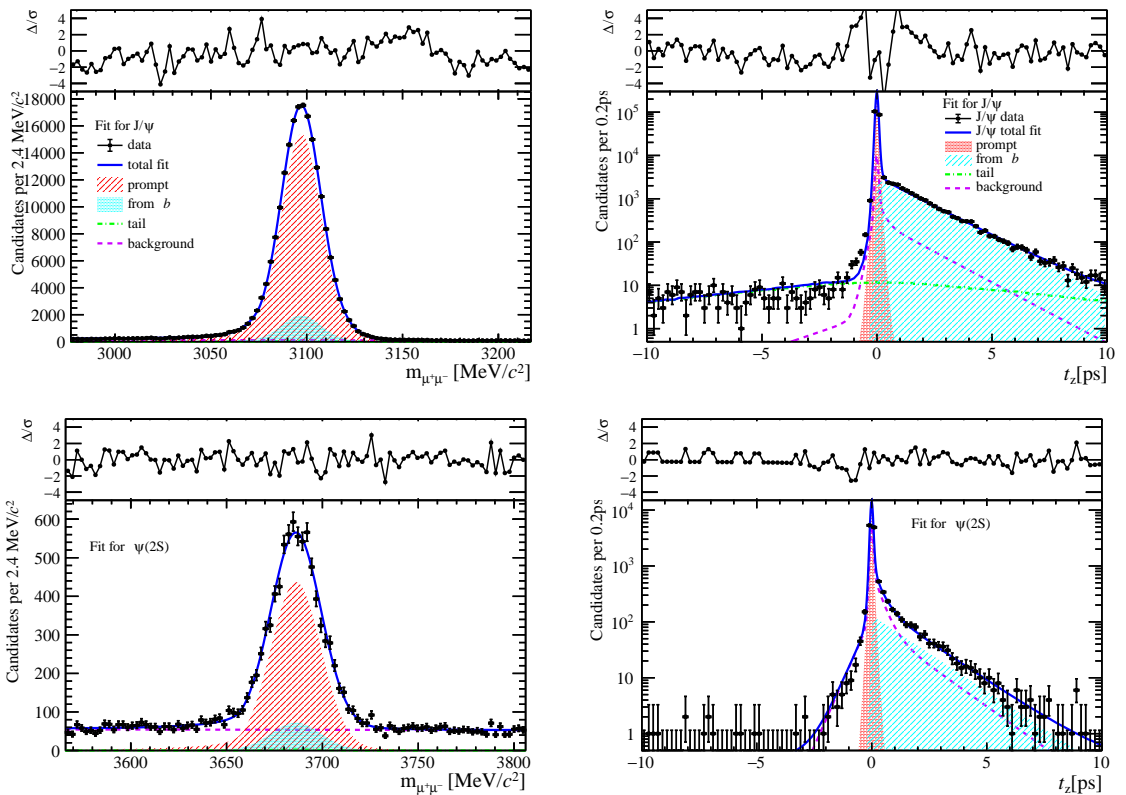


Figure 37: Fit results in  $2 \text{ GeV}/c < p_T < 4 \text{ GeV}/c$ ,  $2.0 < y < 2.8$  and  $0 \leq \text{PVNTRACKS} < 20$ .

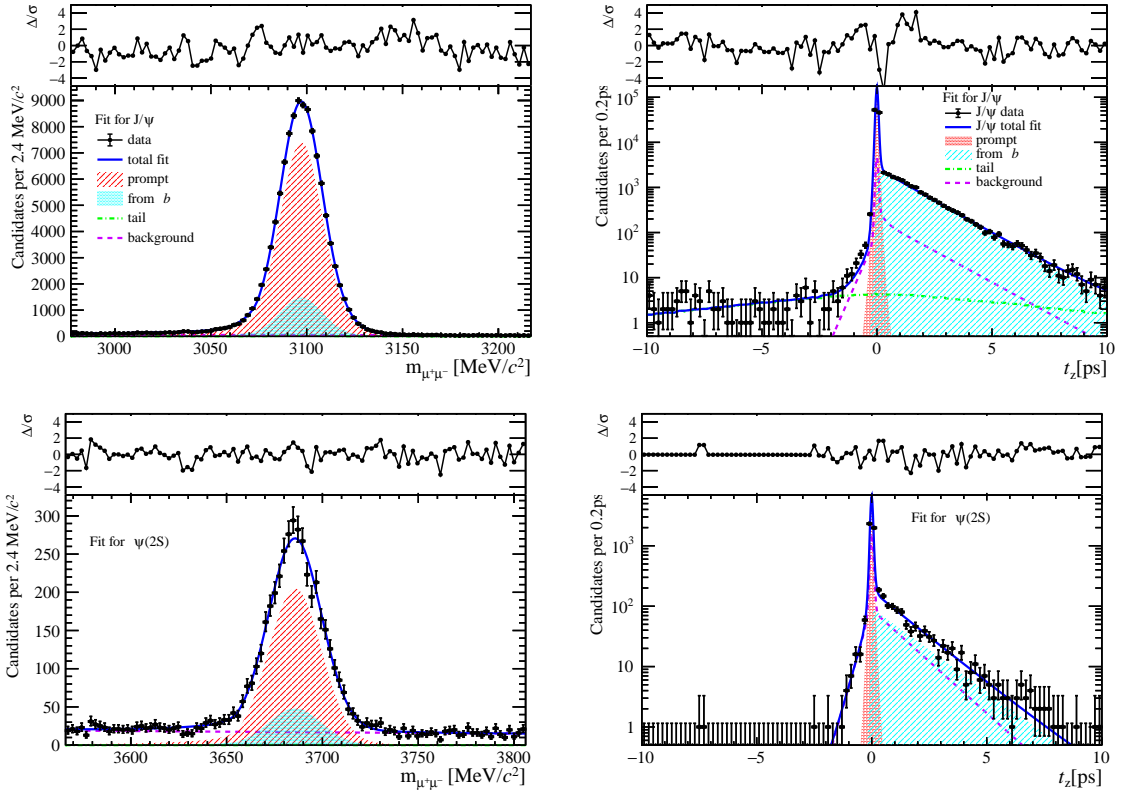


Figure 38: Fit results in  $4 \text{ GeV}/c < p_T < 6 \text{ GeV}/c$ ,  $2.0 < y < 2.8$  and  $0 \leq \text{PVNTRACKS} < 20$ .

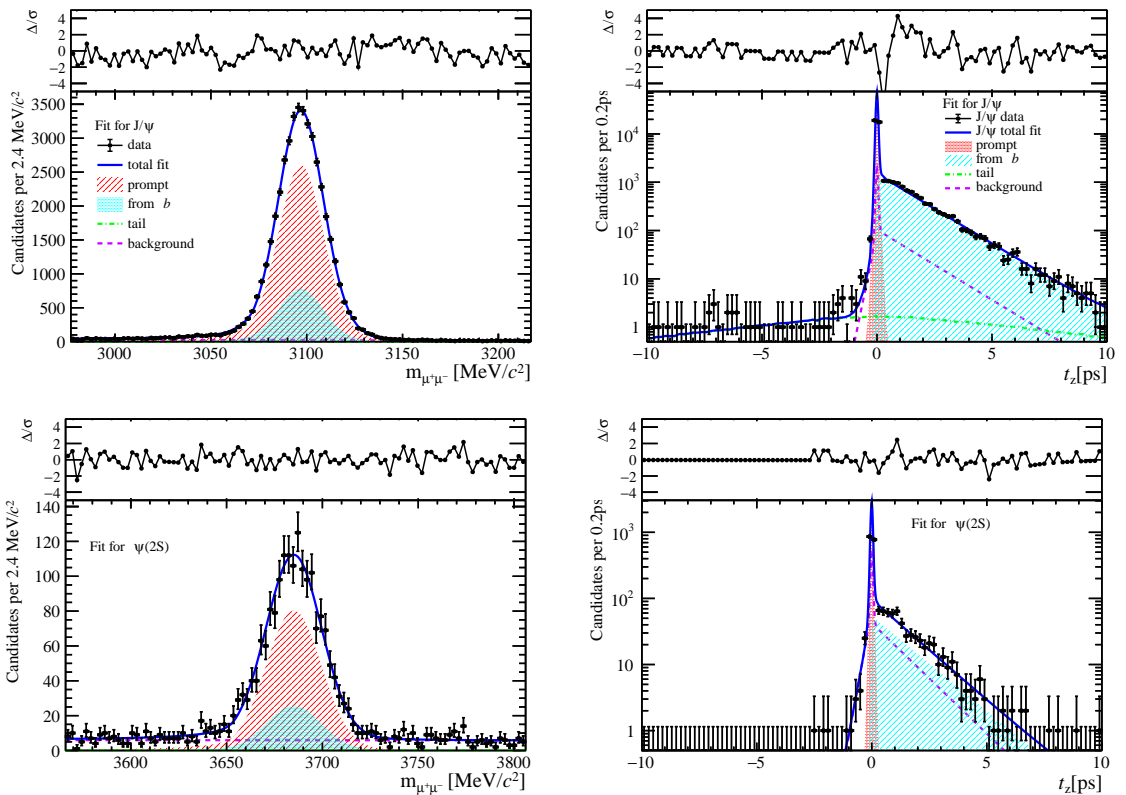


Figure 39: Fit results in  $6 \text{ GeV}/c < p_T < 8 \text{ GeV}/c$ ,  $2.0 < y < 2.8$  and  $0 \leq \text{PVNTRACKS} < 20$ .

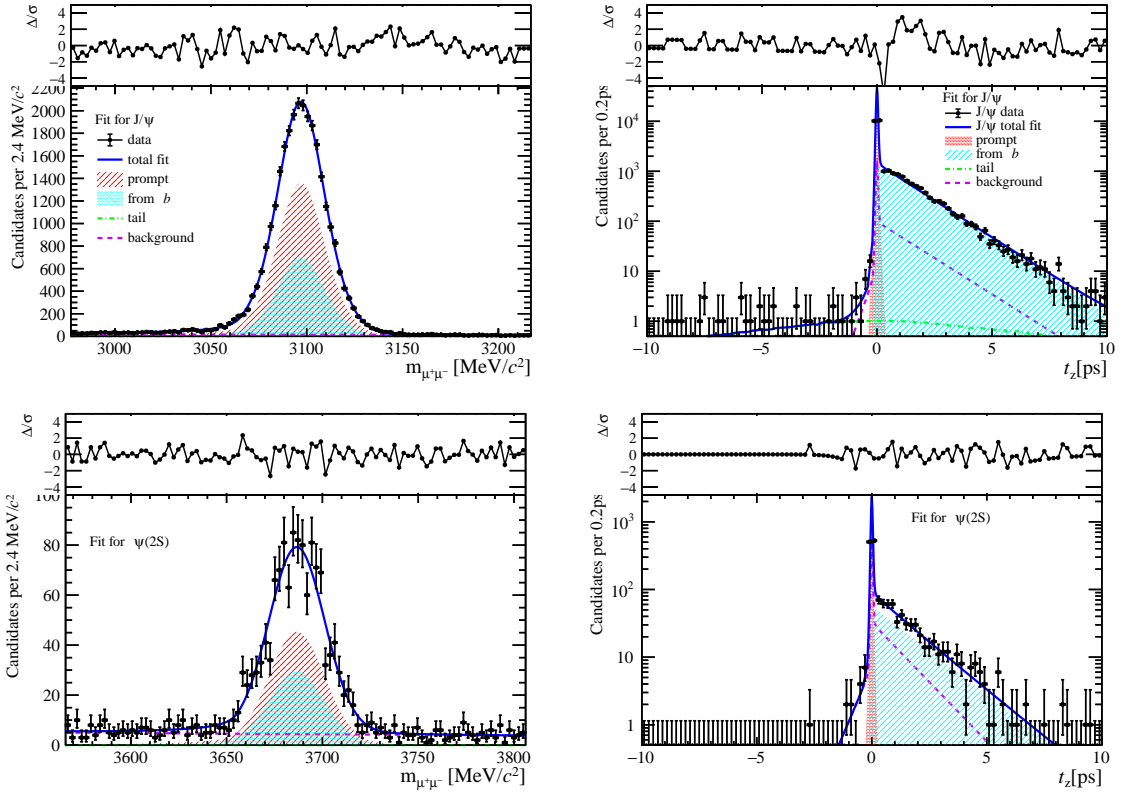


Figure 40: Fit results in  $8 \text{ GeV}/c < p_T < 20 \text{ GeV}/c$ ,  $2.0 < y < 2.8$  and  $0 \leq \text{PVNTRACKS} < 20$ .

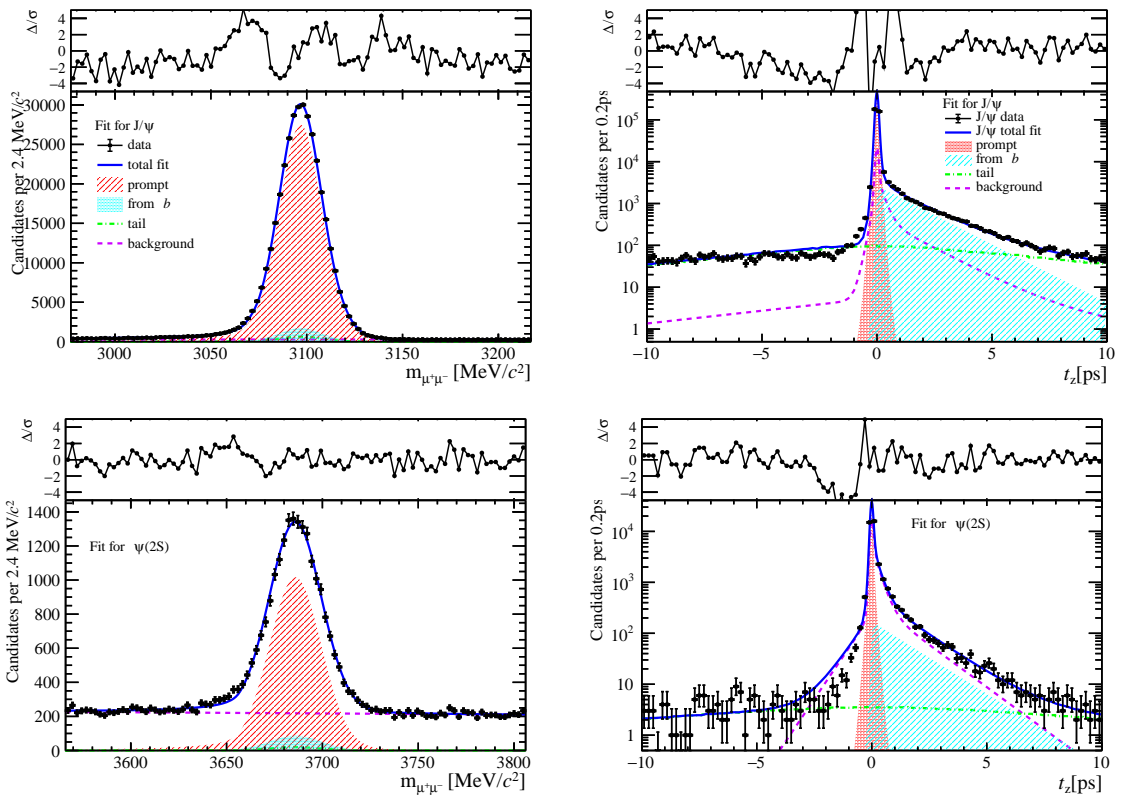


Figure 41: Fit results in  $0 \text{ GeV}/c < p_T < 2 \text{ GeV}/c$ ,  $2.8 < y < 3.5$  and  $0 \leq \text{PVNTRACKS} < 20$ .

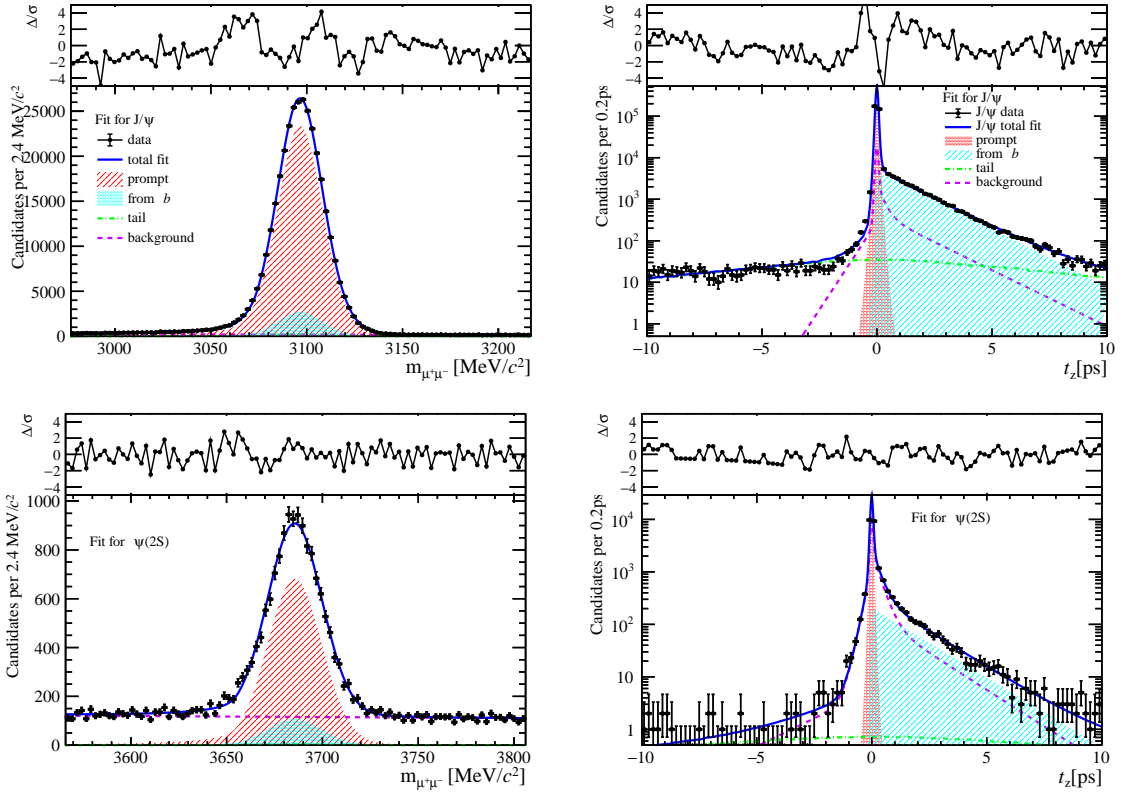


Figure 42: Fit results in  $2 \text{ GeV}/c < p_T < 4 \text{ GeV}/c$ ,  $2.8 < y < 3.5$  and  $0 \leq \text{PVNTRACKS} < 20$ .

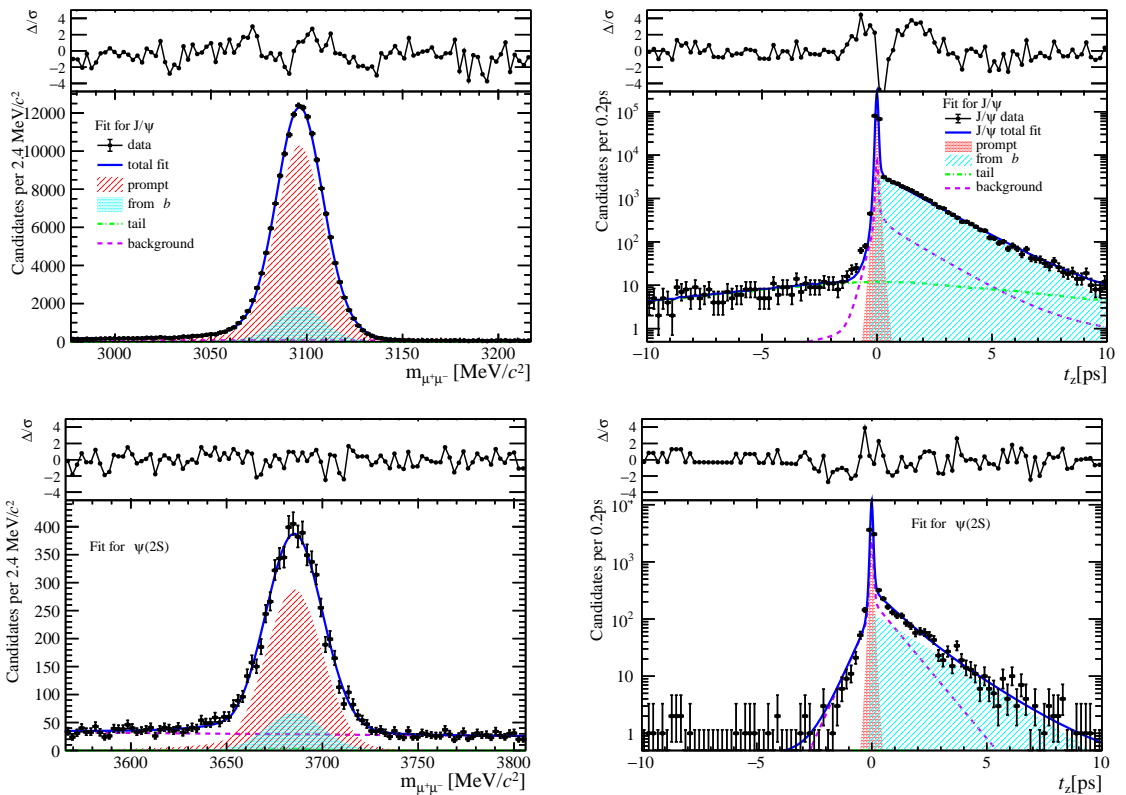


Figure 43: Fit results in  $4 \text{ GeV}/c < p_T < 6 \text{ GeV}/c$ ,  $2.8 < y < 3.5$  and  $0 \leq \text{PVNTRACKS} < 20$ .

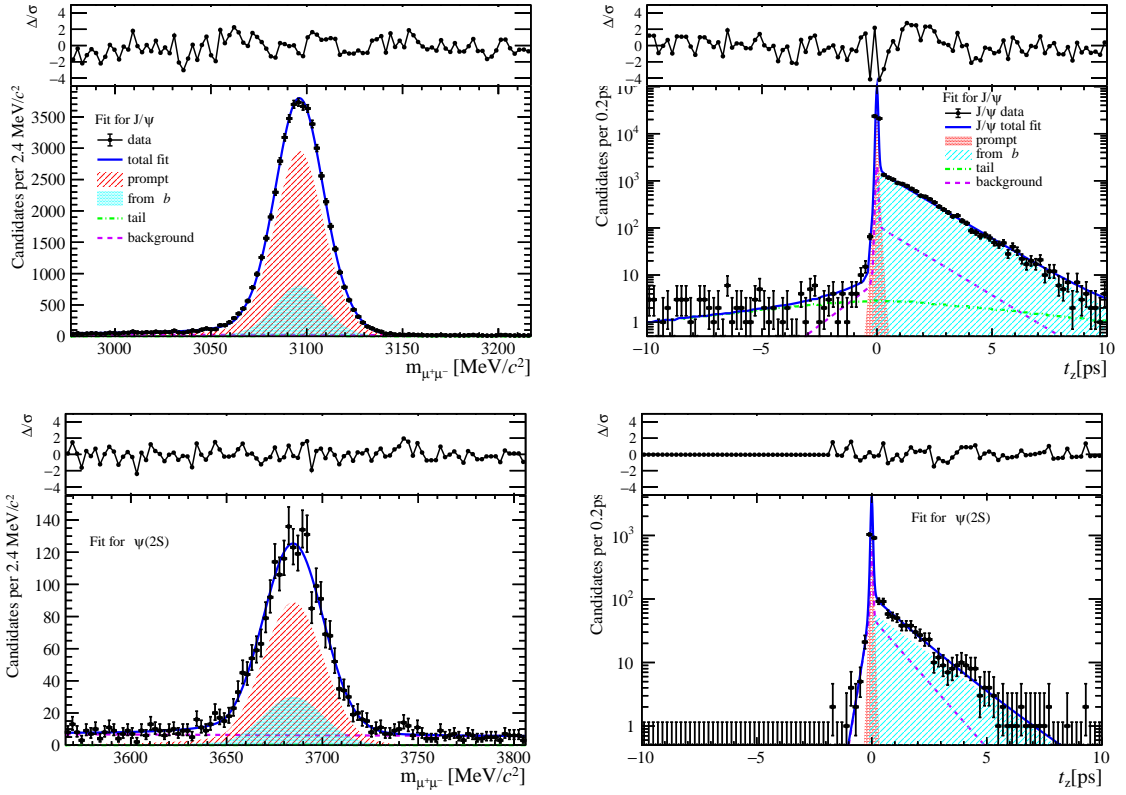


Figure 44: Fit results in  $6 \text{ GeV}/c < p_T < 8 \text{ GeV}/c$ ,  $2.8 < y < 3.5$  and  $0 \leq \text{PVNTRACKS} < 20$ .

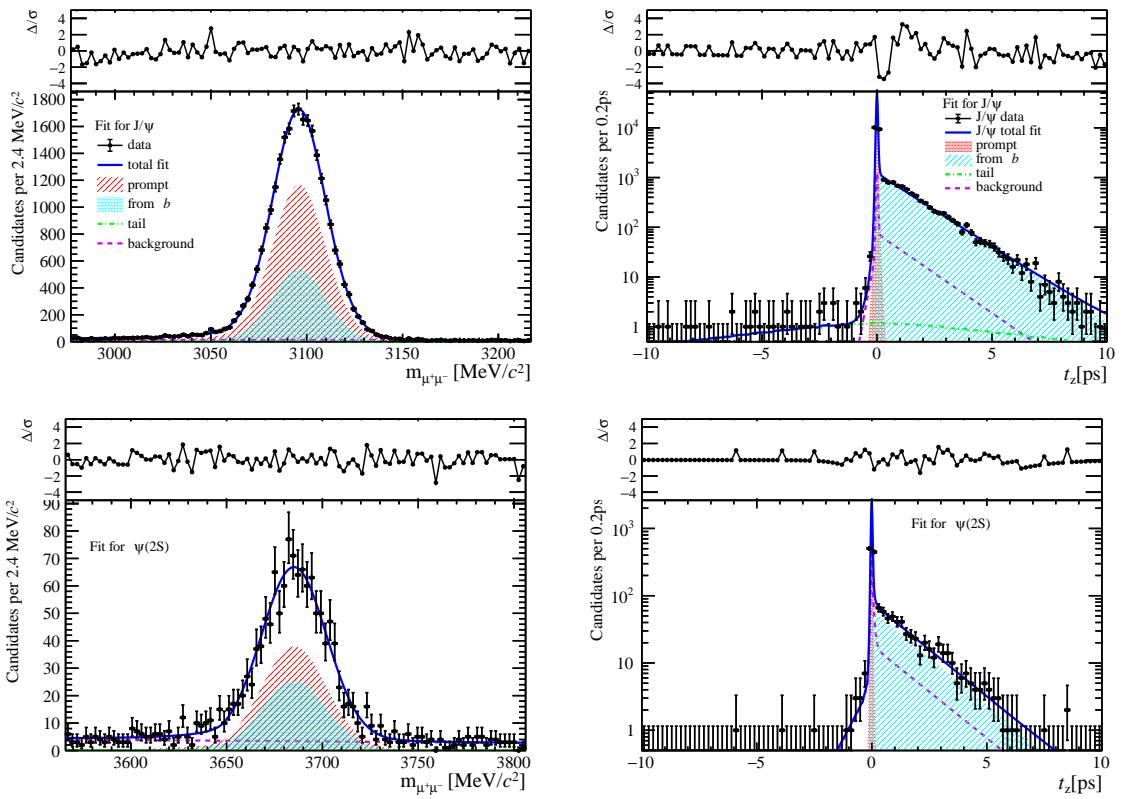


Figure 45: Fit results in  $8 \text{ GeV}/c < p_T < 20 \text{ GeV}/c$ ,  $2.8 < y < 3.5$  and  $0 \leq \text{PVNTRACKS} < 20$ .

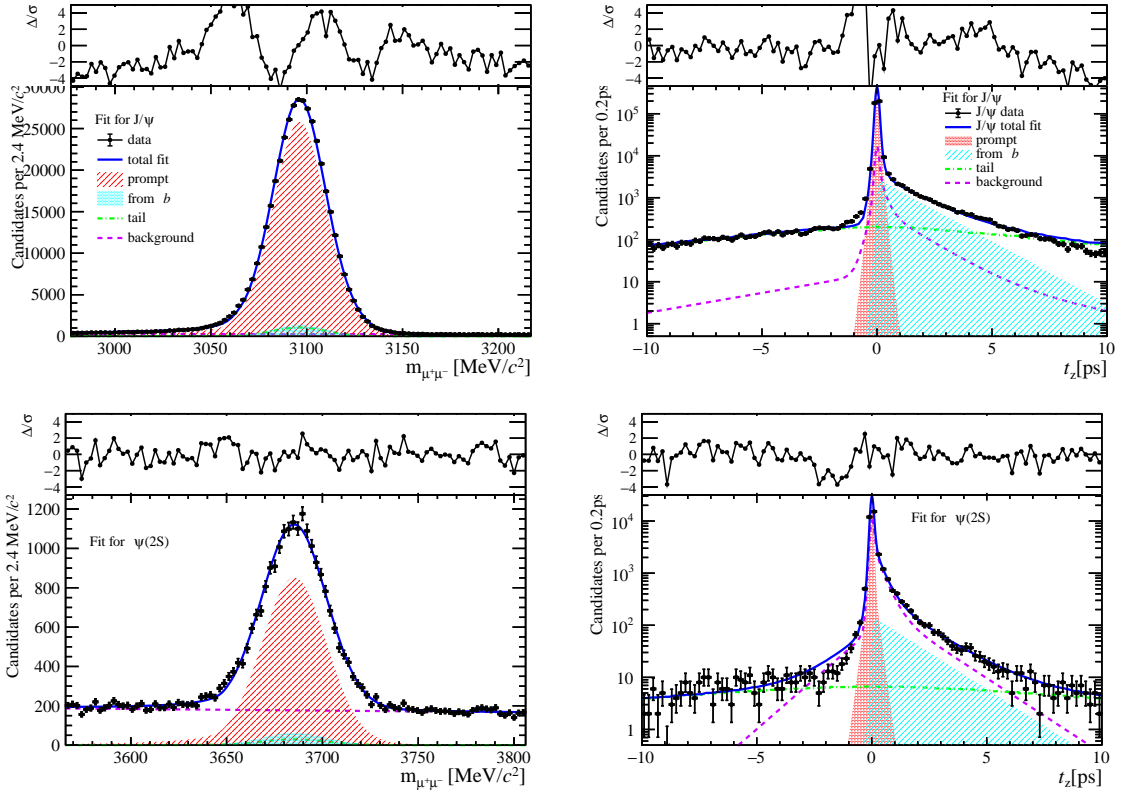


Figure 46: Fit results in  $0 \text{ GeV}/c < p_T < 2 \text{ GeV}/c$ ,  $3.5 < y < 4.5$  and  $0 \leq \text{PVNTRACKS} < 20$ .

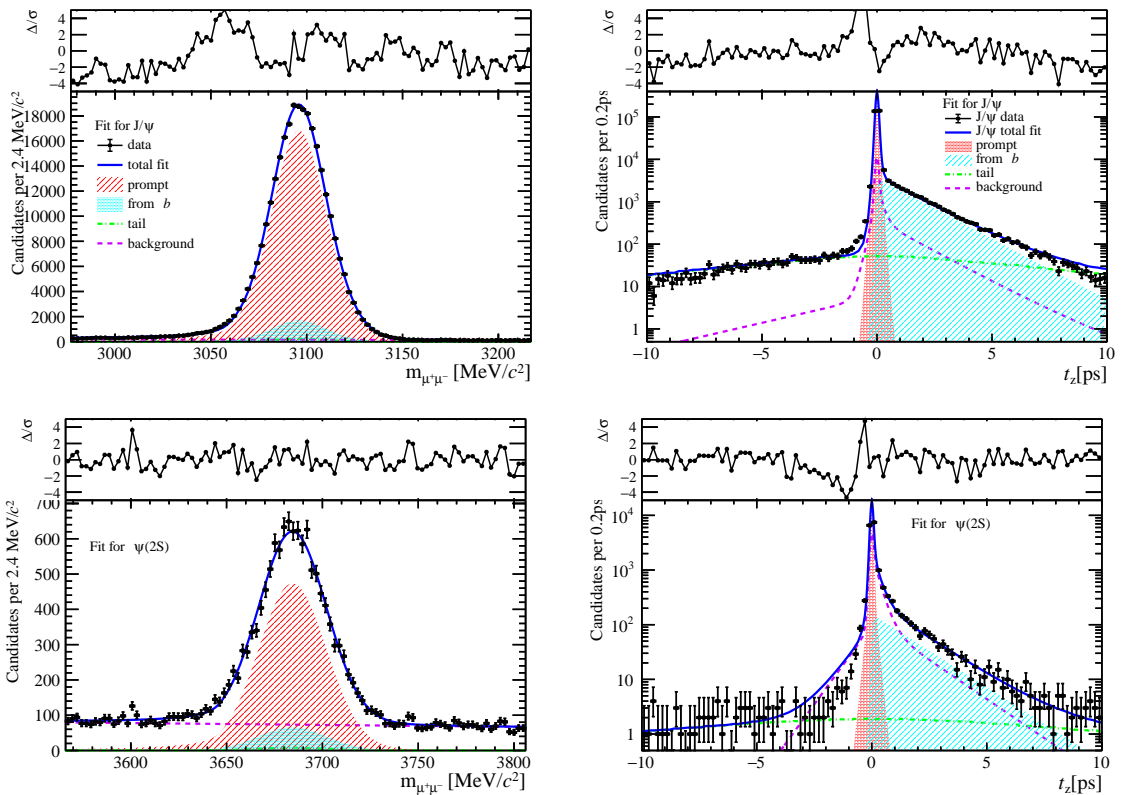


Figure 47: Fit results in  $2 \text{ GeV}/c < p_T < 4 \text{ GeV}/c$ ,  $3.5 < y < 4.5$  and  $0 \leq \text{PVNTRACKS} < 20$ .

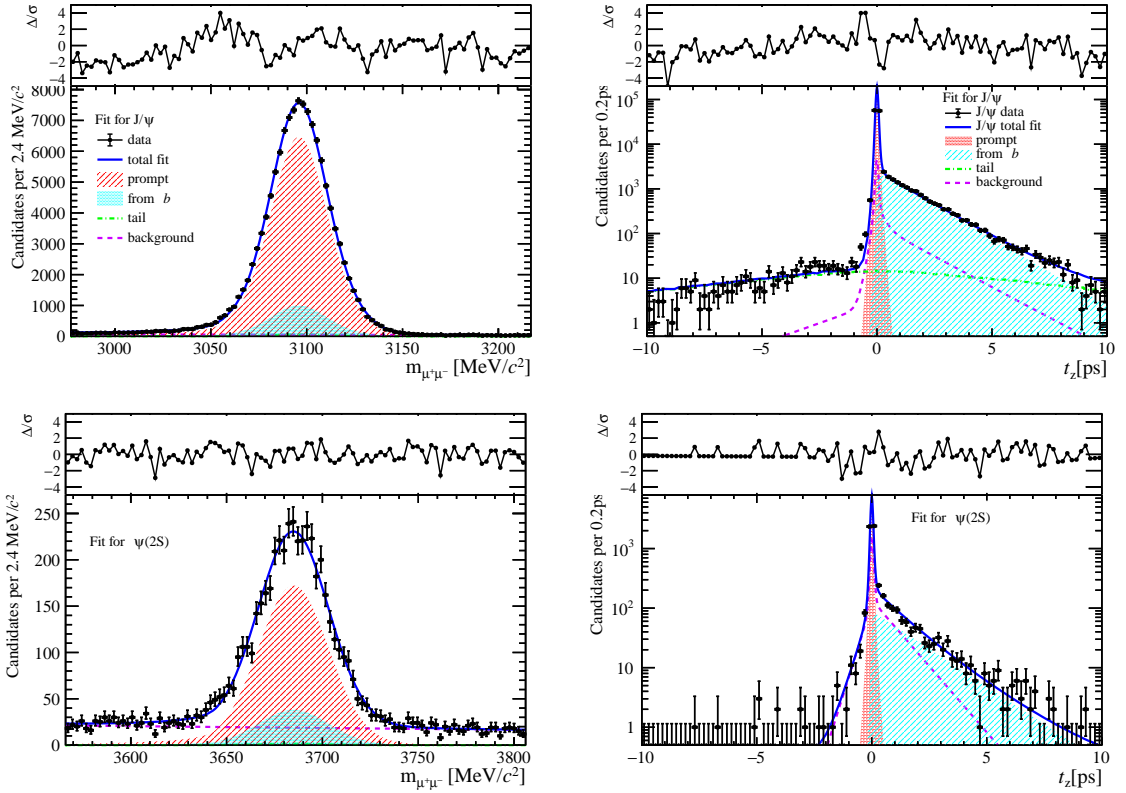


Figure 48: Fit results in  $4 \text{ GeV}/c < p_T < 6 \text{ GeV}/c$ ,  $3.5 < y < 4.5$  and  $0 \leq \text{PVNTRACKS} < 20$ .

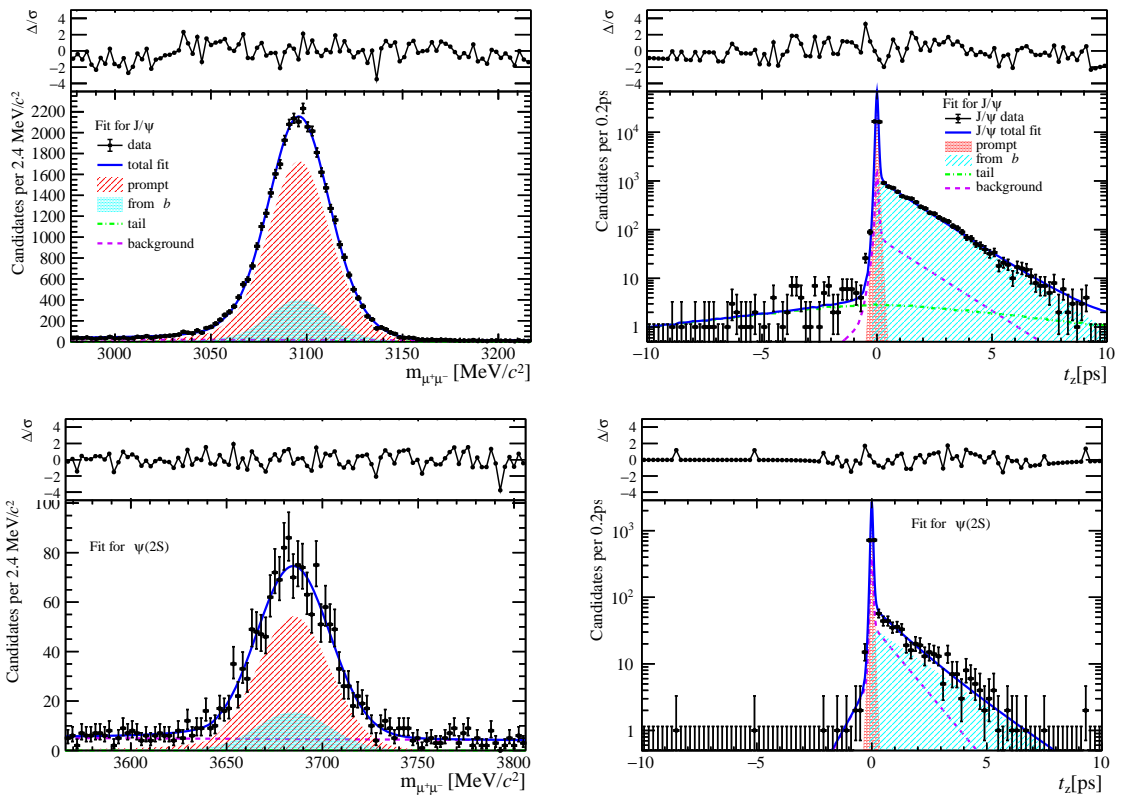


Figure 49: Fit results in  $6 \text{ GeV}/c < p_T < 8 \text{ GeV}/c$ ,  $3.5 < y < 4.5$  and  $0 \leq \text{PVNTRACKS} < 20$ .

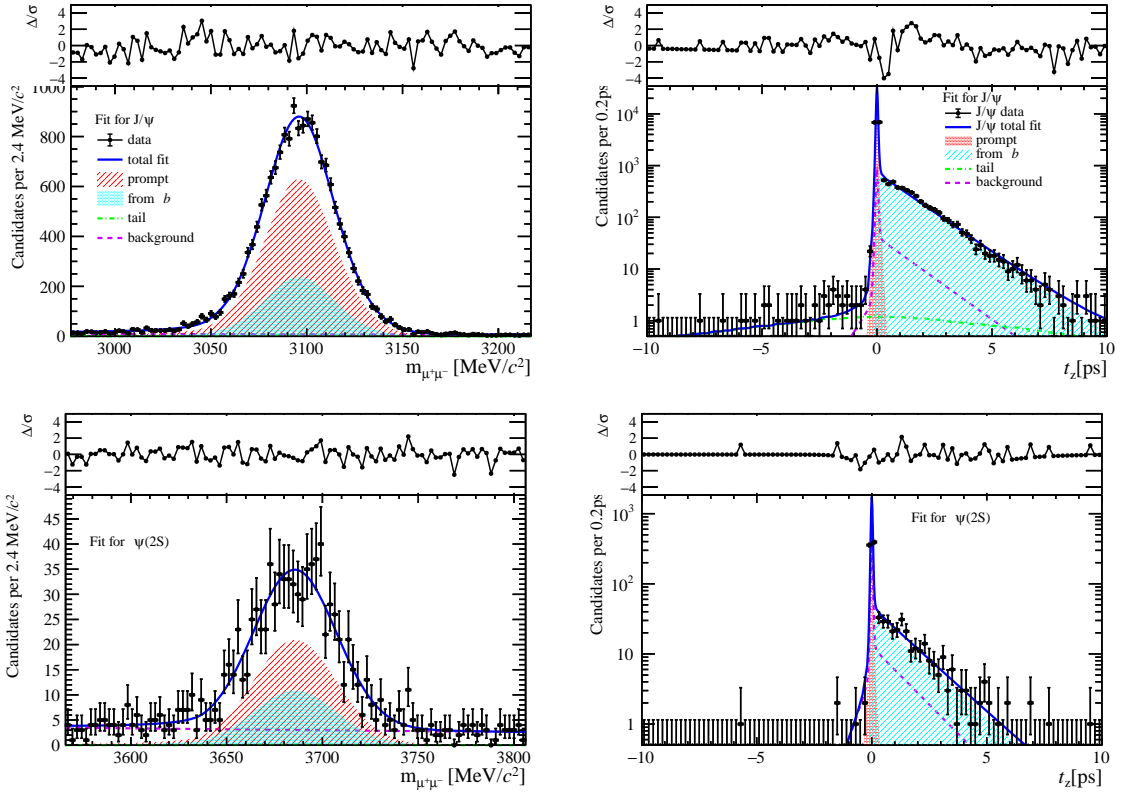


Figure 50: Fit results in  $8 \text{ GeV}/c < p_T < 20 \text{ GeV}/c$ ,  $3.5 < y < 4.5$  and  $0 \leq \text{PVNTRACKS} < 20$ .

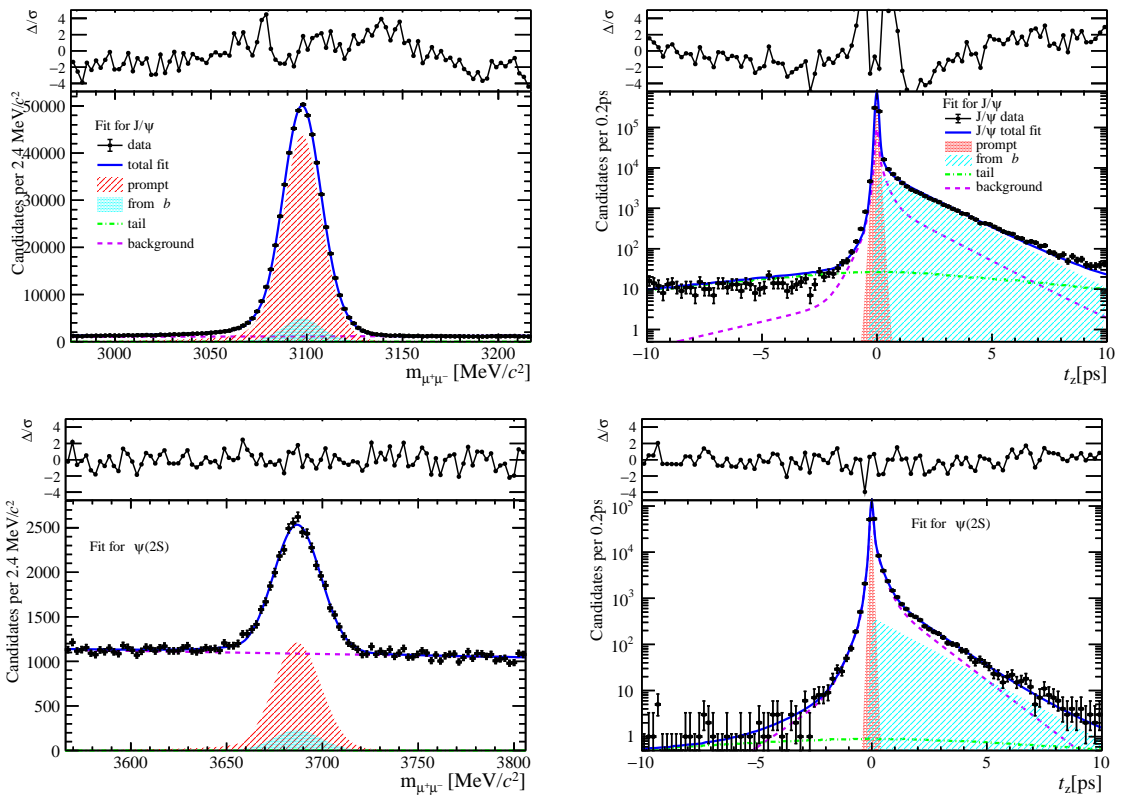


Figure 51: Fit results in  $0 \text{ GeV}/c < p_T < 2 \text{ GeV}/c$ ,  $2.0 < y < 2.8$  and  $20 \leq \text{PVNTRACKS} < 45$ .

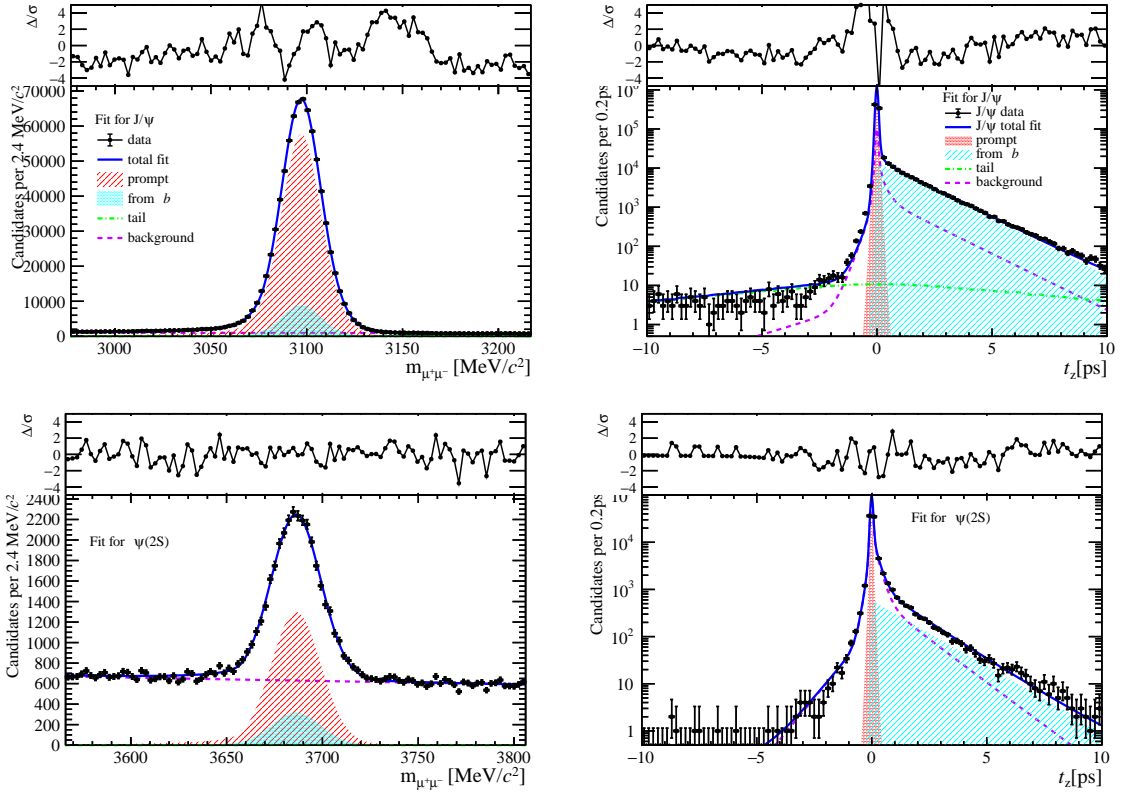


Figure 52: Fit results in  $2 \text{ GeV}/c < p_T < 4 \text{ GeV}/c$ ,  $2.0 < y < 2.8$  and  $20 \leq \text{PVNTRACKS} < 45$ .

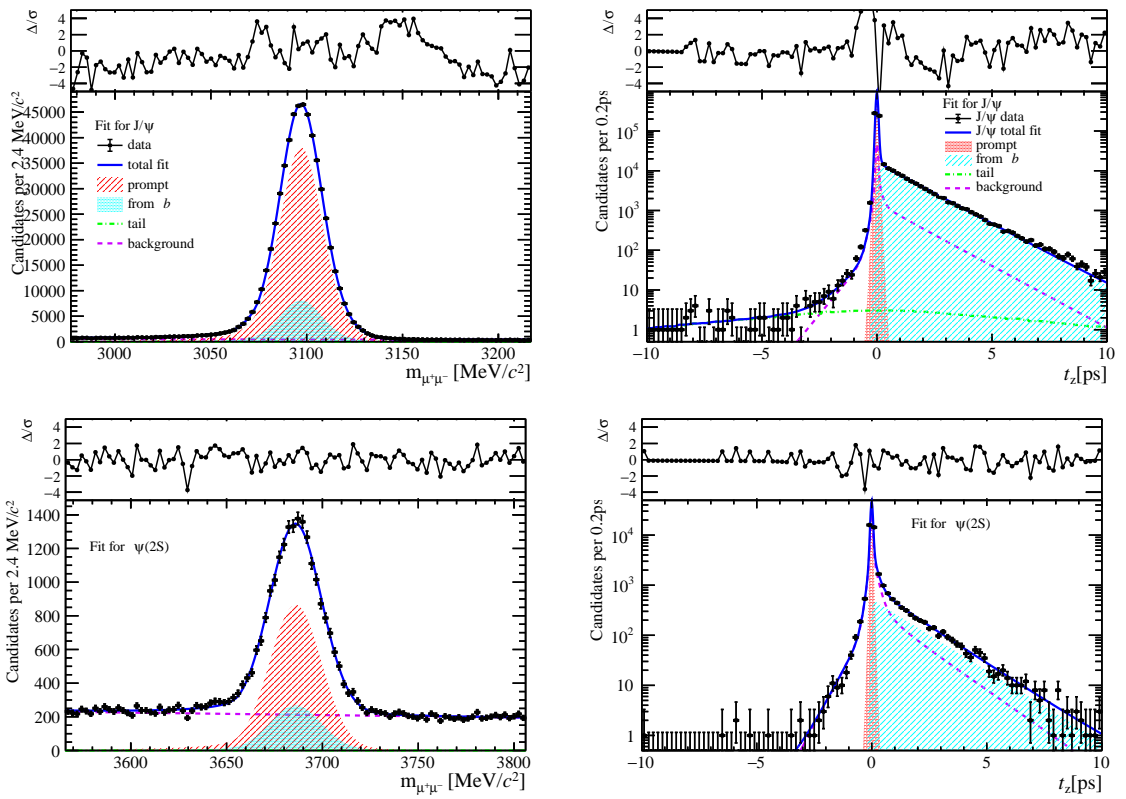


Figure 53: Fit results in  $4 \text{ GeV}/c < p_T < 6 \text{ GeV}/c$ ,  $2.0 < y < 2.8$  and  $20 \leq \text{PVNTRACKS} < 45$ .

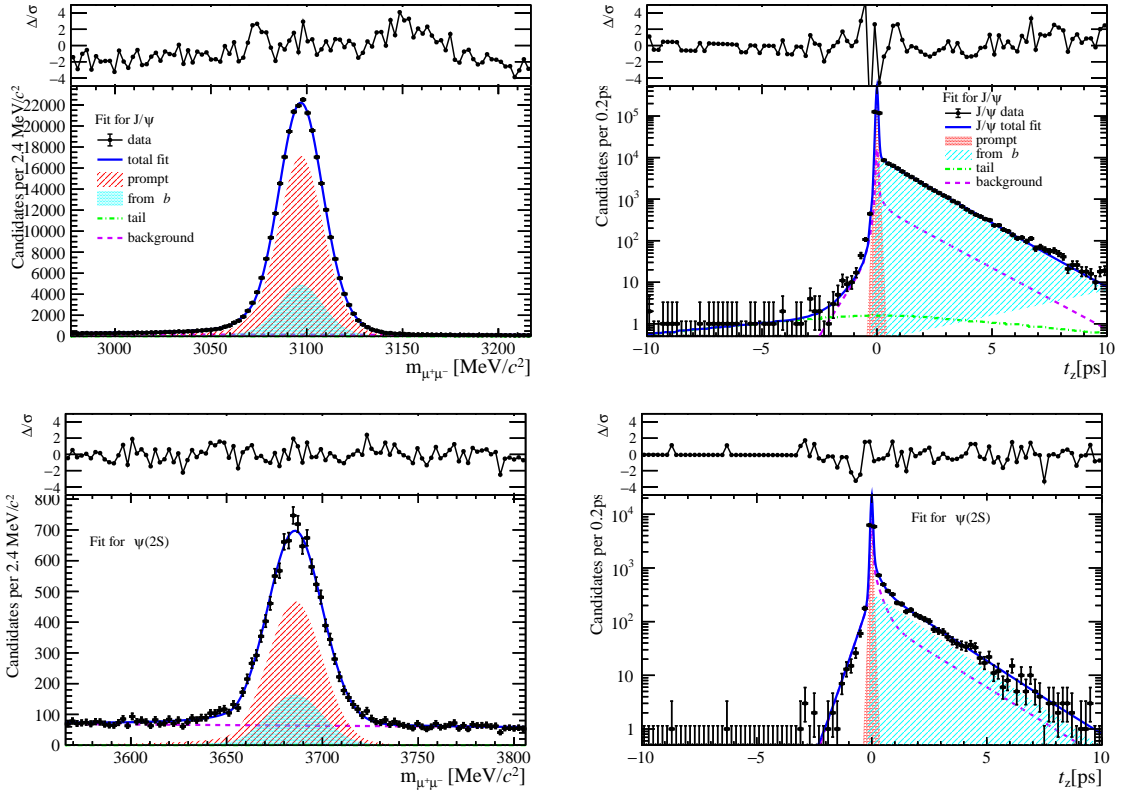


Figure 54: Fit results in  $6 \text{ GeV}/c < p_T < 8 \text{ GeV}/c$ ,  $2.0 < y < 2.8$  and  $20 \leq \text{PVNTRACKS} < 45$ .

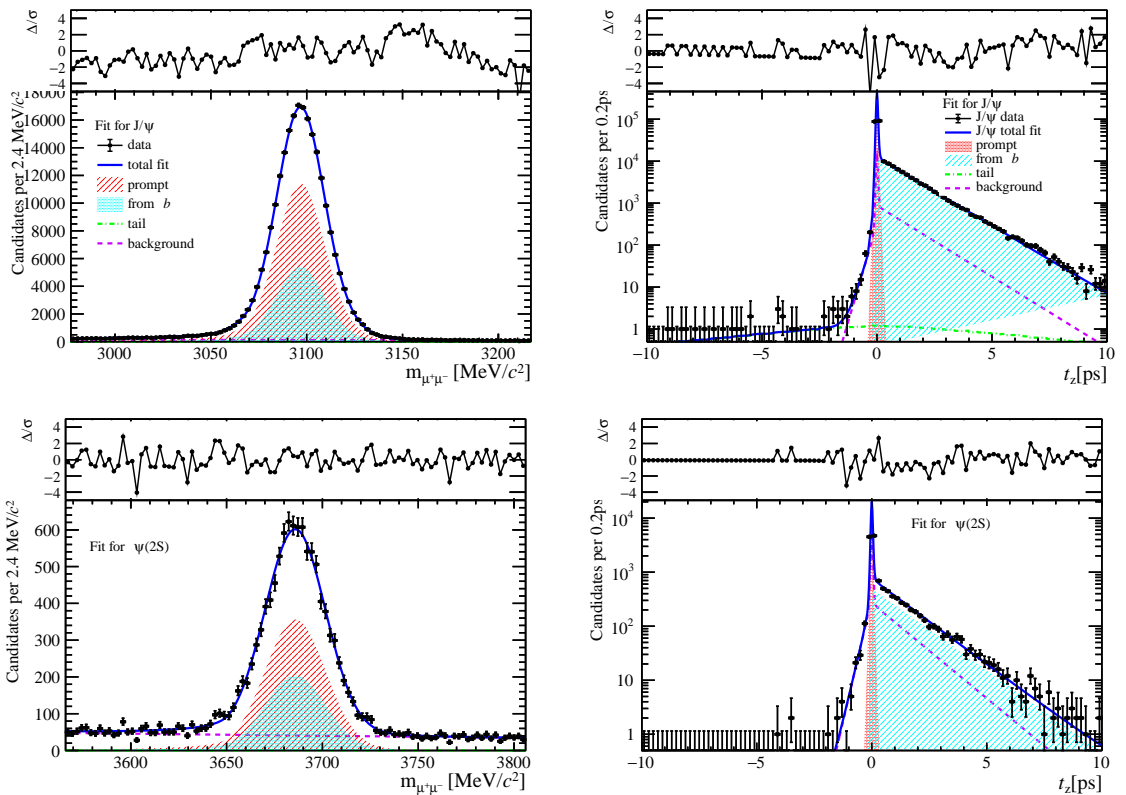


Figure 55: Fit results in  $8 \text{ GeV}/c < p_T < 20 \text{ GeV}/c$ ,  $2.0 < y < 2.8$  and  $20 \leq \text{PVNTRACKS} < 45$ .

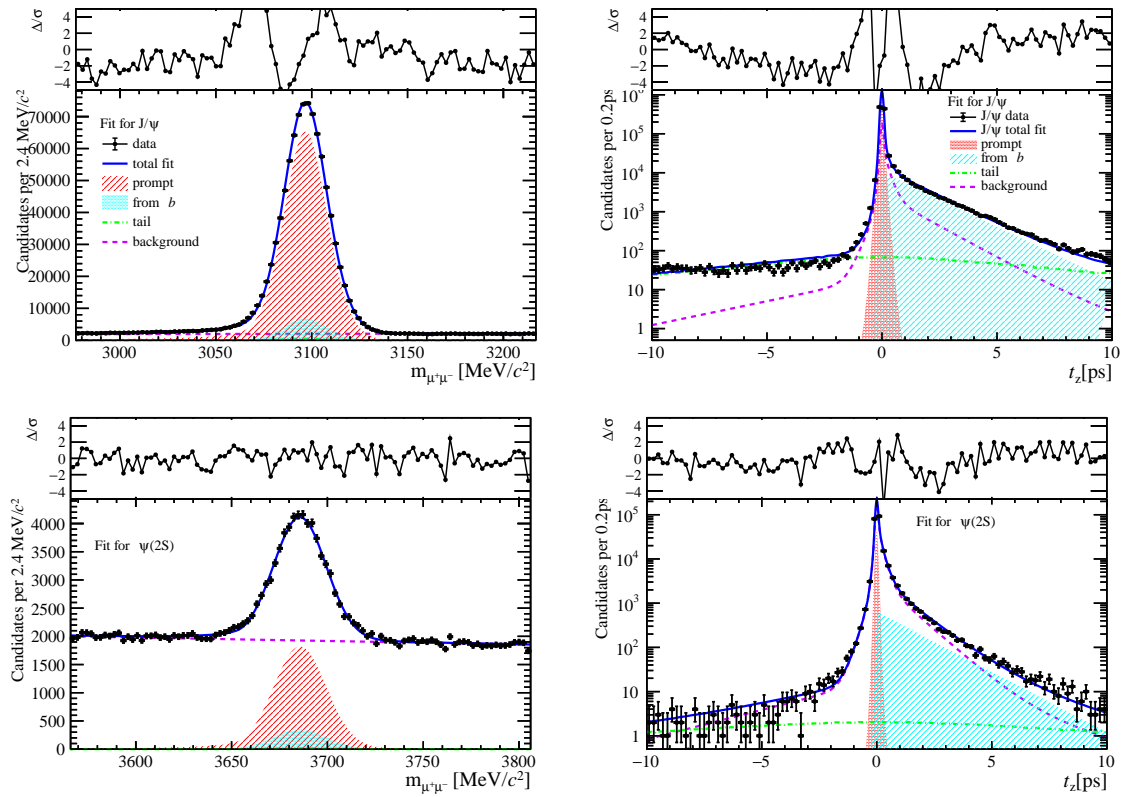


Figure 56: Fit results in  $0 \text{ GeV}/c < p_T < 2 \text{ GeV}/c$ ,  $2.8 < y < 3.5$  and  $20 \leq \text{PVNTRACKS} < 45$ .

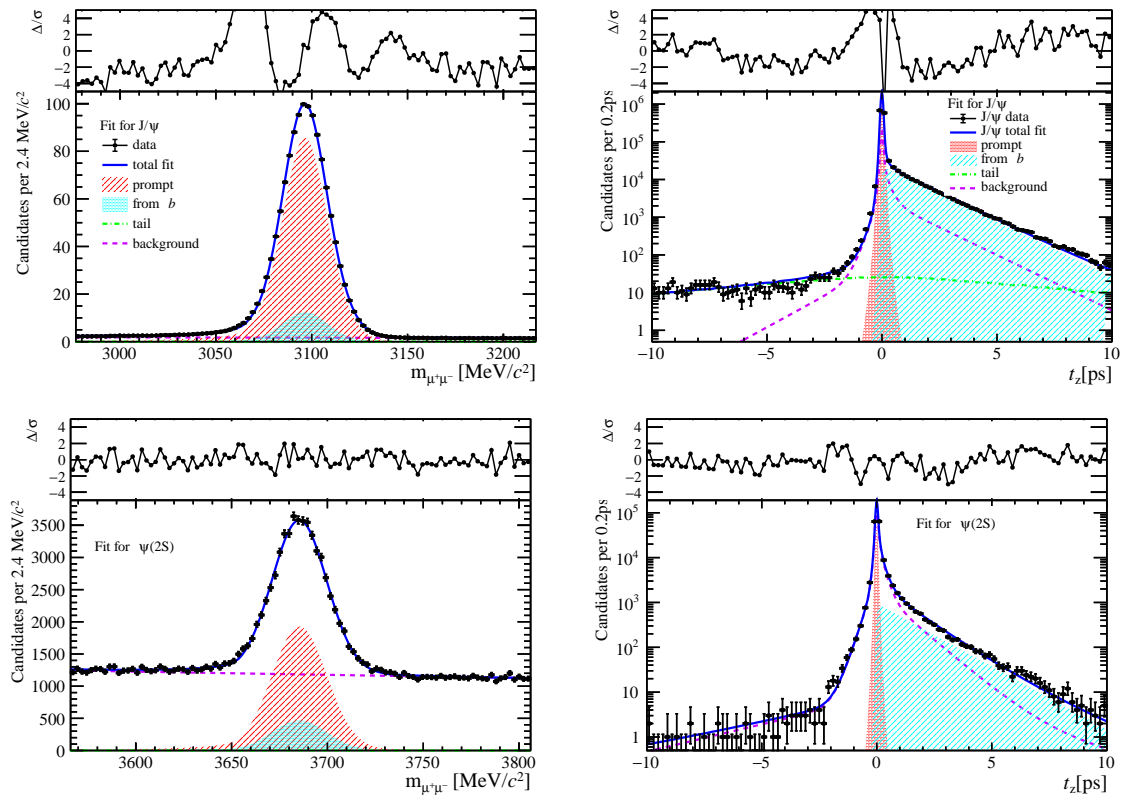


Figure 57: Fit results in  $2 \text{ GeV}/c < p_T < 4 \text{ GeV}/c$ ,  $2.8 < y < 3.5$  and  $20 \leq \text{PVNTRACKS} < 45$ .

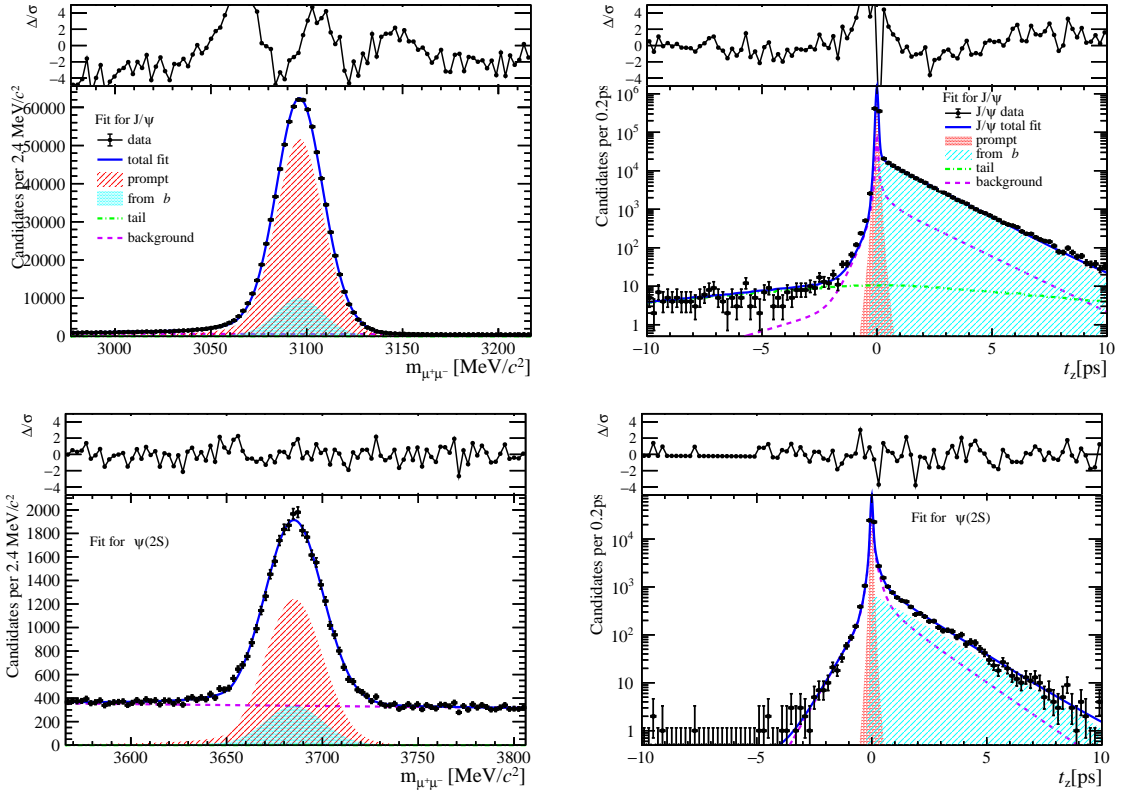


Figure 58: Fit results in  $4 \text{ GeV}/c < p_T < 6 \text{ GeV}/c$ ,  $2.8 < y < 3.5$  and  $20 \leq \text{PVNTRACKS} < 45$ .

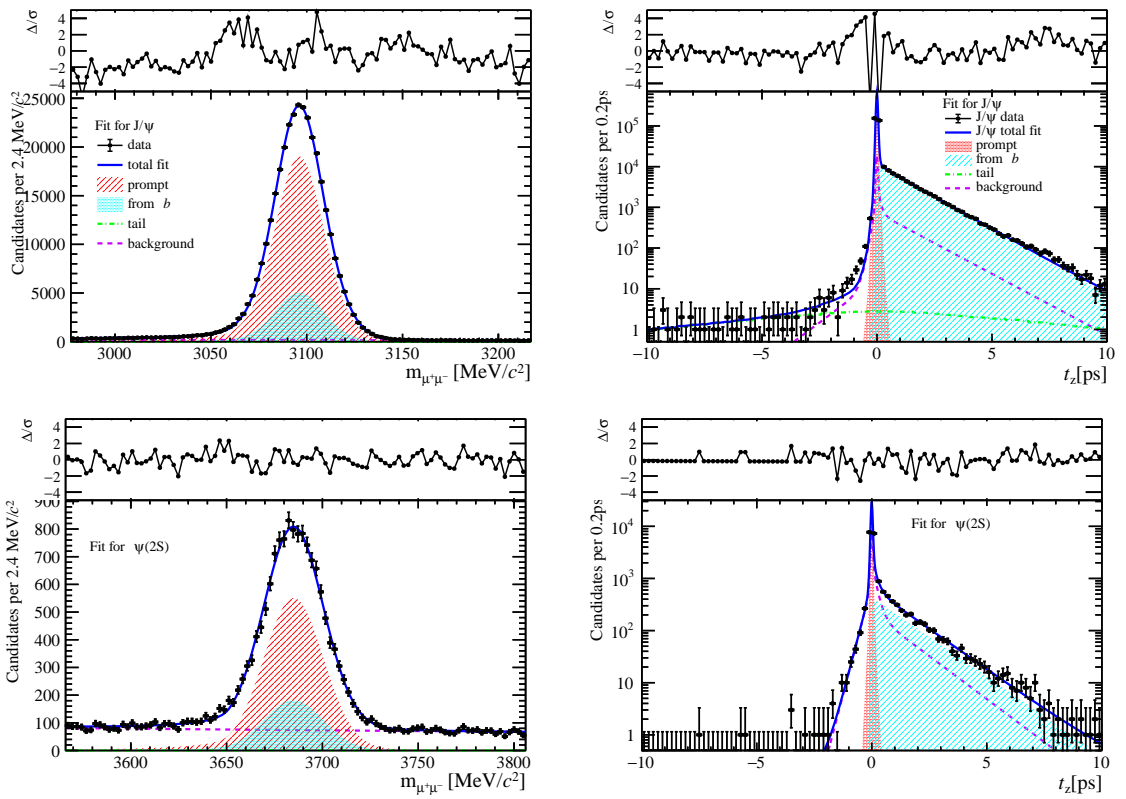


Figure 59: Fit results in  $6 \text{ GeV}/c < p_T < 8 \text{ GeV}/c$ ,  $2.8 < y < 3.5$  and  $20 \leq \text{PVNTRACKS} < 45$ .

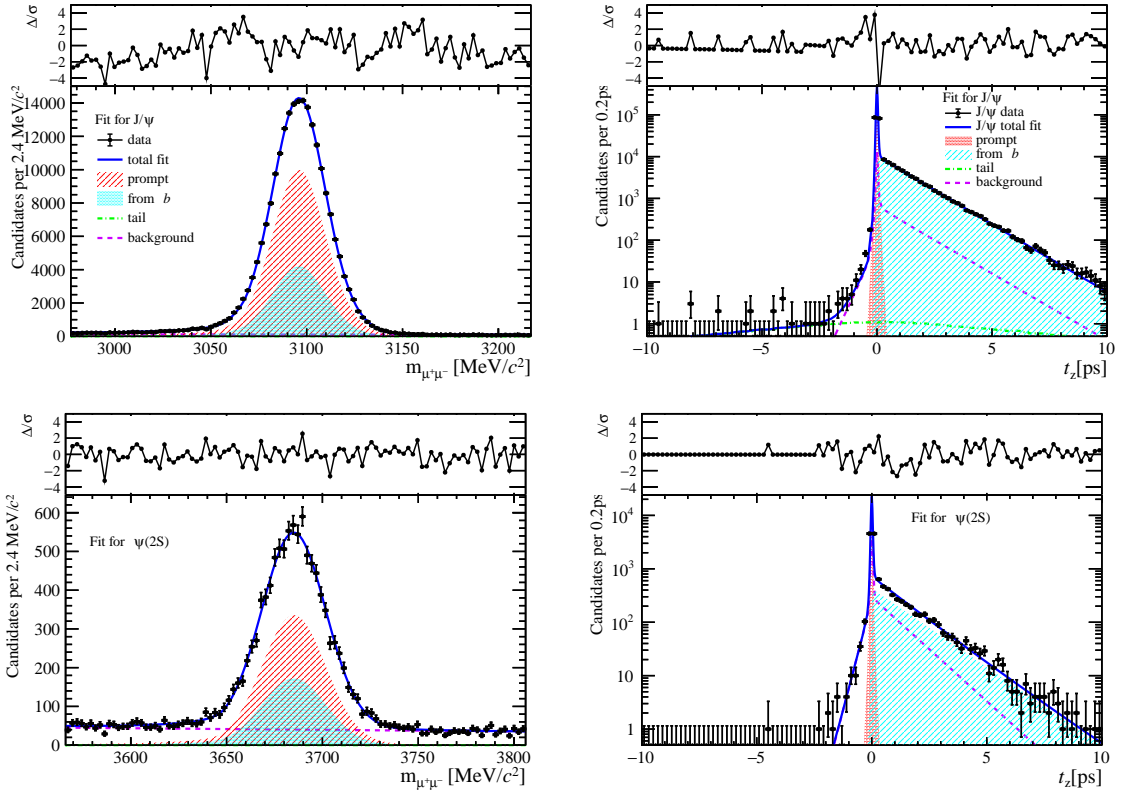


Figure 60: Fit results in  $8 \text{ GeV}/c < p_T < 20 \text{ GeV}/c$ ,  $2.8 < y < 3.5$  and  $20 \leq \text{PVNTRACKS} < 45$ .

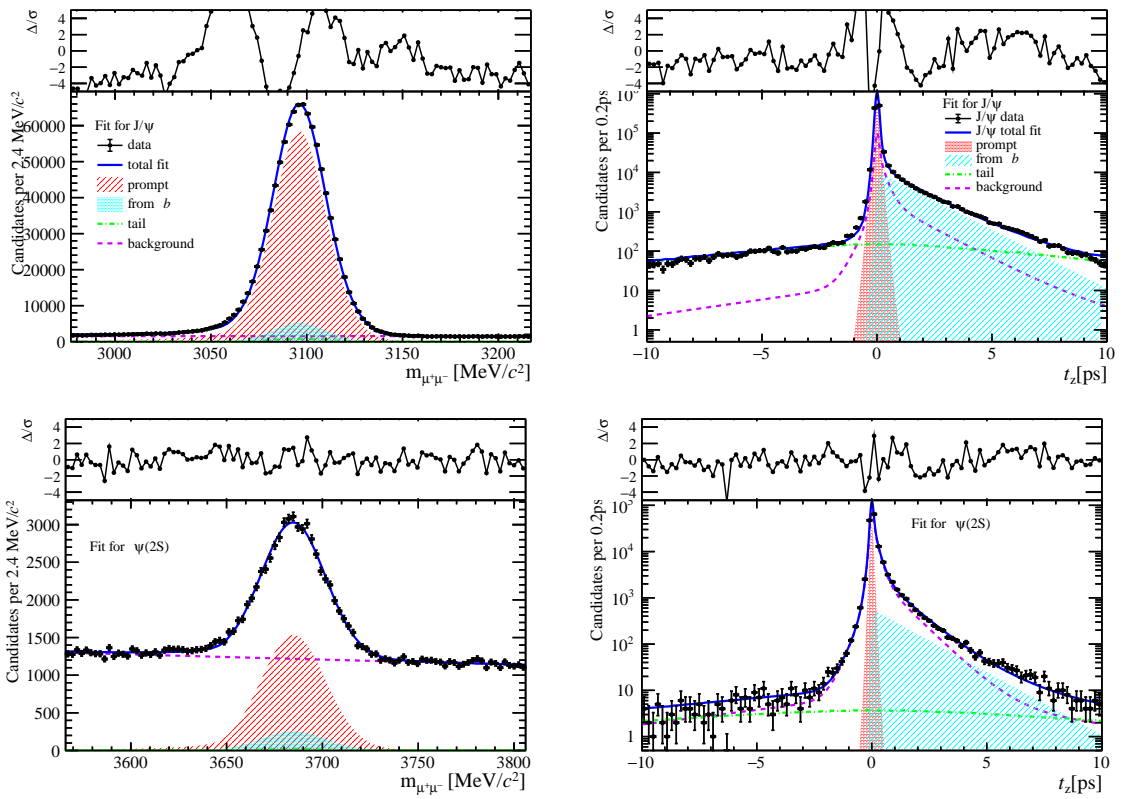


Figure 61: Fit results in  $0 \text{ GeV}/c < p_T < 2 \text{ GeV}/c$ ,  $3.5 < y < 4.5$  and  $20 \leq \text{PVNTRACKS} < 45$ .

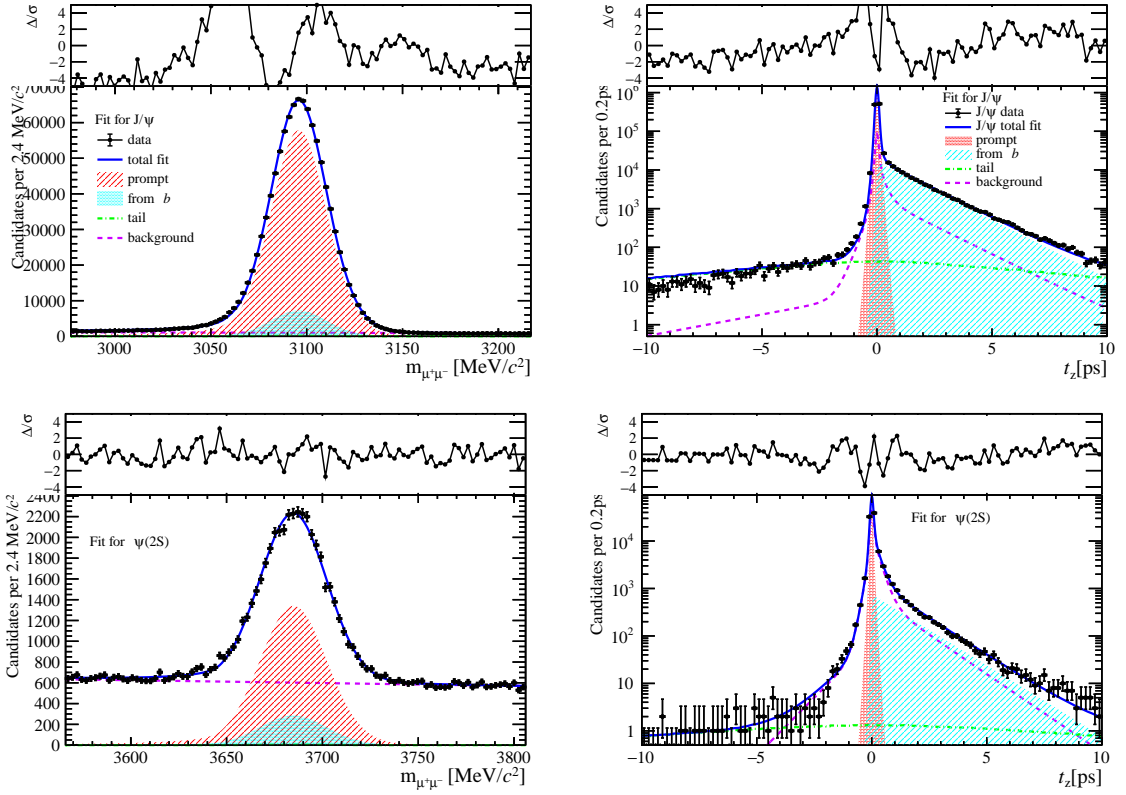


Figure 62: Fit results in  $2 \text{ GeV}/c < p_T < 4 \text{ GeV}/c$ ,  $3.5 < y < 4.5$  and  $20 \leq \text{PVNTRACKS} < 45$ .

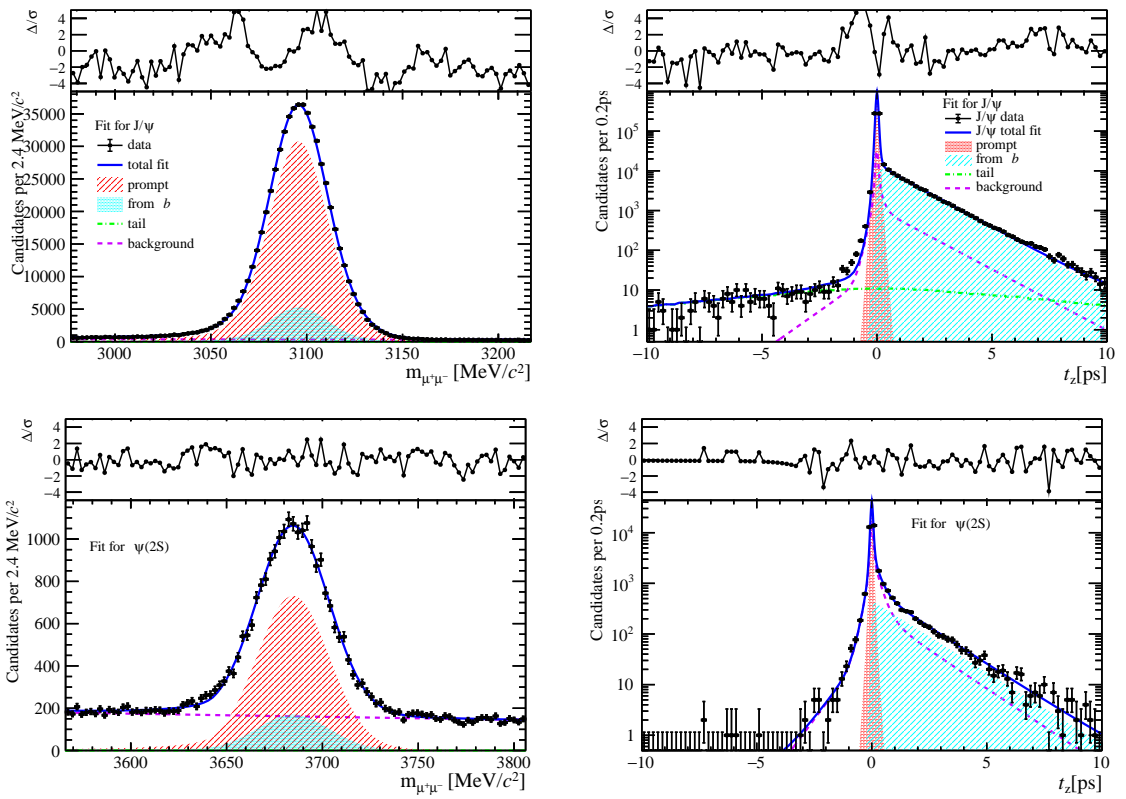


Figure 63: Fit results in  $4 \text{ GeV}/c < p_T < 6 \text{ GeV}/c$ ,  $3.5 < y < 4.5$  and  $20 \leq \text{PVNTRACKS} < 45$ .

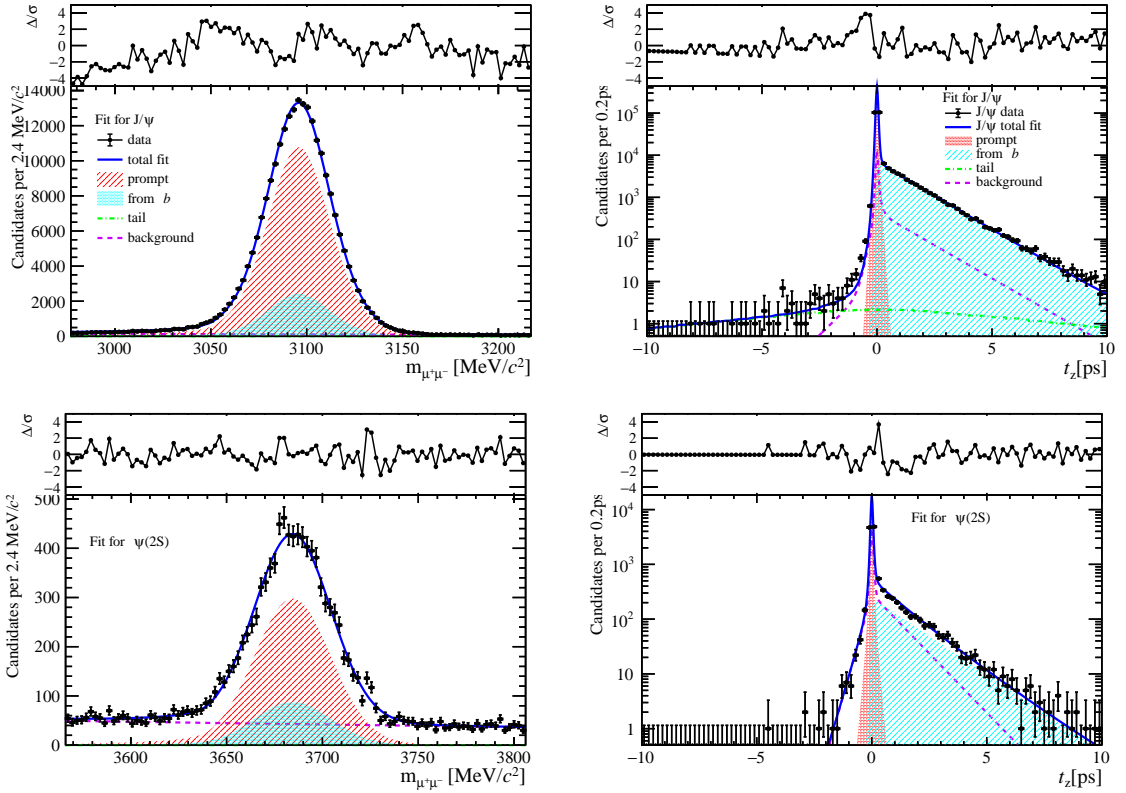


Figure 64: Fit results in  $6 \text{ GeV}/c < p_T < 8 \text{ GeV}/c$ ,  $3.5 < y < 4.5$  and  $20 \leq \text{PVNTRACKS} < 45$ .

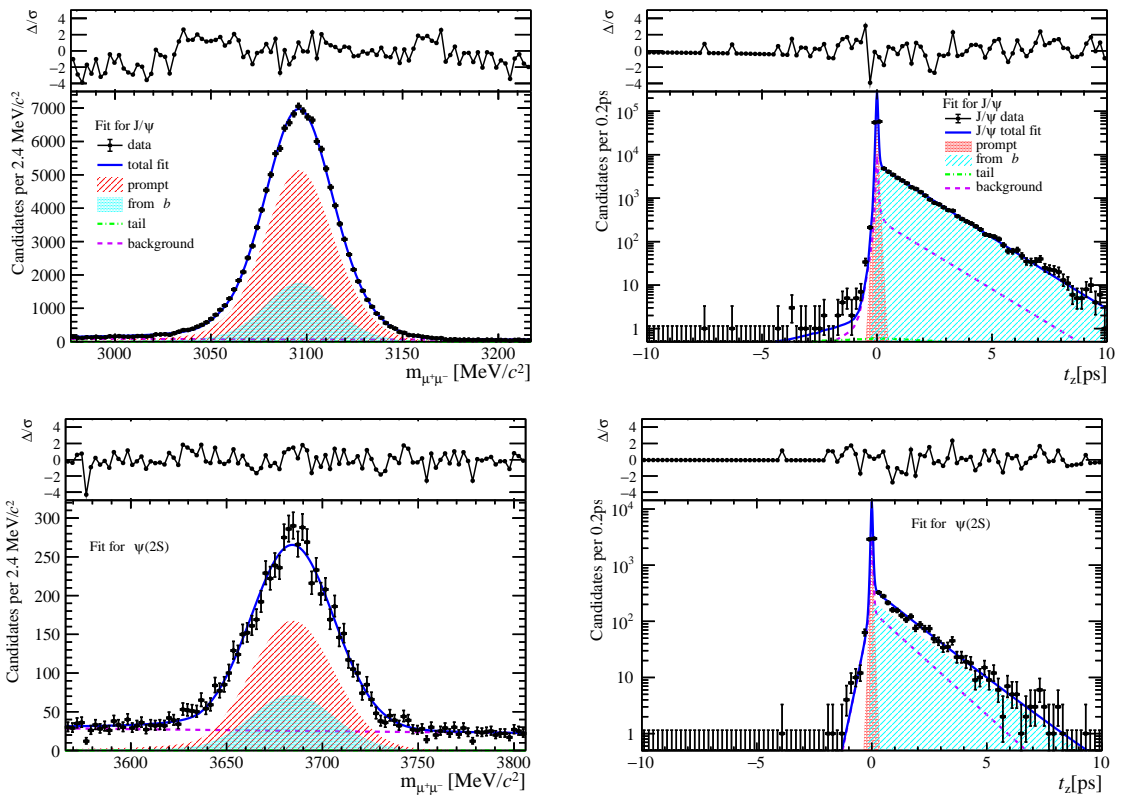


Figure 65: Fit results in  $8 \text{ GeV}/c < p_T < 20 \text{ GeV}/c$ ,  $3.5 < y < 4.5$  and  $20 \leq \text{PVNTRACKS} < 45$ .

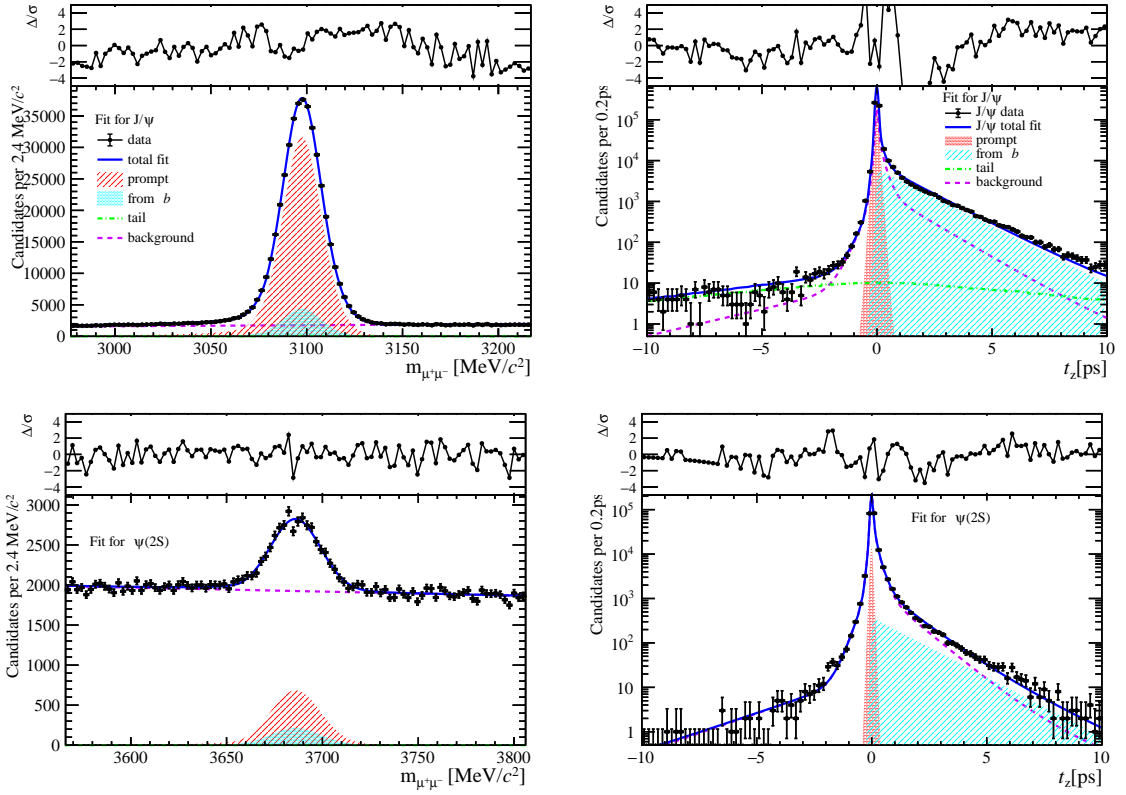


Figure 66: Fit results in  $0 \text{ GeV}/c < p_T < 2 \text{ GeV}/c$ ,  $2.0 < y < 2.8$  and  $45 \leq \text{PVNTRACKS} < 70$ .

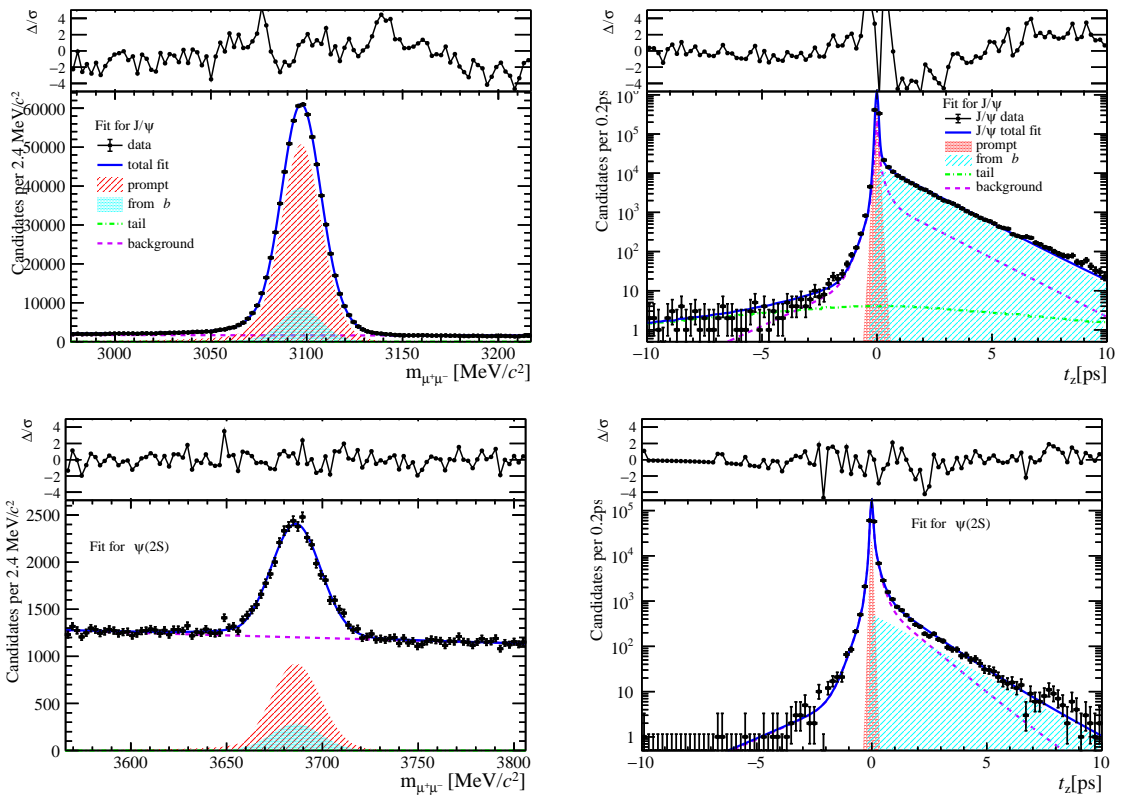


Figure 67: Fit results in  $2 \text{ GeV}/c < p_T < 4 \text{ GeV}/c$ ,  $2.0 < y < 2.8$  and  $45 \leq \text{PVNTRACKS} < 70$ .

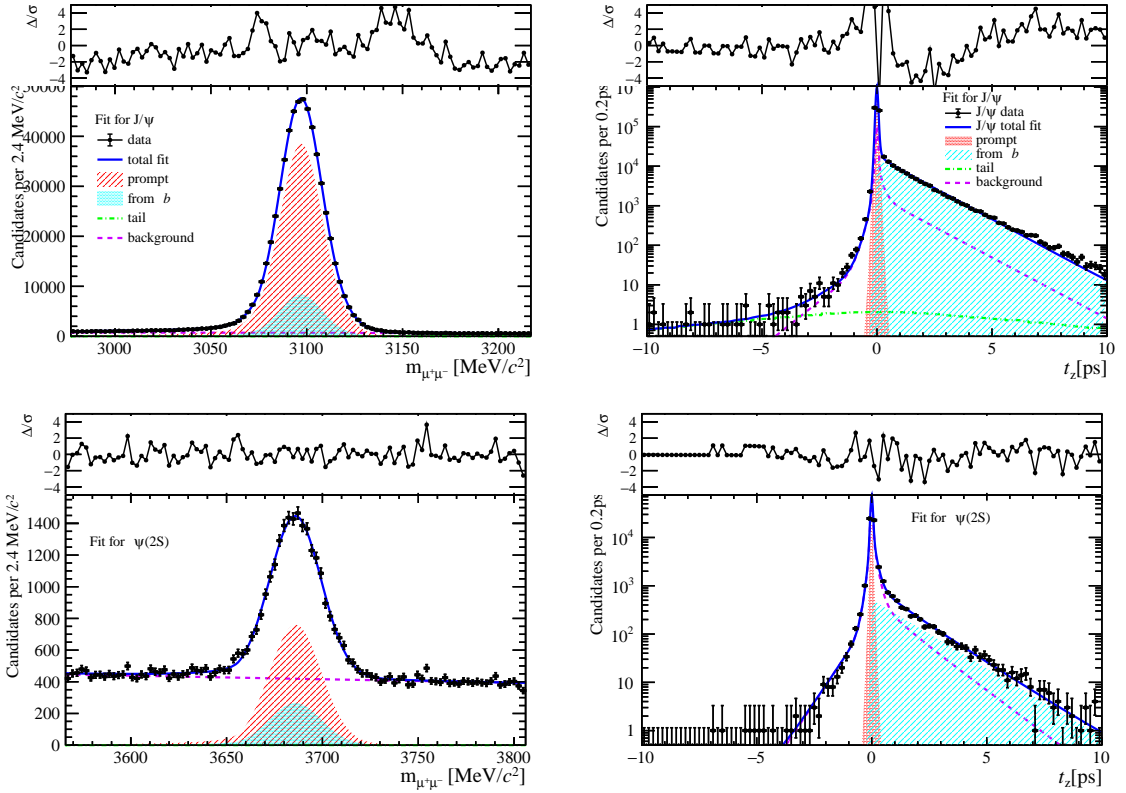


Figure 68: Fit results in  $4 \text{ GeV}/c < p_T < 6 \text{ GeV}/c$ ,  $2.0 < y < 2.8$  and  $45 \leq \text{PVNTRACKS} < 70$ .

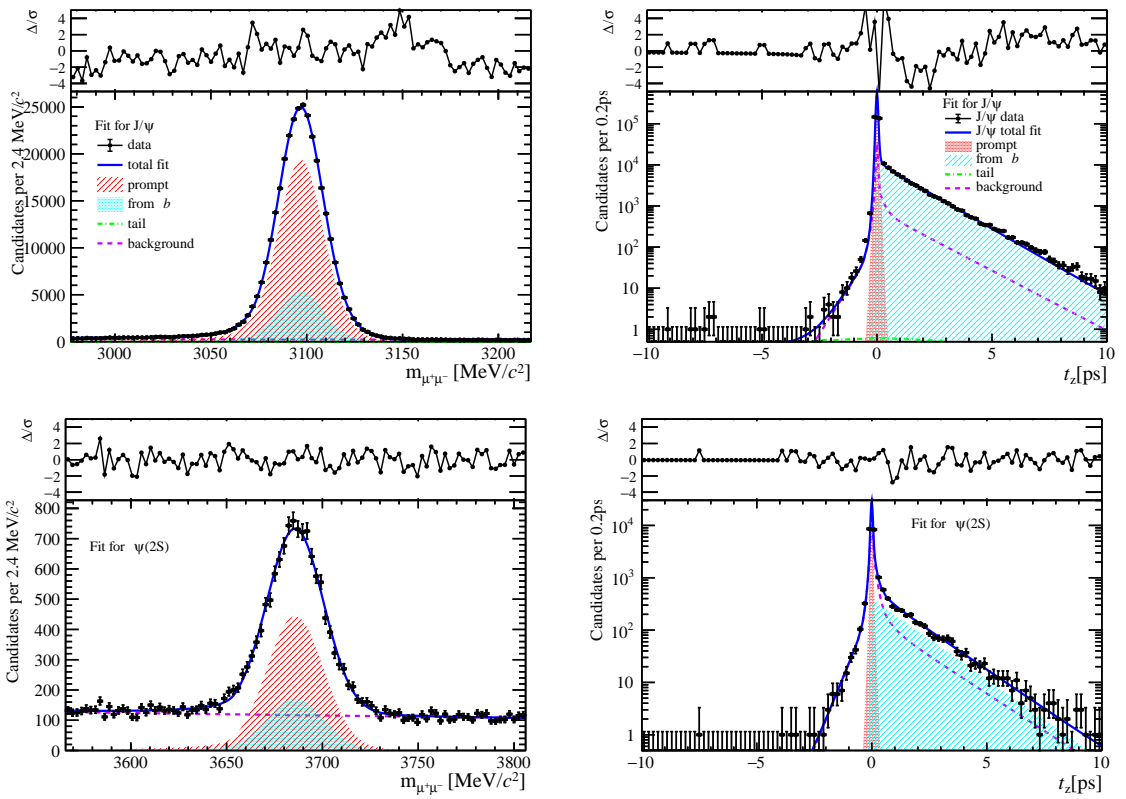


Figure 69: Fit results in  $6 \text{ GeV}/c < p_T < 8 \text{ GeV}/c$ ,  $2.0 < y < 2.8$  and  $45 \leq \text{PVNTRACKS} < 70$ .

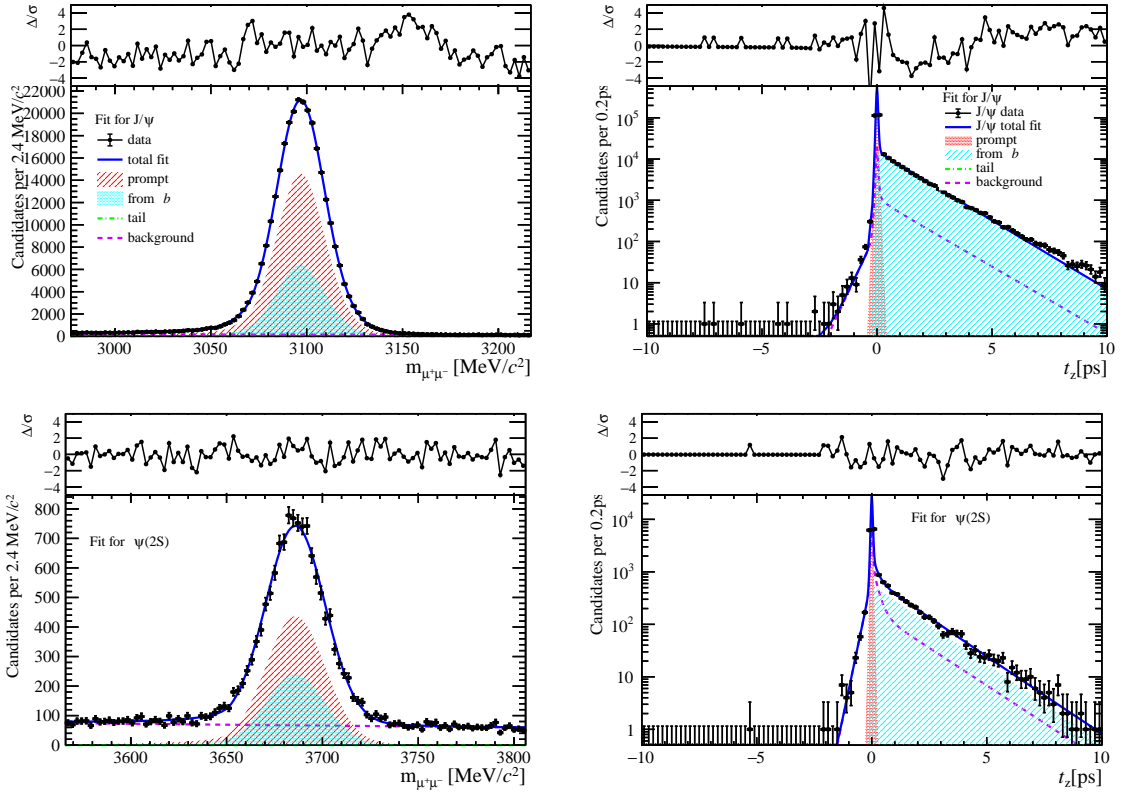


Figure 70: Fit results in  $8 \text{ GeV}/c < p_T < 20 \text{ GeV}/c$ ,  $2.0 < y < 2.8$  and  $45 \leq \text{PVNTRACKS} < 70$ .

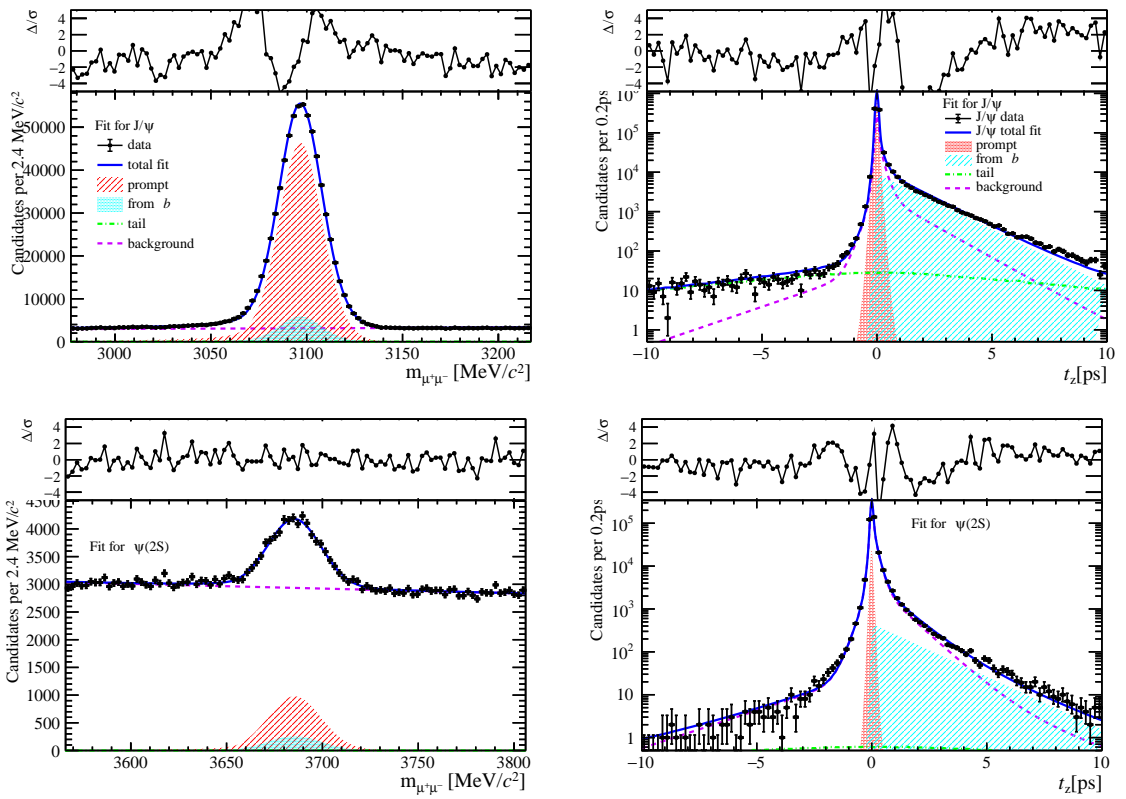


Figure 71: Fit results in  $0 \text{ GeV}/c < p_T < 2 \text{ GeV}/c$ ,  $2.8 < y < 3.5$  and  $45 \leq \text{PVNTRACKS} < 70$ .

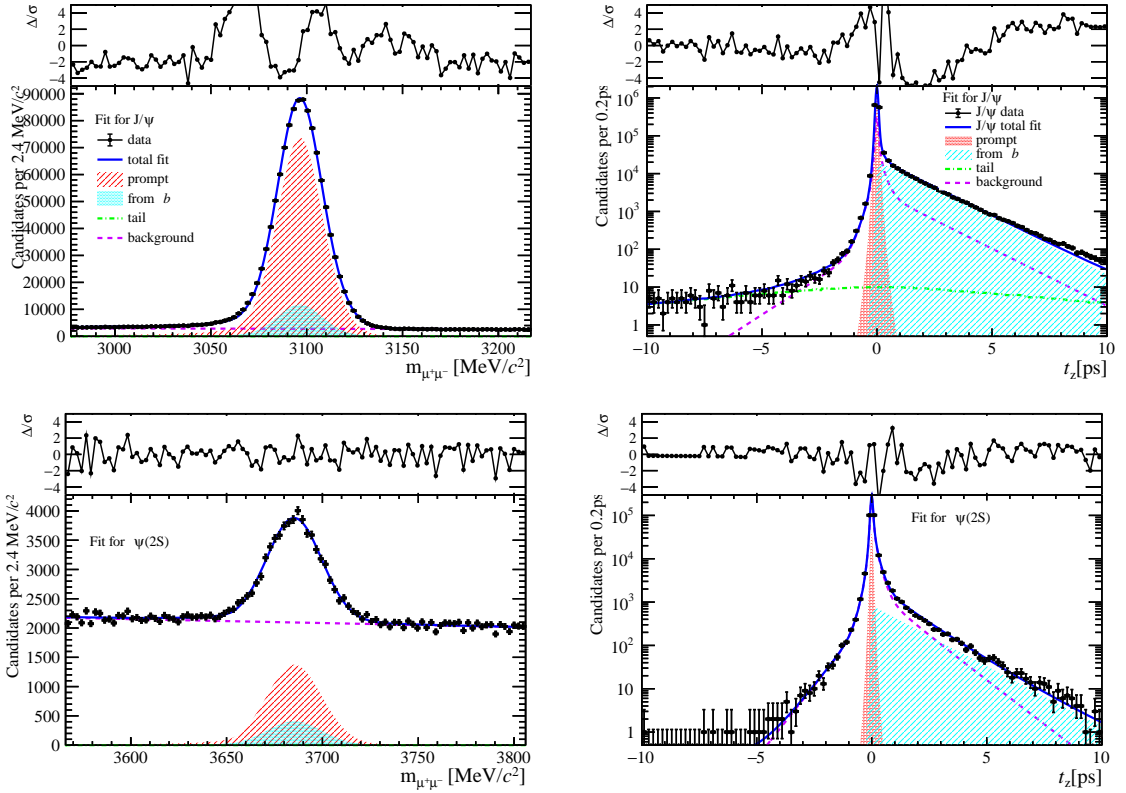


Figure 72: Fit results in  $2 \text{ GeV}/c < p_T < 4 \text{ GeV}/c$ ,  $2.8 < y < 3.5$  and  $45 \leq \text{PVNTRACKS} < 70$ .

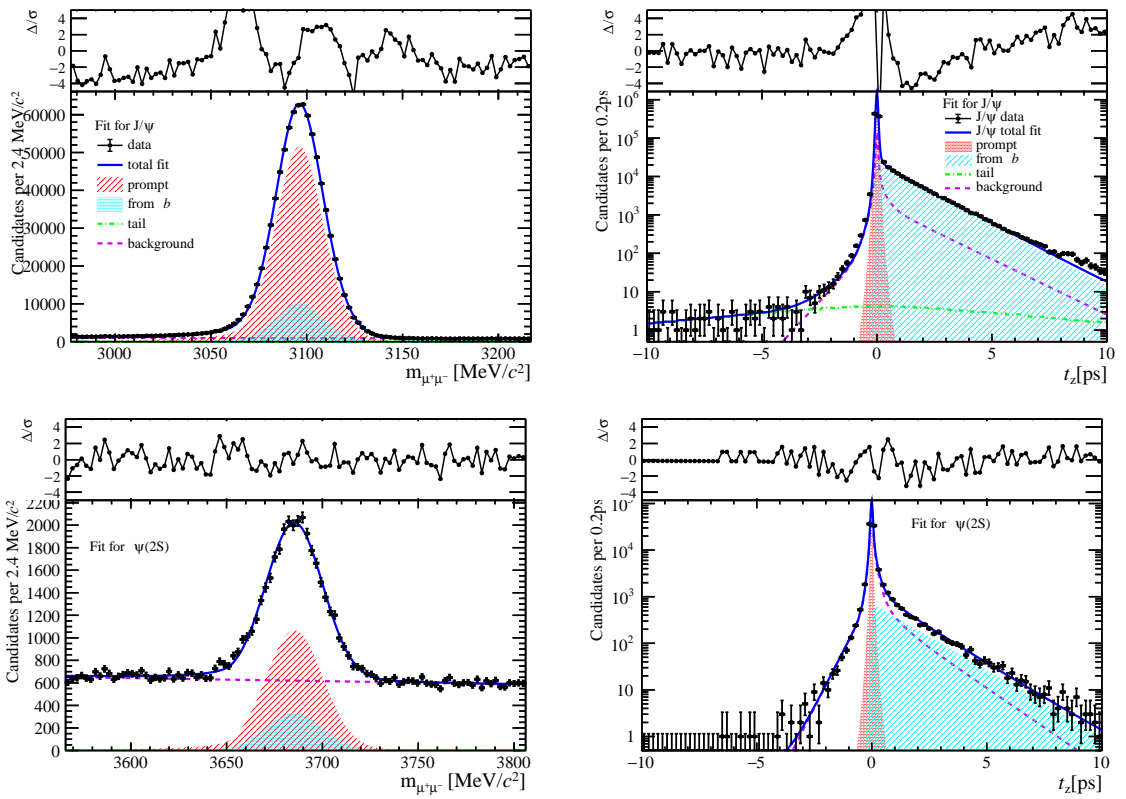


Figure 73: Fit results in  $4 \text{ GeV}/c < p_T < 6 \text{ GeV}/c$ ,  $2.8 < y < 3.5$  and  $45 \leq \text{PVNTRACKS} < 70$ .

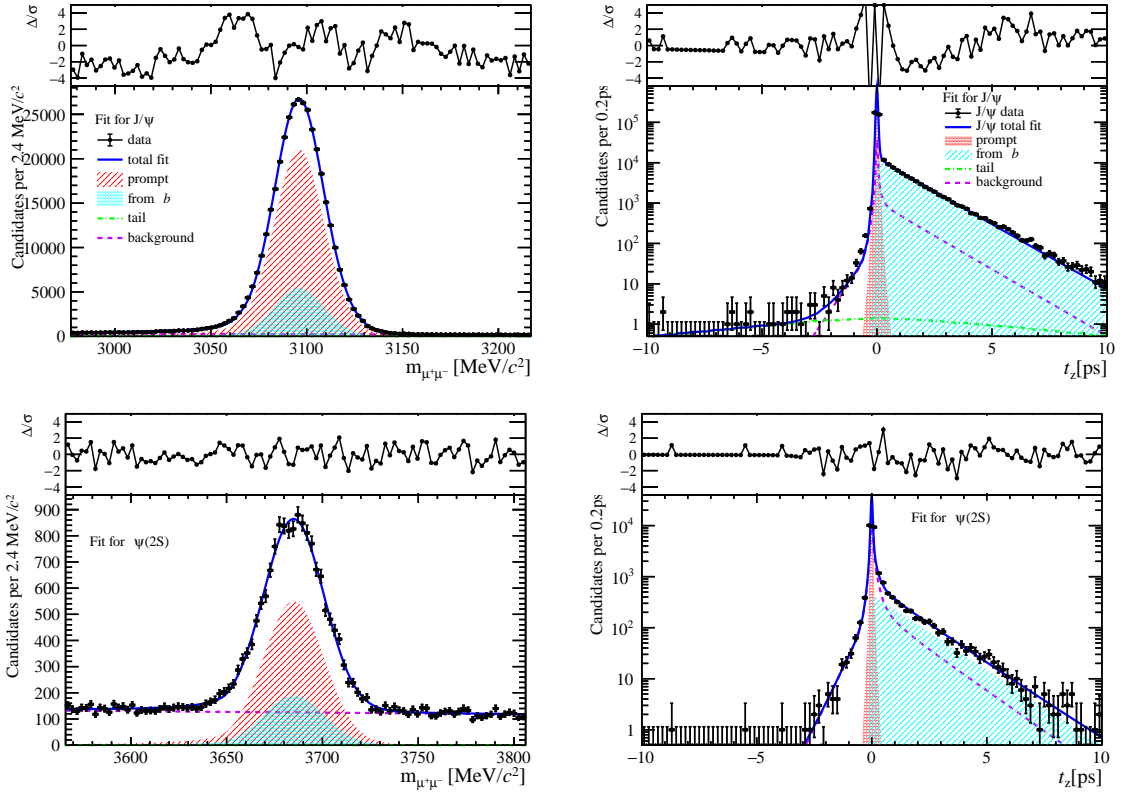


Figure 74: Fit results in  $6 \text{ GeV}/c < p_T < 8 \text{ GeV}/c$ ,  $2.8 < y < 3.5$  and  $45 \leq \text{PVNTRACKS} < 70$ .

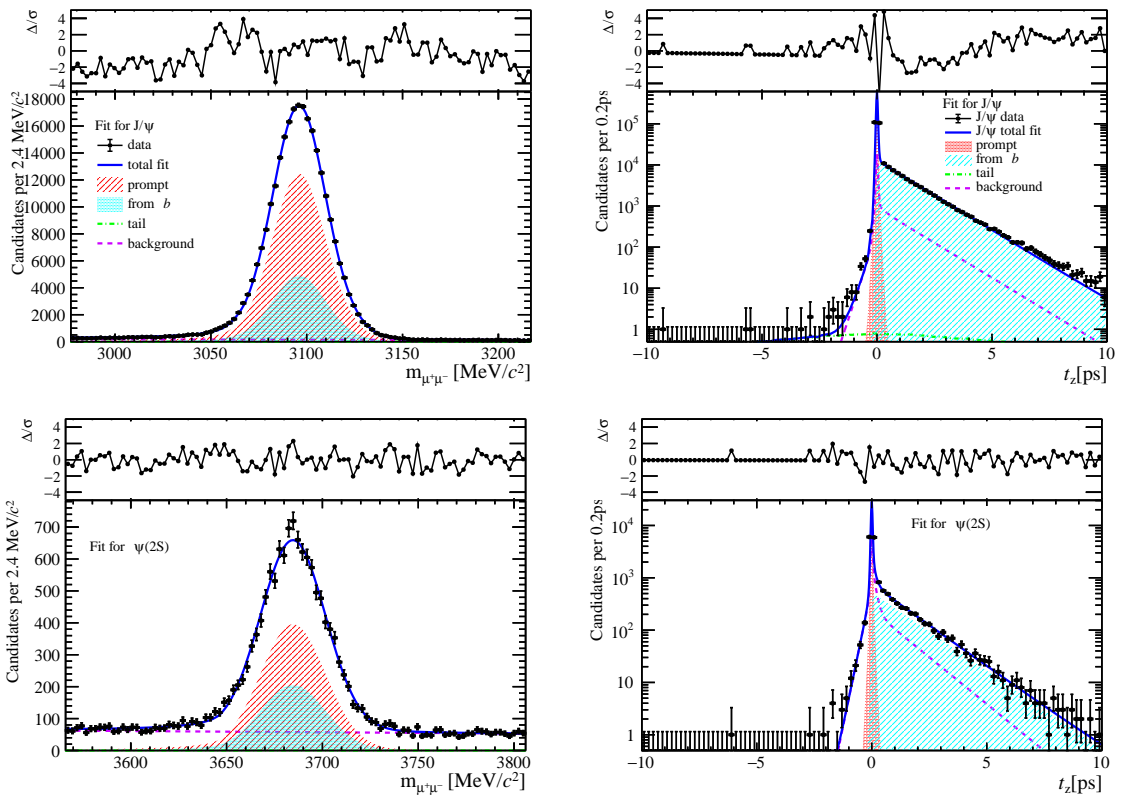


Figure 75: Fit results in  $8 \text{ GeV}/c < p_T < 20 \text{ GeV}/c$ ,  $2.8 < y < 3.5$  and  $45 \leq \text{PVNTRACKS} < 70$ .

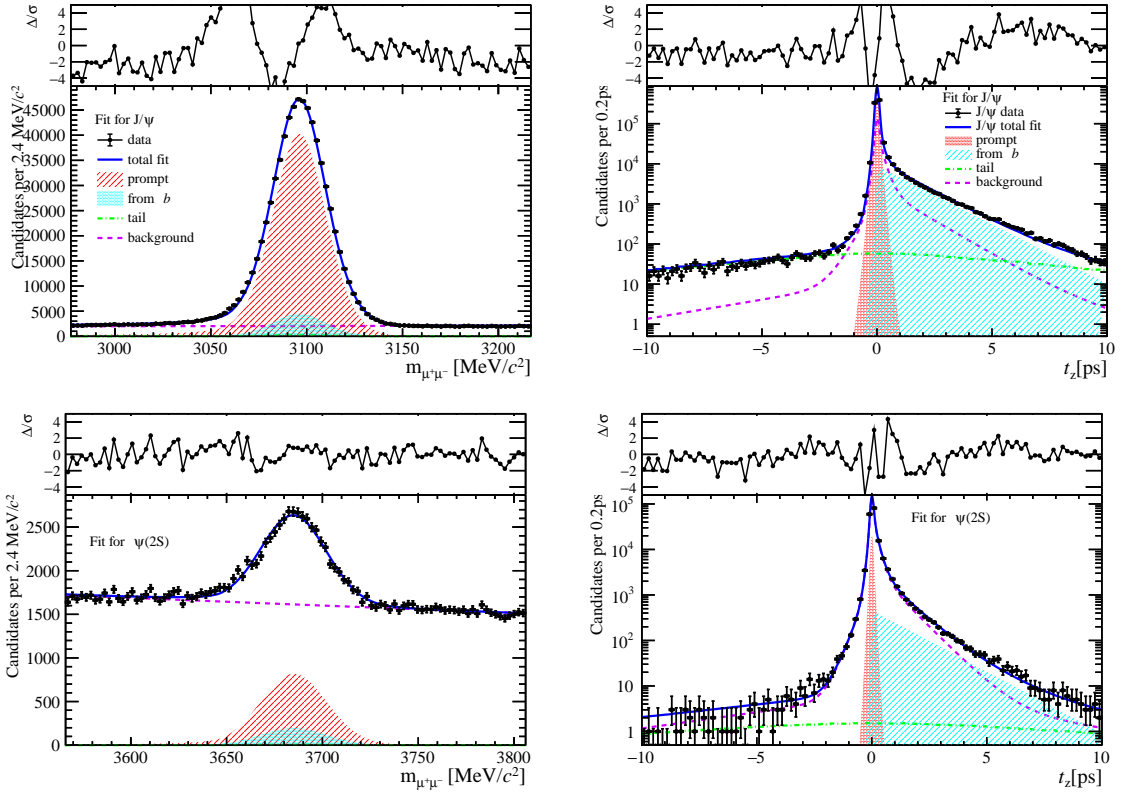


Figure 76: Fit results in  $0 \text{ GeV}/c < p_T < 2 \text{ GeV}/c$ ,  $3.5 < y < 4.5$  and  $45 \leq \text{PVNTRACKS} < 70$ .

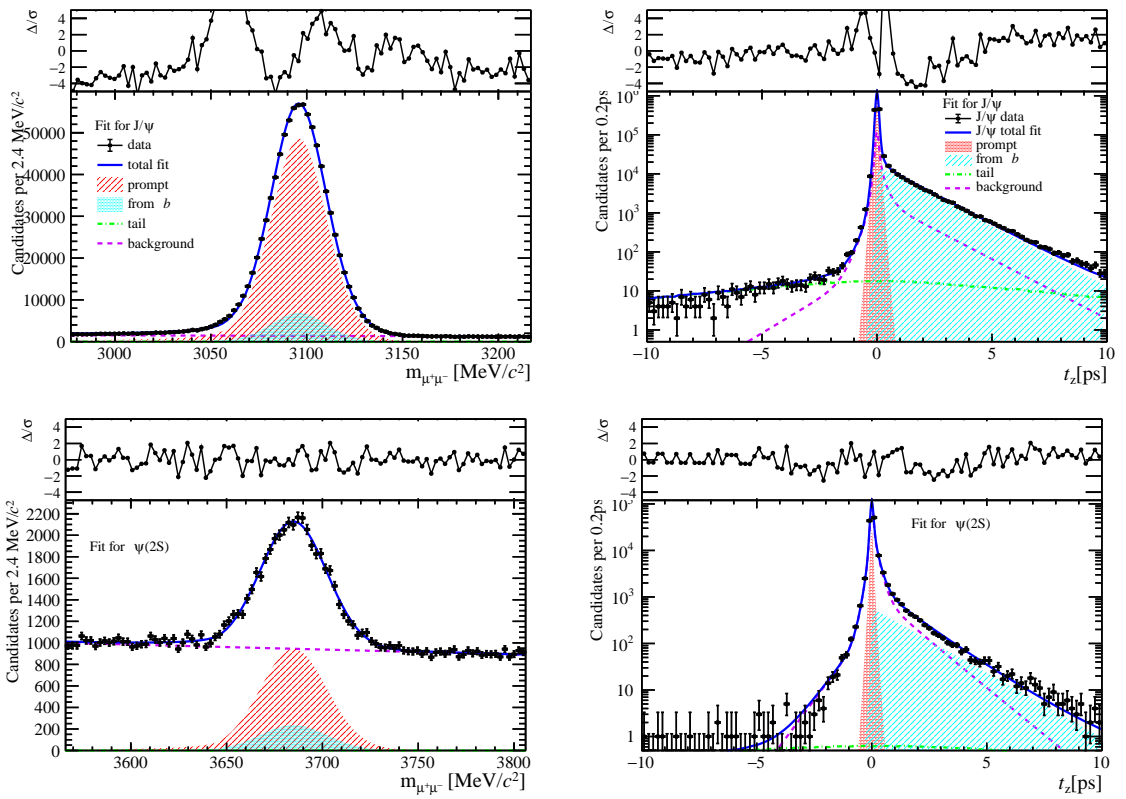


Figure 77: Fit results in  $2 \text{ GeV}/c < p_T < 4 \text{ GeV}/c$ ,  $3.5 < y < 4.5$  and  $45 \leq \text{PVNTRACKS} < 70$ .

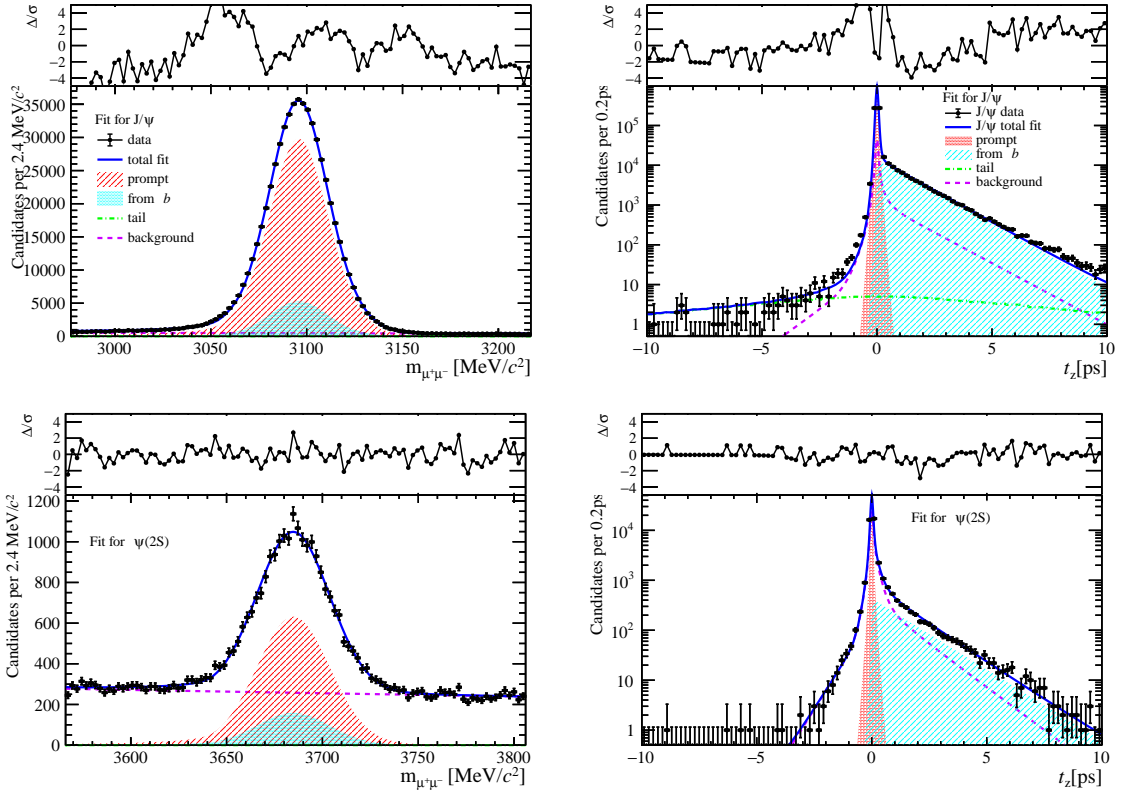


Figure 78: Fit results in  $4 \text{ GeV}/c < p_T < 6 \text{ GeV}/c$ ,  $3.5 < y < 4.5$  and  $45 \leq \text{PVNTRACKS} < 70$ .

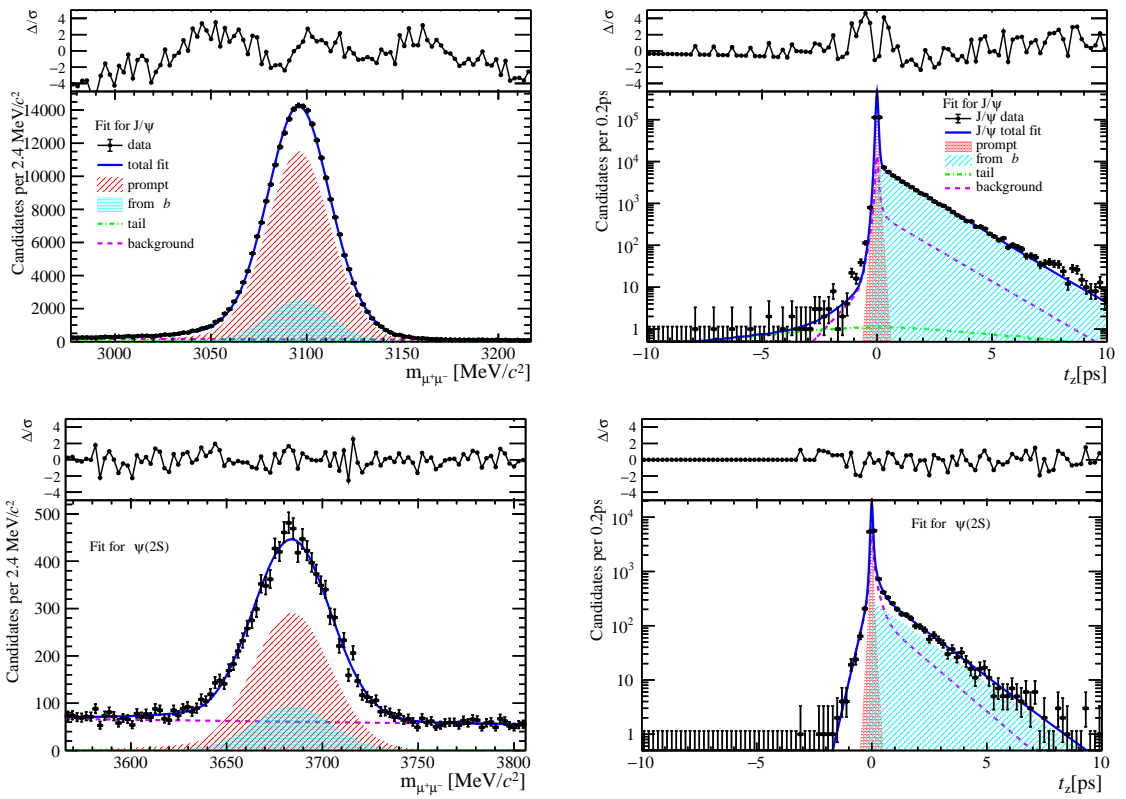


Figure 79: Fit results in  $6 \text{ GeV}/c < p_T < 8 \text{ GeV}/c$ ,  $3.5 < y < 4.5$  and  $45 \leq \text{PVNTRACKS} < 70$ .

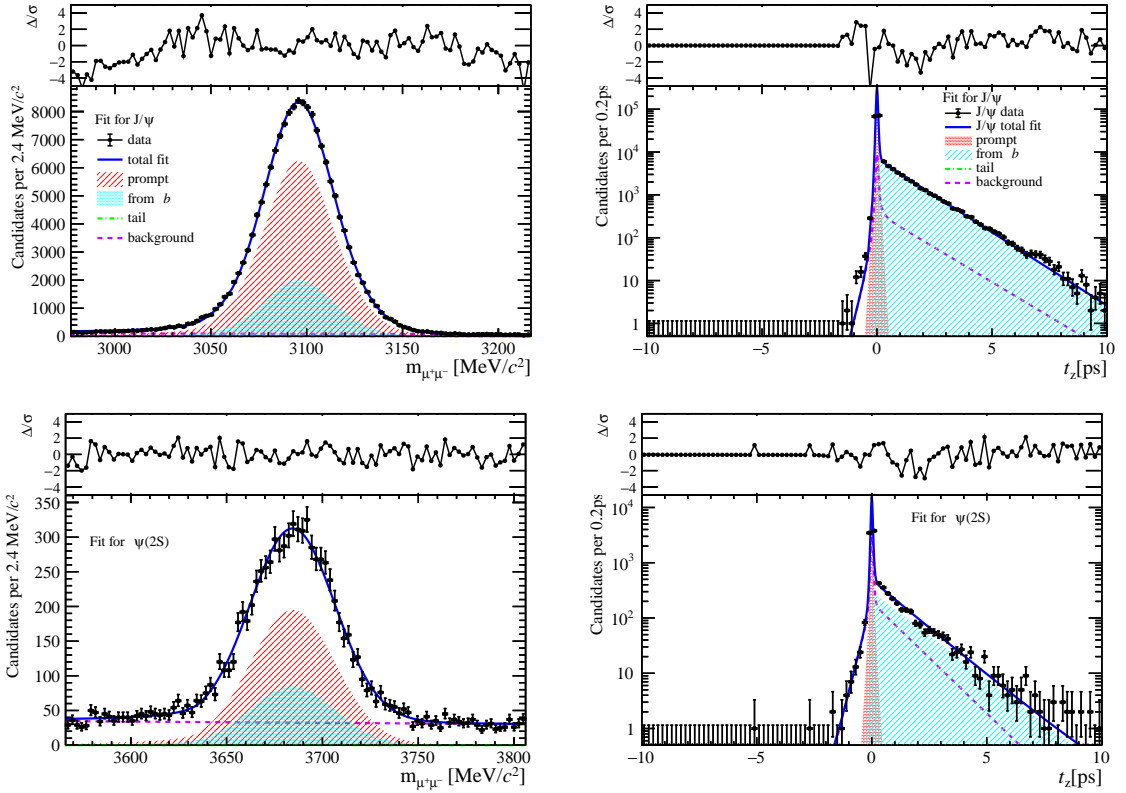


Figure 80: Fit results in  $8 \text{ GeV}/c < p_T < 20 \text{ GeV}/c$ ,  $3.5 < y < 4.5$  and  $45 \leq \text{PVNTRACKS} < 70$ .

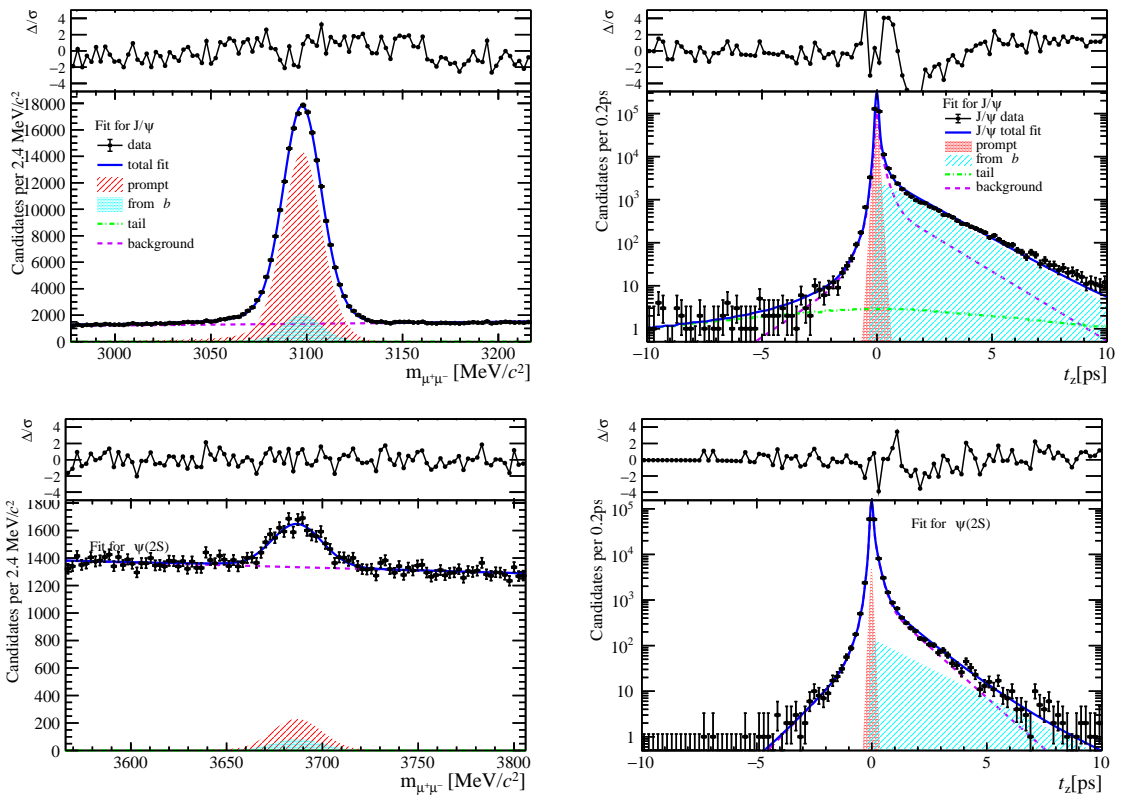


Figure 81: Fit results in  $0 \text{ GeV}/c < p_T < 2 \text{ GeV}/c$ ,  $2.0 < y < 2.8$  and  $70 \leq \text{PVNTRACKS} < 95$ .

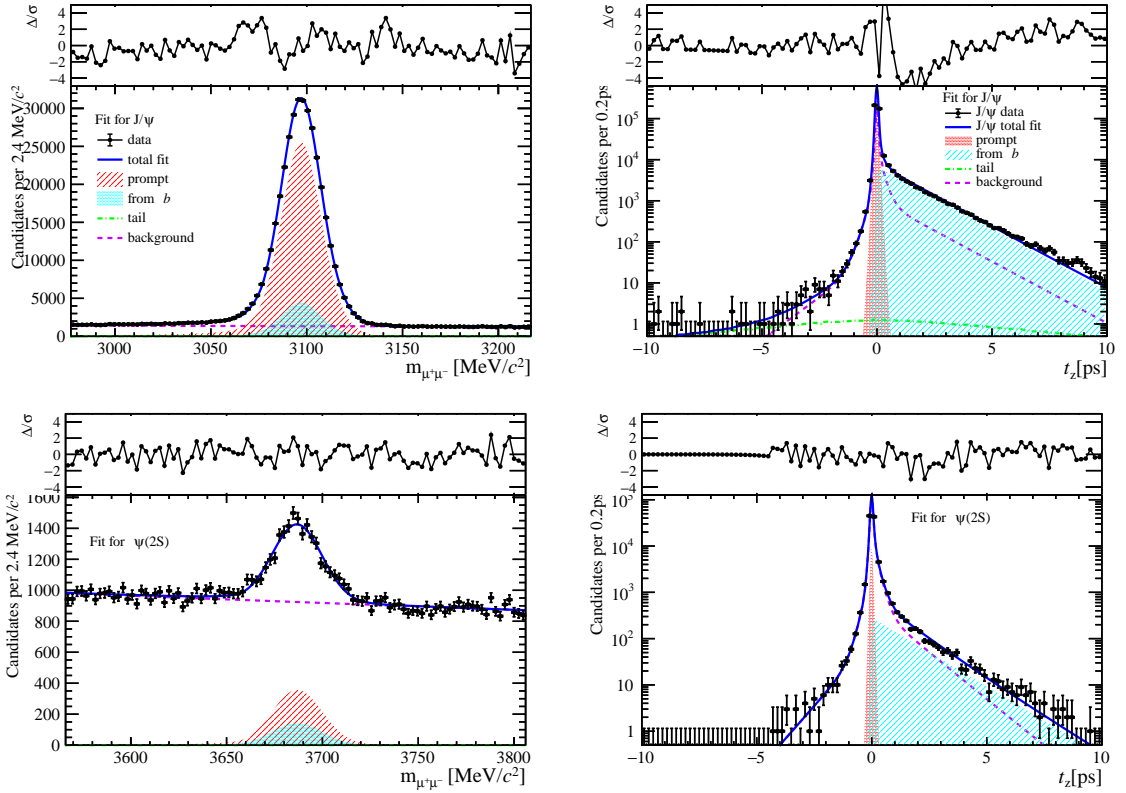


Figure 82: Fit results in  $2 \text{ GeV}/c < p_T < 4 \text{ GeV}/c$ ,  $2.0 < y < 2.8$  and  $70 \leq \text{PVNTRACKS} < 95$ .

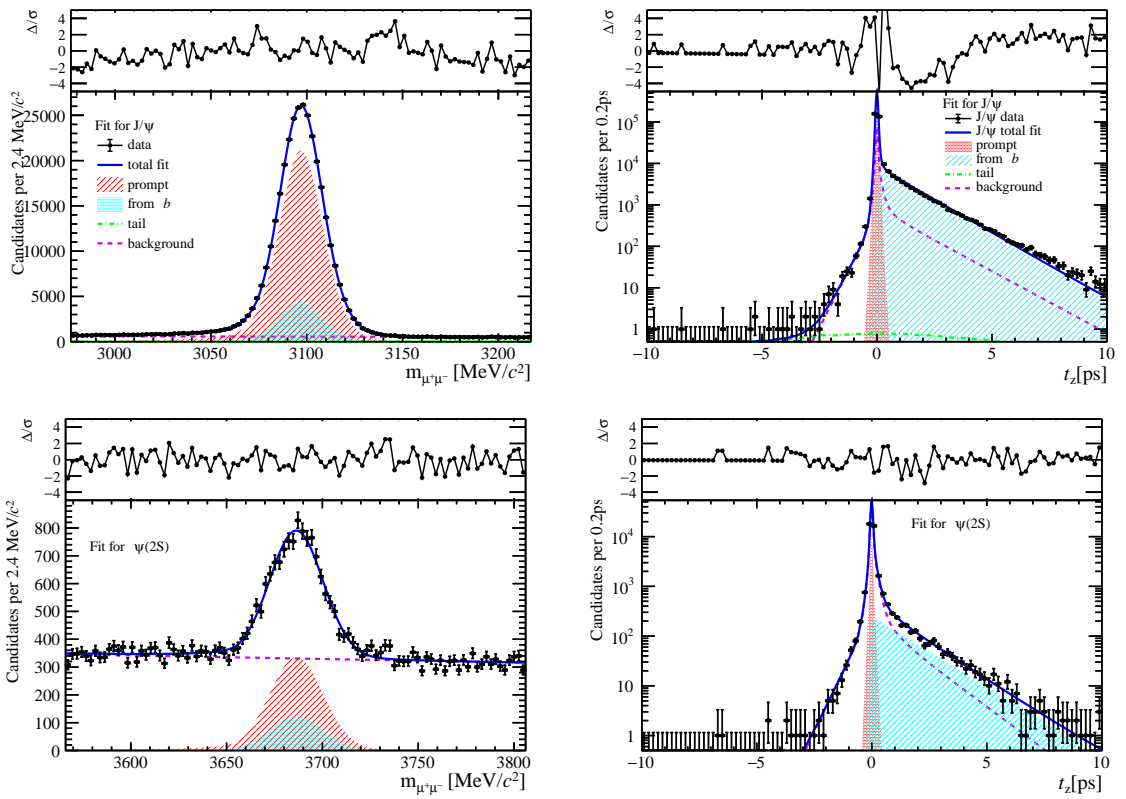


Figure 83: Fit results in  $4 \text{ GeV}/c < p_T < 6 \text{ GeV}/c$ ,  $2.0 < y < 2.8$  and  $70 \leq \text{PVNTRACKS} < 95$ .

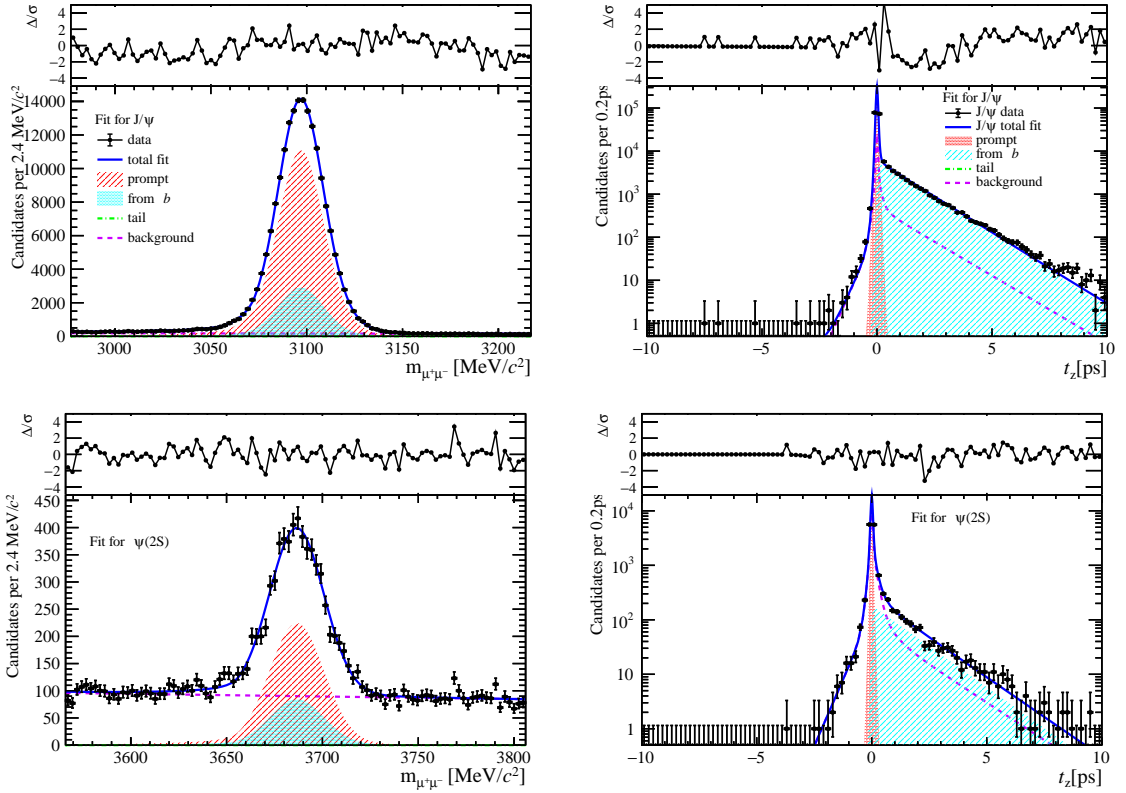


Figure 84: Fit results in  $6 \text{ GeV}/c < p_T < 8 \text{ GeV}/c$ ,  $2.0 < y < 2.8$  and  $70 \leq \text{PVNTRACKS} < 95$ .

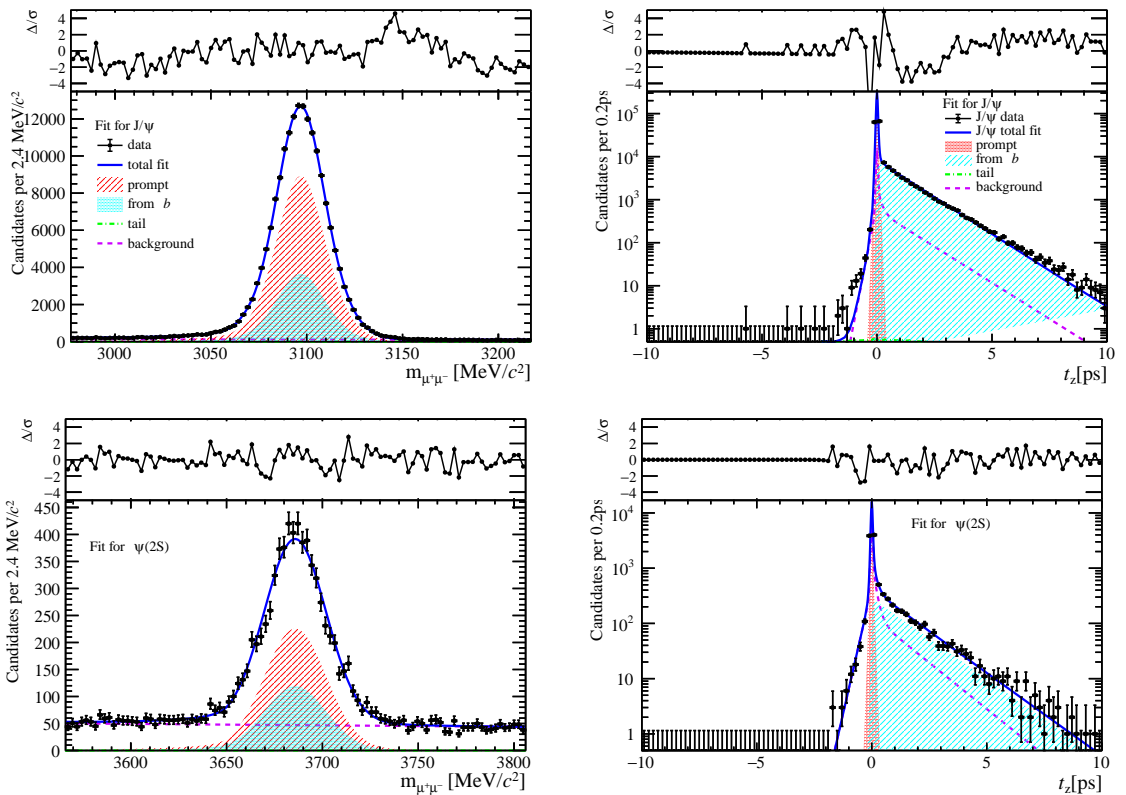


Figure 85: Fit results in  $8 \text{ GeV}/c < p_T < 20 \text{ GeV}/c$ ,  $2.0 < y < 2.8$  and  $70 \leq \text{PVNTRACKS} < 95$ .

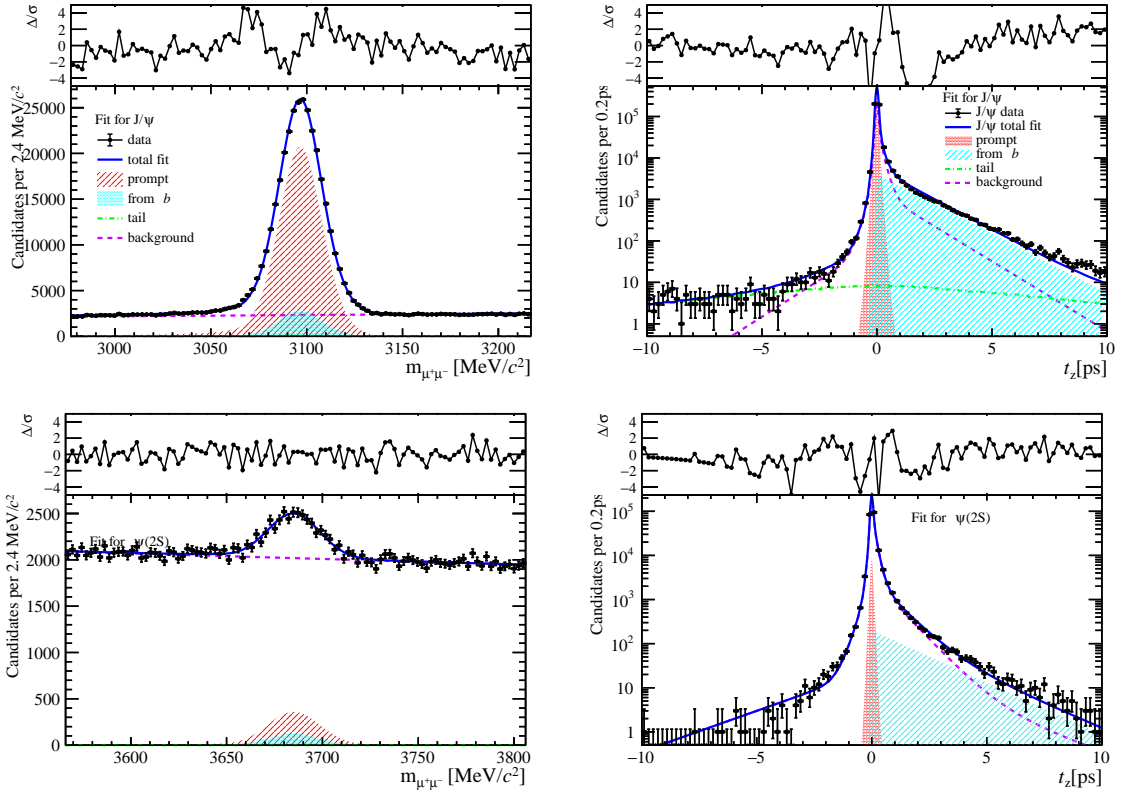


Figure 86: Fit results in  $0 \text{ GeV}/c < p_T < 2 \text{ GeV}/c$ ,  $2.8 < y < 3.5$  and  $70 \leq \text{PVNTRACKS} < 95$ .

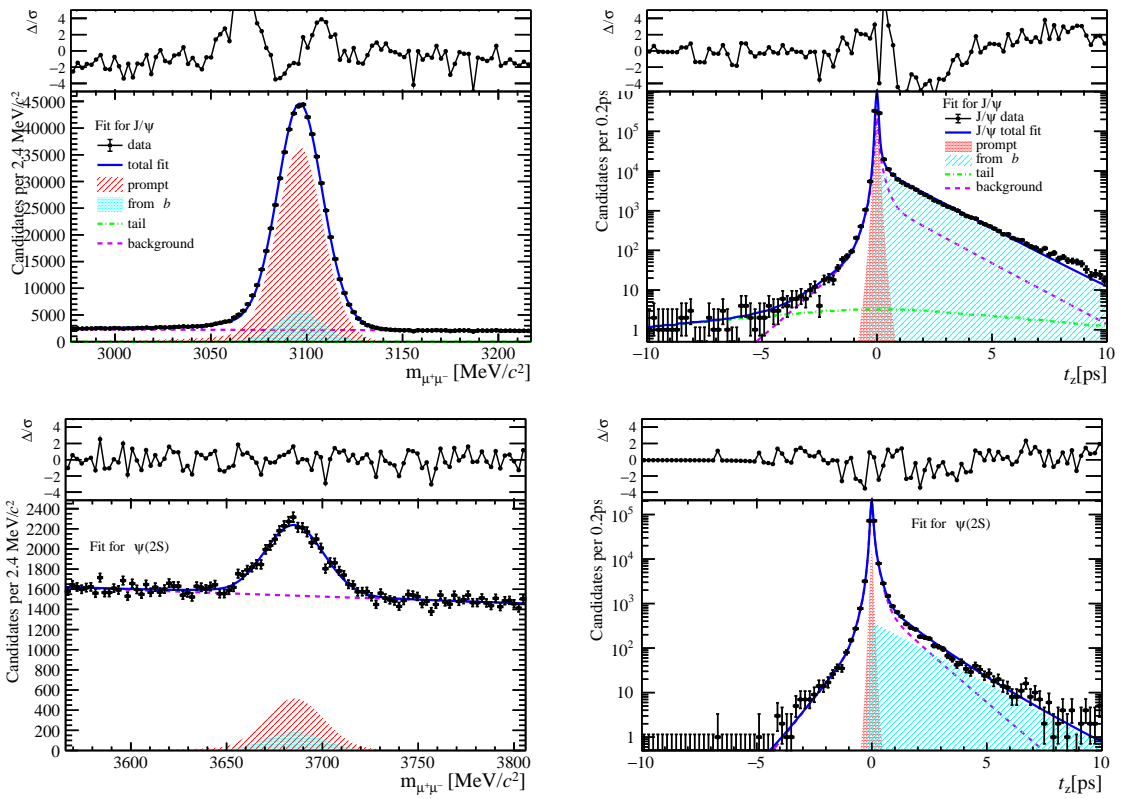


Figure 87: Fit results in  $2 \text{ GeV}/c < p_T < 4 \text{ GeV}/c$ ,  $2.8 < y < 3.5$  and  $70 \leq \text{PVNTRACKS} < 95$ .

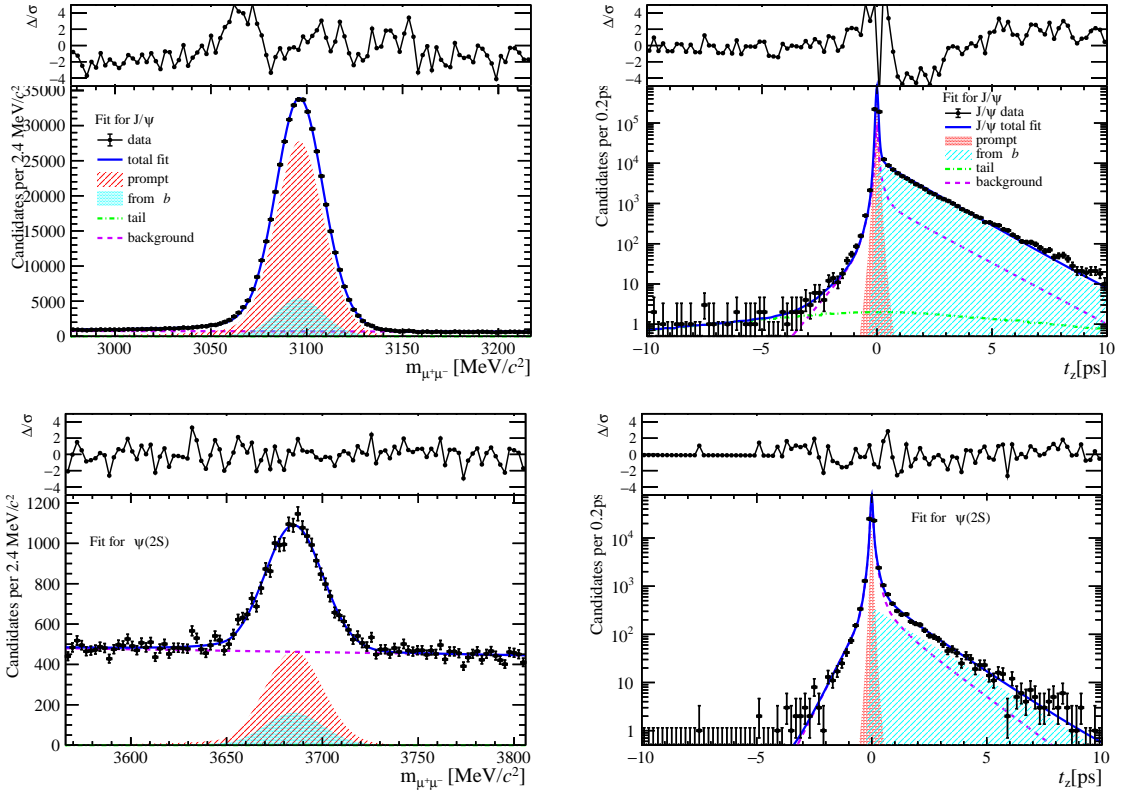


Figure 88: Fit results in  $4 \text{ GeV}/c < p_T < 6 \text{ GeV}/c$ ,  $2.8 < y < 3.5$  and  $70 \leq \text{PVNTRACKS} < 95$ .

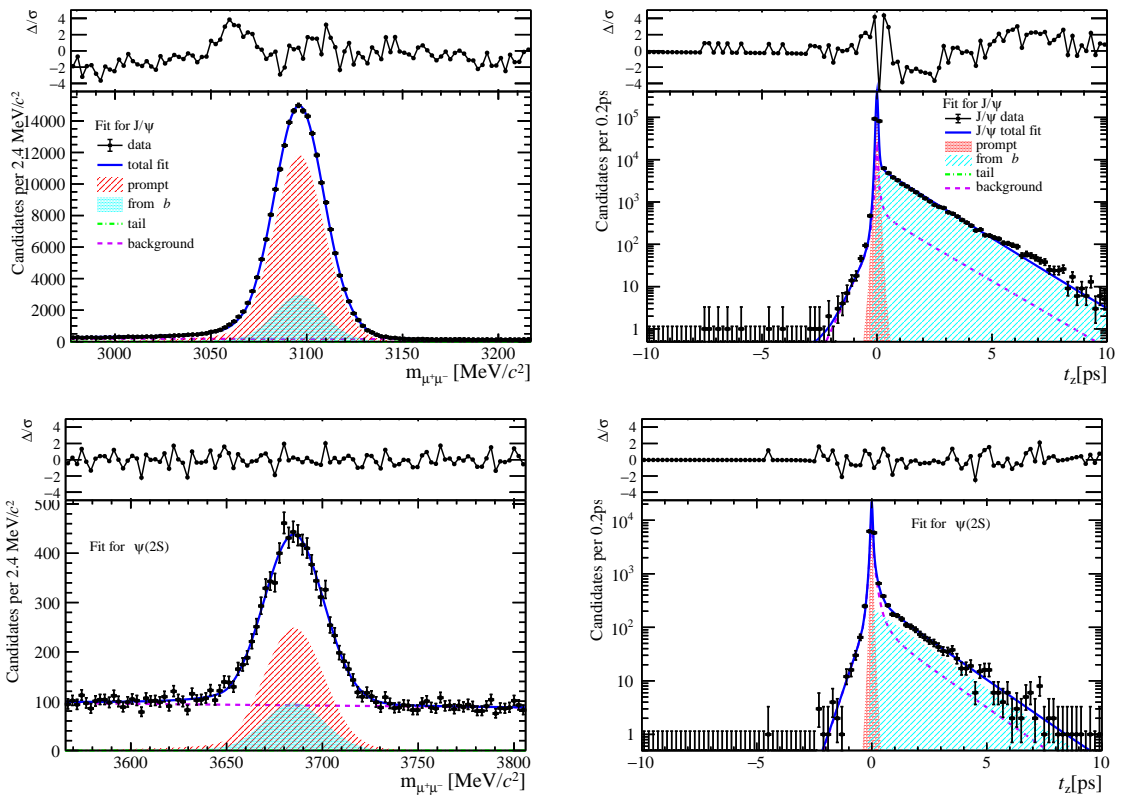


Figure 89: Fit results in  $6 \text{ GeV}/c < p_T < 8 \text{ GeV}/c$ ,  $2.8 < y < 3.5$  and  $70 \leq \text{PVNTRACKS} < 95$ .

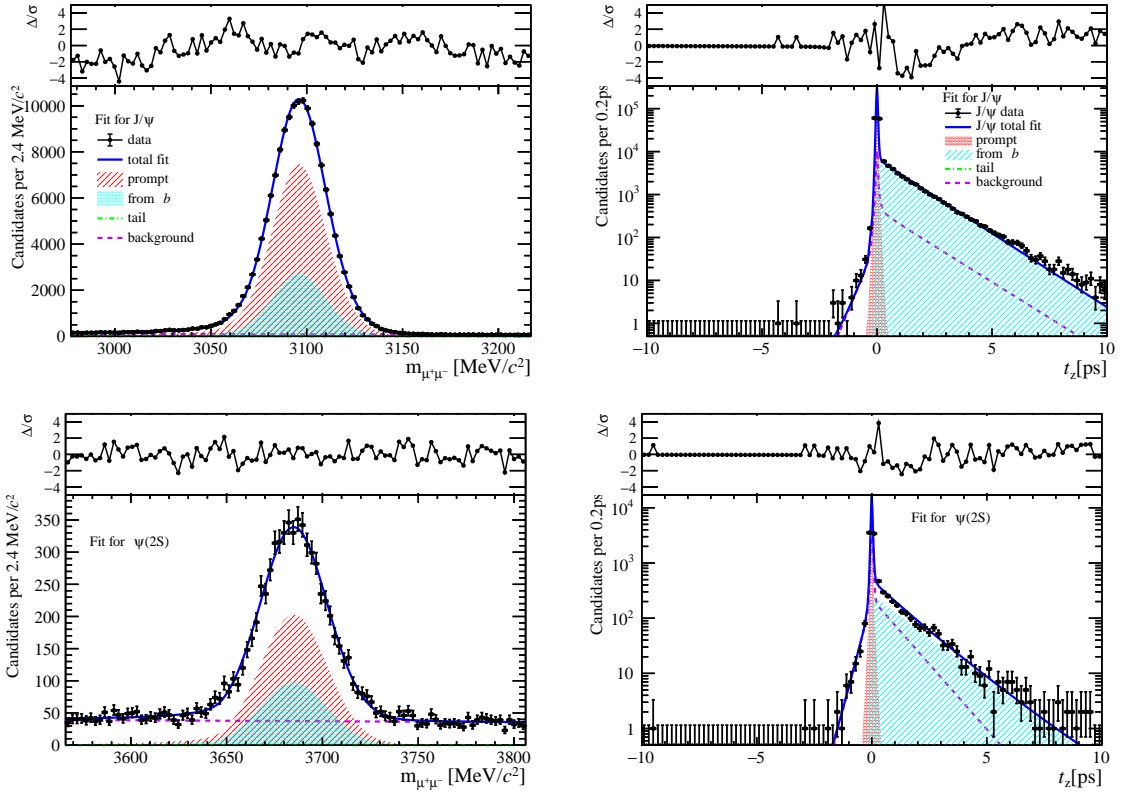


Figure 90: Fit results in  $8 \text{ GeV}/c < p_T < 20 \text{ GeV}/c$ ,  $2.8 < y < 3.5$  and  $70 \leq \text{PVNTRACKS} < 95$ .

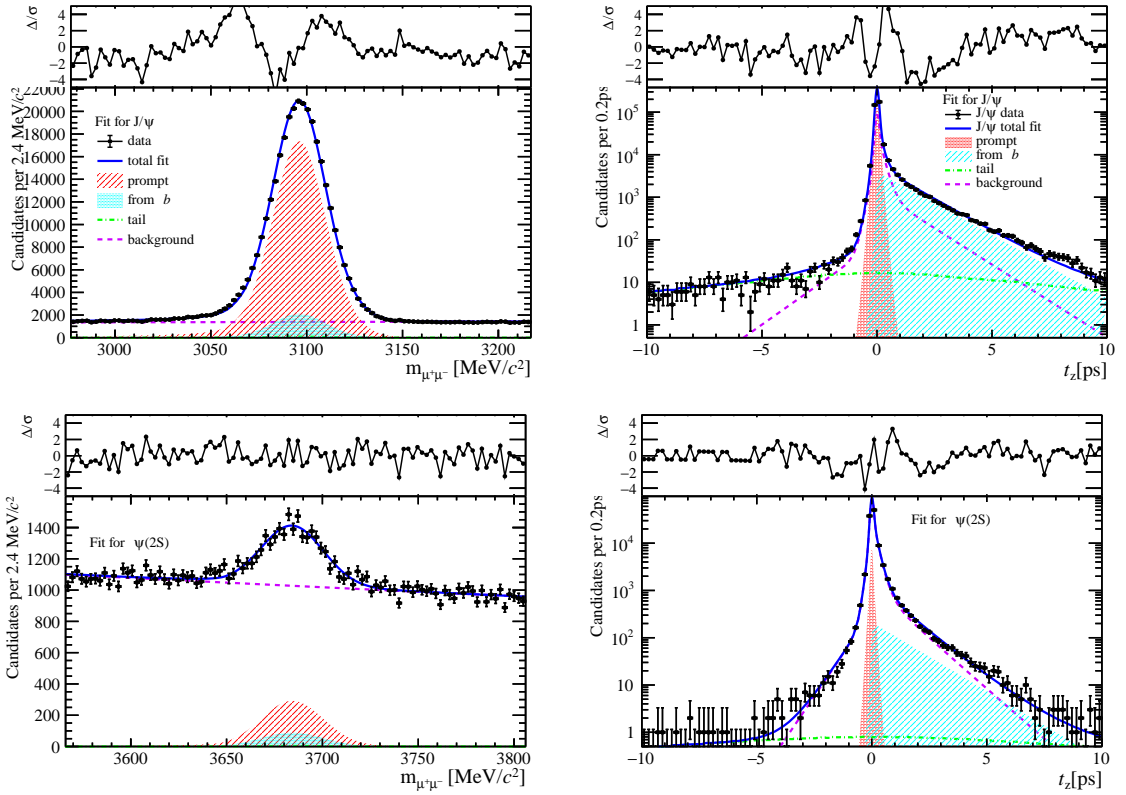


Figure 91: Fit results in  $0 \text{ GeV}/c < p_T < 2 \text{ GeV}/c$ ,  $3.5 < y < 4.5$  and  $70 \leq \text{PVNTRACKS} < 95$ .

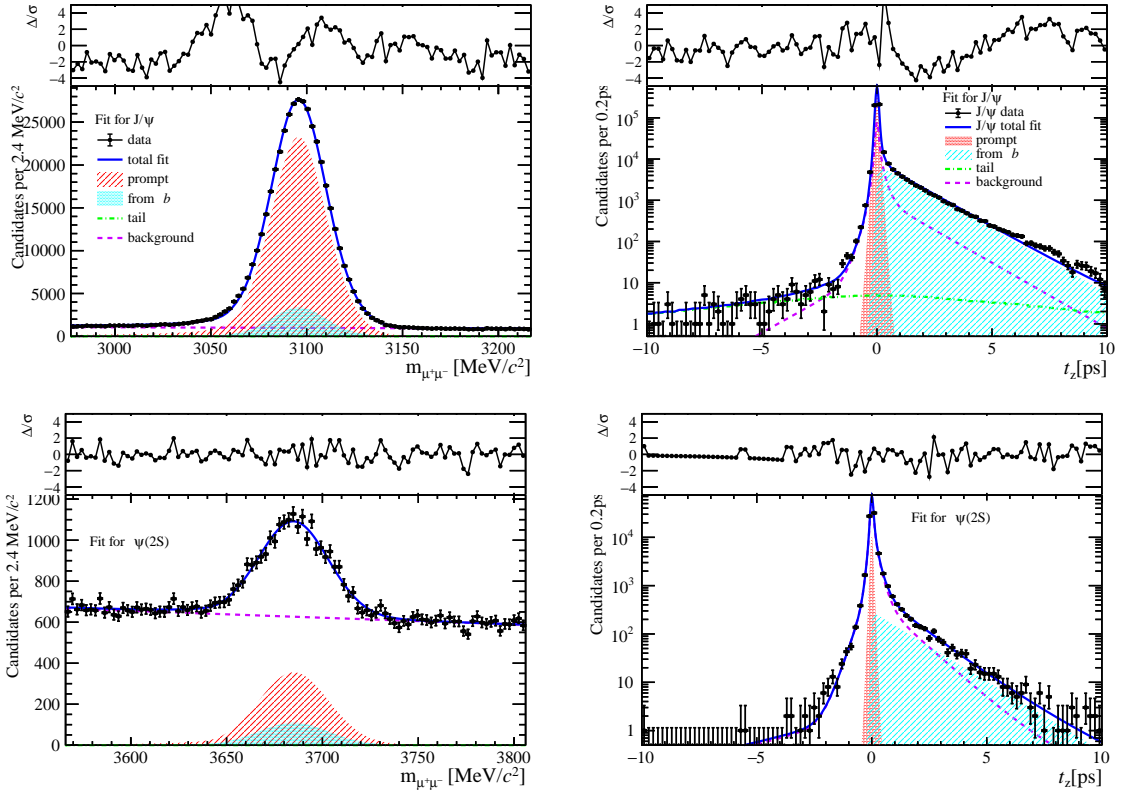


Figure 92: Fit results in  $2 \text{ GeV}/c < p_T < 4 \text{ GeV}/c$ ,  $3.5 < y < 4.5$  and  $70 \leq \text{PVNTRACKS} < 95$ .

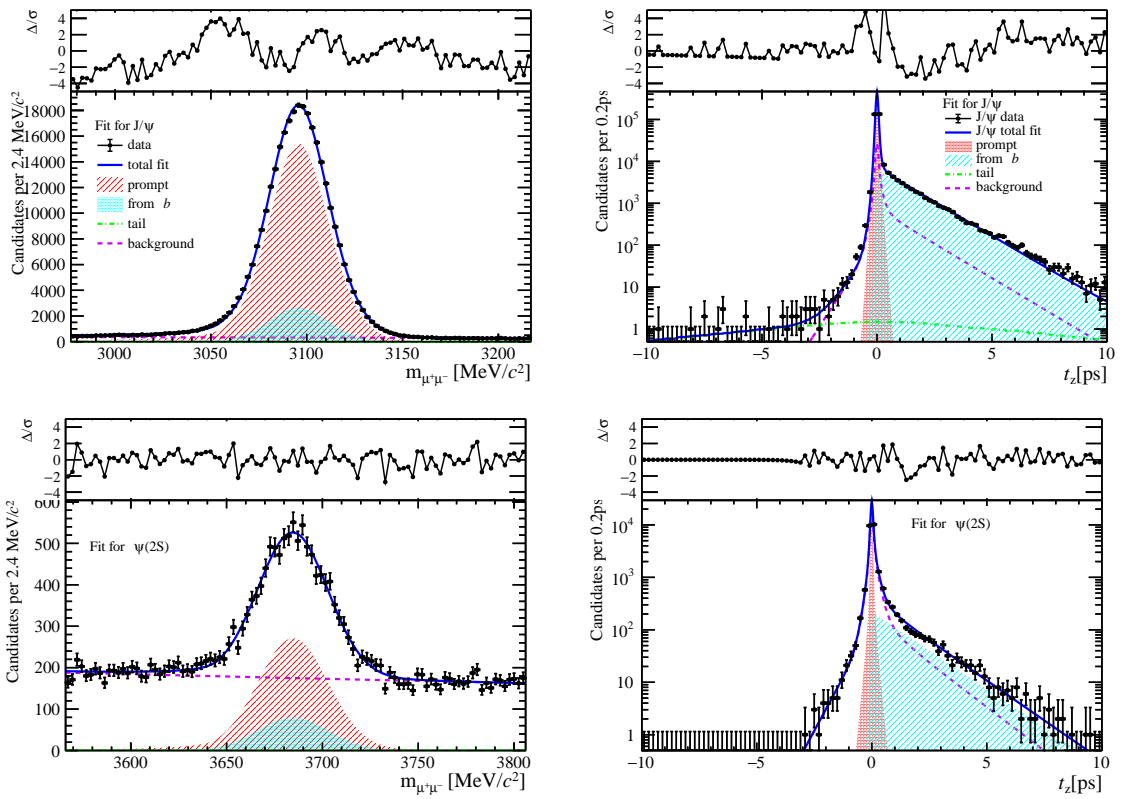


Figure 93: Fit results in  $4 \text{ GeV}/c < p_T < 6 \text{ GeV}/c$ ,  $3.5 < y < 4.5$  and  $70 \leq \text{PVNTRACKS} < 95$ .

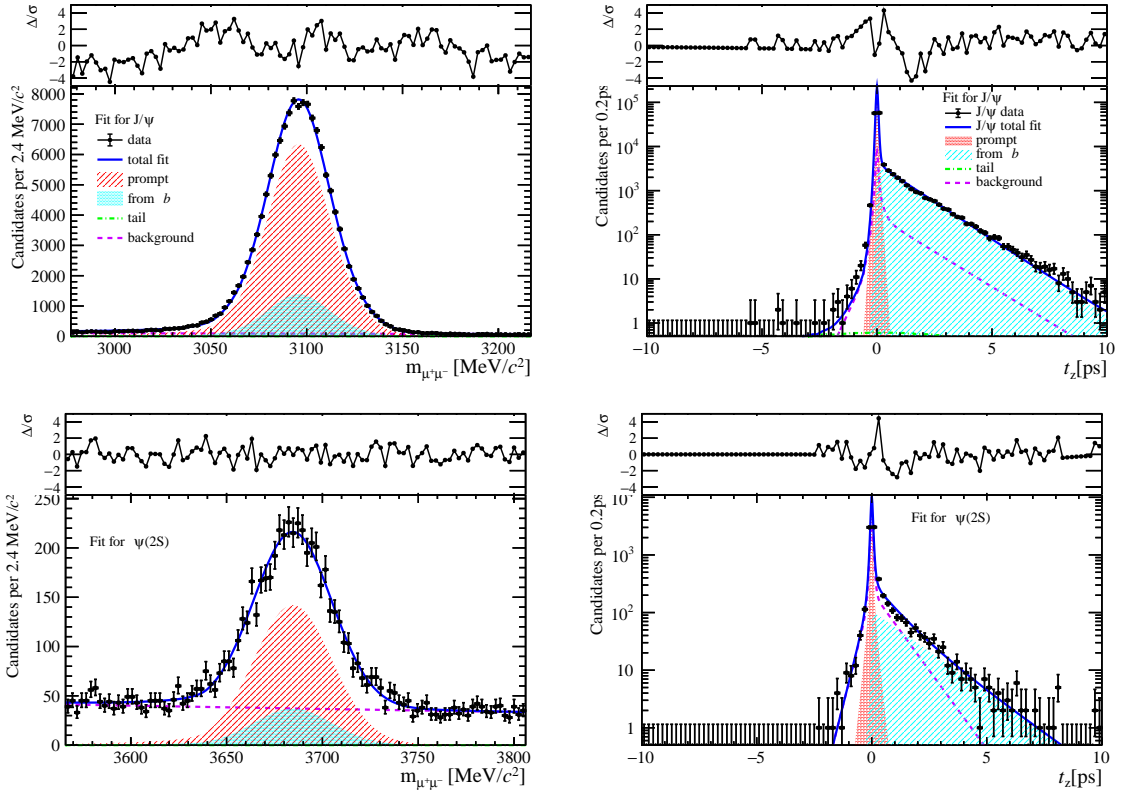


Figure 94: Fit results in  $6 \text{ GeV}/c < p_T < 8 \text{ GeV}/c$ ,  $3.5 < y < 4.5$  and  $70 \leq \text{PVNTRACKS} < 95$ .

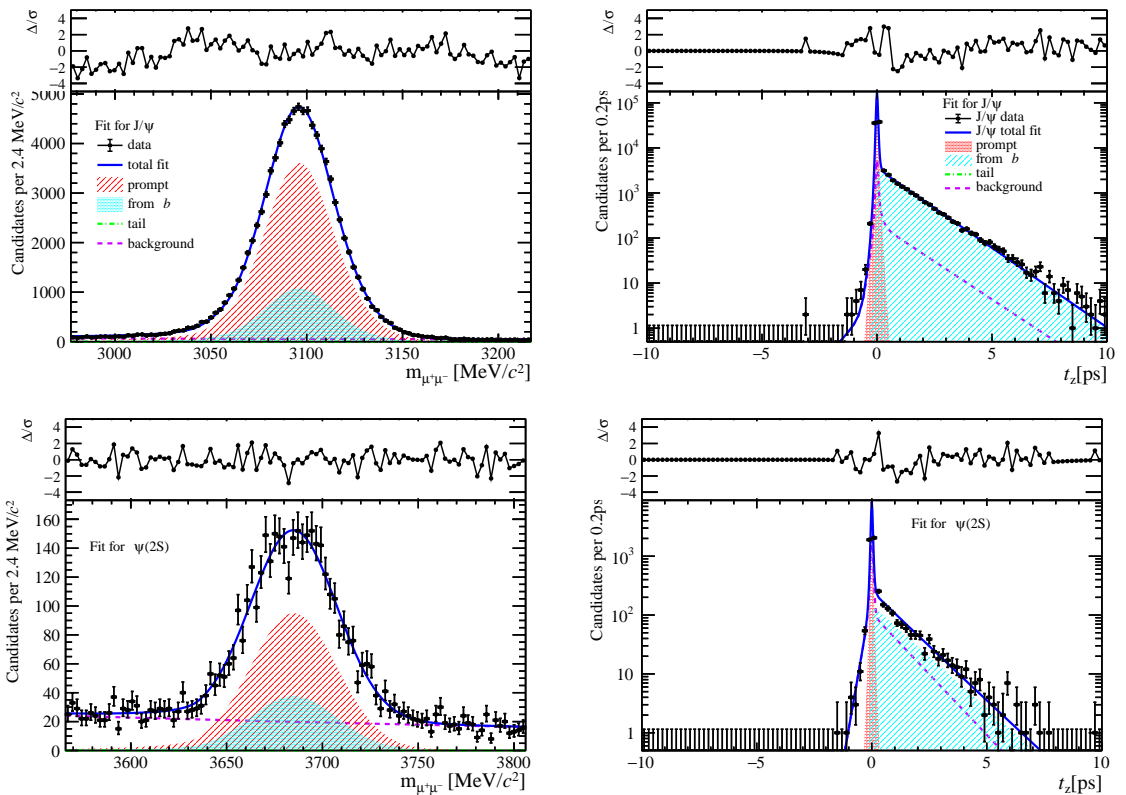


Figure 95: Fit results in  $8 \text{ GeV}/c < p_T < 20 \text{ GeV}/c$ ,  $3.5 < y < 4.5$  and  $70 \leq \text{PVNTRACKS} < 95$ .

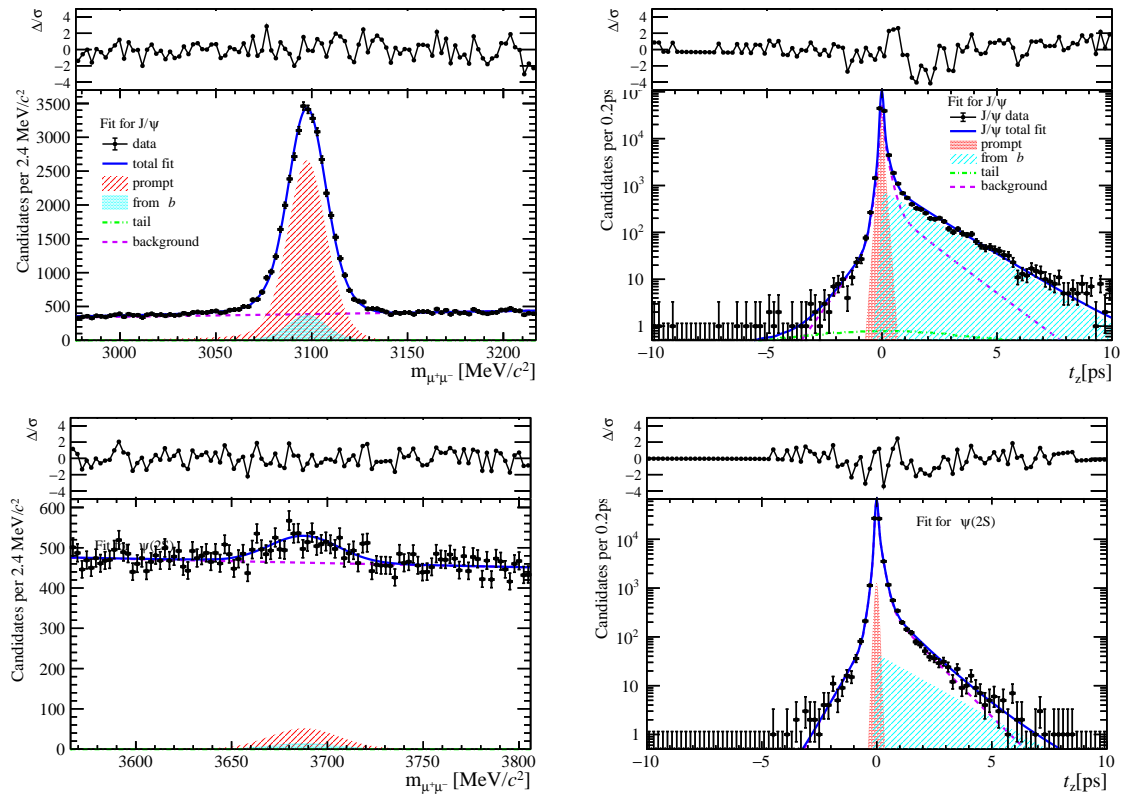


Figure 96: Fit results in  $0 \text{ GeV}/c < p_T < 2 \text{ GeV}/c$ ,  $2.0 < y < 2.8$  and  $95 \leq \text{PVNTRACKS} < 200$ .

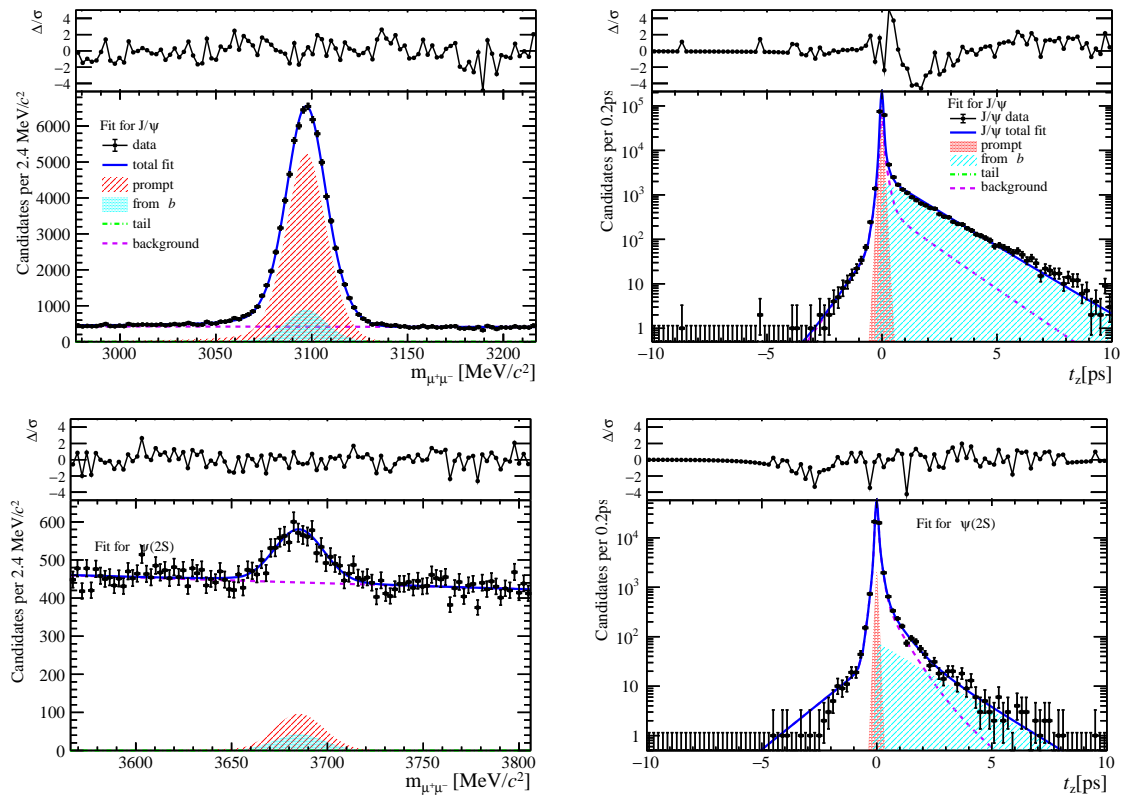


Figure 97: Fit results in  $2 \text{ GeV}/c < p_T < 4 \text{ GeV}/c$ ,  $2.0 < y < 2.8$  and  $95 \leq \text{PVNTRACKS} < 200$ .

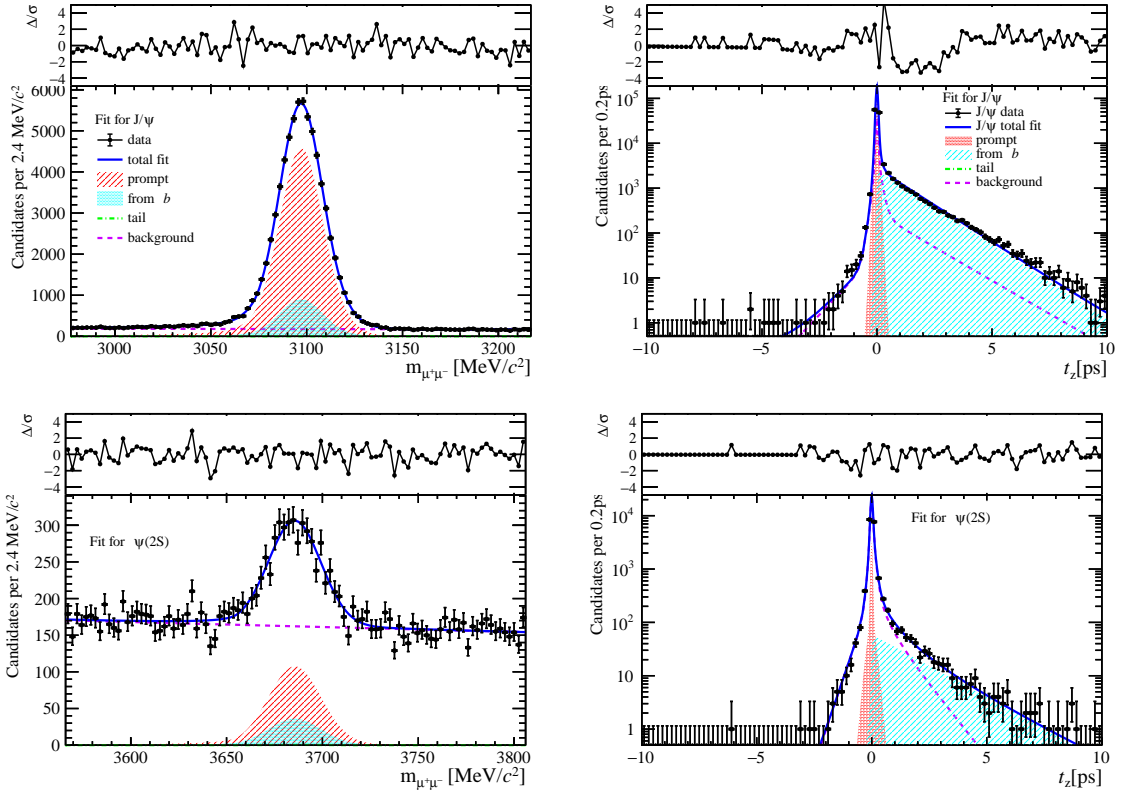


Figure 98: Fit results in  $4 \text{ GeV}/c < p_T < 6 \text{ GeV}/c$ ,  $2.0 < y < 2.8$  and  $95 \leq \text{PVNTRACKS} < 200$ .

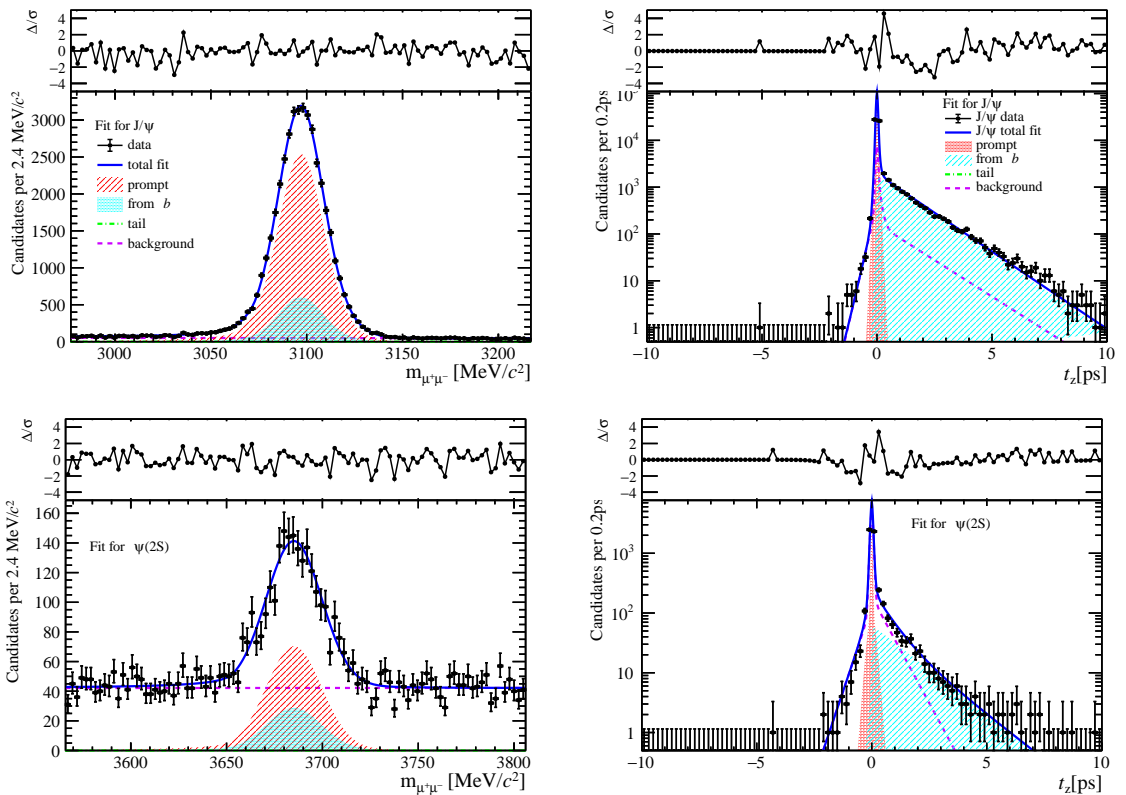


Figure 99: Fit results in  $6 \text{ GeV}/c < p_T < 8 \text{ GeV}/c$ ,  $2.0 < y < 2.8$  and  $95 \leq \text{PVNTRACKS} < 200$ .

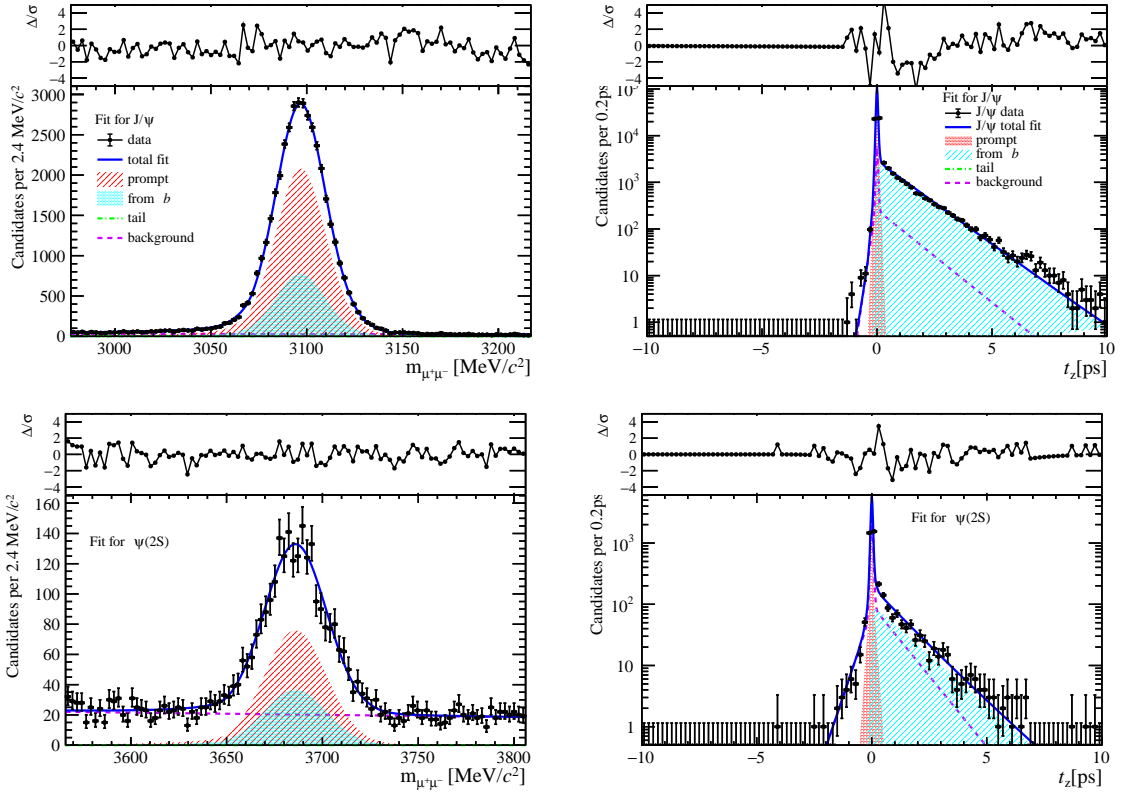


Figure 100: Fit results in  $8 \text{ GeV}/c < p_T < 20 \text{ GeV}/c$ ,  $2.0 < y < 2.8$  and  $95 \leq \text{PVNTRACKS} < 200$ .

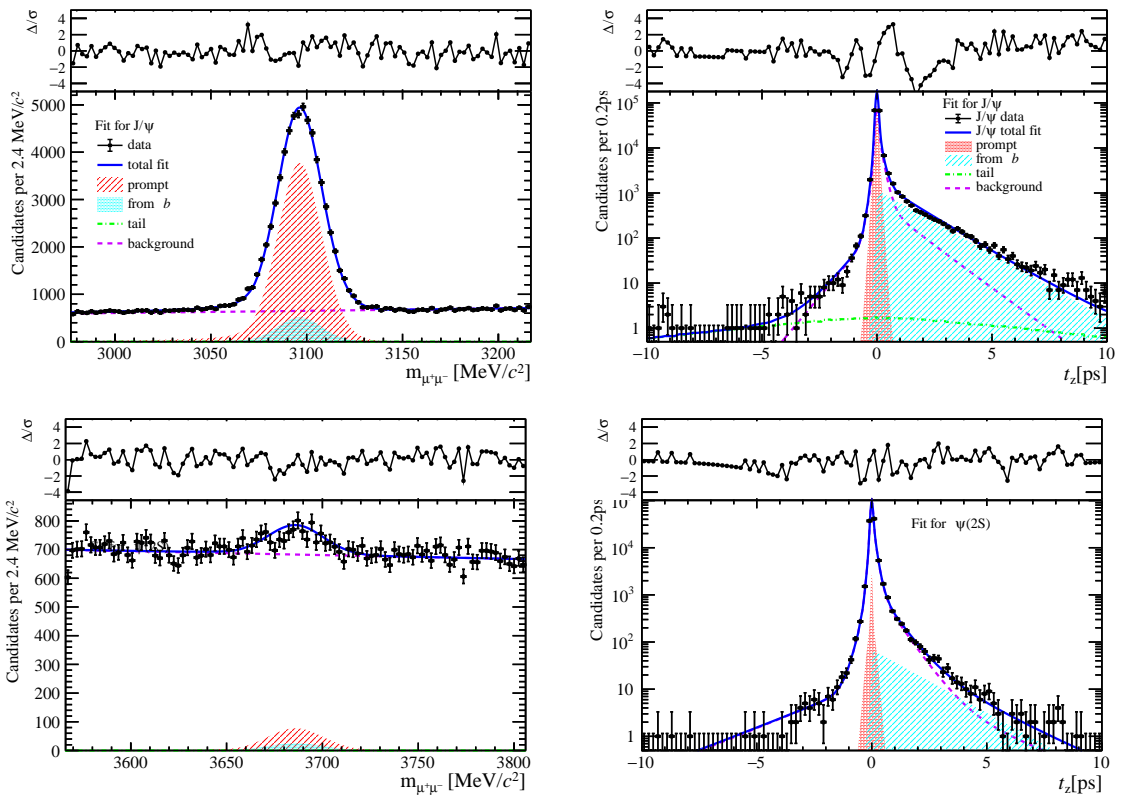


Figure 101: Fit results in  $0 \text{ GeV}/c < p_T < 2 \text{ GeV}/c$ ,  $2.8 < y < 3.5$  and  $95 \leq \text{PVNTRACKS} < 200$ .

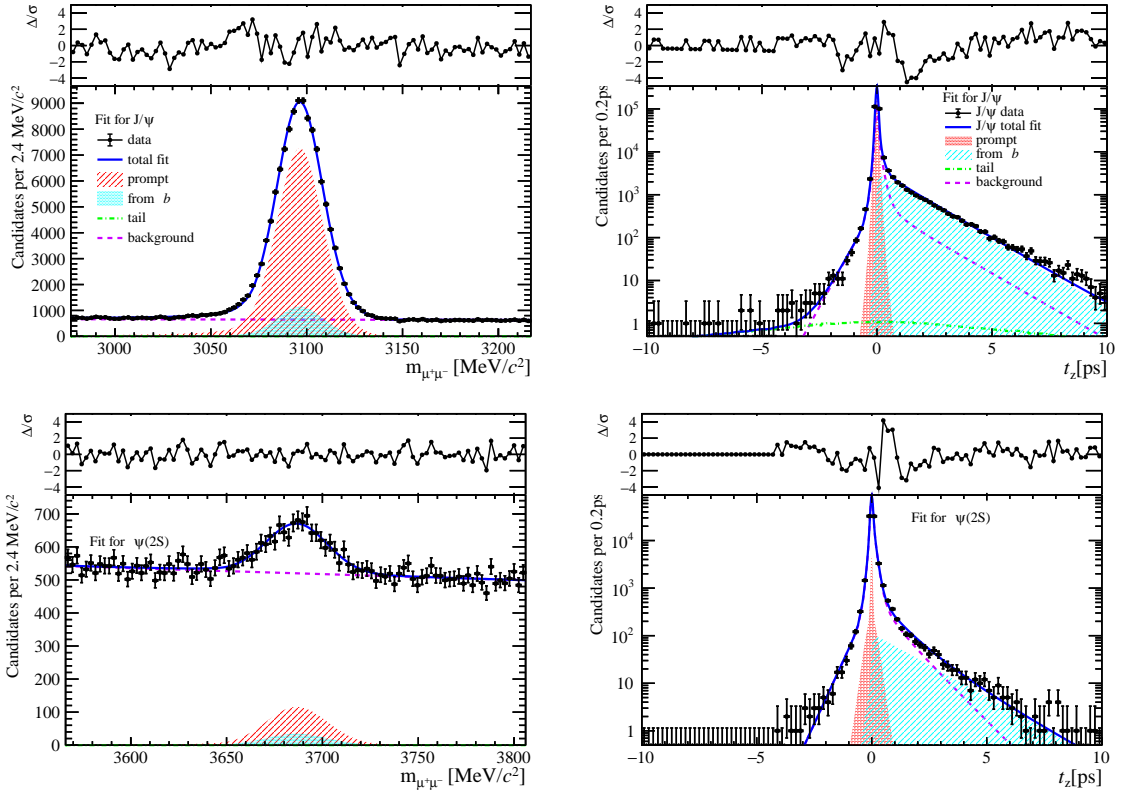


Figure 102: Fit results in  $2 \text{ GeV}/c < p_T < 4 \text{ GeV}/c$ ,  $2.8 < y < 3.5$  and  $95 \leq \text{PVNTRACKS} < 200$ .

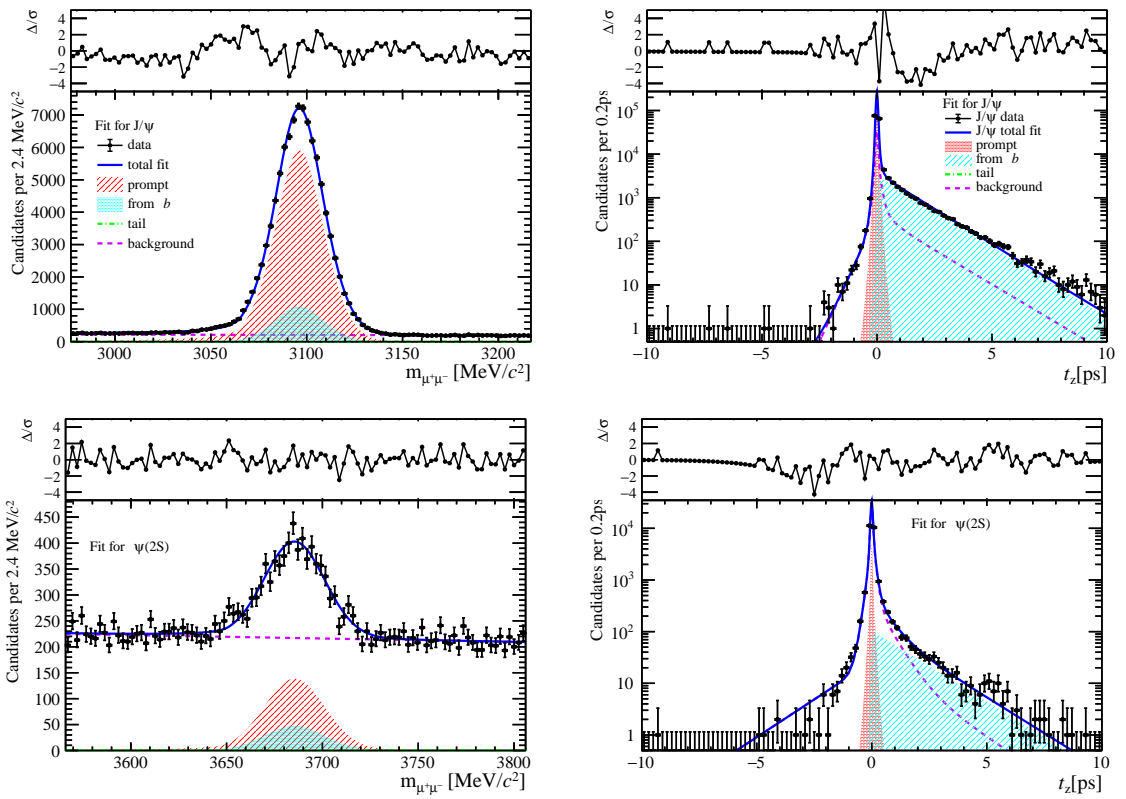


Figure 103: Fit results in  $4 \text{ GeV}/c < p_T < 6 \text{ GeV}/c$ ,  $2.8 < y < 3.5$  and  $95 \leq \text{PVNTRACKS} < 200$ .

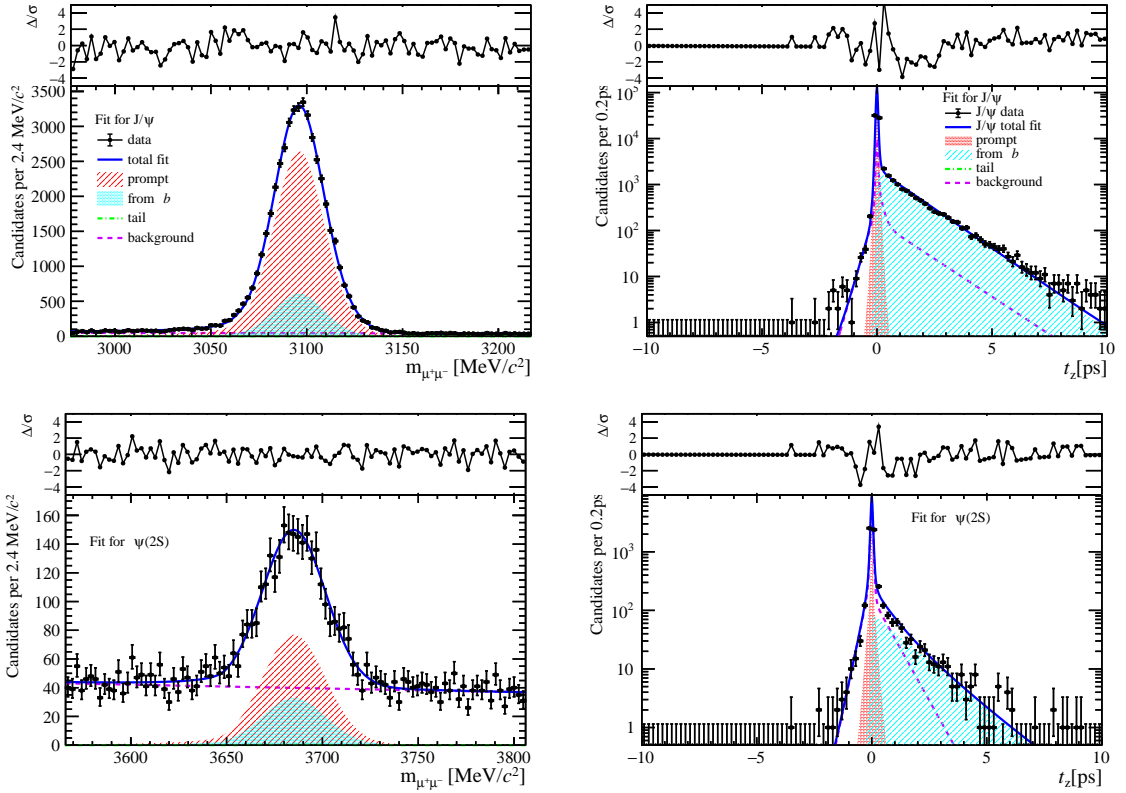


Figure 104: Fit results in  $6 \text{ GeV}/c < p_T < 8 \text{ GeV}/c$ ,  $2.8 < y < 3.5$  and  $95 \leq \text{PVNTRACKS} < 200$ .

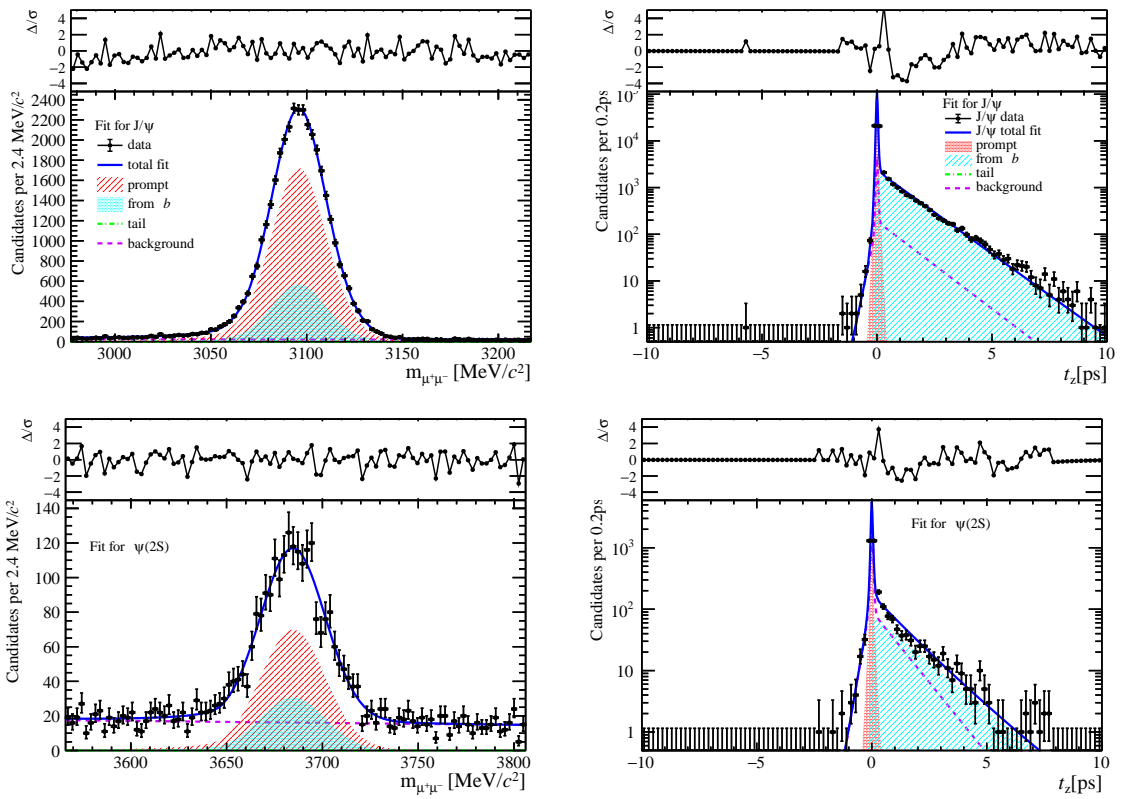


Figure 105: Fit results in  $8 \text{ GeV}/c < p_T < 20 \text{ GeV}/c$ ,  $2.8 < y < 3.5$  and  $95 \leq \text{PVNTRACKS} < 200$ .

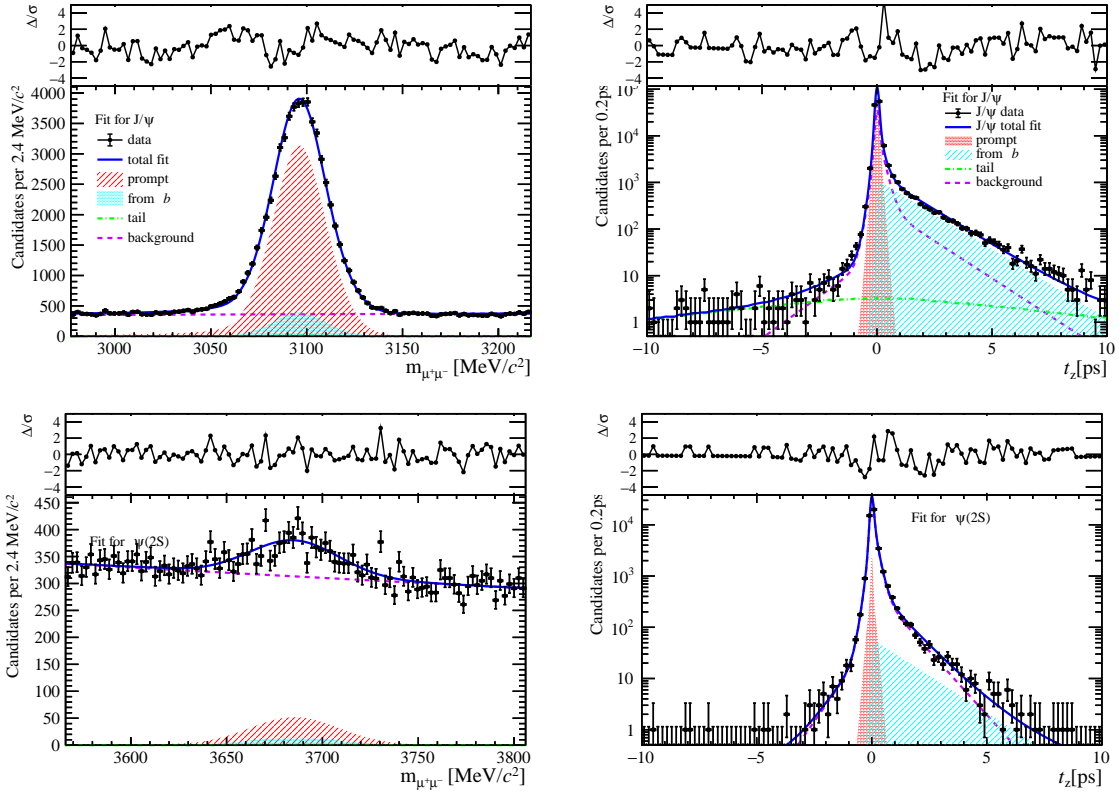


Figure 106: Fit results in  $0 \text{ GeV}/c < p_T < 2 \text{ GeV}/c$ ,  $3.5 < y < 4.5$  and  $95 \leq \text{PVNTRACKS} < 200$ .

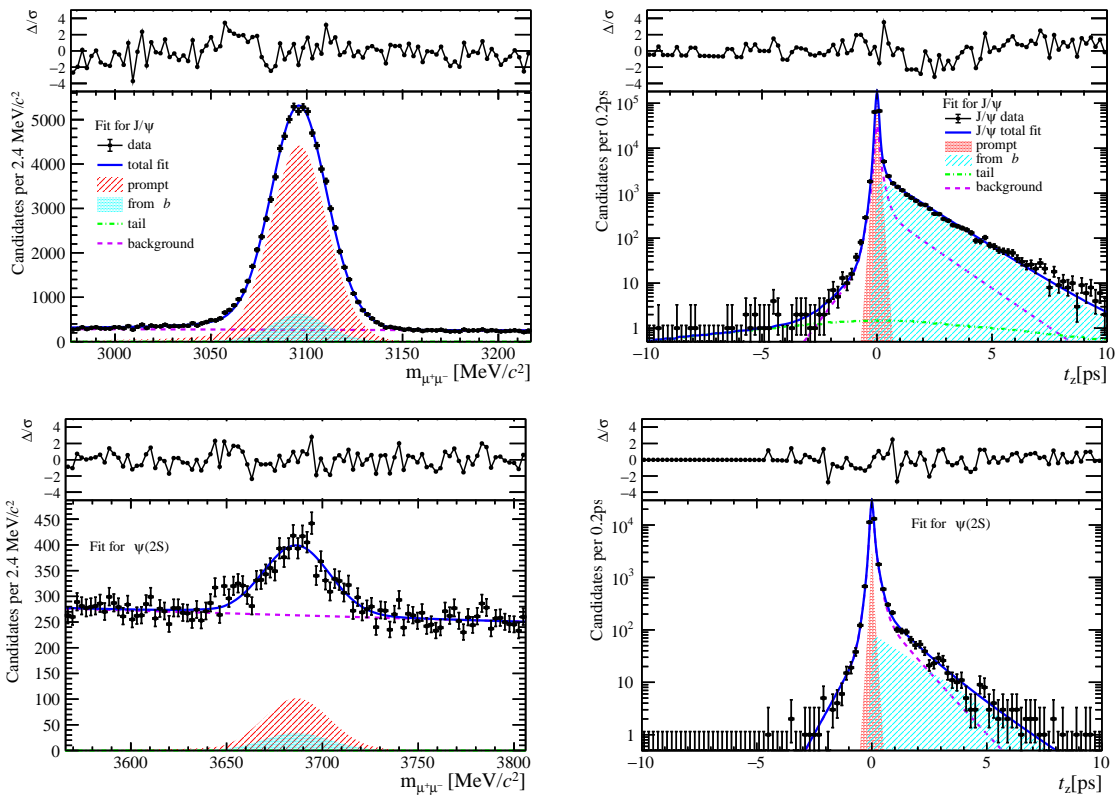


Figure 107: Fit results in  $2 \text{ GeV}/c < p_T < 4 \text{ GeV}/c$ ,  $3.5 < y < 4.5$  and  $95 \leq \text{PVNTRACKS} < 200$ .

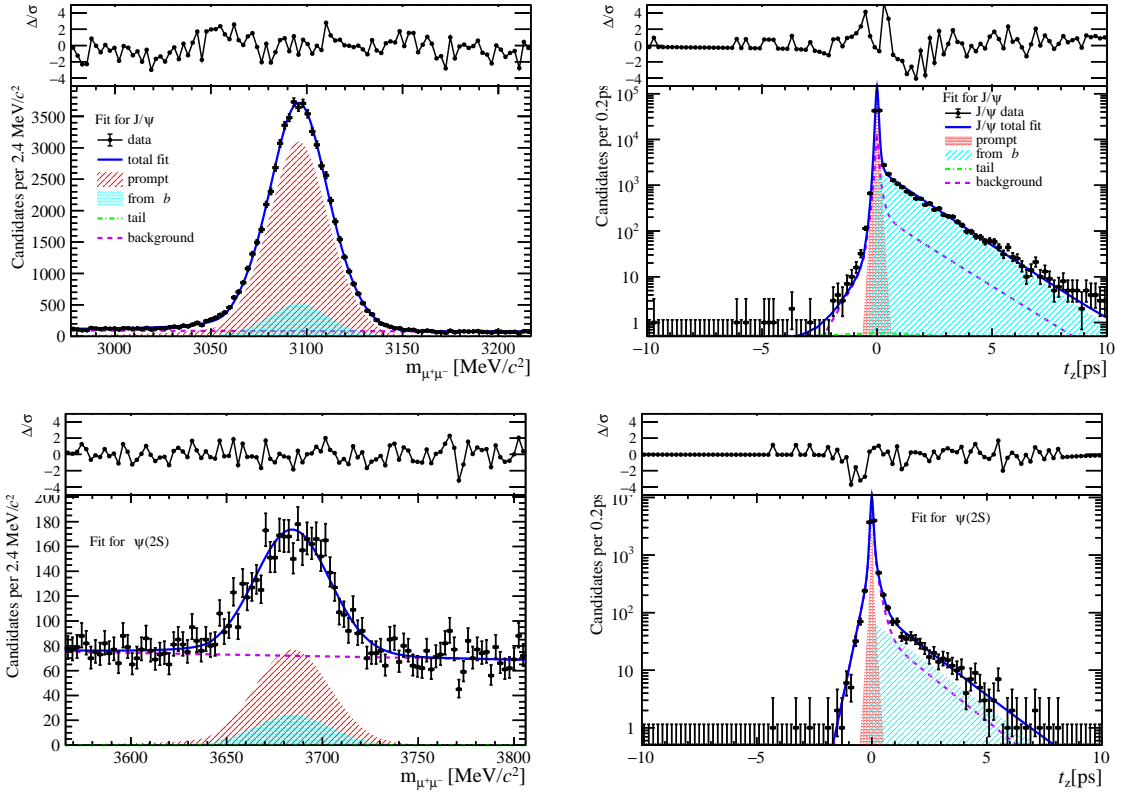


Figure 108: Fit results in  $4 \text{ GeV}/c < p_T < 6 \text{ GeV}/c$ ,  $3.5 < y < 4.5$  and  $95 \leq \text{PVNTRACKS} < 200$ .

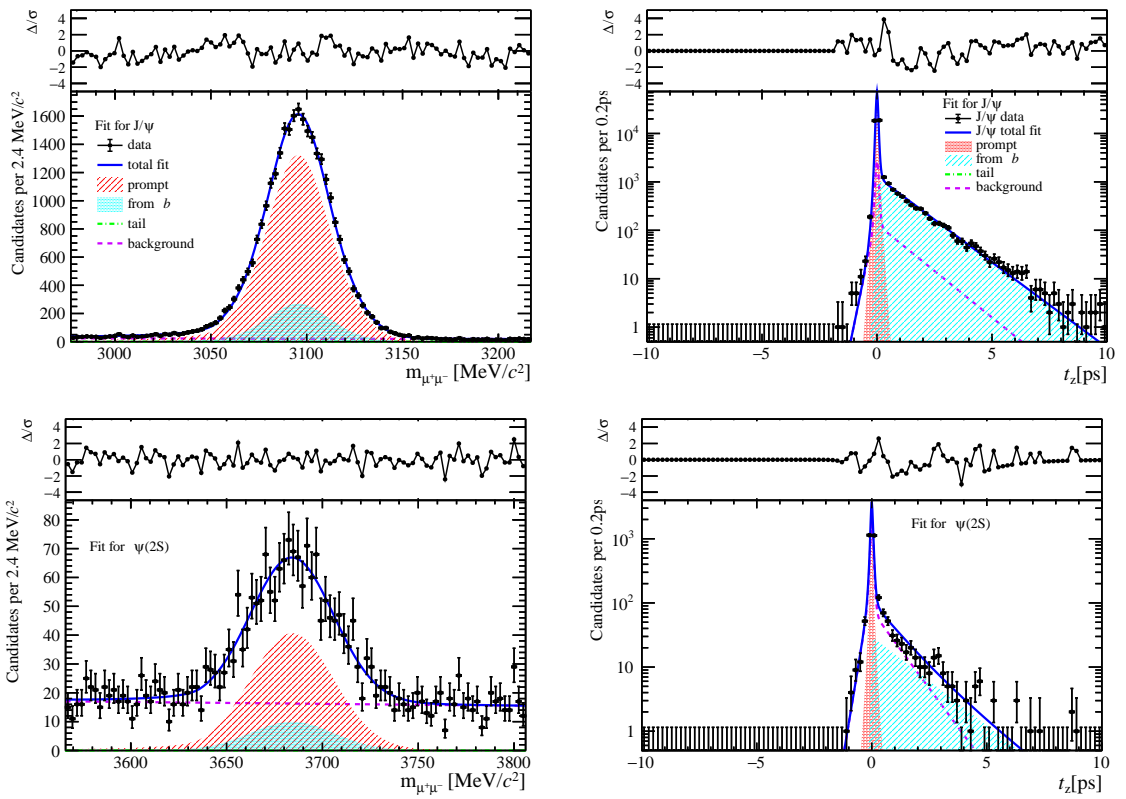


Figure 109: Fit results in  $6 \text{ GeV}/c < p_T < 8 \text{ GeV}/c$ ,  $3.5 < y < 4.5$  and  $95 \leq \text{PVNTRACKS} < 200$ .

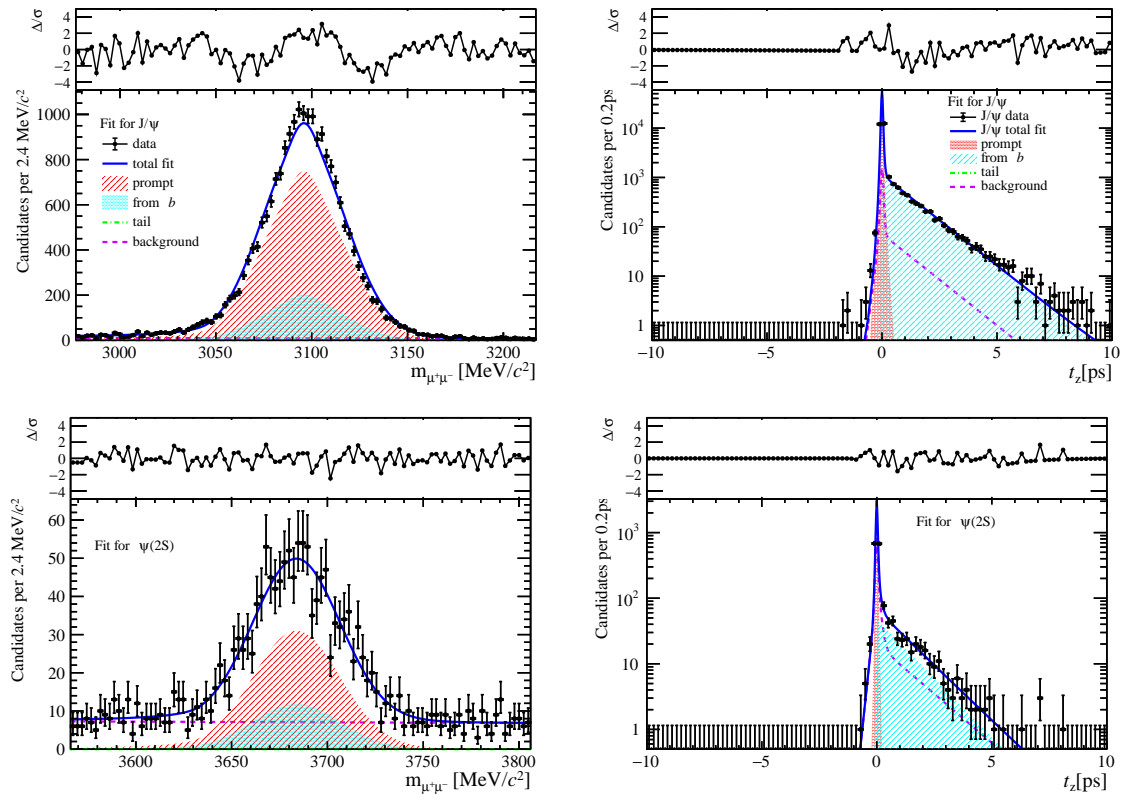


Figure 110: Fit results in  $8 \text{ GeV}/c < p_T < 20 \text{ GeV}/c$ ,  $3.5 < y < 4.5$  and  $95 \leq \text{PVNTRACKS} < 200$ .

## 719 2 Separated by nBackTracks

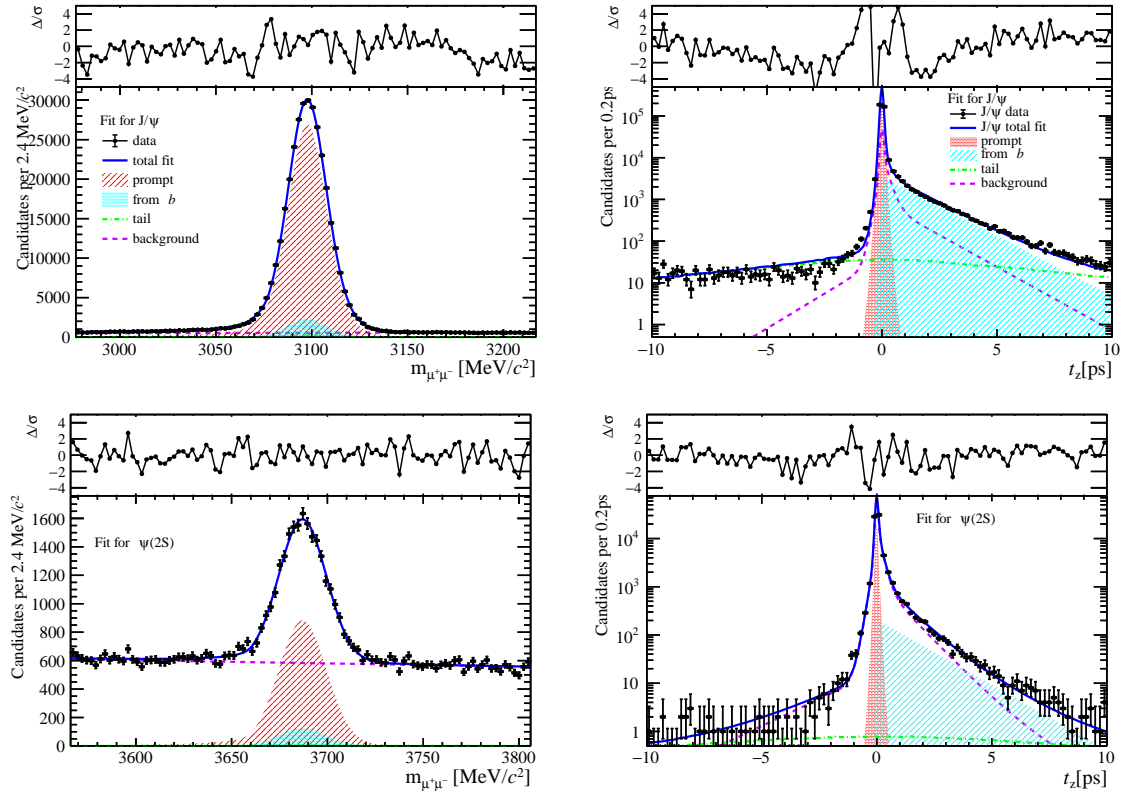


Figure 111: Fit results in  $0 \text{ GeV}/c < p_T < 2 \text{ GeV}/c$ ,  $2.0 < y < 2.8$  and  $0 \leq \text{nBackTracks} < 8$ .

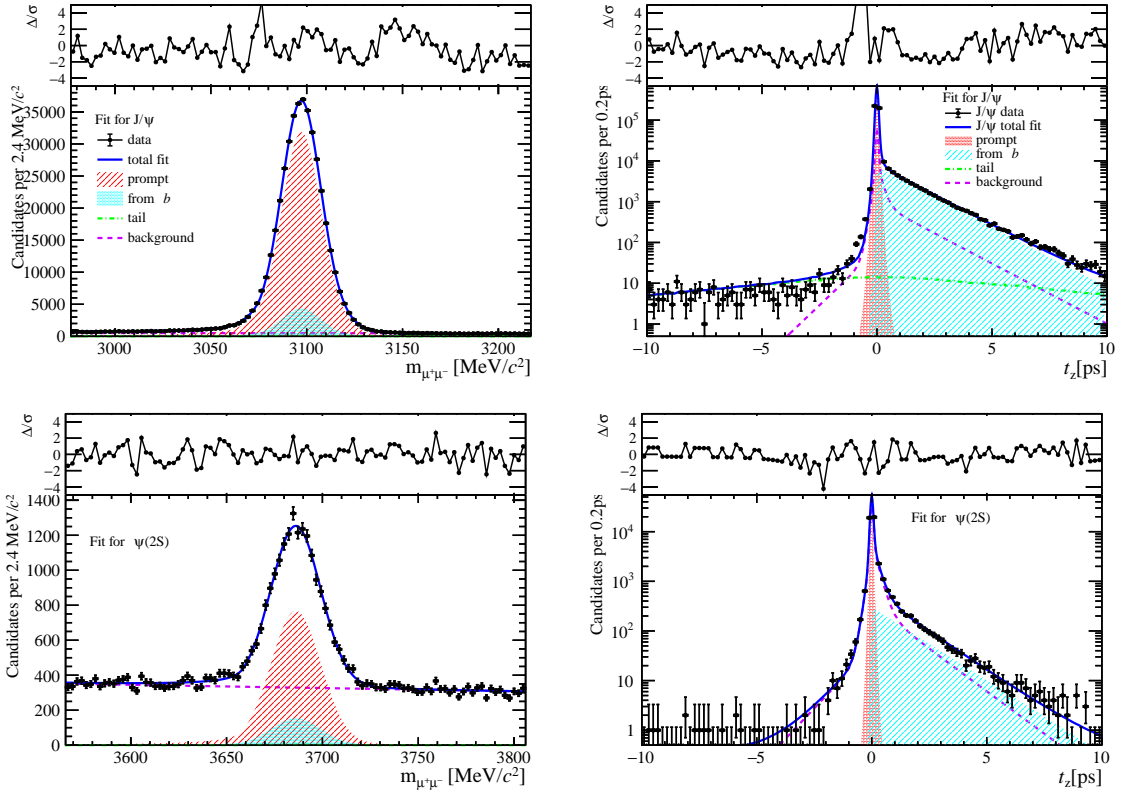


Figure 112: Fit results in  $2 \text{ GeV}/c < p_T < 4 \text{ GeV}/c$ ,  $2.0 < y < 2.8$  and  $0 \leq \text{nBackTracks} < 8$ .

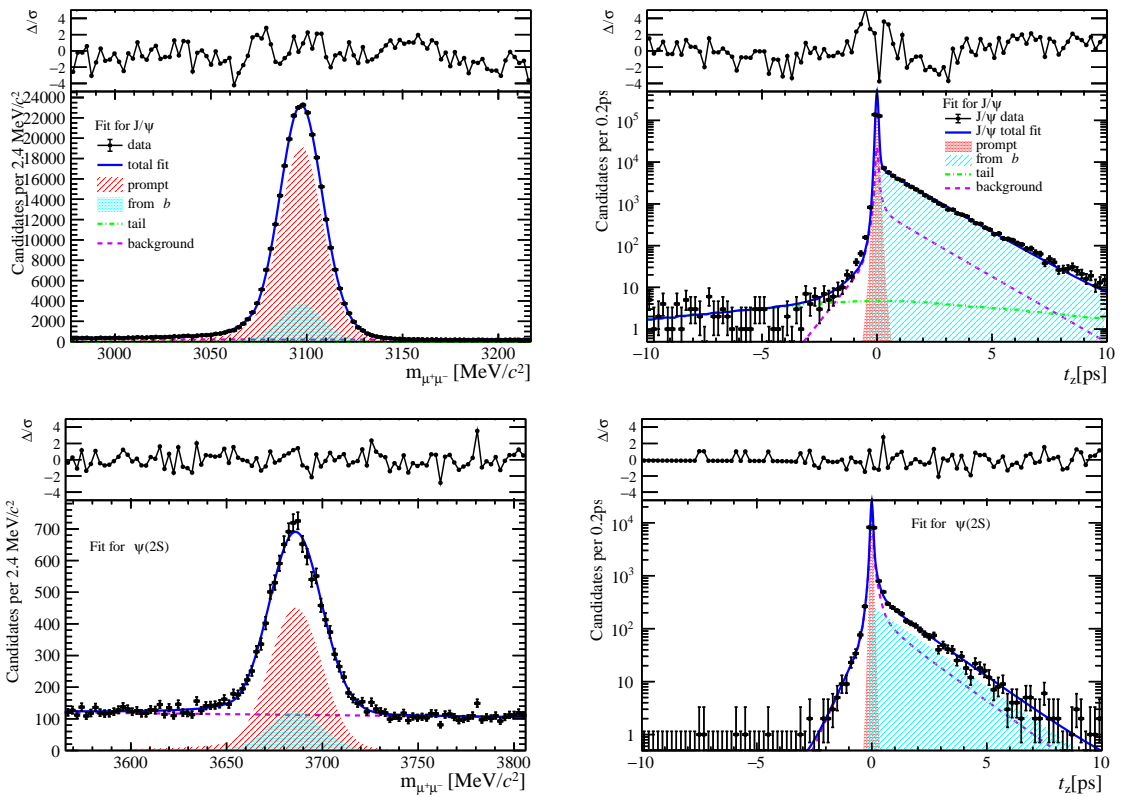


Figure 113: Fit results in  $4 \text{ GeV}/c < p_T < 6 \text{ GeV}/c$ ,  $2.0 < y < 2.8$  and  $0 \leq \text{nBackTracks} < 8$ .

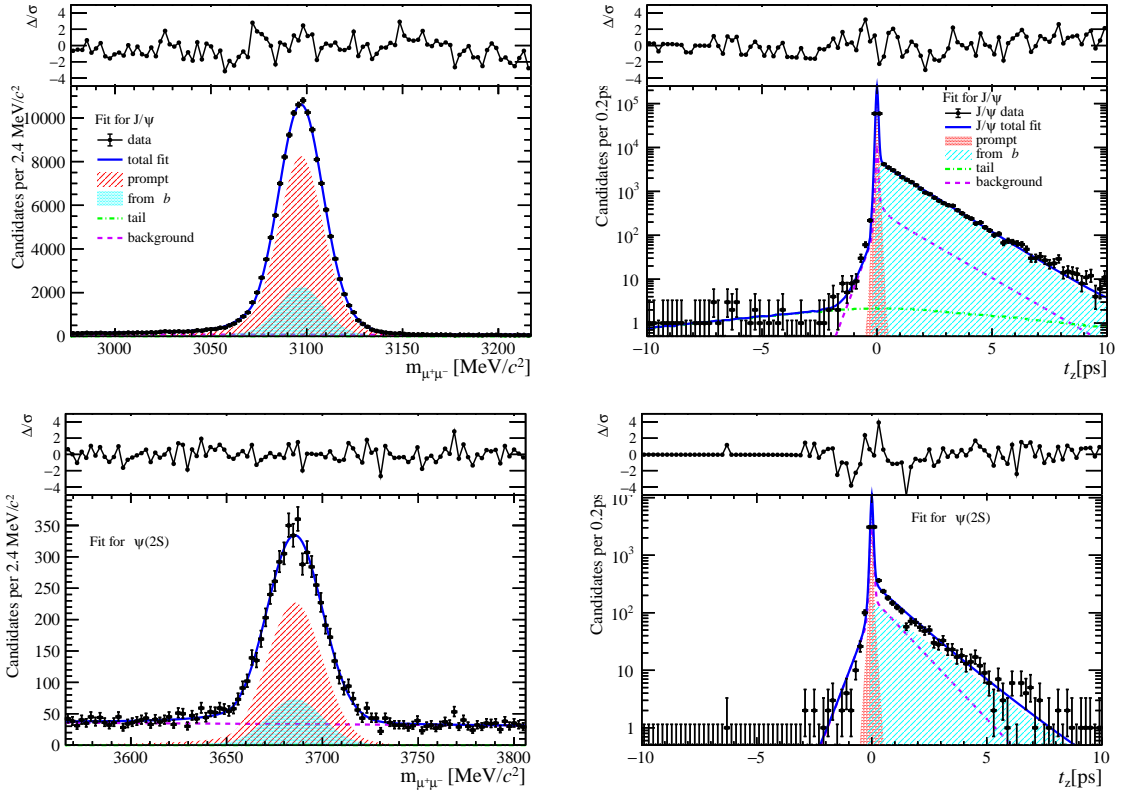


Figure 114: Fit results in  $6 \text{ GeV}/c < p_T < 8 \text{ GeV}/c$ ,  $2.0 < y < 2.8$  and  $0 \leq \text{nBackTracks} < 8$ .

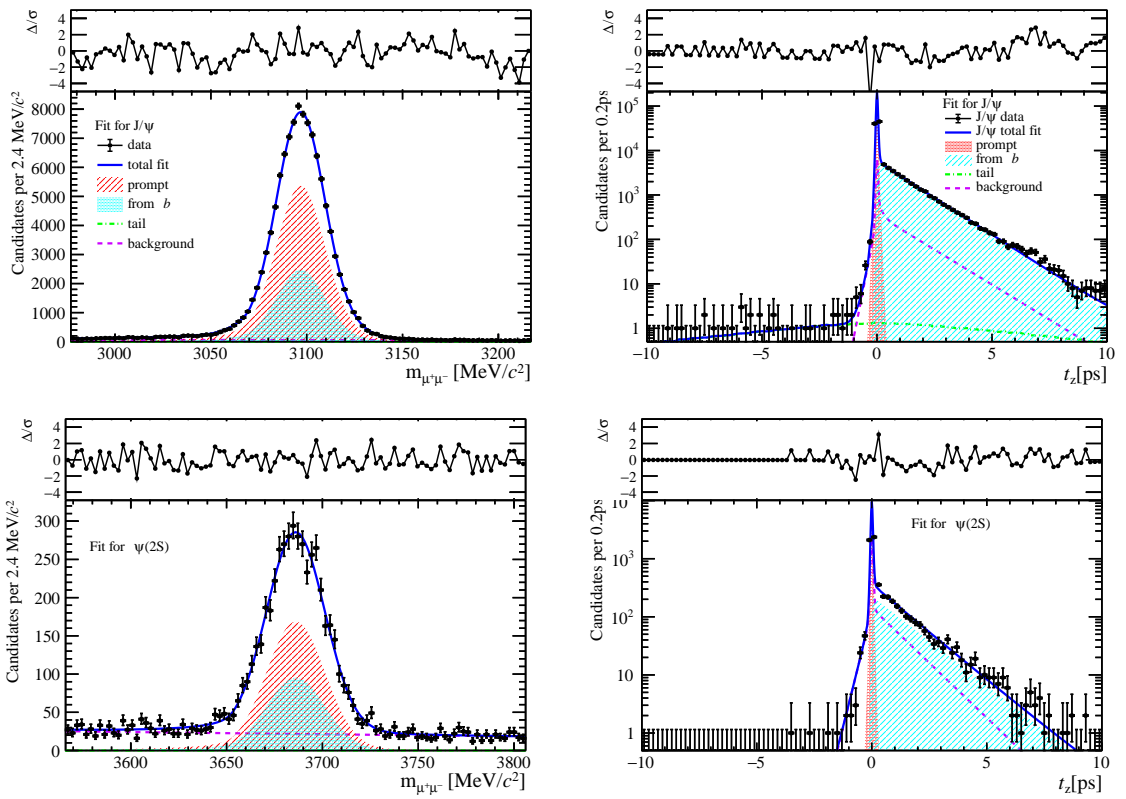


Figure 115: Fit results in  $8 \text{ GeV}/c < p_T < 20 \text{ GeV}/c$ ,  $2.0 < y < 2.8$  and  $0 \leq \text{nBackTracks} < 8$ .

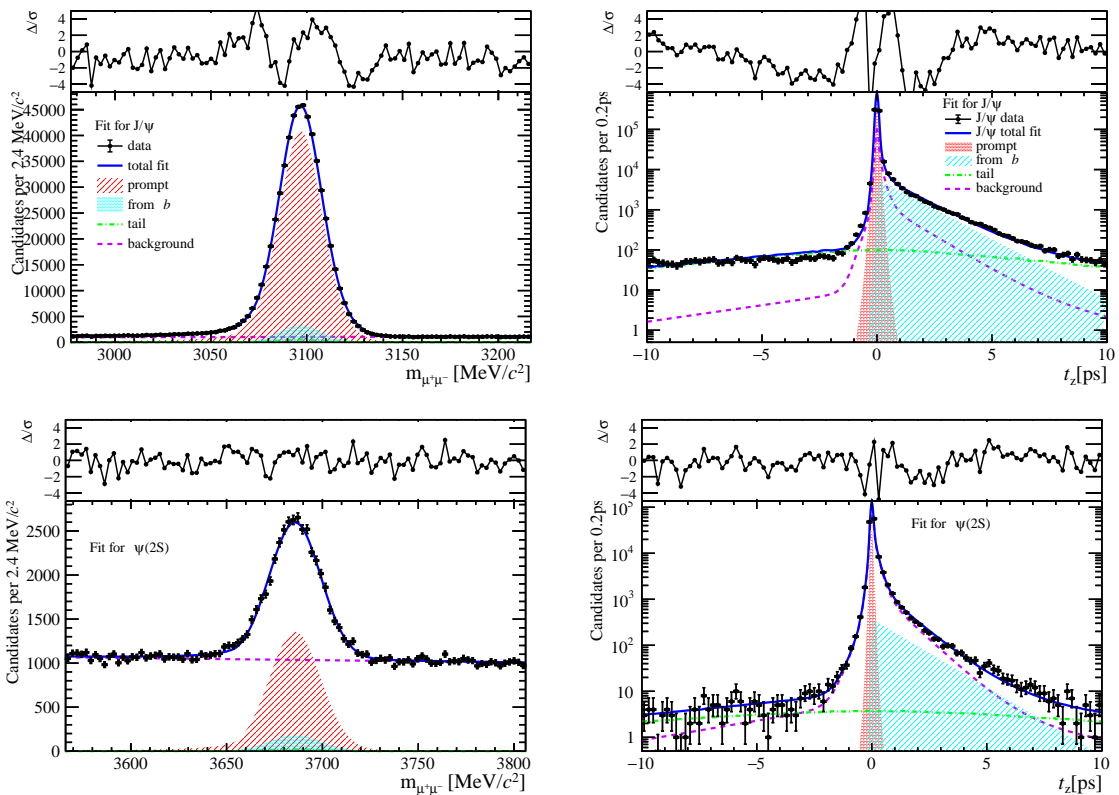


Figure 116: Fit results in  $0 \text{ GeV}/c < p_T < 2 \text{ GeV}/c$ ,  $2.8 < y < 3.5$  and  $0 \leq n\text{BackTracks} < 8$ .

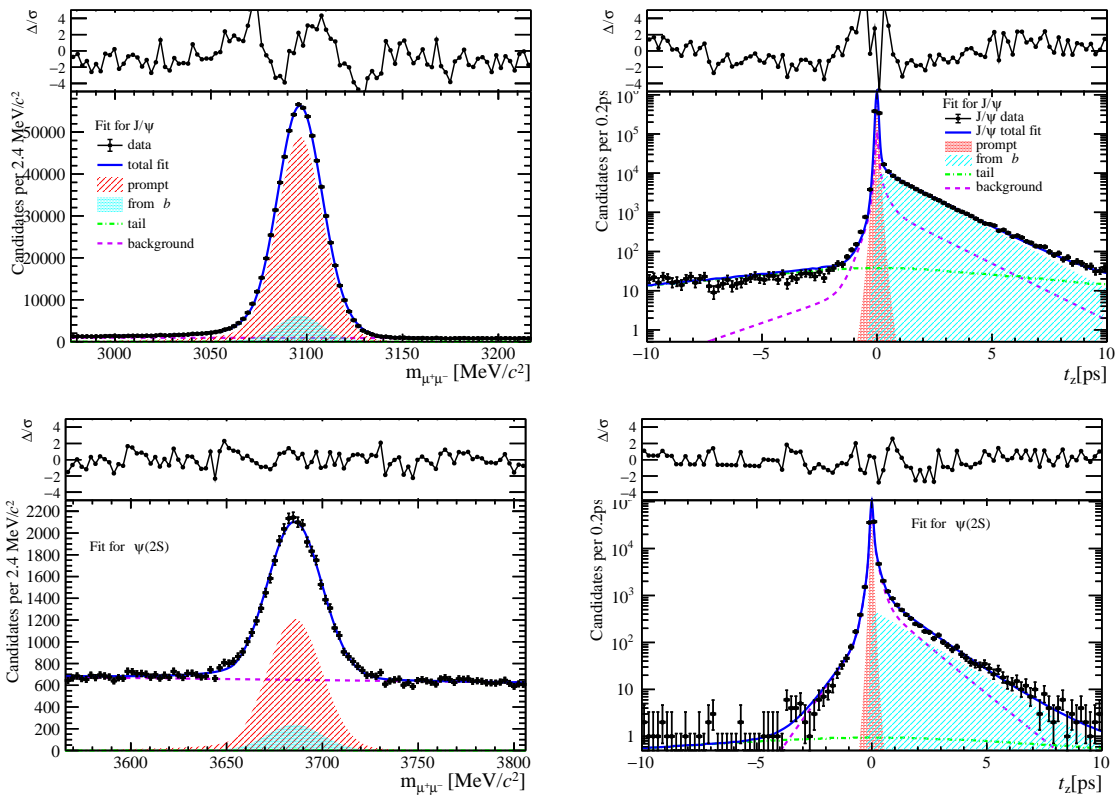


Figure 117: Fit results in  $2 \text{ GeV}/c < p_T < 4 \text{ GeV}/c$ ,  $2.8 < y < 3.5$  and  $0 \leq n\text{BackTracks} < 8$ .

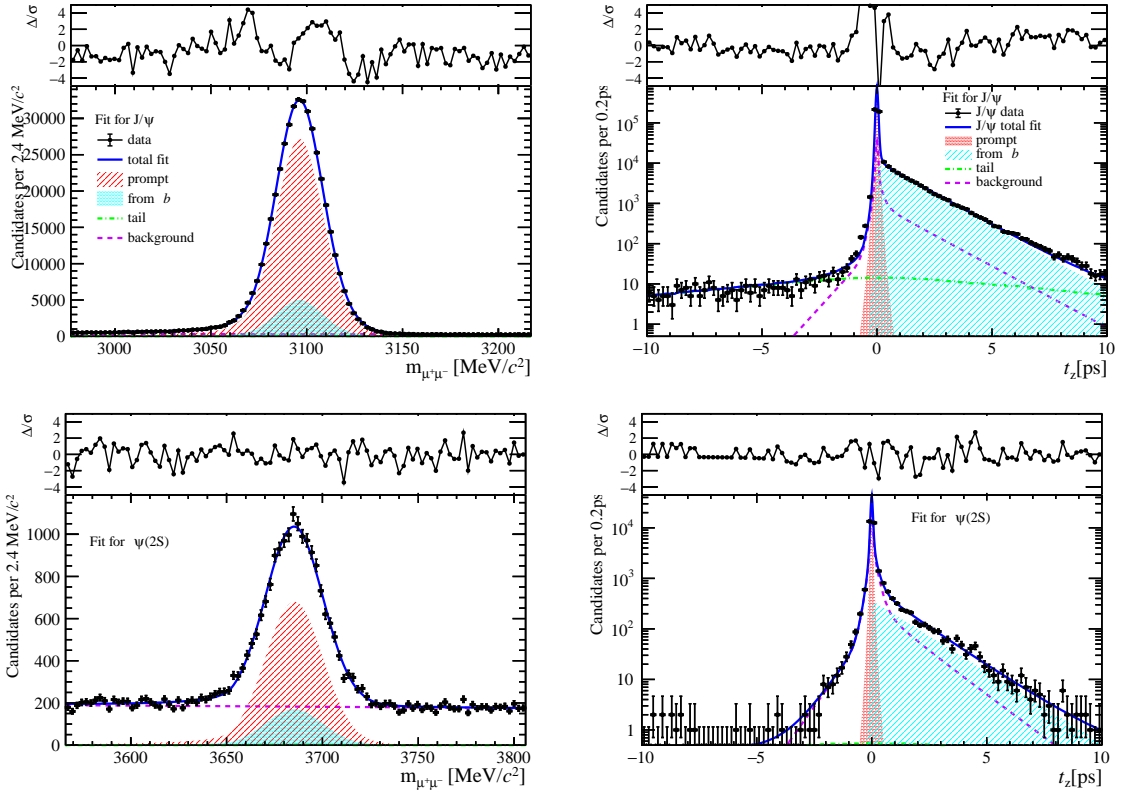


Figure 118: Fit results in  $4 \text{ GeV}/c < p_T < 6 \text{ GeV}/c$ ,  $2.8 < y < 3.5$  and  $0 \leq \text{nBackTracks} < 8$ .

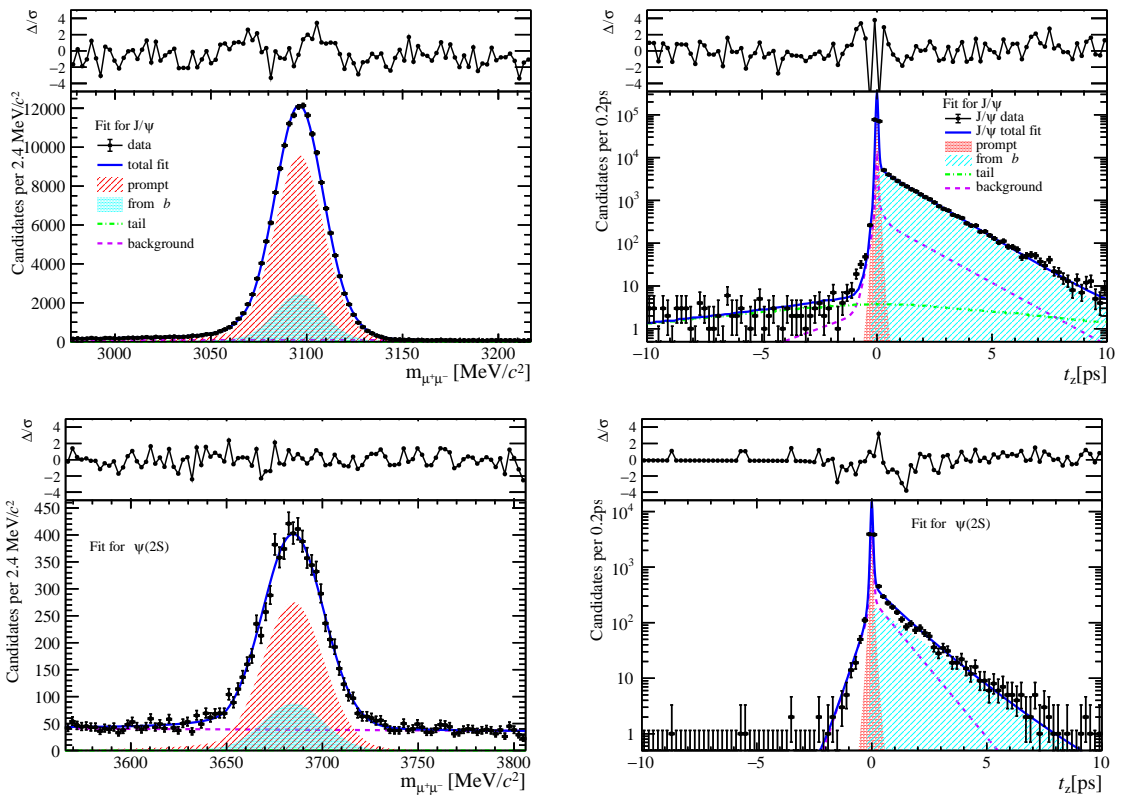


Figure 119: Fit results in  $6 \text{ GeV}/c < p_T < 8 \text{ GeV}/c$ ,  $2.8 < y < 3.5$  and  $0 \leq \text{nBackTracks} < 8$ .

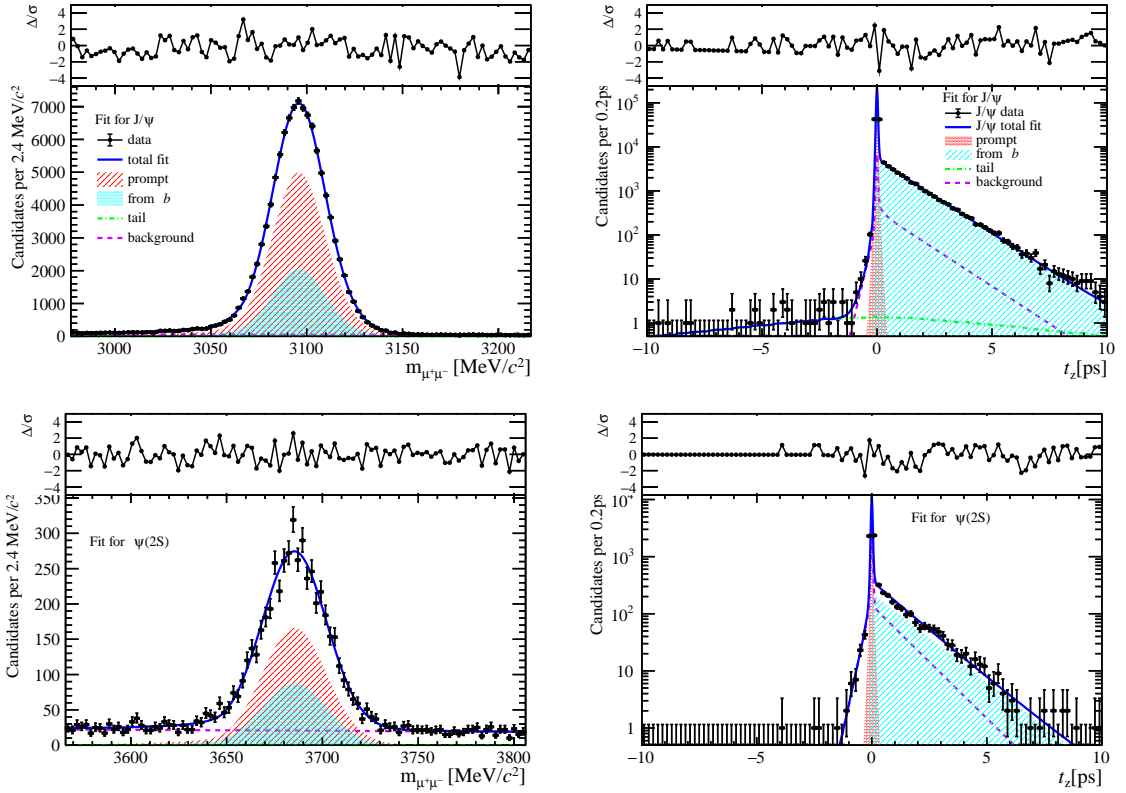


Figure 120: Fit results in  $8 \text{ GeV}/c < p_T < 20 \text{ GeV}/c$ ,  $2.8 < y < 3.5$  and  $0 \leq \text{nBackTracks} < 8$ .

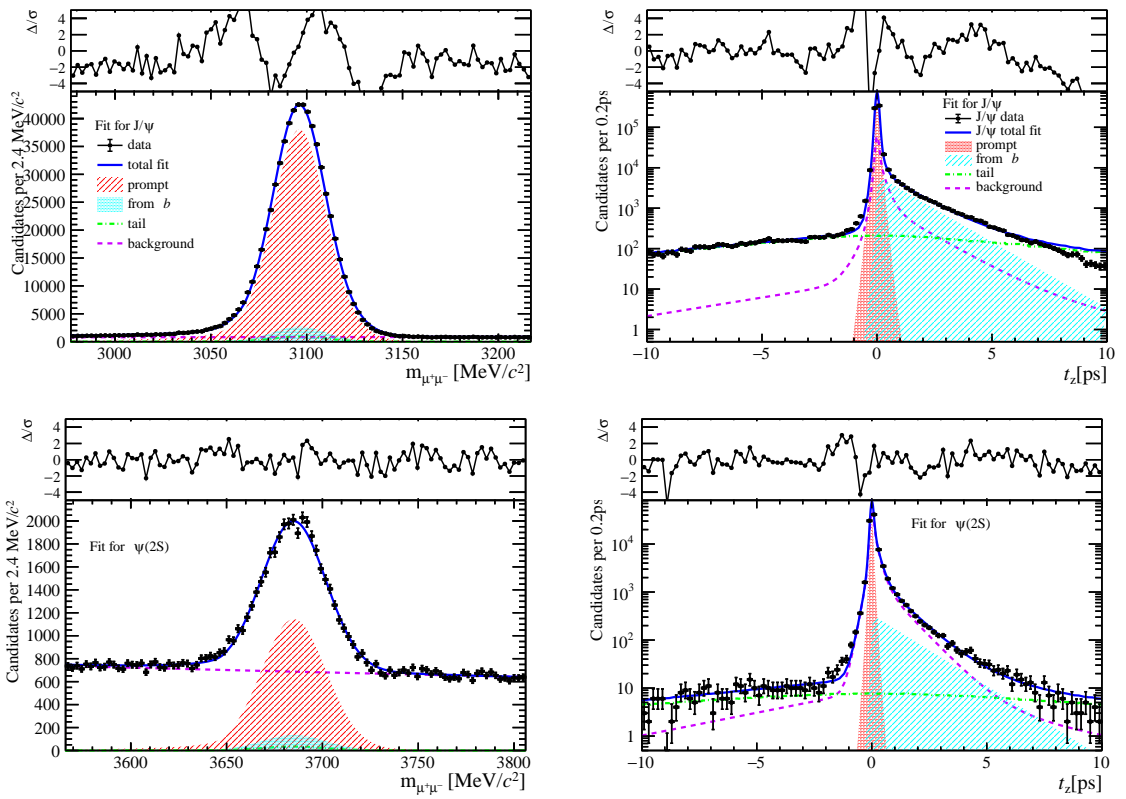


Figure 121: Fit results in  $0 \text{ GeV}/c < p_T < 2 \text{ GeV}/c$ ,  $3.5 < y < 4.5$  and  $0 \leq \text{nBackTracks} < 8$ .

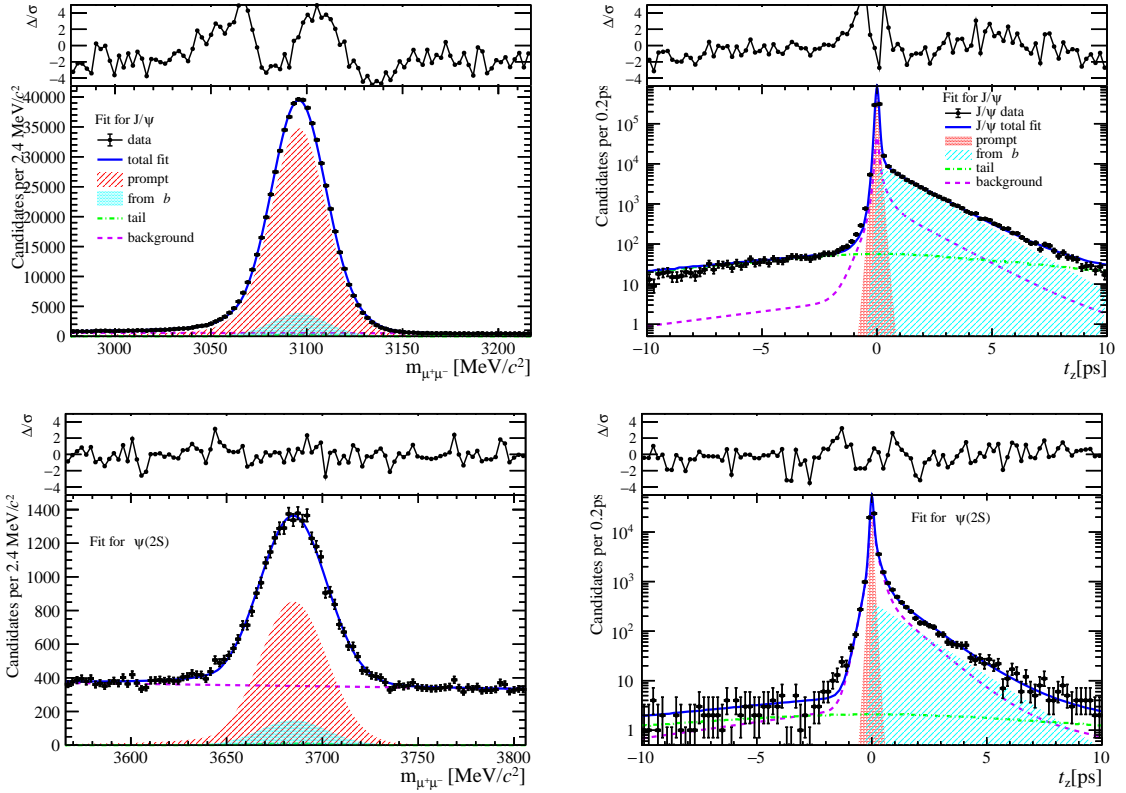


Figure 122: Fit results in  $2 \text{ GeV}/c < p_T < 4 \text{ GeV}/c$ ,  $3.5 < y < 4.5$  and  $0 \leq \text{nBackTracks} < 8$ .

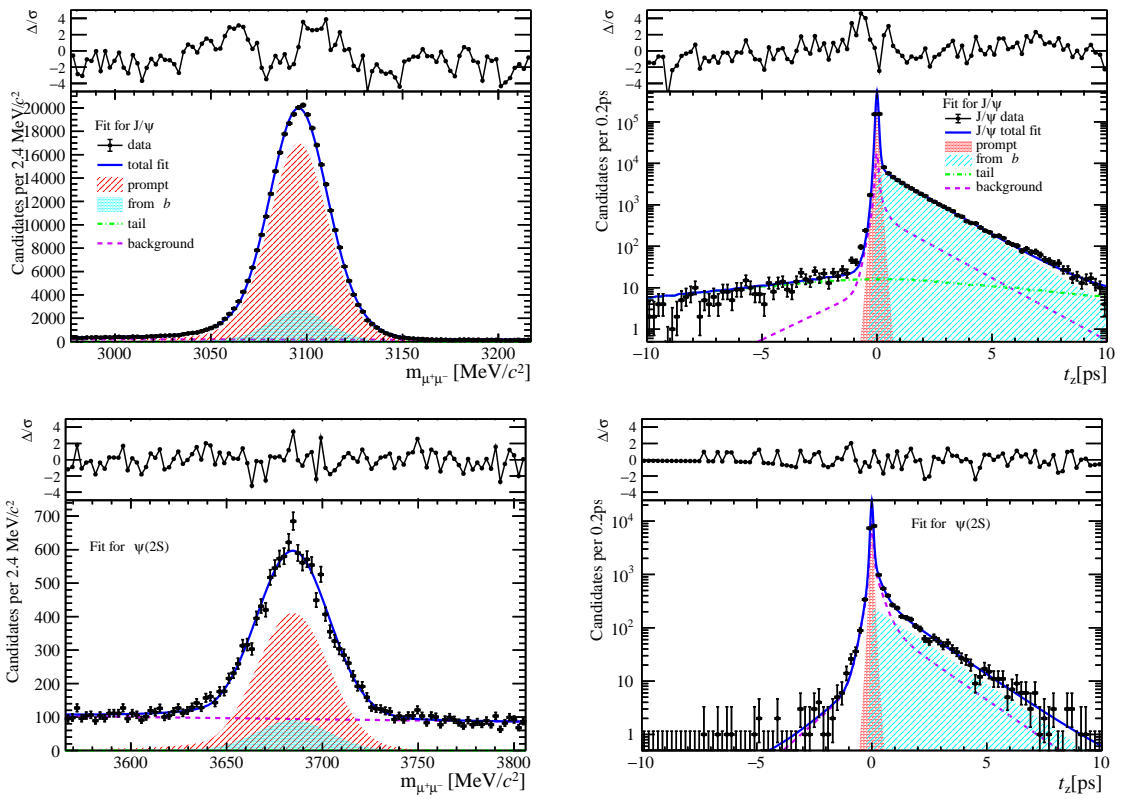


Figure 123: Fit results in  $4 \text{ GeV}/c < p_T < 6 \text{ GeV}/c$ ,  $3.5 < y < 4.5$  and  $0 \leq \text{nBackTracks} < 8$ .

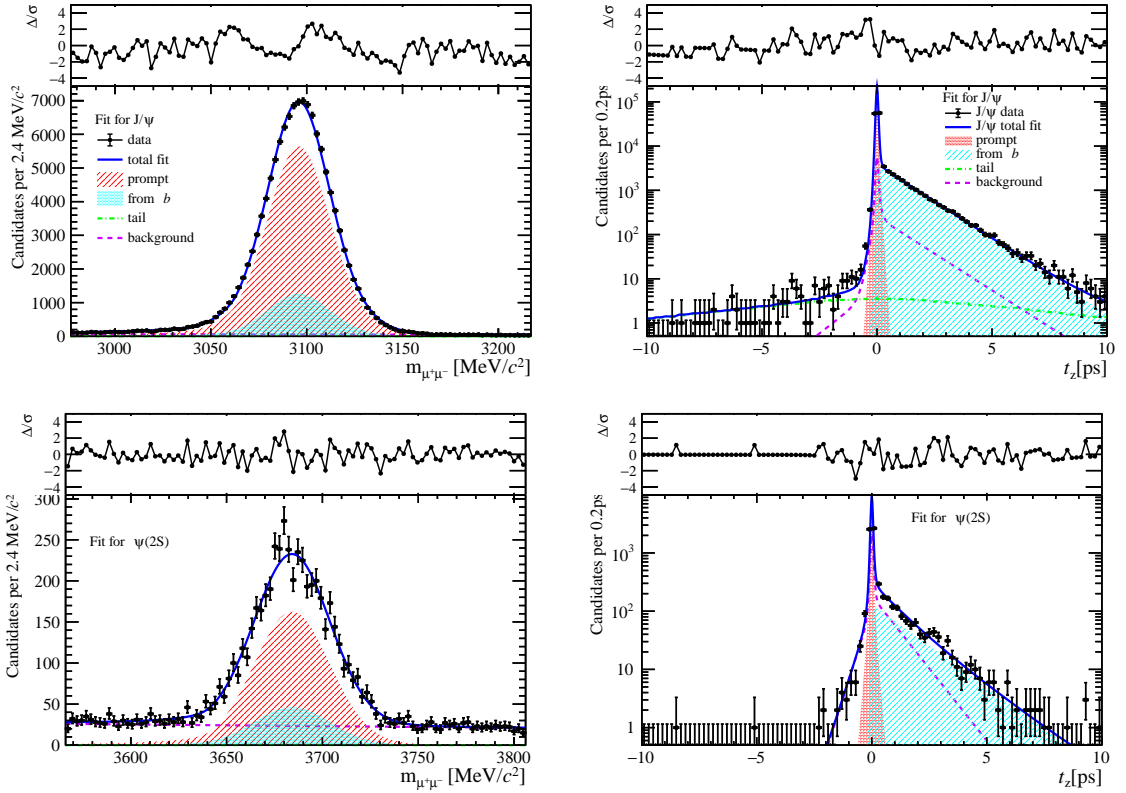


Figure 124: Fit results in  $6 \text{ GeV}/c < p_T < 8 \text{ GeV}/c$ ,  $3.5 < y < 4.5$  and  $0 \leq \text{nBackTracks} < 8$ .

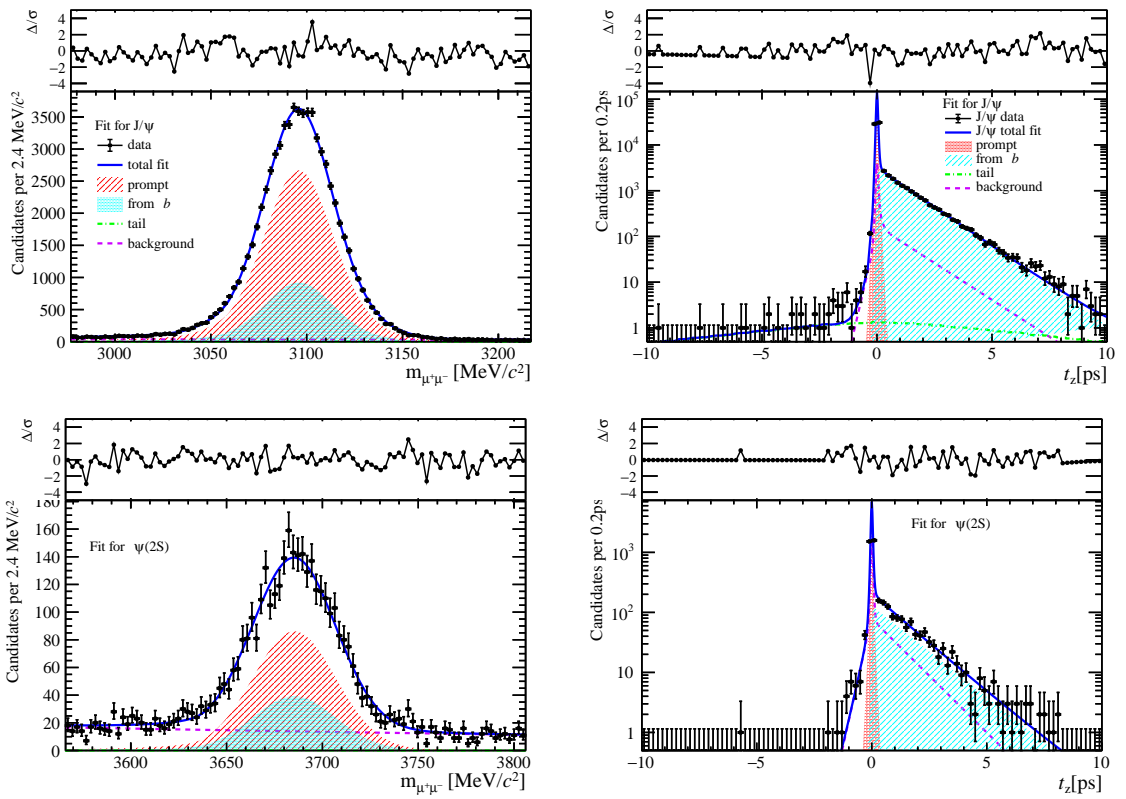


Figure 125: Fit results in  $8 \text{ GeV}/c < p_T < 20 \text{ GeV}/c$ ,  $3.5 < y < 4.5$  and  $0 \leq \text{nBackTracks} < 8$ .

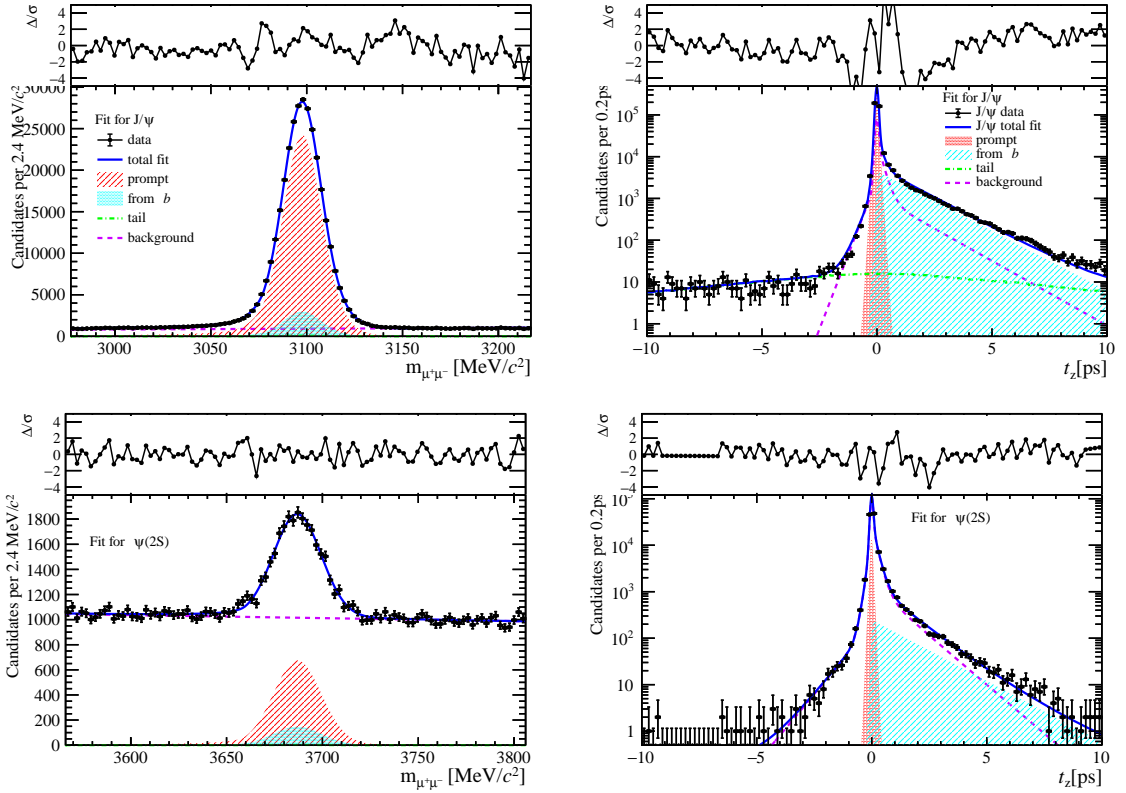


Figure 126: Fit results in  $0 \text{ GeV}/c < p_T < 2 \text{ GeV}/c$ ,  $2.0 < y < 2.8$  and  $8 \leq n\text{BackTracks} < 15$ .

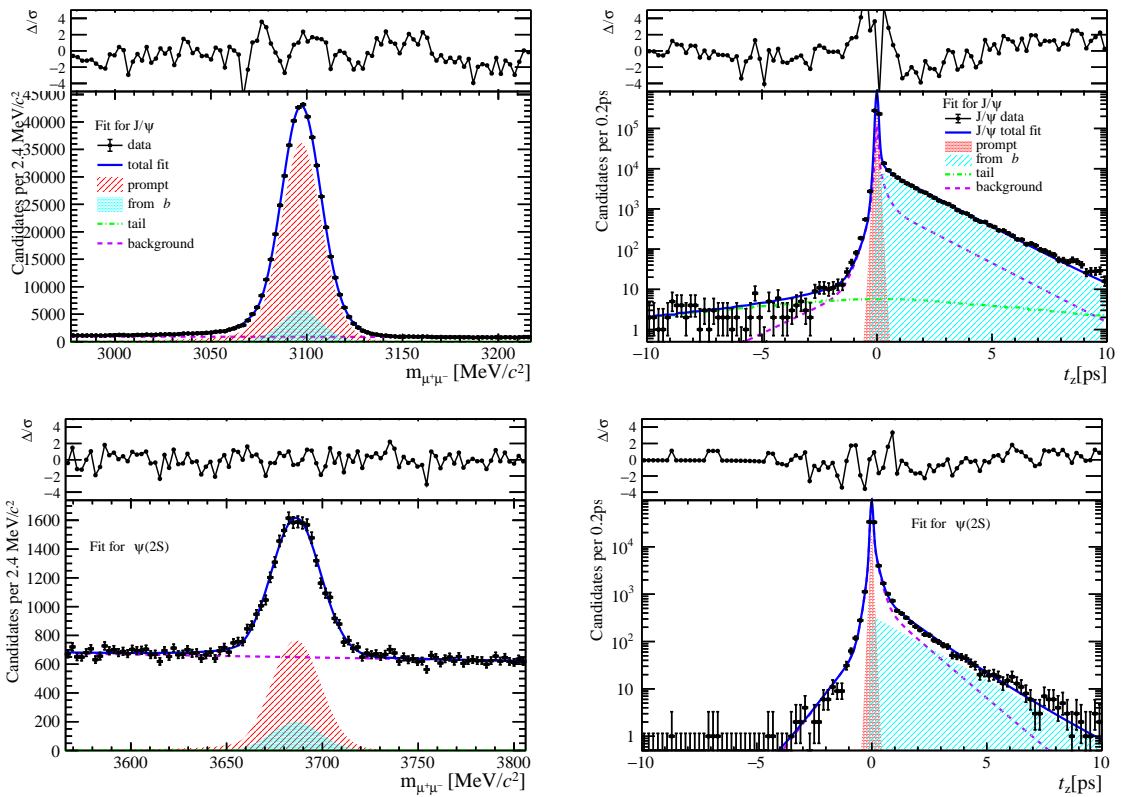


Figure 127: Fit results in  $2 \text{ GeV}/c < p_T < 4 \text{ GeV}/c$ ,  $2.0 < y < 2.8$  and  $8 \leq n\text{BackTracks} < 15$ .

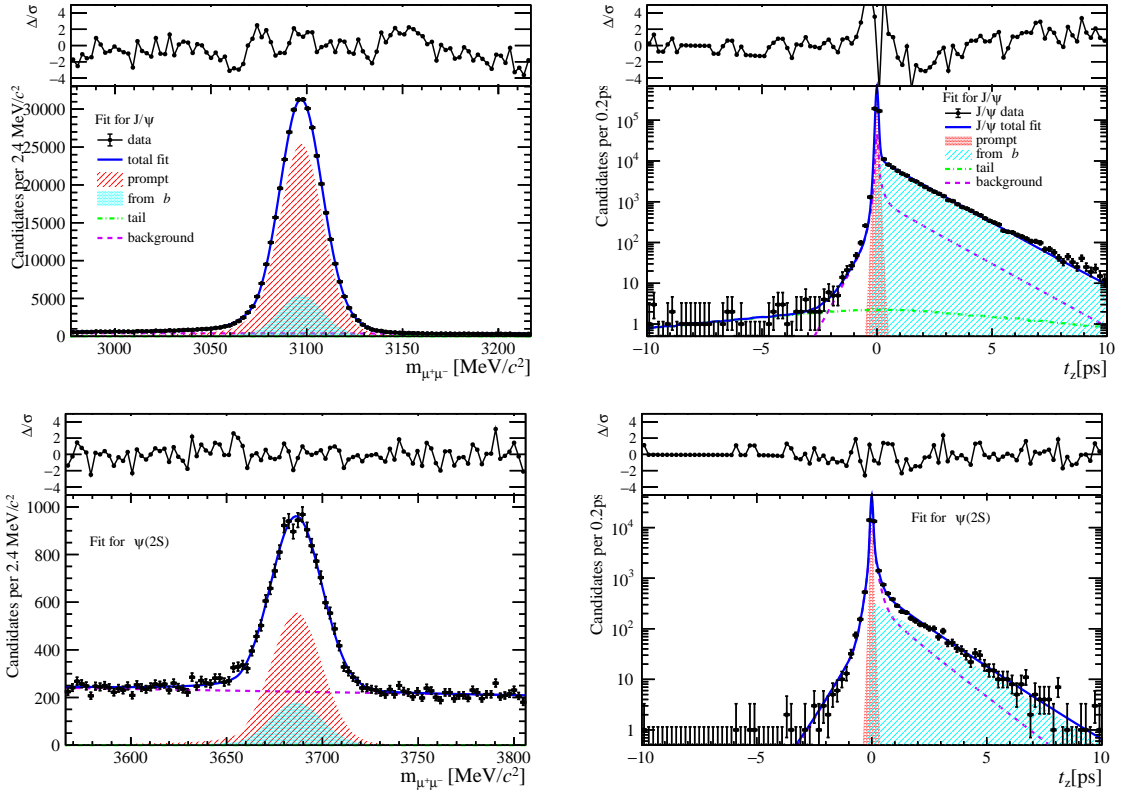


Figure 128: Fit results in  $4 \text{ GeV}/c < p_T < 6 \text{ GeV}/c$ ,  $2.0 < y < 2.8$  and  $8 \leq n\text{BackTracks} < 15$ .

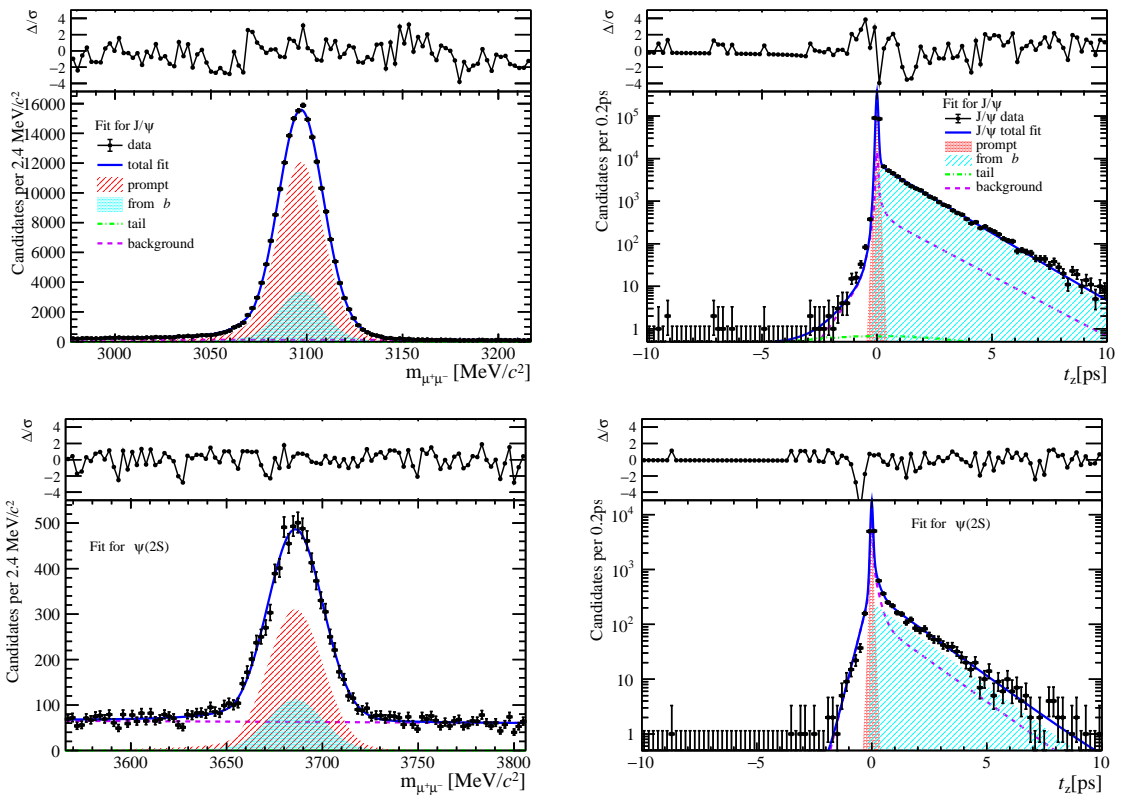


Figure 129: Fit results in  $6 \text{ GeV}/c < p_T < 8 \text{ GeV}/c$ ,  $2.0 < y < 2.8$  and  $8 \leq n\text{BackTracks} < 15$ .

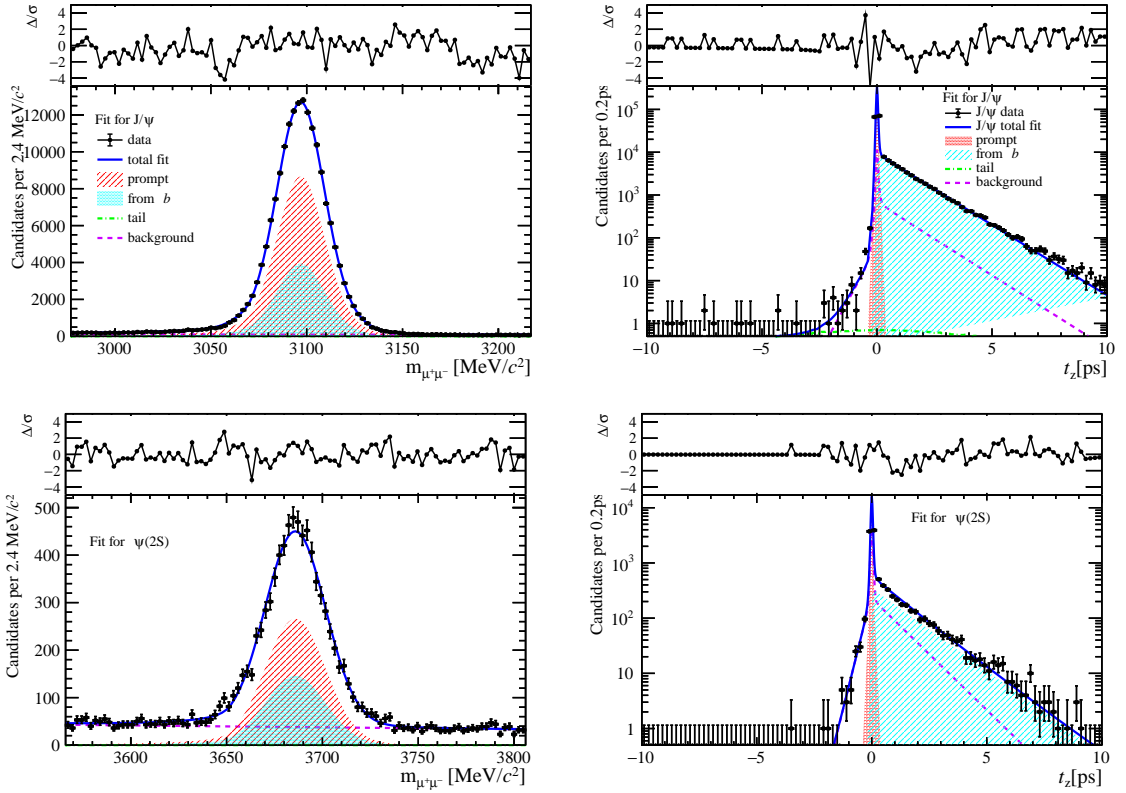


Figure 130: Fit results in  $8 \text{ GeV}/c < p_T < 20 \text{ GeV}/c$ ,  $2.0 < y < 2.8$  and  $8 \leq \text{nBackTracks} < 15$ .

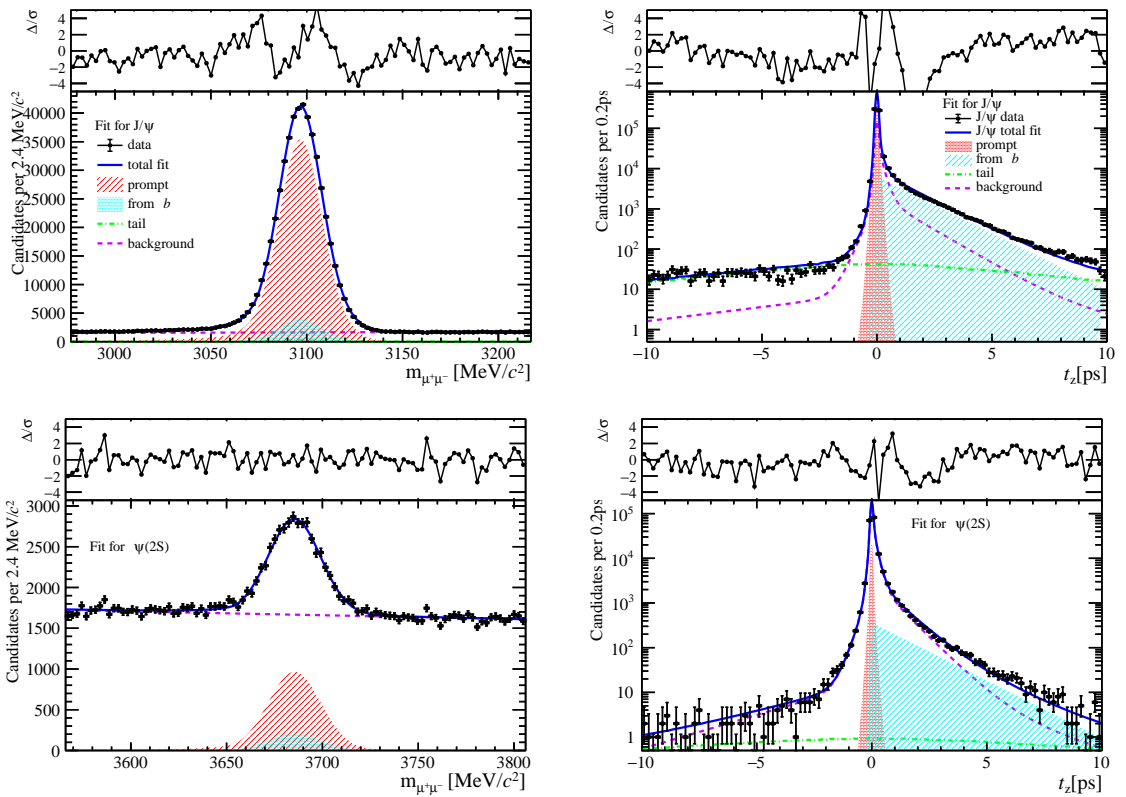


Figure 131: Fit results in  $0 \text{ GeV}/c < p_T < 2 \text{ GeV}/c$ ,  $2.8 < y < 3.5$  and  $8 \leq \text{nBackTracks} < 15$ .

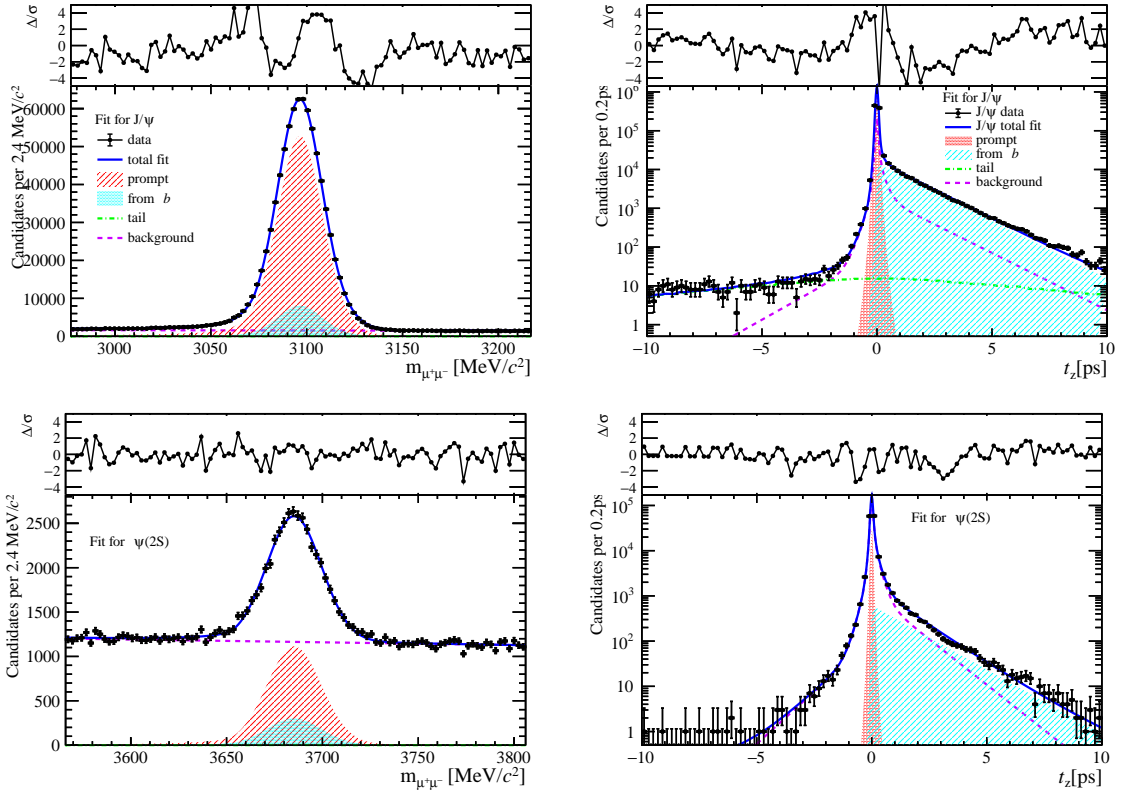


Figure 132: Fit results in  $2 \text{ GeV}/c < p_T < 4 \text{ GeV}/c$ ,  $2.8 < y < 3.5$  and  $8 \leq \text{nBackTracks} < 15$ .

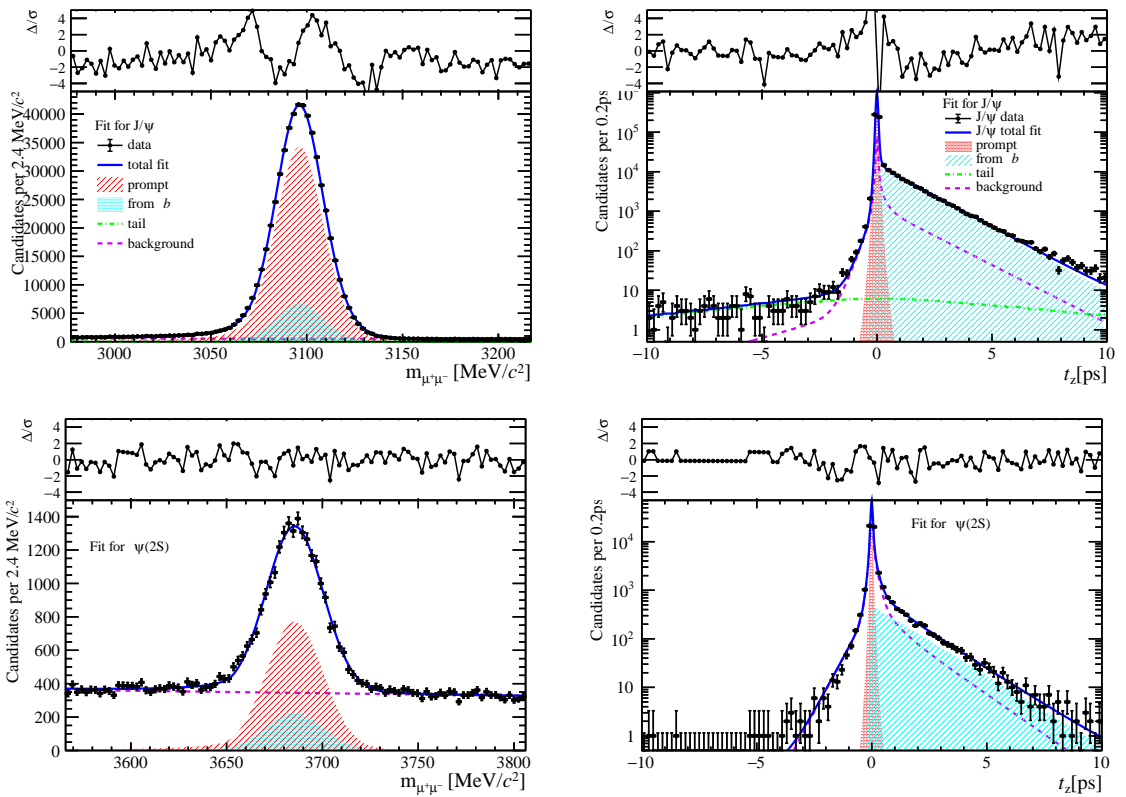


Figure 133: Fit results in  $4 \text{ GeV}/c < p_T < 6 \text{ GeV}/c$ ,  $2.8 < y < 3.5$  and  $8 \leq \text{nBackTracks} < 15$ .

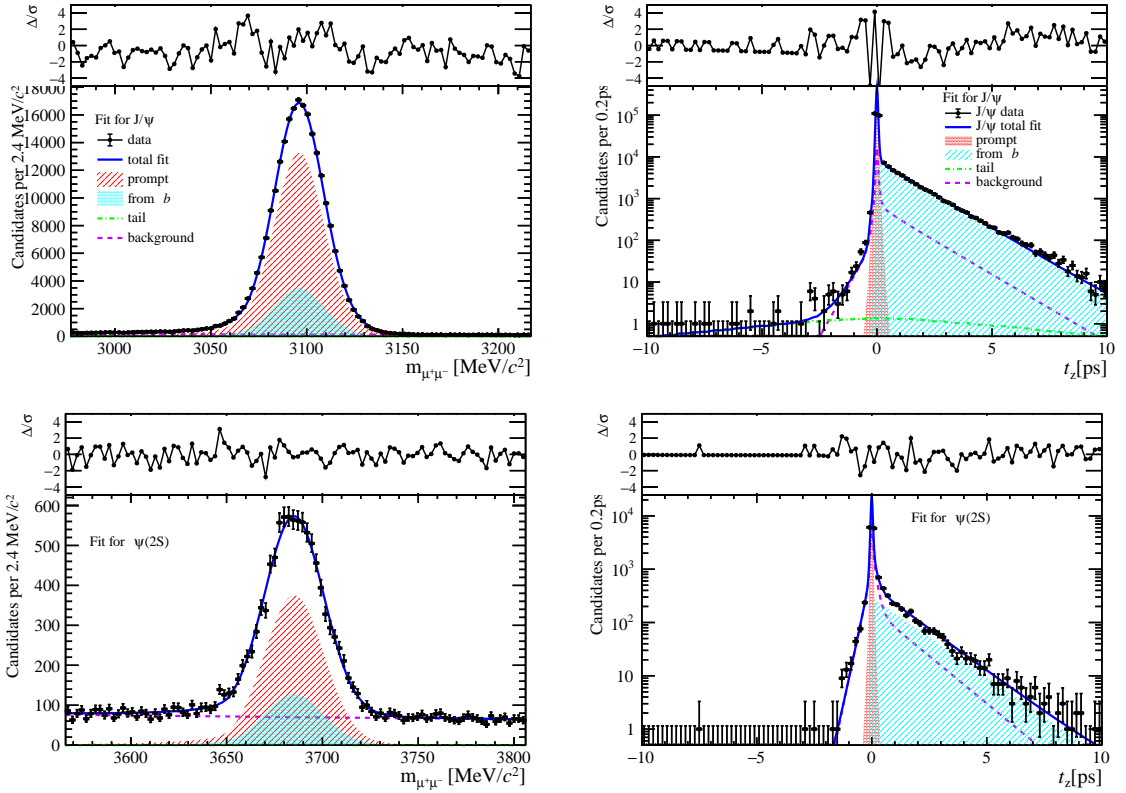


Figure 134: Fit results in  $6 \text{ GeV}/c < p_T < 8 \text{ GeV}/c$ ,  $2.8 < y < 3.5$  and  $8 \leq \text{nBackTracks} < 15$ .

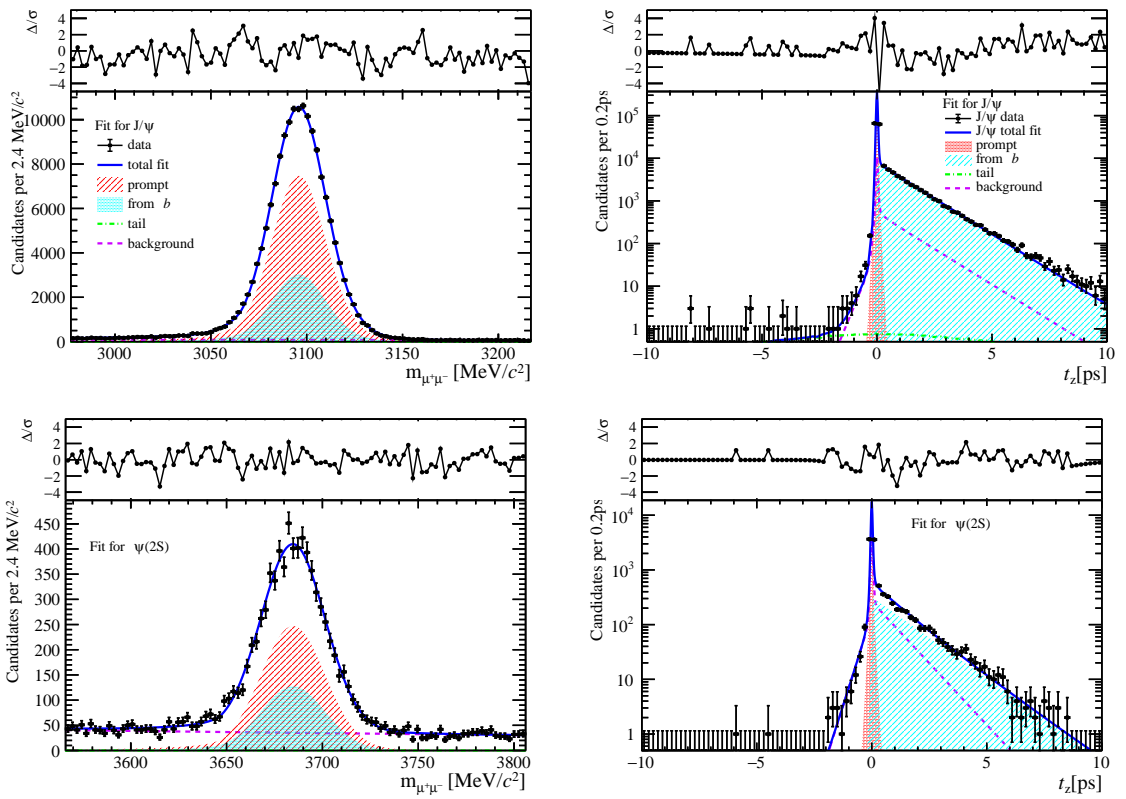


Figure 135: Fit results in  $8 \text{ GeV}/c < p_T < 20 \text{ GeV}/c$ ,  $2.8 < y < 3.5$  and  $8 \leq \text{nBackTracks} < 15$ .

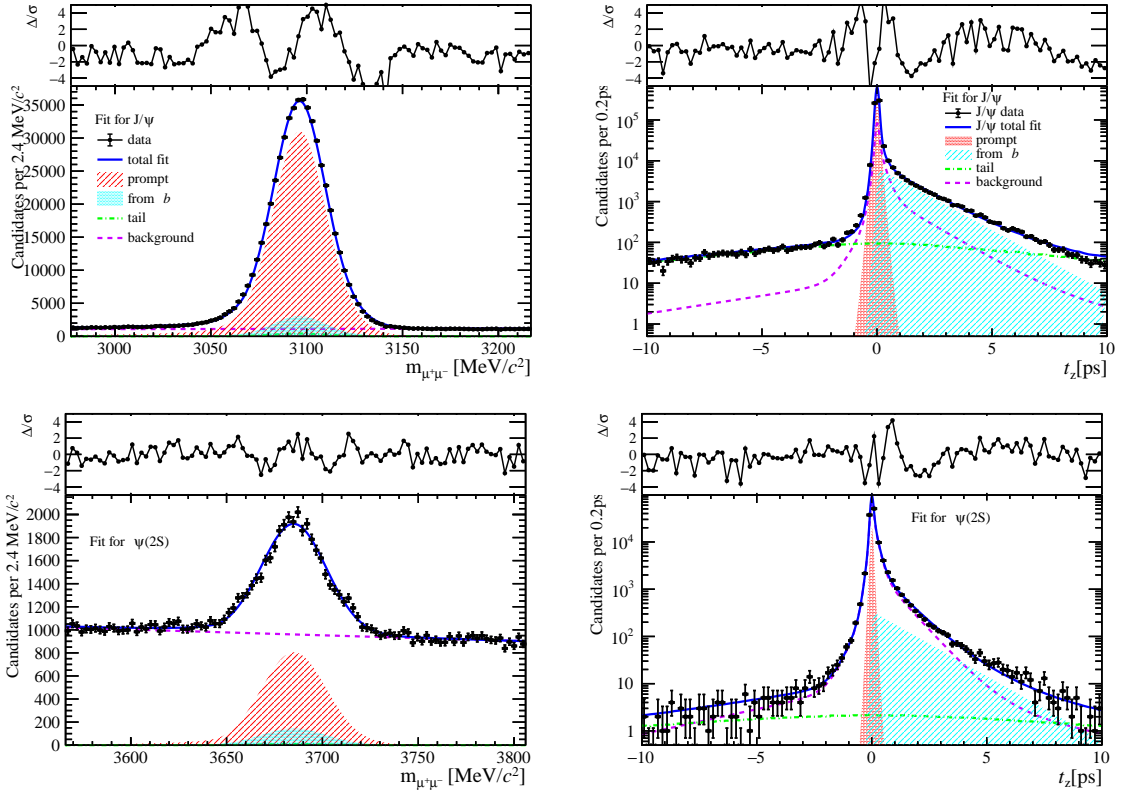


Figure 136: Fit results in  $0 \text{ GeV}/c < p_T < 2 \text{ GeV}/c$ ,  $3.5 < y < 4.5$  and  $8 \leq n\text{BackTracks} < 15$ .

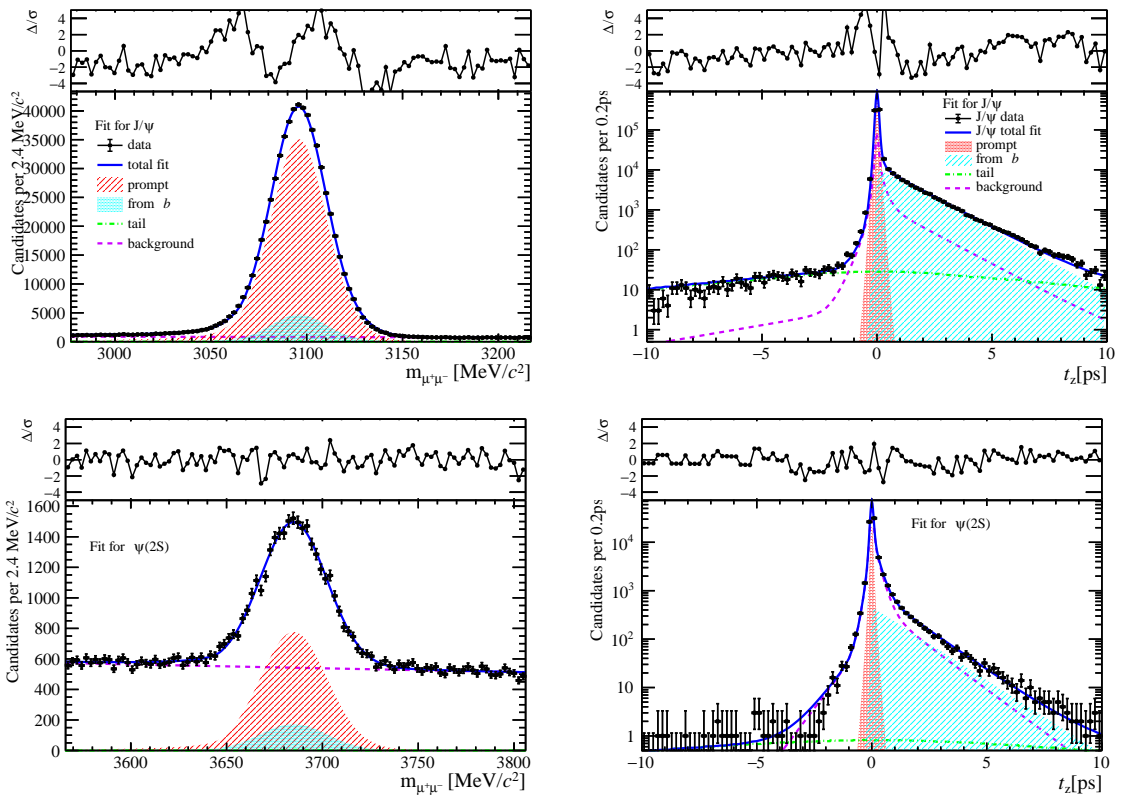


Figure 137: Fit results in  $2 \text{ GeV}/c < p_T < 4 \text{ GeV}/c$ ,  $3.5 < y < 4.5$  and  $8 \leq n\text{BackTracks} < 15$ .

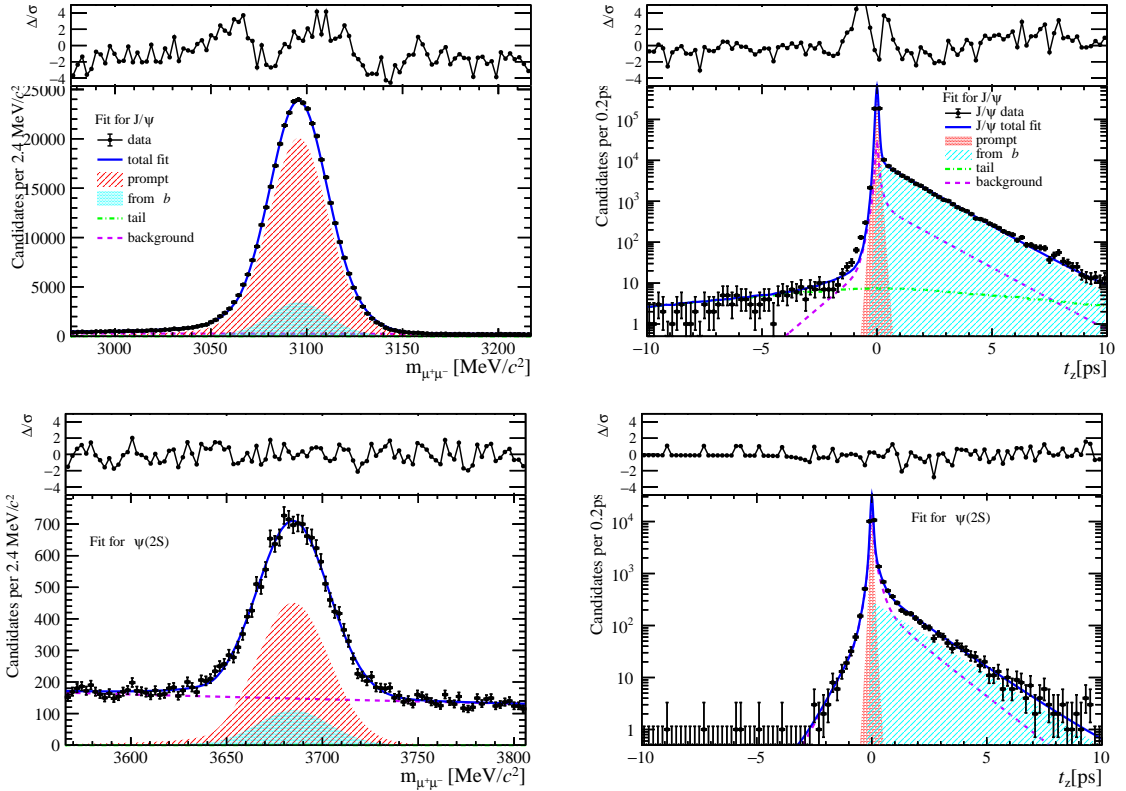


Figure 138: Fit results in  $4 \text{ GeV}/c < p_T < 6 \text{ GeV}/c$ ,  $3.5 < y < 4.5$  and  $8 \leq n\text{BackTracks} < 15$ .

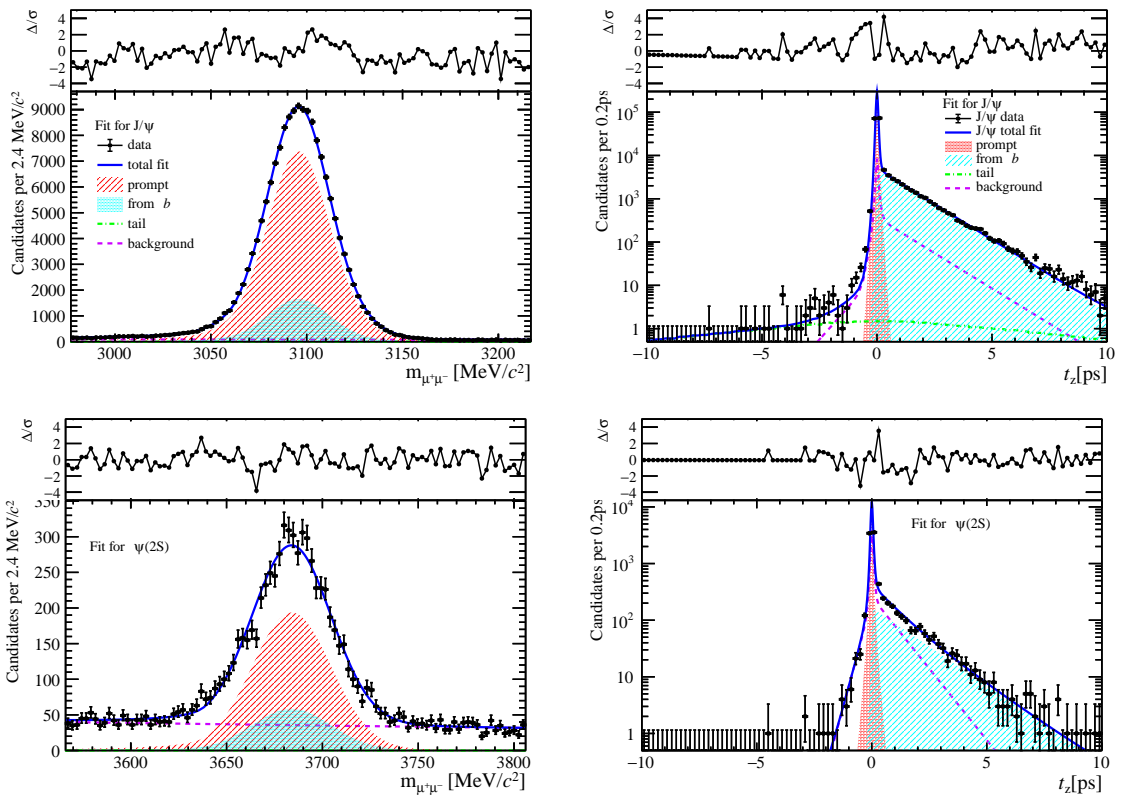


Figure 139: Fit results in  $6 \text{ GeV}/c < p_T < 8 \text{ GeV}/c$ ,  $3.5 < y < 4.5$  and  $8 \leq n\text{BackTracks} < 15$ .

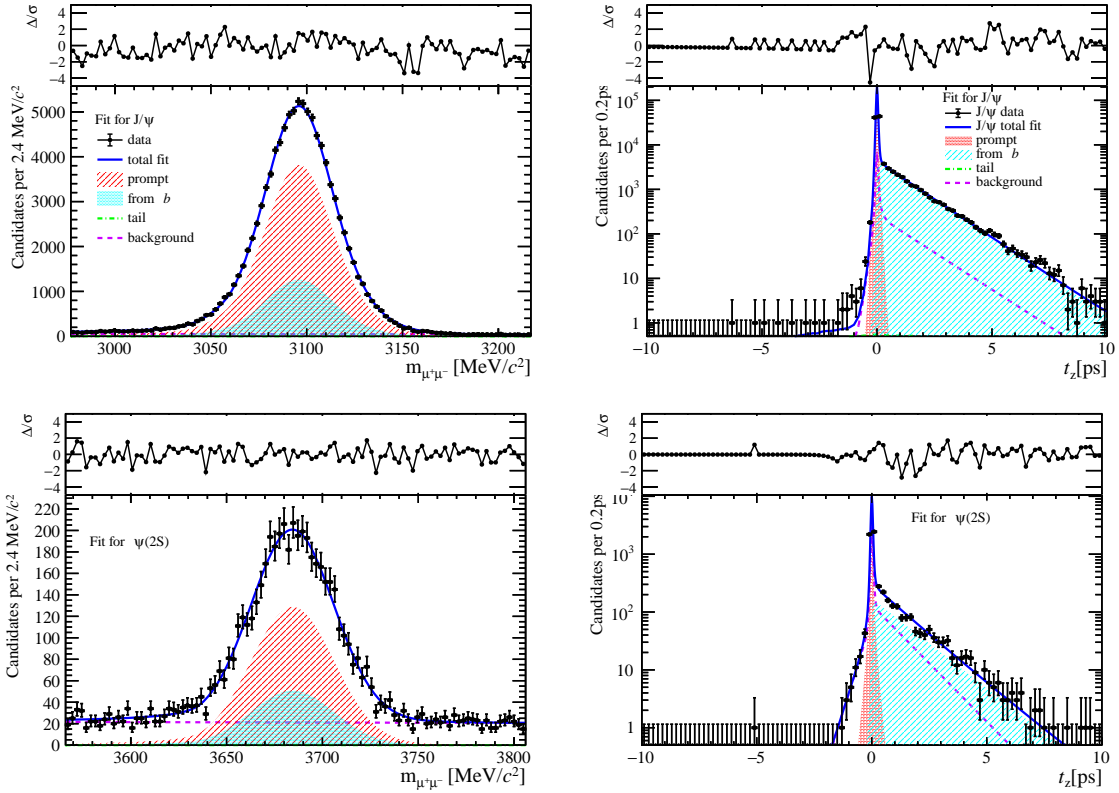


Figure 140: Fit results in  $8 \text{ GeV}/c < p_T < 20 \text{ GeV}/c$ ,  $3.5 < y < 4.5$  and  $8 \leq \text{nBackTracks} < 15$ .

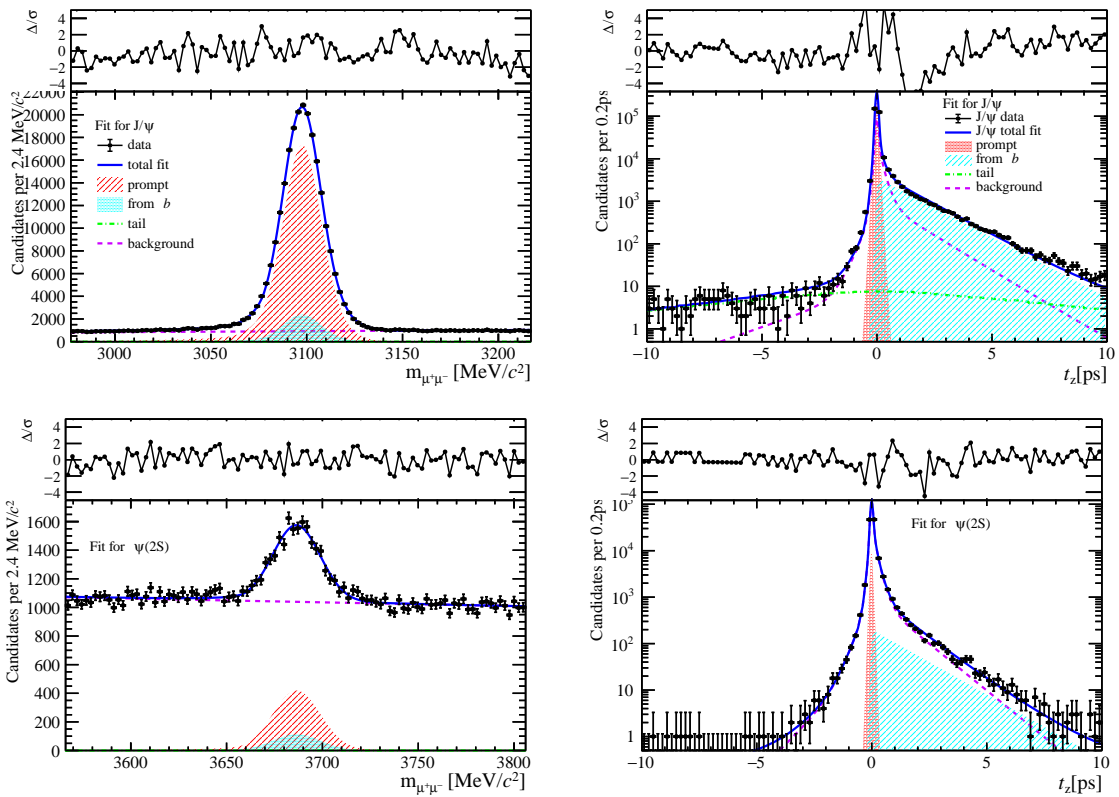


Figure 141: Fit results in  $0 \text{ GeV}/c < p_T < 2 \text{ GeV}/c$ ,  $2.0 < y < 2.8$  and  $15 \leq \text{nBackTracks} < 22$ .

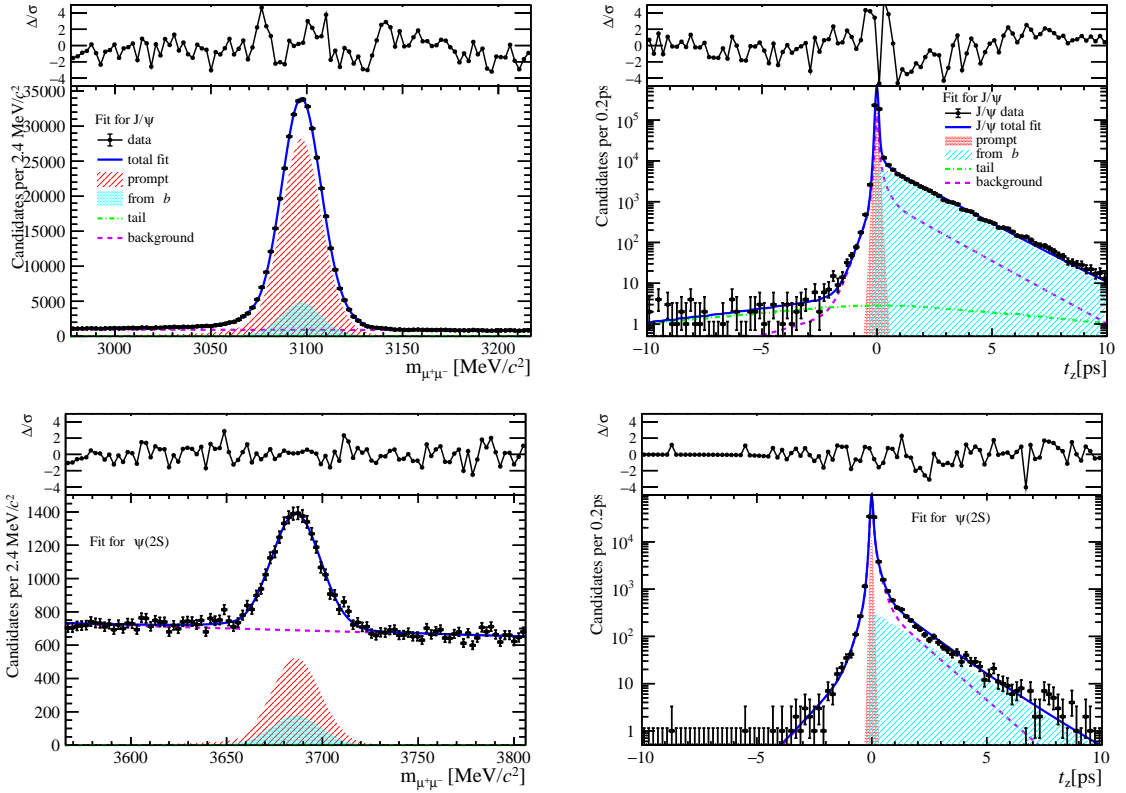


Figure 142: Fit results in  $2 \text{ GeV}/c < p_T < 4 \text{ GeV}/c$ ,  $2.0 < y < 2.8$  and  $15 \leq n\text{BackTracks} < 22$ .

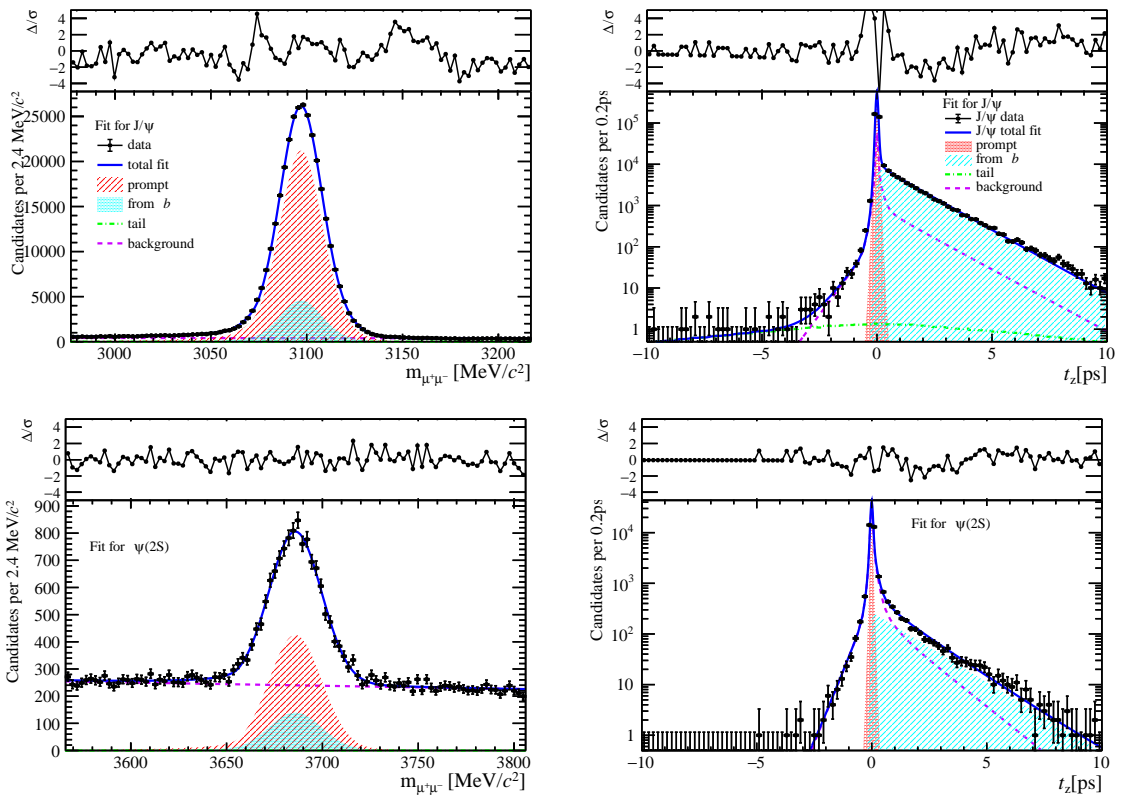


Figure 143: Fit results in  $4 \text{ GeV}/c < p_T < 6 \text{ GeV}/c$ ,  $2.0 < y < 2.8$  and  $15 \leq n\text{BackTracks} < 22$ .

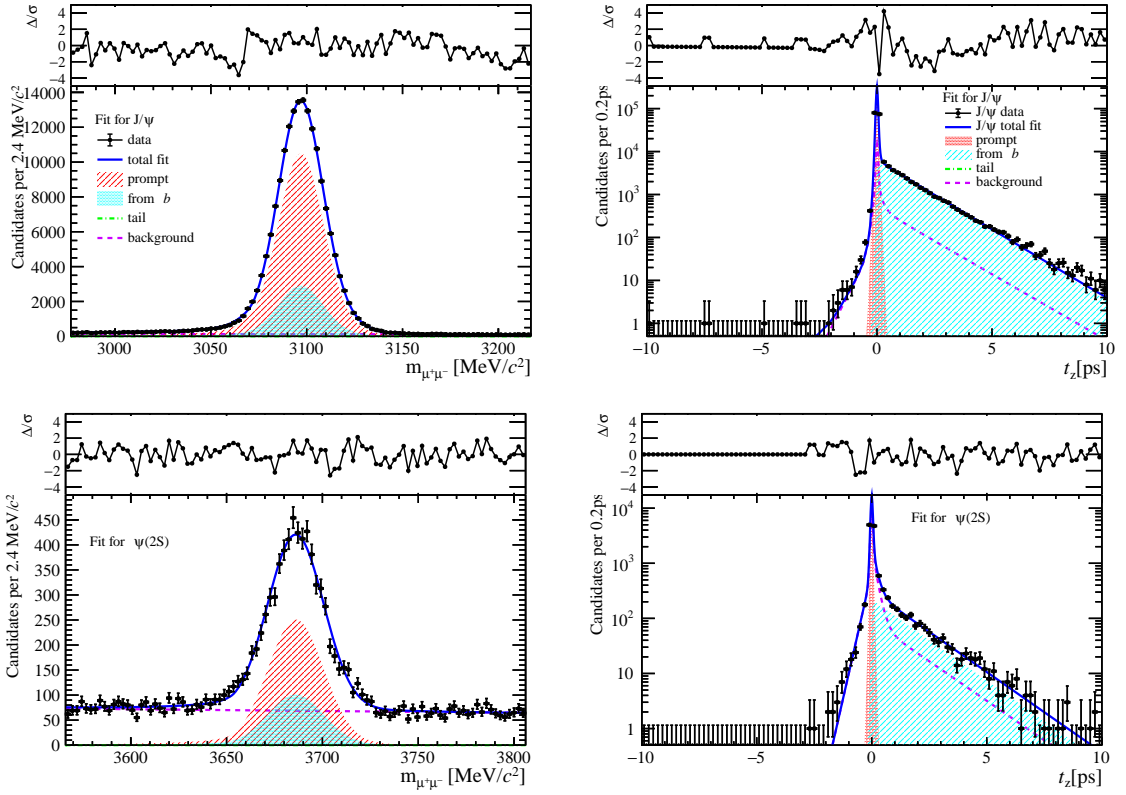


Figure 144: Fit results in  $6 \text{ GeV}/c < p_T < 8 \text{ GeV}/c$ ,  $2.0 < y < 2.8$  and  $15 \leq \text{nBackTracks} < 22$ .

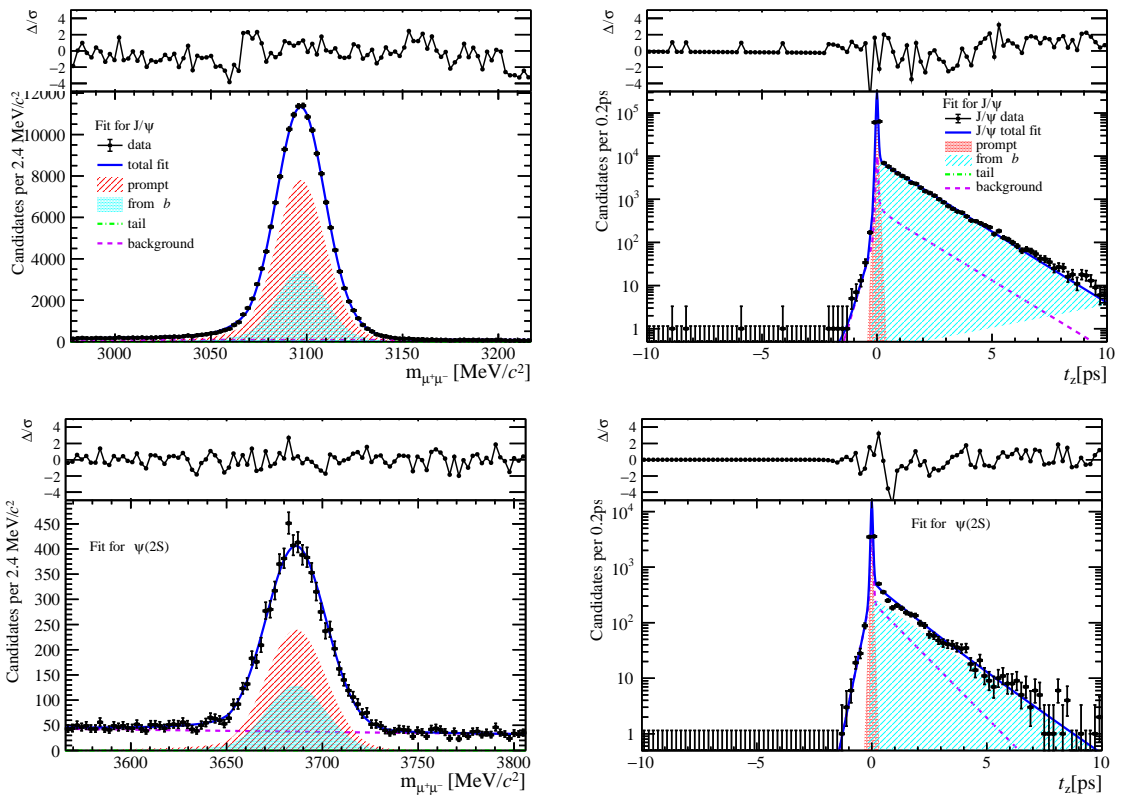


Figure 145: Fit results in  $8 \text{ GeV}/c < p_T < 20 \text{ GeV}/c$ ,  $2.0 < y < 2.8$  and  $15 \leq \text{nBackTracks} < 22$ .

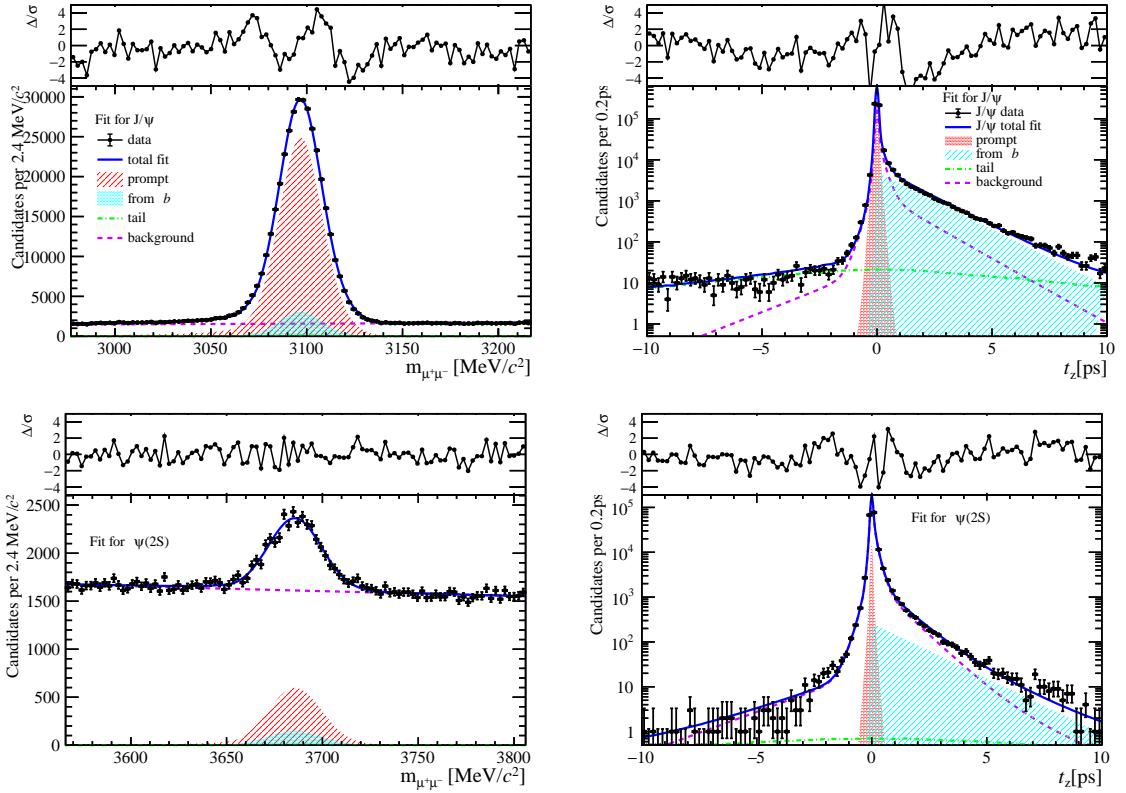


Figure 146: Fit results in  $0 \text{ GeV}/c < p_T < 2 \text{ GeV}/c$ ,  $2.8 < y < 3.5$  and  $15 \leq \text{nBackTracks} < 22$ .

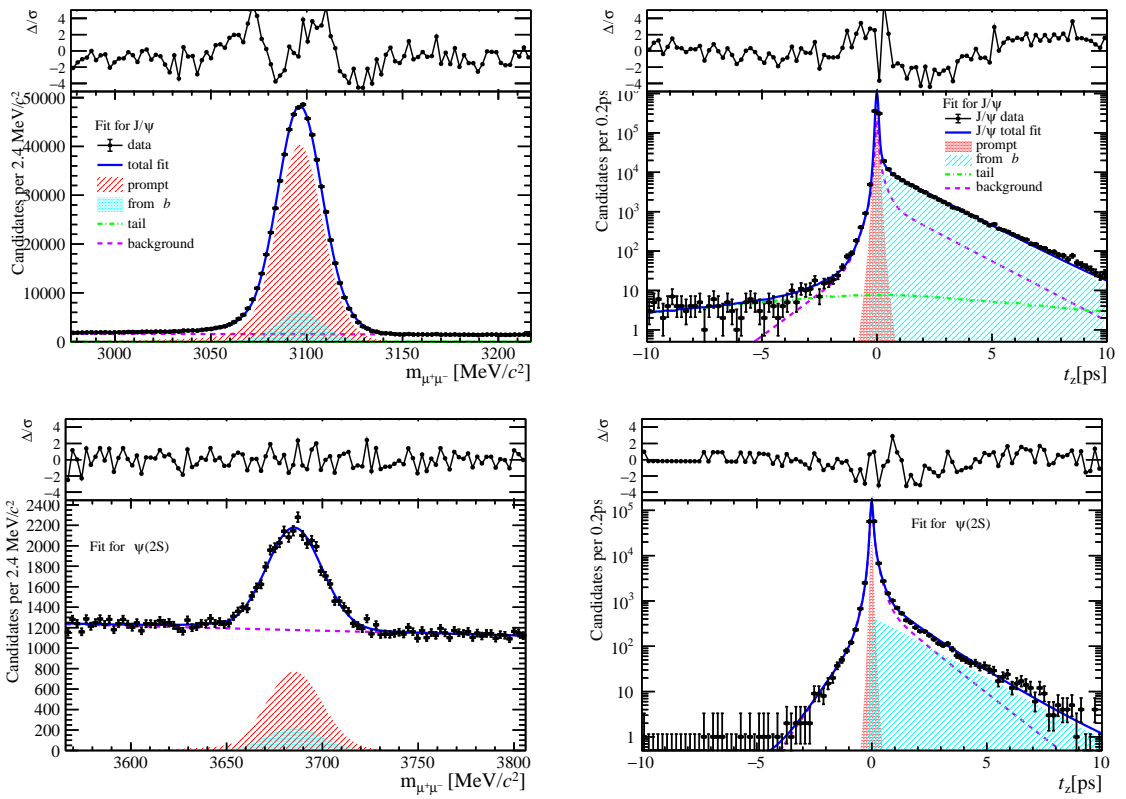


Figure 147: Fit results in  $2 \text{ GeV}/c < p_T < 4 \text{ GeV}/c$ ,  $2.8 < y < 3.5$  and  $15 \leq \text{nBackTracks} < 22$ .

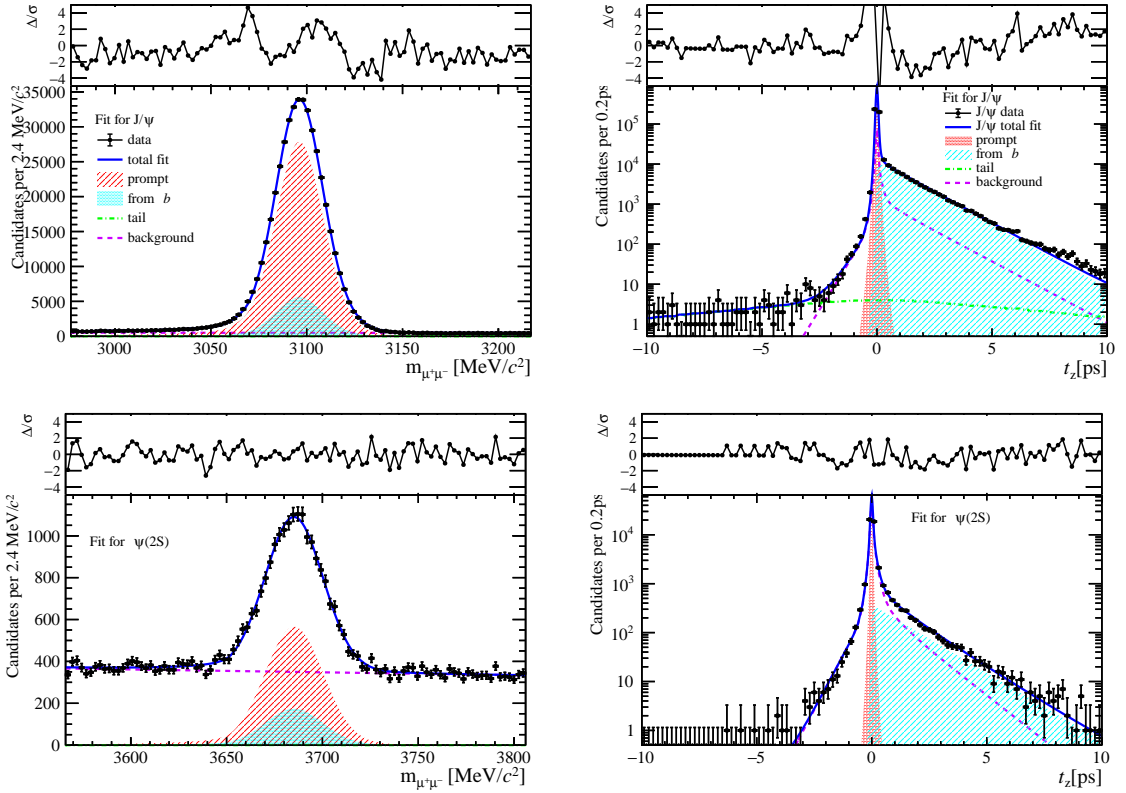


Figure 148: Fit results in  $4 \text{ GeV}/c < p_T < 6 \text{ GeV}/c$ ,  $2.8 < y < 3.5$  and  $15 \leq \text{nBackTracks} < 22$ .

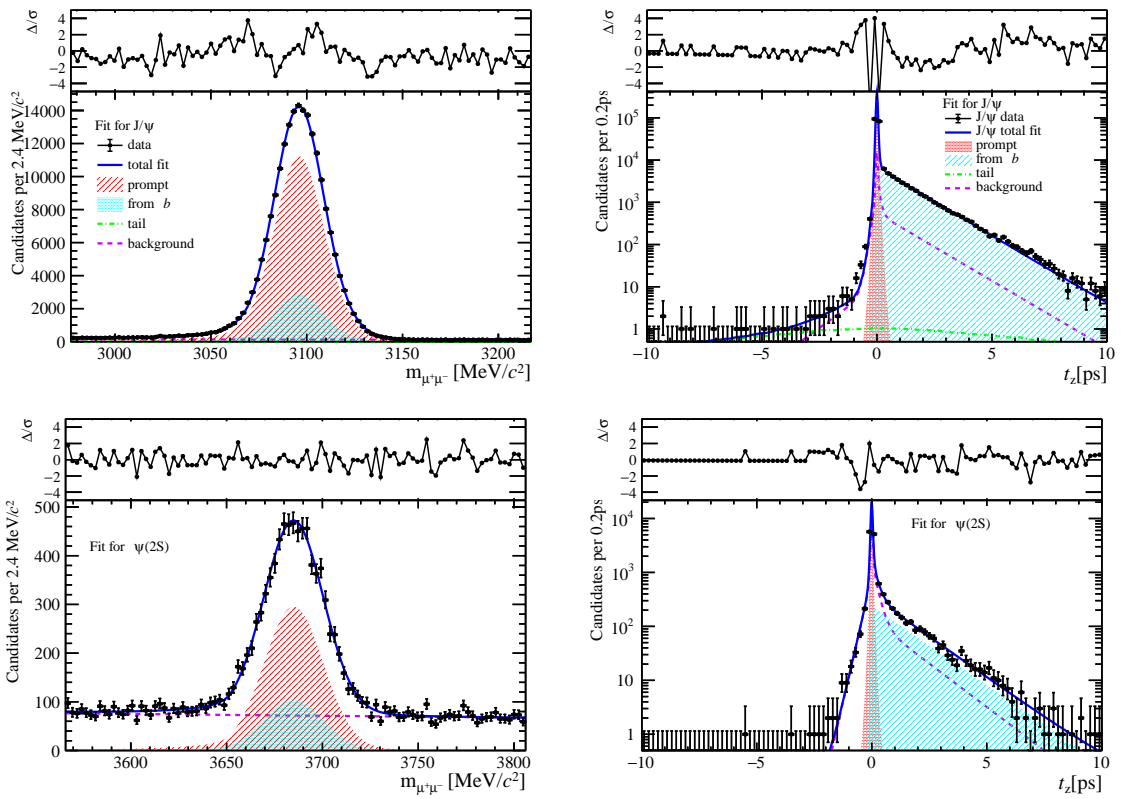


Figure 149: Fit results in  $6 \text{ GeV}/c < p_T < 8 \text{ GeV}/c$ ,  $2.8 < y < 3.5$  and  $15 \leq \text{nBackTracks} < 22$ .

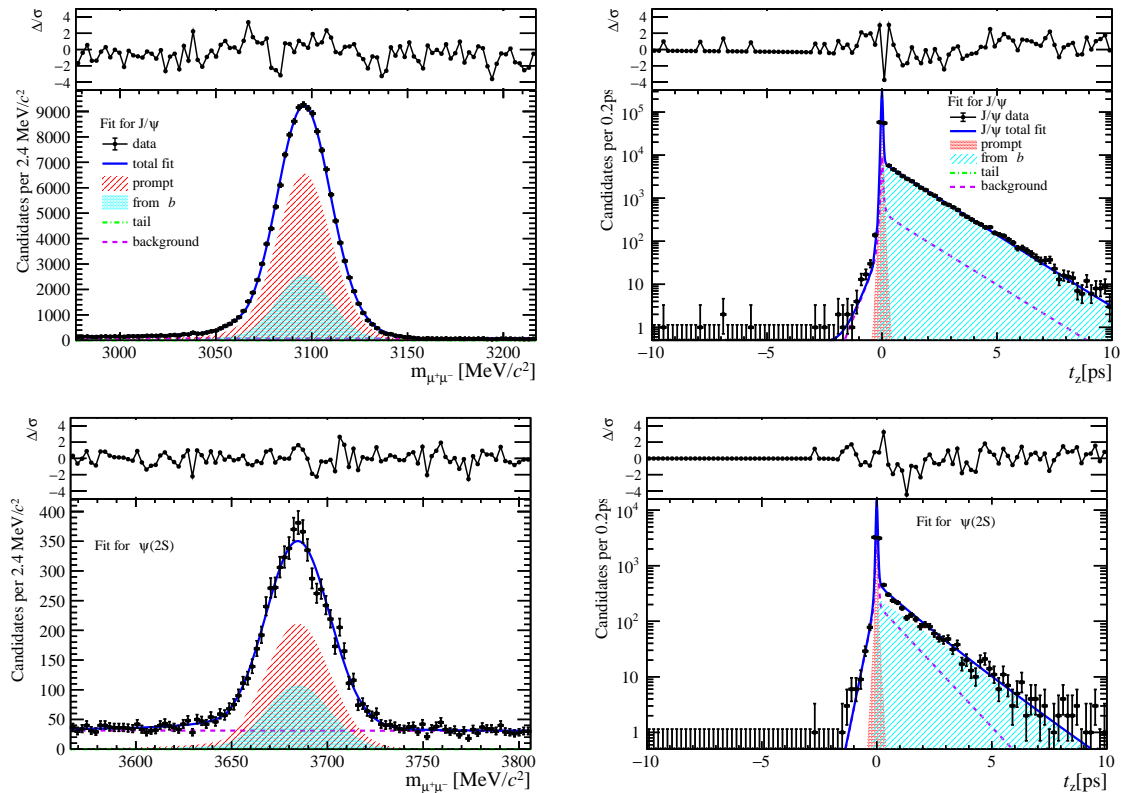


Figure 150: Fit results in  $8 \text{ GeV}/c < p_T < 20 \text{ GeV}/c$ ,  $2.8 < y < 3.5$  and  $15 \leq \text{nBackTracks} < 22$ .

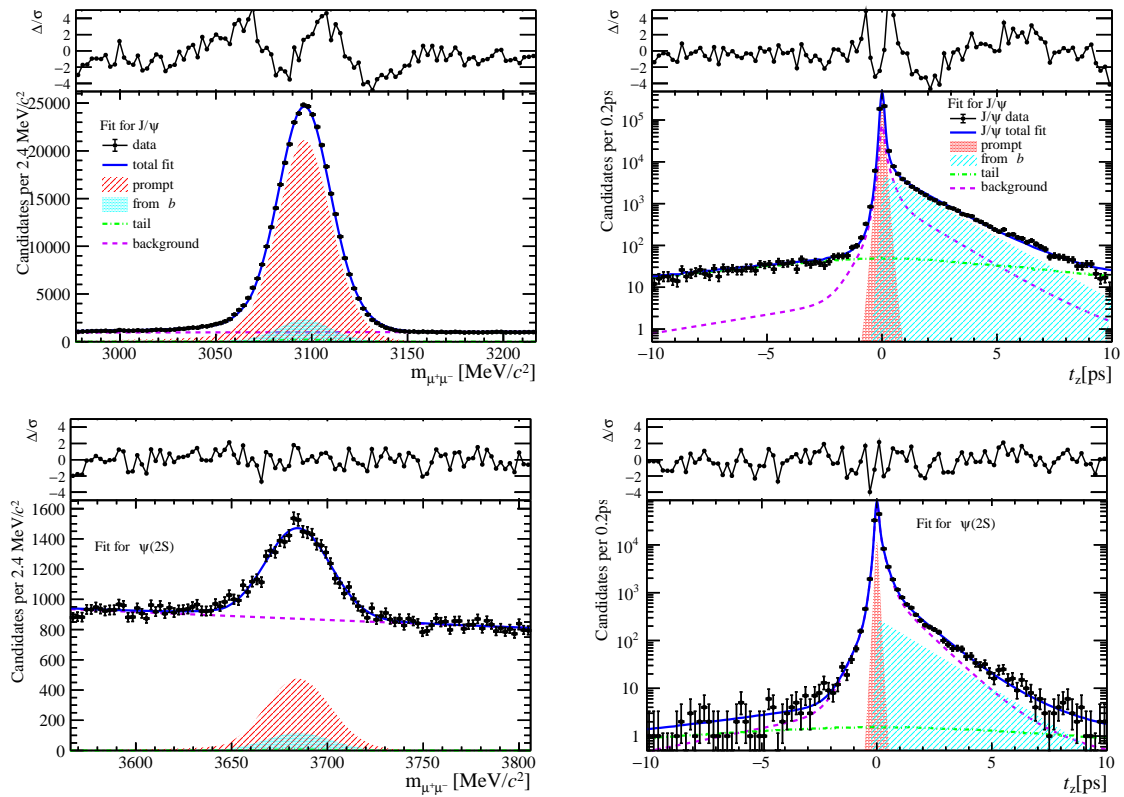


Figure 151: Fit results in  $0 \text{ GeV}/c < p_T < 2 \text{ GeV}/c$ ,  $3.5 < y < 4.5$  and  $15 \leq \text{nBackTracks} < 22$ .

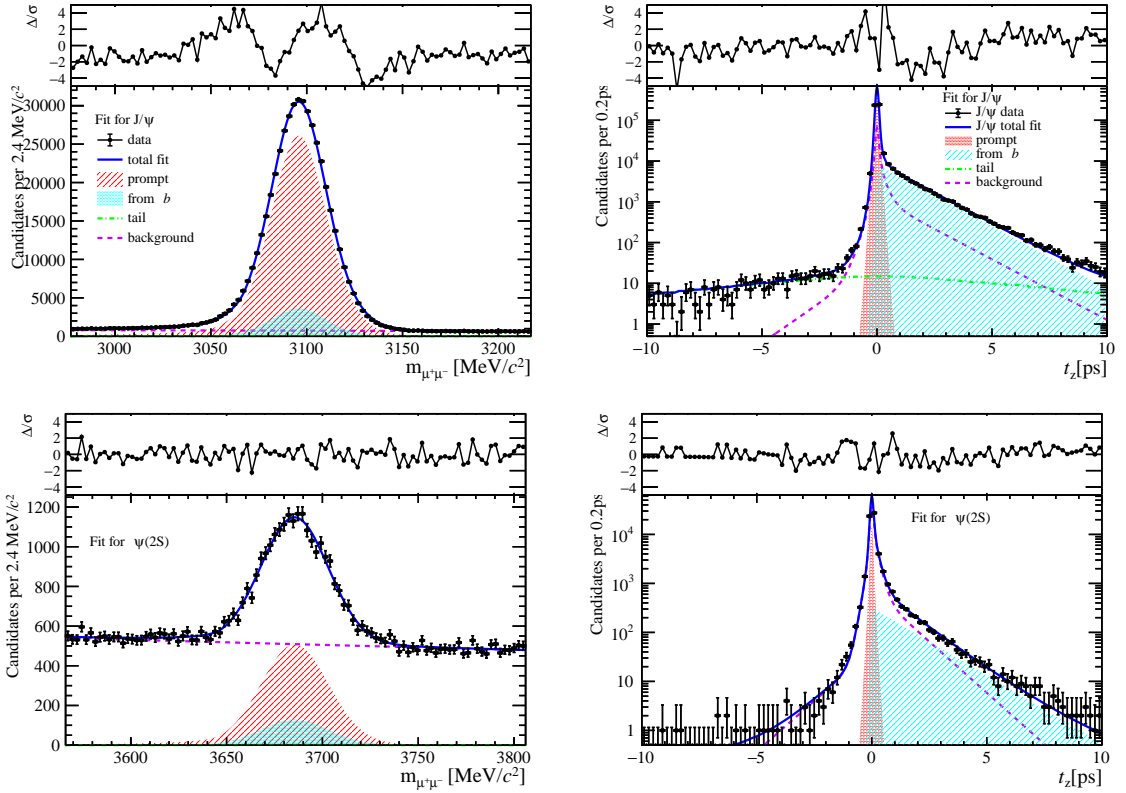


Figure 152: Fit results in  $2 \text{ GeV}/c < p_{\text{T}} < 4 \text{ GeV}/c$ ,  $3.5 < y < 4.5$  and  $15 \leq \text{nBackTracks} < 22$ .

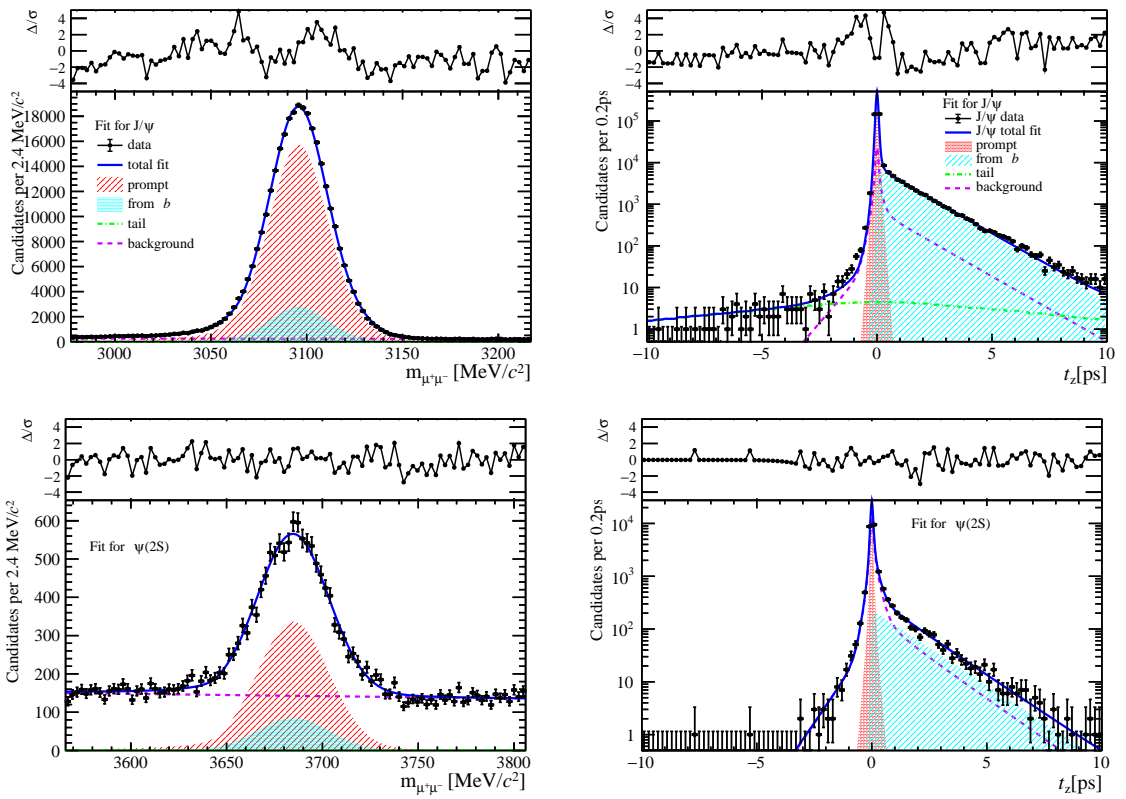


Figure 153: Fit results in  $4 \text{ GeV}/c < p_{\text{T}} < 6 \text{ GeV}/c$ ,  $3.5 < y < 4.5$  and  $15 \leq \text{nBackTracks} < 22$ .

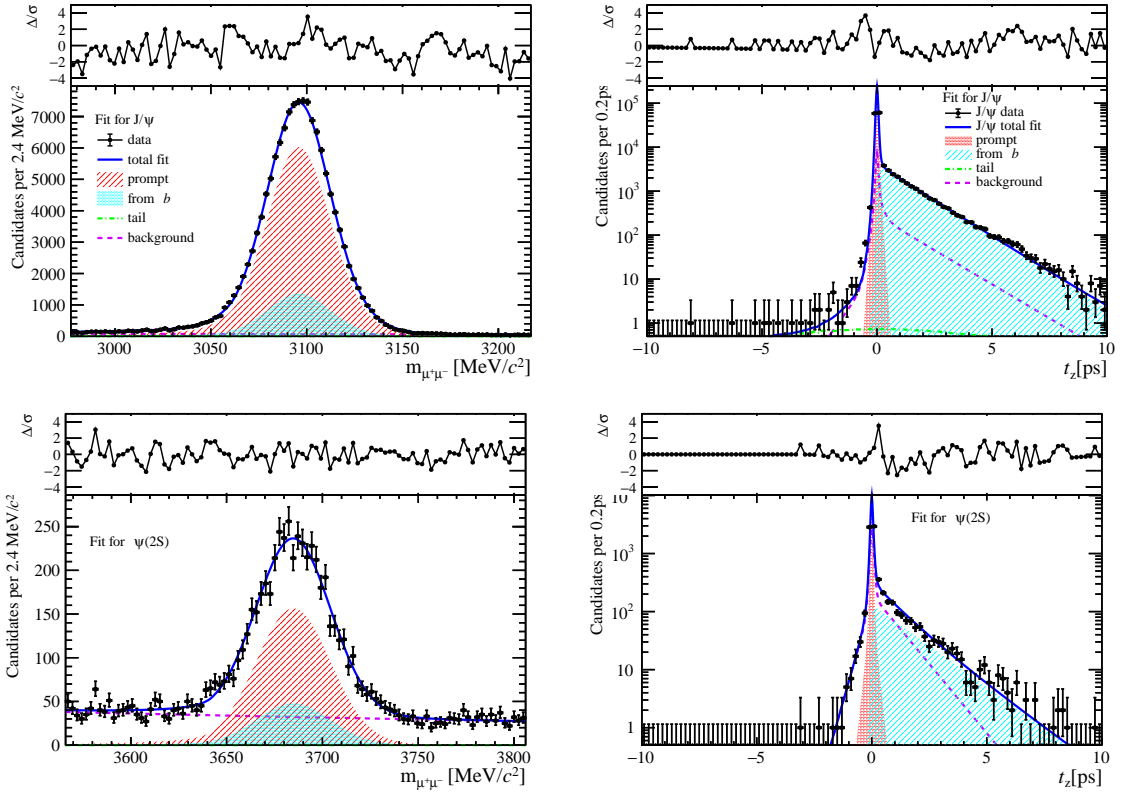


Figure 154: Fit results in  $6 \text{ GeV}/c < p_T < 8 \text{ GeV}/c$ ,  $3.5 < y < 4.5$  and  $15 \leq \text{nBackTracks} < 22$ .

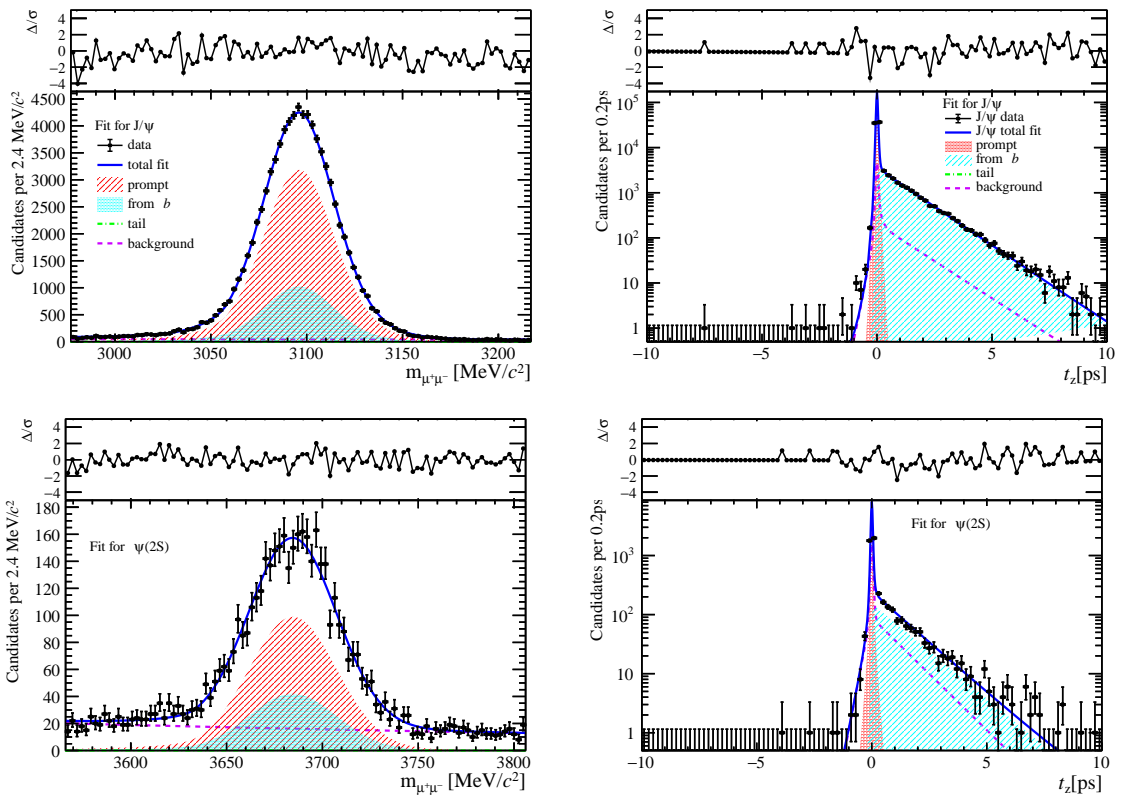


Figure 155: Fit results in  $8 \text{ GeV}/c < p_T < 20 \text{ GeV}/c$ ,  $3.5 < y < 4.5$  and  $15 \leq \text{nBackTracks} < 22$ .

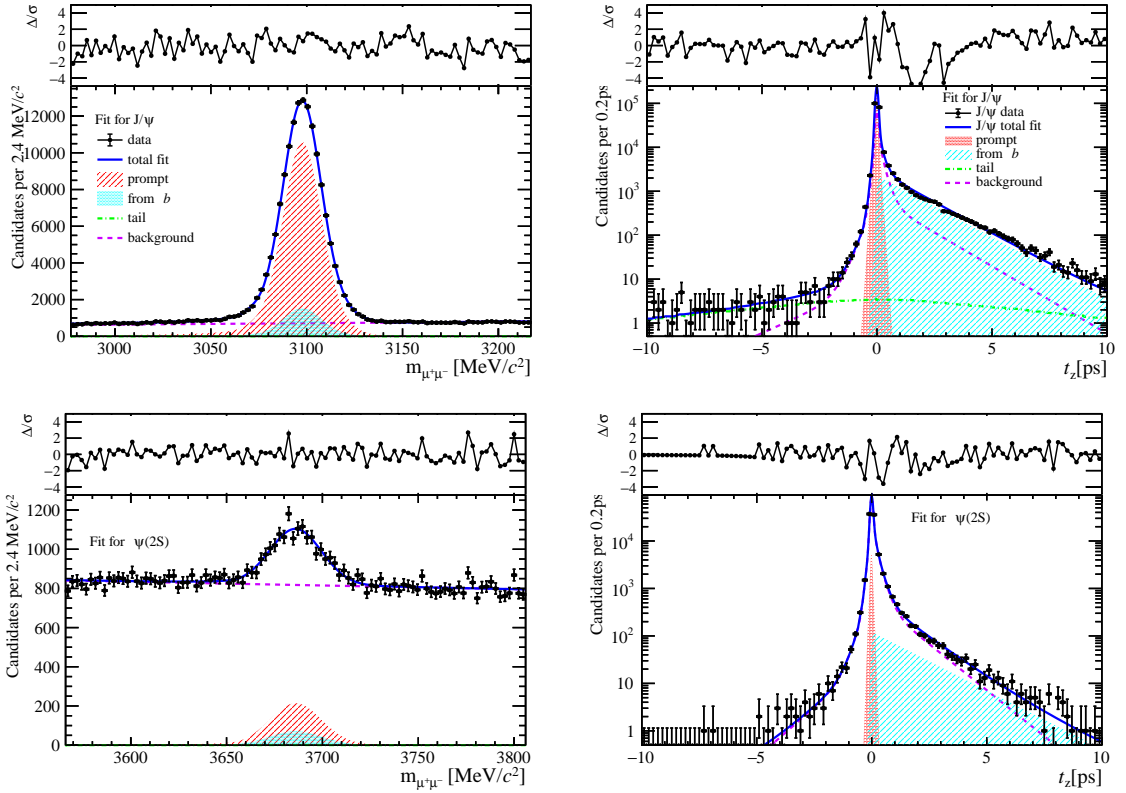


Figure 156: Fit results in  $0 \text{ GeV}/c < p_T < 2 \text{ GeV}/c$ ,  $2.0 < y < 2.8$  and  $22 \leq \text{nBackTracks} < 30$ .

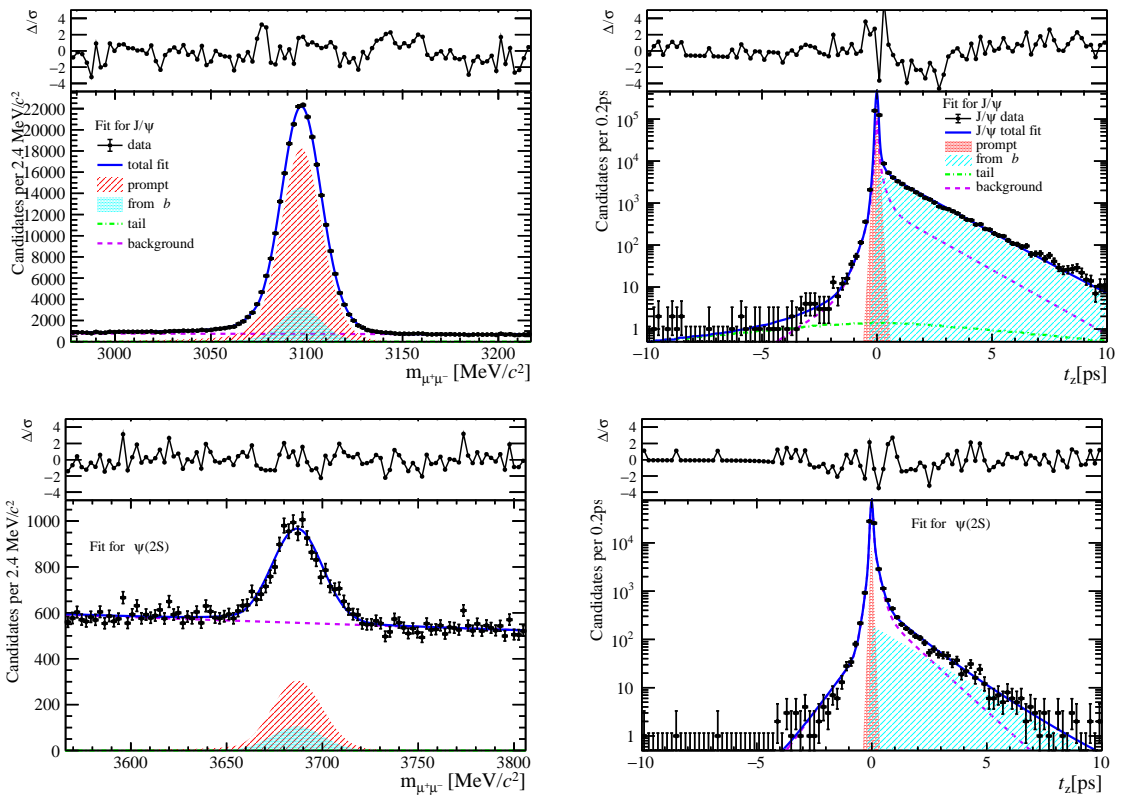


Figure 157: Fit results in  $2 \text{ GeV}/c < p_T < 4 \text{ GeV}/c$ ,  $2.0 < y < 2.8$  and  $22 \leq \text{nBackTracks} < 30$ .

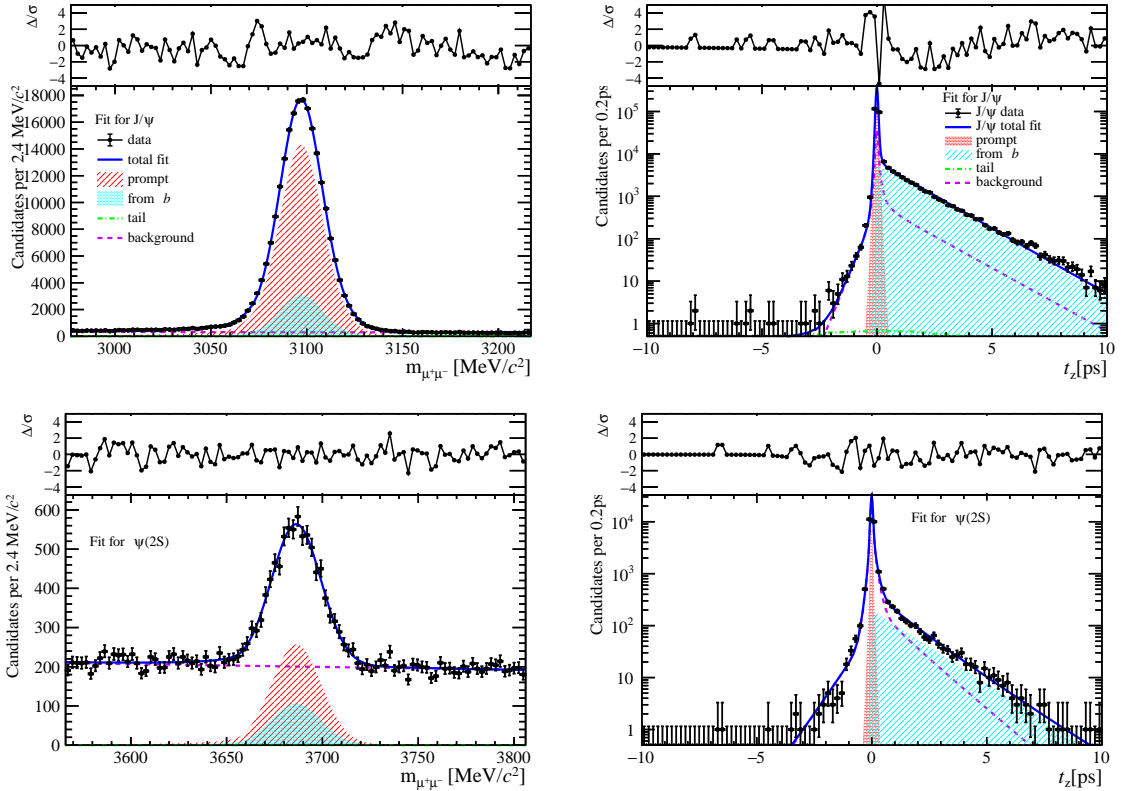


Figure 158: Fit results in  $4 \text{ GeV}/c < p_T < 6 \text{ GeV}/c$ ,  $2.0 < y < 2.8$  and  $22 \leq \text{nBackTracks} < 30$ .

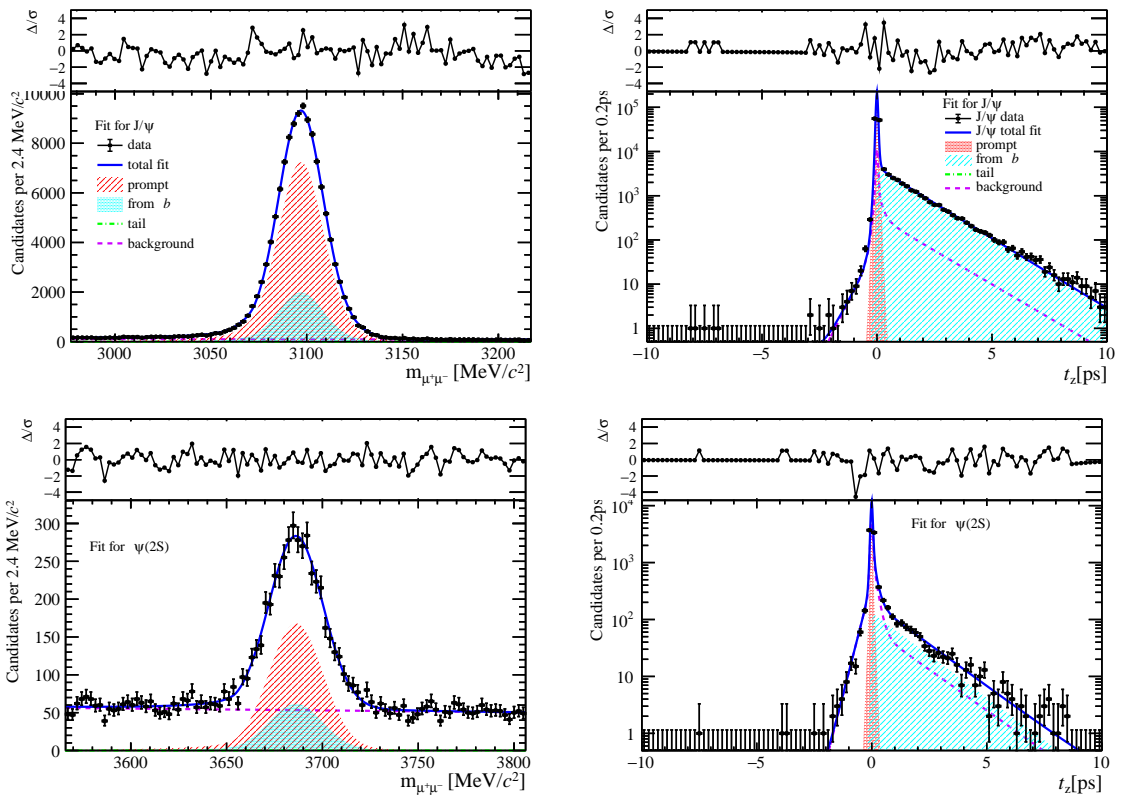


Figure 159: Fit results in  $6 \text{ GeV}/c < p_T < 8 \text{ GeV}/c$ ,  $2.0 < y < 2.8$  and  $22 \leq \text{nBackTracks} < 30$ .

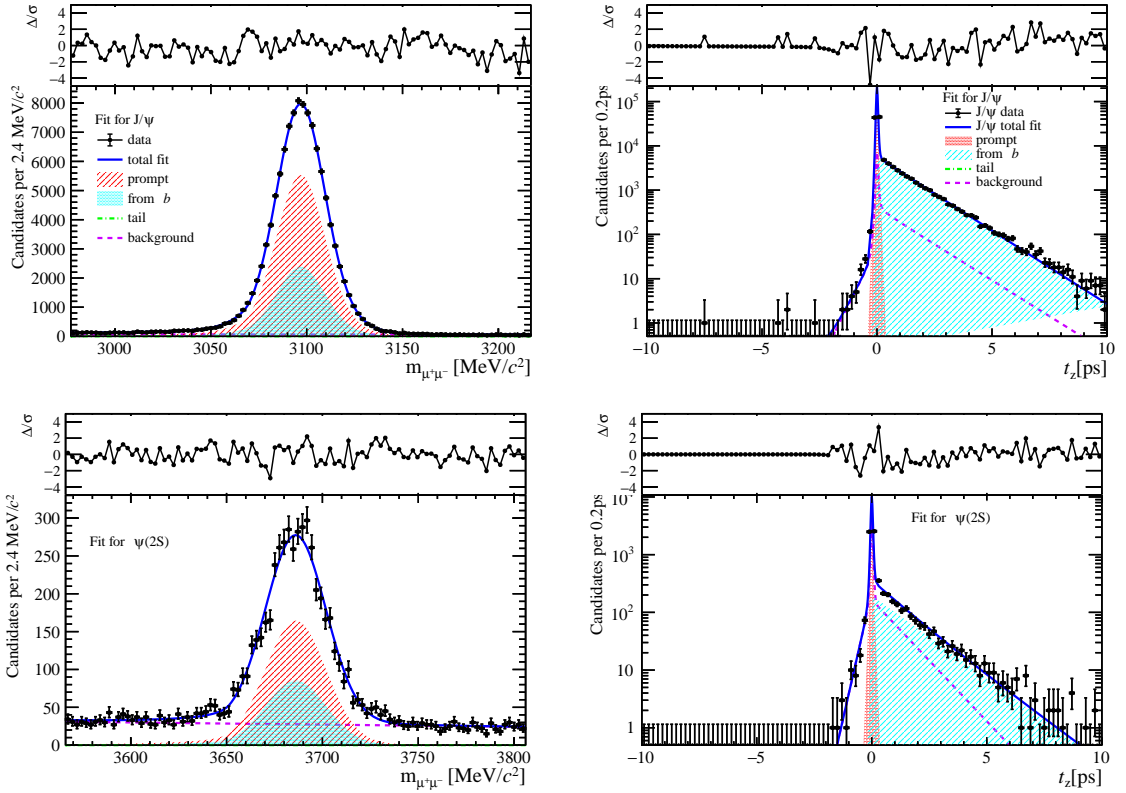


Figure 160: Fit results in  $8 \text{ GeV}/c < p_T < 20 \text{ GeV}/c$ ,  $2.0 < y < 2.8$  and  $22 \leq \text{nBackTracks} < 30$ .

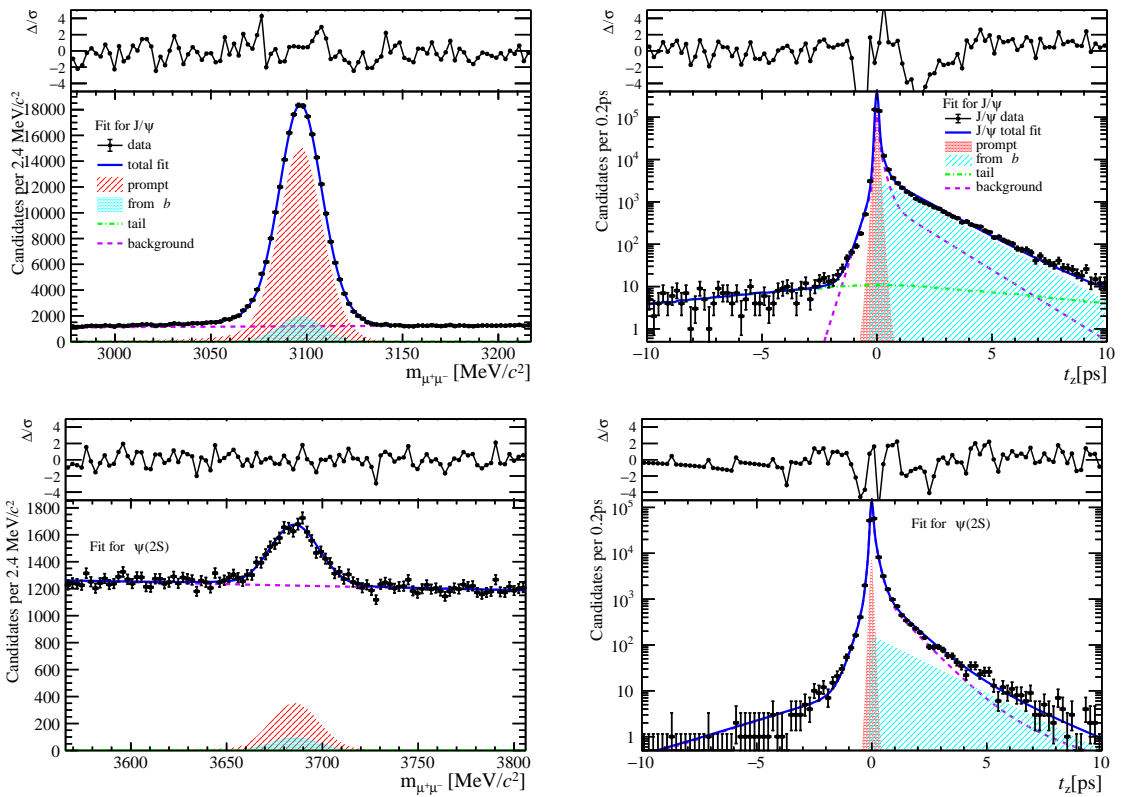


Figure 161: Fit results in  $0 \text{ GeV}/c < p_T < 2 \text{ GeV}/c$ ,  $2.8 < y < 3.5$  and  $22 \leq \text{nBackTracks} < 30$ .

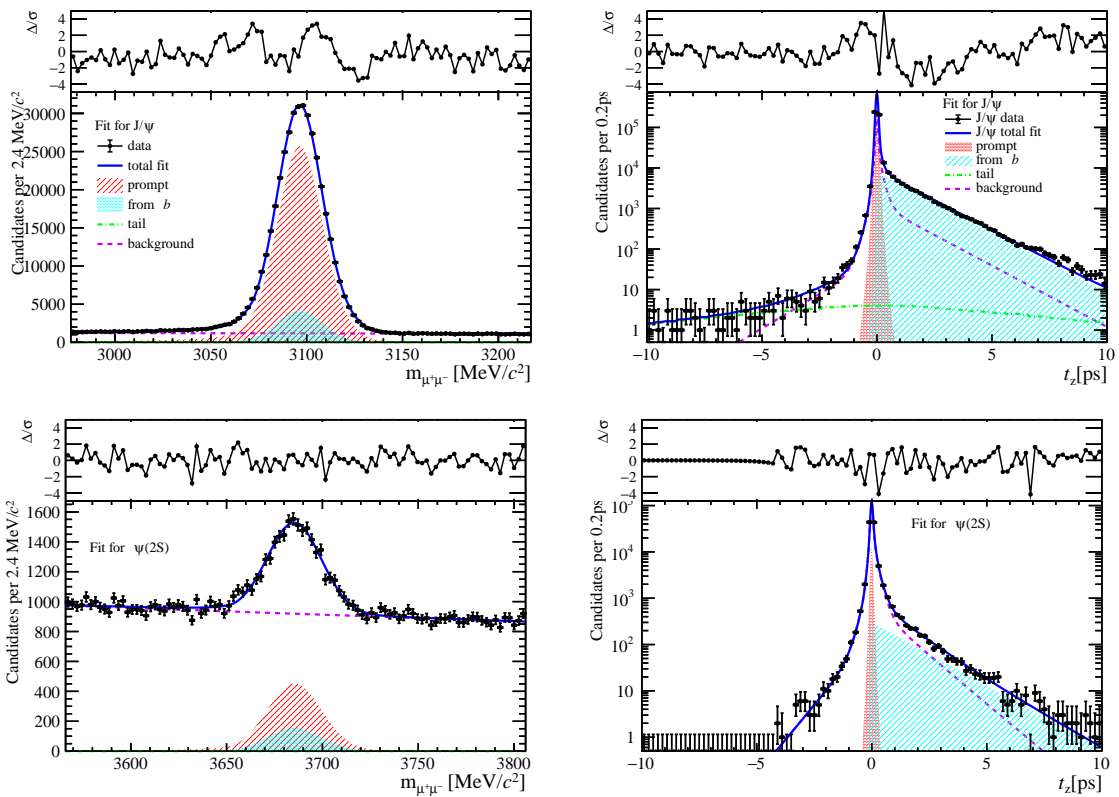


Figure 162: Fit results in  $2 \text{ GeV}/c < p_T < 4 \text{ GeV}/c$ ,  $2.8 < y < 3.5$  and  $22 \leq \text{nBackTracks} < 30$ .

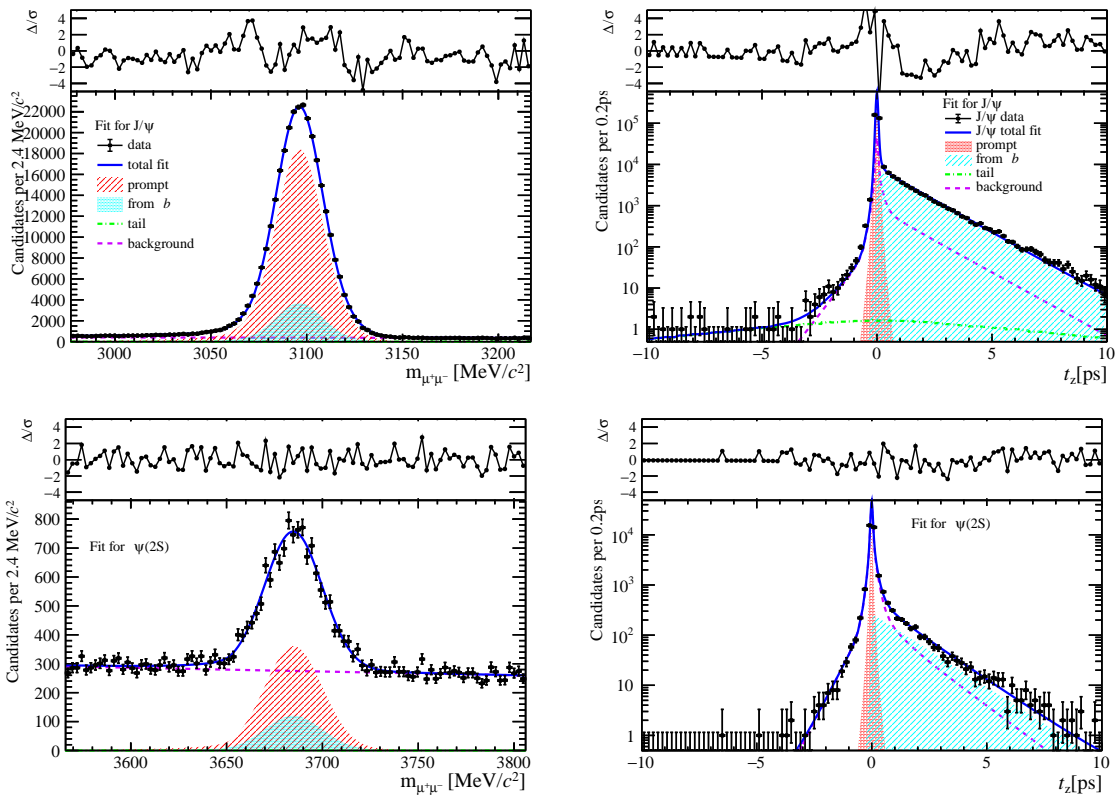


Figure 163: Fit results in  $4 \text{ GeV}/c < p_T < 6 \text{ GeV}/c$ ,  $2.8 < y < 3.5$  and  $22 \leq \text{nBackTracks} < 30$ .

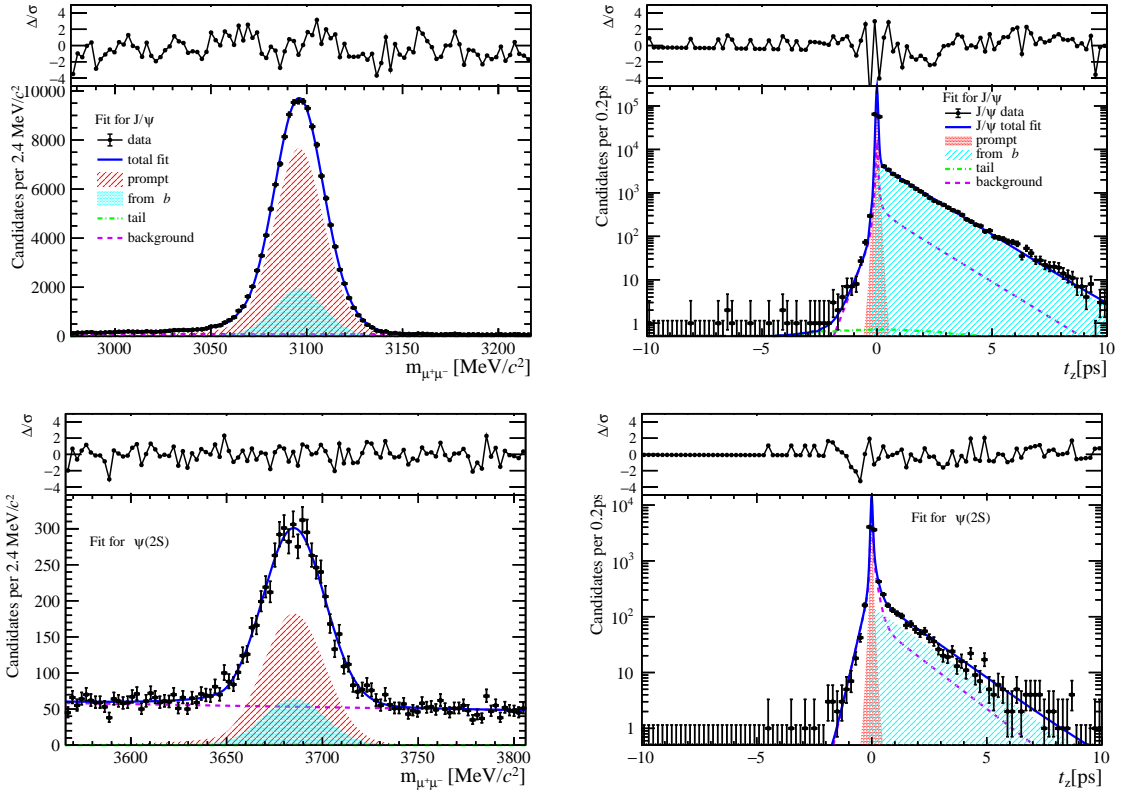


Figure 164: Fit results in  $6 \text{ GeV}/c < p_T < 8 \text{ GeV}/c$ ,  $2.8 < y < 3.5$  and  $22 \leq \text{nBackTracks} < 30$ .

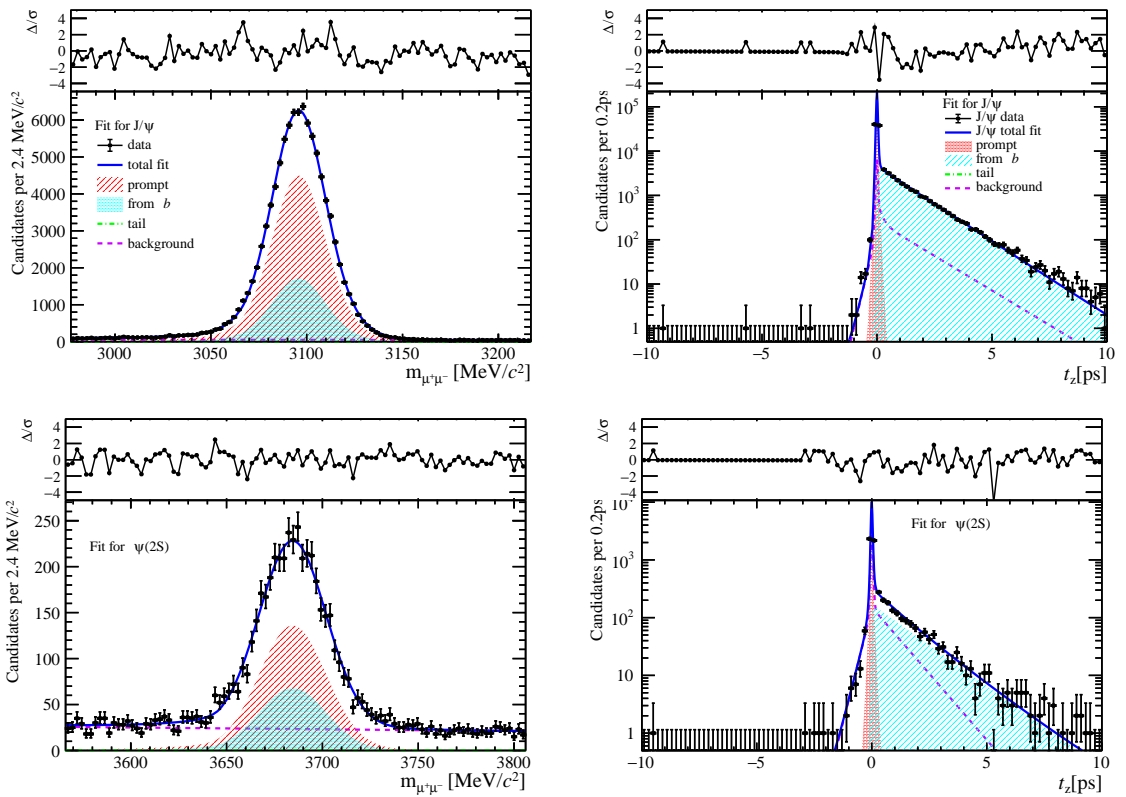


Figure 165: Fit results in  $8 \text{ GeV}/c < p_T < 20 \text{ GeV}/c$ ,  $2.8 < y < 3.5$  and  $22 \leq \text{nBackTracks} < 30$ .

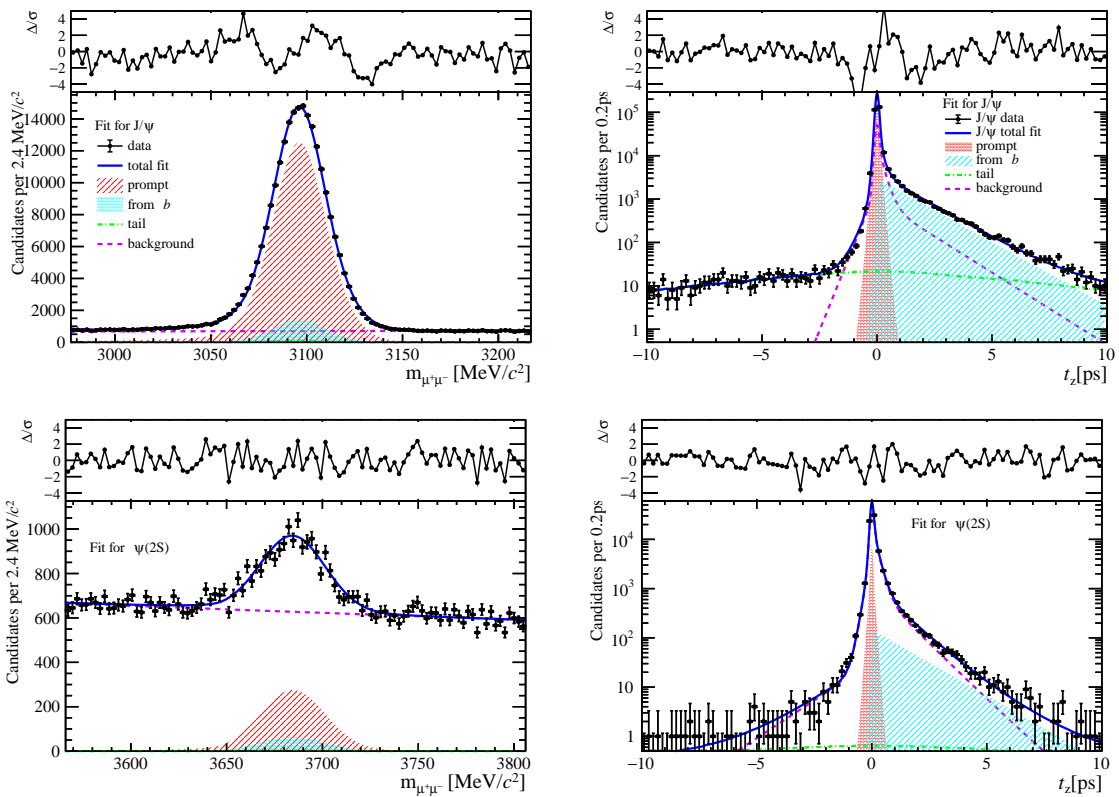


Figure 166: Fit results in  $0 \text{ GeV}/c < p_T < 2 \text{ GeV}/c$ ,  $3.5 < y < 4.5$  and  $22 \leq \text{nBackTracks} < 30$ .

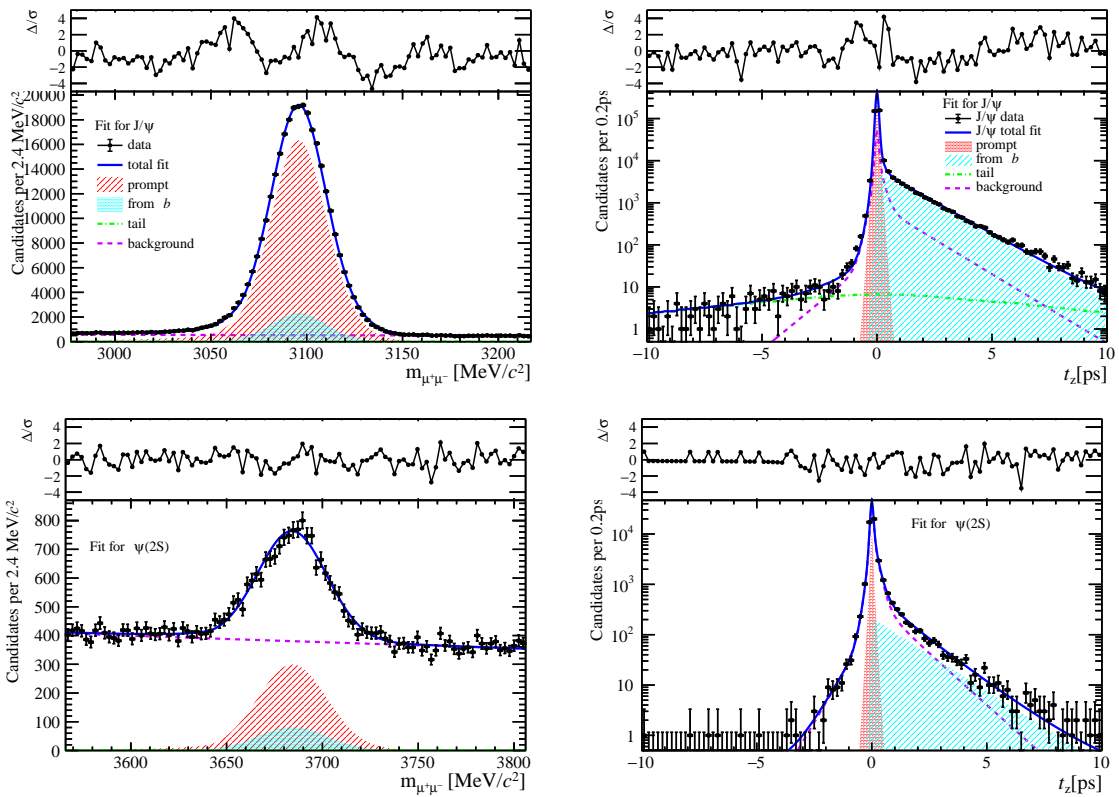


Figure 167: Fit results in  $2 \text{ GeV}/c < p_T < 4 \text{ GeV}/c$ ,  $3.5 < y < 4.5$  and  $22 \leq \text{nBackTracks} < 30$ .

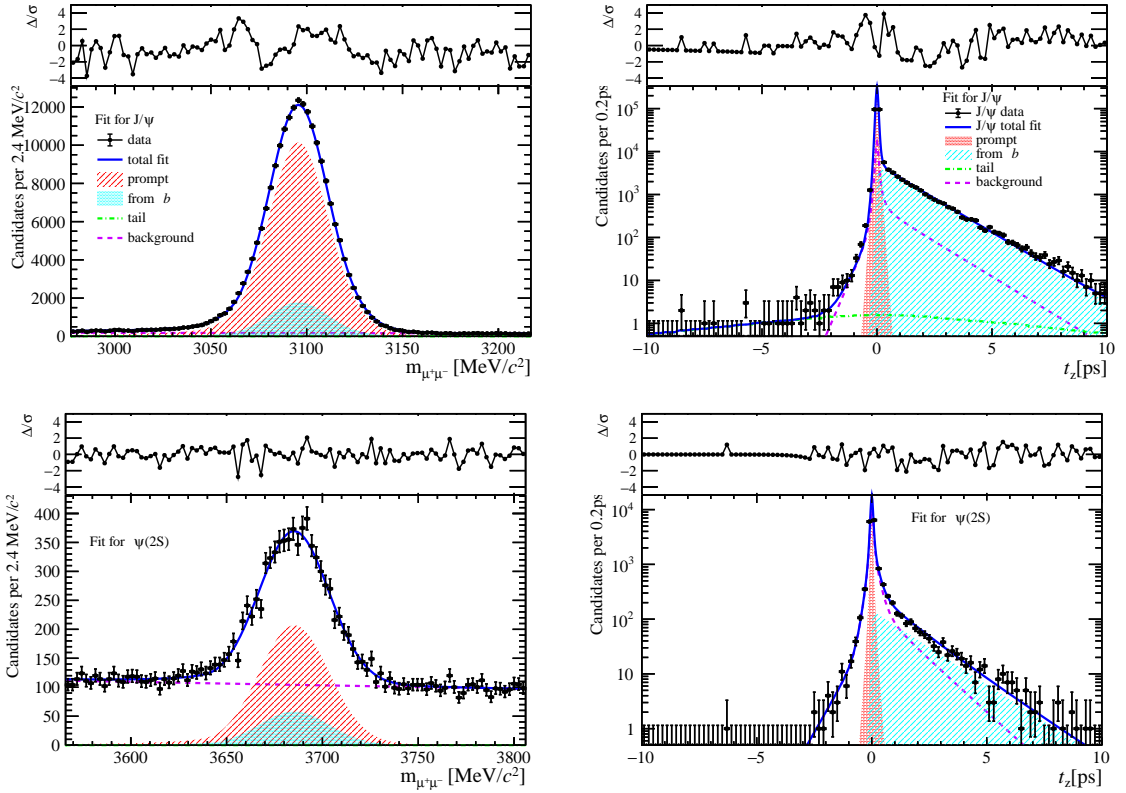


Figure 168: Fit results in  $4 \text{ GeV}/c < p_T < 6 \text{ GeV}/c$ ,  $3.5 < y < 4.5$  and  $22 \leq \text{nBackTracks} < 30$ .

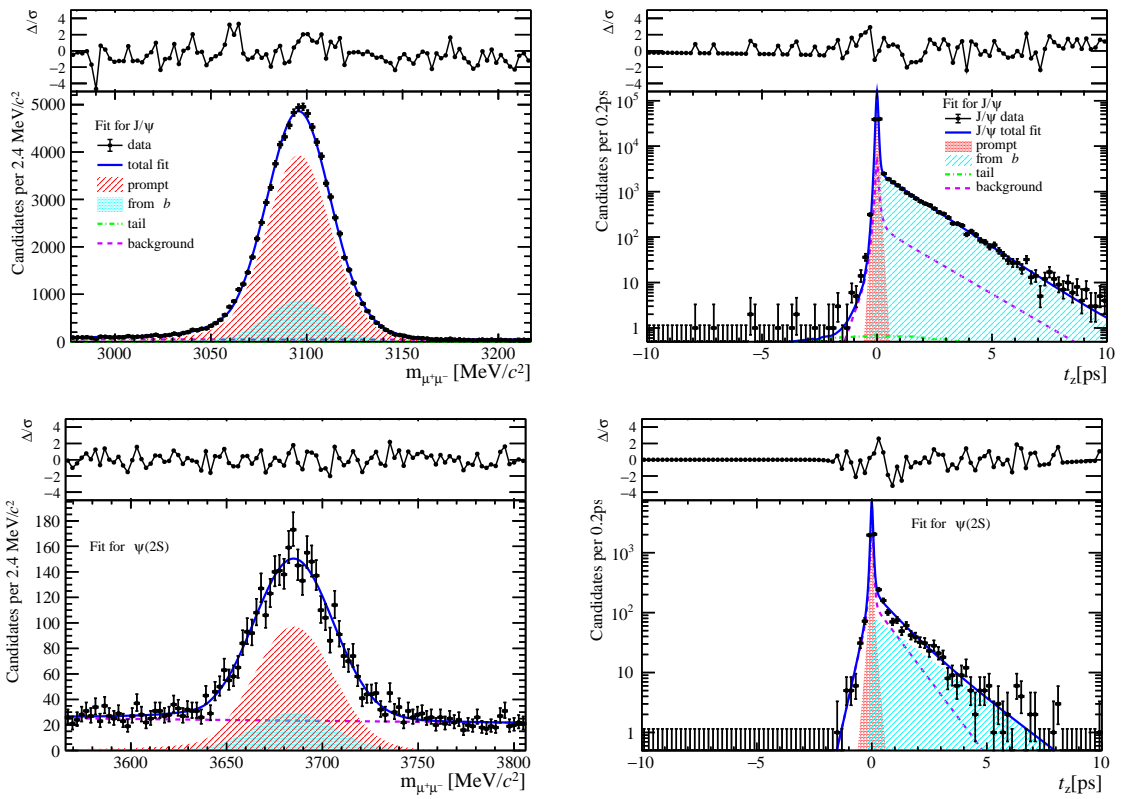


Figure 169: Fit results in  $6 \text{ GeV}/c < p_T < 8 \text{ GeV}/c$ ,  $3.5 < y < 4.5$  and  $22 \leq \text{nBackTracks} < 30$ .

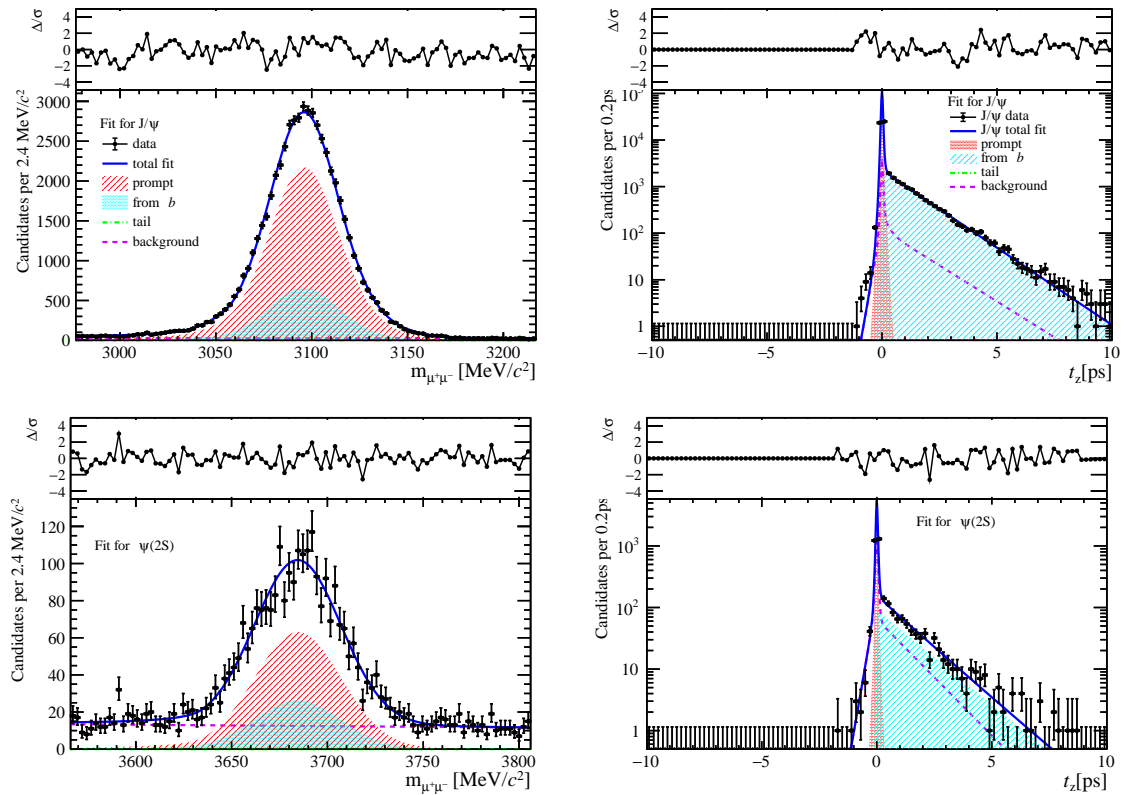


Figure 170: Fit results in  $8 \text{ GeV}/c < p_T < 20 \text{ GeV}/c$ ,  $3.5 < y < 4.5$  and  $22 \leq \text{nBackTracks} < 30$ .

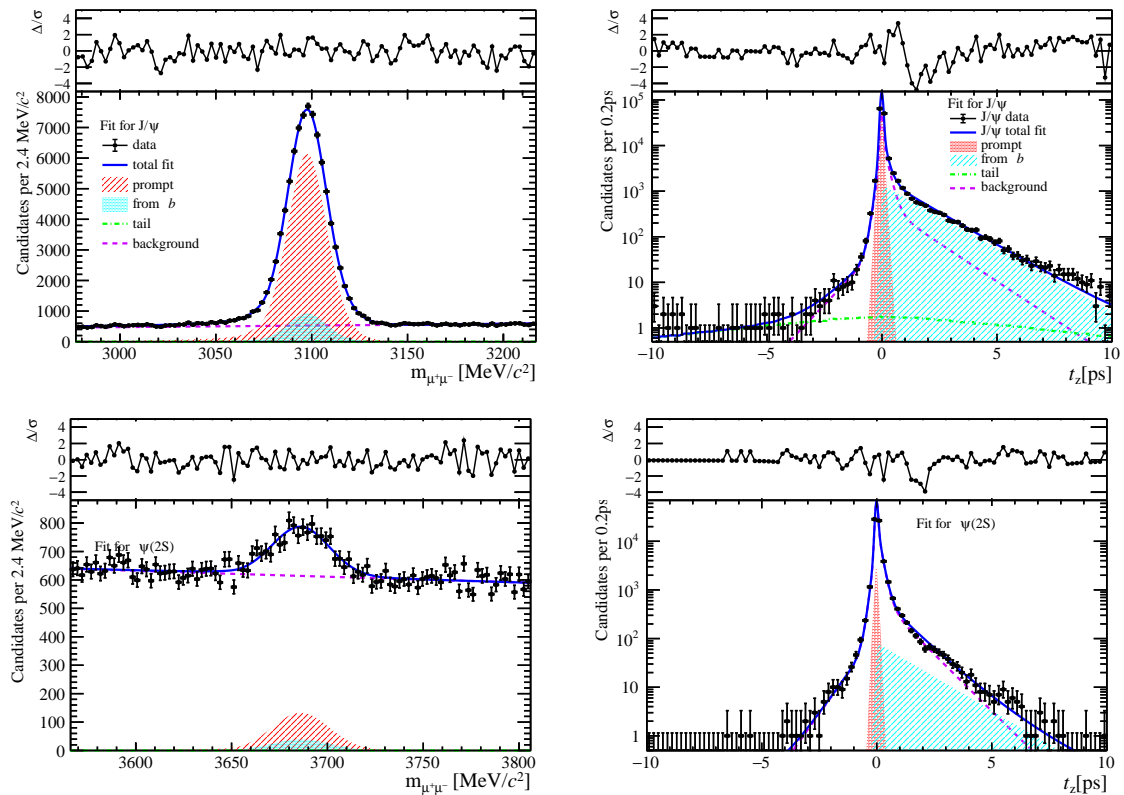


Figure 171: Fit results in  $0 \text{ GeV}/c < p_T < 2 \text{ GeV}/c$ ,  $2.0 < y < 2.8$  and  $30 \leq \text{nBackTracks} < 80$ .

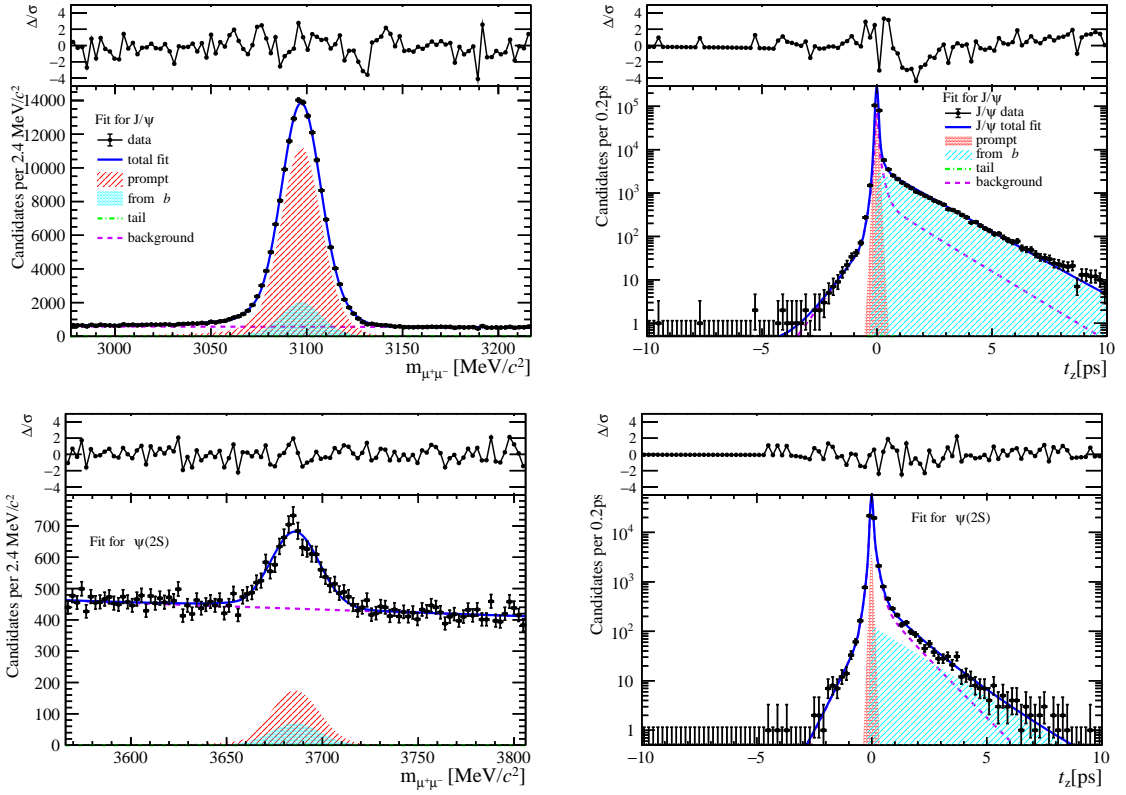


Figure 172: Fit results in  $2 \text{ GeV}/c < p_T < 4 \text{ GeV}/c$ ,  $2.0 < y < 2.8$  and  $30 \leq n\text{BackTracks} < 80$ .

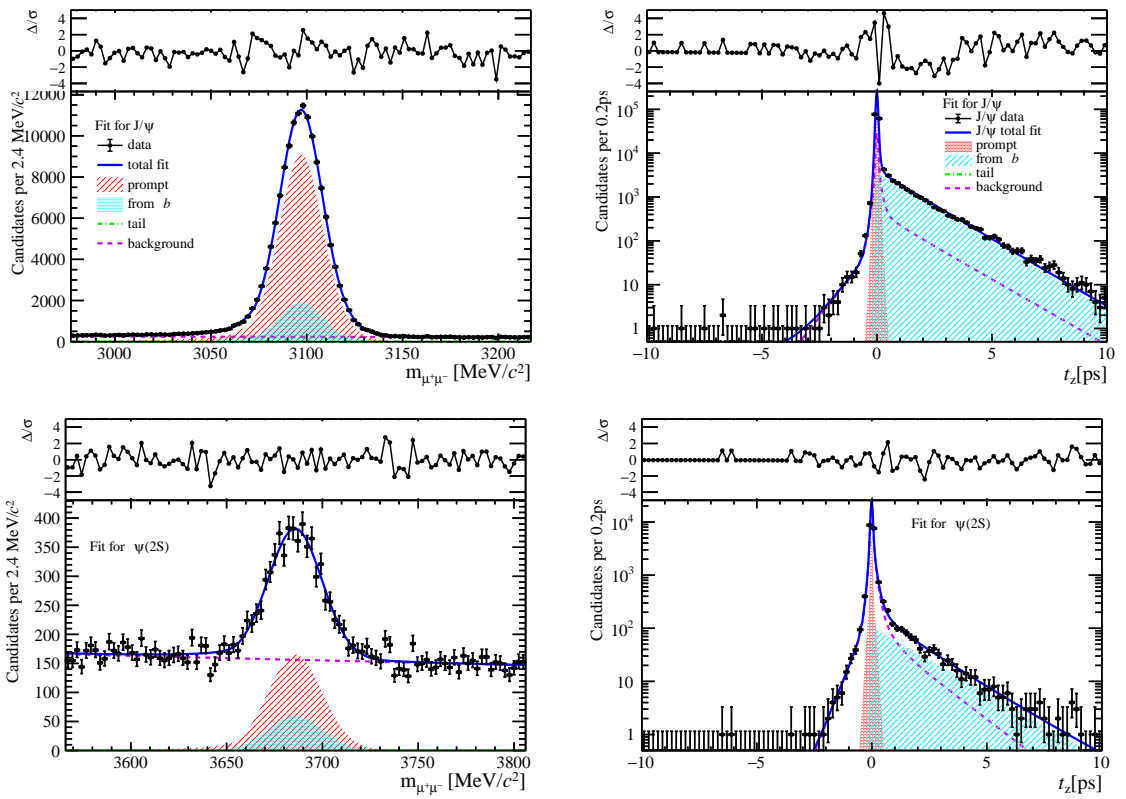


Figure 173: Fit results in  $4 \text{ GeV}/c < p_T < 6 \text{ GeV}/c$ ,  $2.0 < y < 2.8$  and  $30 \leq n\text{BackTracks} < 80$ .

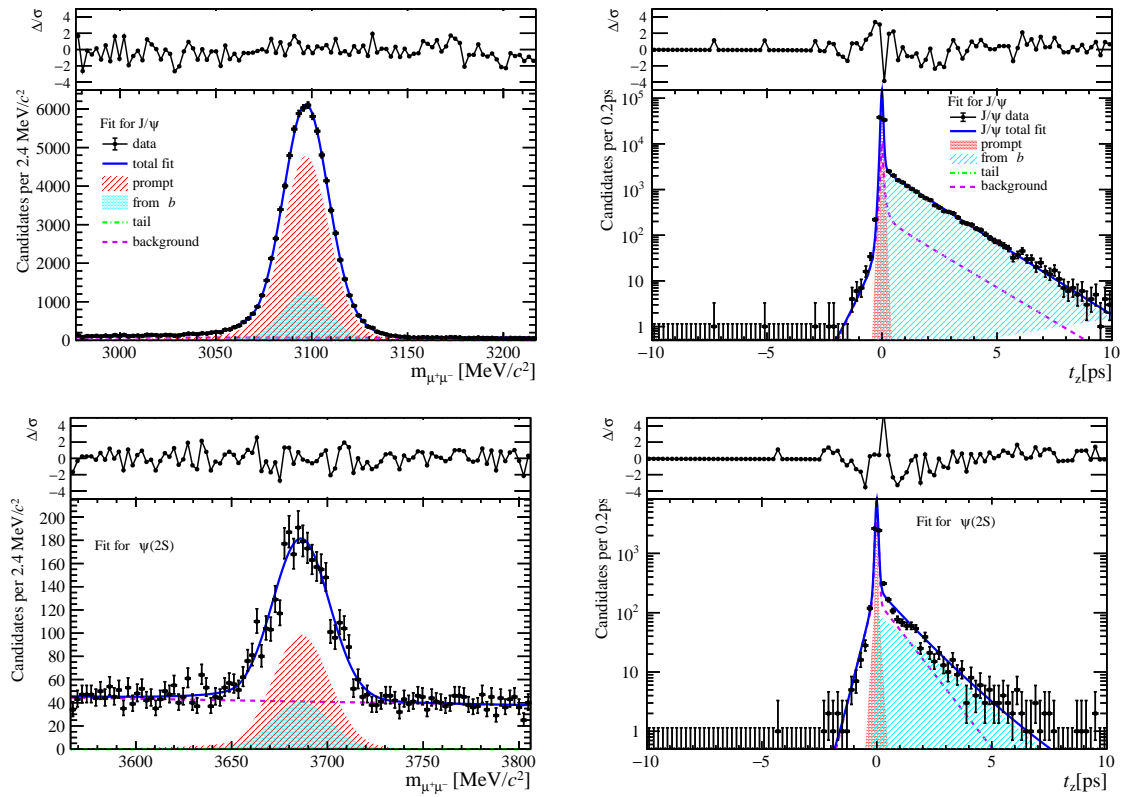


Figure 174: Fit results in  $6 \text{ GeV}/c < p_T < 8 \text{ GeV}/c$ ,  $2.0 < y < 2.8$  and  $30 \leq \text{nBackTracks} < 80$ .

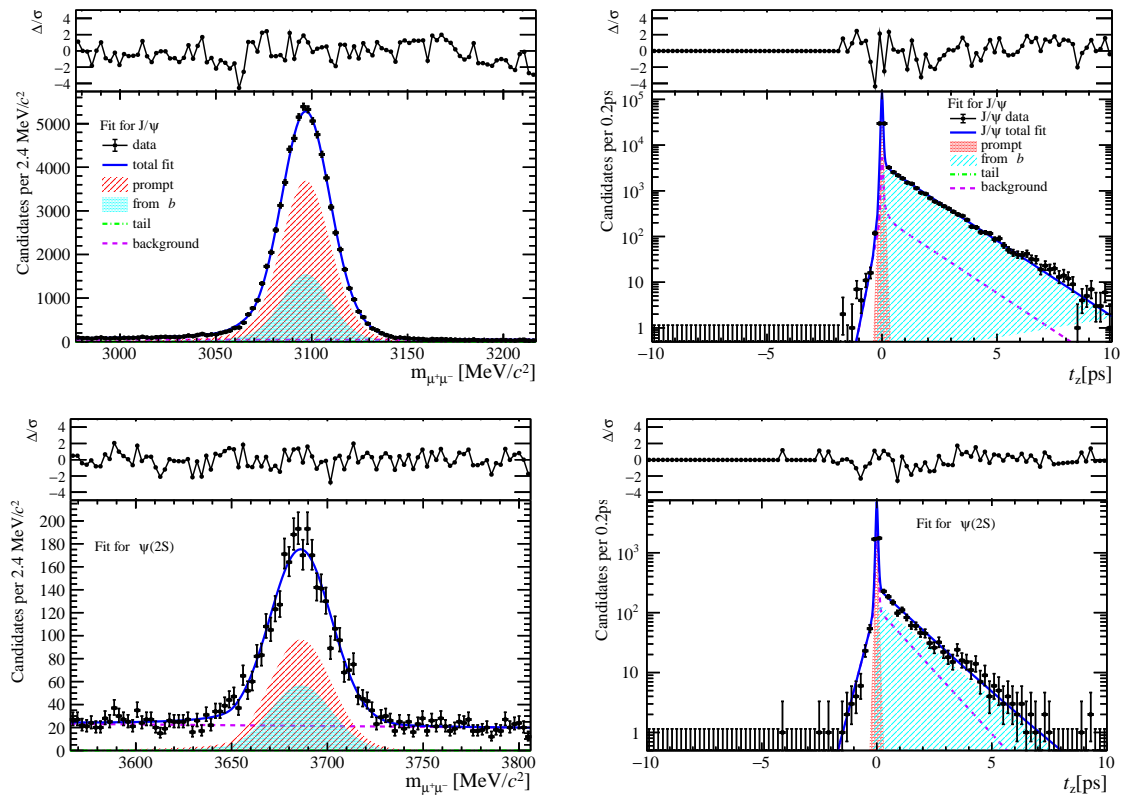


Figure 175: Fit results in  $8 \text{ GeV}/c < p_T < 20 \text{ GeV}/c$ ,  $2.0 < y < 2.8$  and  $30 \leq \text{nBackTracks} < 80$ .

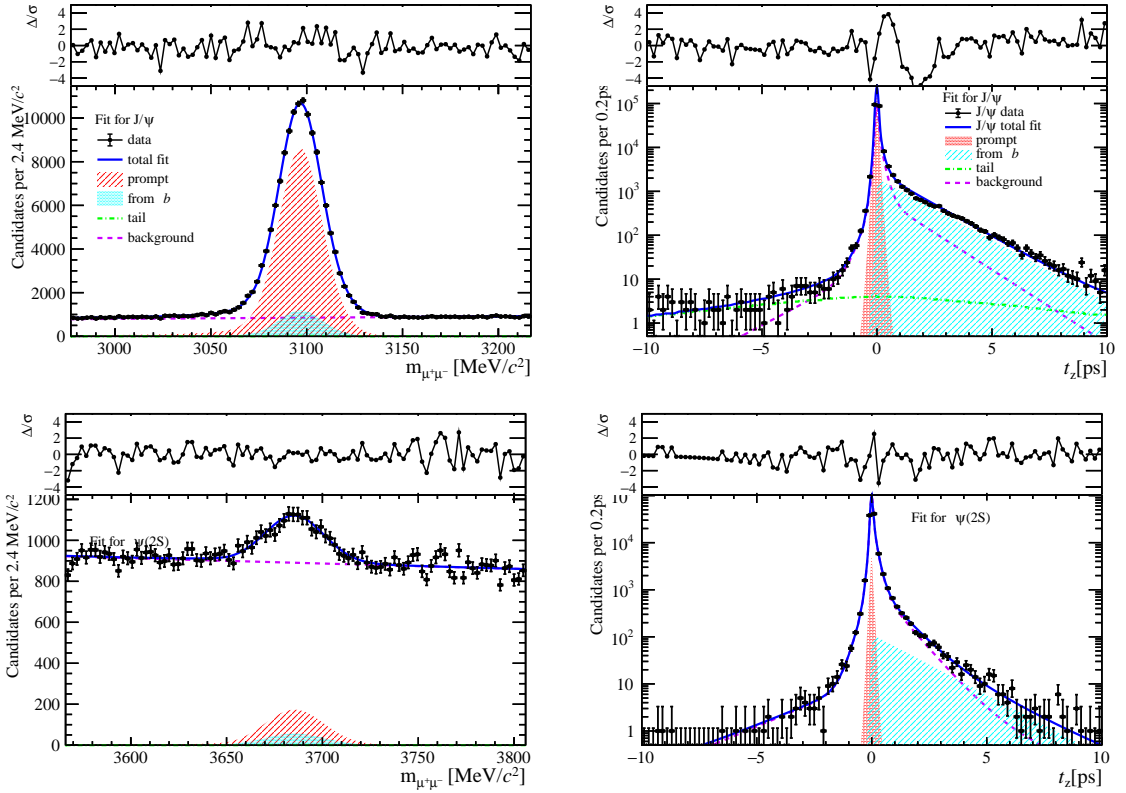


Figure 176: Fit results in  $0 \text{ GeV}/c < p_T < 2 \text{ GeV}/c$ ,  $2.8 < y < 3.5$  and  $30 \leq \text{nBackTracks} < 80$ .

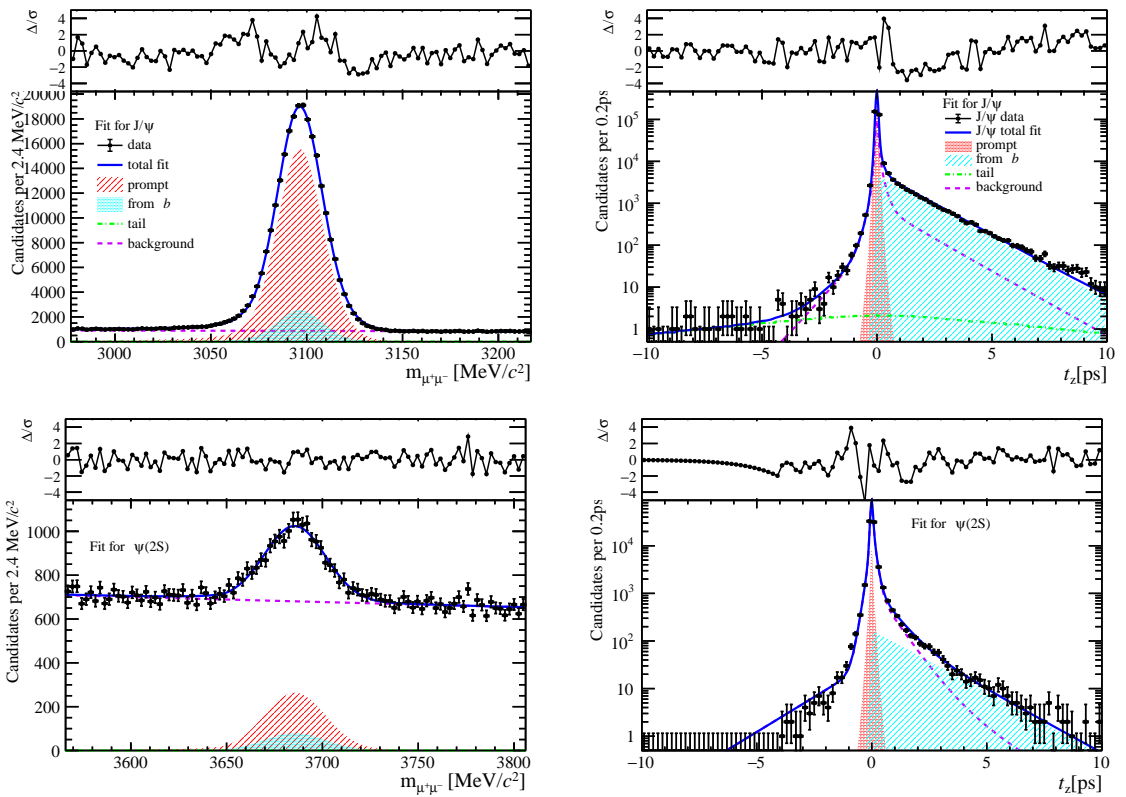


Figure 177: Fit results in  $2 \text{ GeV}/c < p_T < 4 \text{ GeV}/c$ ,  $2.8 < y < 3.5$  and  $30 \leq \text{nBackTracks} < 80$ .

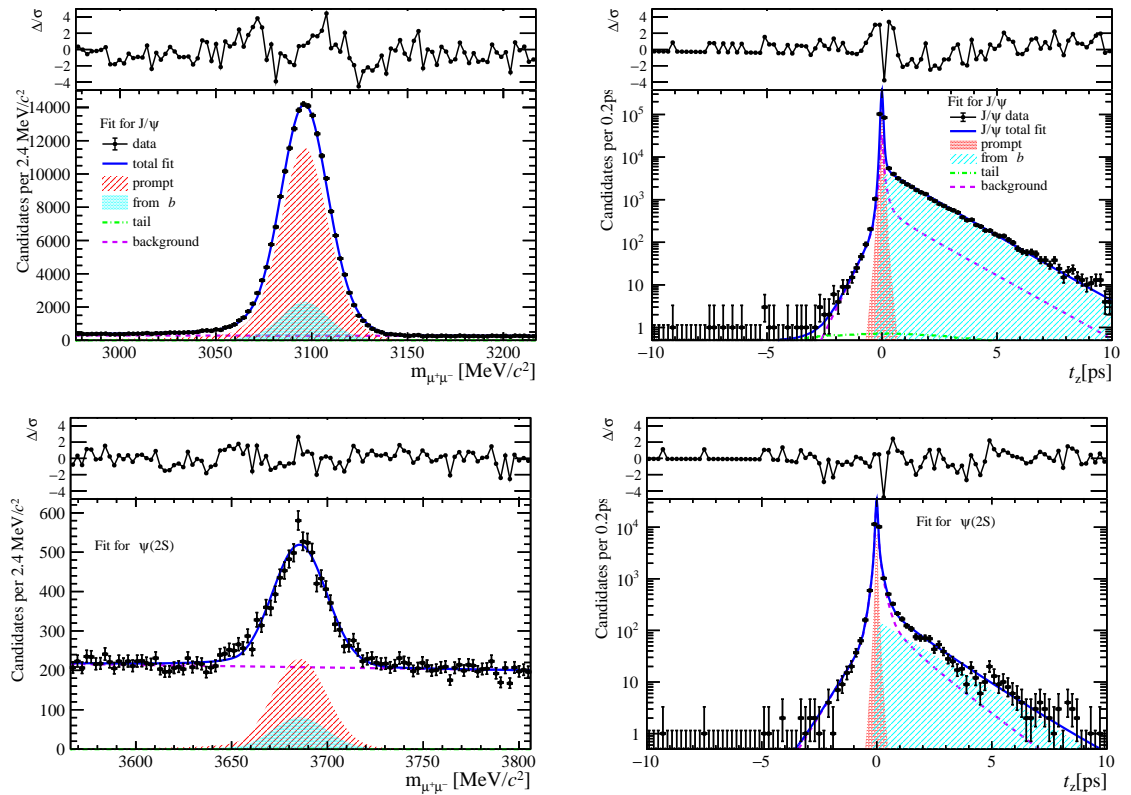


Figure 178: Fit results in  $4 \text{ GeV}/c < p_T < 6 \text{ GeV}/c$ ,  $2.8 < y < 3.5$  and  $30 \leq \text{nBackTracks} < 80$ .

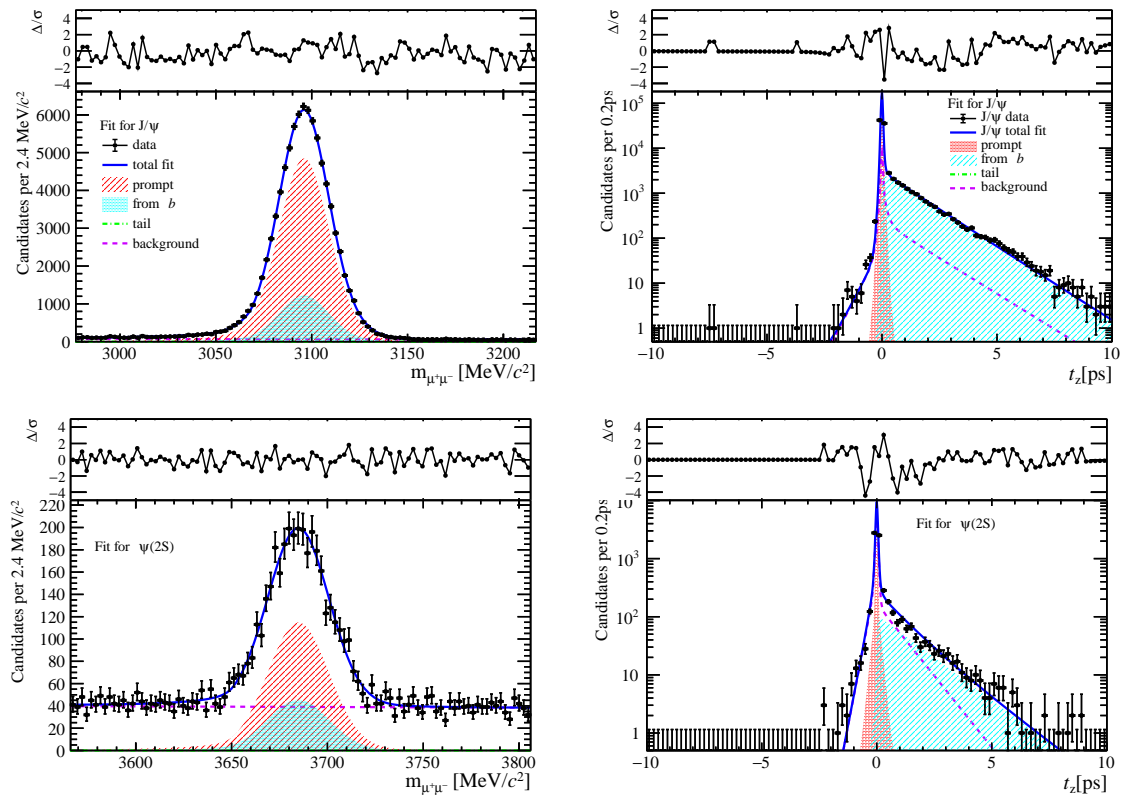


Figure 179: Fit results in  $6 \text{ GeV}/c < p_T < 8 \text{ GeV}/c$ ,  $2.8 < y < 3.5$  and  $30 \leq \text{nBackTracks} < 80$ .

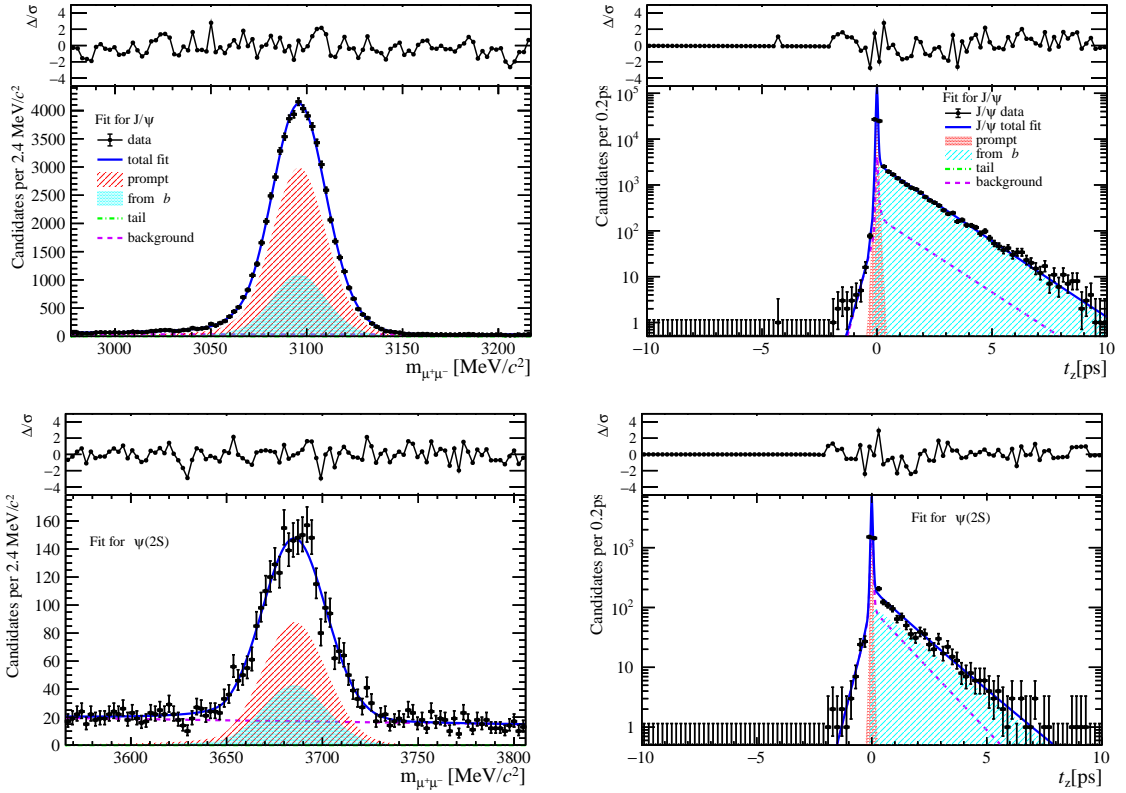


Figure 180: Fit results in  $8 \text{ GeV}/c < p_T < 20 \text{ GeV}/c$ ,  $2.8 < y < 3.5$  and  $30 \leq \text{nBackTracks} < 80$ .

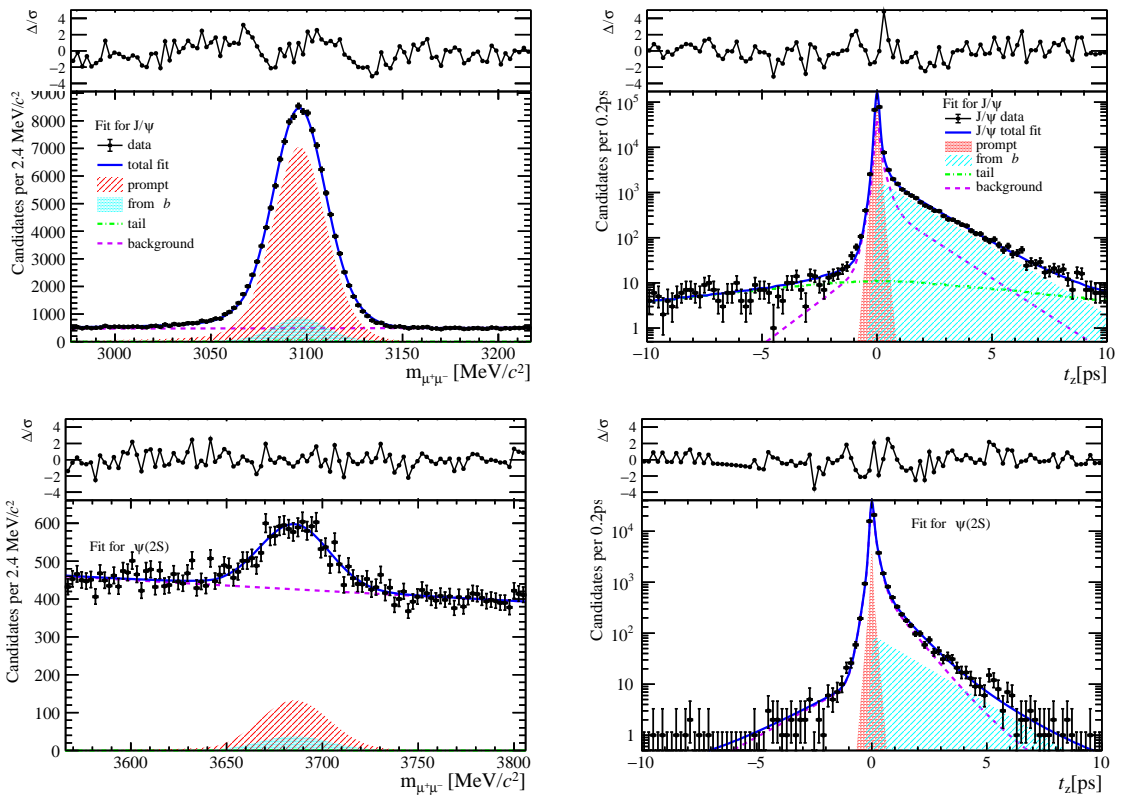


Figure 181: Fit results in  $0 \text{ GeV}/c < p_T < 2 \text{ GeV}/c$ ,  $3.5 < y < 4.5$  and  $30 \leq \text{nBackTracks} < 80$ .

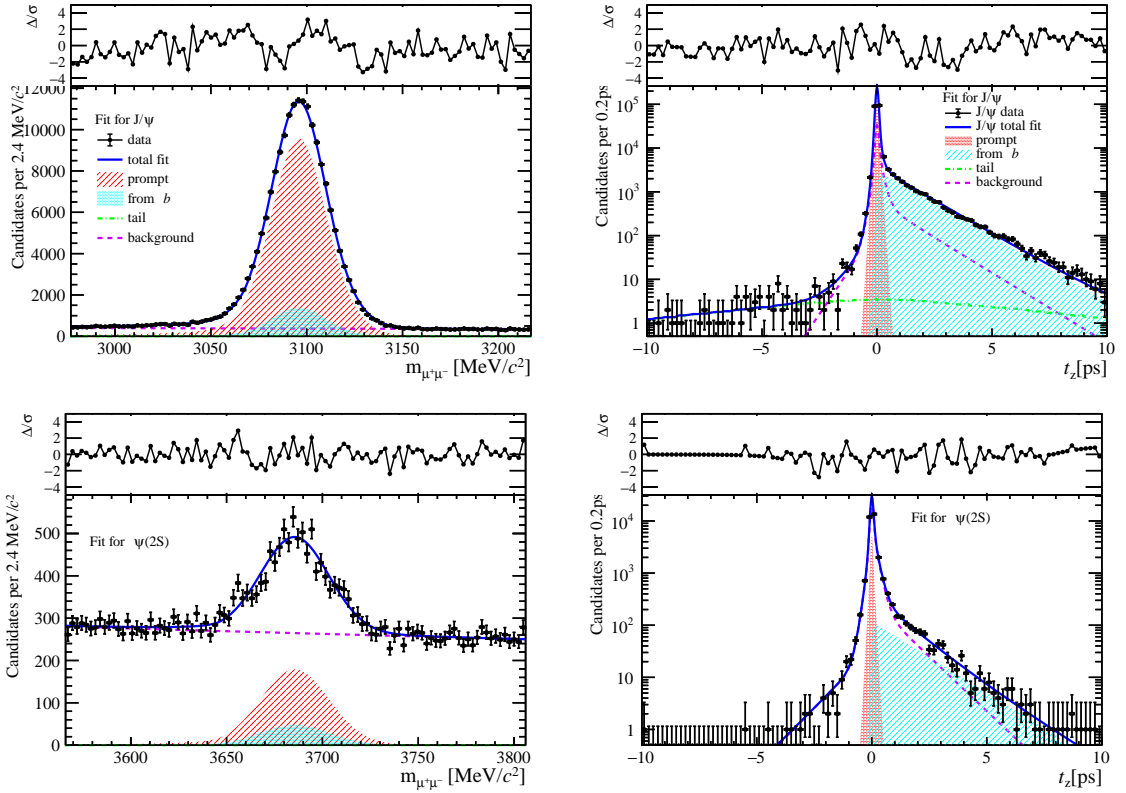


Figure 182: Fit results in  $2 \text{ GeV}/c < p_{\text{T}} < 4 \text{ GeV}/c$ ,  $3.5 < y < 4.5$  and  $30 \leq \text{nBackTracks} < 80$ .

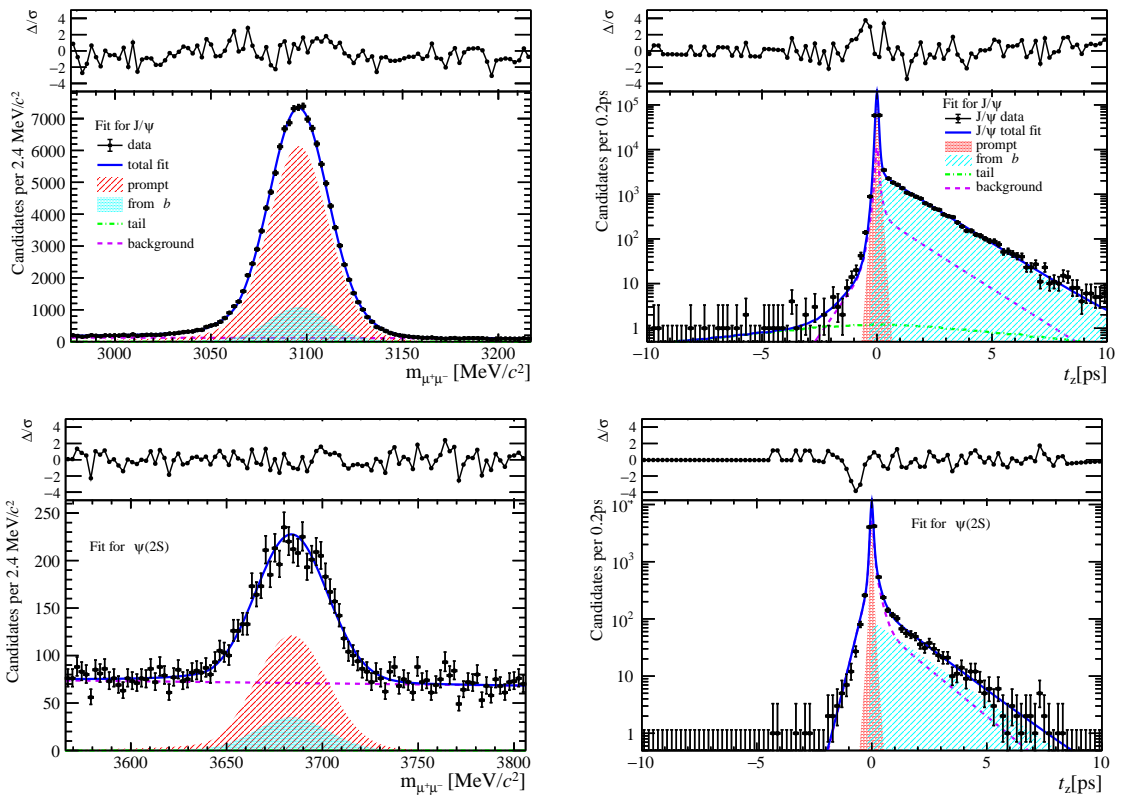


Figure 183: Fit results in  $4 \text{ GeV}/c < p_{\text{T}} < 6 \text{ GeV}/c$ ,  $3.5 < y < 4.5$  and  $30 \leq \text{nBackTracks} < 80$ .

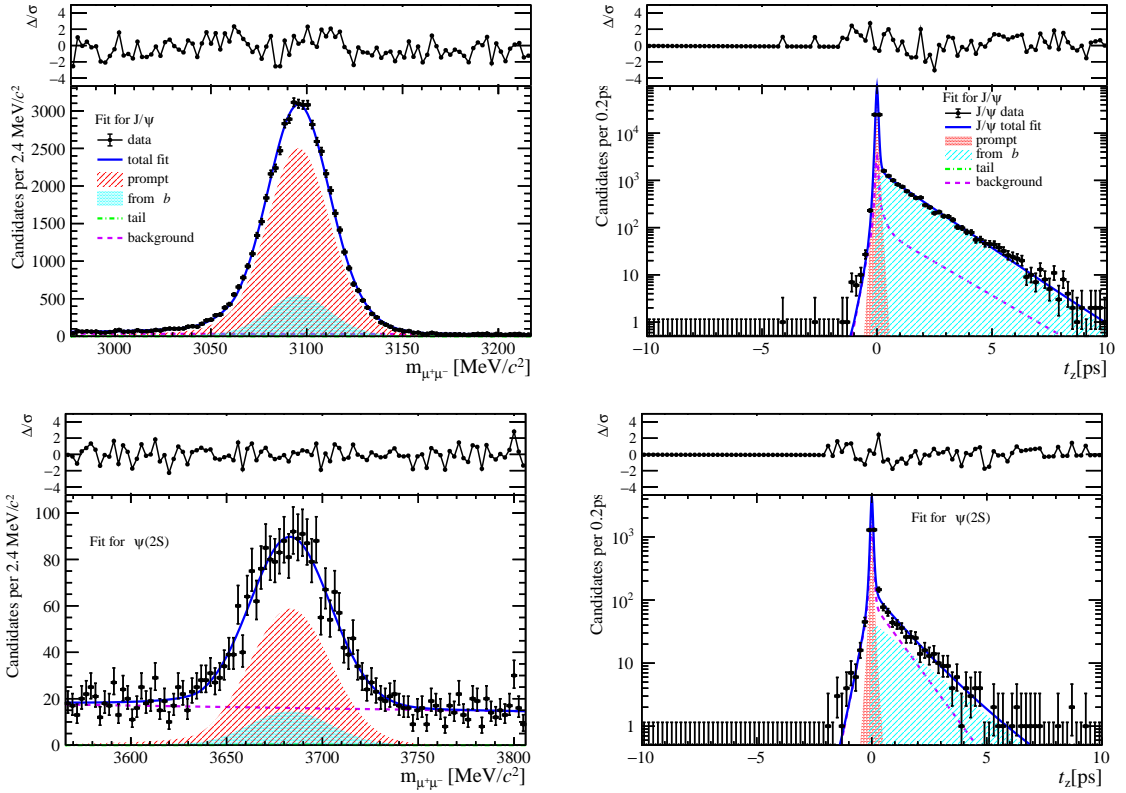


Figure 184: Fit results in  $6 \text{ GeV}/c < p_T < 8 \text{ GeV}/c$ ,  $3.5 < y < 4.5$  and  $30 \leq \text{nBackTracks} < 80$ .

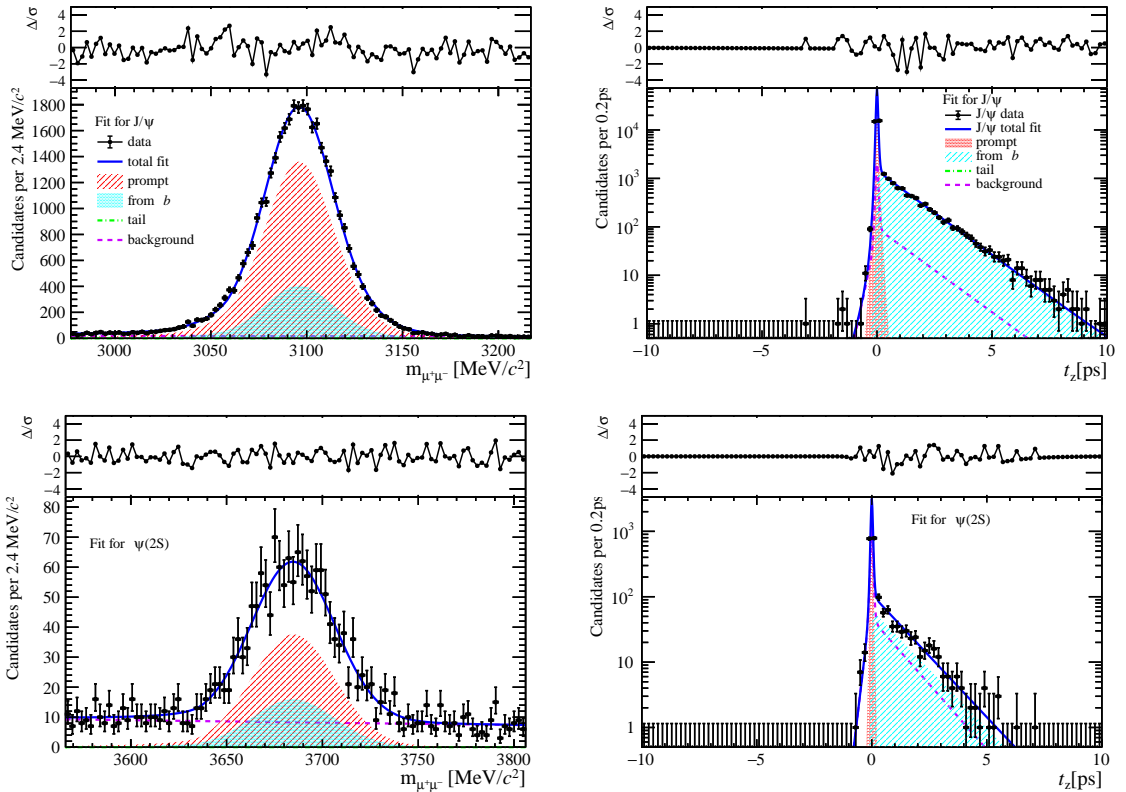


Figure 185: Fit results in  $8 \text{ GeV}/c < p_T < 20 \text{ GeV}/c$ ,  $3.5 < y < 4.5$  and  $30 \leq \text{nBackTracks} < 80$ .

720 **3 Separated by nForwardTracks**

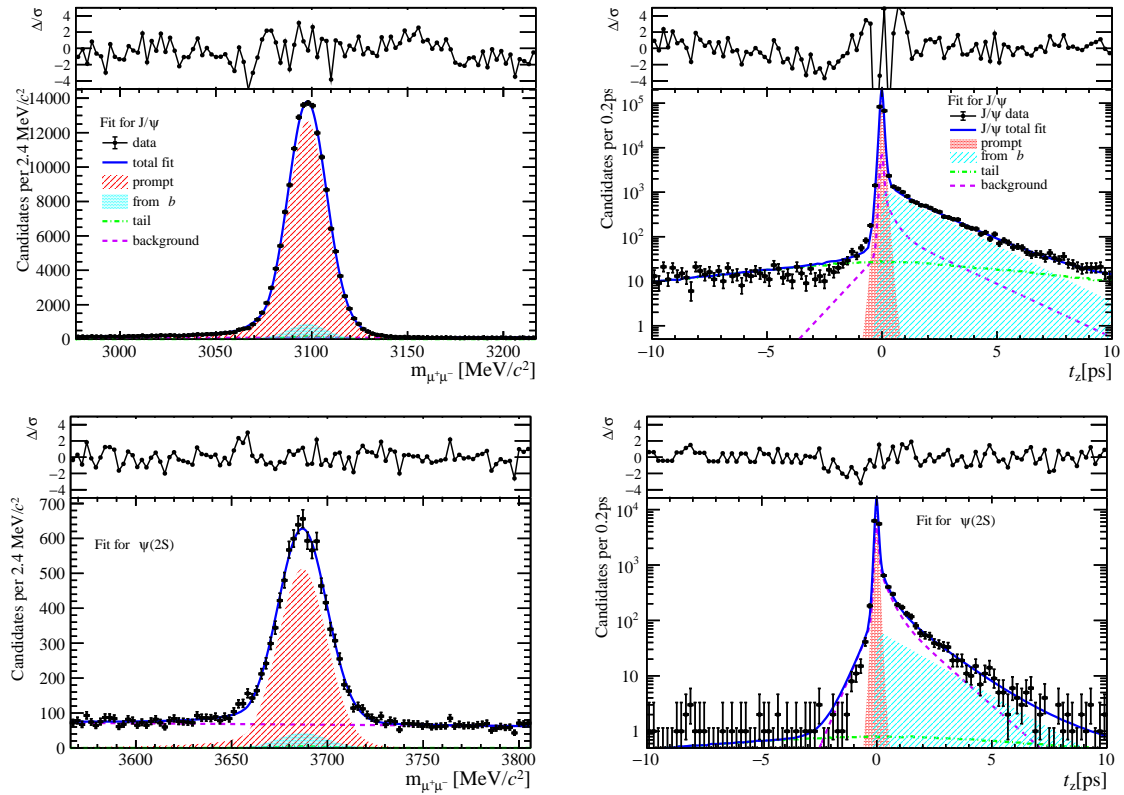


Figure 186: Fit results in  $0 \text{ GeV}/c < p_T < 2 \text{ GeV}/c$ ,  $2.0 < y < 2.8$  and  $0 \leq \text{nForwardTracks} < 12$ .

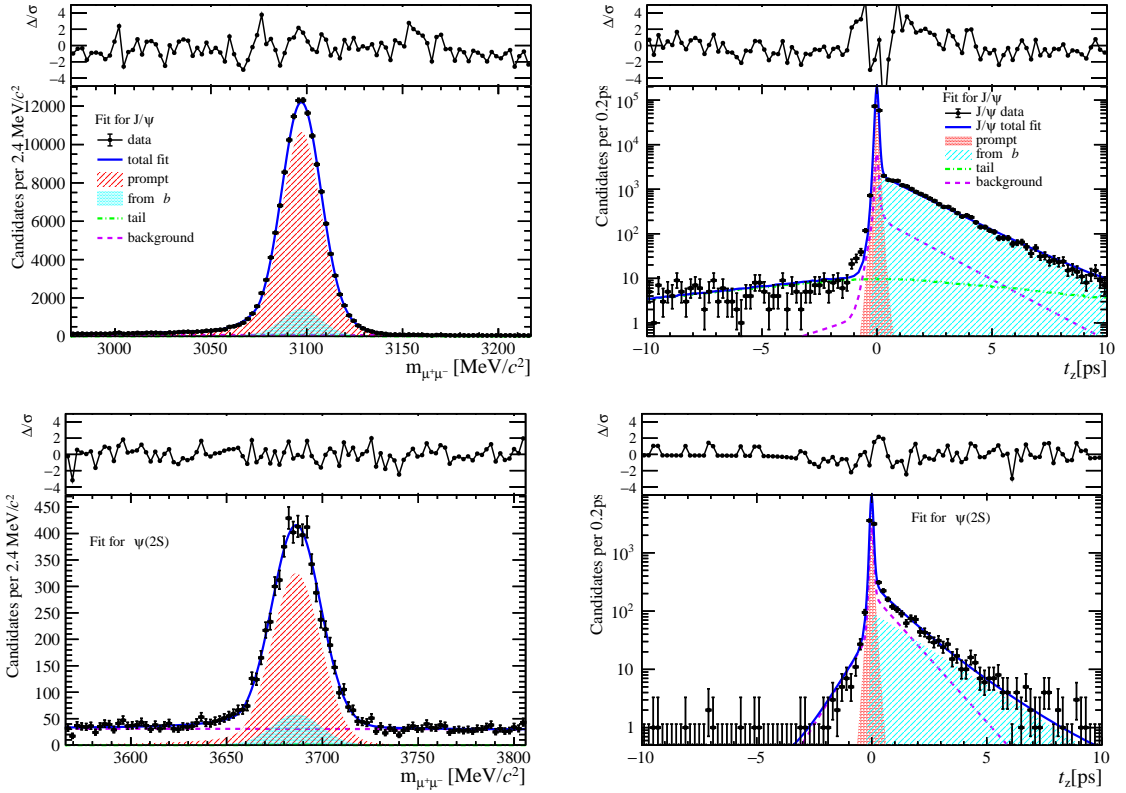


Figure 187: Fit results in  $2 \text{ GeV}/c < p_T < 4 \text{ GeV}/c$ ,  $2.0 < y < 2.8$  and  $0 \leq \text{nForwardTracks} < 12$ .

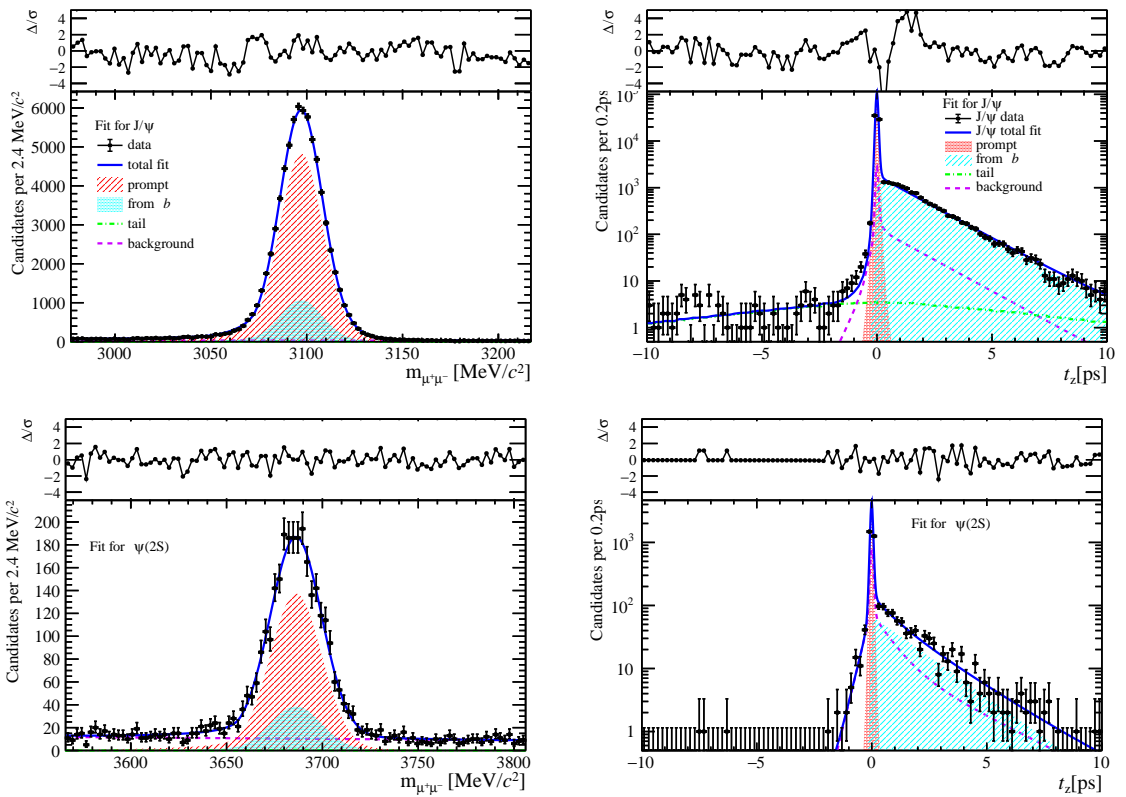


Figure 188: Fit results in  $4 \text{ GeV}/c < p_T < 6 \text{ GeV}/c$ ,  $2.0 < y < 2.8$  and  $0 \leq \text{nForwardTracks} < 12$ .

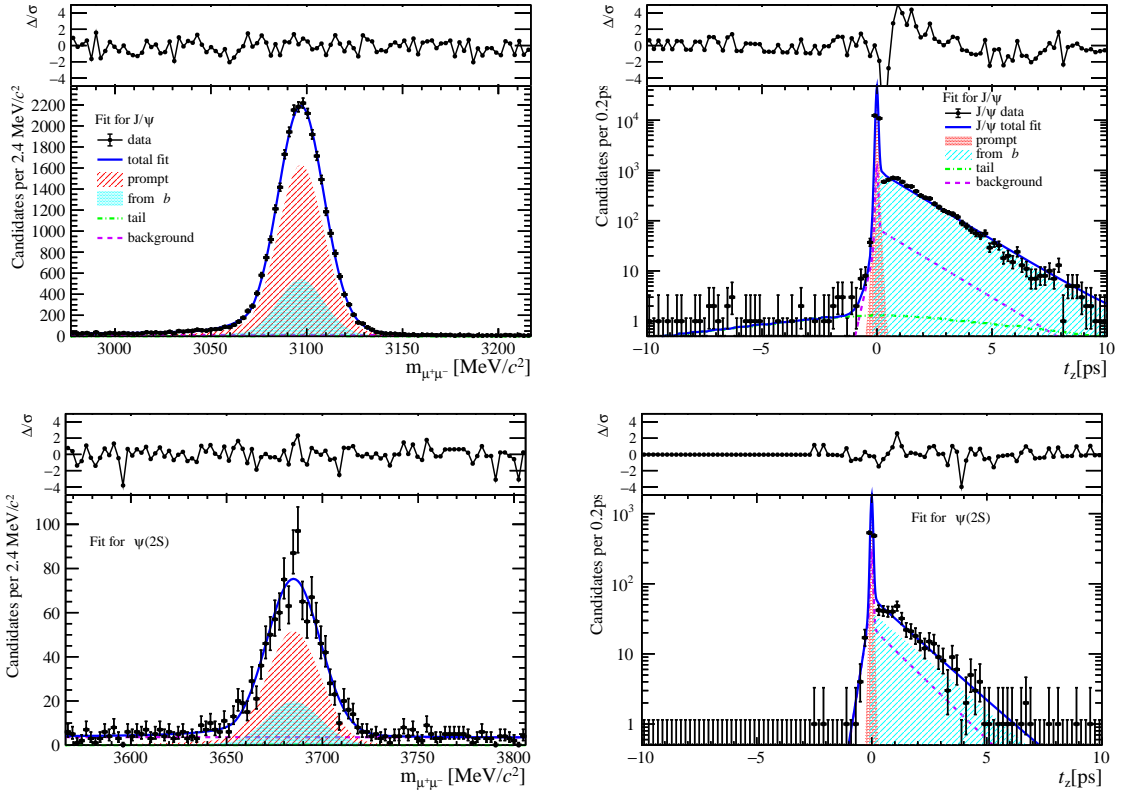


Figure 189: Fit results in  $6 \text{ GeV}/c < p_T < 8 \text{ GeV}/c$ ,  $2.0 < y < 2.8$  and  $0 \leq \text{nForwardTracks} < 12$ .

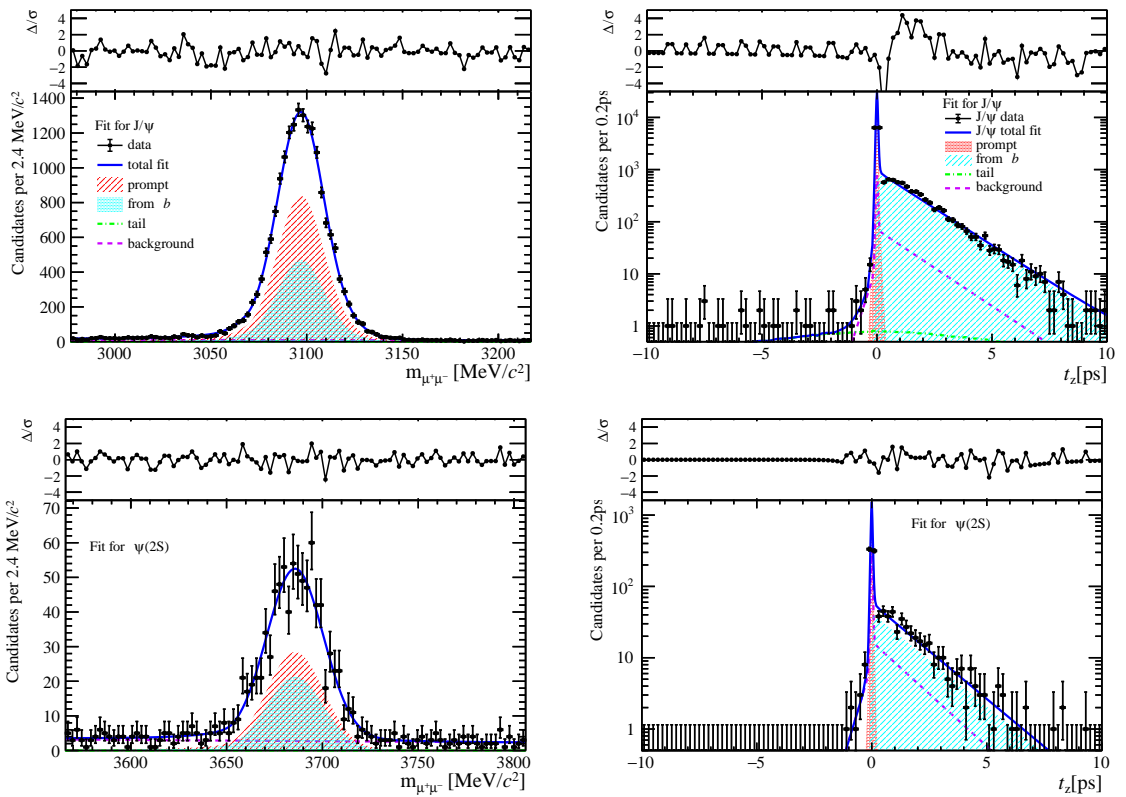


Figure 190: Fit results in  $8 \text{ GeV}/c < p_T < 20 \text{ GeV}/c$ ,  $2.0 < y < 2.8$  and  $0 \leq \text{nForwardTracks} < 12$ .

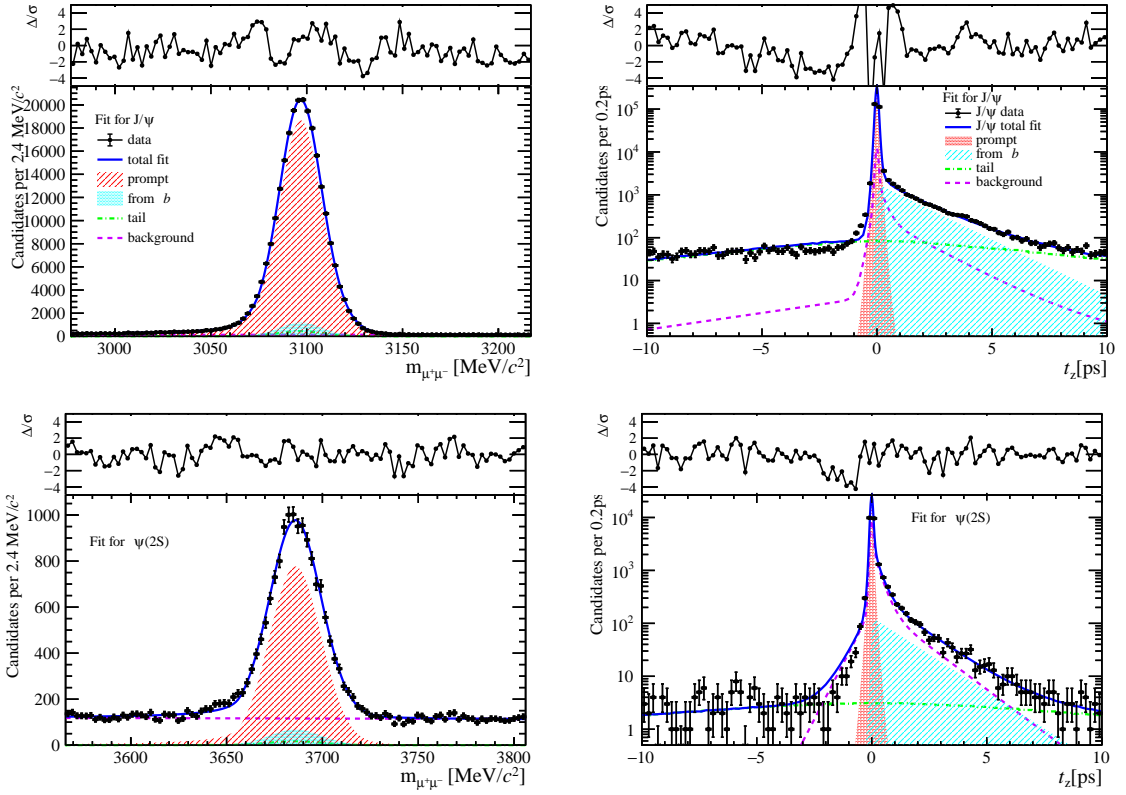


Figure 191: Fit results in  $0 \text{ GeV}/c < p_T < 2 \text{ GeV}/c$ ,  $2.8 < y < 3.5$  and  $0 \leq \text{nForwardTracks} < 12$ .

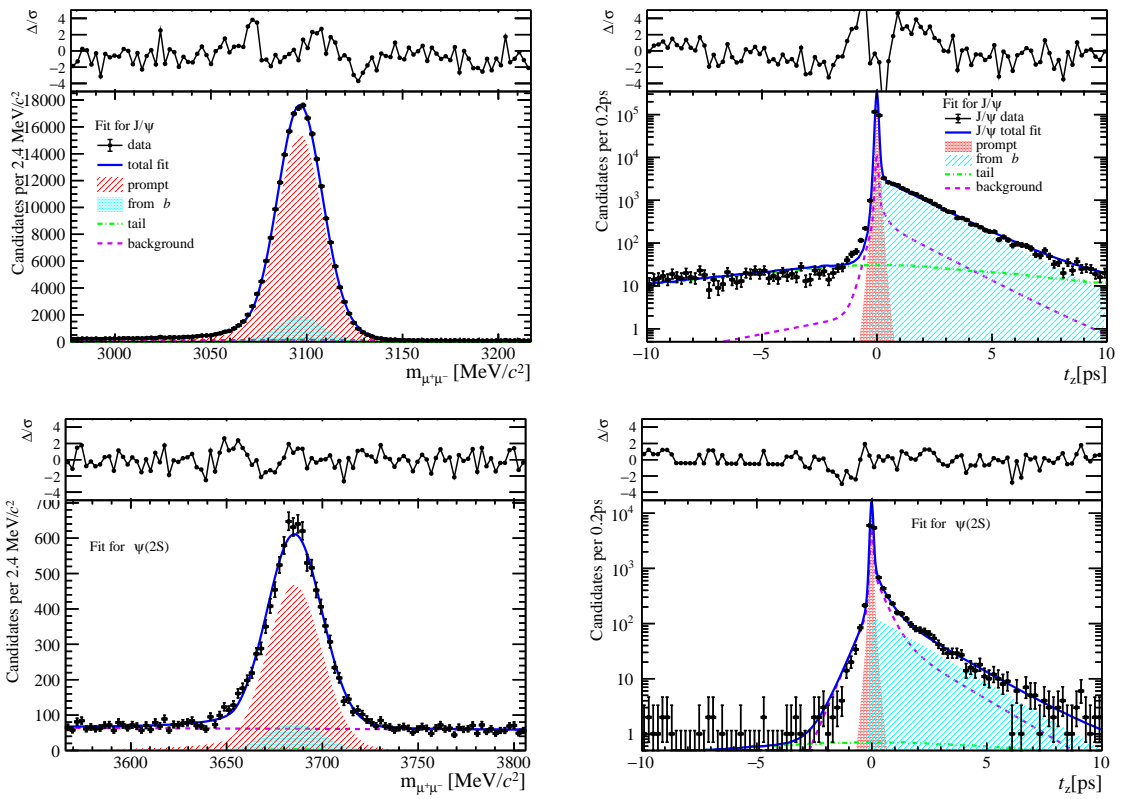


Figure 192: Fit results in  $2 \text{ GeV}/c < p_T < 4 \text{ GeV}/c$ ,  $2.8 < y < 3.5$  and  $0 \leq \text{nForwardTracks} < 12$ .

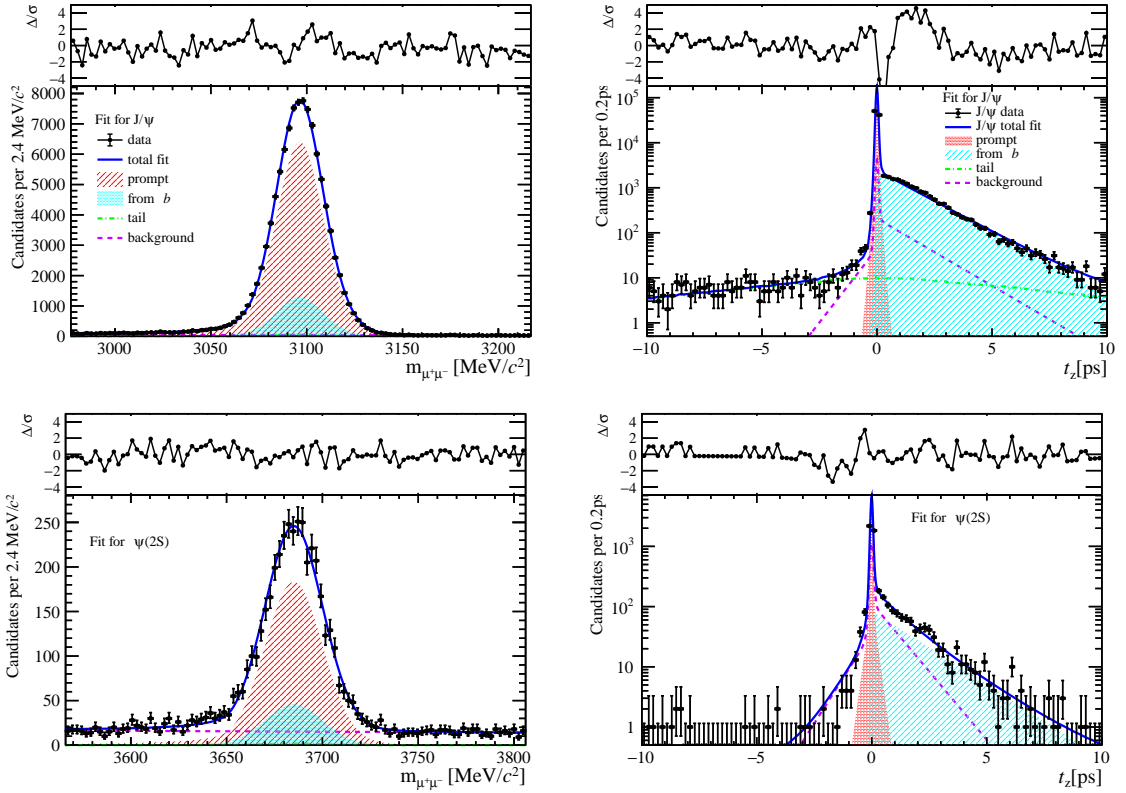


Figure 193: Fit results in  $4 \text{ GeV}/c < p_T < 6 \text{ GeV}/c$ ,  $2.8 < y < 3.5$  and  $0 \leq \text{nForwardTracks} < 12$ .

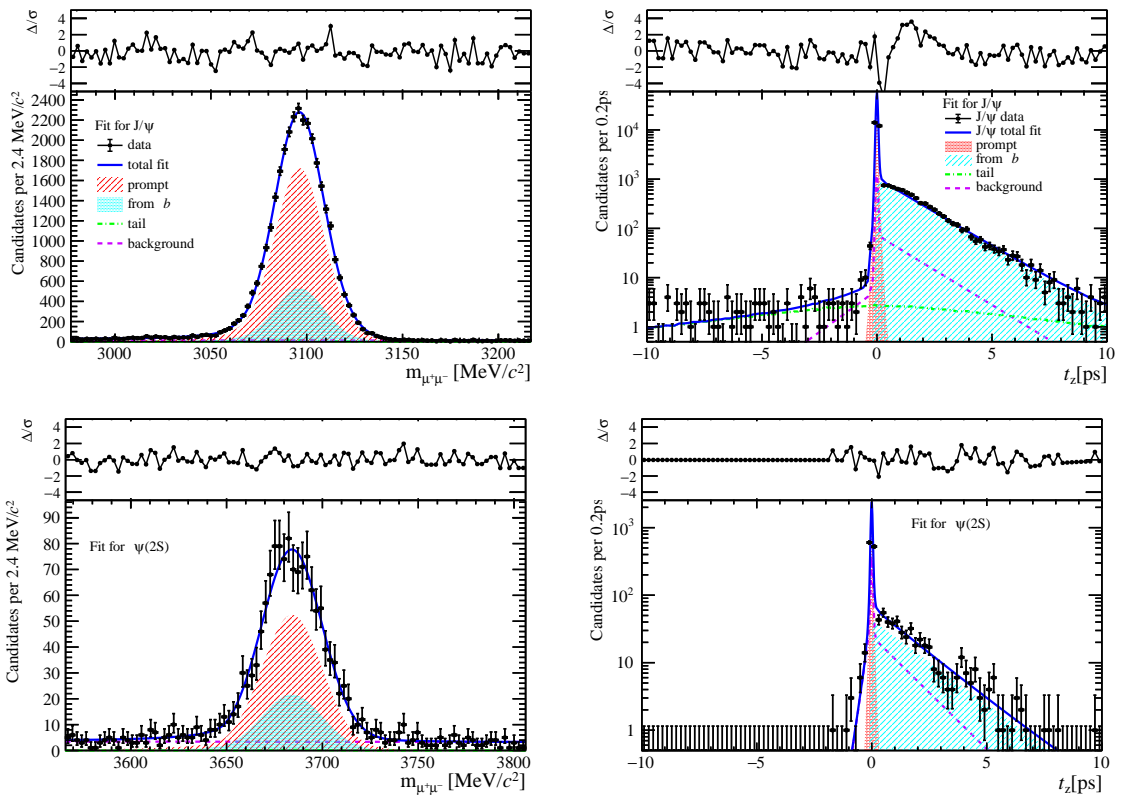


Figure 194: Fit results in  $6 \text{ GeV}/c < p_T < 8 \text{ GeV}/c$ ,  $2.8 < y < 3.5$  and  $0 \leq \text{nForwardTracks} < 12$ .

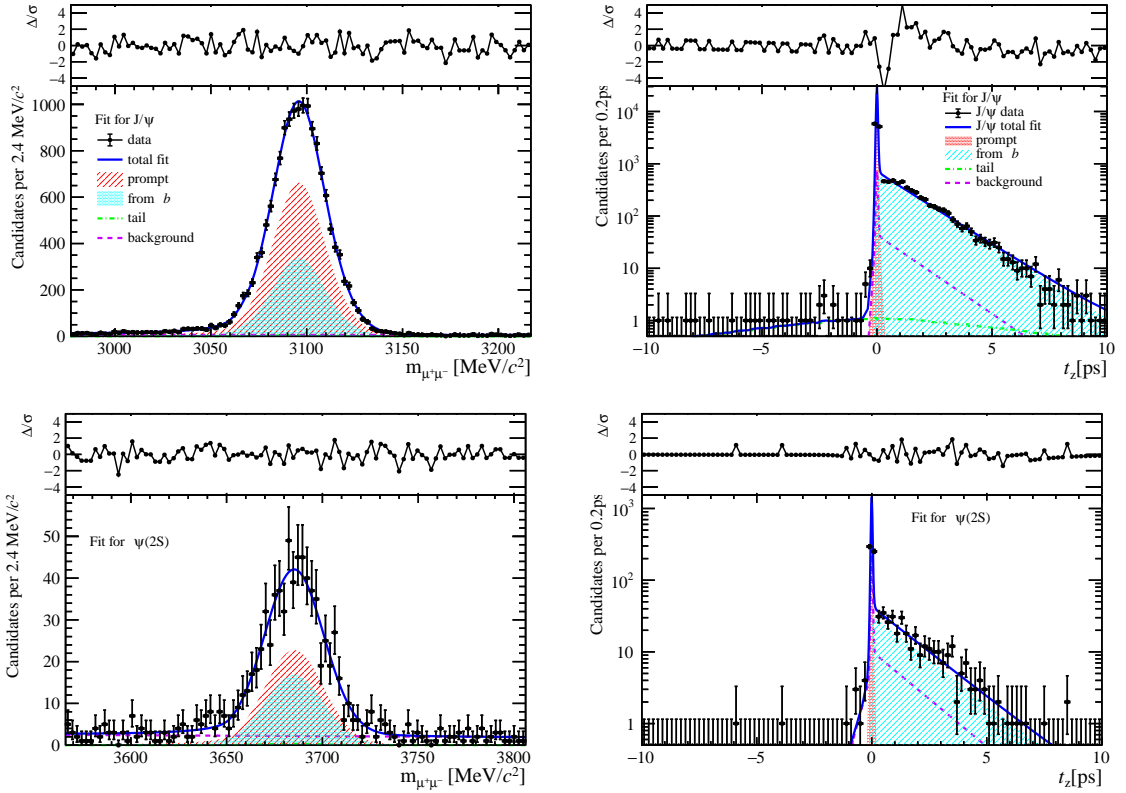


Figure 195: Fit results in  $8 \text{ GeV}/c < p_T < 20 \text{ GeV}/c$ ,  $2.8 < y < 3.5$  and  $0 \leq \text{nForwardTracks} < 12$ .

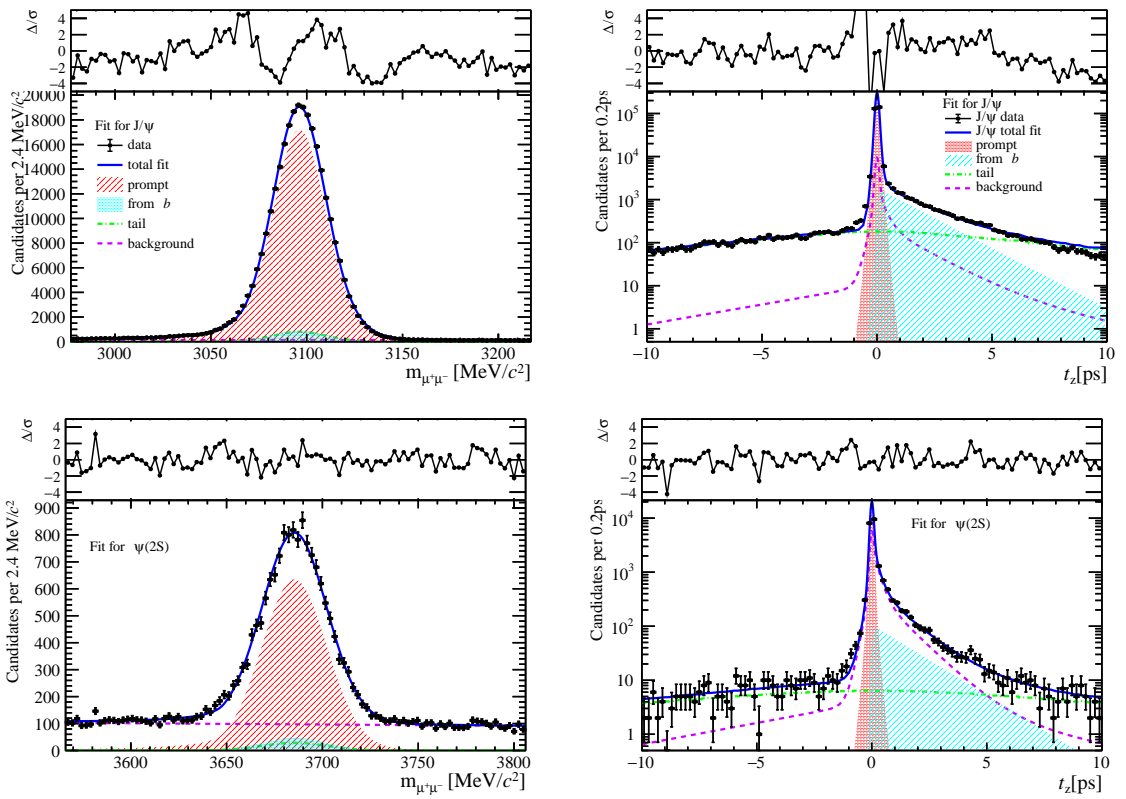


Figure 196: Fit results in  $0 \text{ GeV}/c < p_T < 2 \text{ GeV}/c$ ,  $3.5 < y < 4.5$  and  $0 \leq \text{nForwardTracks} < 12$ .

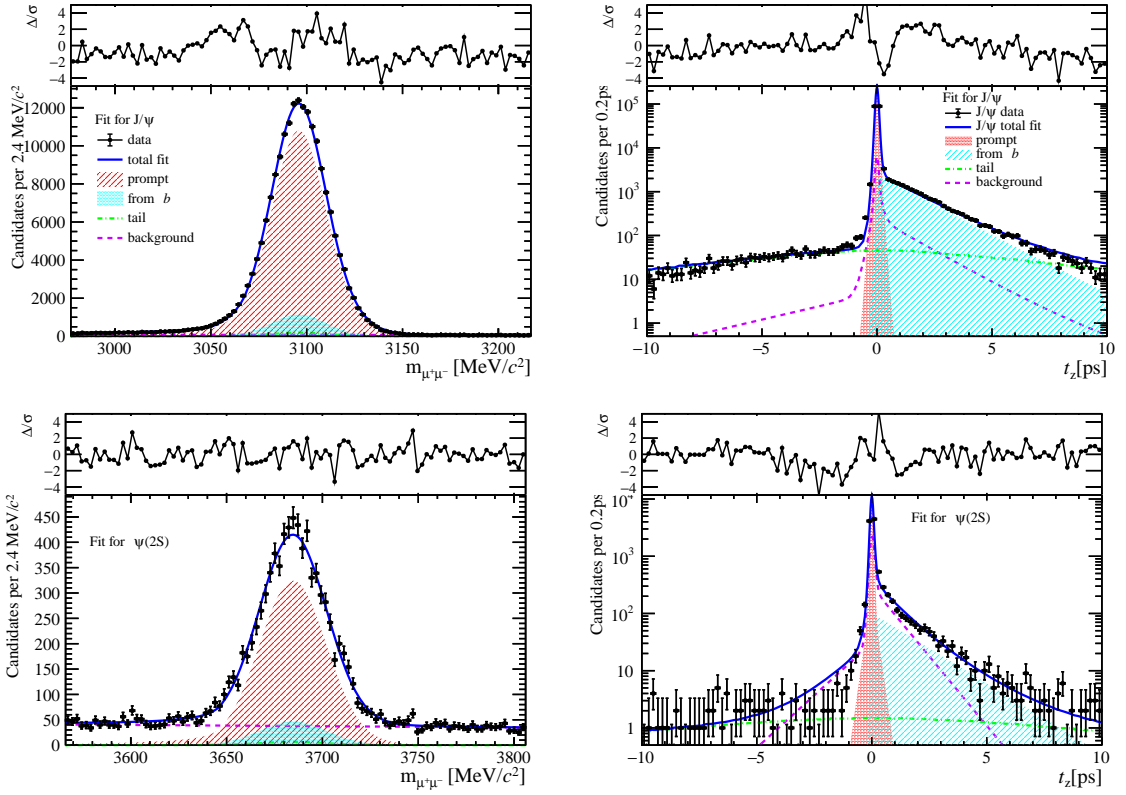


Figure 197: Fit results in  $2 \text{ GeV}/c < p_T < 4 \text{ GeV}/c$ ,  $3.5 < y < 4.5$  and  $0 \leq \text{nForwardTracks} < 12$ .

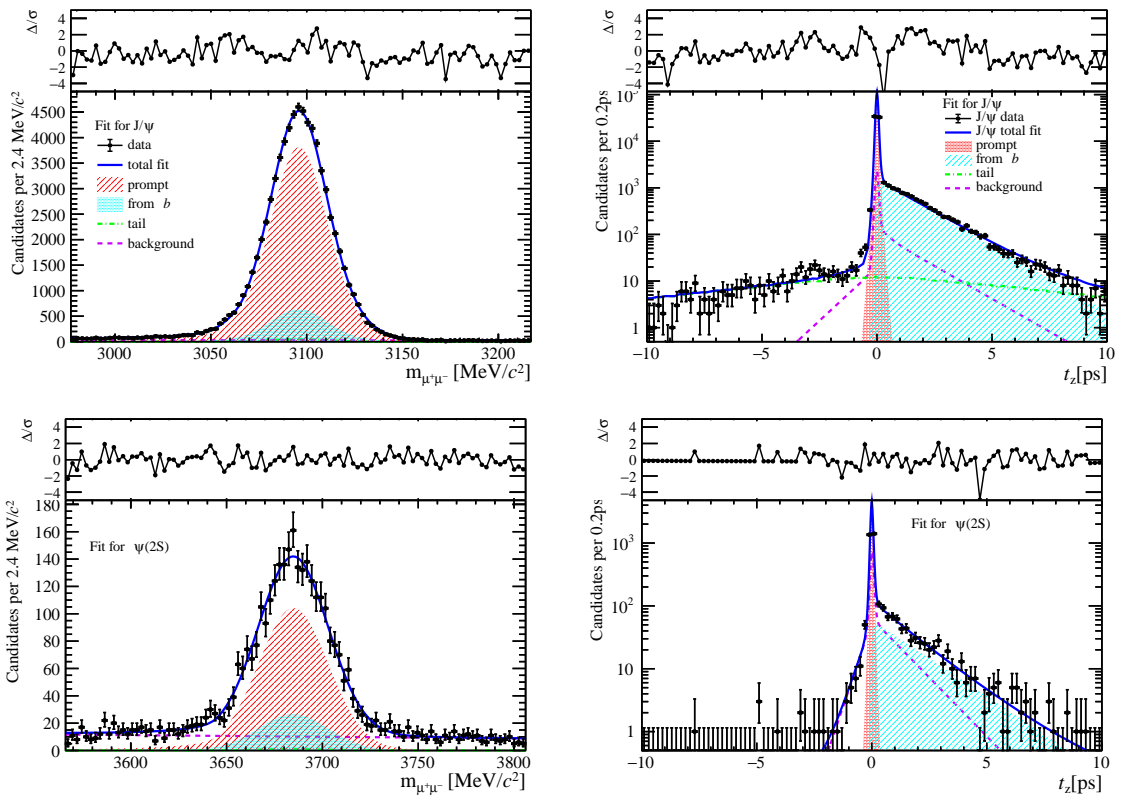


Figure 198: Fit results in  $4 \text{ GeV}/c < p_T < 6 \text{ GeV}/c$ ,  $3.5 < y < 4.5$  and  $0 \leq \text{nForwardTracks} < 12$ .

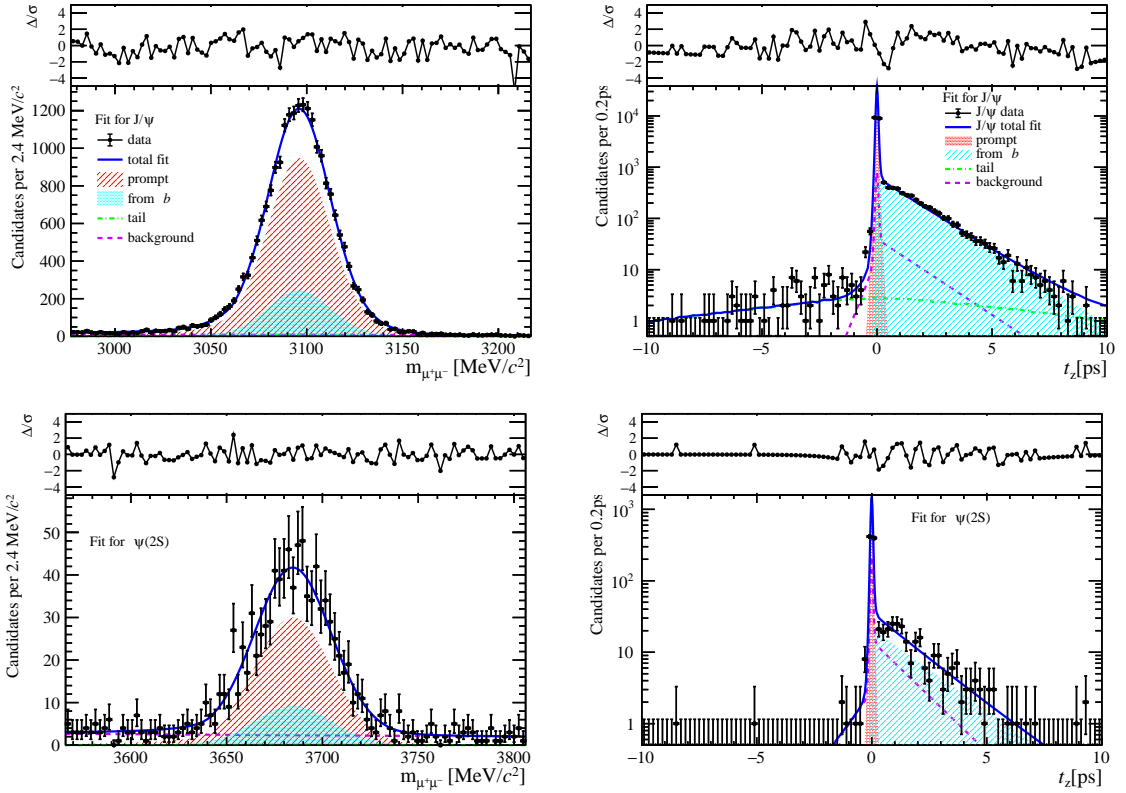


Figure 199: Fit results in  $6 \text{ GeV}/c < p_T < 8 \text{ GeV}/c$ ,  $3.5 < y < 4.5$  and  $0 \leq \text{nForwardTracks} < 12$ .

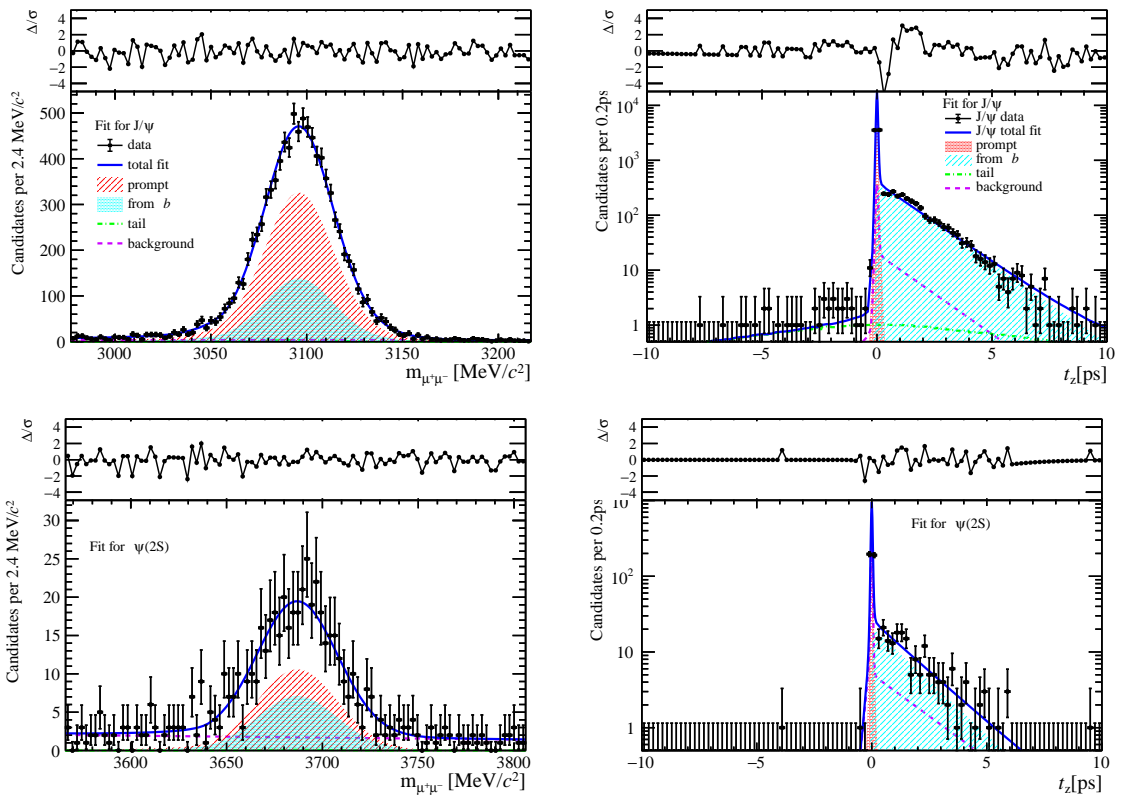


Figure 200: Fit results in  $8 \text{ GeV}/c < p_T < 20 \text{ GeV}/c$ ,  $3.5 < y < 4.5$  and  $0 \leq \text{nForwardTracks} < 12$ .

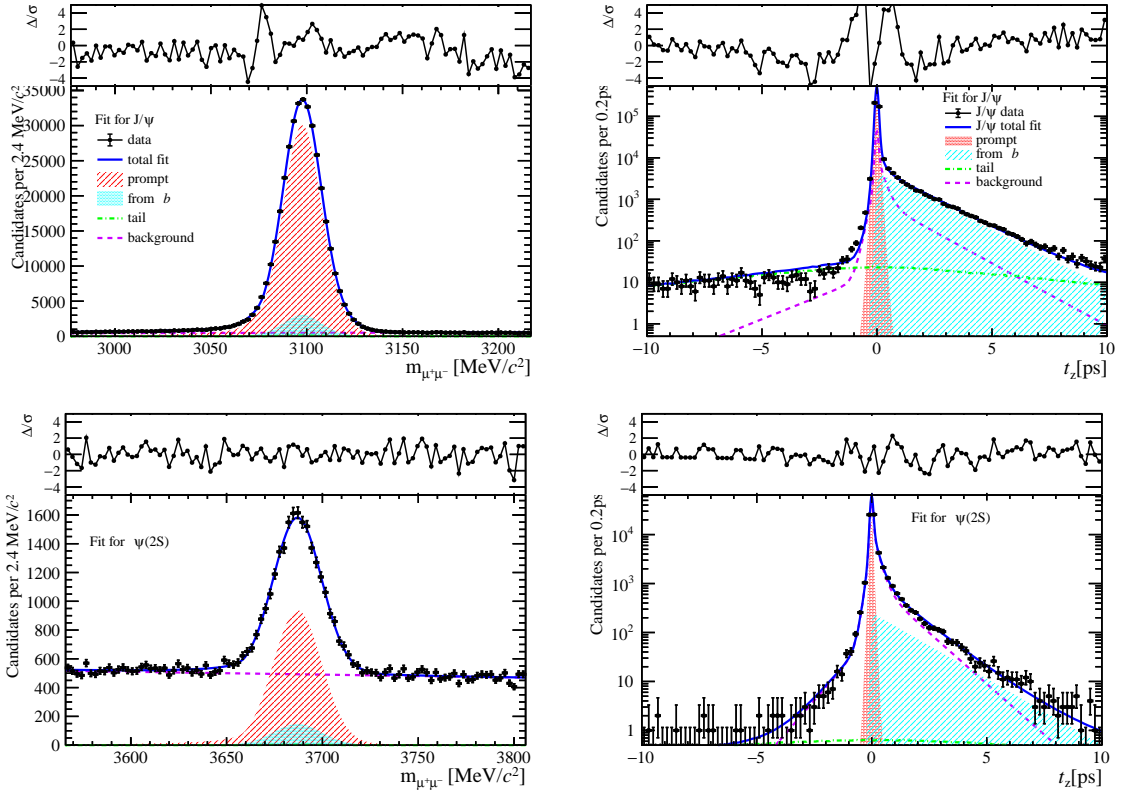


Figure 201: Fit results in  $0 \text{ GeV}/c < p_T < 2 \text{ GeV}/c$ ,  $2.0 < y < 2.8$  and  $12 \leq \text{nForwardTracks} < 24$ .

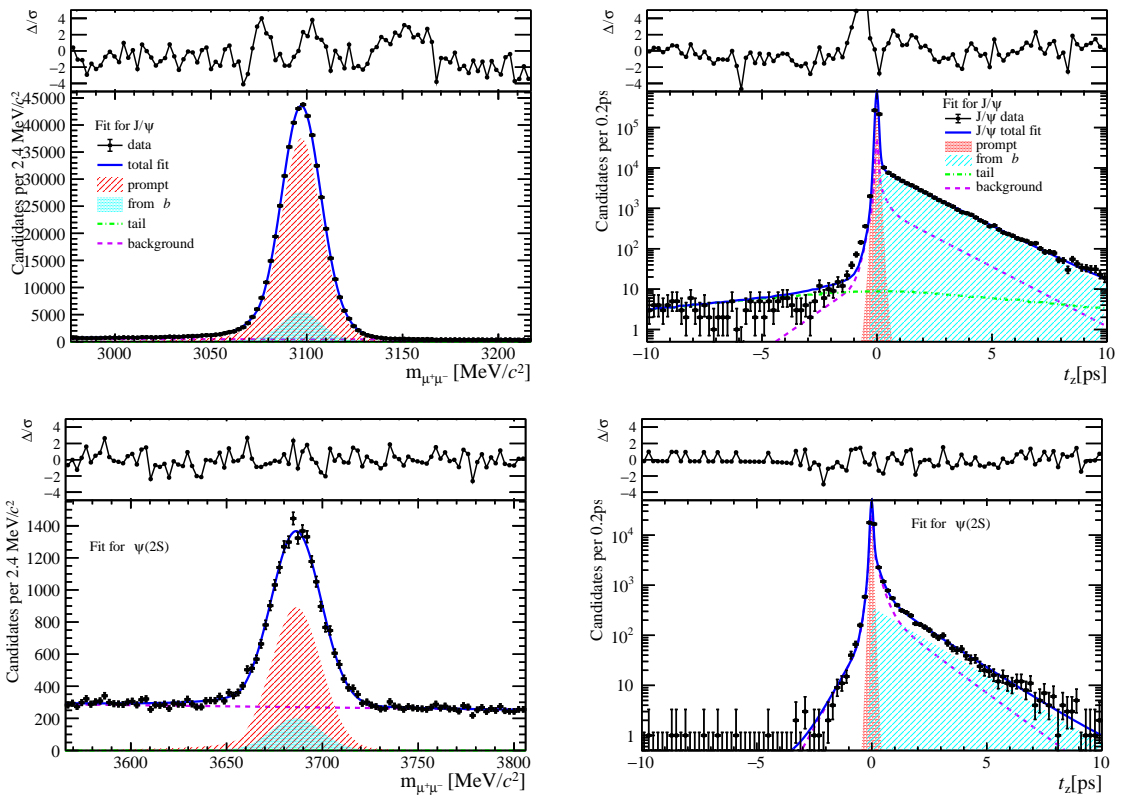


Figure 202: Fit results in  $2 \text{ GeV}/c < p_T < 4 \text{ GeV}/c$ ,  $2.0 < y < 2.8$  and  $12 \leq \text{nForwardTracks} < 24$ .

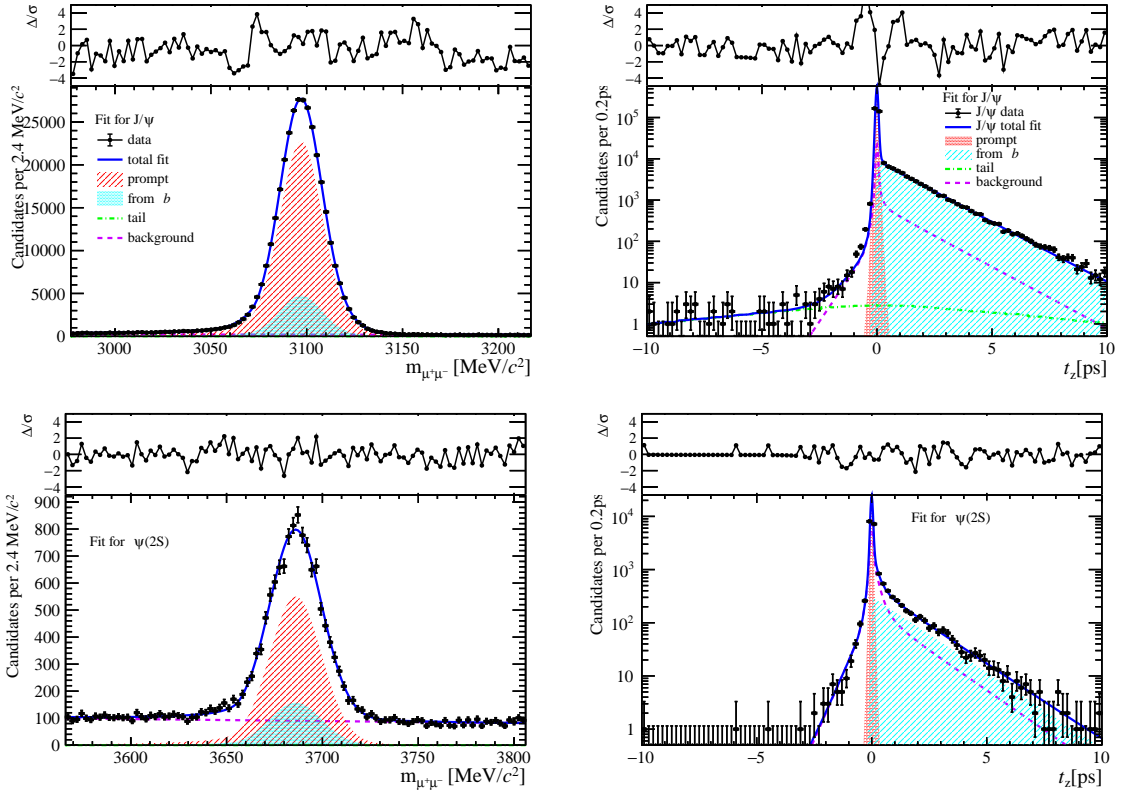


Figure 203: Fit results in  $4 \text{ GeV}/c < p_T < 6 \text{ GeV}/c$ ,  $2.0 < y < 2.8$  and  $12 \leq \text{nForwardTracks} < 24$ .

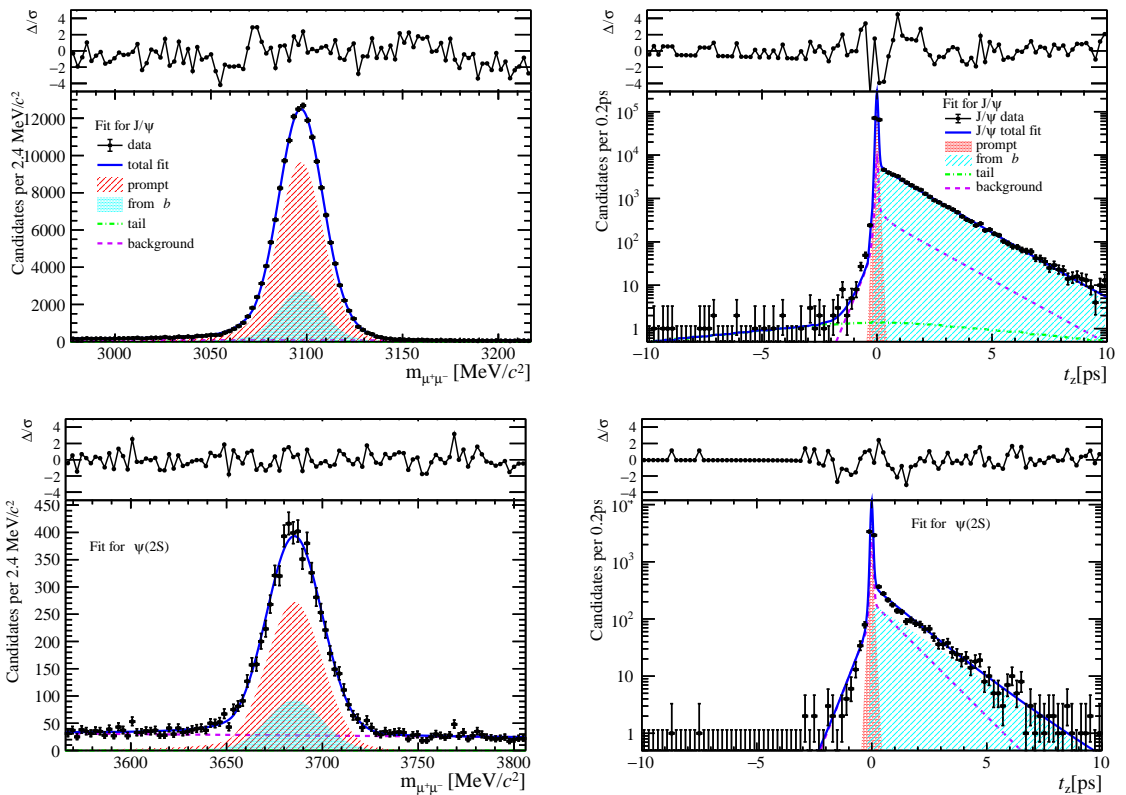


Figure 204: Fit results in  $6 \text{ GeV}/c < p_T < 8 \text{ GeV}/c$ ,  $2.0 < y < 2.8$  and  $12 \leq \text{nForwardTracks} < 24$ .

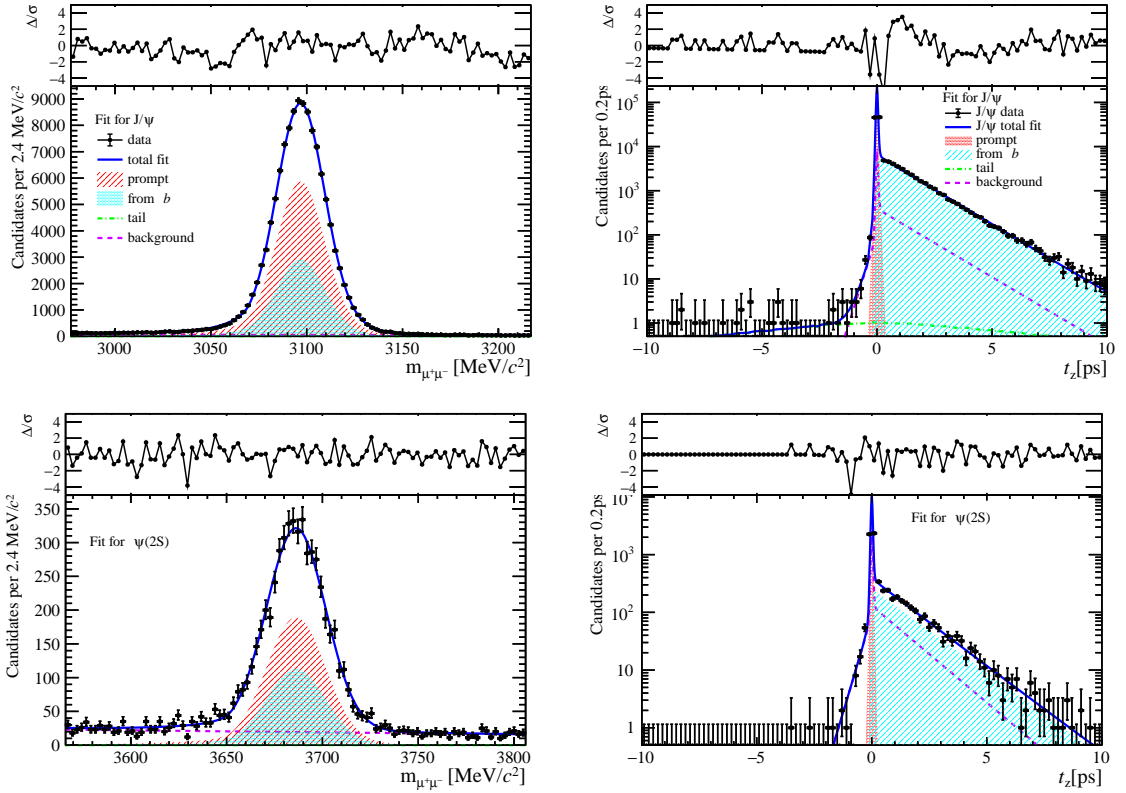


Figure 205: Fit results in  $8 \text{ GeV}/c < p_T < 20 \text{ GeV}/c$ ,  $2.0 < y < 2.8$  and  $12 \leq \text{nForwardTracks} < 24$ .

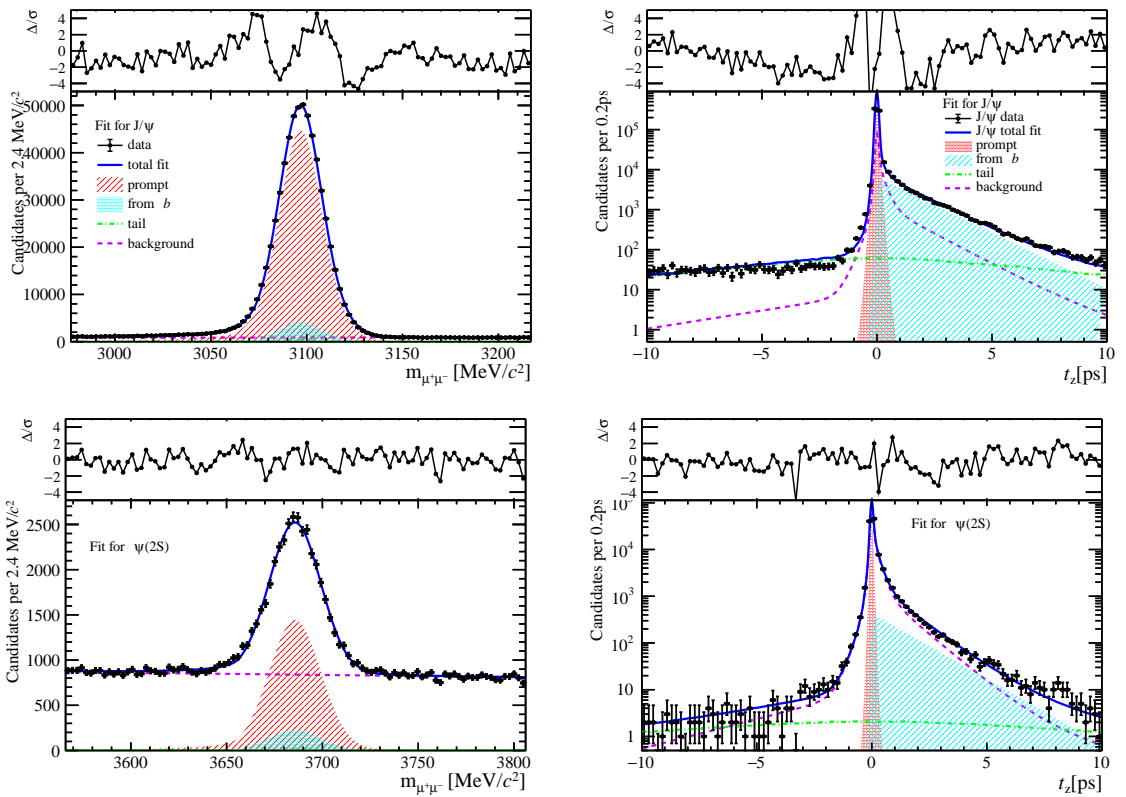


Figure 206: Fit results in  $0 \text{ GeV}/c < p_T < 2 \text{ GeV}/c$ ,  $2.8 < y < 3.5$  and  $12 \leq \text{nForwardTracks} < 24$ .

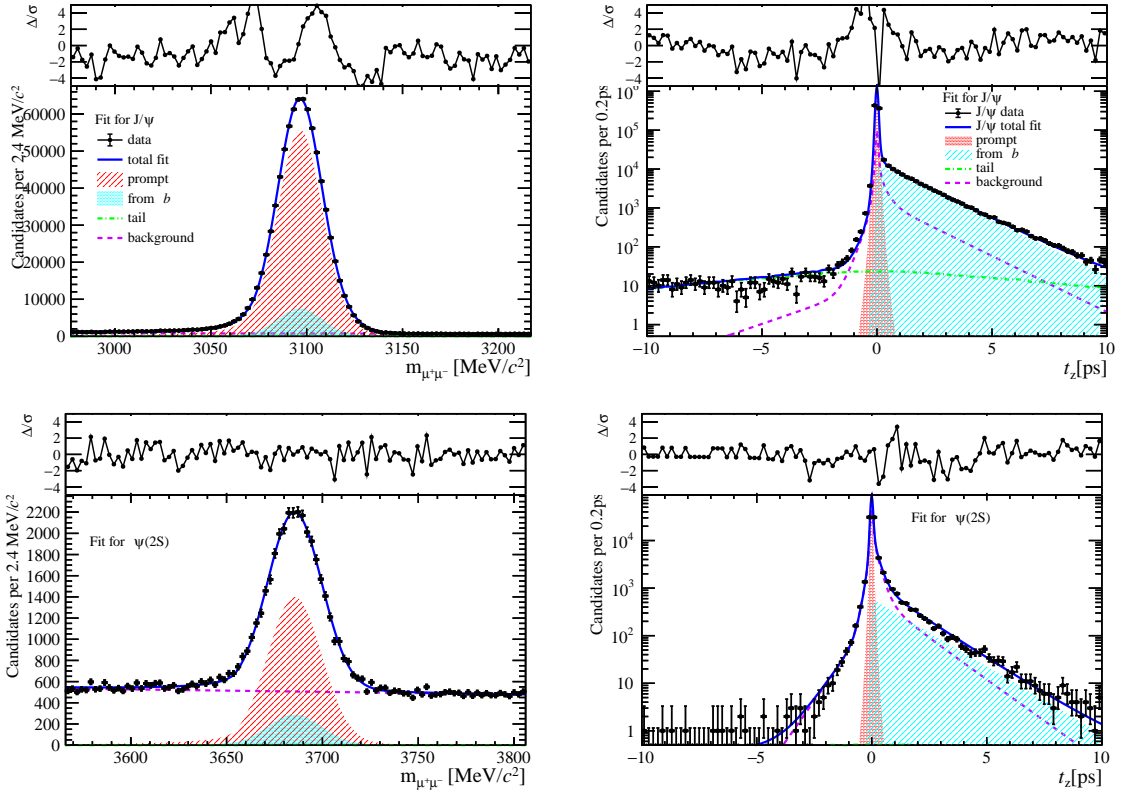


Figure 207: Fit results in  $2 \text{ GeV}/c < p_T < 4 \text{ GeV}/c$ ,  $2.8 < y < 3.5$  and  $12 \leq \text{nForwardTracks} < 24$ .

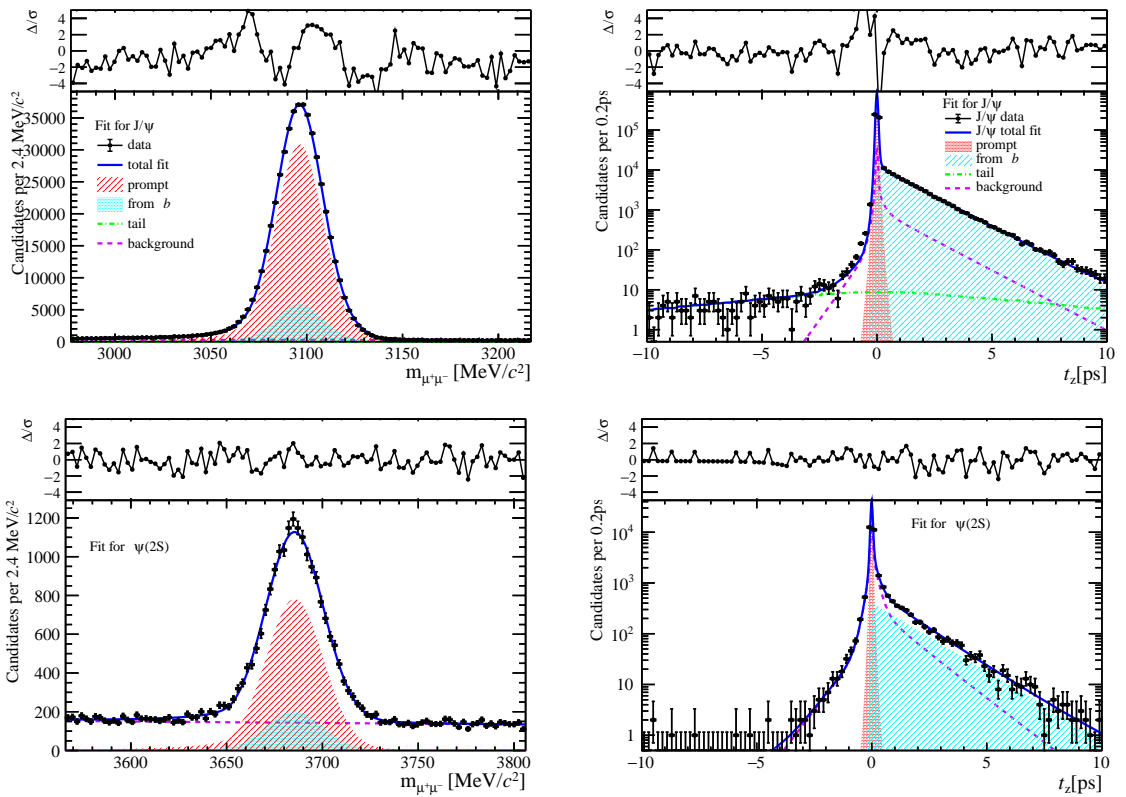


Figure 208: Fit results in  $4 \text{ GeV}/c < p_T < 6 \text{ GeV}/c$ ,  $2.8 < y < 3.5$  and  $12 \leq \text{nForwardTracks} < 24$ .

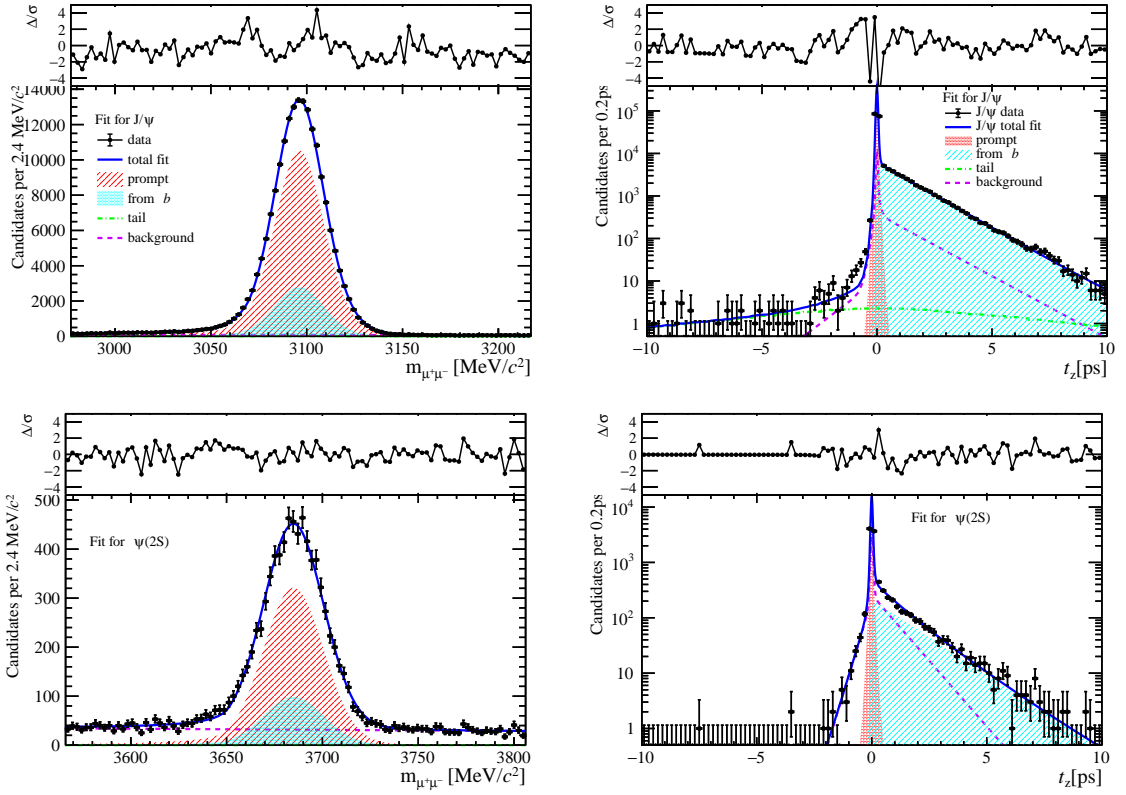


Figure 209: Fit results in  $6 \text{ GeV}/c < p_T < 8 \text{ GeV}/c$ ,  $2.8 < y < 3.5$  and  $12 \leq \text{nForwardTracks} < 24$ .

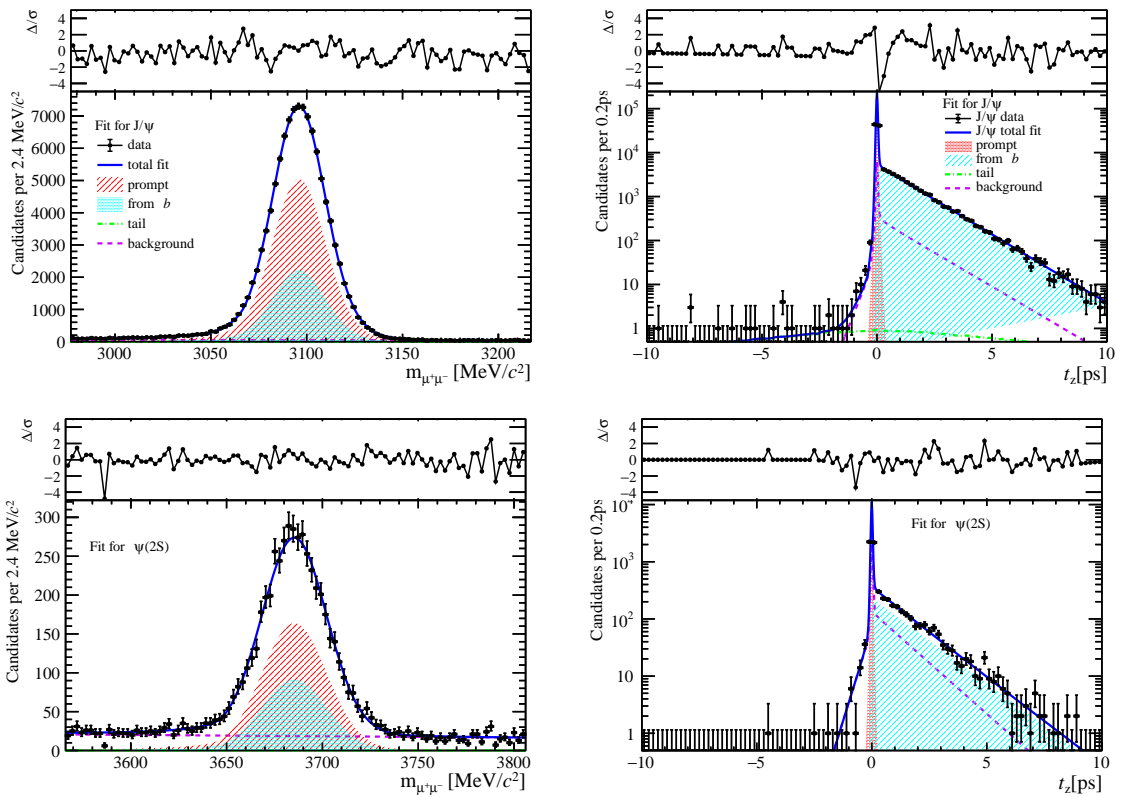


Figure 210: Fit results in  $8 \text{ GeV}/c < p_T < 20 \text{ GeV}/c$ ,  $2.8 < y < 3.5$  and  $12 \leq \text{nForwardTracks} < 24$ .

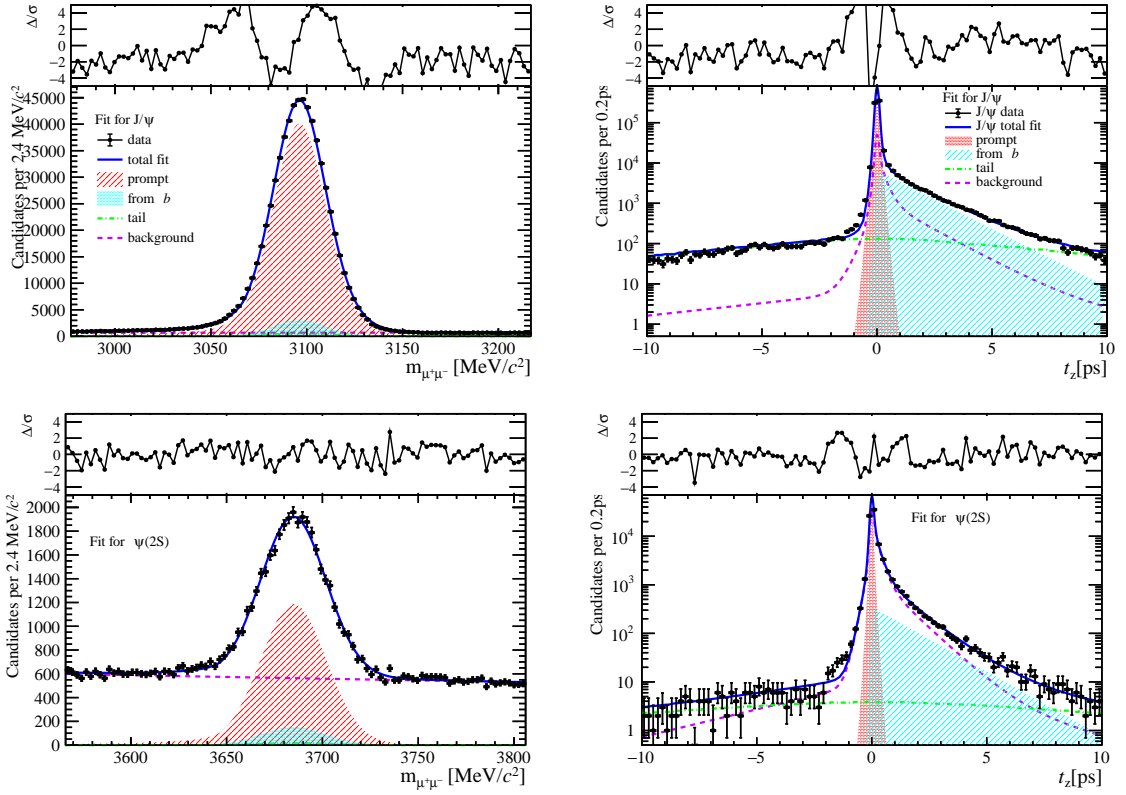


Figure 211: Fit results in  $0 \text{ GeV}/c < p_T < 2 \text{ GeV}/c$ ,  $3.5 < y < 4.5$  and  $12 \leq \text{nForwardTracks} < 24$ .

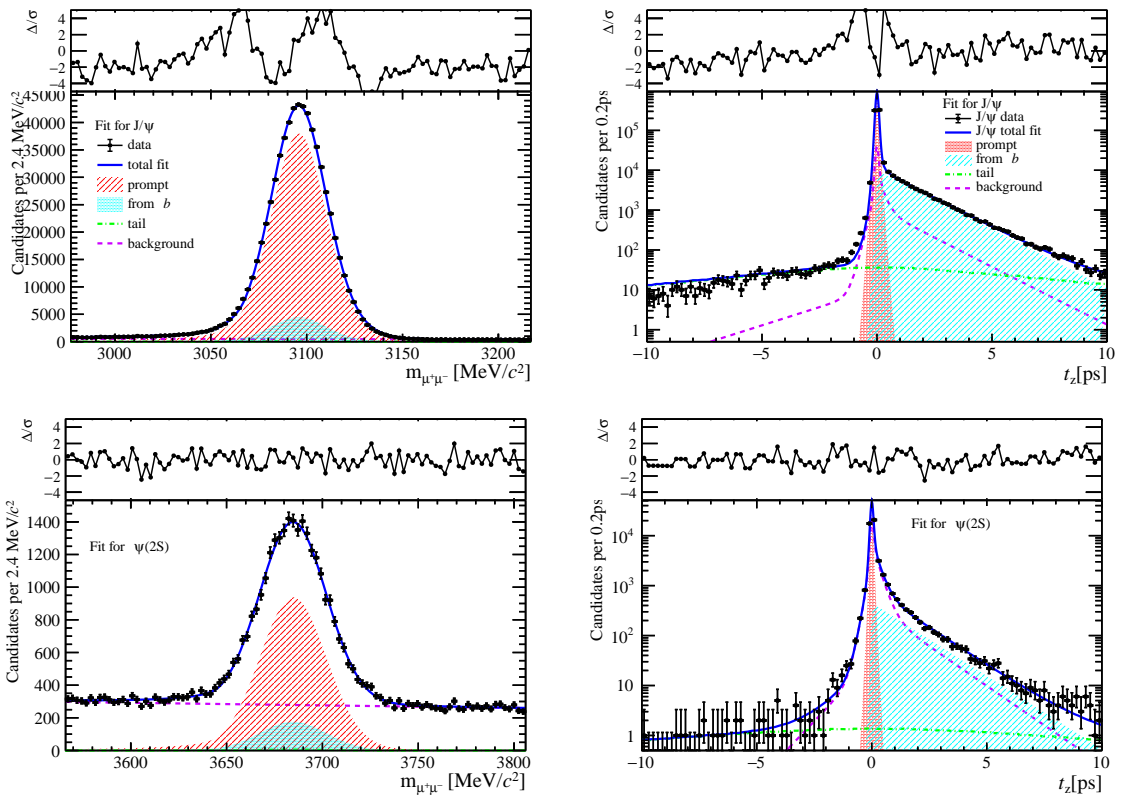


Figure 212: Fit results in  $2 \text{ GeV}/c < p_T < 4 \text{ GeV}/c$ ,  $3.5 < y < 4.5$  and  $12 \leq \text{nForwardTracks} < 24$ .

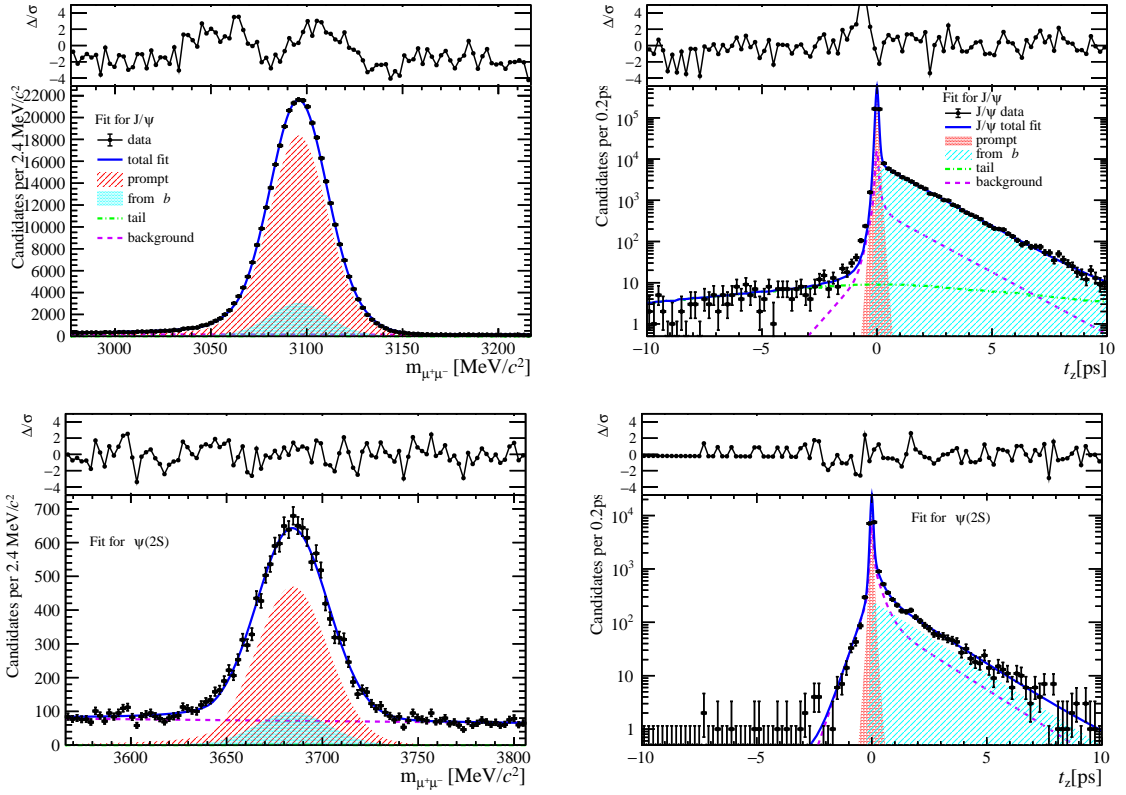


Figure 213: Fit results in  $4 \text{ GeV}/c < p_T < 6 \text{ GeV}/c$ ,  $3.5 < y < 4.5$  and  $12 \leq \text{nForwardTracks} < 24$ .

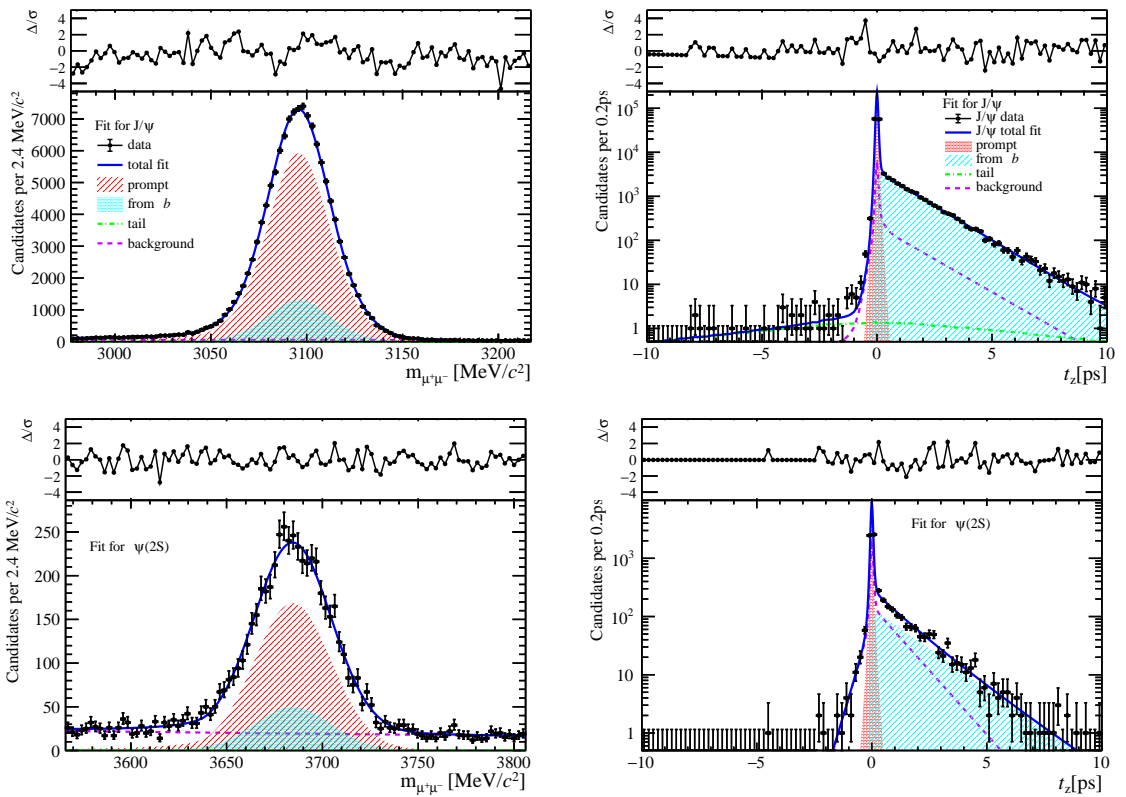


Figure 214: Fit results in  $6 \text{ GeV}/c < p_T < 8 \text{ GeV}/c$ ,  $3.5 < y < 4.5$  and  $12 \leq \text{nForwardTracks} < 24$ .

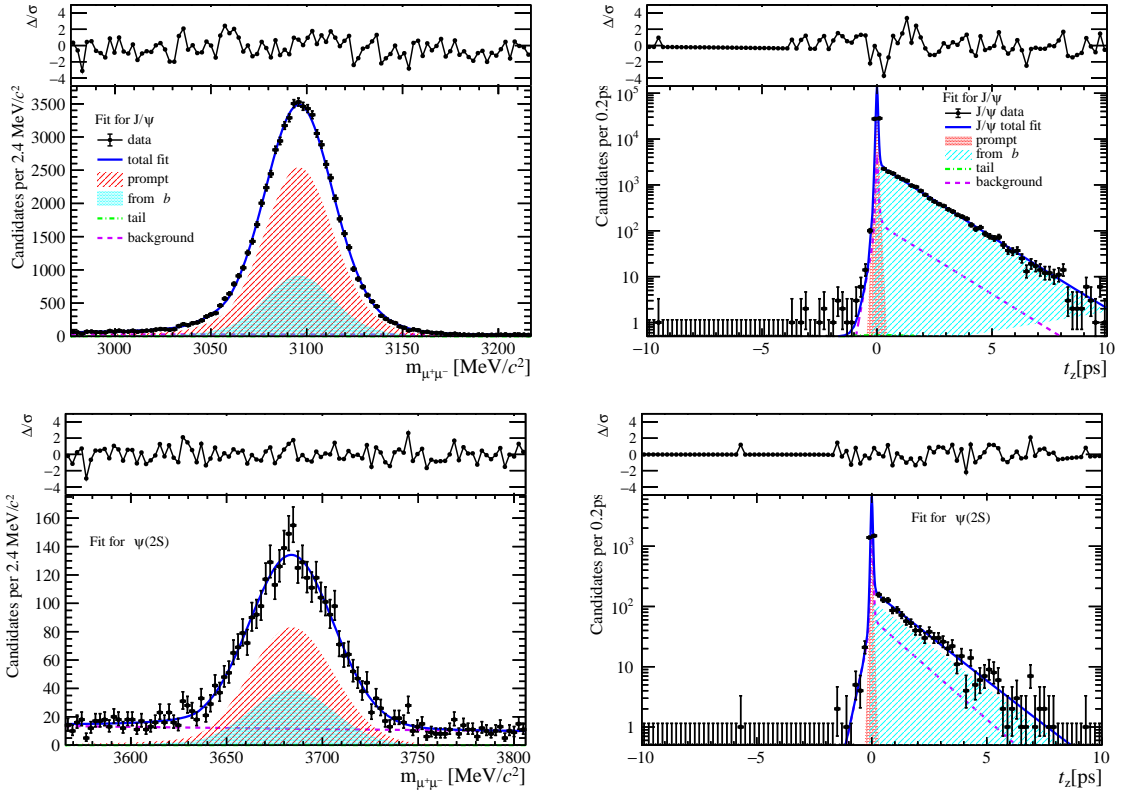


Figure 215: Fit results in  $8 \text{ GeV}/c < p_T < 20 \text{ GeV}/c$ ,  $3.5 < y < 4.5$  and  $12 \leq \text{nForwardTracks} < 24$ .

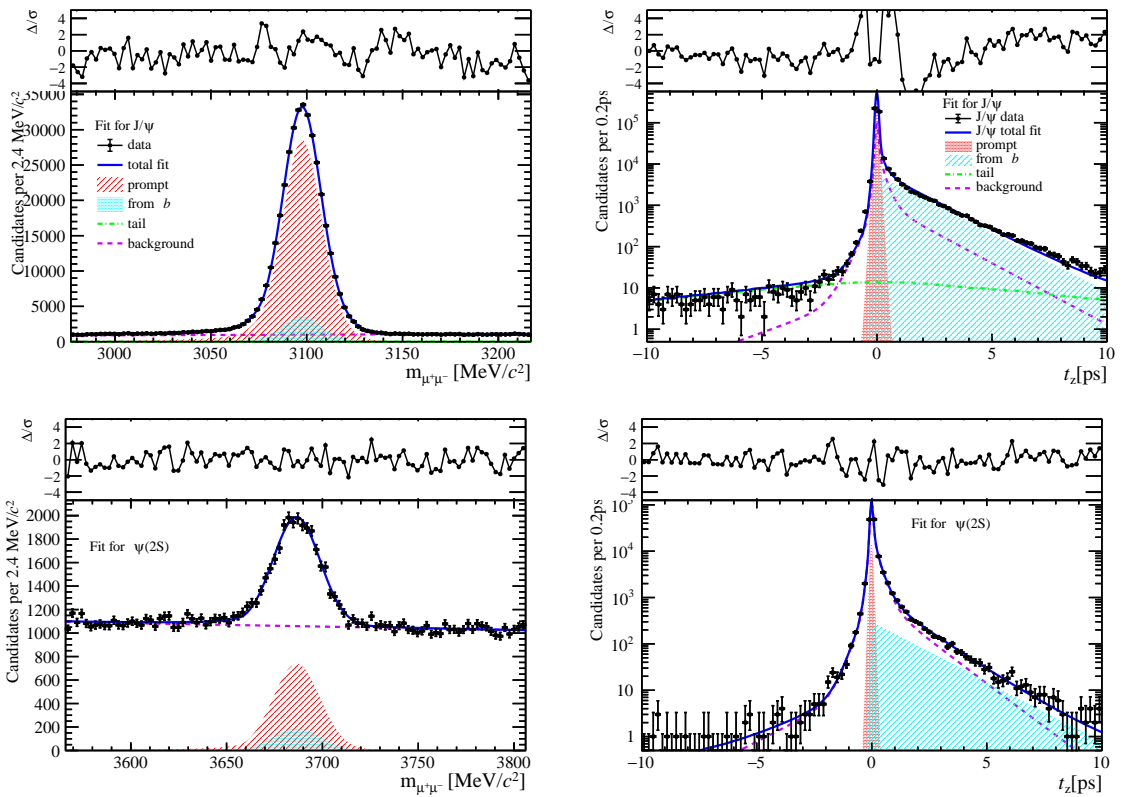


Figure 216: Fit results in  $0 \text{ GeV}/c < p_T < 2 \text{ GeV}/c$ ,  $2.0 < y < 2.8$  and  $24 \leq \text{nForwardTracks} < 36$ .

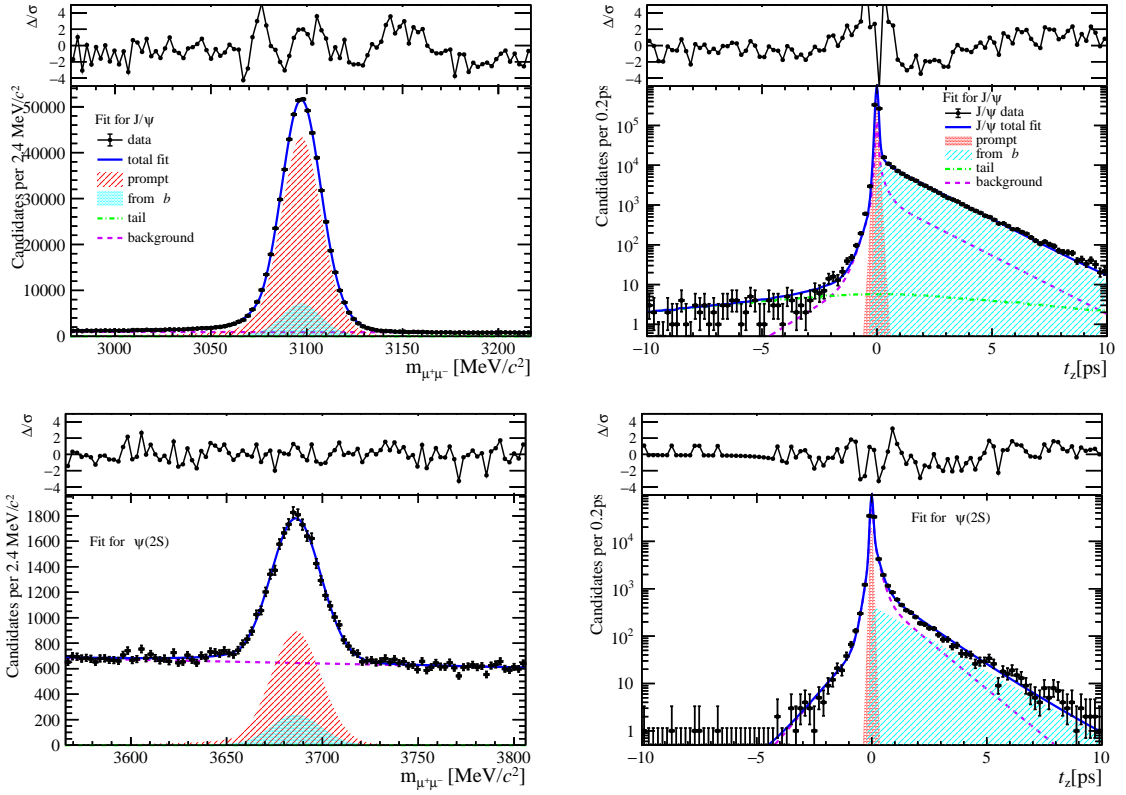


Figure 217: Fit results in  $2 \text{ GeV}/c < p_T < 4 \text{ GeV}/c$ ,  $2.0 < y < 2.8$  and  $24 \leq \text{nForwardTracks} < 36$ .

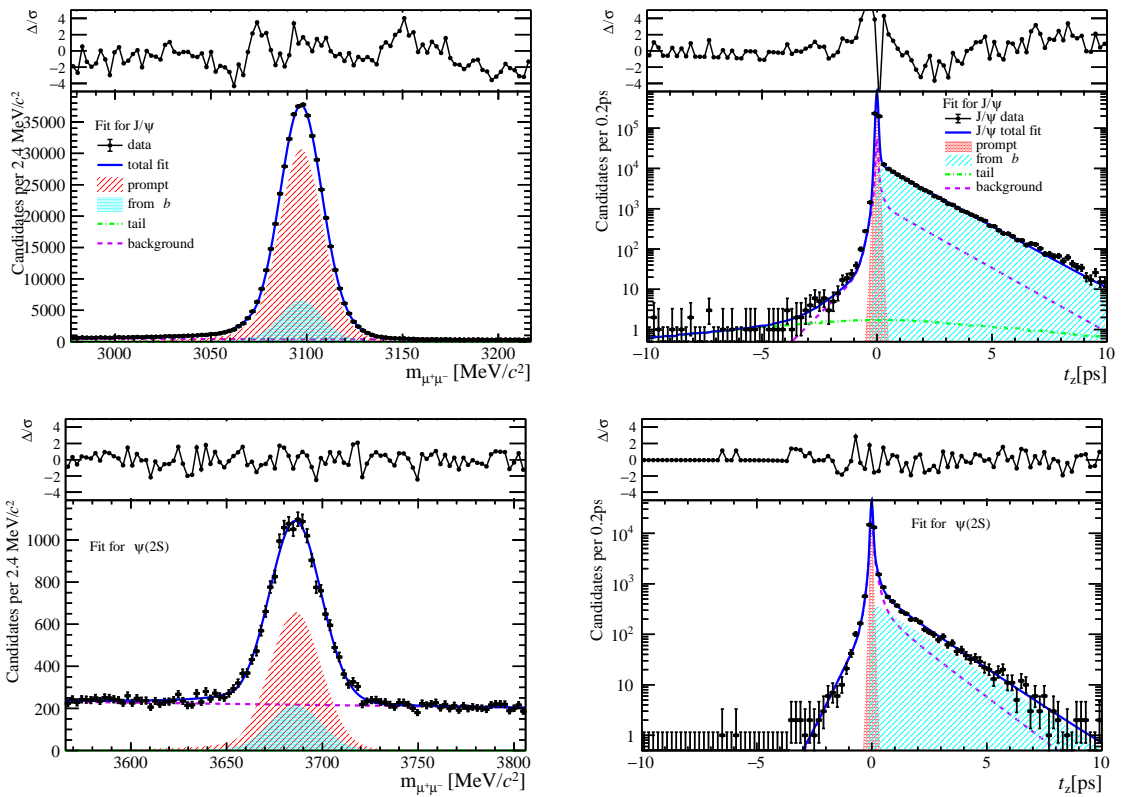


Figure 218: Fit results in  $4 \text{ GeV}/c < p_T < 6 \text{ GeV}/c$ ,  $2.0 < y < 2.8$  and  $24 \leq \text{nForwardTracks} < 36$ .

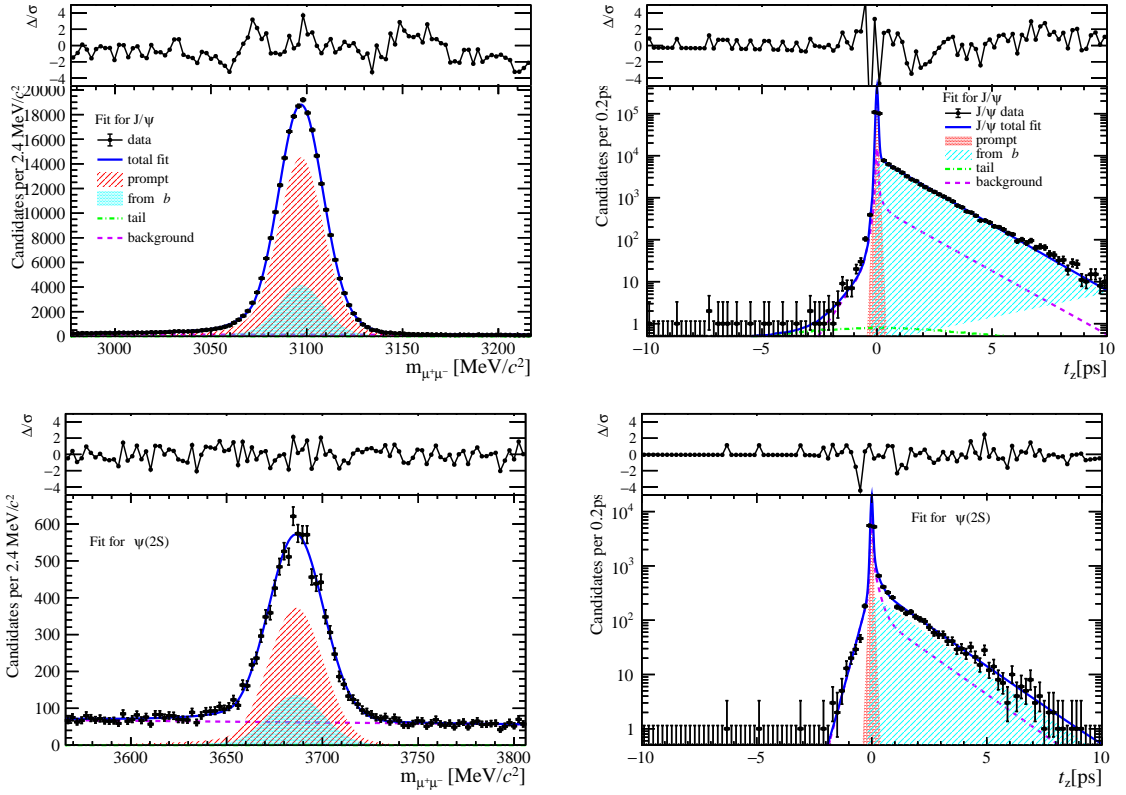


Figure 219: Fit results in  $6 \text{ GeV}/c < p_T < 8 \text{ GeV}/c$ ,  $2.0 < y < 2.8$  and  $24 \leq \text{nForwardTracks} < 36$ .

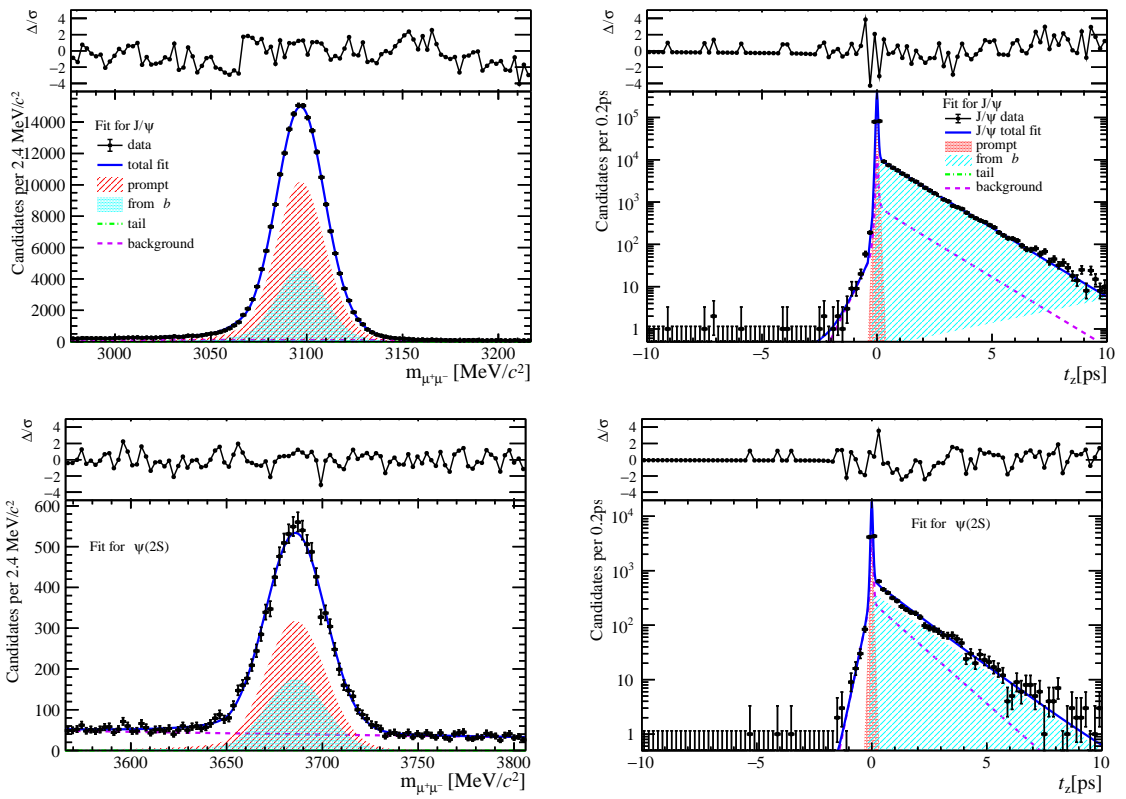


Figure 220: Fit results in  $8 \text{ GeV}/c < p_T < 20 \text{ GeV}/c$ ,  $2.0 < y < 2.8$  and  $24 \leq \text{nForwardTracks} < 36$ .

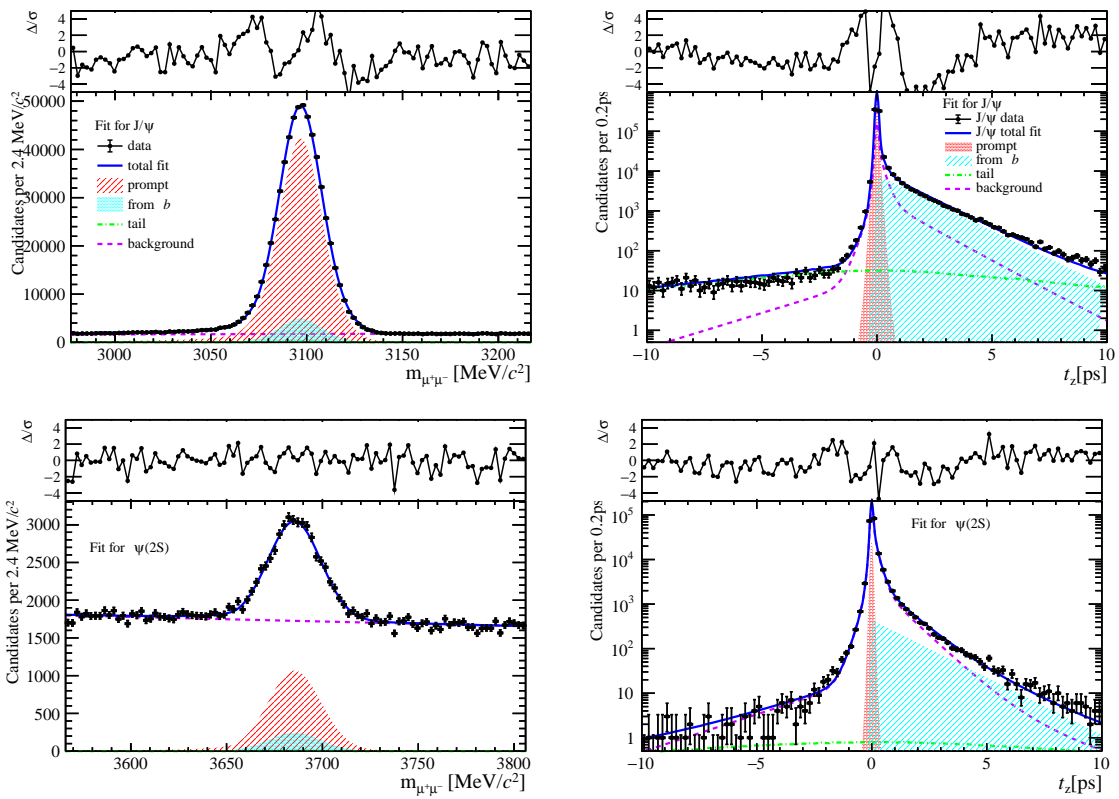


Figure 221: Fit results in  $0 \text{ GeV}/c < p_T < 2 \text{ GeV}/c$ ,  $2.8 < y < 3.5$  and  $24 \leq \text{nForwardTracks} < 36$ .

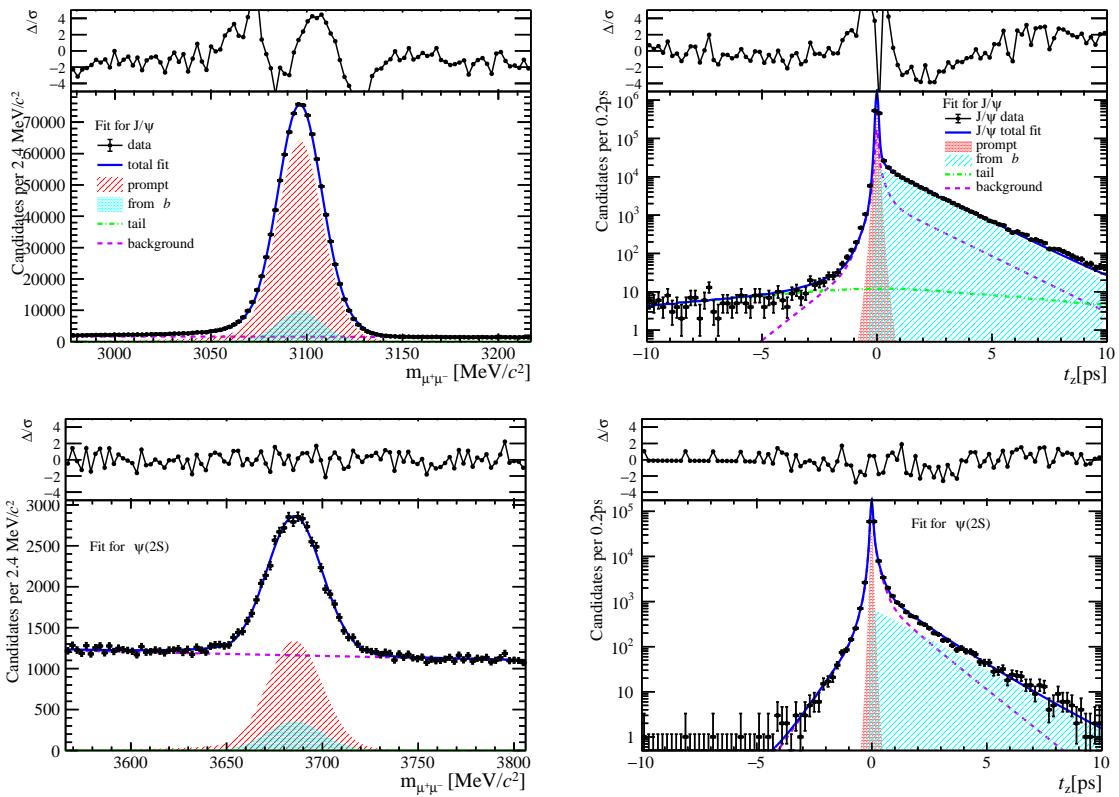


Figure 222: Fit results in  $2 \text{ GeV}/c < p_T < 4 \text{ GeV}/c$ ,  $2.8 < y < 3.5$  and  $24 \leq \text{nForwardTracks} < 36$ .

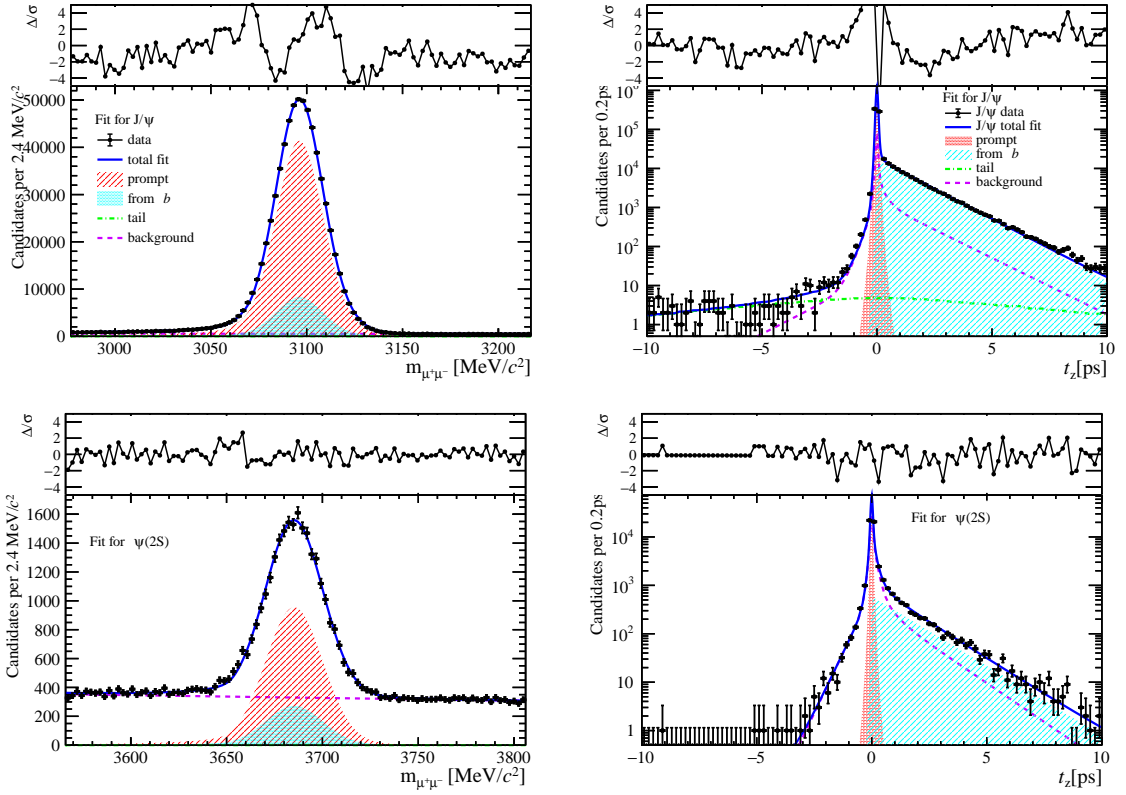


Figure 223: Fit results in  $4 \text{ GeV}/c < p_T < 6 \text{ GeV}/c$ ,  $2.8 < y < 3.5$  and  $24 \leq \text{nForwardTracks} < 36$ .

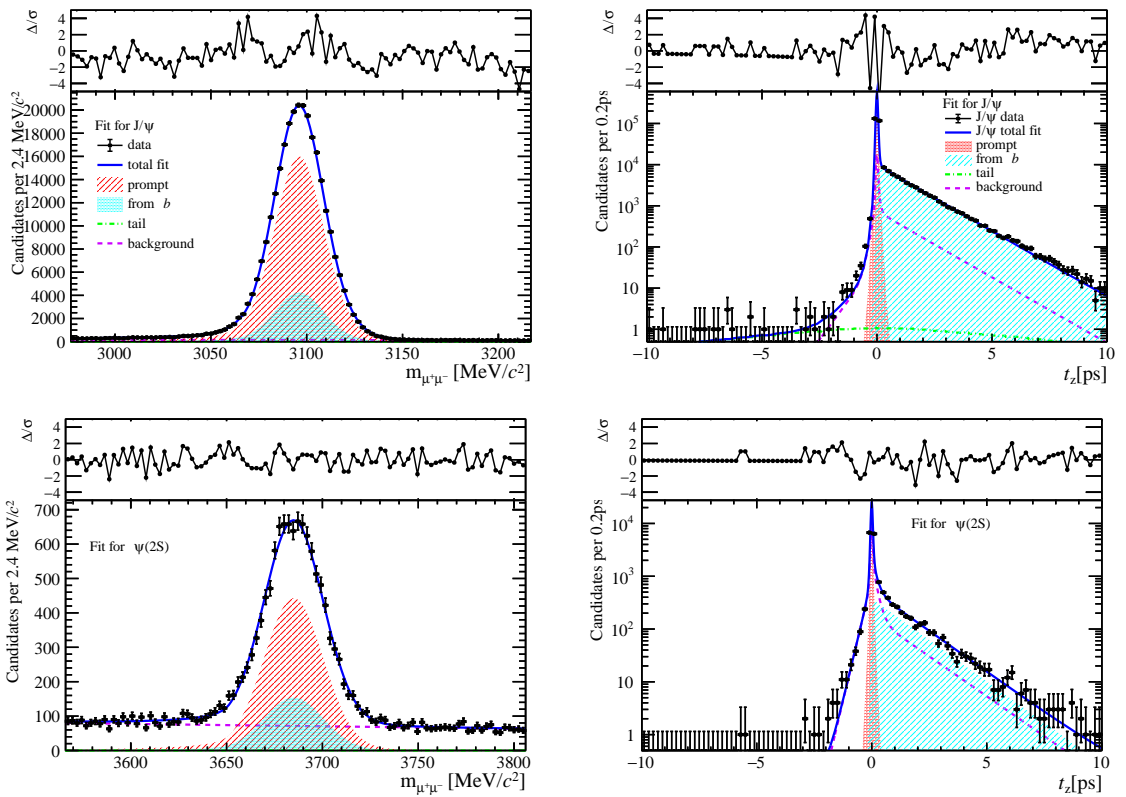


Figure 224: Fit results in  $6 \text{ GeV}/c < p_T < 8 \text{ GeV}/c$ ,  $2.8 < y < 3.5$  and  $24 \leq \text{nForwardTracks} < 36$ .

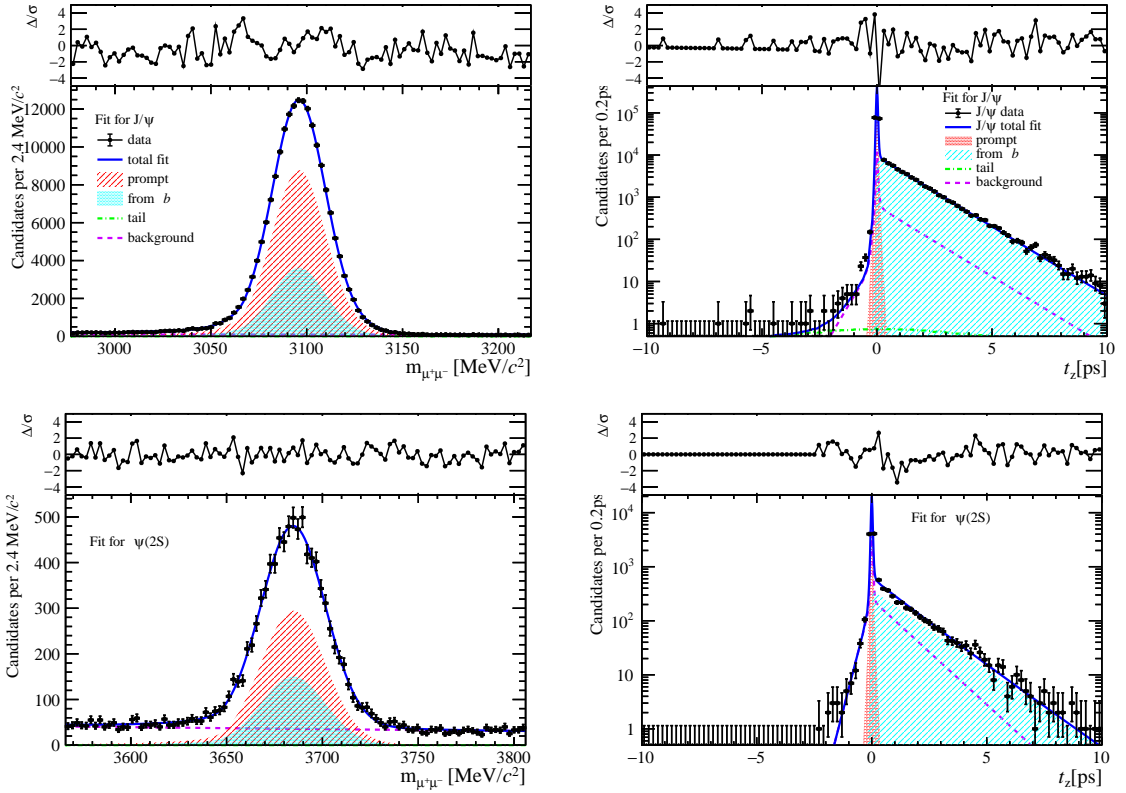


Figure 225: Fit results in  $8 \text{ GeV}/c < p_T < 20 \text{ GeV}/c$ ,  $2.8 < y < 3.5$  and  $24 \leq \text{nForwardTracks} < 36$ .

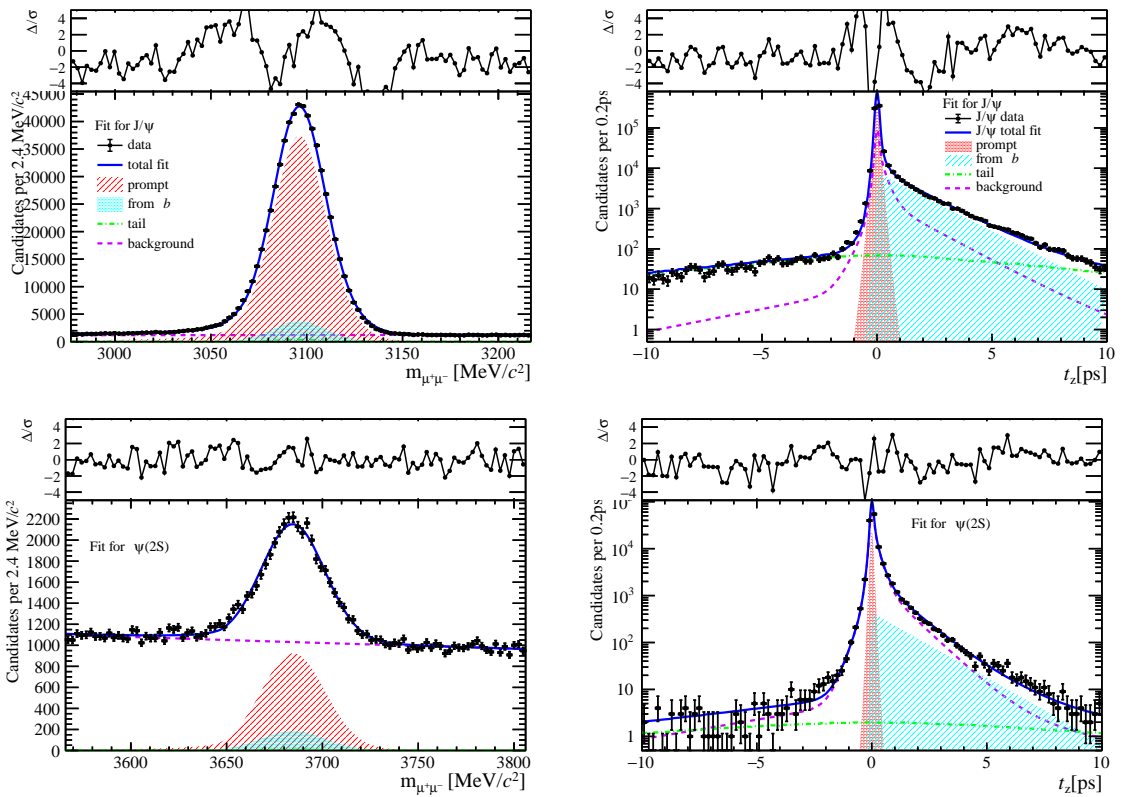


Figure 226: Fit results in  $0 \text{ GeV}/c < p_T < 2 \text{ GeV}/c$ ,  $3.5 < y < 4.5$  and  $24 \leq \text{nForwardTracks} < 36$ .

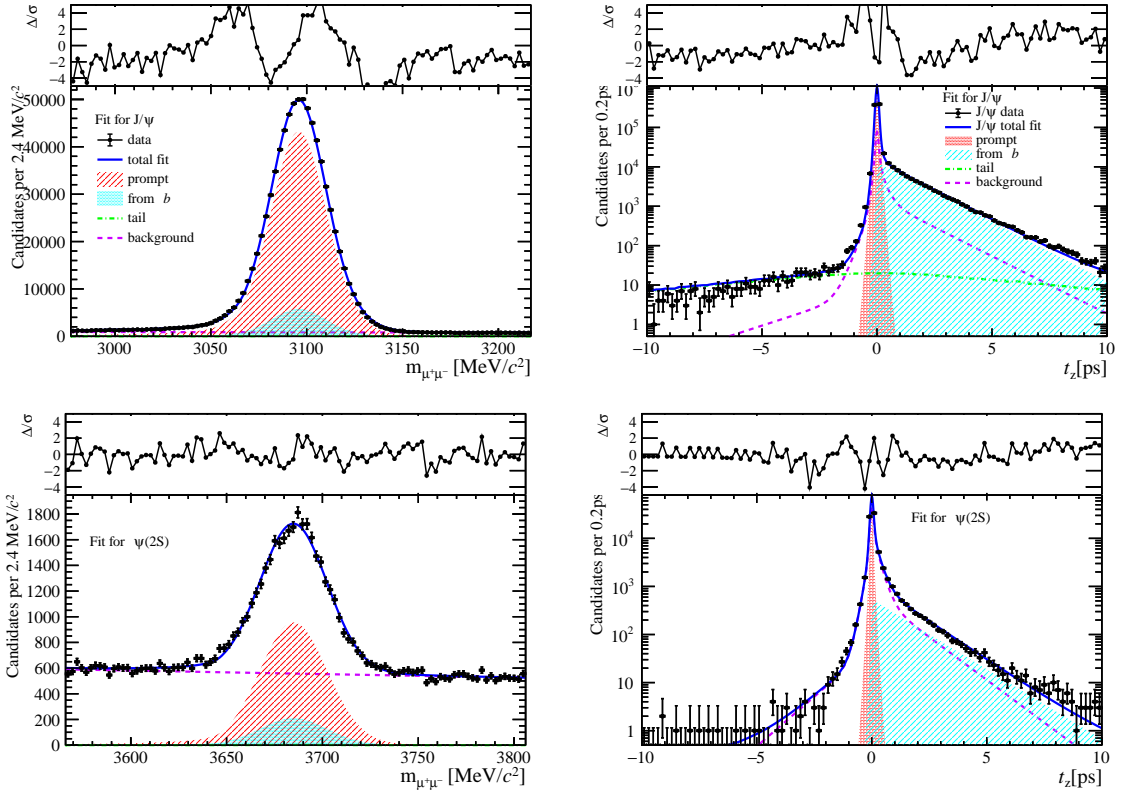


Figure 227: Fit results in  $2 \text{ GeV}/c < p_T < 4 \text{ GeV}/c$ ,  $3.5 < y < 4.5$  and  $24 \leq \text{nForwardTracks} < 36$ .

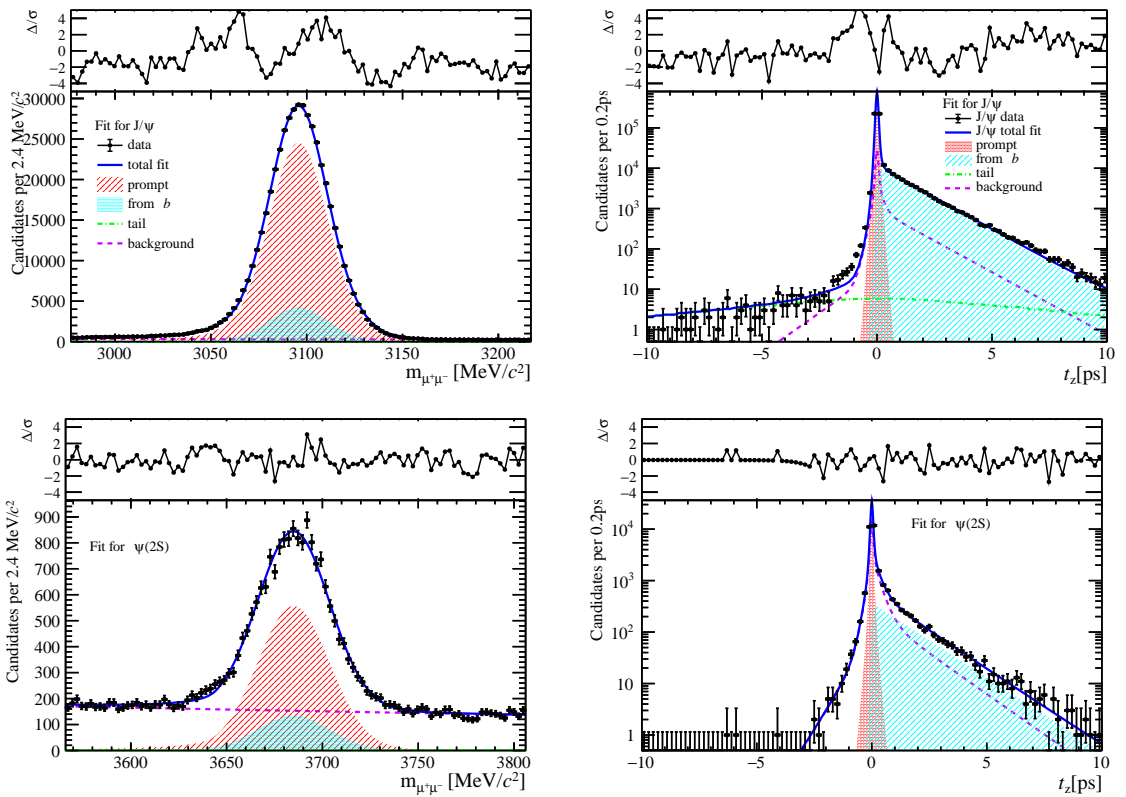


Figure 228: Fit results in  $4 \text{ GeV}/c < p_T < 6 \text{ GeV}/c$ ,  $3.5 < y < 4.5$  and  $24 \leq \text{nForwardTracks} < 36$ .

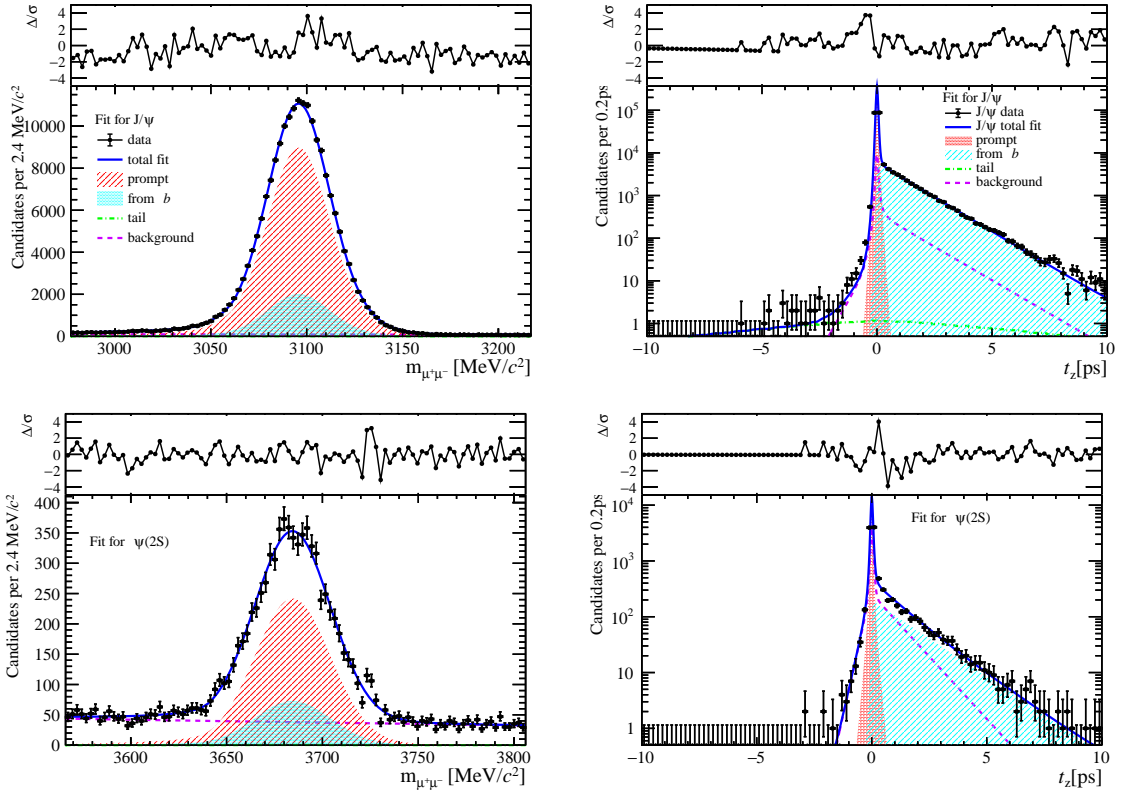


Figure 229: Fit results in  $6 \text{ GeV}/c < p_T < 8 \text{ GeV}/c$ ,  $3.5 < y < 4.5$  and  $24 \leq \text{nForwardTracks} < 36$ .

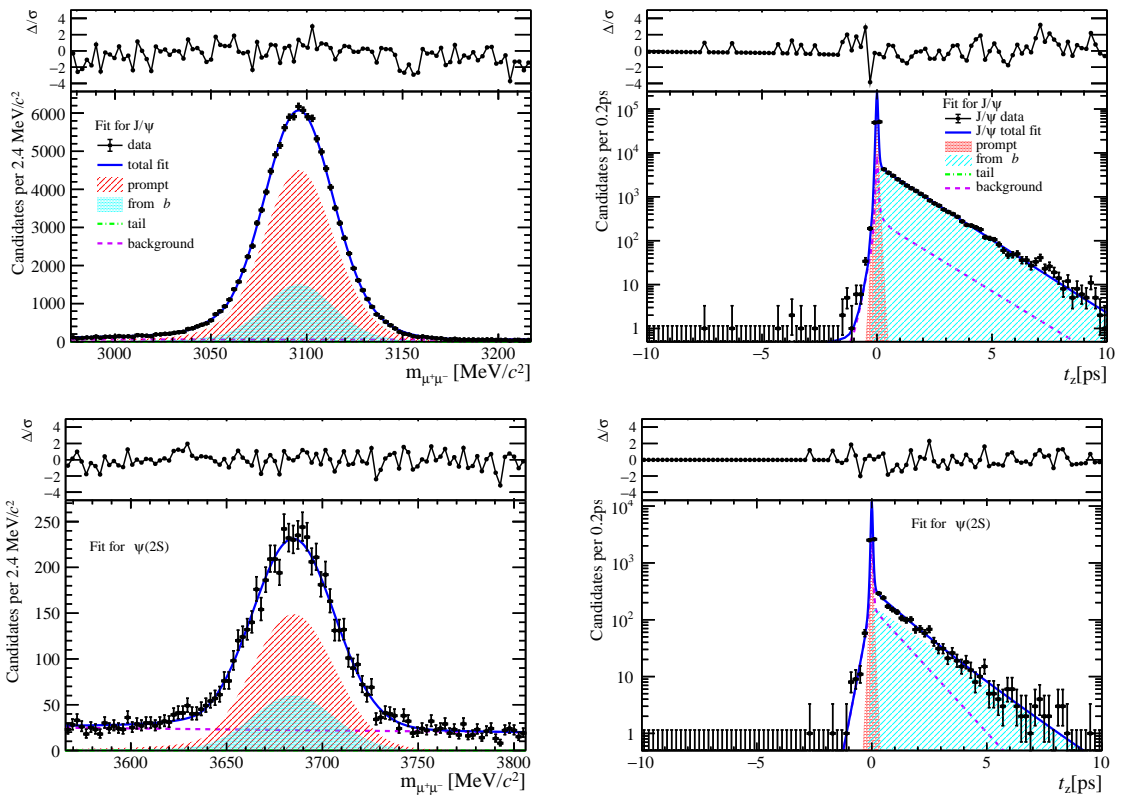


Figure 230: Fit results in  $8 \text{ GeV}/c < p_T < 20 \text{ GeV}/c$ ,  $3.5 < y < 4.5$  and  $24 \leq \text{nForwardTracks} < 36$ .

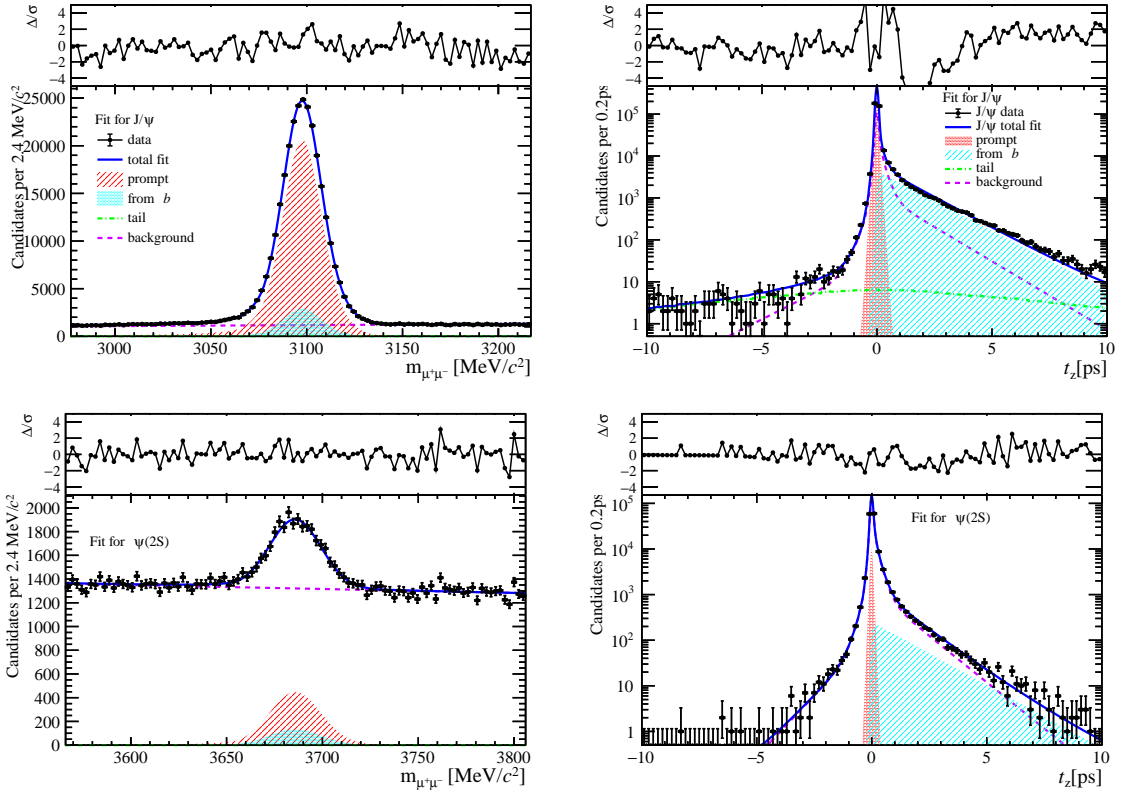


Figure 231: Fit results in  $0 \text{ GeV}/c < p_T < 2 \text{ GeV}/c$ ,  $2.0 < y < 2.8$  and  $36 \leq \text{nForwardTracks} < 48$ .

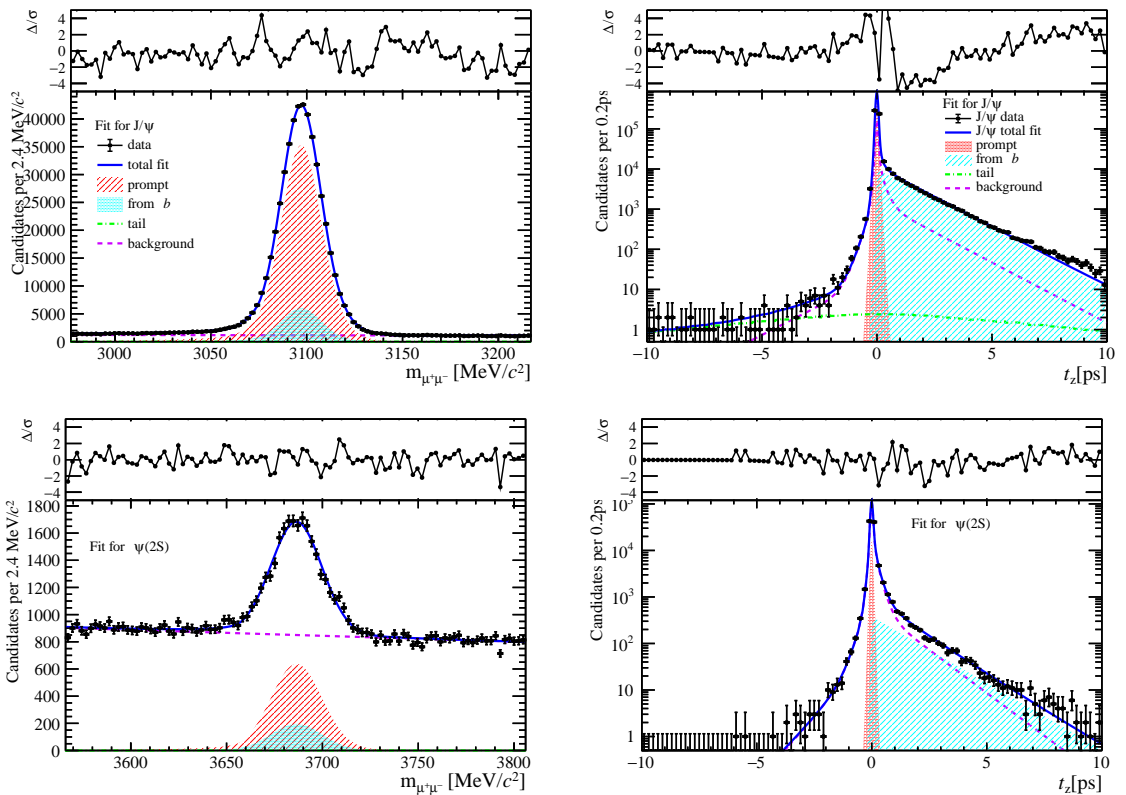


Figure 232: Fit results in  $2 \text{ GeV}/c < p_T < 4 \text{ GeV}/c$ ,  $2.0 < y < 2.8$  and  $36 \leq \text{nForwardTracks} < 48$ .

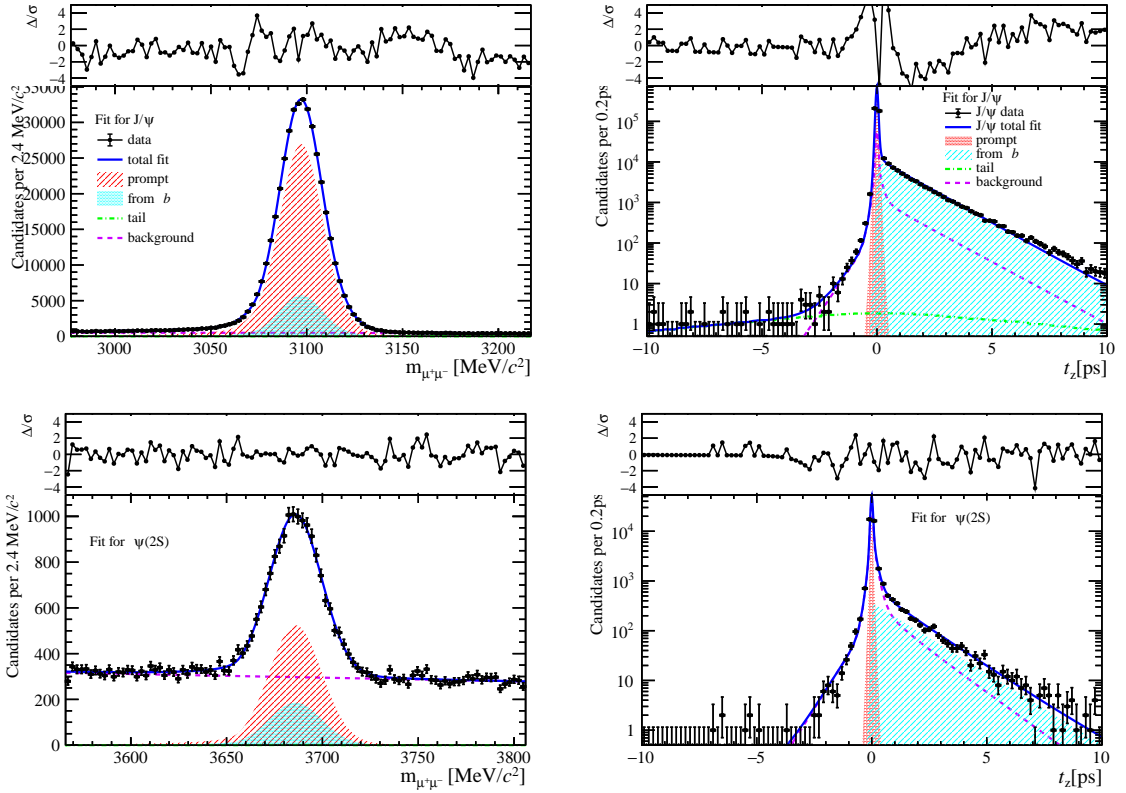


Figure 233: Fit results in  $4 \text{ GeV}/c < p_T < 6 \text{ GeV}/c$ ,  $2.0 < y < 2.8$  and  $36 \leq \text{nForwardTracks} < 48$ .

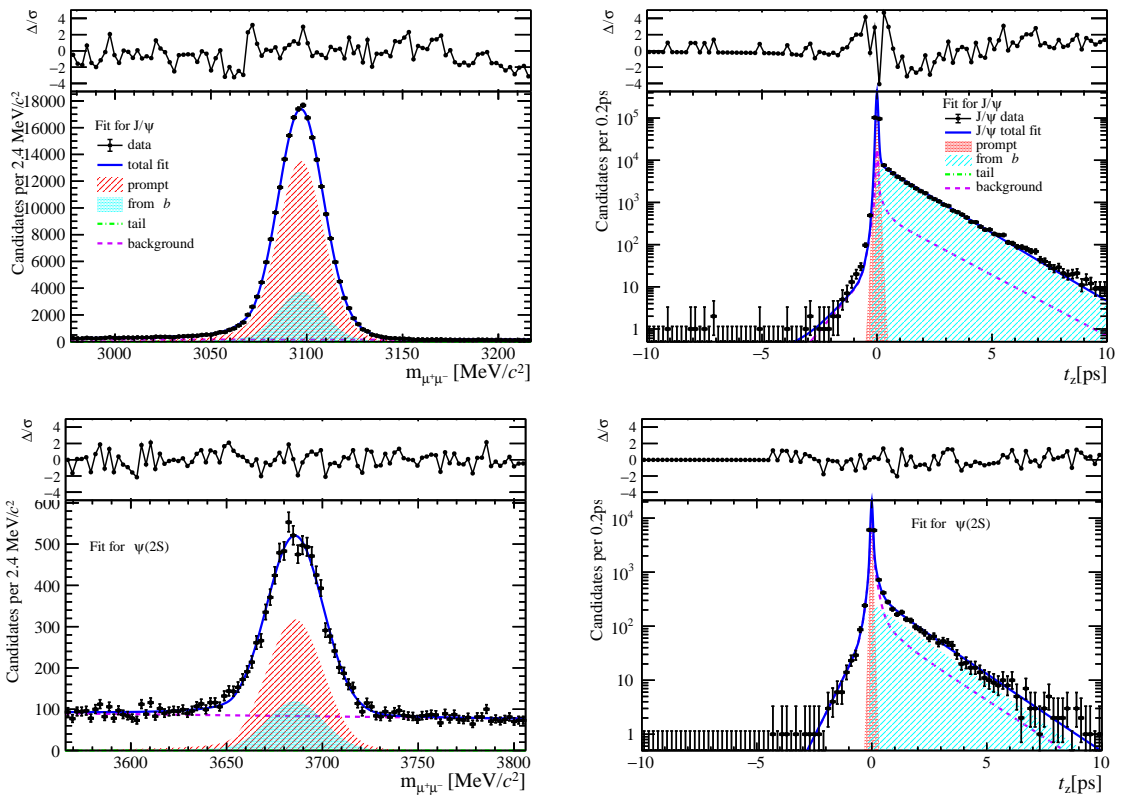


Figure 234: Fit results in  $6 \text{ GeV}/c < p_T < 8 \text{ GeV}/c$ ,  $2.0 < y < 2.8$  and  $36 \leq \text{nForwardTracks} < 48$ .

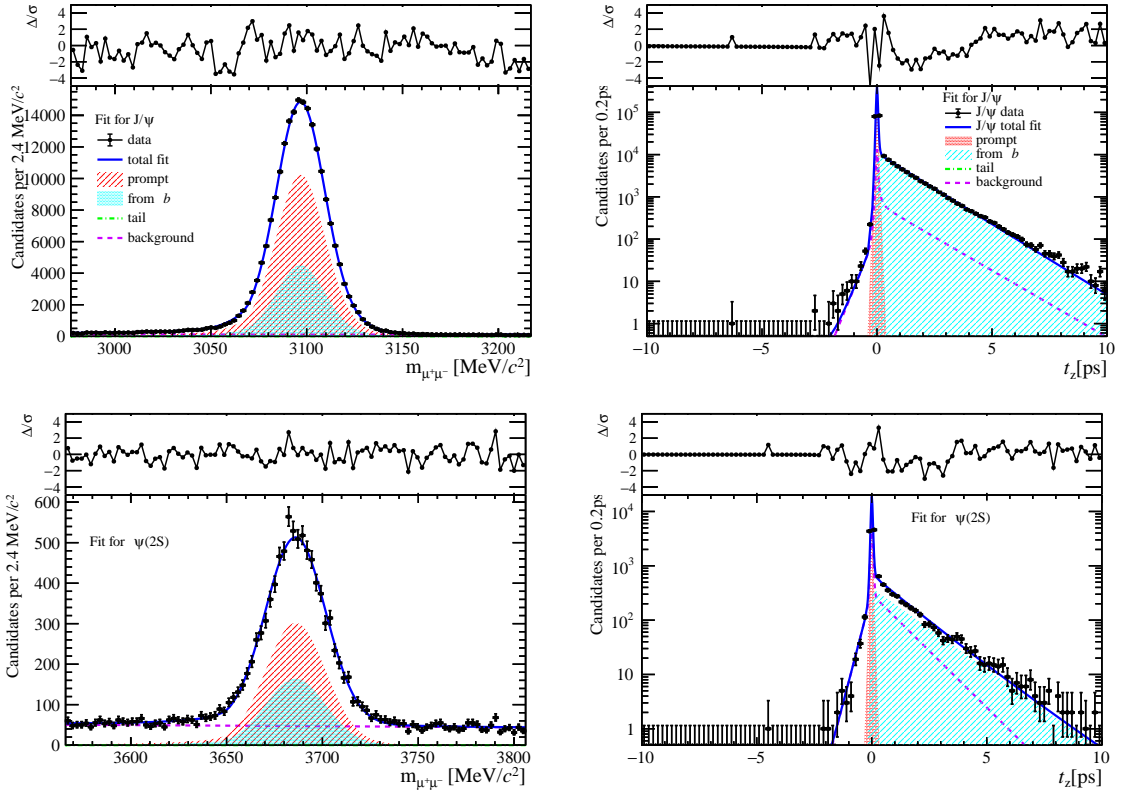


Figure 235: Fit results in  $8 \text{ GeV}/c < p_T < 20 \text{ GeV}/c$ ,  $2.0 < y < 2.8$  and  $36 \leq \text{nForwardTracks} < 48$ .

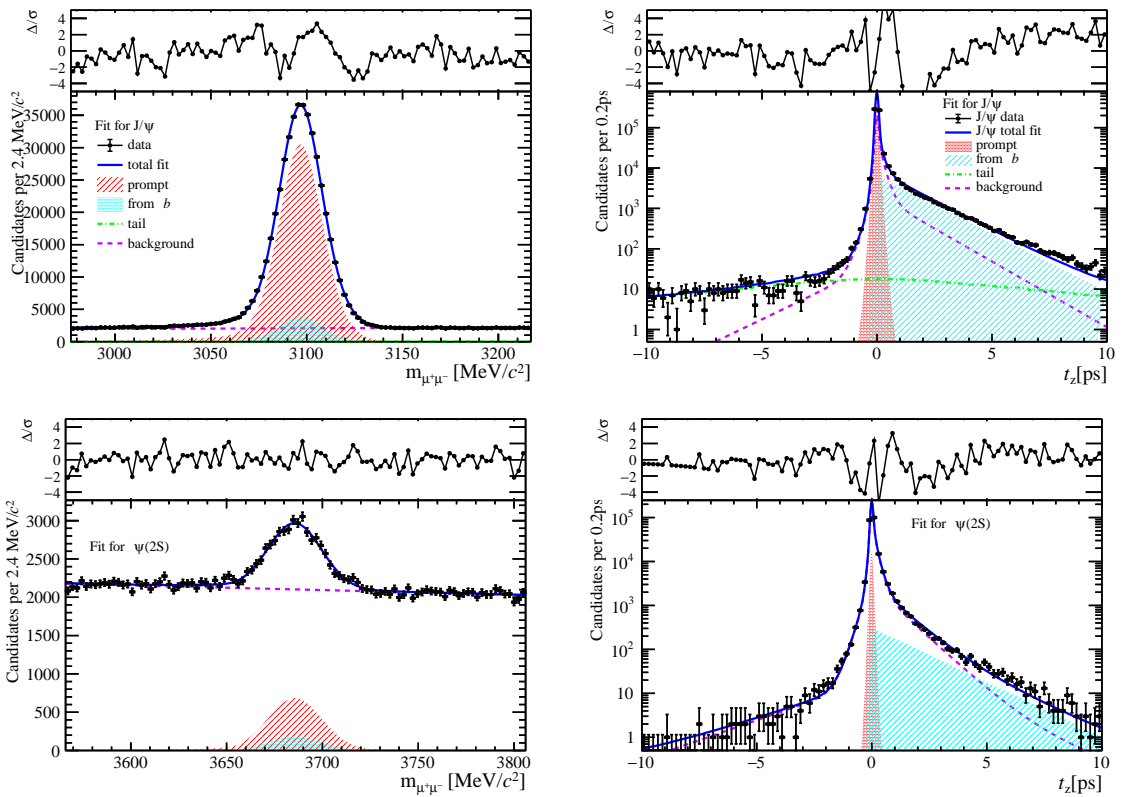


Figure 236: Fit results in  $0 \text{ GeV}/c < p_T < 2 \text{ GeV}/c$ ,  $2.8 < y < 3.5$  and  $36 \leq \text{nForwardTracks} < 48$ .

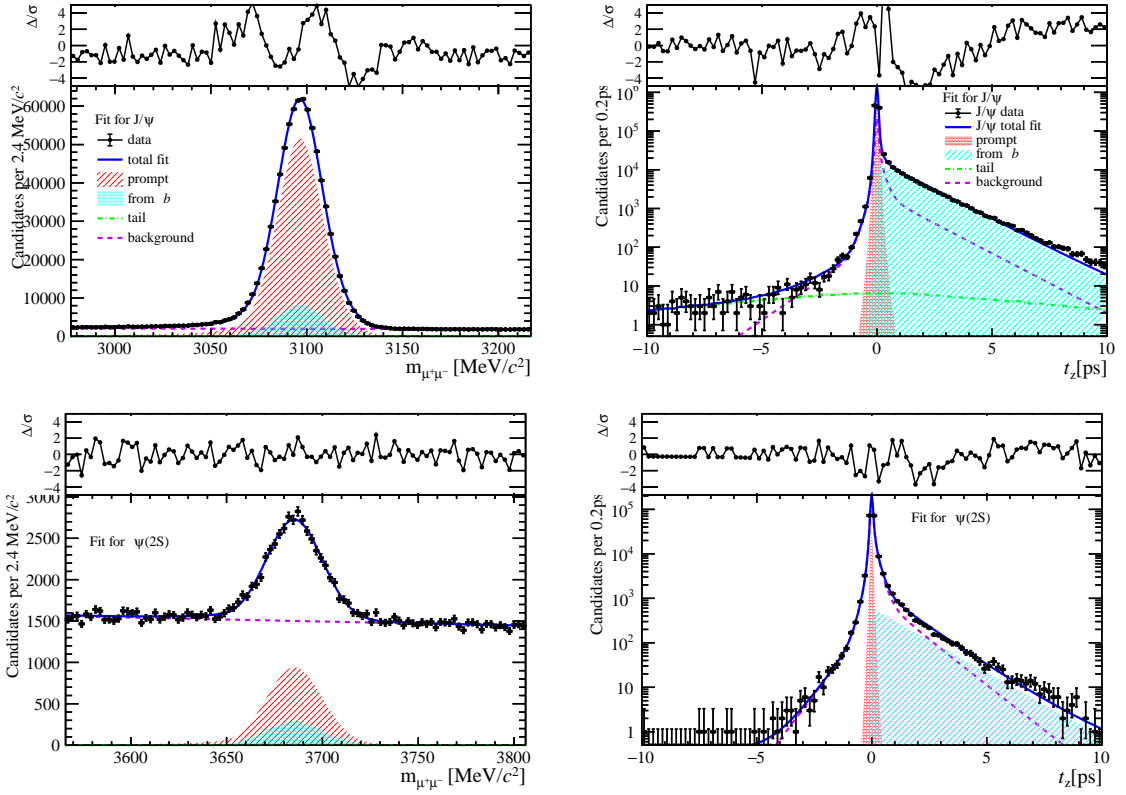


Figure 237: Fit results in  $2 \text{ GeV}/c < p_T < 4 \text{ GeV}/c$ ,  $2.8 < y < 3.5$  and  $36 \leq \text{nForwardTracks} < 48$ .

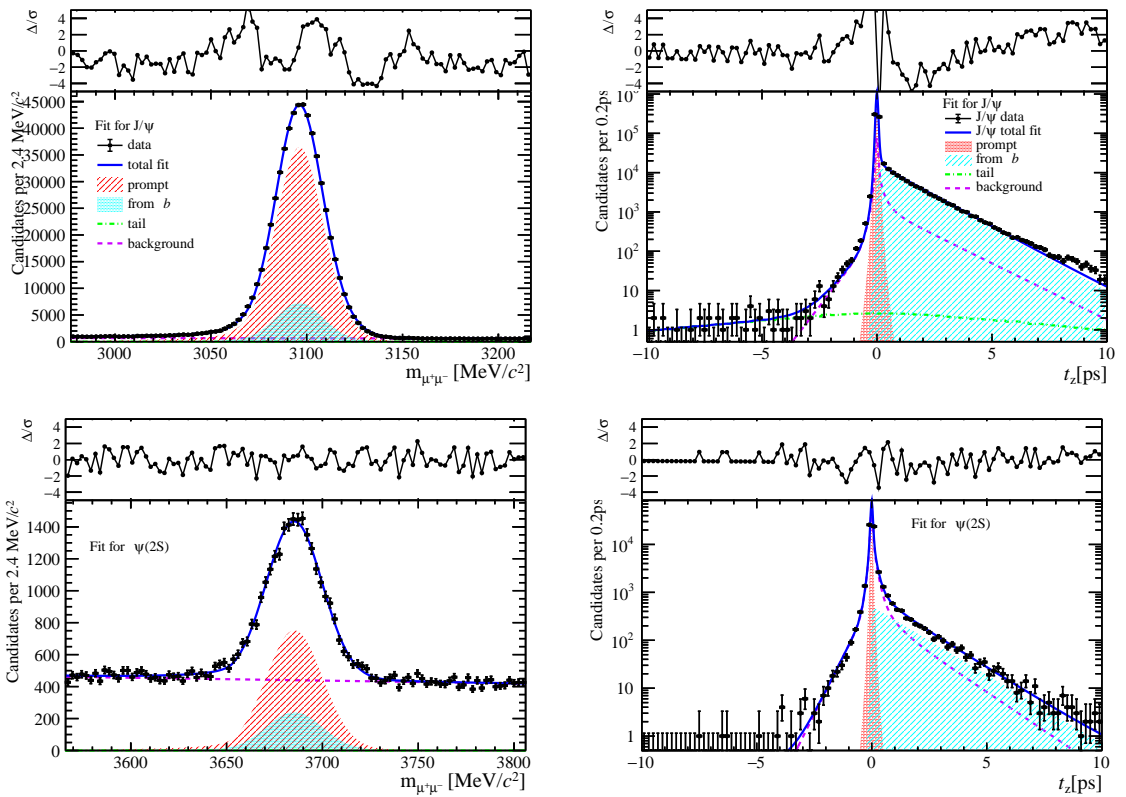


Figure 238: Fit results in  $4 \text{ GeV}/c < p_T < 6 \text{ GeV}/c$ ,  $2.8 < y < 3.5$  and  $36 \leq \text{nForwardTracks} < 48$ .

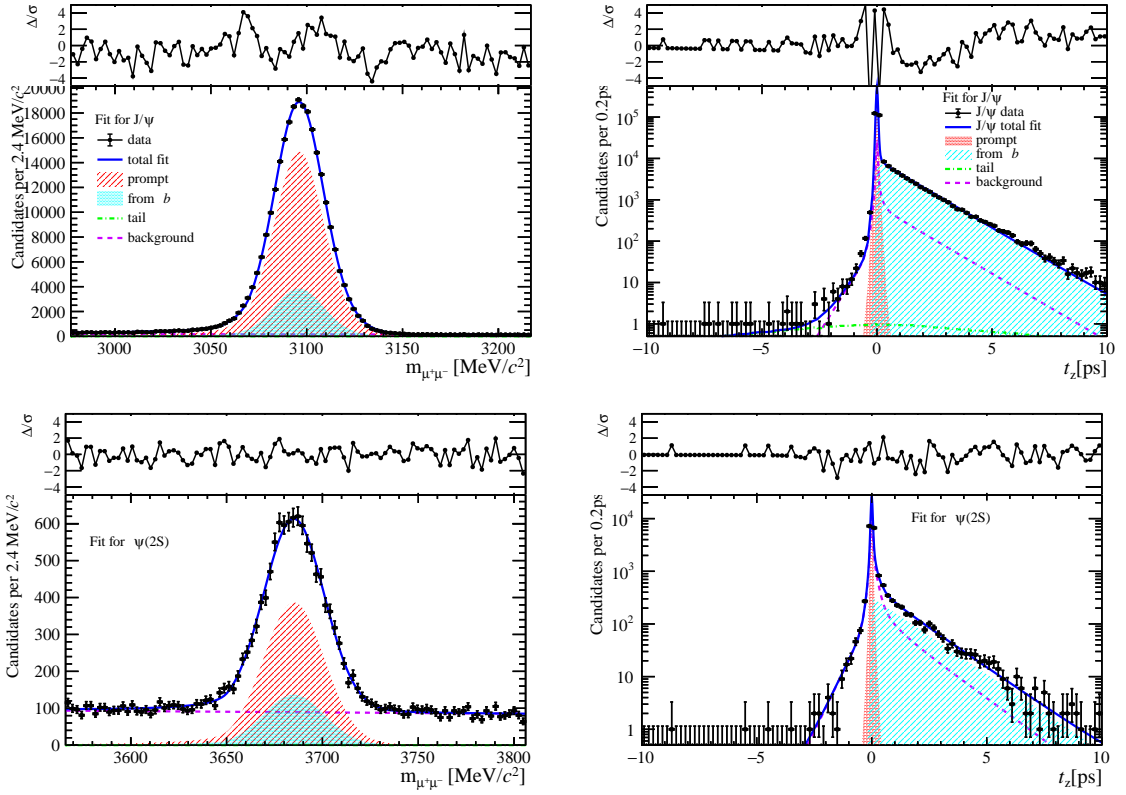


Figure 239: Fit results in  $6 \text{ GeV}/c < p_T < 8 \text{ GeV}/c$ ,  $2.8 < y < 3.5$  and  $36 \leq \text{nForwardTracks} < 48$ .

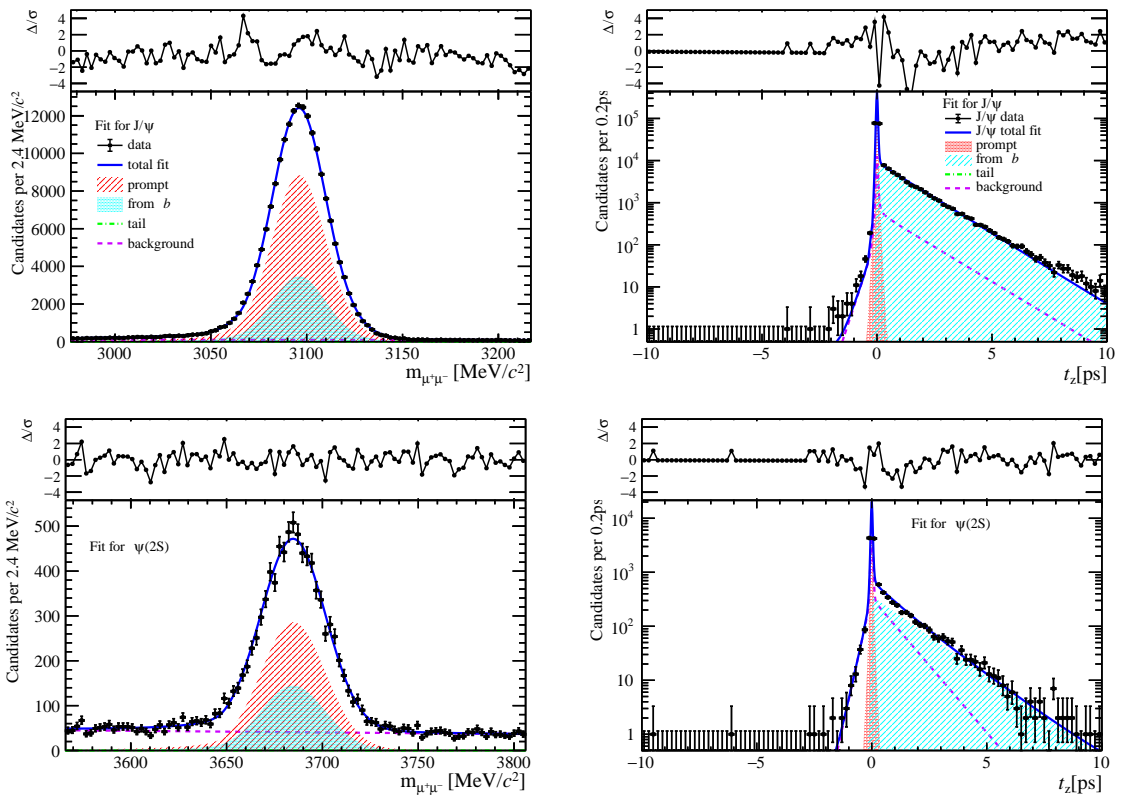


Figure 240: Fit results in  $8 \text{ GeV}/c < p_T < 20 \text{ GeV}/c$ ,  $2.8 < y < 3.5$  and  $36 \leq \text{nForwardTracks} < 48$ .

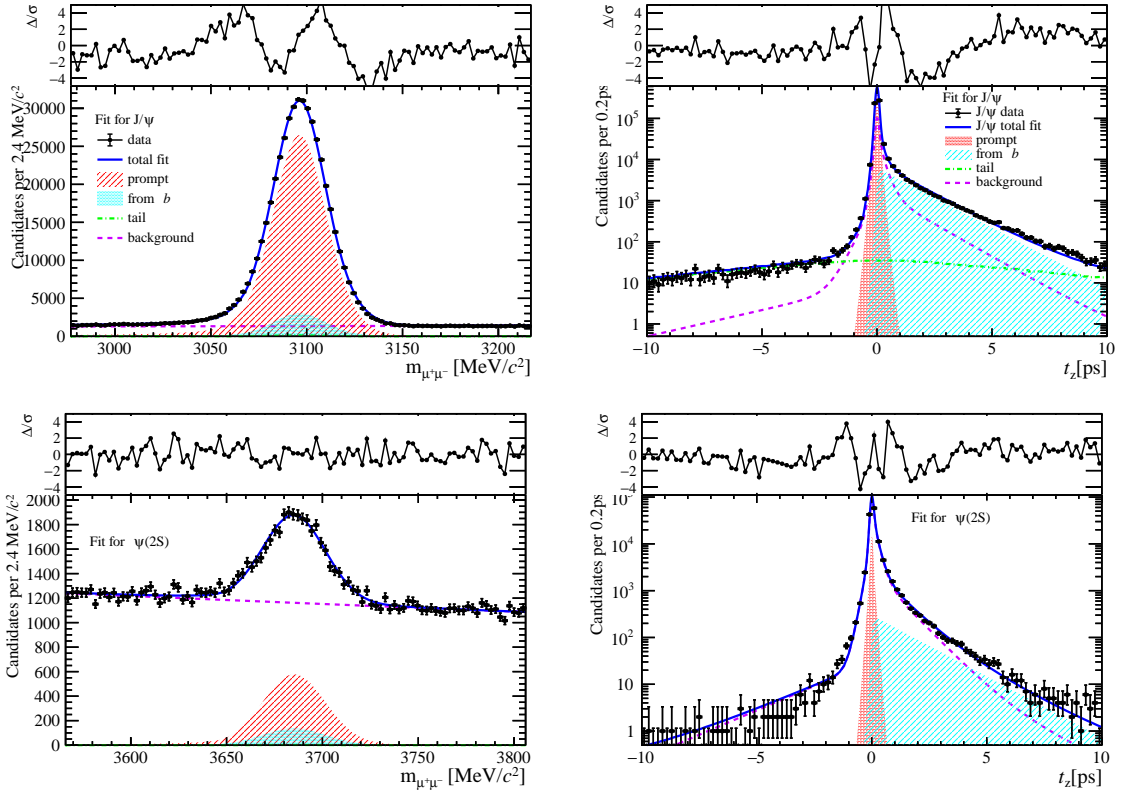


Figure 241: Fit results in  $0 \text{ GeV}/c < p_T < 2 \text{ GeV}/c$ ,  $3.5 < y < 4.5$  and  $36 \leq \text{nForwardTracks} < 48$ .

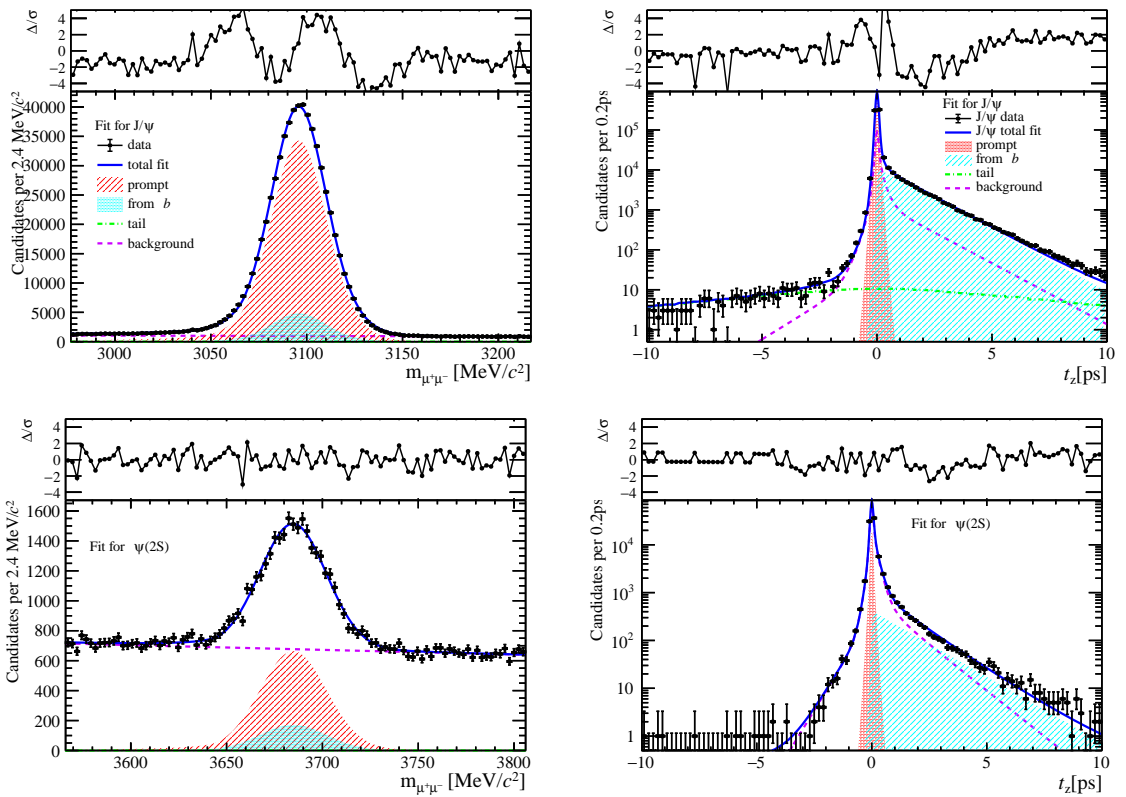


Figure 242: Fit results in  $2 \text{ GeV}/c < p_T < 4 \text{ GeV}/c$ ,  $3.5 < y < 4.5$  and  $36 \leq \text{nForwardTracks} < 48$ .

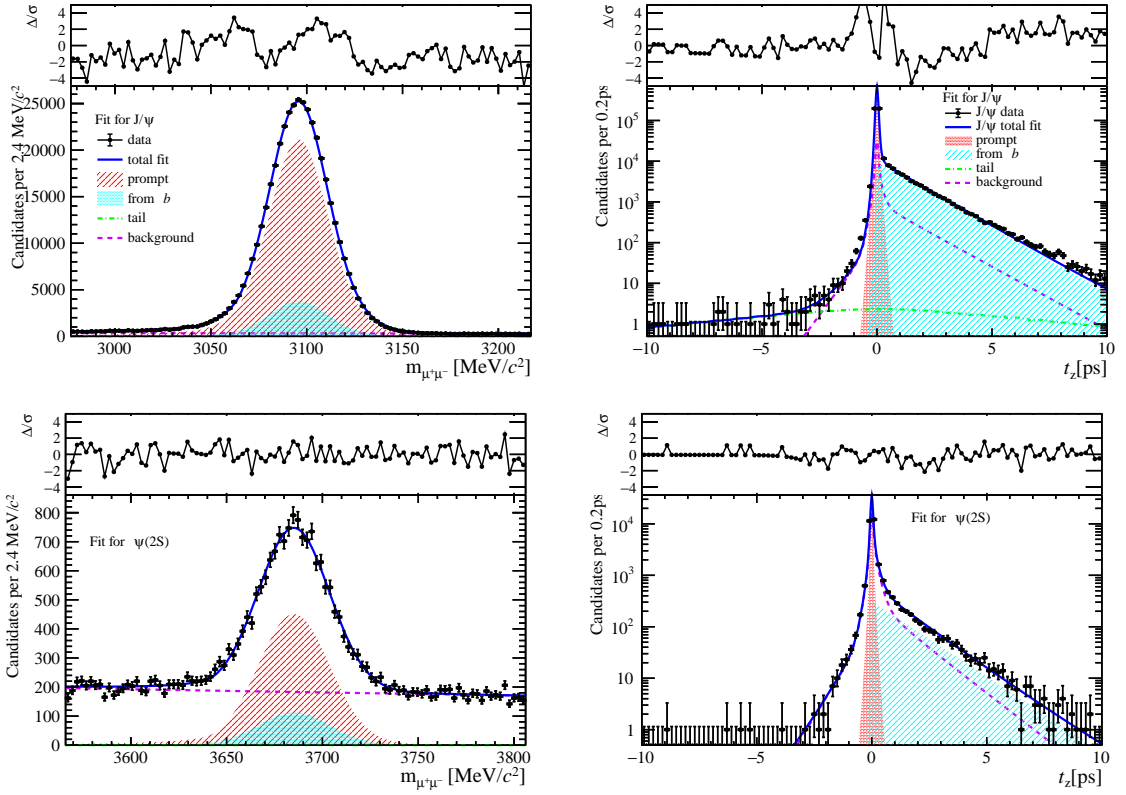


Figure 243: Fit results in  $4 \text{ GeV}/c < p_T < 6 \text{ GeV}/c$ ,  $3.5 < y < 4.5$  and  $36 \leq \text{nForwardTracks} < 48$ .

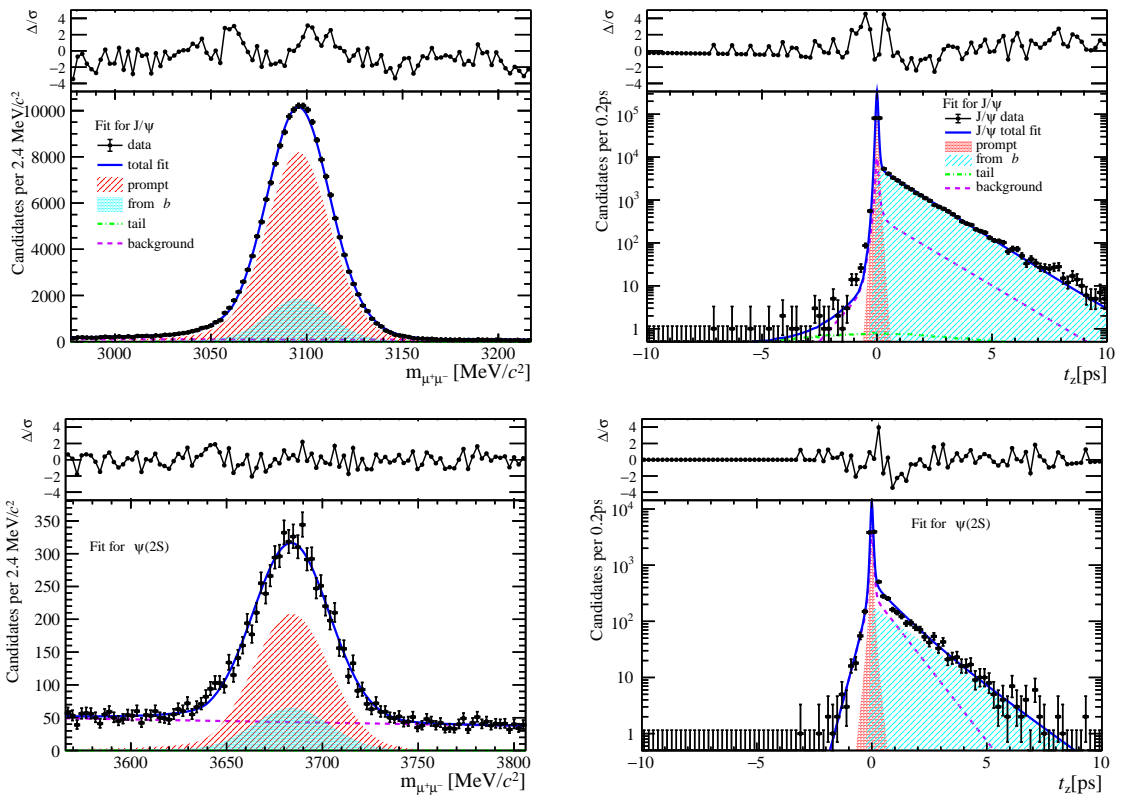


Figure 244: Fit results in  $6 \text{ GeV}/c < p_T < 8 \text{ GeV}/c$ ,  $3.5 < y < 4.5$  and  $36 \leq \text{nForwardTracks} < 48$ .

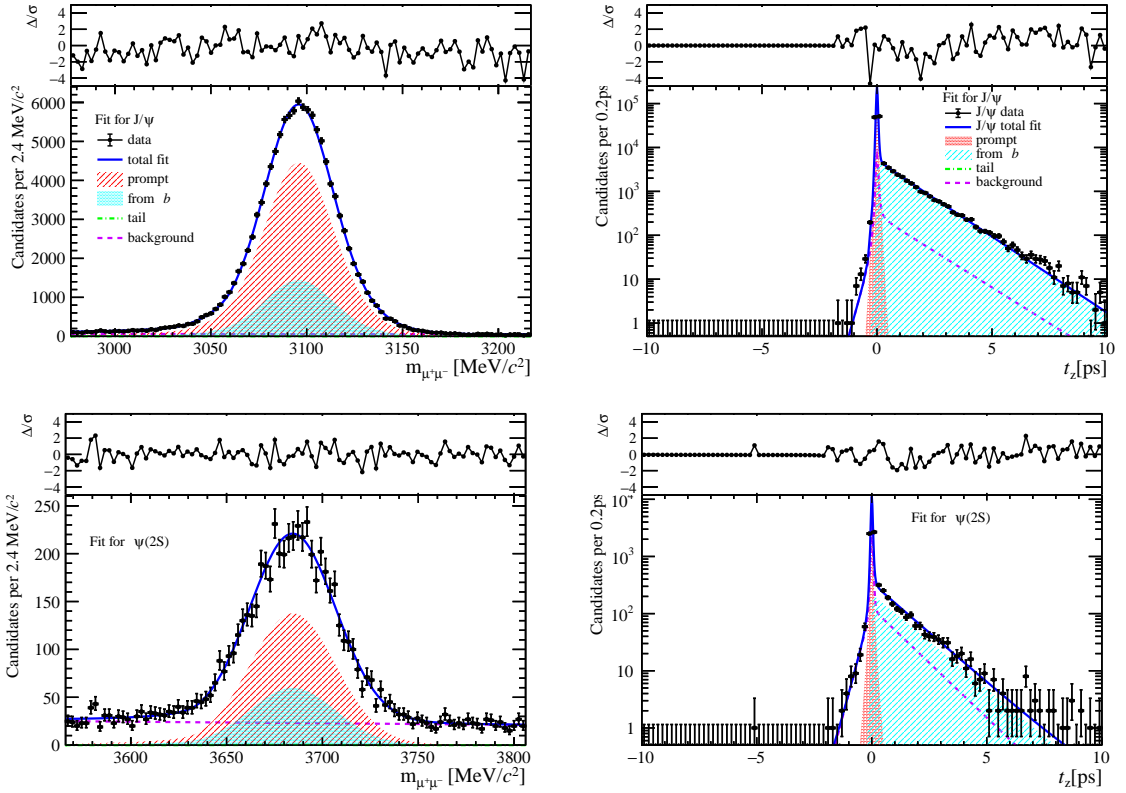


Figure 245: Fit results in  $8 \text{ GeV}/c < p_T < 20 \text{ GeV}/c$ ,  $3.5 < y < 4.5$  and  $36 \leq \text{nForwardTracks} < 48$ .

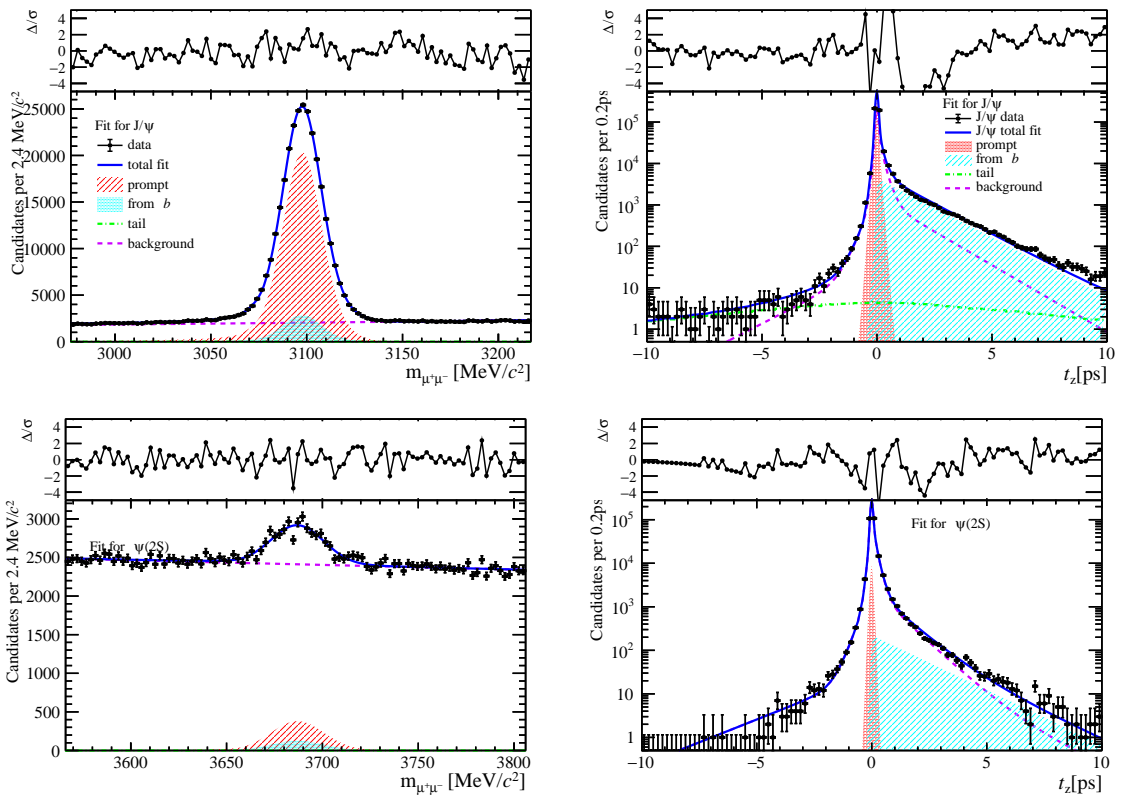


Figure 246: Fit results in  $0 \text{ GeV}/c < p_T < 2 \text{ GeV}/c$ ,  $2.0 < y < 2.8$  and  $48 \leq \text{nForwardTracks} < 130$ .

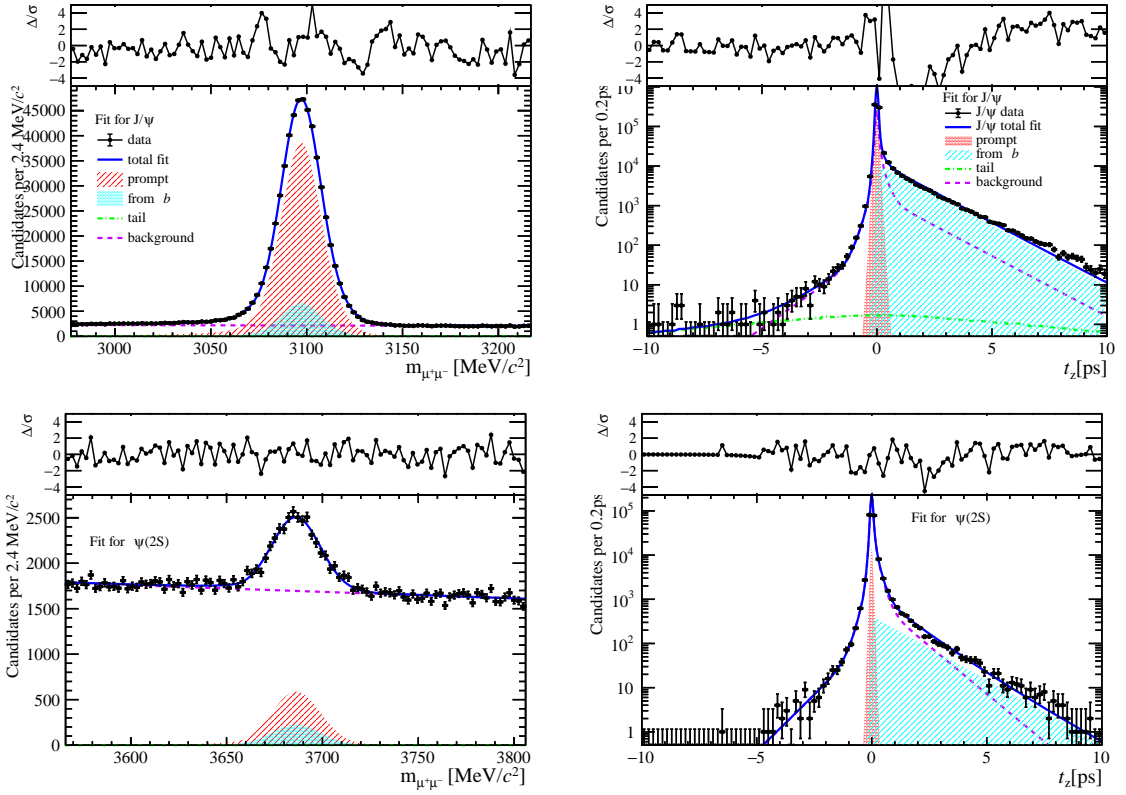


Figure 247: Fit results in  $2 \text{ GeV}/c < p_T < 4 \text{ GeV}/c$ ,  $2.0 < y < 2.8$  and  $48 \leq \text{nForwardTracks} < 130$ .

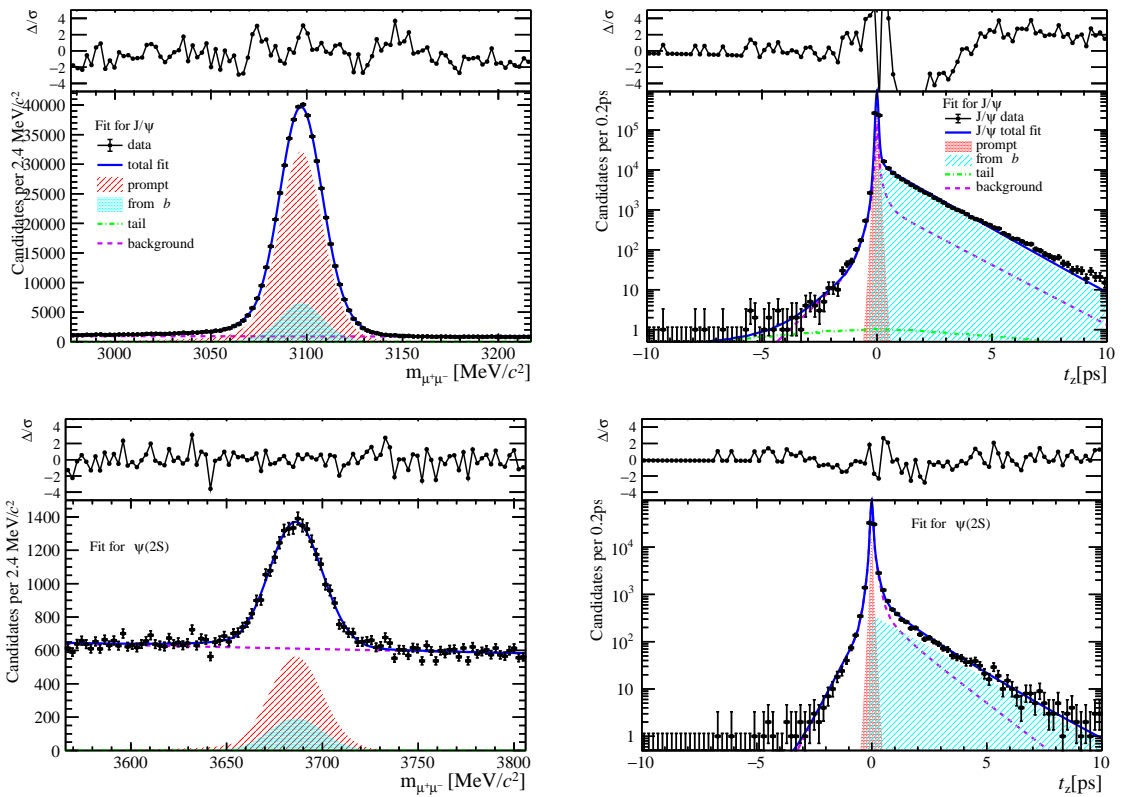


Figure 248: Fit results in  $4 \text{ GeV}/c < p_T < 6 \text{ GeV}/c$ ,  $2.0 < y < 2.8$  and  $48 \leq \text{nForwardTracks} < 130$ .

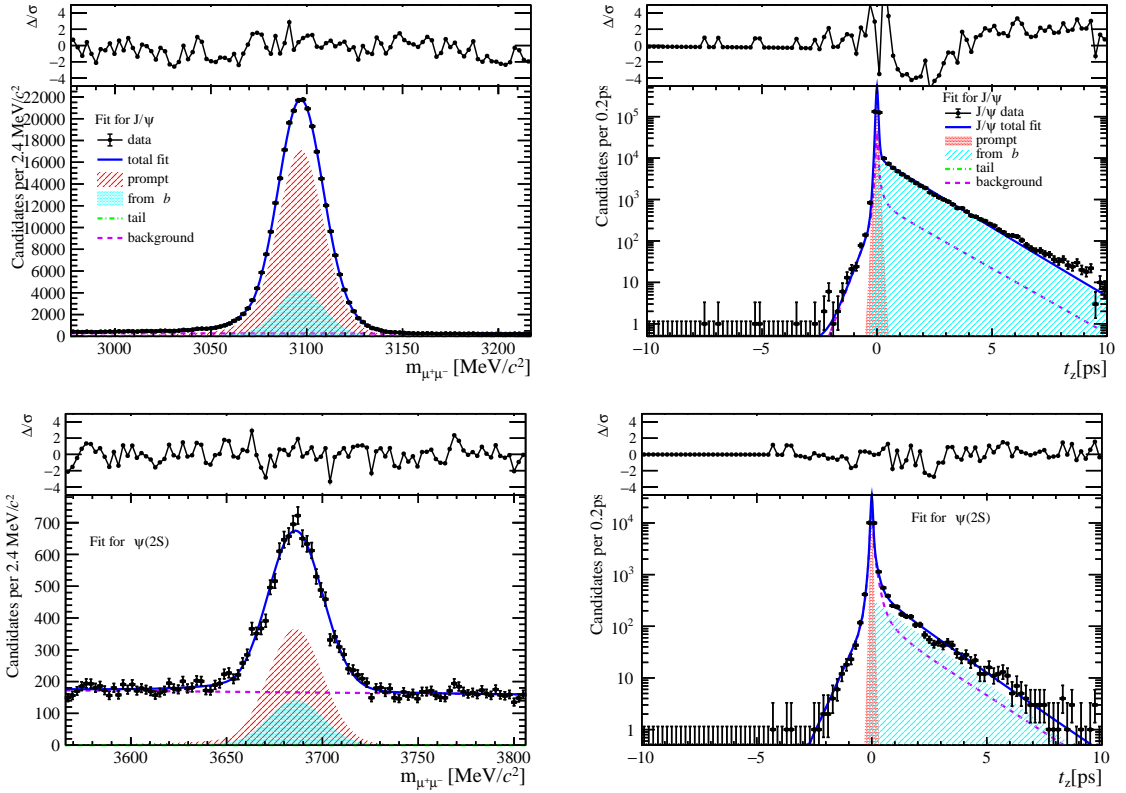


Figure 249: Fit results in  $6 \text{ GeV}/c < p_T < 8 \text{ GeV}/c$ ,  $2.0 < y < 2.8$  and  $48 \leq \text{nForwardTracks} < 130$ .

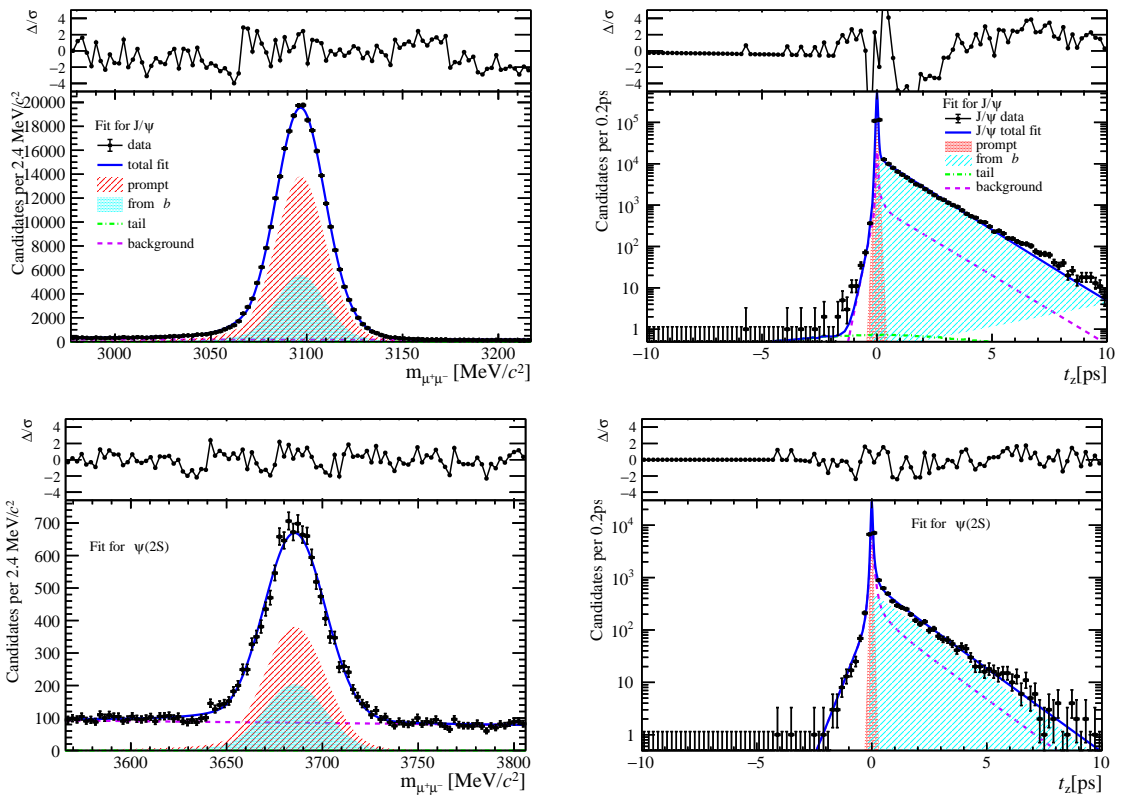


Figure 250: Fit results in  $8 \text{ GeV}/c < p_T < 20 \text{ GeV}/c$ ,  $2.0 < y < 2.8$  and  $48 \leq \text{nForwardTracks} < 130$ .

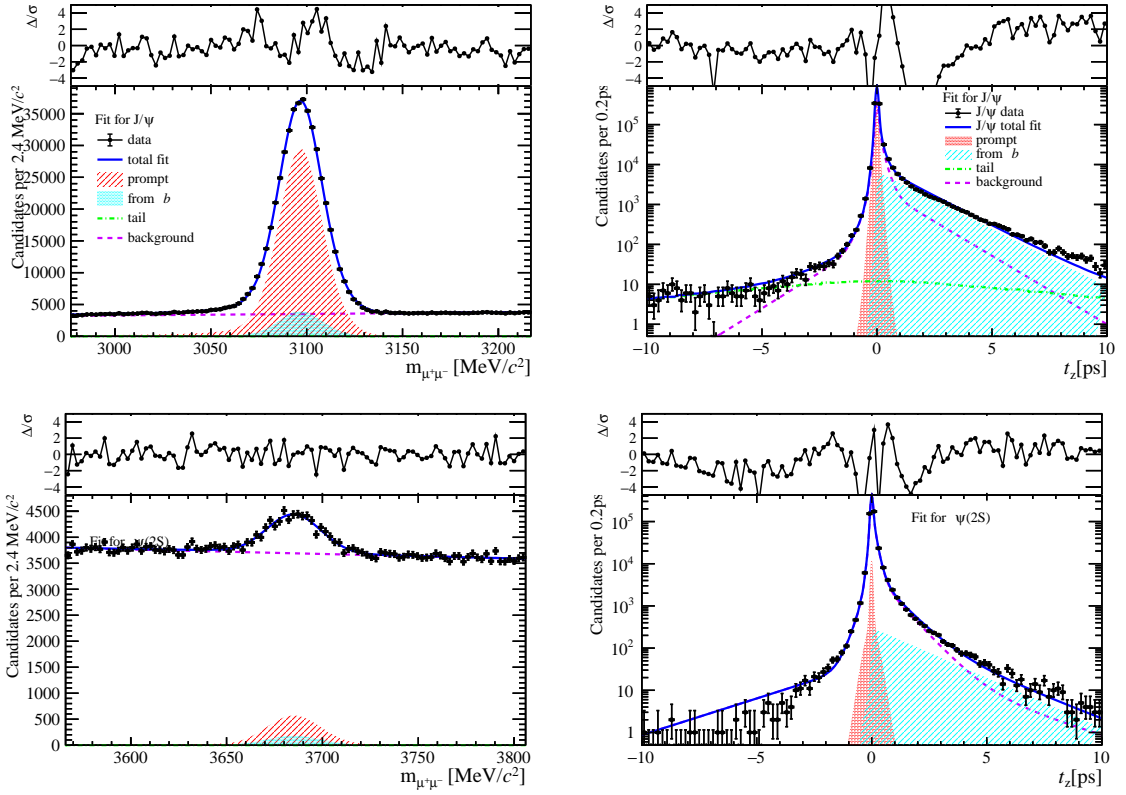


Figure 251: Fit results in  $0 \text{ GeV}/c < p_T < 2 \text{ GeV}/c$ ,  $2.8 < y < 3.5$  and  $48 \leq \text{nForwardTracks} < 130$ .

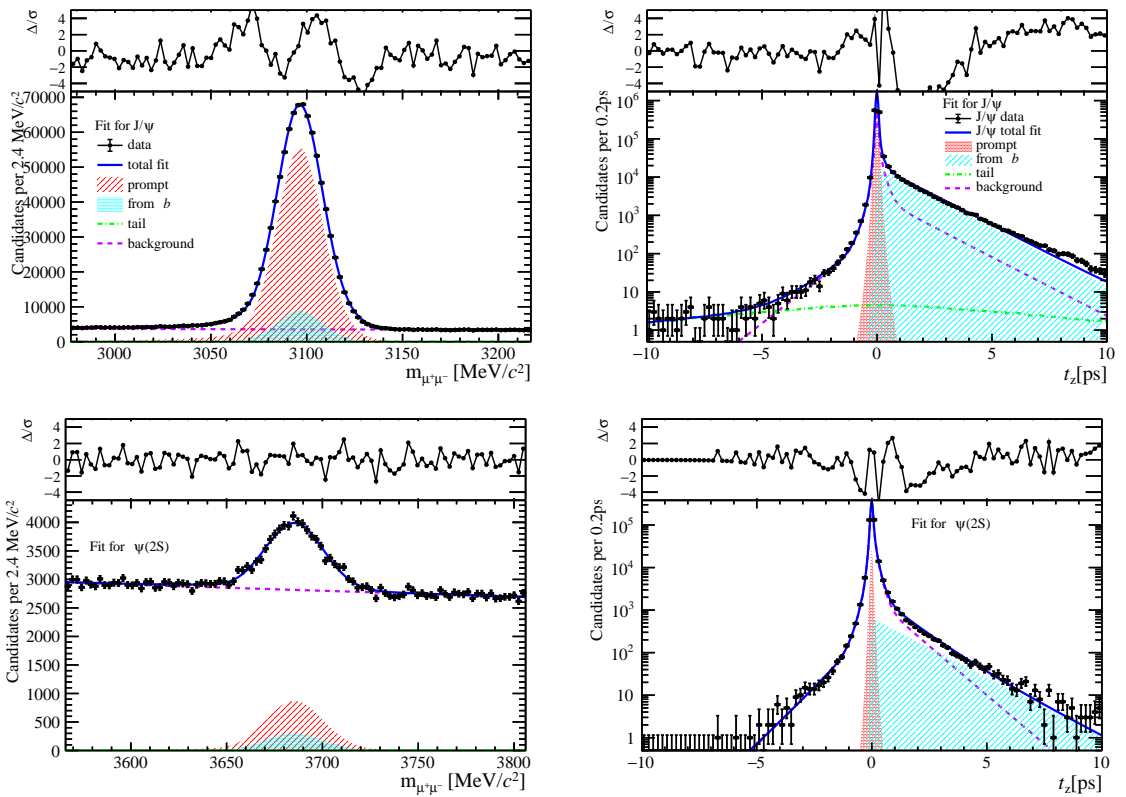


Figure 252: Fit results in  $2 \text{ GeV}/c < p_T < 4 \text{ GeV}/c$ ,  $2.8 < y < 3.5$  and  $48 \leq \text{nForwardTracks} < 130$ .

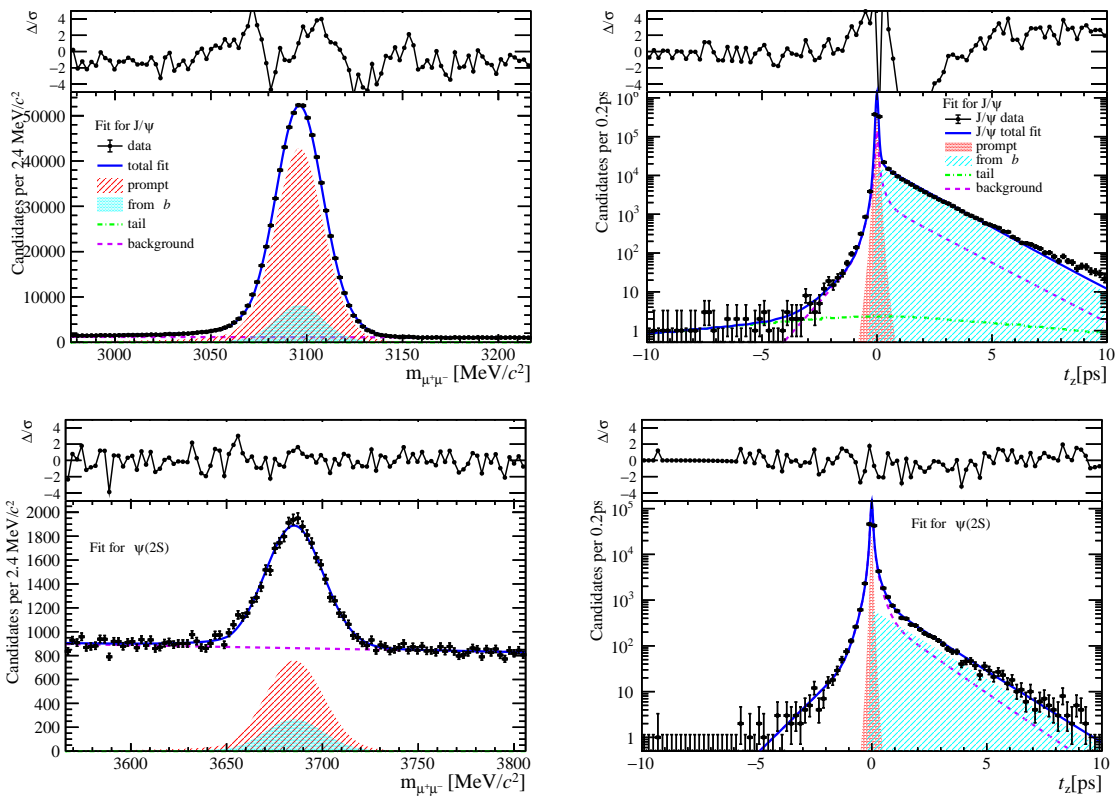


Figure 253: Fit results in  $4 \text{ GeV}/c < p_T < 6 \text{ GeV}/c$ ,  $2.8 < y < 3.5$  and  $48 \leq \text{nForwardTracks} < 130$ .

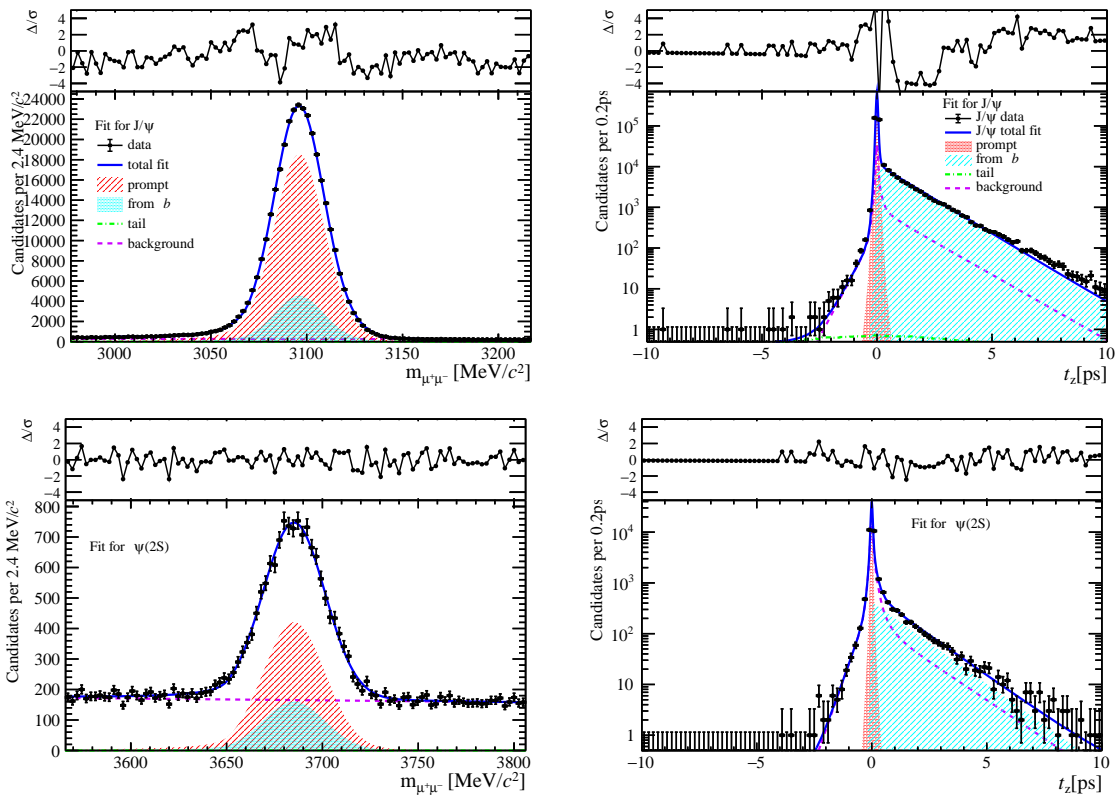


Figure 254: Fit results in  $6 \text{ GeV}/c < p_T < 8 \text{ GeV}/c$ ,  $2.8 < y < 3.5$  and  $48 \leq \text{nForwardTracks} < 130$ .

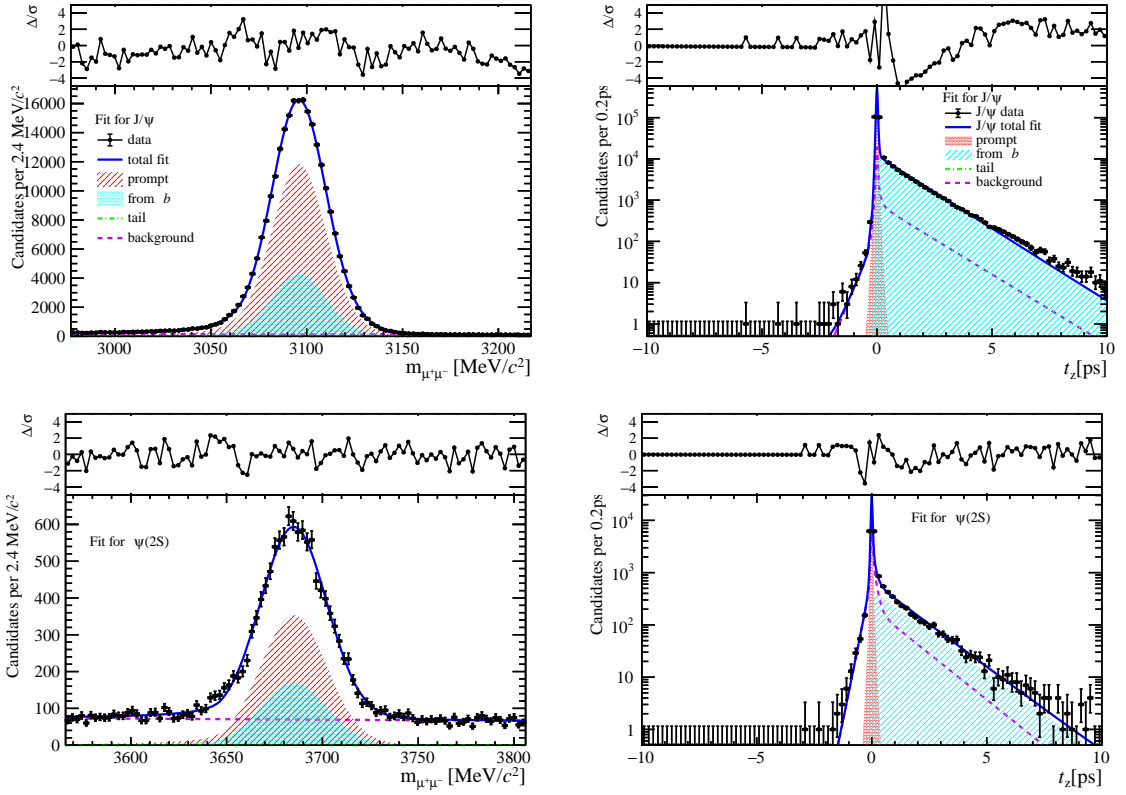


Figure 255: Fit results in  $8 \text{ GeV}/c < p_T < 20 \text{ GeV}/c$ ,  $2.8 < y < 3.5$  and  $48 \leq \text{nForwardTracks} < 130$ .

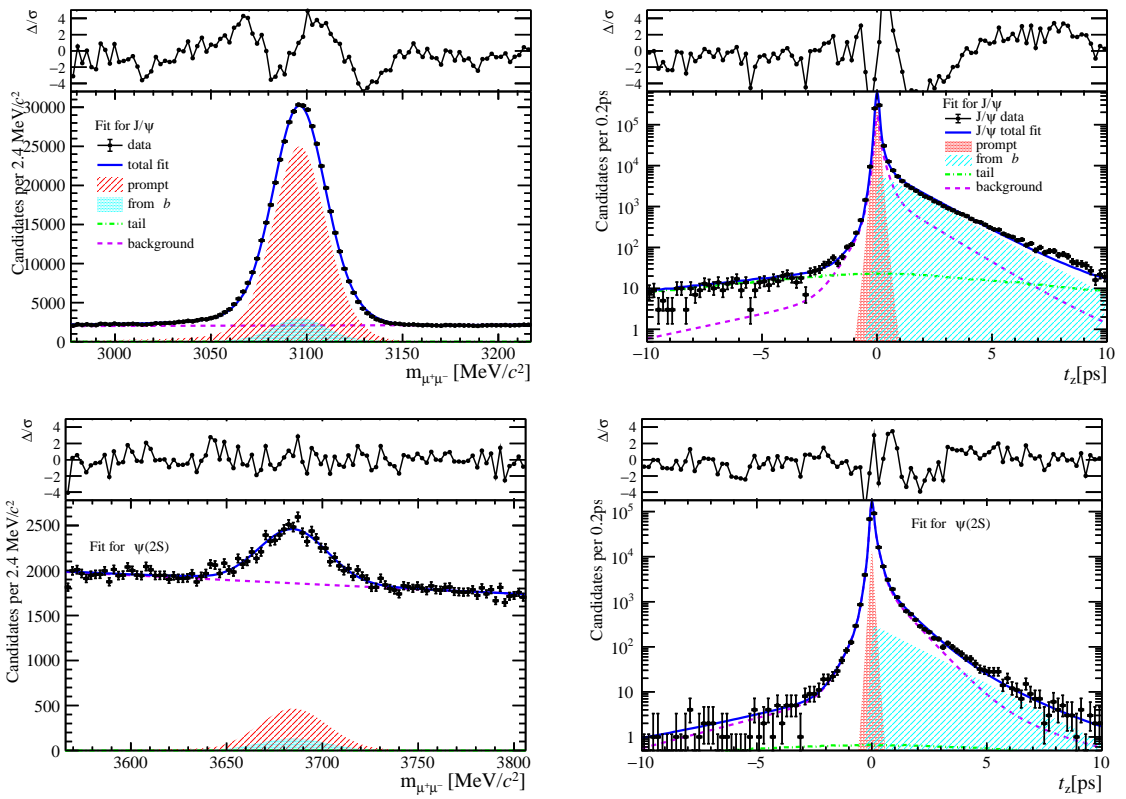


Figure 256: Fit results in  $0 \text{ GeV}/c < p_T < 2 \text{ GeV}/c$ ,  $3.5 < y < 4.5$  and  $48 \leq \text{nForwardTracks} < 130$ .

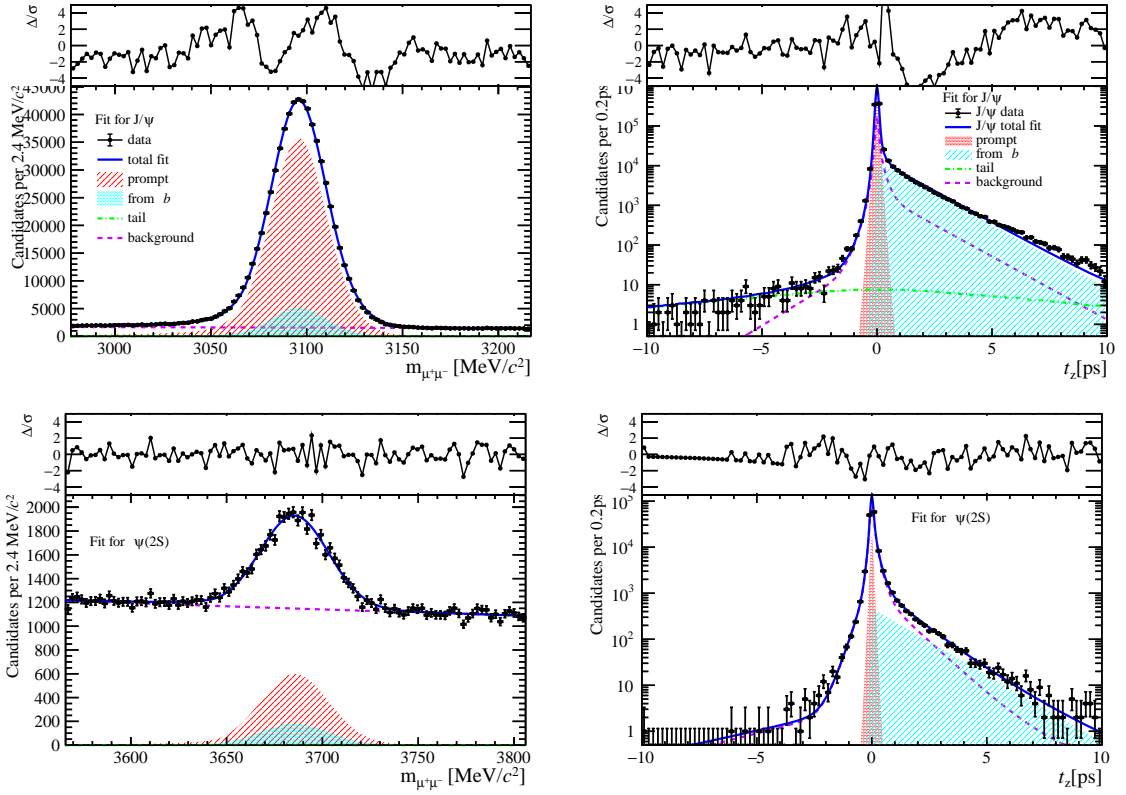


Figure 257: Fit results in  $2 \text{ GeV}/c < p_T < 4 \text{ GeV}/c$ ,  $3.5 < y < 4.5$  and  $48 \leq \text{nForwardTracks} < 130$ .

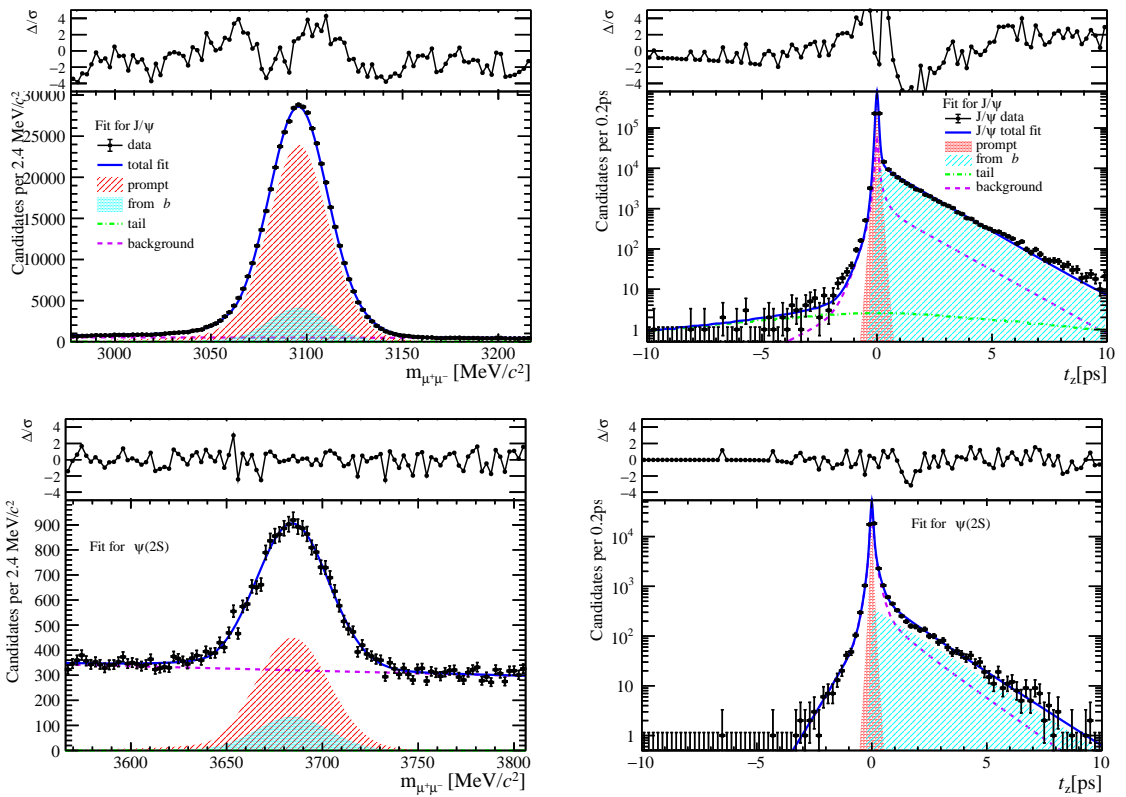


Figure 258: Fit results in  $4 \text{ GeV}/c < p_T < 6 \text{ GeV}/c$ ,  $3.5 < y < 4.5$  and  $48 \leq \text{nForwardTracks} < 130$ .

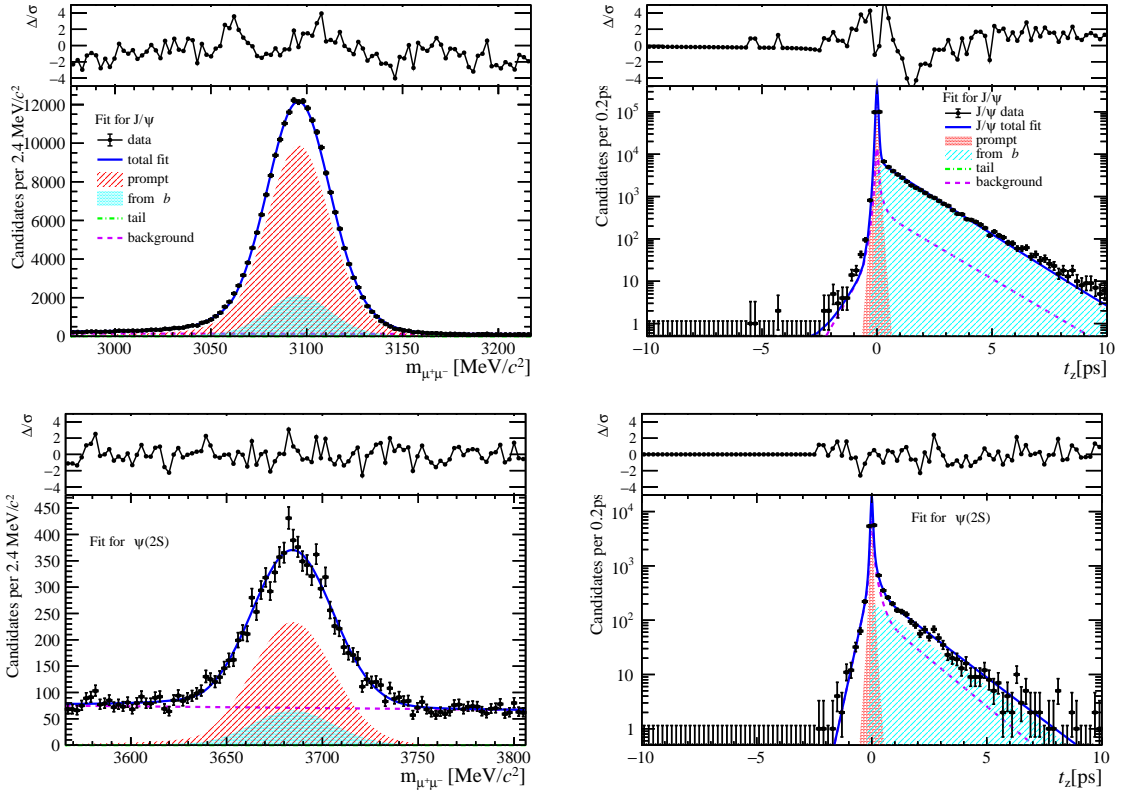


Figure 259: Fit results in  $6 \text{ GeV}/c < p_T < 8 \text{ GeV}/c$ ,  $3.5 < y < 4.5$  and  $48 \leq \text{nForwardTracks} < 130$ .

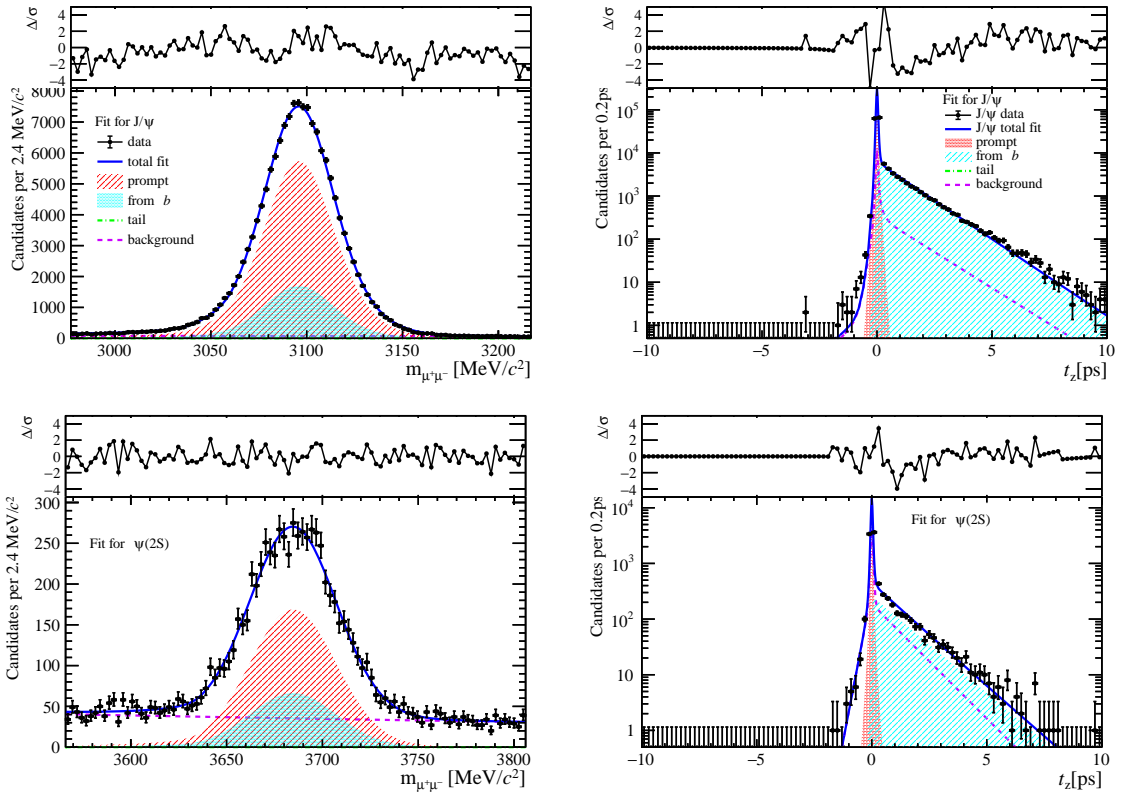


Figure 260: Fit results in  $8 \text{ GeV}/c < p_T < 20 \text{ GeV}/c$ ,  $3.5 < y < 4.5$  and  $48 \leq \text{nForwardTracks} < 130$ .

## 721 References

- 722 [1] T. Matsui and H. Satz, *J/psi suppression by quark-gluon plasma formation*, Physics  
723 Letters B **178** (1986) 416.
- 724 [2] PHENIX collaboration, A. Adare *et al.*, *Cold Nuclear Matter Effects on J/Psi as*  
725 *Constrained by Deuteron-Gold Measurements at s(NN)\*\*(1/2) = 200-GeV*, Phys. Rev.  
726 C **77** (2008) 024912, arXiv:0903.4845, [Erratum: Phys.Rev.C 79, 059901 (2009)].
- 727 [3] LHCb collaboration, R. Aaij *et al.*, *Prompt and nonprompt J/ψ production and*  
728 *nuclear modification in pPb collisions at  $\sqrt{s_{NN}} = 8.16 \text{ TeV}$* , Phys. Lett. B **774** (2017)  
729 159, arXiv:1706.07122.
- 730 [4] S. Atashbar Tehrani, *Nuclear parton distribution functions (nPDFs) and their uncer-*  
731 *tainties in the LHC Era*, KnE Energ. Phys. **3** (2018) 297, arXiv:1712.02153.
- 732 [5] F. Arleo and S. Peigné, *Quarkonium suppression in heavy-ion collisions from coherent*  
733 *energy loss in cold nuclear matter*, JHEP **10** (2014) 073, arXiv:1407.5054.
- 734 [6] E. G. Ferreiro, *Charmonium dissociation and recombination at LHC: Revisiting*  
735 *comovers*, Phys. Lett. B **731** (2014) 57, arXiv:1210.3209.
- 736 [7] ALICE collaboration, J. Adam *et al.*, *Enhanced production of multi-strange*  
737 *hadrons in high-multiplicity proton-proton collisions*, Nature Phys. **13** (2017) 535,  
738 arXiv:1606.07424.
- 739 [8] CMS collaboration, V. Khachatryan *et al.*, *Evidence for collectivity in pp collisions*  
740 *at the LHC*, Phys. Lett. B **765** (2017) 193, arXiv:1606.06198.
- 741 [9] P. Ball, V. M. Braun, and A. Lenz, *Higher-twist distribution amplitudes of the K*  
742 *meson in QCD*, JHEP **05** (2006) 004, arXiv:hep-ph/0603063.
- 743 [10] LHCb collaboration, I. Belyaev *et al.*, *Handling of the generation of primary events*  
744 *in Gauss, the LHCb simulation framework*, J. Phys. Conf. Ser. **331** (2011) 032047.
- 745 [11] D. J. Lange, *The EvtGen particle decay simulation package*, Nucl. Instrum. Meth.  
746 **A462** (2001) 152.
- 747 [12] P. Golonka and Z. Was, *PHOTOS Monte Carlo: A precision tool for QED corrections*  
748 *in Z and W decays*, Eur. Phys. J. **C45** (2006) 97, arXiv:hep-ph/0506026.
- 749 [13] GEANT4 collaboration, S. Agostinelli *et al.*, *GEANT4—a simulation toolkit*, Nucl.  
750 Instrum. Meth. A **506** (2003) 250.
- 751 [14] LHCb collaboration, M. Clemencic *et al.*, *The LHCb simulation application, Gauss:*  
752 *Design, evolution and experience*, J. Phys. Conf. Ser. **331** (2011) 032023.
- 753 [15] M. Bargiotti and V. Vagnoni, *Heavy quarkonia sector in PYTHIA 6.324: Tuning,*  
754 *validation and perspectives at LHCb*, .
- 755 [16] Particle Data Group, R. L. Workman and Others, *Review of Particle Physics*, PTEP  
756 **2022** (2022) 083C01.

- [17] LHCb collaboration, *Evidence for modification of b quark hadronization in high-multiplicity pp collisions at  $\sqrt{s} = 13$  TeV*, arXiv:2204.13042.
- [18] Z. Koba, H. B. Nielsen, and P. Olesen, *Scaling of multiplicity distributions in high-energy hadron collisions*, Nucl. Phys. B **40** (1972) 317.
- [19] LHCb collaboration, R. Aaij *et al.*, *Measurement of forward  $J/\psi$  production cross-sections in pp collisions at  $\sqrt{s} = 13$  TeV*, JHEP **10** (2015) 172, Erratum ibid. **05** (2017) 063, arXiv:1509.00771.
- [20] LHCb collaboration, R. Aaij *et al.*, *Measurement of  $\psi(2S)$  production cross-sections in proton-proton collisions at  $\sqrt{s} = 7$  and 13 TeV*, Eur. Phys. J. C **80** (2020) 185, arXiv:1908.03099.
- [21] T. Skwarnicki, *A study of the radiative cascade transitions between the Upsilon-prime and Upsilon resonances*, PhD thesis, Institute of Nuclear Physics, Krakow, 1986, DESY-F31-86-02.
- [22] J. Lefrancous, *Crystal ball fits*, link.
- [23] M. Pivk and F. R. Le Diberder, *sPlot: A statistical tool to unfold data distributions*, Nucl. Instrum. Meth. **A555** (2005) 356, arXiv:physics/0402083.
- [24] LHCb collaboration, R. Aaij *et al.*, *Measurement of the track reconstruction efficiency at LHCb*, JINST **10** (2015) P02007, arXiv:1408.1251.
- [25] *Tracking correction table*, <https://twiki.cern.ch/twiki/bin/view/LHCb/LHCbTrackingEfficiencies>.
- [26] PHENIX collaboration, A. Adare *et al.*, *Measurement of the relative yields of  $\psi(2S)$  to  $\psi(1S)$  mesons produced at forward and backward rapidity in  $p + p$ ,  $p+Al$ ,  $p+Au$ , and  ${}^3He+Au$  collisions at  $\sqrt{s_{NN}} = 200$  GeV*, Phys. Rev. C **95** (2017) 034904, arXiv:1609.06550.
- [27] NA50 collaboration, B. Alessandro *et al.*,  *$J/\psi$  and  $\psi$ -prime production and their normal nuclear absorption in proton-nucleus collisions at 400-GeV*, Eur. Phys. J. C **48** (2006) 329, arXiv:nucl-ex/0612012.
- [28] PHENIX collaboration, A. Adare *et al.*, *Ground and excited charmonium state production in  $p + p$  collisions at  $\sqrt{s} = 200$  GeV*, Phys. Rev. D **85** (2012) 092004, arXiv:1105.1966.
- [29] E705 collaboration, L. Antoniazzi *et al.*, *Production of  $J/\Psi$  via  $\psi$ -prime and  $\chi_1$  decay in 300-GeV/c proton and pi+- nucleon interactions*, Phys. Rev. Lett. **70** (1993) 383.
- [30] NA51 collaboration, M. C. Abreu *et al.*,  *$J/\psi$ ,  $\psi'$  and Drell-Yan production in  $p$  and  $p\bar{d}$  interactions at 450-GeV/c*, Phys. Lett. B **438** (1998) 35.
- [31] A. G. Clark *et al.*, *Electron Pair Production at the CERN ISR*, Nucl. Phys. B **142** (1978) 29.

- 793 [32] UA1 collaboration, C. Albajar *et al.*, *J / psi and psi-prime production at the CERN*  
794 *p anti-p collider*, Phys. Lett. B **256** (1991) 112.
- 795 [33] CDF collaboration, F. Abe *et al.*, *J/psi and psi(2S) production in pbar-p collisions at*  
796  $\sqrt{s} = 1.8 \text{ TeV}$ , Phys. Rev. Lett. **79** (1997) 572.
- 797 [34] LHCb collaboration, R. Aaij *et al.*, *Exclusive J/psi and psi(2S) production in pp*  
798 *collisions at  $\sqrt{s} = 7 \text{ TeV}$* , J. Phys. G **40** (2013) 045001, [arXiv:1301.7084](https://arxiv.org/abs/1301.7084).